frontiers

RESEARCH TOPICS

THE MICROBIAL FERROUS WHEEL: IRON CYCLING IN TERRESTRIAL, FRESHWATER, AND MARINE ENVIRONMENTS

Hosted by
David Emerson, Eric Roden and
Benjamin Twining

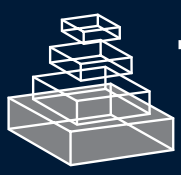

frontiers in
MICROBIOLOGY

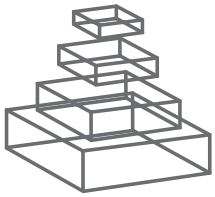

frontiers

FRONTIERS COPYRIGHT STATEMENT

© Copyright 2007-2012
Frontiers Media SA.
All rights reserved.

All content included on this site, such as text, graphics, logos, button icons, images, video/audio clips, downloads, data compilations and software, is the property of or is licensed to Frontiers Media SA ("Frontiers") or its licensees and/or subcontractors. The copyright in the text of individual articles is the property of their respective authors, subject to a license granted to Frontiers.

The compilation of articles constituting this e-book, as well as all content on this site is the exclusive property of Frontiers. Images and graphics not forming part of user-contributed materials may not be downloaded or copied without permission.

Articles and other user-contributed materials may be downloaded and reproduced subject to any copyright or other notices. No financial payment or reward may be given for any such reproduction except to the author(s) of the article concerned.

As author or other contributor you grant permission to others to reproduce your articles, including any graphics and third-party materials supplied by you, in accordance with the Conditions for Website Use and subject to any copyright notices which you include in connection with your articles and materials.

All copyright, and all rights therein, are protected by national and international copyright laws.

The above represents a summary only. For the full conditions see the Conditions for Authors and the Conditions for Website Use.

Cover image provided by Ibbl sarl, Lausanne CH

ISSN 1664-8714
ISBN 978-2-88919-074-4
DOI 10.3389/978-2-88919-074-4

ABOUT FRONTIERS

Frontiers is more than just an open-access publisher of scholarly articles: it is a pioneering approach to the world of academia, radically improving the way scholarly research is managed. The grand vision of Frontiers is a world where all people have an equal opportunity to seek, share and generate knowledge. Frontiers provides immediate and permanent online open access to all its publications, but this alone is not enough to realize our grand goals.

FRONTIERS JOURNAL SERIES

The Frontiers Journal Series is a multi-tier and interdisciplinary set of open-access, online journals, promising a paradigm shift from the current review, selection and dissemination processes in academic publishing.
All Frontiers journals are driven by researchers for researchers; therefore, they constitute a service to the scholarly community. At the same time, the Frontiers Journal Series operates on a revolutionary invention, the tiered publishing system, initially addressing specific communities of scholars, and gradually climbing up to broader public understanding, thus serving the interests of the lay society, too.

DEDICATION TO QUALITY

Each Frontiers article is a landmark of the highest quality, thanks to genuinely collaborative interactions between authors and review editors, who include some of the world's best academicians. Research must be certified by peers before entering a stream of knowledge that may eventually reach the public - and shape society; therefore, Frontiers only applies the most rigorous and unbiased reviews.
Frontiers revolutionizes research publishing by freely delivering the most outstanding research, evaluated with no bias from both the academic and social point of view.
By applying the most advanced information technologies, Frontiers is catapulting scholarly publishing into a new generation.

WHAT ARE FRONTIERS RESEARCH TOPICS?

Frontiers Research Topics are very popular trademarks of the Frontiers Journals Series: they are collections of at least ten articles, all centered on a particular subject. With their unique mix of varied contributions from Original Research to Review Articles, Frontiers Research Topics unify the most influential researchers, the latest key findings and historical advances in a hot research area!
Find out more on how to host your own Frontiers Research Topic or contribute to one as an author by contacting the Frontiers Editorial Office: researchtopics@frontiersin.org

THE MICROBIAL FERROUS WHEEL: IRON CYCLING IN TERRESTRIAL, FRESHWATER, AND MARINE ENVIRONMENTS

Hosted By:
David Emerson, Bigelow Laboratory for Ocean Sciences, USA
Eric Roden, University of Wisconsin-Madison, USA
Benjamin Twining, Bigelow Laboratory for Ocean Sciences, USA

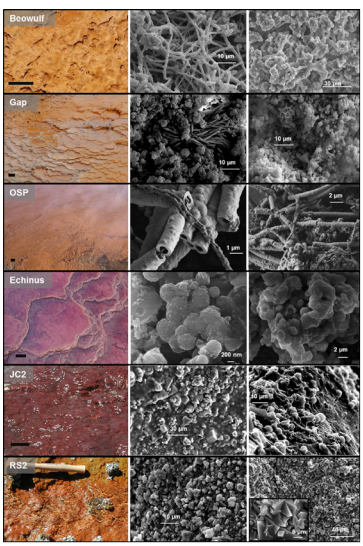

Figure reproduced from Kozubal et al. (2012) (see p. 161).

In the past 15 years, there has been steady growth in work relating to the microbial iron cycle. It is now well established that in anaerobic environments coupling of organic matter utilization to Fe reduction is a major pathway for anaerobic respiration. In iron-rich circumneutral environments that exist at oxic-anoxic boundaries, significant progress has been made in demonstrating that unique groups of microbes can grow either aerobically or anaerobically using Fe as a primary energy source. Likewise, in high iron acidic environments, progress has been made in the study of communities of microbes that oxidize iron, and in understanding the details of how certain of these organisms gain energy from Fe-oxidation. On the iron scarcity side, it is now appreciated that in large areas of the open ocean Fe is a key limiting nutrient; thus, a great deal of research is going into understanding the strategies microbial cells, principally phytoplankton, use to acquire iron, and how the iron cycle may impact other nutrient cycles. Finally, due to its abundance, iron has played an important role in the evolution of Earth's primary biogeochemical cycles through time.

The aim of this Research Topic is to gather contributions from scientists working in diverse disciplines who have common interests in iron cycling at the process level, and at the organismal level, both from the perspective of Fe as an energy source, or as a limiting nutrient for primary productivity in the ocean. The range of disciplines may include: geomicrobiologists, microbial ecologists, microbial physiologists, biological oceanographers, and biogeochemists. Articles can be original research, techniques, reviews, or synthesis papers. An overarching goal is to demonstrate the environmental breadth of the iron cycle, and foster understanding between different scientific communities who may not always be aware of one another's work.

Suggested Topics:
- Microbial Fe oxidation at neutral and acidic pH
- Microbial Fe reduction
- Ecosystem coupling of Fe-oxidation and reduction
- Iron availability in nutrient limited environments (or iron as a limiting nutrient in marine ecosystems)
- Cellular iron acquisition strategies of environmental importance
- Advanced techniques for studying iron biogeochemistry
- Paleo-microbiology of Fe-cycling

Table of Contents

frontiers in
MICROBIOLOGY

EDITORIAL
published: 31 October 2012
doi: 10.3389/fmicb.2012.00383

The microbial ferrous wheel: iron cycling in terrestrial, freshwater, and marine environments

***David Emerson*[1]*, *Eric Roden*[2] *and Benjamin S. Twining*[1]**

[1] *Bigelow Laboratory for Ocean Sciences, East Boothbay, ME, USA*
[2] *Department of Geoscience, University of Wisconsin, Madison, WI, USA*
**Correspondence: demerson@bigelow.org*

Edited by:
Bradley M. Tebo, Oregon Health and Science University, USA

Reviewed by:
Bradley M. Tebo, Oregon Health and Science University, USA

Were Oscar Wilde a devotee of iron biogeochemistry in the twenty-first century (hard as that might be to imagine), he might remark that iron is the most ironic of elements. Those interested in microbes that carry out life-sustaining iron-coupled redox reactions like to point out that iron is, after oxygen, the most abundant redox-active element in the Earth's crust. However, those studying oceanic phytoplankton regard iron as a nutrient that occurs at such vanishingly low concentrations in the surface ocean that it limits the growth of algae in more than 40% of the global ocean. This is because at the pH of seawater oxygen promotes the rapid oxidation of soluble ferrous iron to insoluble ferric iron oxyhydroxides that precipitate and sink out of the water column. As a result, while many marine microbes, and especially the photosynthetic ones, have developed finely-tuned mechanisms for acquiring iron, total primary productivity can be limited by iron.

At oceanic hydrothermal vents, and in terrestrial habitats, iron is not a limiting nutrient. At many oxic-anoxic interfacial habitats, not only is iron not limiting, but it is so abundant that lithotrophic microbes can use it as an electron source to sustain growth, and form robust communities of iron-oxidizing chemolithoautotrophs. In more acidic conditions, such as certain hot springs and acid mine drainage systems, ferrous iron is more stable, concentrations can be in the millmolar range, and specific communities of archaea and bacteria that use iron as an energy source can flourish. Iron-oxidizing microbes are not limited to aerobic habitats, but can also oxidize iron under anaerobic conditions by coupling the oxidation to either anoxygenic photosynthesis or nitrate reduction. Nor does it appear that they are limited to only utilizing soluble ferrous iron as an energy source, but can also acquire iron from insoluble minerals that contain reduced iron.

But iron-oxidation is only one-half of the equation. The utilization of ferric iron, principally in the form of Fe-oxides, to carry out anaerobic respiration is well established as an important pathway for organic carbon metabolism in anaerobic habitats. Furthermore, model organisms such as *Shewanella* and *Geobacter* are utilized to study the biochemical mechanisms of Fe-reduction, and from this we have learned a good deal about processes involved in extracellular electron transfer. Taken as a whole, it is apparent that the iron cycle is a remarkably complex process, dependent upon a wide range of chemical interactions, habitat types and groups of microbes that link it to all of Earth's other important biogeochemical cycles.

In this special topic issue we have gathered contributions from scientists working in diverse disciplines who have common interests in iron cycling at the process level and at the organismal level, from the perspective of iron as an energy source or as a limiting nutrient for primary productivity in the ocean. The hope is that bringing together seemingly disparate lines of research under one cover will result in a more global understanding of the iron cycle, and perhaps draw new insight into the connections within the cycle. We were very fortunate to enlist a varied and talented group of authors to contribute a wide range of articles. In total, 16 papers have been included, with a mixture of 9 original research articles, 6 reviews, and 1 perspective.

Aspects of iron cycling in the open ocean are covered by reviews on organic complexation (Gledhill and Buck, 2012) and on the role of superoxide dismutase (Rose, 2012), as well as in a research article on the role of weak iron-binding ligands in the ocean by Croot and Heller (2012). Oxygen-dependent iron oxidation at circumneutral pH is addressed in a research paper on a potential mechanism for iron oxidation by Liu et al. (2012), a research paper on mineralogy of biogenically-formed oxides at a hydrothermal vent (Toner et al., 2012), and a review of iron-based ecosystems associated with hydrothermal vents and the subsurface in the Pacific by Kato et al. (2012). Iron-cycling in acidic systems is reviewed by Johnson et al. (2012), and original research on a unique iron-rich acidic ecosystem in Yellowstone National Park is presented by Kozubal et al. (2012). A novel spectroscopic technique for biochemical analysis of iron oxidation in *Leptospirillum ferroxidans* is contributed by Blake and Griff (2012). Microbial utilization of iron under anaerobic conditions is dealt with in a review of mechanisms for iron reduction by Shi et al. (2012). Picardal (2012) reviews abiotic and microbial interactions of anaerobic iron oxidation and Carlson et al. (2012) provide an interesting perspective piece on nitrate-dependent iron oxidation. Original research on iron reduction in *Shewanella* is presented by Coursolle and Gralnick (2012), and competition among phototrophic and nitrate-dependent iron-oxidizing microbes is

addressed by Melton et al. (2012). Finally, original work from the laboratory of Eric Roden investigates redox cycling in a typical freshwater iron-rich stream (Roden et al., 2012), as well as the capacity for microbes to use iron minerals as an iron source (Shelobolina et al., 2012).

Taken together these papers present an overview of research on iron from a range of perspectives that indicates the breadth of work that has been done and provides insight into the many exciting avenues of research that continue to enhance our understanding of the iron cycle in nature.

REFERENCES

Blake, I. I. R. C., and Griff, M. N. (2012). *In situ* spectroscopy on intact *Leptospirillum ferrooxidans* reveals that reduced cytochrome 579 is an obligatory intermediate in the aerobic iron respiratory chain. *Front. Microbio.* 3:136. doi: 10.3389/fmicb.2012.00136

Carlson, H. K., Clark, I. C., Melnyk, R. A., and Coates, J. D. (2012). Toward a mechanistic understanding of anaerobic nitrate-dependent iron oxidation: balancing electron uptake and detoxification. *Front. Microbio.* 3:57. doi: 10.3389/fmicb.2012.00057

Coursolle, D., and Gralnick, J. A. (2012). Reconstruction of extracellular respiratory pathways for iron(III). Reduction in *Shewanella oneidensis* strain MR-1. *Front. Microbio.* 3:56. doi: 10.3389/fmicb.2012.00056

Croot, P. L., and Heller, M. I. (2012). The importance of kinetics and redox in the biogeochemical cycling of iron in the surface ocean. *Front. Microbio.* 3:219. doi: 10.3389/fmicb.2012.00219

Gledhill, M., and Buck, K. N. (2012). The organic complexation of iron in the marine environment: a review. *Front. Microbio.* 3:69. doi: 10.3389/fmicb.2012.00069

Johnson, D. B., Kanao, T., and Hedrich, S. (2012). Redox transformations of iron at extremely low pH: fundamental and applied aspects. *Front. Microbio.* 3:96. doi: 10.3389/fmicb.2012.00096

Kato, S., Nakamura, K., Toki, T., Ishibashi, J.-I., Tsunogai, U., Hirota, A., et al. (2012). Iron-based microbial ecosystem on and below the seafloor: a case study of hydrothermal fields of the southern mariana trough. *Front. Microbio.* 3:89. doi: 10.3389/fmicb.2012.00089

Kozubal, M. A., Macur, R. E., Jay, Z. J., Beam, J. P., Malfatti, S. A., Tringe, S. G., et al. (2012). Microbial iron cycling in acidic geothermal springs of Yellowstone National Park: integrating molecular surveys, geochemical processes, and isolation of novel Fe-active microorganisms. *Front. Microbio.* 3:109. doi: 10.3389/fmicb.2012.00109

Liu, J., Wang, Z., Belchik, S. M., Edwards, M. J., Liu, C., Kennedy, D. W., et al. (2012). Identification and characterization of MtoA: a decaheme c-type cytochrome of the neutrophilic Fe(II)-oxidizing bacterium Sideroxydans lithotrophicus ES-1. *Front. Microbio.* 3:37. doi: 10.3389/fmicb.2012.00037

Melton, E. D., Schmidt, C., and Kappler, A. (2012). Microbial iron(II). Oxidation in littoral freshwater lake sediment: the potential for competition between phototrophic vs. nitrate-reducing iron(II)-oxidizers. *Front. Microbio.* 3:197. doi: 10.3389/fmicb.2012.00197

Picardal, F. (2012). Abiotic and microbial interactions during anaerobic transformations of Fe(II) and NO_x^-. *Front. Microbio.* 3:112. doi: 10.3389/fmicb.2012.00112

Roden, E. E., McBeth, J. M., Blöthe, M., Percak-Dennett, E. M., Fleming, E. J., Holyoke, R. R., et al. (2012). The microbial ferrous wheel in a neutral pH groundwater seep. *Front. Microbio.* 3:172. doi: 10.3389/fmicb.2012.00172

Rose, A. L. (2012). The influence of extracellular superoxide on iron redox chemistry and bioavailability to aquatic microorganisms. *Front. Microbio.* 3:124. doi: 10.3389/fmicb.2012.00124

Shelobolina, E., Konishi, H., Xu, H., Benzine, J., Xiong, M. Y., Wu, T., et al. (2012). Isolation of phyllosilicate–iron redox cycling microorganisms from an illite–smectite rich hydromorphic soil. *Front. Microbio.* 3:134. doi: 10.3389/fmicb.2012.00134

Shi, L., Rosso, K. M., Clarke, T. A., Richardson, D. J., Zachara, J. M., and Fredrickson, J. K. (2012). Molecular underpinnings of Fe(III) oxide reduction by *Shewanella oneidensis* MR-1. *Front. Microbio.* 3:50. doi: 10.3389/fmicb.2012.00050

Toner, B. M., Berquó, T. S., Michel, F. M., Sorensen, J. V., Templeton, A. S., and Edwards, K. J. (2012). Mineralogy of iron microbial mats from loihi seamount. *Front. Microbio.* 3:118. doi: 10.3389/fmicb.2012.00118

Received: 02 October 2012; accepted: 14 October 2012; published online: 31 October 2012.

*Citation: Emerson D, Roden E and Twining BS (2012) The microbial ferrous wheel: iron cycling in terrestrial, freshwater, and marine environments. Front. Microbio. **3**:383. doi: 10.3389/fmicb.2012.00383*

This article was submitted to Frontiers in Microbiological Chemistry, a specialty of Frontiers in Microbiology.

Copyright © 2012 Emerson, Roden and Twining. This is an open-access article distributed under the terms of the Creative Commons Attribution License, which permits use, distribution and reproduction in other forums, provided the original authors and source are credited and subject to any copyright notices concerning any third-party graphics etc.

frontiers in
MICROBIOLOGY

REVIEW ARTICLE
published: 11 April 2012
doi: 10.3389/fmicb.2012.00124

The influence of extracellular superoxide on iron redox chemistry and bioavailability to aquatic microorganisms

Andrew L. Rose*

Southern Cross GeoScience, Southern Cross University, Lismore, NSW, Australia

Edited by:
Benjamin Twining, Bigelow Laboratory for Ocean Sciences, USA

Reviewed by:
Colleen Hansel, Harvard University, USA
Kai Waldemar Finster, Aarhus University, Denmark
Yeala Shaked, Hebrew University, Israel

***Correspondence:**
Andrew L. Rose, Southern Cross GeoScience, Southern Cross University, PO Box 157, Lismore, NSW 2480, Australia.
e-mail: andrew.rose@scu.edu.au

Superoxide, the one-electron reduced form of dioxygen, is produced in the extracellular milieu of aquatic microbes through a range of abiotic chemical processes and also by microbes themselves. Due to its ability to promote both oxidative and reductive reactions, superoxide may have a profound impact on the redox state of iron, potentially influencing iron solubility, complex speciation, and bioavailability. The interplay between iron, superoxide, and oxygen may also produce a cascade of other highly reactive transients in oxygenated natural waters. For microbes, the overall effect of reactions between superoxide and iron may be deleterious or beneficial, depending on the organism and its chemical environment. Here I critically discuss recent advances in understanding: (i) sources of extracellular superoxide in natural waters, with a particular emphasis on microbial generation; (ii) the chemistry of reactions between superoxide and iron; and (iii) the influence of these processes on iron bioavailability and microbial iron nutrition.

Keywords: iron, superoxide, bioavailability

INTRODUCTION

Superoxide (O_2^-), an anion resulting from the transfer of one-electron to a molecule of oxygen, was first identified by Edward Neuman, a postdoctoral researcher working with Linus Pauling, in 1934 (Neuman, 1934) as part of Pauling's ongoing interest in the nature of the chemical bond (Pauling, 1979). In aqueous solutions, superoxide exists in equilibrium with its conjugate acid, the hydroperoxyl (or perhydroxyl) radical ($HOO^\bullet$) (Bielski et al., 1985). The anion dominates the equilibrium in solutions whose pH is above the $pK_a = 4.8$ (Bielski et al., 1985). This is the case in the majority of natural surface waters, and at pH ~8.1, which is typical of marine waters and many carbonate-buffered freshwaters, superoxide is ~2000-fold more abundant than hydroperoxyl. To distinguish between the superoxide anion and "total" superoxide (i.e., both O_2^- and $HOO^\bullet$), I will represent "total" superoxide as O_2^{-*}.

O_2^{-*} has two chemical properties that produce a special relationship with Fe in natural aquatic environments. First, it may act as both a reductant (via its oxidation to O_2) and oxidant (via its reduction to H_2O_2), with the redox potentials of the O_2/O_2^{-*} and O_2^{-*}/H_2O_2 couples in natural waters around neutral pH poised in such a way that O_2^{-*} is thermodynamically able to react with a vast range of Fe complexes (Pierre et al., 2002). The second property arises from its unusual electronic structure. Despite possessing an odd number of valence shell electrons, the O_2^- anion is resonance stabilized by virtue of its symmetry and exhibits very little free radical character (Pauling, 1931; Neuman, 1934; Sawyer, 1991); hence I follow the convention here of omitting the free radical symbol and representing the superoxide anion as O_2^-. Thus in natural waters around pH 8 where the relatively unreactive O_2^- dominates over $HOO^\bullet$, and in the absence of other suitably reactive partners, O_2^{-*} has a half-life of tens of seconds to hours and has been measured to accumulate to typical concentrations in the range of 10–1000 pM (Rose et al., 2008b, 2010; Hansard et al., 2010; Shaked et al., 2010). These lifetimes are sufficiently long to ensure that O_2^{-*} can diffuse well away from the site of its production, enabling it to influence local redox chemistry on a spatial scale that is biologically significant, while typical concentrations are sufficiently high to ensure that it can react at environmentally relevant rates. It is this critical balance between longevity and reactivity that renders O_2^{-*} one of a select few extracellular reducing agents in natural waters that are able to exert a biologically significant influence on local redox chemistry. The combination of the overlapping redox potentials of the O_2/O_2^{-*} couple with the redox potentials of wide range of couples of Fe(II)/Fe(III) species, and the ability of O_2^{-*} to persist at sufficiently high concentrations, ensures that the fates of O_2^{-*} and Fe are often closely tied in environmental systems, and also in many intracellular biological systems, to the extent that they have been called "partners in crime" (Liochev and Fridovich, 1999).

The existence of O_2^{-*} has thus been known for nearly 90 years, initially being studied largely as a chemical curiosity due to its unusual electronic structure. In the 1960s, its importance in the aqueous intracellular environment was established with the discovery of superoxide dismutase (SOD), an enzyme whose role is to destroy O_2^{-*}. The biological importance of O_2^{-*} has been further reinforced by the discovery that SOD appears essential in aerobic organisms (McCord et al., 1971), and is found in nearly all aerobic forms of life (Wolfe-Simon et al., 2005) as well as many anaerobes (Gregory et al., 1978). Production of O_2^{-*} in the intracellular environment, its reactions with Fe, and effects on biological processes, have consequently been extensively studied over the past 50 years (see, for example, Sawyer and Gibian, 1979; Sawyer and Valentine, 1981; Fridovich, 1986; Afanas'ev, 1989; Winterbourn, 1995). However it is only since the 1980s that the potential role of O_2^{-*} in the aqueous extracellular environment has been examined in detail. Baxter and Carey (1983) established that O_2^{-*} was formed

during photolysis of humic substances in natural waters, while further pioneering work by Zika (Petasne and Zika, 1987; Micinski et al., 1993) and Zafiriou (1990) established that O_2^{-*} occurs in marine waters, where it may participate in reactions with a range of biologically important compounds. There has been renewed interest in the role of O_2^{-*} as a redox agent in natural waters in the last decade primarily because the development of new highly sensitive, rapid, and convenient analytical techniques (e.g., chemiluminescence of MCLA and its derivatives, with detection limits on the order of a few picomolar; Nakano et al., 1986; Nakano, 1998; Teranishi, 2007), has allowed determination of O_2^{-*} concentrations (Rose et al., 2008a) and production rates (Godrant et al., 2009; Milne et al., 2009) at environmentally relevant values. The role of O_2^{-*} was first accounted for in models of Fe speciation and bioavailability in natural waters by Miller et al. (1995), with increasing recognition of its potential importance reflected by inclusion of reactions between O_2^{-*} and Fe in several more recent models (Weber et al., 2005, 2007; Fan, 2008).

The primary purpose of this paper is to provide a detailed overview of the ways in which O_2^{-*} in the external milieu of microorganisms can modulate the chemical speciation of Fe, and thereby influence its biological availability. While drawing on some of the pioneering work on aqueous O_2^{-*} chemistry in the intracellular environment (including its reactions with Fe), the scope of the paper will be limited primarily to the extracellular environment in natural waters. In addition, while the paper is intended to consider the influence of extracellular superoxide on iron redox chemistry and bioavailability to aquatic microorganisms in all natural waters, it is relatively biased toward marine systems, because it is in these systems that most recent advances on the subject have occurred. While many other aspects of O_2^{-*} chemistry in natural waters are still being unraveled, including its role in cycles of other elements, this paper will consider only the role of O_2^{-*} in modulating Fe chemistry. In particular, the following issues will be addressed with an attempt to identify major knowledge gaps and critical research questions where possible:

1. How is O_2^{-*} produced in the extracellular milieu in natural waters?
2. By what mechanisms, and to what degree, can O_2^{-*} modulate Fe chemistry in the extracellular environment?
3. How can O_2^{-*} influence Fe bioavailability to microorganisms in aquatic environments, through direct and indirect means?

SOURCES OF EXTRACELLULAR SUPEROXIDE IN NATURAL WATERS

OVERVIEW

Theoretically, O_2^{-*} can be produced via either the one-electron reduction of O_2 or the one-electron oxidation of H_2O_2. In practice, reduction of O_2 appears to be the dominant pathway for O_2^{-*} production in natural waters, though oxidation of H_2O_2 has been shown to occur under some conditions (Moffett and Zafiriou, 1990). Like O_2^-, the dioxygen molecule also possesses an unusual electronic structure, with its lowest energetic state (ground state) possessing two unpaired electrons with parallel spins, i.e., its ground state is a triplet state biradical (Sawyer, 1991). Quantum mechanical restrictions (the Pauli exclusion principle) dictate that, under typical environmental conditions, triplet state dioxygen can react only extremely slowly with molecules possessing singlet state electronic configurations (e.g., most organic compounds), but much more readily with free radicals (e.g., organic radicals and transition metal ions), such that the reduction of dioxygen must proceed primarily via single electron transfer steps (Fridovich, 1998). This implies that reduction of dioxygen should always result in O_2^{-*} production.

Attempting to identify sources of O_2^{-*} in oxygenated waters is complicated, because the redox cycling of a range of relatively labile redox couples are intimately coupled in oxygenated natural waters; thus, trying to establish which redox reaction governs the system behavior is like the "chicken and egg" question of which came first. A common property of these labile redox-active compounds (LRACs) is that they are sufficiently labile to accept and donate their cargo of electrons, but also sufficiently long-lived to enable transport on biologically relevant spatial scales. Three major processes result in the occurrence of reduced LRACs in oxygenated surface waters: abiotic photochemistry, biological activity, and transport of reduced LRACs into (at least partially) oxygenated surface waters from other environments (e.g., at sediment-water interfaces, discharge of anoxic groundwaters, rainwater deposition, etc.). In the case of biological processes, the "ultimate" source of electrons is usually (but not always) water; in the case of abiotic photochemistry it is usually organic compounds, which are themselves often (although not always) derived from biological activity. Biological reduction in oxygenated waters is also predominantly powered ultimately via solar energy (either through photosynthesis, or respiration of reduced substrates that have been previously been produced by photosynthesis). In oxygenated waters, O_2^{-*} can then be produced by reduction of O_2 directly through one of these processes, or through reduction of another LRAC that then reacts with O_2 to yield O_2^{-*}. Thus the vast majority of O_2^{-*} production in natural waters is driven ultimately by solar radiation, but the path by which this solar energy ultimately induces reduction of O_2 to O_2^{-*} varies (**Figure 1**).

The main pathways for reduction of O_2 to O_2^{-*} can thus be broadly grouped into abiotic thermal ("dark") processes, abiotic photochemical processes, and biologically mediated processes. Until recently, abiotic photochemistry in surface waters was thought to be the major pathway for O_2^{-*} production in the extracellular environment (Cooper et al., 1989). A growing body of work has shown that aquatic microorganisms can also produce O_2^{-*} extracellularly, and that the flux via this pathway may be at least as great as that via abiotic photochemistry (Hansard et al., 2010; Rose et al., 2010). However abiotic photochemistry is still likely to result in a non-negligible contribution to total extracellular superoxide production (ESP) in most sunlit waters, and in some cases may be the dominant source. The contribution of abiotic thermal production (through oxygenation of reduced LRACs) to overall rates of ESP in natural waters is unknown, although the observation that filtration to remove cells (and other particulates) does not always completely inhibit ESP (e.g., Rose et al., 2010) suggests that it may be substantial in some environments. These pathways are now considered in more detail.

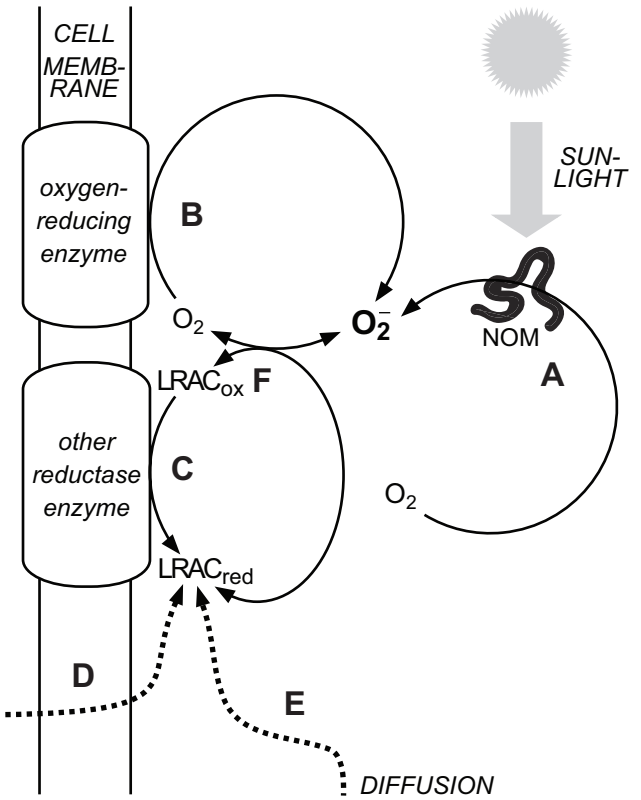

FIGURE 1 | Major sources of O_2^{-*} in natural waters. (A) Abiotic, photochemical oxidation of natural organic matter (NOM) with concomitant reduction of O_2. **(B)** Biological reduction of O_2 in the extracellular milieu via cell surface enzymes. **(C)** Biological reduction of oxidized labile redox-active compounds ($LRAC_{ox}$) in the extracellular milieu to form reduced labile redox-active compounds ($LRAC_{red}$) that subsequently reduce O_2 to O_2^{-*}. **(D)** Biological release of $LRAC_{red}$ into the extracellular milieu that subsequently reduce O_2 to O_2^{-*}. **(E)** Diffusion of $LRAC_{red}$ produced under suboxic conditions into more oxygenated waters. **(F)** The O_2/O_2^{-*} couple readily exchanges electrons with a range of other labile redox-active compounds in the extracellular milieu. Decay pathways for O_2^{-*} are not shown.

ABIOTIC THERMAL ("DARK") PRODUCTION

O_2^{-*} can theoretically be produced by oxygenation of a range of reduced LRACs that may occur in natural waters. The oxygenation of reduced metals [e.g., Fe(II), Mn(II), V(II), Cr(II), Cu(I), and Co(II)] has been proposed to generally occur via the Haber–Weiss mechanism (Haber and Weiss, 1934), resulting in the production of O_2^- after the first step:

$$M^{n+} + O_2 \rightarrow M^{(n+1)+} + O_2^- \quad (1)$$

Where M^{n+} represents the reduced form of the metal and $M^{(n+1)+}$ its oxidized form.

However it is not certain that these electron transfer steps always result in release of the free intermediate, as O_2^- and peroxide anions (O_2^{2-}) both possess coordinative properties and may potentially remain bound in the inner coordination sphere of the oxidized metal center. Using computational chemistry methods, Rosso and Morgan (2002) concluded that V^{2+}, Co^{2+}, and Fe^{2+} were likely to react with O_2 via an outer-sphere mechanism, such that O_2^- would be formed outside the inner coordination sphere (and presumably be able to diffuse into the bulk medium as the free anion), while Mn^{2+}, Cr^{2+}, and hydrolyzed Fe(II) species were suggested to react with O_2 via an inner-sphere process, such that O_2^- would initially be coordinated to the metal center (Rosso and Morgan, 2002). Fe(II) complexed by EDTA and similar ligands also appears to react with O_2 via an inner-sphere process (Zang and van Eldik, 1990; Seibig and van Eldik, 1997).

Whether O_2^{-*} formed in this way could subsequently participate in other reactions likely depends on how rapidly it can escape from the inner coordination sphere after electron transfer is complete. It is unclear how Fe(II) in natural waters might behave, but complexation of Fe(II) by natural organic matter (NOM) appears to substantially modify its oxygenation kinetics (e.g., Rose and Waite, 2003a and references therein), suggesting that further investigation of this issue is needed, ideally through both experimental and computational means. Hereafter, it will be assumed that reduction of O_2 ultimately results in production of unbound O_2^{-*}, even if it is initially formed in the inner coordination sphere of a metal complex. However, this uncertainty in our understanding of O_2^{-*} behavior needs to be resolved in order to fully evaluate the relationship between O_2^{-*} and Fe bioavailabilty in natural waters.

Other reduced LRACs in natural waters include reduced sulfur species (RSS) such as thiols and sulfides, and some reduced organic moieties. While the contribution of such species to ESP has not yet been evaluated, RSS may be found at measurable concentrations in oxic waters (Bowles et al., 2003; Luther and Rickard, 2005; Rickard and Luther, 2006) and at least some RSS yield O_2^{-*} as a result of oxygenation (Rao et al., 1990). Certain redox-active moieties within NOM also react readily with oxygen (Ratasuk and Nanny, 2007; Aeschbacher et al., 2010), potentially yielding O_2^{-*} (discussed further in the following section). The oxygenation chemistry (particularly thermodynamics) of a range of major LRACs present in natural waters has recently been described in considerable detail by Luther (2010), while the thermodynamics of the $Fe/O_2/O_2^{-*}$ system is discussed in detail by Pierre et al. (Pierre and Fontecave, 1999; Pierre et al., 2002).

PHOTOCHEMICAL PRODUCTION

Measured rates of photochemical O_2^{-*} production in natural marine waters have typically been in the range of ∼0.3–500 nM h^{-1} (Petasne and Zika, 1987; Micinski et al., 1993; Shaked et al., 2010). Rates of O_2^{-*} production in natural freshwaters have not been reported in the literature, although laboratory experiments using simulated freshwater systems yielded similar rates (Garg et al., 2011a). The mechanism of abiotic photochemical O_2^{-*} production from NOM has usually been represented by a reaction in which NOM is photoexcited to a triplet state, which subsequently transfers an electron to O_2 to yield O_2^{-*} and an oxidized organic moiety (Cooper et al., 1988, 1989):

$$NOM + h\nu + O_2 \rightarrow NOM^+ + O_2^{-*} \quad (2)$$

The pathway(s) by which this overall reaction occurs are still not certain, although the details are slowly being unraveled. While it was thought that photoexcited NOM may eject free aquated

electrons, this now appears unlikely (Thomas-Smith and Blough, 2001). Instead, the photoexcited organic moiety can undergo a range of possible energetic and redox transitions, particularly in humic and fulvic substances that possess a wide range of functional groups and redox potentials. The mechanism of organic radical formation in photoexcited NOM was first studied in detail by Blough (1988) but, despite considerable advances over the last 20 years, the precise details of O_2^{-*} formation still remain elusive. The mechanisms were thought to be similar to those involved in O_2^{-*} production from photoexcited quinones, which have been studied extensively (e.g., Garg et al., 2007b and references therein), however the situation in humic and fulvic-type NOM is complicated considerably by the existence of multiple chromophores (Del Vecchio and Blough, 2002, 2004; Boyle et al., 2009) and redox-active moieties (Aeschbacher et al., 2010), many of which may be linked under exposure to light through charge-transfer complexes (Del Vecchio and Blough, 2004). More recently, Garg et al. (2011b) proposed a mechanism in which quinone-like moieties within NOM are reduced by some other electron donor within the NOM structure under solar radiation, with the reduced organic moiety then reacting with dissolved oxygen (in either the triplet or singlet state) to yield O_2^{-*}:

$$\mathrm{NOM} + h\nu \xrightarrow{\text{organic electron donor}} \mathrm{NOM}^- \quad (3)$$

$$\mathrm{NOM}^- + \mathrm{O_2} \longrightarrow \mathrm{NOM} + \mathrm{O_2^{-*}} \quad (4)$$

The overall process is complicated considerably by formation of a range of other radical sinks for O_2^{-*}, but the net result is that NOM is oxidized by O_2 to yield O_2^{-*} through the involvement of several moieties within the NOM, some of which may act as photocatalysts.

Consistent with the concept of labile transfer of electrons between the range of LRACs present in oxygenated waters, a second indirect mechanism of photochemical superoxide formation involves formation of reduced metals via ligand-to-metal charge-transfer reactions, with subsequent oxygenation of the reduced metal. The role of such reactions involving iron–organic complexes in marine systems has been recently reviewed by Barbeau (2006), and similar reactions can also occur with complexes of copper (Jones et al., 1985).

BIOLOGICAL PRODUCTION

Biological production of O_2^{-*} in the extracellular milieu has been reported from culture studies involving a wide range of environmentally occurring aquatic microorganisms, including eukaryotic microalgae from the class Raphidophyceae (Oda et al., 1997; Marshall et al., 2002, 2005; Yamasaki et al., 2004; Garg et al., 2007a); dinoflagellates and prymnesiophytes (Yamasaki et al., 2004; Marshall et al., 2005); marine diatoms from the genus *Thalassiosira* (Kustka et al., 2005); marine cyanobacteria from the genera *Synechococcus* (Rose et al., 2008b), *Lyngbya* (Rose et al., 2005) and *Trichodesmium* (Godrant et al., 2009); a marine alphaproteobacterium from the genus *Roseobacter* (Learman et al., 2011); the freshwater cyanobacterium *Microcystis aeruginosa* (Fujii et al., 2011); the unicellular protozoan coral symbiont *Symbiodinium* (Saragosti et al., 2010); fungi and yeasts including *Aspergillus nidulans* (Lara-Ortíz et al., 2003) and *Saccharomyces cerevisiae* (Shatwell et al., 1996), as reviewed by Aguirre et al. (2005); and the heterotrophic bacteria *Paracoccus denitrificans* (Henry and Vignais, 1980) and *Escherichia coli* (Korshunov and Imlay, 2006). Rates of ESP vary enormously between these different organisms, with the maximum reported rates being from the marine Raphidophycean *Chattonella marina* of up to ∼5 pmol cell^{-1} h^{-1} (Oda et al., 1997; Garg et al., 2007a). Additionally, recent field studies have provided evidence from several marine environments suggesting that a significant proportion of ESP occurs via biologically mediated processes, with measured rates of biological ESP up to 1 nM h^{-1} in the Great Barrier Reef lagoon (Rose et al., 2010) and up to 20 nM h^{-1} in the Gulf of Alaska (Hansard et al., 2010). These studies have predominantly involved either field studies in marine environments, or culture studies of organisms that typically inhabit marine environments, with notable exceptions being the studies involving *M. aeruginosa*, *P. denitrificans* (which is typically rather ubiquitous in soils), *A. nidulans*, *S. cerevisiae*, and *E. coli*. While there is still insufficient evidence to make definitive generalizations, the occurrence of these processes across such a wide range of microorganisms in the marine environment, coupled with evidence for ESP by a range of terrestrial multicellular organisms such as lichens (Beckett et al., 2003) and plants (Bolwell, 1999), suggests that microbial ESP probably occurs to at least some extent in the vast majority of surface waters.

Biological production of O_2^{-*} in the intracellular environment has been studied for several decades and many of the processes involved are well understood. In eukaryotic organisms, intracellular O_2^{-*} production is believed to be highly compartmentalized, with the majority occurring via reduction of O_2 inside the mitochondria and through the action of NADPH oxidase (NOX) enzymes, which are typically located inside vesicles (Auchère and Rusnak, 2002). In photosynthetic eukaryotes, O_2^{-*} is also produced in significant amounts in the chloroplasts (Lesser, 2006). In prokaryotic organisms, which lack intracellular compartments separated by cellular membranes, the majority of intracellular O_2^{-*} production is thought to occur during O_2 reduction by the respiratory electron transport chain (Auchère and Rusnak, 2002), which is also used for electron transport during photosynthesis in photosynthetic prokaryotes such as cyanobacteria (Lesser, 2006). It is extremely unlikely that such intracellular processes can be the direct source of ESP because the polar O_2^- anion is unable to readily diffuse through the lipid bilayer that isolates the cytoplasm from the external milieu (Korshunov and Imlay, 2002). HOO$^\bullet$ can diffuse at a rate approaching that of water (permeability of $P = 9 \times 10^{-4}$ cm s^{-1} $= 3.2 \times 10^{-2}$ m h^{-1}; Korshunov and Imlay, 2002), but as HOO$^\bullet$ is only a small proportion of O_2^{-*} around neutral pH, this flux is limited. The flux of O_2^{-*} out of the cell is given by:

$$\mathrm{Flux} = \alpha_{\mathrm{HOO}^\bullet} P A \Delta \left[\mathrm{O_2^{-*}}\right] \quad (5)$$

Where $\alpha_{\mathrm{HOO}^\bullet}$ is the fraction of O_2^{-*} that is in the HOO$^\bullet$ form, P is the permeability of HOO$^\bullet$, A is the cell surface area, and $\Delta[O_2^{-*}]$ is the difference between the intracellular and extracellular O_2^{-*} concentrations. In a typical "healthy" cell, the steady-state intracellular O_2^{-*} concentration is around 100 pM (Imlay and Fridovich,

1991). Considering an exemplary spherical cell with a diameter of 20 μm, and assuming that the steady-state extracellular O_2^{-*} concentration ≪100 pM, the calculated flux is 8 zmol cell h^{-1}. Even if we assume that the cell is suffering from severe oxidative stress, resulting in an intracellular O_2^{-*} concentration of 10 nM, the flux is still only 800 zmol cell h^{-1}. This is several orders of magnitude less than measured rates of ESP from the range of aquatic microorganisms surveyed to date. Additionally, O_2^{-*} concentrations in the external milieu may be similar to, if not greater than, intracellular O_2^{-*} concentrations, such that diffusion of O_2^{-*} across the lipid bilayer, even if it could occur at substantial rates, would in fact occur into the cell under these conditions by virtue of the concentration gradient.

Another possible source of ESP is release of intracellular O_2^{-*} during cell lysis. Assuming that the rate of cell lysis = rate of cell division to maintain a steady-state population, with spherical cells 20 μm in diameter under severe oxidative stress such that the intracellular O_2^{-*} concentration was again 10 nM, then even in a rapidly growing population with a division rate of 1 h^{-1} the rate of ESP by this pathway would be only 4 zmol cell h^{-1}. Of course more rapid lysis could temporarily result in a more rapid release of intracellular O_2^{-*} by this pathway, but such rates could not be sustained to yield the steady-state concentrations of O_2^{-*} that have been measured in natural waters to date. Thus the majority of O_2^{-*} found in the extracellular milieu of aquatic microorganisms must, in general, be produced extracellularly.

While mechanisms of biological ESP have been reasonably well studied in human cells, mechanisms of biological ESP in aquatic microorganisms are generally not well understood. Enzymes from the NOX and dual oxidase (DUOX) families located at the cytoplasmic membrane are known to be responsible for ESP in the majority of human cells, notably including phagocytes responsible for the "respiratory burst" immunological defense phenomenon (Vignais, 2002; Lambeth, 2004). Cell surface located NOX enzymes have also been shown to be responsible for ESP in *C. marina* (Kim et al., 2000), the fungus *A. nidulans* (Lara-Ortíz et al., 2003) and numerous other fungi and yeasts (Aguirre et al., 2005), certain plant cells (Torres et al., 1998; Sagi and Fluhr, 2001), and the coral *Stylophora pistillata* and its symbiont *Symbiodinium* sp. (Saragosti et al., 2010). Addition of diphenyleneiodonium chloride (DPI), which is a specific inhibitor of NOX enzymes, has also been shown to dramatically inhibit ESP in cultures of the diatoms *Thalassiosira weissflogii* and *T. pseudonana* (Kustka et al., 2005). BLAST searches of sequenced genomes reveal the presence of genes encoding for polypeptide sequences similar to those found in NOX proteins in these two diatoms (Kustka et al., 2005) and in a wide range of other eukaryotic aquatic microorganisms, however this does not necessarily indicate the occurrence of ESP mediated by NOX enzymes in these organisms, since NOX enzymes are also found intracellularly as discussed previously. BLAST searches of the genomes of prokaryotic aquatic microorganisms reveal that such genes are not always present, suggesting that ESP by prokaryotes may occur via one or more other mechanisms.

Finally, it is worth reiterating that it is often difficult to establish which species is reduced first during ESP; in the case of biological ESP, it is not always clear whether O_2 is reduced to O_2^{-*} directly by enzymes, or whether O_2^{-*} is produced through oxygenation of some other reduced LRAC formed directly by enzymatic reduction. In the case of *E. coli*, O_2^{-*} production in the organism's periplasm has been inferred to occur through the oxidation of soluble, reduced quinones, with electrons originating from transfer across the cytoplasmic membrane via the respiratory electron transport chain (Korshunov and Imlay, 2006). The cell surface ferric reductase system of the yeast *S. cerevisiae* possesses similarities to the NOX system at the genetic level (Shatwell et al., 1996), and is capable of reducing a range of LRACs (Kosman, 2003) including O_2 to yield O_2^{-*} (Lesuisse et al., 1996). The biogeochemical significance (if any) of which LRAC is reduced first is not yet certain, however it is clear that caution should be used when assigning a particular mechanism for cell surface reductase activity on the basis of genetic homology or biochemical studies conducted under a limited set of chemical conditions.

CHEMISTRY OF REACTIONS BETWEEN SUPEROXIDE AND IRON

OVERVIEW

In aqueous solutions, O_2^{-*} can react in three major ways (Sawyer and Gibian, 1979; Sawyer and Valentine, 1981; Sawyer, 1991):

1. As a reductant. The O_2^- anion is a mild reducing agent capable of directly donating electrons via an outer-sphere process to suitable electron acceptors (e.g., transition metals and their complexes).
2. As an oxidant. $HOO^\bullet$ is capable of oxidizing suitable electron donors via direct electron transfer, but this is highly unfavorable for the O_2^- anion due to the extreme instability of the O_2^{2-} anion in aqueous solution at most pH values. However, O_2^- is capable of indirectly inducing oxidation by either hydrogen atom or proton extraction from suitable substrates, with subsequent reactions resulting in their net oxidation.
3. As a Lewis base (electron pair donor). The O_2^- anion may be coordinated in the inner sphere of various metal ions in aqueous solution, and can also participate in radical–radical coupling with a range of organic radical cations.

The role of O_2^{-*} as a Lewis base is restricted in natural aquatic environments because the maximum concentration of O_2^{-*} that is attainable is typically too low (due to its consumption via other reactions) in comparison to other species to have any significant effect. In practice, therefore, O_2^{-*} behaves primarily as a reductant or oxidant in natural waters. Early laboratory studies of reactions between aqueous Fe and O_2^{-*} typically used pulse radiolysis to generate O_2^{-*} and UV–visible spectrophotometry to observe the subsequent reactions (Jayson et al., 1969, 1973; Buettner et al., 1983; Bull et al., 1983; Rush and Bielski, 1985). While useful in understanding the chemistry of Fe and O_2^{-*}, results from these studies must be applied to environmental systems with caution because the use of high concentrations of both Fe and O_2^{-*} could favor reactions that are not important at lower, environmentally relevant concentrations. This is particularly true for oxidation of Fe(II) by O_2^{-*}, where the initial step appears to typically involve coordination of O_2^- in the inner sphere of Fe(II). Furthermore, natural systems involve a host of other competing reactions due to the range of other species present.

The potential effect of O_2^{-*} on Fe in environmental systems was first specifically studied by Voelker and Sedlak (1995). They concluded that O_2^{-*} functioned primarily as a reductant of Fe(III) over the pH range 5–8 (where O_2^- dominates over $HOO^\bullet$), and that substantial amounts of Fe(II) could be expected to be produced in certain environmental systems as a result of this process. More recent studies have typically used lower concentrations of Fe and O_2^{-*} that are more representative of what is typically found in natural systems, largely due to the possibilities afforded by the development of new techniques such as the MCLA chemiluminescence method, and have considered a range of different conditions that are more relevant to natural waters. Fe species can be broadly classified in such systems into three main groups:

1. Mononuclear inorganic complexes, which include hydrolysis species and a range of relatively weak complexes with small, commonly occurring inorganic ligands such as chloride, sulfate, bromide, fluoride, carbonate, and phosphate. These complexes interconvert rapidly compared to the other reactions we will consider, and may thus be assumed to be at equilibrium at all times.
2. Mononuclear organic complexes, which occur with a wide range of naturally occurring organic ligands such as humic and fulvic-type materials, polysaccharides, siderophores, and other biologically produced compounds.
3. Polynuclear complexes, which include amorphous oxyhydroxide solids, various iron minerals, and aggregates containing varying proportions of iron, organic material, and potentially other species.

Within each of these classes, individual Fe atoms may be present in either the Fe(II) or Fe(III) redox state, and the transformations between these redox states may be mediated by O_2^{-*} (**Figure 2**).

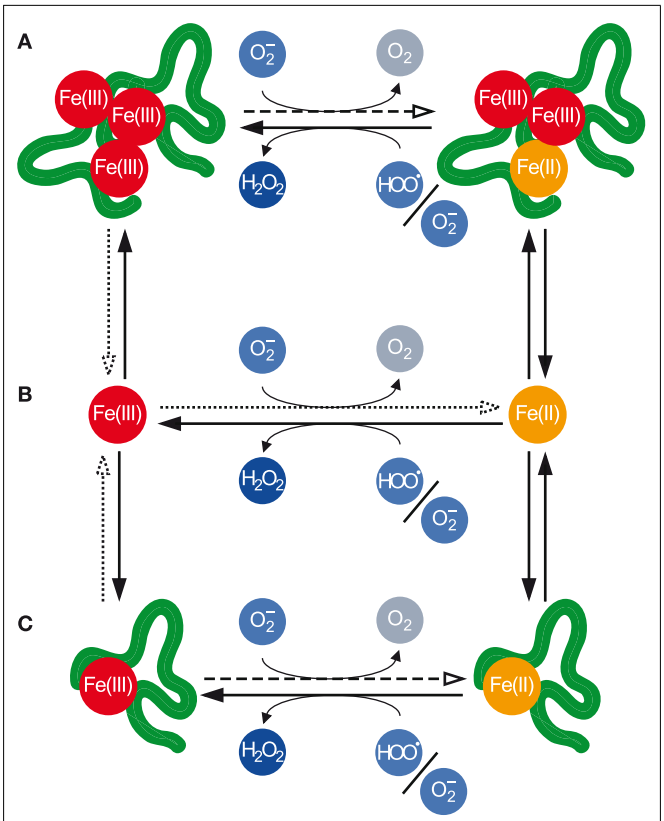

FIGURE 2 | Transformations between various pools of Fe as mediated by O_2^{-*}. (A) Polynuclear complexes, which contain multiple Fe atoms and may also contain other inorganic and organic ligands. **(B)** Mononuclear inorganic complexes. **(C)** Mononuclear organic complexes. Fe(III) in all pools may be reduced by the O_2^- anion to Fe(II), while Fe(II) in all pools may be oxidized to Fe(III) primarily by $HOO^\bullet$, but also indirectly by O_2^-. The dotted arrows denote the dissociative reduction (DR) pathway, while the dashed arrows denote the non-dissociative reduction (NDR) pathway for Fe(III) reduction by O_2^{-*}.

THERMODYNAMICS

Due to pK_a of $O_2^-/HOO^\bullet$ being in the environmentally relevant range, and $HOO^\bullet$ being considerably more oxidizing than O_2^-, the standard redox potential of the O_2/O_2^{-*} couple can vary considerably from +120 mV at pH ≪ 4.8 to −160 mV at pH ≫ 4.8 (Sawyer, 1991). In the majority of natural surface waters, which are in the neutral to slightly alkaline pH range, the standard redox potential of the O_2/O_2^{-*} couple is thus −160 mV. Therefore, under standard conditions at around neutral pH, O_2^{-*} is a mild reducing agent. In contrast, the standard redox potentials of various Fe(II)/Fe(III) couples vary from <−1000 to >+1000 mV depending on pH and complex speciation (Pierre and Fontecave, 1999; Pierre et al., 2002). Despite the overlap between the standard redox potentials of the O_2/O_2^{-*} couple and those of many Fe(II)/Fe(III) species redox couples, an important caveat when considering the feasibility of redox reactions is that these redox potentials apply to standard conditions, i.e., $[O_2] = [O_2^{-*}] =$ [Fe(II)] species = [Fe(III)] species. As discussed in detail by Pierre et al. (2002), such conditions are irrelevant in most natural systems. Under conditions typical for a neutral air-saturated surface water (pH 7 and $[O_2] = 250\ \mu M$), the actual redox potential of the O_2/O_2^{-*} couple is +335 mV when $[O_2^{-*}] = 1$ pM and +158 mV when $[O_2^{-*}] = 1$ nM. An equally important consideration for the thermodynamic reducibility of a particular form of Fe by O_2^{-*} is the concentration of relevant Fe(II) and Fe(III) species. The reduction of an organic Fe complex [denoted as Fe(II)L in the reduced state and Fe(III)L in the oxidized state] is thermodynamically feasible if:

$$\log([\text{Fe (II) L}]/[\text{Fe (III) L}]) < \left(E^0_{Fe^{3+}\rightarrow Fe^{2+}} - E_{O_2\rightarrow O_2^{-*}}\right)\Big/59 + \log\left(\left(K_{Fe(II)L}\alpha_{Fe^{3+}}\right)/\left(K_{Fe(III)L}\alpha_{Fe^{2+}}\right)\right) \quad (6)$$

where the stability constants are mixed constants expressed as:

$$K_{Fe(II)L} = \frac{[\text{Fe (II) L}]}{[\text{Fe (II)}'][L']} \quad (7)$$

$$K_{Fe(III)L} = \frac{[\text{Fe (III) L}]}{[\text{Fe (III)}'][L']} \quad (8)$$

and where, under particular medium conditions, Fe(II)′ represents the sum of all monomeric inorganic Fe(II) species, Fe(III)′ represents the sum of all monomeric inorganic Fe(III) species, L′

represents the sum of all ligand species, $\alpha_{Fe^{2+}}$ represents the ratio of $[Fe^{2+}]/[Fe(II)']$, $\alpha_{Fe^{3+}}$ represents the ratio of $[Fe^{3+}]/[Fe(III)']$, and redox potentials are in millivolt (see Thermodynamics for the full derivation in Appendix).

Calculated values for some typical complexes around pH 8, where $\alpha_{Fe^{2+}} = 0.5$ and $\alpha_{Fe^{3+}} = 10^{-10}$ (Millero et al., 1995), are shown in **Table 1**. It is thermodynamically feasible to reduce a substantial proportion of Fe(III)L to Fe(II)L for some relatively strong Fe(III) complexes, such as that formed with EDTA in freshwater, provided that the ligand also forms a relatively strong Fe(II) complex. This contrasts with the case of DFB, which forms a much stronger complex with Fe(III) than with Fe(II), where reduction of Fe(III)L to Fe(II)L is thermodynamically feasible only at exceedingly low Fe(II)L:Fe(III)L ratios.

However reduction of Fe(III) by O_2^{-*} may be still environmentally important even when the thermodynamically permissible concentration of Fe(II)L is much less than that of Fe(III)L, because many microorganisms acquire iron from the dissolved inorganic pool rather than directly from organically complexes species. A more useful thermodynamic test, then, is whether O_2^{-*} can increase the proportion of dissolved inorganic Fe, given that it is these forms of Fe that are usually the immediate substrate for uptake by aquatic microorganisms (Morel et al., 2008). According to the Nernst equation, reduction of Fe^{3+} to Fe^{2+} is thermodynamically feasible when:

$$\log\left(\left[\text{Fe (II)}'\right]/\left[\text{Fe (III)}'\right]\right) < \log\left(\alpha_{Fe^{3+}}/\alpha_{Fe^{2+}}\right) + \left(E^0_{Fe^{3+}\rightarrow Fe^{2+}} - E_{O_2\rightarrow O_2^{-*}}\right)\Big/59 \quad (9)$$

Thus at pH 8.1, it is thermodynamically feasible to attain ratios of $[Fe(II)']/[Fe(III)']$ of up to ∼0.005 with 1 pM O_2^{-*} and up to ∼5 with 1 nM O_2^{-*}. Consequently, regardless of organic complex speciation, nanomolar concentrations of O_2^{-*} can theoretically result in more Fe(II)′ than Fe(III)′ in an equilibrium or pseudo-equilibrium scenario.

While these types of calculations are useful for assessing the thermodynamic driving force and consequent feasibility of O_2^{-*} as a reductant for Fe, they are really only useful to provide a general context for such reactions. It is often overlooked that environmental systems are not always at equilibrium (and in some environments, are never at equilibrium), and as a consequence, the usefulness of thermodynamics in such systems is limited. In particular, processes that can perturb the system can increase the thermodynamic feasibility, such as removal of Fe(II) by biological uptake (Pierre and Fontecave, 1999). In this case, a lower Fe(II) concentration can be maintained, increasing the driving force for reduction (Eq. 9). Because such systems are at steady-state rather than a true equilibrium, thermodynamics cannot be used to predict what the final system will look like, but if the composition [e.g., concentrations of O_2^{-*}, O_2, Fe(II), and Fe(III)] of the steady-state system is known, it can be used to understand the energetics of the system. However being able to predict what this steady-state system will look like is usually a major objective in environmental systems, and this can only be achieved by a more rigorous kinetic analysis.

KINETICS AND MECHANISMS

Within the three classes shown in **Figure 2**, there is potentially a multitude of individual Fe species. Speciation of the dissolved

Table 1 | Calculated ratios of [Fe(II)L]/[Fe(III)L] below which reduction of Fe(III)L to Fe(II)L by O_2^{-*} is thermodynamically feasible for various Fe complexes in natural waters around pH 8.

Ligand (L)	Medium conditions	$[O_2^{-*}]$ (pM)	$\log K_{Fe(II)L}$	$\log K_{Fe(III)L}$	Maximum [Fe(II)L]/[Fe(III)L]
Desferrioxamine B (DFB)	pH 8.0, freshwater ($I = 0.1$ M)	1	7.0[a]	18.1[a]	3.7×10^{-14}
		1000	7.0[a]	18.1[a]	3.7×10^{-11}
	pH 8.0, seawater ($I = 0.7$ M)	1	4.05[b]	12.1[c]	4.2×10^{-11}
		1000	4.05[b]	12.1[c]	4.2×10^{-8}
Ethylenediaminetetraacetate (EDTA)	pH 8.0, freshwater ($I = 2$ mM)	1	9.24[d]	10.54[e]	2.4×10^{-4}
		1000	9.24[d]	10.54[e]	0.24
	pH 8.0, seawater ($I = 0.7$ M)	1	5.37[b]	7.36[f]	4.8×10^{-5}
		1000	5.37[b]	7.36[f]	4.8×10^{-2}
Citrate	pH 8.2, seawater ($I = 0.7$ M)	1	5.40[g]	8.12[h]	9.0×10^{-6}
		1000	5.40[g]	8.12[h]	9.0×10^{-3}
Suwannee River fulvic acid (SRFA)	pH 8.1, seawater ($I = 0.7$ M)	1	7.5[g]	10.4[g]	5.9×10^{-6}
		1000	7.5[g]	10.4[g]	5.9×10^{-3}

[a] *Calculated at $I = 0.1$ M, ignoring formation of any other complexes using stability constants from Farkas et al. (2003).*

[b] *Calculated as $\log K = p/(p-1)[L]_T$ where $[L]_T$ is total ligand concentration and p is proportion complexed as reported in Table 2 of Hudson et al. (1992).*

[c] *Measured value at pH 8.1 reported by Witter et al. (2000).*

[d] *Calculated from complex formation and dissociation rate constants measured by Fujii et al. (2011).*

[e] *Calculated from complex formation and dissociation rate constants measured by Fujii et al. (2010a).*

[f] *Measured value at pH 7.98 reported by Sunda and Huntsman (2003).*

[g] *Calculated from complex formation and dissociation rate constants measured by Rose and Waite (2003b).*

[h] *Calculated from complex formation and dissociation rate constants measured by Fujii et al. (2010a) for a citrate concentration of 100 μM (the apparent conditional stability constant varies with ligand concentration due to the existence of multiple complex species).*

inorganic pool depends on pH and major ion composition of the aquatic system; in the case of the other two pools, speciation depends on these two factors and also the presence of various organic ligands (see Kinetics and Mechanisms for kinetic equations in Appendix).

Rush and Bielski (1985) studied the reactivity of Fe(II)′ and Fe(III)′ with O_2^{-*} as a function of pH in the acidic to neutral range in detail. They determined that conditional rate constants for Fe(II) oxidation varied with pH over the range 1–7 primarily due to faster reactivity of Fe(II) with O_2^- (rate constant $= 1.0 \times 10^7\ M^{-1}\ s^{-1}$) than $HOO^\bullet$ (rate constant $= 1.2 \times 10^6\ M^{-1}\ s^{-1}$), with no apparent influence of Fe(II) speciation on oxidation kinetics in this pH range. Similarly, over the pH range 0–7, Fe(III) was reduced rapidly by O_2^- (rate constant $= 1.5 \times 10^8\ M^{-1}\ s^{-1}$) but negligibly slowly by $HOO^\bullet$ (rate constant $< 10^3\ M^{-1}\ s^{-1}$), again with no apparent influence of Fe(III) speciation. Similar values under acidic conditions have since been confirmed in more recent studies (Khaikin et al., 1996; Mansano-Weiss et al., 2002). Conditional rate constants for overall Fe(II) oxidation by O_2^{-*} of $k_{ox,inorg} = 1.0 \times 10^7\ M^{-1}\ s^{-1}$ and Fe(III) reduction by O_2^{-*} of $k_{red,inorg} = 1.5 \times 10^8\ M^{-1}\ s^{-1}$ are thus frequently used in kinetic studies of environmental systems at circum neutral pH, implicitly assuming that the values derived by Rush and Bielski can be extrapolated to systems with higher pH, lower Fe and O_2^{-*} concentrations, and considerably more variable ionic composition (the original study considered only effects of Fe hydrolysis and sulfate complexation). Extrapolation of these values appears consistent with results in these studies, suggesting that this is valid, however with the advent of new, more sensitive techniques for O_2^{-*} determination, these fundamental reactions warrant further attention.

In systems where organic complexation and/or polynuclear complex formation occur, a single conditional rate constant for Fe(III) reduction and another for Fe(II) oxidation by O_2^{-*} cannot be derived; it is necessary to separately account for the reactions of O_2^{-*} with mononuclear inorganic Fe and at least one organic and/or polynuclear Fe complex. Studies in model systems containing a single, well characterized synthetic ligand have confirmed that reduction of Fe(III) by O_2^{-*} around neutral pH can occur via direct reduction of the complex (denoted "non-dissociative reduction," or NDR), or via dissociation of the complex with subsequent reduction of the liberated Fe(III)′ (denoted "dissociative reduction," or DR; Garg et al., 2007c,d; Fujii et al., 2008), as shown in **Figure 2**. The relative importance of these two pathways for Fe(III) reduction depends on the relative rates of complex dissociation, complex formation, Fe(III)′ reduction by O_2^{-*}, and Fe(III)L reduction by O_2^{-*}. Under steady-state conditions where most Fe(III) is present in complexed form, the net rate of Fe(III) reduction by NDR is simply:

$$k_{red,Fe(III)L}\,[\text{Fe (III) L}]\left[O_2^{-*}\right] \approx k_{red,Fe(III)L}[\text{Fe (III)}]_T\left[O_2^{-*}\right] \quad (10)$$

where $k_{red,Fe(III)L}$ represents the rate constant for reduction of a particular Fe(III)L complex and the subscript T denotes the total concentration of all Fe(III) species. Thus, the apparent rate constant for NDR is simply $k_{NDR} = k_{red,Fe(III)L}$. Also, at steady-state:

$$\frac{d}{dt}\left[\text{Fe (III)}'\right] = k_{d,Fe(III)L}\,[\text{Fe (III) L}] - k_{f,Fe(III)L}\left[\text{Fe (III)}'\right][\text{L}] - k_{red,inorg}\left[\text{Fe (III)}'\right]\left[O_2^{-*}\right] = 0 \quad (11)$$

$$\Rightarrow \left[\text{Fe (III)}'\right] = \frac{k_{d,Fe(III)L}\,[\text{Fe (III) L}]}{k_{f,Fe(III)L}\,[\text{L}] + k_{red,inorg}\left[O_2^{-*}\right]} \quad (12)$$

where $k_{d,Fe(III)L}$ and $k_{f,Fe(III)L}$ represent rate constants for the dissociation and formation, respectively, of a particular Fe(III)L complex. Hence the apparent rate constant for net Fe(III) reduction by DR is obtained from the equation:

$$k_{red,inorg}\left[\text{Fe (III)}'\right]\left[O_2^{-*}\right] = \frac{k_{red,inorg}k_{d,Fe(III)L}}{k_{f,Fe(III)L}\,[\text{L}] + k_{red,inorg}\left[O_2^{-*}\right]} \times [\text{Fe (III) L}]\left[O_2^{-*}\right] \quad (13)$$

$$\Rightarrow k_{DR} = \frac{k_{red,inorg}k_{d,Fe(III)L}}{k_{f,Fe(III)L}\,[\text{L}] + k_{red,inorg}\left[O_2^{-*}\right]} \quad (14)$$

Thus the relative importance of the two processes is given by:

$$k_{NDR}/k_{DR} = \frac{k_{red,Fe(III)L}\left(k_{f,Fe(III)L}\,[\text{L}] + k_{red,inorg}\left[O_2^{-*}\right]\right)}{k_{red,inorg}k_{d,Fe(III)L}} \quad (15)$$

All parameters in this equation will be influenced to varying extents by medium conditions (e.g., pH and ionic strength). Additionally, for a given ligand, the system pH, major ion composition, ligand concentration, and O_2^{-*} concentration will have specific effects on particular parameters. The relative importance of NDR compared to DR will be increased by:

1. Decreasing concentrations of H^+ (i.e., higher pH) or cations such as Ca^{2+} and Mg^{2+}; the presence of these species will lower "free" ligand concentration, [L], by occupying sites within ligands that might otherwise complex Fe, thus decreasing the numerator of Eq. 15.
2. Increasing ligand concentrations; this will increase the numerator of Eq. 15.
3. Increasing O_2^{-*} concentrations; this will increase the numerator of Eq. 15.

The affinity of the ligand for Fe(III) also has a major effect on the relative importance of DR and NDR, but this effect is complicated because two factors act in opposite ways. First, increasing the Fe(III) binding strength of the ligand will tend to increase $k_{f,Fe(III)L}$ (increasing the numerator of Eq. 15) and/or decrease $k_{d,Fe(III)L}$ (decreasing the denominator of Eq. 15); this leads to a relative increase in the importance of NDR relative to DR. However weaker Fe(III) complexes typically react faster with O_2^{-*} than stronger complexes, as observed empirically for a range of synthetic Fe-binding ligands (Rose and Waite, 2005), such that increasing Fe(III) binding strength of the ligand will tend to decrease $k_{red,Fe(III)L}$. Rate constants for reduction of organic complexes of Fe(III) by O_2^{-*} at pH 8 were found to be several orders of magnitude smaller than those for reduction of Fe(III)′, ranging

from $\sim 10^4\ M^{-1}\ s^{-1}$ for reduction of the strong complex Fe(III)–DFB to $\sim 2 \times 10^6\ M^{-1}\ s^{-1}$ for reduction of the relatively weak complex Fe(III)-salicylate (Rose and Waite, 2005). This trend is consistent with Marcus Theory for outer-sphere electron transfer processes (see Marcus and Sutin (1985) for a detailed review), which is the process by which reduction of transition metal complexes by O_2^{-*} is thought to occur (Weinstock, 2008). In fact Marcus Theory relates the rate constant to the ratio of stability constants for the Fe(II) and Fe(III) complexes, not just the stability of the Fe(III) complex alone (Marcus and Sutin, 1985); however as ligands that form stronger complexes with Fe(III) often form weaker complexes with Fe(II), there is generally a consistent trend for slower reduction of stronger Fe(III) complexes by O_2^{-*}.

Polynuclear complexes are also able to be reduced by O_2^{-*}, as demonstrated in laboratory studies with amorphous ferric oxyhydroxide (AFO; Fujii et al., 2006) and in field studies with Saharan dust in seawater (Heller and Croot, 2011). A similar competition between DR and NDR would be expected to occur for polynuclear complexes. Fujii et al. (2006) found that in both very freshly formed AFO (which has a relatively small conditional stability constant) and aged AFO (which has a much larger conditional stability constant), Fe(II) production during reduction of AFO by O_2^{-*} occurred almost entirely via DR. These experiments were performed in seawater at pH 8.2 using total Fe concentrations of 50–500 nM, which is a reasonable range in coastal marine systems, but using higher steady-state O_2^{-*} concentrations than would be expected in most environments (~20 nM cf. 0.1–1 nM measured in marine waters). These higher O_2^{-*} concentrations would tend to increase the importance of NDR, which implies that at the lower O_2^{-*} concentrations measured in natural waters to date, the process will almost certainly occur via DR. Given that aged AFO has a relatively large conditional stability constant, NDR might be expected to play a more substantial role, however polynuclear complexes (unlike mononuclear complexes) may permit extremely rapid intramolecular electron transfer from relatively labile Fe atoms (e.g., at the AFO surface) to less labile Fe atoms within the polymeric structure (Katz et al., 2010), inhibiting the release of Fe(II) potentially formed through this pathway. Whether this or some other phenomenon is responsible for the dominance of DR during reduction of aged AFO remains untested, however, and will require further experimental studies to resolve.

At lower pH values (3 and 5), $HOO^\bullet$ is a major oxidant of Fe(II) (Voelker et al., 1997). Around pH 8, where O_2^- dominates over $HOO^\bullet$, Fujii et al. (2010b) determined rate constants for oxidation of complexes between Fe(II) and humic-type organic ligands by O_2^{-*} in the range $6.9–23 \times 10^5\ M^{-1}\ s^{-1}$, which were ~4–5 orders of magnitude greater than corresponding rate constants for oxidation of the complexes by O_2. Given a typical dissolved O_2 concentration of ~250 μM for natural waters in equilibrium with atmospheric O_2, this implies that O_2^{-*} would be a negligibly minor oxidant of these Fe(II) complexes at the picomolar O_2^{-*} concentrations that have been measured in natural waters. In contrast, Heller and Croot (2010) suggested that O_2^{-*} may react with naturally occurring organic Fe(II) complexes found in the Southern Ocean with rate constants of up to $\sim 5 \times 10^7\ M^{-1}\ s^{-1}$, which is around an order of magnitude greater than those for the humic-type complexes (Fujii et al., 2010b). This would suggest that O_2^{-*} might contribute significantly to Fe(II) oxidation at the higher range of environmentally relevant O_2^{-*} concentrations; however this can not be evaluated directly without also knowing the kinetics of reaction between the Fe(II) complexes and O_2, which were not determined in the Southern Ocean study. To date, oxidation of polynuclear Fe(II) by O_2^{-*} has not been studied directly, although such a reaction would seem less environmentally relevant than reduction of polynulcear Fe(III) by O_2^{-*}, given the weaker tendency of Fe(II) to form polynuclear species. However, it is clear that more studies of the oxidation of organically complexed and polynuclear Fe(II) by O_2^{-*} are required to better constrain the potential importance of O_2^{-*} as an oxidant of Fe(II) in natural waters.

INDIRECT EFFECTS OF REACTIONS BETWEEN SUPEROXIDE AND IRON

While being primarily concerned with the effect of O_2^{-*} on Fe speciation, it is also worth briefly considering the ability of reactions between O_2^{-*} and Fe to generate other reactive intermediates, which may be biologically important. Perhaps the major such process is the Haber–Weiss cycle, in which O_2^{-*} and Fe promote the formation of hydroxyl radicals ($HO^\bullet$). It was initially thought that O_2^{-*} could reduce H_2O_2 to yield $HO^\bullet$:

$$O_2^{-*} + H_2O_2 \rightarrow O_2 + HO^\bullet + HO^- \quad (16)$$

It has since been shown that this reaction does not occur directly, but represents the net result of a series of reactions involving O_2^{-*} and Fe (Winterbourn, 1995; Koppenol, 2001):

$$O_2^{-*} + \text{Fe (III)} \rightarrow O_2 + \text{Fe (II)} \quad (17)$$

$$O_2^{-*} + \text{Fe (II)} \xrightarrow{2H^+} H_2O_2 + \text{Fe (III)} \quad (18)$$

$$H_2O_2 + \text{Fe (II)} \rightarrow HO^\bullet + HO^- + \text{Fe (III)} \quad (19)$$

The reaction in Eq. 19 (the Fenton reaction) may produce Fe(IV) (ferryl iron) rather than $OH^\bullet$ under some conditions (Remucal and Sedlak, 2011):

$$H_2O_2 + \text{Fe (II)} \rightarrow H_2O + \text{Fe (IV)}\ O_2^{2+} \quad (20)$$

The biological importance of these processes lies in the ability of $HO^\bullet$ and/or Fe(IV) to oxidize a wide range of biologically important molecules, and constitutes one of the main pathways to oxidative stress. This only occurs when O_2^{-*} is reduced by Fe(II) to form H_2O_2 [i.e., when O_2^{-*} acts as an oxidant of Fe(II)] which, as discussed in the previous section, appears to be negligible at O_2^{-*} concentrations that have so far been measured in natural waters. A second potential consequence of this series of reactions is the possibility that O_2 formed in the reaction shown in Eq. 17 is in the excited singlet state rather than the triplet ground state. Singlet state dioxygen ($^1O_2$) is a powerful, but rather selective, oxidant of a range of biologically important molecules (Briviba et al., 1997). Formation of $^1O_2$ from oxidation of O_2^{-*} is only possible with a sufficiently powerful oxidant (Koppenol, 1976), which may or may not be satisfied by different Fe(II) species (Nanni et al., 1981).

INFLUENCE OF EXTRACELLULAR SUPEROXIDE ON IRON BIOAVAILABILITY AND MICROBIAL IRON NUTRITION

SUPEROXIDE: A FORCE FOR GOOD OR EVIL?

O_2^{-*} is frequently associated with the concept of oxidative stress in cells, and has consequently developed a reputation as an enemy of healthy biological functioning. The detrimental effect of intracellular O_2^{-*} can largely be attributed to two main types of processes (Fridovich, 1986, 1998; Cadenas, 1989; Auchère and Rusnak, 2002; Lesser, 2006):

1. interference with critical redox processes by adversely influencing the redox state of enzymes (particularly including enzymes containing iron) and other smaller molecules with specific biochemical functions; and
2. initiation of radical chain reactions, including as a precursor to much more reactive species such as $HO^{\bullet}$, Fe(IV), and $^1O_2$ via the processes described previously.

Adverse effects caused by extracellular O_2^{-*} in a typical aquatic environment near neutral pH could presumably result from similar processes that cause adverse effects inside the cell. The potential for processes in the extracellular environment to adversely affect cells is limited by the inability of O_2^{-*} and many of its more reactive derivatives to cross cell membranes, which inhibits or prevents these species from reacting with the vast majority of enzymes and other biological molecules used for normal cellular function. Additionally, concentrations of Fe (and other promoters of free radical production) are usually much lower in the extracellular environment than the intracellular environment, which decreases formation rates of potentially damaging reactive derivatives by slowing reaction kinetics. The presence of other potential sinks can also help scavenge these reactive derivatives and thus confer additional protection to the cell.

However, in some cases, extracellular O_2^{-*} is capable of inflicting cellular damage and may even be deliberately used in this fashion either to defend against invasions by other cells [e.g., the "oxidative burst" produced by human phagocyte cells (Vignais, 2002)] or as an agent of cellular warfare, as has been suggested some raphidophyceans such as *C. marina* (Oda et al., 1992). A frequently observed factor in these situations is the production of large amounts of O_2^{-*} at relatively rapid rates. This can be rationalized on the basis that in order to produce H_2O_2 and subsequently $HO^{\bullet}$ and/or Fe(IV) at substantial rates, O_2^{-*} must be reduced at substantial rates, as O_2^{-*} production rates need to be fast enough to sustain relatively rapid formation of both H_2O_2 (through reduction of O_2^{-*}) and Fe(II) (or other reduced species) to oxidize H_2O_2 to $HO^{\bullet}$ [or to yield Fe(IV)]. In contrast, relatively low O_2^{-*} production rates will result in relatively low H_2O_2 production rates and also relatively low concentrations of Fe(II) (or other reduced species), such that H_2O_2 is more likely to decay via pathways that do not result in $HO^{\bullet}$ or Fe(IV) formation. Thus, at the picomolar concentrations typically encountered in natural waters, O_2^{-*} is unlikely to be particularly detrimental for aquatic microorganisms. This notion is further supported by evidence that a wide range of cells use O_2^{-*} as a signaling molecule at low concentrations (Buetler et al., 2004), although given the limited number of studies on the roles and/or effects of extracellular O_2^{-*} on living organisms, it is difficult to make definitive conclusions regarding this issue at present.

Nonetheless, picomolar concentrations of O_2^{-*} have the potential to maintain mild reducing capacity in the extracellular environment. As discussed previously, under these conditions O_2^{-*} is both thermodynamically and kinetically capable of reducing a wide range of Fe(III) species to Fe(II), thereby potentially increasing Fe bioavailability.

CAN EXTRACELLULAR SUPEROXIDE PRODUCTION INCREASE Fe BIOAVAILABILITY?

The analysis in Section "Kinetics and Mechanisms" separately considered rates of Fe(III) reduction and rates of Fe(II) oxidation by O_2^{-*} for a range of different forms of Fe. While this provides useful insight into the mechanisms by which O_2^{-*} can influence Fe speciation, and the relative importance of these various pathways under various conditions, the most important factor from the perspective of Fe bioavailability is the net result of these processes. Most organisms in natural waters are thought to use the mononuclear inorganic complexes, collectively represented as Fe(II)′ and Fe(III)′, as the substrate that is directly internalized by the cell (Morel et al., 2008). Thus while Fe from the other pools may be bioavailable in the sense that Fe contained within them may ultimately find its way into the cell, this can only occur after conversion to Fe(II)′ or Fe(III)′. The ability of O_2^{-*} to influence Fe bioavailability therefore depends largely on whether its production increases the concentration of Fe(II)′ and/or Fe(III)′ at or near the sites of cellular uptake of these species.

A spatially homogeneous steady-state system in which Fe exists predominantly as a single type of organic complex, O_2 is assumed to be the only oxidant of Fe(II), and O_2^{-*} is assumed to be the only reductant of Fe(III), is shown schematically in **Figure 3**. While such a system is highly simplified, it provides a useful basis to understand when O_2^{-*} might increase Fe bioavailability. The number of variables can be further simplified by assuming a 1:1 Fe:L ratio

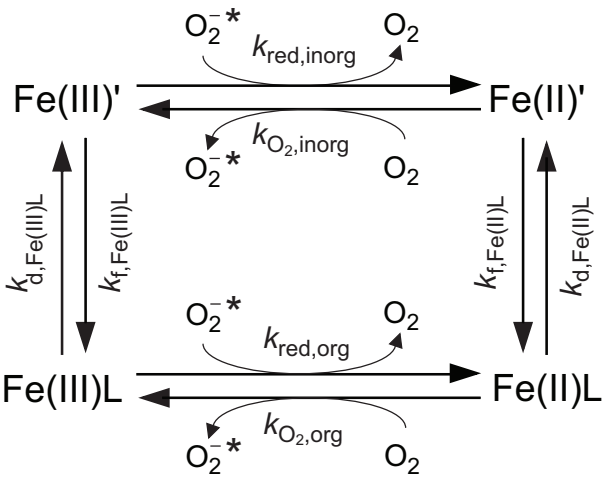

FIGURE 3 | Simplified steady-state model for Fe chemistry in a spatially homogeneous system containing O_2^{-*} and a single ligand (L) that forms a 1:1 complex with Fe, showing relevant rate constants.

for Fe(II)L and Fe(III)L, that the complex formation rate constants are independent of ligand type (consistent with control of complex formation by water loss kinetics, i.e., the complexes form via a perfect Eigen–Wilkins mechanism (Eigen and Wilkins, 1965) in which the electrostatic charge on L does not vary between different ligand types), and that the oxidation of Fe(II)L by O_2 and reduction of Fe(III)L by O_2^{-*} are outer-sphere electron transfer processes that obey Marcus Theory perfectly. With these simplifications, analytical solutions for the steady-state concentrations of the Fe species can be derived as a function of the eight kinetic parameters shown in **Figure 3**. Four of these kinetic parameters ($k_{f,Fe(III)L}$, $k_{f,Fe(II)L}$, $k_{O_2,inorg}$, and $k_{red,inorg}$) are constants for specified [L], [O_2], and [O_2^{-*}], while the remaining four kinetic parameters can all be expressed as functions of $K_{Fe(III)L}$ and $K_{Fe(II)L}$ (see Details of Spatially Homogeneous Steady-State Model For Fe′ Concentrations as a Function of Superoxide Concentrations for the full derivation in Appendix).

Consider an illustrative typical coastal marine water in equilibrium with the atmosphere at pH 8.1, temperature 25°C, ionic strength of 0.7 M, constant ionic composition, $[Fe]_T = 100$ nM, and [L] = 1 μM. Steady-state [Fe(III)′], [Fe(II)′], and $[Fe']_T$ were calculated in Microsoft Excel from the relationships in Eqs A28 and A29 (see Appendix) at steady-state [O_2^{-*}] of 0, 10, 100 pM, and 1 nM, considering a range of stability constants for Fe(III)L and Fe(II)L that are representative of what might be encountered in coastal marine waters (**Figure 4**). Provided Fe(II) forms relatively weak complexes, 1 nM O_2^{-*} increases steady-state $[Fe']_T$ by nearly an order of magnitude compared to the absence of O_2^{-*} across the whole range of $K_{Fe(III)L}$ considered; the effect is smaller at 100 pM O_2^{-*} and negligible at 10 pM O_2^{-*} under the particular conditions in this example. In all cases, the increase in steady-state $[Fe']_T$ is due to production of Fe(II)′; steady-state [Fe(III)′] is mostly affected to a negligibly small extent by O_2^{-*}. When Fe(II) forms relatively strong complexes while Fe(III) forms relatively weak complexes, the steady-state $[Fe']_T$ actually decreases due to the influence of O_2^{-*}; this is intuitively reasonable, as in this case the reduction of Fe(III) to Fe(II) would result in transformation to a less labile form (predominantly as the Fe(II)L complex). This effect is more pronounced at higher [O_2^{-*}], as would be expected from such a mechanism. There is little evidence for naturally occurring ligands that form strong complexes with Fe(II) but weak complexes with Fe(III), however, suggesting that this latter scenario is unlikely to be important in most natural waters.

Under the conditions of the example above, it is clear that steady-state concentrations of O_2^{-*} that are typical of those measured in natural waters have the potential to significantly increase Fe bioavailability. The same approach can be readily applied to natural waters with differing Fe concentrations, because the steady-state concentrations of Fe(II)′ and Fe(III)′ are simply proportional to $[Fe]_T$ when all other parameters remain constant (Eqs A28 and A29 in Appendix). However, there are several other factors that must also be considered when attempting to apply this approach to other conditions:

1. Different values of [L] will influence $k^*_{f,Fe(III)L} = k_{f,Fe(III)L}[L]$ and $k^*_{f,Fe(II)L} = k_{f,Fe(II)L}[L]$, which will influence steady-state [Fe(II)′] and [Fe(III)′] in a non-linear manner.
2. Parameter values will vary independently with medium conditions (e.g., pH, ionic strength and ionic composition), which will also influence steady-state [Fe(II)′] and [Fe(III)′] in a non-linear manner.
3. Real ligands do not all form 1:1 complexes with Fe, nor do they all possess equal electrostatic charges. For this and other reasons, real complexes do not conform precisely to the Eigen–Wilkins mechanism, which means that values of $k_{f,Fe(III)L}$ and $k_{f,Fe(II)L}$ will not be independent of ligand type, and values of $k_{d,Fe(III)L}$ and $k_{d,Fe(II)L}$ will differ even between ligands with identical values of $K_{Fe(III)L}$ and $K_{Fe(II)L}$. Similarly, real complexes do not conform precisely to Marcus Theory, such that values of $k_{O_2,org}$ and $k_{red,org}$ will also differ between ligands with identical values of $K_{Fe(III)L}$ and $K_{Fe(II)L}$.
4. In natural waters, a range of Fe complexes are likely to coexist.
5. In natural waters, oxidants other than O_2 and reductants other than O_2^{-*} may influence Fe speciation. In particular,

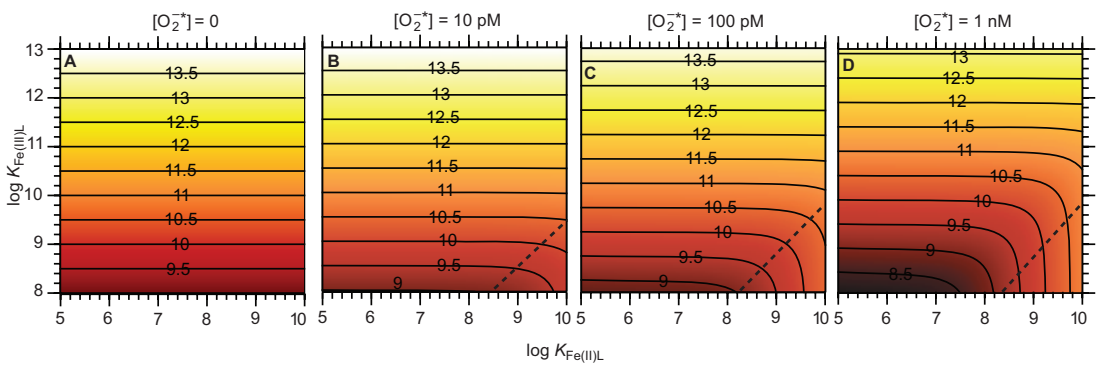

FIGURE 4 | Effect of O_2^{-*} on Fe bioavailability in a system containing a single Fe complexing ligand. (A) Steady-state [O_2^{-*}] = 0. **(B)** Steady-state [O_2^{-*}] = 10 pM. **(C)** Steady-state [O_2^{-*}] = 100 pM. **(D)** Steady-state [O_2^{-*}] = 1 nM. Panels show the resulting pFe′ [= −log[Fe′]$_T$ = −log([Fe(II)′] + [Fe(III)′]) at steady-state. The contours shown in each panel represent constant pFe′ values, as indicated by the numbers marked on the contour lines. The region to the bottom right of the dashed lines in each panel approximately indicates conditions where the strength of the Fe(II) complex relative to that of the Fe(III) complex is sufficiently high that the presence of O_2^{-*} decreases Fe bioavailability.

the possible role of O_2^{-*} as an oxidant of Fe(II) has been ignored here.

This simplified model also neglects biological uptake of Fe(II)′ and/or Fe(III)′ as an additional sink of these species. While this is unlikely to be important at low cell densities, under bloom conditions or in laboratory cultures it may become important. Additionally, the assumption of spatial homogeneity neglects any role of transport processes. In reality, it is highly likely that spatial gradients for several of the species involved (e.g., O_2^{-*}, Fe(II)′, and Fe(III)′) will exist under some conditions at least.

In summary, while this analysis demonstrates that O_2^{-*} can potentially increase Fe bioavailability under some conditions, whether this will actually occur depends strongly on the specific chemical conditions.

DO ORGANISMS EXPLOIT SUPEROXIDE CHEMISTRY TO FACILITATE Fe ACQUISITION?

Since O_2^{-*} can persist in circumneutral natural waters at picomolar concentrations due to biological and other processes, and can increase bioavailable Fe(II)′ and Fe(III)′ concentrations under some such conditions, the potential exists for organisms to exploit this chemistry to facilitate Fe acquisition. A simple test for the involvement of O_2^{-*} in Fe uptake is whether addition of SOD to the external milieu decreases Fe uptake by an organism, on the basis that SOD will scavenge O_2^{-*} and thereby prevent its reaction with Fe. This assay has been used to demonstrate the involvement of O_2^{-*} in Fe uptake under particular conditions by several aquatic microorganisms in culture studies, including *C. marina* (Garg et al., 2007a), *L. majuscula* (Rose et al., 2005), and *M. aeruginosa* (Fujii et al., 2010a). The assay has also been used to demonstrate that O_2^{-*} was apparently not involved in Fe uptake in experiments with cultures of the diatoms *T. weissflogii* and *T. pseudonana* (Kustka et al., 2005), and the green alga *Chlorella kessleri* (Middlemiss et al., 2001).

While the SOD addition assay would seem robust, care must be taken when interpreting and extrapolating results for three main reasons. First, in organisms possessing compartments external to the cytoplasmic membrane (e.g., the periplasm of Gram negative bacteria) or producing extracellular microenvironments (e.g., the glycocalyx of *C. marina*), SOD may not be able to access the site(s) of extracellular O_2^{-*} production or Fe reduction due to the large size of the molecule (molecular mass ∼32 kDa). Thus if, for example, O_2^{-*} production and subsequent Fe reduction and uptake were occurring in the periplasm of a Gram negative organism, the SOD addition assay would not result in inhibition of Fe uptake. Second, SOD concentrations employed in these assays are often much greater than those theoretically needed to ensure O_2^{-*} concentrations are negligibly small in homogeneous solution. The need to use such large SOD concentrations may be partly related to failure to account for compartmentalization or other spatial heterogeneity, but may potentially be due to as yet unknown non-specific interference with or inhibition of Fe uptake. Finally, as seen above, O_2^{-*} is only able to substantially increase Fe bioavailability under certain conditions. Therefore it is risky to generalize the potential role of O_2^{-*} in Fe uptake based on culture studies under only a few conditions. This has been well demonstrated in studies on *C. marina* (Garg et al., 2007a) and *M. aeruginosa* (Fujii et al., 2010a) in which $O_2^{-*}$was found to aid Fe uptake under some conditions, but not others. To date there have been no reports of field experiments to test the role of O_2^{-*} in Fe uptake under more environmentally relevant conditions than those used in culture studies, but such experiments would seem essential to truly test the potential role of O_2^{-*} in Fe uptake by aquatic microorganisms in their natural habitats.

Understanding the potential role of O_2^{-*} in Fe uptake is further complicated by the issue of which comes first: Fe reduction with subsequent O_2^{-*} generation by oxygenation of the resulting Fe(II), or O_2^{-*} generation with subsequent reduction of Fe. Reductive Fe uptake is now recognized to be a major strategy for Fe acquisition by a wide range of aquatic microorganisms (e.g., Maldonado and Price, 2001; Davey et al., 2003), facilitated by a general class of enzymes known as ferrireductases (Schröder et al., 2003; Kranzler et al., 2011). While extracellular ferrireductases vary in structure and location, in some cases at least they are capable of reducing O_2 to O_2^{-*} in addition to reducing Fe(III) to Fe(II) (Lesuisse et al., 1996). Middlemiss et al. (2001) demonstrated in experiments with *C. kessleri* that while both Fe(II) and O_2^{-*} were generated by the organism, SOD addition had no effect on Fe uptake rates, implying that Fe reduction by cell surface reductases was the first step in the process. It was thus suggested that rates of Fe reduction at the cell surface far exceeded rates of Fe uptake, and that the fate of Fe(II) in the bulk solution had no discernible influence on the kinetics of Fe uptake by the organism. Kustka et al. (2005) also found that addition of exogenous SOD had no effect on Fe uptake rates by *T. weissflogii* and *T. pseudonana*, despite a measurable increase in Fe(II) production in the bulk solution due to the presence of O_2^{-*}. It was thus suggested that under these experimental conditions, O_2^{-*} simply converted existing Fe(III)′ into Fe(II)′ without changing the total Fe′ concentration, which is ultimately the substrate for uptake. In these cases, it would appear that O_2^{-*} was neither required nor helpful for reductive Fe uptake, despite being produced in the process.

Regardless of whether the initial process is Fe reduction or O_2^{-*} production, its occurrence at or near the cell surface will likely lead to gradients in Fe(II) and O_2^{-*} concentrations away from the cell. If Fe(II) is released from a ferrireductase enzyme into solution prior to uptake, and the timescale of diffusive processes is faster than that of reactive processes, then the spatial distributions of Fe(II) and O_2^{-*} at steady-state should be similar in both cases. However if the diffusive timescale is slower than the reactive timescale, then we would expect significantly higher Fe(II) concentrations near the cell surface in the former case, leading to faster Fe uptake kinetics and implying that reactions between Fe and O_2^{-*} should have only a limited effect on Fe uptake kinetics. In the former case, it may also be possible that Fe(II) is passed directly from the ferrireductase enzyme to an uptake site, in which case we might expect very little (if any) Fe(II) to diffuse into the bulk solution. At present, the only model for reductive Fe uptake that considers spatial heterogeneity at the cellular scale is the Fe(II)s model of Shaked et al. (2005), which considers two pools of Fe: a pool near the cell surface, and another in the bulk solution. More detailed reacto-diffusive modeling would appear needed to quantitatively understand differences in behavior of the ferrireductase system

versus a system in which Fe reduction is driven initially by O_2^{-*} generation at the cell surface.

UNDER WHAT CONDITIONS CAN EXTRACELLULAR SUPEROXIDE PRODUCTION AID IRON ACQUISITION?

From the analysis and discussion in the previous sections, an attempt can be made to answer the general question of when will O_2^{-*} assist in Fe uptake? Generally, O_2^{-*} is unlikely to aid Fe uptake when:

1. $[Fe']_T$ is already high relative to cellular needs. Under these conditions, Fe uptake systems are likely to be near saturation, such that further increasing $[Fe']_T$ will not substantially increase Fe uptake rates.
2. Organic ligands form strong complexes with Fe(II) relative to those formed with Fe(III). Under these conditions, reduction of Fe(III) to Fe(II) will decrease $[Fe']_T$ and therefore hinder Fe acquisition.
3. The rate at which O_2^{-*} is reduced to H_2O_2 is relatively fast. Under these conditions, a high rate of O_2^{-*} production (by whatever means) is required to sustain a steady-state concentration of O_2^{-*} that is sufficient to increase $[Fe']_T$. Furthermore, relatively rapid production of H_2O_2 may promote formation of biologically harmful species such as $HO^{\bullet}$.
4. A large proportion of O_2^{-*} is consumed through reactions with species that outcompete Fe(III) for O_2^{-*} and remove electrons from the reactive pool by formation of relatively stable reduced species, e.g., other trace metals and organic radicals. In this case, the efficiency of electron transfer from O_2^{-*} to Fe may again be relatively low and the process expensive for cells.

Thus, extracellular O_2^{-*} is likely to aid Fe uptake when Fe′ concentrations in the absence of O_2^{-*} would be low in terms of biological requirements; reduction of any Fe(III) complexes results in formation of relatively weak Fe(II) complexes; and rates of reduction of O_2^{-*} to H_2O_2 are relatively low. However while these conditions would appear beneficial for cells in terms of promoting Fe bioavailability, this does not mean that cells would necessarily deliberately use ESP to assist in Fe acquisition; establishing the use of ESP in such a way would at least require evidence of regulation at the genetic level, which has not been convincingly demonstrated to date.

What types of environments would meet these criteria? Many marine waters are likely to do so, given that Fe′ is often present at low concentrations due to limited Fe supply and strong organic complexation of Fe(III) (e.g., Rue and Bruland, 1995). It is not certain that the corresponding Fe(II) complexes would always be relatively weak in comparison, but limited measurements of the strength of natural complexes in coastal waters suggests this is likely in some cases at least. Additionally, rates of O_2^{-*} reduction to H_2O_2 would appear relatively low in relatively "clean" marine waters based on reported rates of H_2O_2 production (Palenik and Morel, 1988; Herut et al., 1998) and O_2^{-*} decay (Hansard et al., 2010; Rose et al., 2010; Shaked et al., 2010). Many carbonate-buffered freshwaters might also satisfy these criteria, but there is insufficient information in the literature to draw definitive conclusions. Extracellular O_2^{-*} might also be able to increase Fe bioavailability in some oxygenated sedimentary and soil environments with neutral to alkaline pH where $[Fe(III)']$ would be expected to be very low. In contrast, extracellular O_2^{-*} is unlikely to increase Fe bioavailability in acidic environments (where Fe solubility would be higher and rates of O_2^{-*} reduction to H_2O_2 relatively rapid) or waters rich in trace metal and/or organic species that could scavenge O_2^{-*} much more effectively than Fe (e.g., highly polluted natural waters or some engineered aquatic systems). Finally, these criteria may not always be met in laboratory cultures. In particular, the widely used ligand EDTA forms rather strong complexes with Fe(II) in comparison to complexes with Fe(III) at pH 8 (**Table 1**), which will limit the ability of extracellular O_2^{-*} to increase $[Fe']_T$ under some conditions. O_2^{-*} has previously been observed to have little or no effect on Fe bioavailability in cultures where Fe is complexed by EDTA (Kustka et al., 2005; Garg et al., 2007a), which may be at least partly attributable to this effect, although factors including spatial heterogeneity may also be involved. Therefore, while useful for understanding particular processes, care must be taken in extrapolating such results to natural aquatic systems where ligands with similar properties are unlikely to dominate.

CONCLUDING REMARKS

O_2^{-*} is produced in the extracellular environment predominantly through univalent reduction of oxygen. This occurs mostly through (i) the oxygenation of relatively labile reduced compounds such as Fe(II) and Cu(I); (ii) abiotic photochemical oxidation of organic compounds; and (iii) biological production by a wide range of eukaryotic and prokaryotic organisms. Biological ESP appears primarily due to the activity of cell surface reductase enzymes that export electrons from the cell either directly to O_2, or to other labile electron acceptors that subsequently react with O_2 to yield O_2^{-*}.These processes can together maintain an environmentally significant concentration of O_2^{-*}in the extracellular milieu. The chemistry of Fe and O_2^{-*} is intimately coupled in many oxygenated waters. O_2^{-*} is thermodynamically and mechanistically capable of reducing a wide range of forms of Fe(III) under typical environmental conditions, including inorganic $Fe(III)'$, organically complexed Fe(III), and even solid (polynuclear) forms of Fe(III). Conversely, the oxidation of Fe(II) by O_2 is thought to produce O_2^{-*} (although this has not yet been conclusively demonstrated). While O_2^{-*} can also oxidize Fe(II), at sub-nanomolar O_2^{-*} concentrations in neutral to alkaline solutions, this is likely to be a relatively unimportant reaction because O_2 will oxidize Fe(II) at much faster rates.

The net effect of O_2^{-*} on Fe bioavailability depends not so much on the thermodynamic ability of O_2^{-*} to reduce various forms of Fe(III), but on the net effect of O_2^{-*} on steady-state concentrations of $Fe(II)'$ and $Fe(III)'$, which are the species actually internalized by most cells. In a spatially homogeneous steady-state system, O_2^{-*} at concentrations >10 pM can increase $[Fe']_T$ $(=[Fe(II)'] + [Fe(III)'])$, provided that the dominant form(s) of Fe(II) (e.g., organic Fe(II) complexes) are relatively labile compared to the dominant form(s) of Fe(III). In a spatially homogeneous system, it is unimportant whether cell surface ferrireductases reduce Fe(III) to Fe(II) that then reacts with O_2 to yield O_2^{-*}, or whether cell surface oxygen reductases reduce O_2 to O_2^{-*} that

then reacts with Fe(III) to yield Fe(II), unless ferrireductases pass Fe(II) directly to the uptake site without release of free Fe(II). In such a system, direct reduction of O_2 by cells maybe more effective in increasing Fe bioavailability, since rates of O_2 reduction by an oxygen reductase may be faster than rates of Fe(III) reduction by a ferrireductase simply because the concentration of O_2 is much greater than that of Fe(III) in most oxygenated environments. However in a spatially heterogeneous system, a ferrireductase mechanism would likely be more efficient due to biological compartmentalization and diffusion resulting in higher concentrations of Fe(II)′ near the site of cellular uptake compared to in the bulk solution. Understanding the chemistry of Fe and O_2^{-*} at a detailed mechanistic level, and a more rigorous understanding of the role of physical transport processes, is needed to fully assess the potential role of O_2^{-*} in increasing Fe bioavailability in a range of aquatic environments. On the basis of the information presently available, however, it seems that extracellular O_2^{-*} has the potential to significantly increase Fe bioavailability under some conditions at least and may therefore be an important part of the complicated process of Fe acquisition by aquatic organisms.

ACKNOWLEDGMENTS

I wish to acknowledge the contributions over the past decade of my close colleague Prof. T. David Waite and his research group at the University of New South Wales to the work that underpinned the development of many of the ideas discussed in this paper. I also gratefully acknowledge funding from the Australian Research Council through projects DP0987188 and DP0987351 that partly supported the writing of this paper.

REFERENCES

Aeschbacher, M., Sander, M., and Schwarzenbach, R. P. (2010). Novel electrochemical approach to assess the redox properties of humic substances. *Environ. Sci. Technol.* 44, 87–93.

Afanas'ev, I. B. (1989). *Superoxide Ion Chemistry and Biological Implications*. Boca Raton, FL: CRC Press.

Aguirre, J., Rios-Momberg, M., Hewitt, D., and Hansberg, W. (2005). Reactive oxygen species and development in microbial eukaryotes. *Trends Microbiol.* 13, 111–118.

Auchère, F., and Rusnak, F. (2002). What is the ultimate fate of superoxide anion in vivo? *J. Biol. Inorg. Chem.* 7, 664–667.

Barbeau, K. A. (2006). Photochemistry of organic iron(III) complexing ligands in oceanic systems. *Photochem. Photobiol.* 82, 1505–1516.

Baxter, R. M., and Carey, J. H. (1983). Evidence for photochemical generation of superoxide ion in humic waters. *Nature* 306, 575–576.

Beckett, R. P., Minibayeva, F. V., Vylegzhanina, N. N., and Tolpysheva, T. (2003). High rates of extracellular superoxide production by lichens in the suborder Peltigerineae correlate with indices of high metabolic activity. *Plant Cell Environ.* 26, 1827–1837.

Bielski, B. H. J., Cabelli, D. E., Arudi, R. L., and Ross, A. B. (1985). Reactivity of HO_2/O_2^- radicals in aqueous solution. *J. Phys. Chem. Ref. Data* 14, 1041–1100.

Blough, N. V. (1988). Electron paramagnetic resonance measurements of photochemical radical production in humic substances. 1. Effects of oxygen and charge on radical scavenging by nitroxides. *Environ. Sci. Technol.* 22, 77–82.

Bolwell, G. P. (1999). Role of active oxygen species and NO in plant defence responses. *Curr. Opin. Plant Biol.* 2, 287–294.

Bowles, K. C., Ernste, M. J., and Kramer, J. R. (2003). Trace sulfide determination in oxic freshwaters. *Anal. Chim. Acta* 477, 113–124.

Boyle, E. S., Guerriero, N., Thiallet, A., Vecchio, R. D., and Blough, N. V. (2009). Optical properties of humic substances and CDOM: relation to structure. *Environ. Sci. Technol.* 43, 2262–2268.

Briviba, K., Klotz, L. O., and Sies, H. (1997). Toxic and signaling effects of photochemically or chemically generated singlet oxygen in biological systems. *Biol. Chem.* 378, 1259–1265.

Buetler, T. M., Krauskopf, A., and Ruegg, U. T. (2004). Role of superoxide as a signaling molecule. *Physiology* 19, 120–123.

Buettner, G. R., Doherty, T. P., and Patterson, L. K. (1983). The kinetics of the reaction of superoxide radical with Fe(III) complexes of EDTA, DETAPAC and HEDTA. *FEBS Lett.* 158, 143–146.

Bull, C., Mcclune, G. J., and Fee, J. A. (1983). The mechanism of iron EDTA catalyzed superoxide dismutation. *J. Am. Chem. Soc.* 105, 5290–5300.

Cadenas, E. (1989). Biochemistry of oxygen toxicity. *Annu. Rev. Biochem.* 58, 79–110.

Cooper, W. J., Zika, R. G., Petasne, R. G., and Fischer, A. M. (1989). "Sunlight-induced photochemistry of humic substances in natural waters: major reactive species," in *Aquatic Humic Substances: Influence on Fate and Treatment of Pollutants*, eds I. H. Suffet and P. MacCarthy (Washington: American Chemical Society), 333–362.

Cooper, W. J., Zika, R. G., Petasne, R. G., and Plane, J. M. C. (1988). Photochemical formation of hydrogen peroxide in natural waters exposed to sunlight. *Environ. Sci. Technol.* 22, 1156–1160.

Davey, M. S., Suggett, D. J., Geider, R. J., and Taylor, A. R. (2003). Phytoplankton plasma membrane redox activity: effect of iron limitation and interaction with photosynthesis. *J. Phycol.* 39, 1132–1144.

Del Vecchio, R., and Blough, N. V. (2002). Photobleaching of chromophoric dissolved organic matter in natural waters: kinetics and modeling. *Mar. Chem.* 78, 231–253.

Del Vecchio, R., and Blough, N. V. (2004). On the origin of the optical properties of humic substances. *Environ. Sci. Technol.* 38, 3885–3891.

Eigen, M., and Wilkins, R. G. (1965). "Kinetics and mechanisms of formation of metal complexes," in *Mechanisms of Inorganic Reactions*, eds R. K. Marmann, R. T. Fraser, and J. Bouman (Washington: American Chemical Society), 55–80.

Fan, S.-M. (2008). Photochemical and biochemical controls on reactive oxygen and iron speciation in the pelagic surface ocean. *Mar. Chem.* 109, 152–164.

Farkas, E., Enyedy, É. A., and Fábián, I. (2003). New insight into the oxidation of Fe(II) by desferrioxamine B (DFB): spectrophotometric and capillary electrophoresis (CE) study. *Inorg. Chem. Commun.* 6, 131–134.

Fridovich, I. (1986). Biological effects of the superoxide radical. *Arch. Biochem. Biophys.* 247, 1–11.

Fridovich, I. (1998). Oxygen toxicity: a radical explanation. *J. Exp. Biol.* 201, 1203–1209.

Fujii, M., Dang, T. C., Rose, A. L., Omura, T., and Waite, T. D. (2011). Effect of light on iron uptake by the freshwater cyanobacterium *Microcystis aeruginosa*. *Environ. Sci. Technol.* 45, 1391–1398.

Fujii, M., Ito, H., Rose, A. L., Waite, T. D., and Omura, T. (2008). Superoxide-mediated Fe(II) formation from organically complexed Fe(III) in coastal waters. *Geochim. Cosmochim. Acta* 72, 6079–6089.

Fujii, M., Rose, A. L., Omura, T., and Waite, T. D. (2010a). Effect of Fe(II) and Fe(III) transformation kinetics on iron acquisition by a toxic strain of *Microcystis aeruginosa*. *Environ. Sci. Technol.* 44, 1980–1986.

Fujii, M., Rose, A. L., Waite, T. D., and Omura, T. (2010b). Oxygen and superoxide-mediated redox kinetics of iron complexed by humic substances in coastal seawater. *Environ. Sci. Technol.* 44, 9337–9342.

Fujii, M., Rose, A. L., Waite, T. D., and Omura, T. (2006). Superoxide-mediated dissolution of amorphous ferric oxyhydroxide in seawater. *Environ. Sci. Technol.* 40, 880–887.

Garg, S., Rose, A. L., Godrant, A., and Waite, T. D. (2007a). Iron uptake by the ichthyotoxic *Chattonella marina* (Raphidophyceae): impact of superoxide generation. *J. Phycol.* 43, 978–991.

Garg, S., Rose, A. L., and Waite, T. D. (2007b). Production of reactive oxygen species on photolysis of dilute aqueous quinone solutions. *Photochem. Photobiol.* 83, 904–913.

Garg, S., Rose, A. L., and Waite, T. D. (2007c). Superoxide mediated reduction of organically complexed iron(III): comparison of non-dissociative and dissociative reduction pathways. *Environ. Sci. Technol.* 41, 3205–3212.

Garg, S., Rose, A. L., and Waite, T. D. (2007d). Superoxide-mediated reduction of organically complexed iron(III): impact of pH and competing cations (Ca^{2+}). *Geochim. Cosmochim. Acta* 71, 5620–5634.

Garg, S., Rose, A. L., and Waite, T. D. (2011a). Photochemical production of superoxide and hydrogen peroxide from natural organic matter. *Geochim. Cosmochim. Acta* 75, 4310–4320.

Garg, S., Rose, A. L., and Waite, T. D. (2011b). "Pathways contributing to the formation and decay of ferrous iron in sunlit natural waters," in *Aquatic Redox Chemistry*, eds P. G. Tratnyek, T. J. Grundl, and S. B. Haderlein. (Washington: American Chemical Society), 153–176.

Godrant, A., Rose, A. L., Sarthou, G., and Waite, T. D. (2009). A new method for the determination of extracellular production of superoxide from phytoplankton cells using MCLA and red-CLA as chemiluminescent probes. *Limnol. Oceanogr. Methods* 7, 682–692.

Gregory, E. M., Moore, W. E., and Holdeman, L. V. (1978). Superoxide dismutase in anaerobes: survey. *Appl. Environ. Microbiol.* 35, 988–991.

Haber, F., and Weiss, J. (1934). The catalytic decomposition of hydrogen peroxide by iron salts. *Proc. R. Soc. Lond. A Math. Phys. Sci.* 147, 332–351.

Hansard, S. P., Vermilyea, A. W., and Voelker, B. M. (2010). Measurements of superoxide radical concentration and decay kinetics in the Gulf of Alaska. *Deep Sea Res. Part I Oceanogr. Res. Pap.* 57, 1111–1119.

Heller, M. I., and Croot, P. L. (2010). Superoxide decay kinetics in the Southern Ocean. *Environ. Sci. Technol.* 44, 191–196.

Heller, M. I., and Croot, P. L. (2011). Superoxide decay as a probe for speciation changes during dust dissolution in Tropical Atlantic surface waters near Cape Verde. *Mar. Chem.* 126, 37–55.

Henry, M.-F., and Vignais, P. M. (1980). Production of superoxide anions in *Paracoccus denitrificans*. *Arch. Biochem. Biophys.* 203, 365–371.

Herut, B., Shoham-Frider, E., Kress, N., Fiedler, U., and Angel, D. L. (1998). Hydrogen peroxide production rates in clean and polluted coastal marine waters of the Mediterranean, Red and Baltic Seas. *Mar. Pollut. Bull.* 36, 994–1003.

Hudson, R. J. M., Covault, D. T., and Morel, F. M. M. (1992). Investigations of iron coordination and redox reactions in seawater using ^{59}Fe radiometry and ion-pair solvent extraction of amphiphilic iron complexes. *Mar. Chem.* 38, 209–235.

Imlay, J. A., and Fridovich, I. (1991). Assay of metabolic superoxide production in *Escherichia coli*. *J. Biol. Chem.* 266, 6957–6965.

Jayson, G. G., Keene, J. P., Stirling, D. A., and Swallow, A. J. (1969). Pulse-radiolysis study of some unstable complexes of iron. *Trans. Faraday Soc.* 65, 2453–2464.

Jayson, G. G., Parsons, B. J., and Swallow, A. J. (1973). Oxidation of ferrous ions by perhydroxyl radicals. *J. Chem. Soc. Faraday Trans.* 1 69, 236–242.

Jones, G. J., Waite, T. D., and Smith, J. D. (1985). Light-dependent reduction of copper(II) and its effect on cell-mediated thiol-dependent superoxide production. *Biochem. Biophys. Res. Commun.* 128, 1031–1036.

Katz, J. E., Gilbert, B., Zhang, X., Attenkofer, K., Falcone, R. W., and Waychunas, G. A. (2010). Observation of transient iron(II) formation in dye-sensitized iron oxide nanoparticles by time-resolved X-ray spectroscopy. *J. Phys. Chem. Lett.* 1, 1372–1376.

Khaikin, G. I., Alfassi, Z. B., Huie, R. E., and Neta, P. (1996). Oxidation of ferrous and ferrocyanide ions by peroxyl radicals. *J. Phys. Chem.* 100, 7072–7077.

Kim, D., Nakamura, A., Okamoto, T., Komatsu, N., Oda, T., Iida, T., Ishimatsu, A., and Muramatsu, T. (2000). Mechanism of superoxide anion generation in the toxic red tide phytoplankton *Chattonella marina*: possible involvement of NAD(P)H oxidase. *Biochim. Biophys. Acta* 1524, 220–227.

Koppenol, W. H. (1976). Reactions involving singlet oxygen and the superoxide anion. *Nature* 262, 420–421.

Koppenol, W. H. (2001). The Haber-Weiss cycle – 70 years later. *Redox Rep.* 6, 229–234.

Korshunov, S., and Imlay, J. A. (2006). Detection and quantification of superoxide formed within the periplasm of *Escherichia coli*. *J. Bacteriol.* 188, 6326–6334.

Korshunov, S. S., and Imlay, J. A. (2002). A potential role for periplasmic superoxide dismutase in blocking the penetration of external superoxide into the cytosol of Gram-negative bacteria. *Mol. Microbiol.* 43, 95–106.

Kosman, D. J. (2003). Molecular mechanisms of iron uptake in fungi. *Mol. Microbiol.* 47, 1185–1197.

Kranzler, C., Lis, H., Shaked, Y., and Keren, N. (2011). The role of reduction in iron uptake processes in a unicellular, planktonic cyanobacterium. *Environ. Microbiol.* 13, 2990–2999.

Kustka, A., Shaked, Y., Milligan, A., King, D. W., and Morel, F. M. M. (2005). Extracellular production of superoxide by marine diatoms: contrasting effects on iron redox chemistry and bioavailability. *Limnol. Oceanogr.* 50, 1172–1180.

Lambeth, J. D. (2004). NOX enzymes and the biology of reactive oxygen. *Nat. Rev. Immunol.* 4, 181–189.

Lara-Ortíz, T., Riveros-Rosas, H., and Aguirre, J. (2003). Reactive oxygen species generated by microbial NADPH oxidase NoxA regulate sexual development in *Aspergillus nidulans*. *Mol. Microbiol.* 50, 1241–1255.

Learman, D. R., Voelker, B. M., Vazquez-Rodriguez, A. I., and Hansel, C. M. (2011). Formation of manganese oxides by bacterially generated superoxide. *Nat. Geosci.* 4, 95–98.

Lesser, M. P. (2006). Oxidative stress in marine environments: biochemistry and physiological ecology. *Annu. Rev. Physiol.* 68, 253–278.

Lesuisse, E., Casteras-Simon, M., and Labbe, P. (1996). Evidence for the *Saccharomyces cerevisiae* ferrireductase system being a multicomponent electron transport chain. *J. Biol. Chem.* 271, 13578–13583.

Liochev, S. I., and Fridovich, I. (1999). Superoxide and iron: partners in crime. *IUBMB Life* 48, 157–161.

Luther, G. W. III, and Rickard, D. T. (2005). Metal sulfide cluster complexes and their biogeochemical importance in the environment. *J. Nanopart. Res.* 7, 389–407.

Luther, G. W. III. (2010). The role of one- and two-electron transfer reactions in forming thermodynamically unstable intermediates as barriers in multi-electron redox reactions. *Aquat. Geochem.* 16, 395–420.

Maldonado, M. T., and Price, N. M. (2001). Reduction and transport of organically bound iron by *Thalassiosira oceanica* (Bacillariophyceae). *J. Phycol.* 37, 298–310.

Mansano-Weiss, C., Cohen, H., and Meyerstein, D. (2002). Reactions of peroxyl radicals with $Fe(H_2O)_6^{2+}$. *J. Inorg. Biochem.* 91, 199–204.

Marcus, R. A., and Sutin, N. (1985). Electron transfers in chemistry and biology. *Biochim. Biophys. Acta* 811, 265–322.

Marshall, J.-A., De Salas, M., Oda, T., and Hallegraeff, G. (2005). Superoxide production by marine microalgae. I. Survey of 37 species from 6 classes. *Mar. Biol.* 147, 533–540.

Marshall, J.-A., Hovenden, M., Oda, T., and Hallegraeff, G. M. (2002). Photosynthesis does influence superoxide production in the ichthyotoxic alga *Chattonella marina* (Raphidophyceae). *J. Plankton Res.* 24, 1231–1236.

McCord, J. M., Keele, B. B., and Fridovich, I. (1971). An enzyme-based theory of obligate anaerobiosis: the physiological function of superoxide dismutase. *Proc. Natl. Acad. Sci. U.S.A.* 68, 1024–1027.

Micinski, E., Ball, L. A., and Zafiriou, O. C. (1993). Photochemical oxygen activation: superoxide radical detection and production rates in the eastern Caribbean. *J. Geophys. Res.* 98, 2299–2306.

Middlemiss, J. K., Anderson, A. M., Stratilo, C. W., and Weger, H. G. (2001). Oxygen consumption associated with ferric reductase activity and iron uptake by iron-limited cells of *Chlorella kessleri* (Cholophyceae). *J. Phycol.* 37, 393–399.

Miller, W. L., King, D. W., Lin, J., and Kester, D. R. (1995). Photochemical redox cycling of iron in coastal seawater. *Mar. Chem.* 50, 63–77.

Millero, F. J., Yao, W., and Aicher, J. (1995). The speciation of Fe(II) and Fe(III) in natural waters. *Mar. Chem.* 50, 21–39.

Milne, A., Davey, M. S., Worsfold, P. J., Achterberg, E. P., and Taylor, A. R. (2009). Real-time detection of reactive oxygen species generation by marine phytoplankton using flow injection-chemiluminescence. *Limnol. Oceanogr. Methods* 7, 706–715.

Moffett, J. W., and Zafiriou, O. C. (1990). An investigation of hydrogen peroxide chemistry in surface waters of Vineyard Sound with $H_2{}^{18}O_2$ and $^{18}O_2$. *Limnol. Oceanogr.* 35, 1221–1229.

Morel, F. M. M., Kustka, A. B., and Shaked, Y. (2008). The role of unchelated Fe in the iron nutrition of phytoplankton. *Limnol. Oceanogr.* 53, 400–404.

Nakano, M. (1998). Detection of active oxygen species in biological systems. *Cell. Mol. Neurobiol.* 18, 565–579.

Nakano, M., Sugioka, K., Ushijima, Y., and Goto, T. (1986). Chemiluminescence probe with *Cypridina luciferin* analog, 2-methyl-6-phenyl-3,7-dihydroimidazo[1,2-a]pyrazin-3-one, for estimating the ability of human granulocytes to generate O_2^-. *Anal. Biochem.* 159, 363–369.

Nanni, E. J., Birge, R. R., Hubbard, L. M., Morrison, M. M., and Sawyer, D. T. (1981). Oxidation and dismutation of superoxide ion solutions to molecular oxygen. Singlet vs. triplet state. *Inorg. Chem.* 20, 737–741.

Neuman, E. W. (1934). Potassium superoxide and the three-electron bond. *J. Chem. Phys.* 2, 31–33.

Oda, T., Akaike, T., Sato, K., Ishimatsu, A., Takeshita, S., Muramatsu, T., and Maeda, H. (1992). Hydroxyl radical generation by red tide algae. *Arch. Biochem. Biophys.* 294, 38–43.

Oda, T., Nakamura, A., Shikayama, M., Kawano, I., Ishimatsu, A., and Muramatsu, T. (1997). Generation of reactive oxygen species by raphidophycean phytoplankton. *Biosci. Biotechnol. Biochem.* 61, 1658–1662.

Palenik, B., and Morel, F. M. M. (1988). Dark production of H_2O_2 in the Sargasso Sea. *Limnol. Oceanogr.* 33, 1606–1611.

Pauling, L. (1931). The nature of the chemical bond. II. The one-electron bond and the three-electron bond. *J. Am. Chem. Soc.* 53, 3225–3237.

Pauling, L. (1979). The discovery of the superoxide radical. *Trends Biochem. Sci.* 4, N270–N271.

Petasne, R. G., and Zika, R. G. (1987). Fate of superoxide in coastal sea water. *Nature* 325, 516–518.

Pierre, J. L., and Fontecave, M. (1999). Iron and activated oxygen species in biology: the basic chemistry. *Biometals* 12, 195–199.

Pierre, J. L., Fontecave, M., and Crichton, R. R. (2002). Chemistry for an essential biological process: the reduction of ferric iron. *Biometals* 15, 341–346.

Rao, D. N. R., Fischer, V., and Mason, R. P. (1990). Glutathione and ascorbate reduction of the acetaminophen radical formed by peroxidase. Detection of the glutathione disulfide radical anion and the ascorbyl radical. *J. Biol. Chem.* 265, 844–847.

Ratasuk, N., and Nanny, M. A. (2007). Characterization and quantification of reversible redox sites in humic substances. *Environ. Sci. Technol.* 41, 7844–7850.

Remucal, C. K., and Sedlak, D. L. (2011). "The role of iron coordination in the production of reactive oxidants from ferrous iron oxidation by oxygen and hydrogen peroxide," in *Aquatic Redox Chemistry*, eds P. G. Tratnyek, T. J. Grundl, and S. B. Haderlein (Washington: American Chemical Society), 177–197.

Rickard, D., and Luther, G. W. III. (2006). Metal sulfide complexes and clusters. *Rev. Mineral. Geochem.* 61, 421–504.

Rose, A. L., Godrant, A., Furnas, M., and Waite, T. D. (2010). Dynamics of nonphotochemical superoxide production in the Great Barrier Reef lagoon. *Limnol. Oceanogr.* 55, 1521–1536.

Rose, A. L., Moffett, J. W., and Waite, T. D. (2008a). Determination of superoxide in seawater using 2-methyl-6-(4-methoxyphenyl)-3,7-dihydroimidazo[1,2-a]pyrazin-3(7*H*)-one chemiluminescence. *Anal. Chem.* 80, 1215–1227.

Rose, A. L., Webb, E. A., Waite, T. D., and Moffett, J. W. (2008b). Measurement and implications of nonphotochemically generated superoxide in the equatorial Pacific Ocean. *Environ. Sci. Technol.* 42, 2387–2393.

Rose, A. L., Salmon, T. P., Lukondeh, T., Neilan, B. A., and Waite, T. D. (2005). Use of superoxide as an electron shuttle for iron acquisition by the marine cyanobacterium *Lyngbya majuscula*. *Environ. Sci. Technol.* 39, 3708–3715.

Rose, A. L., and Waite, T. D. (2003a). Effect of dissolved natural organic matter on the kinetics of ferrous iron oxygenation in seawater. *Environ. Sci. Technol.* 37, 4877–4886.

Rose, A. L., and Waite, T. D. (2003b). Kinetics of iron complexation by dissolved natural organic matter in coastal waters. *Mar. Chem.* 84, 85–103.

Rose, A. L., and Waite, T. D. (2005). Reduction of organically complexed ferric iron by superoxide in a simulated natural water. *Environ. Sci. Technol.* 39, 2645–2650.

Rosso, K. M., and Morgan, J. J. (2002). Outer-sphere electron transfer kinetics of metal ion oxidation by molecular oxygen. *Geochim. Cosmochim. Acta* 66, 4223–4233.

Rue, E. L., and Bruland, K. W. (1995). Complexation of iron(III) by natural organic ligands in the Central North Pacific as determined by a new competitive ligand equilibration/adsorptive cathodic stripping voltammetric method. *Mar. Chem.* 50, 117–138.

Rush, J. D., and Bielski, B. H. J. (1985). Pulse radiolytic studies of the reactions of HO_2/O_2^- with Fe(II)/Fe(III) ions. The reactivity of HO_2/O_2^- with ferric ions and its implication on the occurrence of the Haber-Weiss reaction. *J. Phys. Chem.* 89, 5062–5066.

Sagi, M., and Fluhr, R. (2001). Superoxide production by plant homologues of the gp91^{phox} NADPH oxidase. Modulation of activity by calcium and by tobacco mosaic virus infection. *Plant Physiol.* 126, 1281–1290.

Saragosti, E., Tchernov, D., Katsir, A., and Shaked, Y. (2010). Extracellular production and degradation of superoxide in the coral *Stylophora pistillata* and cultured *Symbiodinium*. *PLoS ONE* 5, e12508. doi:10.1371/journal.pone.0012508

Sawyer, D. T. (1991). *Oxygen Chemistry*. New York: Oxford University Press.

Sawyer, D. T., and Gibian, M. J. (1979). The chemistry of superoxide ion. *Tetrahedron* 35, 1471–1481.

Sawyer, D. T., and Valentine, J. S. (1981). How super is superoxide? *Acc. Chem. Res.* 14, 393–400.

Schröder, I., Johnson, E., and De Vries, S. (2003). Microbial ferric iron reductases. *FEMS Microbiol. Rev.* 27, 427–447.

Seibig, S., and van Eldik, R. (1997). Kinetics of [Fe^{II}(edta)] oxidation by molecular oxygen revisited. New evidence for a multistep mechanism. *Inorg. Chem.* 36, 4115–4120.

Shaked, Y., Harris, R., and Klein-Kedem, N. (2010). Hydrogen peroxide photocycling in the Gulf of Aqaba, Red Sea. *Environ. Sci. Technol.* 44, 3238–3244.

Shaked, Y., Kustka, A. B., and Morel, F. M. M. (2005). A general kinetic model for iron acquisition by eukaryotic phytoplankton. *Limnol. Oceanogr.* 50, 872–882.

Shatwell, K. P., Dancis, A., Cross, A. R., Klausner, R. D., and Segal, A. W. (1996). The FRE1 ferric reductase of *Saccharomyces cerevisiae* is a cytochrome *b* similar to that of NADPH oxidase. *J. Biol. Chem.* 271, 14240–14244.

Sunda, W., and Huntsman, S. (2003). Effect of pH, light, and temperature on Fe-EDTA chelation and Fe hydrolysis in seawater. *Mar. Chem.* 84, 35–47.

Teranishi, K. (2007). Development of imidazopyrazinone red-chem iluminescent probes for detecting superoxide anions via a chemiluminescence resonance energy transfer method. *Luminescence* 22, 147–156.

Thomas-Smith, T. E., and Blough, N. V. (2001). Photoproduction of hydrated electron from constituents of natural waters. *Environ. Sci. Technol.* 35, 2721–2726.

Torres, M. A., Onouchi, H., Hamada, S., Machida, C., Hammond-Kosack, K. E., and Jones, J. D. G. (1998). Six *Arabidopsis thaliana* homologues of the human respiratory burst oxidase (*gp91^{phox}*). *Plant J.* 14, 365–370.

Vignais, P. V. (2002). The superoxide-generating NADPH oxidase: structural aspects and activation mechanism. *Cell. Mol. Life Sci.* 59, 1428–1459.

Voelker, B. M., Morel, F. M. M., and Sulzberger, B. (1997). Iron redox cycling in surface waters: effects of humic substances and light. *Environ. Sci. Technol.* 31, 1004–1011.

Voelker, B. M., and Sedlak, D. L. (1995). Iron reduction by photoproduced superoxide in seawater. *Mar. Chem.* 50, 93–102.

Weber, L., Völker, C., Oschlies, A., and Burchard, H. (2007). Iron profiles and speciation of the upper water column at the Bermuda Atlantic Time-series Study site: a model based sensitivity study. *Biogeosciences* 4, 689–706.

Weber, L., Völker, C., Schartau, M., and Wolf-Gladrow, D. A. (2005). Modeling the speciation and biogeochemistry of iron at the Bermuda Atlantic Time-series Study site. *Global Biogeochem. Cycles* 19, GB1019.

Weinstock, I. A. (2008). Outer-sphere oxidation of the superoxide radical anion. *Inorg. Chem.* 47, 404–406.

Winterbourn, C. C. (1995). Toxicity of iron and hydrogen peroxide: the Fenton reaction. *Toxicol. Lett.* 82–83, 969–974.

Witter, A. E., Hutchins, D. A., Butler, A., and Luther, G. W. (2000). Determination of conditional stability constants and kinetic constants for strong model Fe-binding ligands in seawater. *Mar. Chem.* 69, 1–17.

Wolfe-Simon, F., Grzebyk, D., Schofield, O., and Falkowski, P. G. (2005). The role and evolution of superoxide dismutases in algae. *J. Phycol.* 41, 453–465.

Yamasaki, Y., Kim, D.-I., Matsuyama, Y., Oda, T., and Honjo, T. (2004). Production of superoxide anion and hydrogen peroxide by the red tide dinoflagellate *Karenia mikimotoi*. *J. Biosci. Bioeng.* 97, 212–215.

Zafiriou, O. C. (1990). Chemistry of superoxide ion-radical (O_2^{-}) in seawater. I. pKa_{sw^*} (HOO) and uncatalyzed dismutation kinetics studied by pulse radiolysis. *Mar. Chem.* 30, 31–43.

Zang, V., and van Eldik, R. (1990). Kinetics and mechanism of the

autoxidation of iron(II) induced through chelation by ethylenediaminetetraacetate and related ligands. *Inorg. Chem.* 29, 1705–1711.

Conflict of Interest Statement: The author declares that the research was conducted in the absence of any commercial or financial relationships that could be construed as a potential conflict of interest.

Received: 11 November 2011; accepted: 15 March 2012; published online: 11 April 2012.

Citation: Rose AL (2012) The influence of extracellular superoxide on iron redox chemistry and bioavailability to aquatic microorganisms. Front. Microbio. ***3****:124. doi: 10.3389/fmicb.2012.00124*
This article was submitted to Frontiers in Microbiological Chemistry, a specialty of Frontiers in Microbiology.

Copyright © 2012 Rose. This is an open-access article distributed under the terms of the Creative Commons Attribution Non Commercial License, which permits non-commercial use, distribution, and reproduction in other forums, provided the original authors and source are credited.

APPENDIX

ADDITIONAL DETAILS OF CHEMISTRY OF REACTIONS BETWEEN SUPEROXIDE AND IRON

Thermodynamics

Application of the Nernst equation, using measured or estimated values for the concentrations of the various species, is required to determine the environmental redox potential at 25°C:

$$E = E^0 + 59\log([\mathrm{Ox}]/[\mathrm{Red}]) \tag{A1}$$

where Ox represents the oxidized form of the species, Red the reduced form, and E and E^0 are in millivolt.

Consequently, under conditions typical for a neutral air-saturated surface water (pH 7 and $[O_2] = 250\,\mu M$), the actual redox potential of the O_2/O_2^{-*} couple is +335 mV when $[O_2^{-*}] = 1$ pM and +158 mV when $[O_2^{-*}] = 1$ nM. While Pierre et al. (2002) emphasize the importance of using actual concentrations of O_2 and O_2^{-*} to calculate relevant redox potentials, an equally important consideration for the thermodynamic reducibility of a particular form of Fe by O_2^{-*} is the concentration of relevant Fe(II) and Fe(III) species. This is well demonstrated by considering the case of some organic Fe complexes, which we denote as Fe(II)L in the reduced state and Fe(III)L in the oxidized state. Since:

$$E^0 = 59\log K \tag{A2}$$

where K is the equilibrium constant for the equilibrium redox reaction:

$$\mathrm{Ox} + ne^- \Leftrightarrow \mathrm{Red} \tag{A3}$$

we obtain the relationship:

$$\begin{aligned} E^0_{\mathrm{Fe^{3+}L}\rightarrow\mathrm{Fe^{2+}L}} &= E^0_{\mathrm{Fe^{3+}}\rightarrow\mathrm{Fe^{2+}}} + 59\log\left(K_{\mathrm{Fe^{2+}L}}/K_{\mathrm{Fe^{3+}L}}\right) \\ &= E^0_{\mathrm{Fe^{3+}}\rightarrow\mathrm{Fe^{2+}}} + 59\log\left(\left(K_{\mathrm{Fe(II)L}}\alpha_{\mathrm{Fe^{3+}}}\right)/\left(K_{\mathrm{Fe(III)L}}\alpha_{\mathrm{Fe^{2+}}}\right)\right) \end{aligned} \tag{A4}$$

where the stability constants are mixed constants expressed as:

$$K_{\mathrm{Fe^{2+}L}} = \frac{[\mathrm{Fe\ (II)\ L}]}{\left[\mathrm{Fe^{2+}}\right]\left[\mathrm{L'}\right]} \tag{A5}$$

$$K_{\mathrm{Fe^{3+}L}} = \frac{[\mathrm{Fe\ (III)\ L}]}{\left[\mathrm{Fe^{3+}}\right]\left[\mathrm{L'}\right]} \tag{A6}$$

$$K_{\mathrm{Fe(II)L}} = \frac{[\mathrm{Fe\ (II)\ L}]}{\left[\mathrm{Fe\ (II)'}\right]\left[\mathrm{L'}\right]} \tag{A7}$$

$$K_{\mathrm{Fe(III)L}} = \frac{[\mathrm{Fe\ (III)\ L}]}{\left[\mathrm{Fe\ (III)'}\right]\left[\mathrm{L'}\right]} \tag{A8}$$

and where, under particular medium conditions, Fe(II)′ represents the sum of all monomeric inorganic Fe(II) species, Fe(III)′ represents the sum of all monomeric inorganic Fe(III) species, L′ represents the sum of all ligand species, $\alpha_{\mathrm{Fe^{2+}}}$ represents the ratio of $[\mathrm{Fe^{2+}}]/[\mathrm{Fe(II)'}]$, and $\alpha_{\mathrm{Fe^{3+}}}$ represents the ratio of $[\mathrm{Fe^{3+}}]/[\mathrm{Fe(III)'}]$.

It is then relatively straightforward to rewrite the Nernst equation in terms of the stability constants of the Fe(III) complex and Fe(II) complex:

$$\begin{aligned} E_{\mathrm{Fe^{3+}L}\rightarrow\mathrm{Fe^{2+}L}} &= E^0_{\mathrm{Fe^{3+}L}\rightarrow\mathrm{Fe^{2+}L}} + 59\log\left([\mathrm{Fe\ (II)\ L}]\ /\ [\mathrm{Fe\ (III)\ L}]\right) \\ &= E^0_{\mathrm{Fe^{3+}}\rightarrow\mathrm{Fe^{2+}}} + 59\log\left(\left(K_{\mathrm{Fe(II)L}}\alpha_{\mathrm{Fe^{3+}}}\right)/\left(K_{\mathrm{Fe(III)L}}\alpha_{\mathrm{Fe^{2+}}}\right)\right) + 59\log\left([\mathrm{Fe\ (II)\ L}]\ /\ [\mathrm{Fe\ (III)\ L}]\right) \end{aligned} \tag{A9}$$

The criterion that must be satisfied for a thermodynamic driving force toward Fe(III)L reduction is:

$$E_{\mathrm{Fe^{3+}L}\rightarrow\mathrm{Fe^{2+}L}} > E_{\mathrm{O_2}\rightarrow\mathrm{O_2^{-*}}} \tag{A10}$$

which, in combination with Eq. A9, yields the necessary condition:

$$\log\left([\mathrm{Fe\ (II)\ L}]\ /\ [\mathrm{Fe\ (III)\ L}]\right) < \left(E^0_{\mathrm{Fe^{3+}}\rightarrow\mathrm{Fe^{2+}}} - E_{\mathrm{O_2}\rightarrow\mathrm{O_2^{-*}}}\right)/59 + \log\left(\left(K_{\mathrm{Fe(II)L}}\alpha_{\mathrm{Fe^{3+}}}\right)/\left(K_{\mathrm{Fe(III)L}}\alpha_{\mathrm{Fe^{2+}}}\right)\right) \tag{A11}$$

According to the Nernst equation, reduction of Fe^{3+} to Fe^{2+} is thermodynamically feasible when:

$$E_{Fe^{3+}\rightarrow Fe^{2+}} = E^0_{Fe^{3+}\rightarrow Fe^{2+}} + 59\log\left(\left[Fe^{3+}\right]/\left[Fe^{2+}\right]\right) > E_{O_2\rightarrow O_2^{-*}} \tag{A12}$$

$$\text{i.e. } \log\left(\left[Fe^{3+}\right]/\left[Fe^{2+}\right]\right) > \left(E_{O_2\rightarrow O_2^{-*}} - E^0_{Fe^{3+}\rightarrow Fe^{2+}}\right)/59 \tag{A13}$$

$$\Rightarrow \log\left(\left[Fe\ (II)'\right]/\left[Fe\ (III)'\right]\right) < \log\left(\alpha_{Fe^{3+}}/\alpha_{Fe^{2+}}\right) + \left(E^0_{Fe^{3+}\rightarrow Fe^{2+}} - E_{O_2\rightarrow O_2^{-*}}\right)/59 \tag{A14}$$

Kinetics and mechanisms

The reduction of each Fe(III) species by O_2^{-*} can be represented by the following two general reactions:

$$Fe(III)_i + O_2^- \rightarrow Fe(II)_i + O_2 \tag{A15}$$

$$Fe(III)_i + HOO^\bullet \rightarrow Fe(II)_i + O_2 + H^+ \tag{A16}$$

where $Fe(III)_i$ represents an individual Fe(III) species. The corresponding rate law equation is given by:

$$-\frac{d}{dt}\left[Fe(III)_i\right] = k_{red,O_2^-,i}\left[Fe(III)_i\right]\left[O_2^-\right] + k_{red,HOO^\bullet,i}\left[Fe(III)_i\right]\left[HOO^\bullet\right] \tag{A17}$$

Since O_2^- and $HOO^\bullet$ equilibrate much faster than the timescale of this reaction, we can write $[O_2^-] = \alpha_{O_2^-}[O_2^{-*}]$ and $[HOO^\bullet] = \alpha_{HOO^\bullet}[O_2^{-*}]$ where $\alpha_{O_2^-}$ and $\alpha_{HOO^\bullet}$ are constants under constant medium conditions (pH, ionic strength, etc.). Thus the rate law equation becomes:

$$-\frac{d}{dt}\left[Fe(III)_i\right] = \left(k_{red,O_2^-,i}\alpha_{O_2^-} + k_{red,HOO^\bullet,i}\alpha_{HOO^\bullet}\right)\left[Fe(III)_i\right]\left[O_2^{-*}\right] = k_{red,i}\left[Fe(III)_i\right]\left[O_2^{-*}\right] \tag{A18}$$

where O_2^{-*} exhibits constant speciation under given constant medium conditions, and $k_{red,i}$ is a conditional rate constant for reduction of $Fe(III)_i$ under those conditions. The overall rate law for reduction of all Fe(III) species is then given by:

$$\begin{aligned} -\frac{d}{dt}[Fe\ (III)]_T &= -\frac{d}{dt}\left[Fe\ (III)'\right] - \frac{d}{dt}[Fe\ (III)]_{org} - \frac{d}{dt}[Fe\ (III)]_{poly} \\ &= \sum_{all\ x} k_{red,x}\left[Fe(III)_x\right]\left[O_2^{-*}\right] + \sum_{all\ y} k_{red,y}\left[Fe(III)_y\right]\left[O_2^{-*}\right] + \sum_{all\ z} k_{red,z}\left[Fe(III)_z\right]\left[O_2^{-*}\right] \end{aligned} \tag{A19}$$

where $[Fe(III)]_T$ denotes the total concentration of Fe(III) in all classes; $[Fe(III)']$ denotes the total concentration of all Fe(III) species in the mononuclear inorganic class, $[Fe(III)]_{org}$ denotes the total concentration of all Fe(III) species in the mononuclear organic class, and $[Fe(III)]_{poly}$ denotes the total concentration of all Fe(III) species in the polynuclear class; and $Fe(III)_x$, $Fe(III)_y$, and $Fe(III)_z$ denote individual Fe(III) species in the mononuclear inorganic, mononuclear organic, and polynuclear classes, respectively.

A similar analysis yields the rate law for oxidation of all Fe(II) species by O_2^{-*}:

$$\begin{aligned} -\frac{d}{dt}[Fe\ (II)]_T &= -\frac{d}{dt}\left[Fe\ (II)'\right] - \frac{d}{dt}[Fe\ (II)]_{org} - \frac{d}{dt}[Fe\ (II)]_{poly} \\ &= \sum_{all\ x} k_{ox,x}\left[Fe(II)_x\right]\left[O_2^{-*}\right] + \sum_{all\ y} k_{ox,y}\left[Fe(II)_y\right]\left[O_2^{-*}\right] + \sum_{all\ z} k_{ox,z}\left[Fe(II)_z\right]\left[O_2^{-*}\right] \end{aligned} \tag{A20}$$

where $[Fe(II)]_T$ denotes the total concentration of Fe(II) in all classes; $[Fe(II)']$ denotes the total concentration of all Fe(II) species in the mononuclear inorganic class, $[Fe(II)]_{org}$ denotes the total concentration of all Fe(II) species in the mononuclear organic class, and $[Fe(II)]_{poly}$ denotes the total concentration of all Fe(II) species in the polynuclear class; and $Fe(II)_x$, $Fe(II)_y$, and $Fe(II)_z$ denote individual Fe(II) species in the mononuclear inorganic, mononuclear organic, and polynuclear classes, respectively.

Mononuclear inorganic Fe(III) species equilibrate much faster than the timescale of their reactions with O_2^{-*}. Thus we can further simplify Eq. A19 using the relationship:

$$\sum_{all\ x} k_{red,x}\left[Fe(III)_x\right]\left[O_2^{-*}\right] = \sum_{all\ x} k_{red,x}\alpha_{Fe(III)_x}\left[Fe\ (III)'\right]\left[O_2^{-*}\right] = k_{red,inorg}\left[Fe\ (III)'\right]\left[O_2^{-*}\right] \tag{A21}$$

where $\alpha_{Fe(III)_x}$ represents the ratio of $[Fe(III)_x]/[Fe(III)']$ and $k_{red,inorg}$ is a conditional rate constant for reduction of all mononuclear inorganic Fe(III) species under particular, constant medium conditions.

Hence overall:

$$-\frac{\mathrm{d}}{\mathrm{d}t}[\mathrm{Fe\ (III)}]_\mathrm{T} = k_{\mathrm{red,inorg}}\left[\mathrm{Fe\ (III)}'\right]\left[\mathrm{O_2^{-*}}\right] + \sum_{\mathrm{all}\ y} k_{\mathrm{red},y}\left[\mathrm{Fe(III)}_y\right]\left[\mathrm{O_2^{-*}}\right] + \sum_{\mathrm{all}\ z} k_{\mathrm{red},z}\left[\mathrm{Fe(III)}_z\right]\left[\mathrm{O_2^{-*}}\right] \tag{A22}$$

Similarly for oxidation of Fe(II) by $\mathrm{O_2^{-*}}$:

$$-\frac{\mathrm{d}}{\mathrm{d}t}[\mathrm{Fe\ (II)}]_\mathrm{T} = k_{\mathrm{ox,inorg}}\left[\mathrm{Fe\ (II)}'\right]\left[\mathrm{O_2^{-*}}\right] + \sum_{\mathrm{all}\ y} k_{\mathrm{ox},y}\left[\mathrm{Fe(II)}_y\right]\left[\mathrm{O_2^{-*}}\right] + \sum_{\mathrm{all}\ z} k_{\mathrm{ox},z}\left[\mathrm{Fe(II)}_z\right]\left[\mathrm{O_2^{-*}}\right] \tag{A23}$$

DETAILS OF SPATIALLY HOMOGENEOUS STEADY-STATE MODEL FOR Fe′ CONCENTRATIONS AS A FUNCTION OF SUPEROXIDE CONCENTRATIONS

The steady-state concentrations of the Fe species for the system shown in **Figure 3** are controlled by eight parameters: $k_{\mathrm{f,Fe(III)L}}$, $k_{\mathrm{d,Fe(III)L}}$, $k_{\mathrm{f,Fe(II)L}}$, $k_{\mathrm{d,Fe(II)L}}$, $k_{\mathrm{O_2,inorg}}$, $k_{\mathrm{red,inorg}}$, $k_{\mathrm{O_2,org}}$, and $k_{\mathrm{red,org}}$, and can be determined by solving the resulting rate law equations for each Fe species subject to the steady-state condition $\mathrm{d}/\mathrm{d}t = 0$. The four resulting equations are not independent, so we also need to invoke a mass balance equation for Fe, leading to the following system of independent equations that must be solved in order to calculate the steady-state concentrations of the Fe species in the system:

$$\frac{\mathrm{d}}{\mathrm{d}t}\left[\mathrm{Fe\ (II)}'\right] = k_{\mathrm{red,inorg}}\left[\mathrm{O_2^{-*}}\right]\left[\mathrm{Fe\ (III)}'\right] - k_{\mathrm{O_2,inorg}}\left[\mathrm{O_2}\right]\left[\mathrm{Fe\ (II)}'\right] + k_{\mathrm{d,Fe(II)L}}\left[\mathrm{Fe\ (II)\ L}\right] - k_{\mathrm{f,Fe(II)L}}\left[\mathrm{L}\right]\left[\mathrm{Fe\ (II)}'\right] \tag{A24}$$

$$\frac{\mathrm{d}}{\mathrm{d}t}\left[\mathrm{Fe\ (III)}'\right] = k_{\mathrm{O_2,inorg}}\left[\mathrm{O_2}\right]\left[\mathrm{Fe\ (II)}'\right] - k_{\mathrm{red,inorg}}\left[\mathrm{O_2^{-*}}\right]\left[\mathrm{Fe\ (III)}'\right] + k_{\mathrm{d,Fe(III)L}}\left[\mathrm{Fe\ (III)\ L}\right] - k_{\mathrm{f,Fe(III)L}}\left[\mathrm{L}\right]\left[\mathrm{Fe\ (III)}'\right] \tag{A25}$$

$$\frac{\mathrm{d}}{\mathrm{d}t}\left[\mathrm{Fe\ (II)\ L}\right] = k_{\mathrm{red,org}}\left[\mathrm{O_2^{-*}}\right]\left[\mathrm{Fe\ (III)\ L}\right] - k_{\mathrm{O_2,org}}\left[\mathrm{O_2}\right]\left[\mathrm{Fe\ (II)\ L}\right] + k_{\mathrm{f,Fe(II)L}}\left[\mathrm{L}\right]\left[\mathrm{Fe\ (II)}'\right] - k_{\mathrm{d,Fe(II)L}}\left[\mathrm{Fe\ (II)\ L}\right] \tag{A26}$$

$$\left[\mathrm{Fe\ (III)}'\right] + \left[\mathrm{Fe\ (II)}'\right] + \left[\mathrm{Fe\ (III)\ L}\right] + \left[\mathrm{Fe\ (II)\ L}\right] = [\mathrm{Fe}]_\mathrm{T} \tag{A27}$$

This can be simplified to a system of linear equations by treating the steady-state concentrations of the other species in the system (L, $\mathrm{O_2}$, and $\mathrm{O_2^{-*}}$) as constants. In oxygen-saturated waters at 25°C, $[\mathrm{O_2}] = 250\ \mu\mathrm{M} \gg [\mathrm{Fe}]_\mathrm{T}$ in most cases. Assuming [L] is constant is also reasonable provided $[\mathrm{L}] \gg [\mathrm{Fe}]_\mathrm{T}$, which is frequently the case, but even if not we can specify a constant amount of free, excess ligand for the present purposes provided the majority of Fe remains organically complexed under the range of scenarios investigated (which will be seen to be the case, as shown in **Figure 4**). Finally, we will specify a constant steady-state $[\mathrm{O_2^{-*}}]$ and consider the effect of this value on steady-state [Fe(III)′], [Fe(II)′], and $[\mathrm{Fe}']_\mathrm{T} = [\mathrm{Fe(III)}'] + [\mathrm{Fe(II)}']$.

Under these conditions, it is straightforward to solve the system of linear Eqs A24–A27 using a symbolic mathematics software package (the MATLAB Symbolic Math Toolbox in this case) to yield rather complicated analytical solutions for steady-state [Fe(II)′] and [Fe(III)′]:

$$\left[\mathrm{Fe\ (II)}'\right] = \frac{k_{\mathrm{d,Fe(II)L}}k_{\mathrm{d,Fe(III)L}}k^*_{\mathrm{red,inorg}} + k_{\mathrm{d,Fe(II)L}}k^*_{\mathrm{f,Fe(III)L}}k^*_{\mathrm{red,org}} + k_{\mathrm{d,Fe(III)L}}k^*_{\mathrm{red,org}}k^*_{\mathrm{red,inorg}} + k_{\mathrm{d,Fe(II)L}}k^*_{\mathrm{red,inorg}}k^*_{\mathrm{red,org}}}{\left(\begin{array}{c} k_{\mathrm{d,Fe(II)L}}k_{\mathrm{d,Fe(III)L}}k^*_{\mathrm{O_2,inorg}} + k_{\mathrm{d,Fe(II)L}}k^*_{\mathrm{f,Fe(III)L}}k^*_{\mathrm{O_2,inorg}} + k_{\mathrm{d,Fe(III)L}}k^*_{\mathrm{f,Fe(II)L}}k^*_{\mathrm{O_2,org}} + k_{\mathrm{d,Fe(II)L}}k_{\mathrm{d,Fe(III)L}}k^*_{\mathrm{red,inorg}} + \\ k^*_{\mathrm{f,Fe(II)L}}k^*_{\mathrm{f,Fe(III)L}}k^*_{\mathrm{O_2,org}} + k_{\mathrm{d,Fe(III)L}}k^*_{\mathrm{f,Fe(II)L}}k^*_{\mathrm{red,inorg}} + k_{\mathrm{d,Fe(II)L}}k^*_{\mathrm{f,Fe(III)L}}k^*_{\mathrm{red,org}} + k^*_{\mathrm{f,Fe(II)L}}k^*_{\mathrm{f,Fe(III)L}}k^*_{\mathrm{red,org}} + \\ k_{\mathrm{d,Fe(III)L}}k^*_{\mathrm{O_2,inorg}}k^*_{\mathrm{O_2,org}} + k^*_{\mathrm{f,Fe(III)L}}k^*_{\mathrm{O_2,inorg}}k^*_{\mathrm{O_2,org}} + k_{\mathrm{d,Fe(II)L}}k^*_{\mathrm{O_2,inorg}}k^*_{\mathrm{red,org}} + k_{\mathrm{d,Fe(III)L}}k^*_{\mathrm{O_2org}}k^*_{\mathrm{red,inorg}} + \\ k^*_{\mathrm{f,Fe(II)L}}k^*_{\mathrm{O_2,org}}k^*_{\mathrm{red,inorg}} + k^*_{\mathrm{f,Fe(III)L}}k^*_{\mathrm{O_2,inorg}}k^*_{\mathrm{red,org}} + k_{\mathrm{d,Fe(II)L}}k^*_{\mathrm{red,inorg}}k^*_{\mathrm{red,org}} + k^*_{\mathrm{f,Fe(II)L}}k^*_{\mathrm{red,inorg}}k^*_{\mathrm{red,org}} \end{array}\right)}[\mathrm{Fe}]_\mathrm{T} \tag{A28}$$

$$[\mathrm{Fe(III')}] = \frac{k_{\mathrm{d,Fe(II)L}}k_{\mathrm{d,Fe(III)L}}k^*_{\mathrm{O_2,inorg}} + k_{\mathrm{d,Fe(III)L}}k^*_{\mathrm{f,Fe(II)L}}k^*_{\mathrm{O_2,org}} + k_{\mathrm{d,Fe(III)L}}k^*_{\mathrm{O_2,inorg}}k^*_{\mathrm{O_2,org}} + k_{\mathrm{d,Fe(II)L}}k^*_{\mathrm{O_2,inorg}}k^*_{\mathrm{red,org}}}{\left(\begin{array}{c} k_{\mathrm{d,Fe(II)L}}k_{\mathrm{d,Fe(III)L}}k^*_{\mathrm{O_2,inorg}} + k_{\mathrm{d,Fe(II)L}}k^*_{\mathrm{f,Fe(III)L}}k^*_{\mathrm{O_2,inorg}} + k_{\mathrm{d,Fe(III)L}}k^*_{\mathrm{f,Fe(II)L}}k^*_{\mathrm{O_2,org}} + k_{\mathrm{d,Fe(II)L}}k_{\mathrm{d,Fe(III)L}}k^*_{\mathrm{red,inorg}} + \\ k^*_{\mathrm{f,Fe(II)L}}k^*_{\mathrm{f,Fe(III)L}}k^*_{\mathrm{O_2,org}} + k_{\mathrm{d,Fe(III)L}}k^*_{\mathrm{f,Fe(II)L}}k^*_{\mathrm{red,inorg}} + k_{\mathrm{d,Fe(II)L}}k^*_{\mathrm{f,Fe(III)L}}k^*_{\mathrm{red,org}} + k^*_{\mathrm{f,Fe(II)L}}k^*_{\mathrm{f,Fe(III)L}}k^*_{\mathrm{red,org}} + \\ k_{\mathrm{d,Fe(III)L}}k^*_{\mathrm{O_2,inorg}}k^*_{\mathrm{O_2,org}} + k^*_{\mathrm{f,Fe(III)L}}k^*_{\mathrm{O_2,inorg}}k^*_{\mathrm{O_2,org}} + k_{\mathrm{d,Fe(II)L}}k^*_{\mathrm{O_2,inorg}}k^*_{\mathrm{red,org}} + k_{\mathrm{d,Fe(III)L}}k^*_{\mathrm{O_2,org}}k^*_{\mathrm{red,inorg}} + \\ k^*_{\mathrm{f,Fe(II)L}}k^*_{\mathrm{O_2,org}}k^*_{\mathrm{red,inorg}} + k^*_{\mathrm{f,Fe(III)L}}k^*_{\mathrm{O_2,inorg}}k^*_{\mathrm{red,inorg}} + k_{\mathrm{d,Fe(II)L}}k^*_{\mathrm{red,inorg}}k^*_{\mathrm{red,org}} + k^*_{\mathrm{f,Fe(II)L}}k^*_{\mathrm{red,inorg}}k^*_{\mathrm{red,org}} \end{array}\right)}[\mathrm{Fe}]_\mathrm{T} \tag{A29}$$

where $k^*_{\mathrm{f,Fe(III)L}} = k_{\mathrm{f,Fe(III)L}}[\mathrm{L}]$, $k^*_{\mathrm{f,Fe(II)L}} = k_{\mathrm{f,Fe(II)L}}[\mathrm{L}]$, $k^*_{\mathrm{O_2,inorg}} = k_{\mathrm{O_2,inorg}}[\mathrm{O_2}]$, $k^*_{\mathrm{red,inorg}} = k_{\mathrm{red,inorg}}[\mathrm{O_2^{-*}}]$, $k^*_{\mathrm{O_2,org}} = k_{\mathrm{O_2,org}}[\mathrm{O_2}]$, and $k^*_{\mathrm{red,org}} = k_{\mathrm{red,org}}[\mathrm{O_2^{-*}}]$.

The number of variables can be further simplified by assuming a 1:1 Fe:L ratio for Fe(II)L and Fe(III)L, that the complex formation rate constants are independent of ligand type (consistent with control of complex formation by water loss kinetics, i.e., the complexes form via a perfect Eigen–Wilkins mechanism (Eigen and Wilkins, 1965) in which the electrostatic charge on L does not vary between

different ligand types), and that the oxidation of Fe(II)L by O_2 and reduction of Fe(III)L by O_2^{-*} are outer-sphere electron transfer processes that obey Marcus Theory perfectly. With these simplifications, we will consider an illustrative typical coastal marine water in equilibrium with the atmosphere at pH 8.1, temperature 25°C, ionic strength of 0.7 M, and constant ionic composition, specifying the following parameter values:

$k_{f,Fe(III)L} = 5 \times 10^6\ M^{-1}\ s^{-1}$, a typical value from Rose and Waite (2003b)
$k_{f,Fe(II)L} = 5 \times 10^4\ M^{-1}\ s^{-1}$, a typical value from Rose and Waite (2003b)
$k_{d,Fe(III)L} = k_{f,Fe(III)L}/K_{Fe(III)L}\ s^{-1}$ where $K_{Fe(III)L}$ (M^{-1}) is as defined previously
$k_{d,Fe(II)L} = k_{f,Fe(II)L}/K_{Fe(II)L}\ s^{-1}$ where $K_{Fe(II)L}$ (M^{-1}) is as defined previously
$k_{O_2,inorg} = 13\ M^{-1}\ s^{-1}$ (Rose and Waite, 2002)
$k_{red,inorg} = 1.5 \times 10^8\ M^{-1}\ s^{-1}$ (Bielski et al., 1985).

The remaining two parameters $k_{O_2,org}$ and $k_{red,org}$ are specified by the Marcus relationship:

$$k_{O_2,org} = \frac{k_{diff}}{1 + \frac{k_{diff}}{K_d Z} \exp\left(\frac{\lambda}{4RT}\left(1 + \frac{\Delta G^0_{ox,org}}{\lambda}\right)^2\right)} \tag{A30}$$

$$k_{red,org} = \frac{k_{diff}}{1 + \frac{k_{diff}}{K_d Z} \exp\left(\frac{\lambda}{4RT}\left(1 + \frac{\Delta G^0_{red,org}}{\lambda}\right)^2\right)} \tag{A31}$$

where $\Delta G^0_{ox,org}$ and $\Delta G^0_{red,org}$ (kJ mol^{-1}) are expressed in terms of the conditional stability constants $K_{Fe(III)L}$ and $K_{Fe(II)L}$, as described in Rose and Waite (2003a):

$$\Delta G^0_{red,org} = -\Delta G^0_{ox,org} = 10^{-6} F \left(E^0_{O_2 \to O_2^{-*}} - E^0_{Fe^{3+} \to Fe^{2+}} - 59 \log\left(K_{Fe(II)L}\right) / \left(K_{Fe(III)L}\right)\right) \tag{A32}$$

and $E^0_{O_2 \to O_2^{-*}} = -160$ mV (Sawyer, 1991), $E^0_{Fe^{3+} \to Fe^{2+}} = +770$ mV (Morel and Hering, 1993), $F = 9.649 \times 10^4$ C mol^{-1} (Morel and Hering, 1993), and we assume values of $k_{diff} = 10^{10}\ M^{-1}\ s^{-1}$, $k_{diff}/(K_d\ Z) = 0.1$, and $\lambda = 135$ kJ mol^{-1} as per Rose and Waite (2003a).

Consequently the parameters $k_{f,Fe(III)L}$, $k_{f,Fe(II)L}$, $k_{O_2,inorg}$, and $k_{red,inorg}$ are constants (for a specified [L], [O_2], and $\left[O_2^{-*}\right]$), while the parameters $k_{d,Fe(III)L}$, $k_{d,Fe(II)L}$, $k_{O_2,org}$, and $k_{red,org}$ are functions of $K_{Fe(III)L}$ and $K_{Fe(II)L}$.

REFERENCES

Morel, F. M. M., and Hering, J. G. (1993). *Principles and Applications of Aquatic Chemistry*. New York: Wiley.
Rose, A. L., and Waite, T. D. (2002). Kinetic model for Fe(II) oxidation in seawater in the absence and presence of natural organic matter. *Environ. Sci. Technol.* 36, 433–444.

frontiers in
MICROBIOLOGY

REVIEW ARTICLE
published: 28 February 2012
doi: 10.3389/fmicb.2012.00069

The organic complexation of iron in the marine environment: a review

***Martha Gledhill*[1]*† *and Kristen N. Buck*[2]*†**

[1] *Ocean and Earth Science, National Oceanography Centre – Southampton, University of Southampton, Southampton, UK*
[2] *Bermuda Institute of Ocean Sciences, St. George's, Bermuda*

Edited by:
Benjamin Twining, Bigelow Laboratory for Ocean Sciences, USA

Reviewed by:
Sylvia G. Sander, University of Otago, New Zealand
Alessandro Tagliabue, Council for Scientific and Industrial Research, South Africa

***Correspondence:**
Martha Gledhill, Ocean and Earth Science, National Oceanography Centre – Southampton, University of Southampton, Southampton SO14 3ZH, UK.
e-mail: martha@soton.ac.uk;
Kristen N. Buck, Bermuda Institute of Ocean Sciences, Ferry Reach, St. George's GE 01, Bermuda.
e-mail: kristen.buck@bios.edu

†Martha Gledhill and Kristen N. Buck have contributed equally to this work.

Iron (Fe) is an essential micronutrient for marine organisms, and it is now well established that low Fe availability controls phytoplankton productivity, community structure, and ecosystem functioning in vast regions of the global ocean. The biogeochemical cycle of Fe involves complex interactions between lithogenic inputs (atmospheric, continental, or hydrothermal), dissolution, precipitation, scavenging, biological uptake, remineralization, and sedimentation processes. Each of these aspects of Fe biogeochemical cycling is likely influenced by organic Fe-binding ligands, which complex more than 99% of dissolved Fe. In this review we consider recent advances in our knowledge of Fe complexation in the marine environment and their implications for the biogeochemistry of Fe in the ocean. We also highlight the importance of constraining the dissolved Fe concentration value used in interpreting voltammetric titration data for the determination of Fe speciation. Within the published Fe speciation data, there appear to be important temporal and spatial variations in Fe-binding ligand concentrations and their conditional stability constants in the marine environment. Excess ligand concentrations, particularly in the truly soluble size fraction, seem to be consistently higher in the upper water column, and especially in Fe-limited, but productive, waters. Evidence is accumulating for an association of Fe with both small, well-defined ligands, such as siderophores, as well as with larger, macromolecular complexes like humic substances, exopolymeric substances, and transparent exopolymers. The diverse size spectrum and chemical nature of Fe ligand complexes corresponds to a change in kinetic inertness which will have a consequent impact on biological availability. However, much work is still to be done in coupling voltammetry, mass spectrometry techniques, and process studies to better characterize the nature and cycling of Fe-binding ligands in the marine environment.

Keywords: seawater, speciation, colloids, siderophores, exopolymeric substances, humic substances, nanoparticles, ligands

INTRODUCTION – IRON BIOGEOCHEMISTRY IN THE OCEAN AND THE IMPORTANCE OF IRON SPECIATION

Approximately 30% of surface waters in the open ocean are known as high nutrient low chlorophyll (HNLC) regions (Boyd et al., 2007). These areas are replete in the macronutrients nitrate and phosphate, but present lower phytoplankton biomass, in terms of chlorophyll concentrations, than expected from residual macronutrient concentrations (**Figure 1**). The restriction of phytoplankton growth in these regions is now acknowledged to be the result of iron (Fe) limitation (Martin and Fitzwater, 1988; Boyd et al., 2007). Fe is a micronutrient required for proteins involved in fundamental cellular processes, including both photosynthesis and respiration (Raven et al., 1999). Despite being the fourth most abundant element in the Earth's crust (Liu and Millero, 2002), dissolved Fe (dFe: <0.2 or 0.45 μm) concentrations in open ocean surface waters typically fall below 0.2 nM, (De Baar and De Jong, 2001; Boyd and Ellwood, 2010) and dFe generally exhibits a nutrient-type depth profile in the ocean, depicting removal in surface waters by biological uptake, and increased concentrations at depth from remineralization processes occurring through the water column (Boyd and Ellwood, 2010). Although low, dFe concentrations in the ocean can be much higher than might be predicted given that the solubility of ferric hydroxide in seawater at pH 8.1 and 25°C has been determined to be as low as 0.01 nM (Liu and Millero, 2002). The presence of dFe at concentrations beyond the inorganic solubility of Fe is thought to be facilitated by organic complexation of Fe with stabilizing ligands, which buffer dFe in seawater against hydrolysis and ensuing precipitation (Hunter and Boyd, 2007; Boyd and Ellwood, 2010). However, the overall physico-chemical speciation of dFe, which encompasses all of its possible physical and chemical forms in seawater, is more complex than implied by the consideration of organic complexation alone. The different physico-chemical fractions of dFe include Fe(II), colloidal, truly soluble, and inorganic iron in addition to organically complexed iron. These different fractions have different environmental and biological mobility (Kuma et al., 1996; Maldonado et al., 2005; Hunter and Boyd, 2007; Kitayama et al., 2009; Boyd and Ellwood, 2010; Hassler et al., 2011b). The motivation for understanding the

physico-chemical speciation of Fe, therefore, results from a desire to understand how these different fractions influence the overall biogeochemistry of Fe in the oceans.

It is important to note that dissolved iron (dFe) is operationally defined by filtration, with early studies employing 0.45 μm or, more recently, 0.2 μm membrane filters (De Baar and De Jong, 2001; Cutter et al., 2010). However, it has been shown that a significant proportion of dFe is colloidal ($Fe_{colloidal}$; Wu and Luther, 1994; Cullen et al., 2006; Bergquist et al., 2007; Kondo et al., 2008; Schlosser and Croot, 2008; Boye et al., 2010). Colloidal Fe is characterized as the difference between the Fe concentration determined in the <0.2 μm fraction (dFe) and the >1 kDa or >0.02 μm fraction, depending on whether cross flow filtration or membrane filtration techniques are used for the determination (Schlosser and Croot, 2008). The colloidal fraction is not measured directly, but inferred from the difference between dissolved (<0.2 μm) and soluble (<1 kDa or <0.02 μm) fractions.

The mass balances for Fe when considering its physical distribution can be described as

$$Fe_{total} = Fe_{particulate} + Fe_{colloidal} + Fe_{soluble}$$

while the mass balance from a chemical perspective might be described as

$$Fe_{total} = Fe' + FeL + Fe_{inert},$$

where Fe′ represents labile inorganic Fe complexes, FeL represents Fe organic ligand complexes exchangeable within a time scale of <1 day, and Fe_{inert} represents the Fe fraction bound up in matrices that are essentially non-labile. As our analytical methods for the determination of the physico-chemical speciation of Fe tend to focus on either the physical (e.g., Schlosser and Croot, 2008; Baalousha et al., 2011) or the chemical (e.g., Gledhill and van den Berg, 1994; Rue and Bruland, 1995; van den Berg, 1995; Wu and Luther, 1995; Laglera et al., 2007; Mawji et al., 2008a; Velasquez et al., 2011) perspective, reconciling these two approaches remains a major challenge to Fe biogeochemists.

In recent years there has been a concerted effort to understand more about both the physical partitioning of Fe in the marine environment, and the chemical nature of the Fe ligand pool. The application of filtration with trace metal clean 0.02 μm pore size membrane filtration, ultrafiltration (10 kDa cut offs), and flow field flow fractionation (FFFF) coupled to ultra-violet (UV) and inductively coupled plasma-mass spectrometry (ICP-MS) detection techniques have considerably improved our knowledge of the physical partitioning of Fe in marine waters (Schlosser and Croot, 2008; Baalousha et al., 2011). Characterization of the FeL pool has been tackled through the utilization of high performance liquid chromatography–electrospray ionization-mass spectrometry (HPLC–ESI-MS) and development of novel electroanalytical techniques (McCormack et al., 2003; Laglera et al., 2007; Velasquez et al., 2011). In parallel to these advances a concerted effort is being made to improve our understanding of the robustness of competitive ligand exchange–adsorptive cathodic stripping voltammetry (CLE–ACSV), the technique most commonly used to determine Fe complexation in seawater (Buck et al., under review;Laglera et al., 2011). These advances have indicated that although the absolute physical partitioning determined varies from study to study as a result of the different techniques and filter cut offs, the colloidal Fe pool makes up between 30 and 91% of the dFe pool (Wu and Luther, 1994; Nishioka et al., 2001; Cullen et al., 2006; Bergquist et al., 2007; Hurst and Bruland, 2008; Kondo et al., 2008; Schlosser and Croot, 2008; Boye et al., 2010). The presence of Fe-binding ligands has been inferred in colloidal and measured in soluble fractions (Wu et al., 2001; Boye et al., 2010; Thuroczy et al., 2010), but both FFFF and ultrafiltration studies indicate that not all of the colloidal Fe (organic or inorganic) is exchangeable or under saturated with respect to Fe (Wu et al., 2001; Boye et al., 2010; Stolpe and Hassellov, 2010; Stolpe et al., 2010; Thuroczy et al., 2010). The existence of an inert colloidal fraction has broad implications for our understanding of Fe biogeochemistry and its significance in the ocean has yet to be properly assessed. Thus, while $Fe_{soluble}$ might reasonably be expected to include Fe′, FeL, or Fe_{inert} are unlikely to be discreet to $Fe_{soluble}$, $Fe_{colloidal}$, or $Fe_{particulate}$.

Even though we have not fully characterized either colloidal or organic Fe associations, efforts to understand the overall effects of Fe speciation on Fe biogeochemistry have been made (Archer and Johnson, 2000; Moore et al., 2004; Parekh et al., 2005; Weber et al., 2005; Fan, 2008; Moore and Braucher, 2008; Tagliabue et al., 2009; Fan and Dunne, 2011; Tagliabue and Voelker, 2011). Modelers have made considerable progress toward capturing the complexity of iron speciation, incorporating inorganic iron scavenging and up to two ligand classes, in order to investigate the large scale implications of iron speciation on ocean productivity and the potential effects of a changing climate (Tagliabue et al., 2009; Ye et al., 2009; Tagliabue and Voelker, 2011). Fe biogeochemical models incorporating Fe speciation tend to highlight the importance of photoreduction processes in determining the dissolved concentrations of Fe in surface waters, while indicating that organic ligands are likely to strongly influence the thermodynamic solubility of Fe (Weber et al., 2005; Fan, 2008; Tagliabue et al., 2009; Tagliabue and Voelker, 2011). Furthermore, variations in organic ligand concentration and conditional stability constants have also been shown to influence the residence time and potential bioavailability of Fe in models (Tagliabue et al., 2009). Other studies have shown that different organic ligands have different chemical labilities and different susceptibilities to photoreduction (Hutchins et al., 1999; Barbeau et al., 2001, 2003; Maldonado et al., 2005; Hassler et al., 2011b). Overall, such studies highlight the need to characterize more fully the physico-chemical speciation of dFe.

In this paper, we will review current knowledge of the organic complexation of Fe, the characterization and distributions of specific FeL complexes, and the characterization of colloidal Fe fractions as a first attempt at reconciling the different approaches to understanding the physico-chemical speciation of dFe in seawater. We will not consider the reduced Fe pool, Fe(II), in this review as our understanding of the interactions between Fe(II), Fe(III), and organic matter (e.g., Toner et al., 2009; Bligh and Waite, 2010) require further investigation. However, it should be born in mind that Fe(II) is likely important to Fe biogeochemistry as it is thought to be highly biologically available and can make up 50–60% of the dFe pool in illuminated surface waters or near sediments, hydrothermal vent systems, or oxygen minimum zones

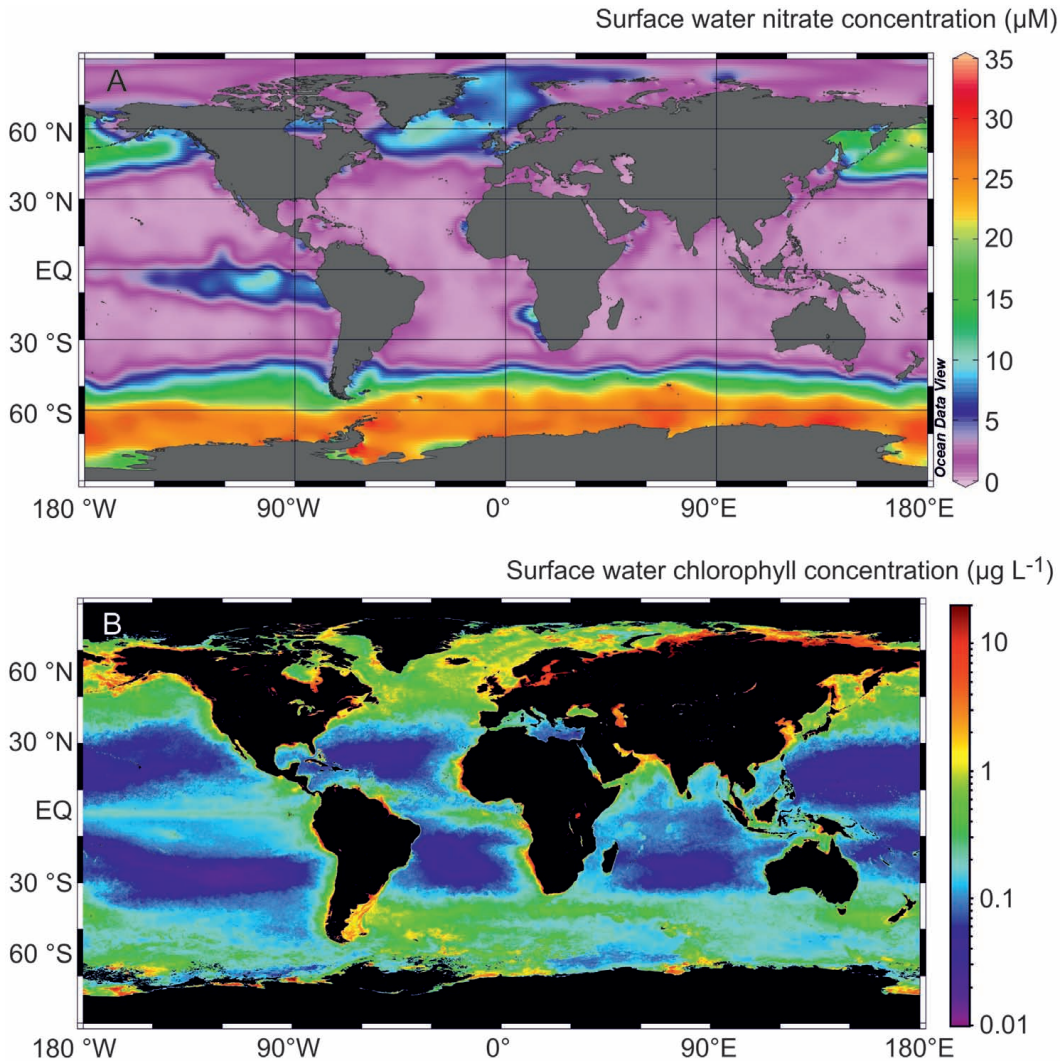

FIGURE 1 | (A) Annualized average nitrate (μM) and **(B)** composite chlorophyll *a* (mg L^{-1}) distributions observed in surface waters in the global ocean. The nitrate distribution was obtained using data from the World Ocean Atlas 2009 (http://www.nodc.noaa.gov/OC5/WOA09/pr_woa09.html), while the chlorophyll *a* distribution represents the 2009 Aqua MODIS chlorophyll composite (http://oceancolor.gsfc.nasa.gov/cgi/l3).

(Hong and Kester, 1986; Kuma et al., 1992; Johnson et al., 1994; Gledhill and van den Berg, 1995; Croot et al., 2005; Ussher et al., 2007; Hansard et al., 2009; Sarthou et al., 2011).

IRON COMPLEXATION AS DETERMINED BY COMPETITIVE EQUILIBRIUM EXPERIMENTS

The organic complexation of dFe, including organic Fe-binding ligand concentrations ($[L_i]$) and their associated conditional stability constants ($K^{cond}_{FeL_i,Fe'}$ or $K^{cond}_{FeL_i,Fe^{3+}}$), is primarily measured in seawater using the electrochemical technique CLE–ACSV. The ambient Fe-binding ligands determined by this technique are typically described as ligand "classes," which are operationally defined by the associated conditional stability constant measured. Ligand classes are denoted as L_i, where $i = 1$ for stronger ligand classes and $i = 2$, 3, etc., for progressively weaker ligand classes. Conditional stability constants for these ligand classes are expressed as either $K^{cond}_{FeL_i,Fe'}$ or $K^{cond}_{FeL_i,Fe^{3+}}$, where $K^{cond}_{FeL_i,Fe^{3+}} = K^{cond}_{FeL_i,Fe'} \bullet \alpha_{Fe'}$ and $\alpha_{Fe'}$ is the inorganic side reaction coefficient for Fe, with $\alpha_{Fe'} = [Fe']/[Fe^{3+}]$. $\alpha_{Fe'}$ varies with pH (Byrne et al., 1988), but a value of 10^{10} is commonly used for $\alpha_{Fe'}$ in pH 8 seawater (Hudson et al., 1992; Sunda and Huntsman, 2003), although other values have been used (Gledhill and van den Berg, 1994; Rue and Bruland, 1997; Gledhill et al., 1998; Nolting et al., 1998). In CLE–ACSV, samples are buffered prior to analyses, typically to pH 8, and mostly equilibrated and measured at room temperature, so the use of an $\alpha_{Fe'} = 10^{10}$ is reasonable for these cases, regardless of original sample pH or temperature. To better facilitate comparisons across studies, we encourage analysts to consider adjusting their $K^{cond}_{FeL_i,Fe^{3+}}$ to $K^{cond}_{FeL_i,Fe'}$ using the appropriate $\alpha_{Fe'}$ for the analytical pH employed. Similarly, those who report $K^{cond}_{FeL_i,Fe'}$ are encouraged to specify the $\alpha_{Fe'}$ used.

COMPETITIVE LIGAND EXCHANGE–ADSORPTIVE CATHODIC STRIPPING VOLTAMMETRY

Aliquots of a filtered, but otherwise unaltered, seawater sample are first buffered to maintain pH near 8, and then titrated with increasing additions of dissolved Fe (dFe) from +0 to typically 10×–20× the ambient dFe concentration. It is recommended to have two +0 Fe additions in the titration, with at least eight Fe amendments, for a total of 10 or more titration points to provide the best data structure for interpretation (Garnier et al., 2004; Sander et al., 2011). DFe additions are left to equilibrate with ambient Fe-binding ligands, often for several hours, before each aliquot is amended with a given concentration of a well-characterized added ligand (AL) and allowed an additional equilibration time of minutes to hours. Once equilibrated with both added dFe and AL, each sample aliquot of the titration is analyzed sequentially by ACSV on a hanging mercury drop electrode (HMDE).

Over a deposition time predetermined to allow sufficient preconcentration of $Fe(AL)_x$ in the sample, the $Fe(AL)_x$ complex formed in the titrations is adsorbed at a set initial potential to the surface of the HMDE while stirring the solution. As the deposition time employed is applied to all aliquots in a given titration, it is essential that the length of time chosen is long enough to distinguish the small increases in the added dFe between vials early in the titration, but not so long that the larger amendments of dFe at the end of the titration saturates the HMDE surface. After the deposition time concludes, there is often a few seconds of "quiet time," when stirring is stopped, before the voltage applied to the HMDE is ramped in the negative direction (cathodic stripping) following the optimal excitation signal wave form (differential pulse, linear sweep, Osteryoung square wave) for the $Fe(AL)_x$ chosen.

At the reduction potential of Fe, roughly −0.5 V (depending on AL chosen), Fe is reduced from the $Fe(AL)_x$ complex, or, in some cases, the $Fe(AL)_x$ itself may reduce, generating a peak in current measured at the HMDE. The height of this peak in current, typically expressed in absolute nA units, is recorded for each aliquot as a titration point and plotted against the added dFe to generate a titration curve. This raw titration data is then interpreted using either linear (Scatchard, 1949; Ružic, 1982; Van Den Berg, 1982) or non-linear (Gerringa et al., 1995) transformations to determine ambient Fe-binding ligand concentrations and their thermodynamic conditional stability constants.

The concentration and choice of AL employed, along with the thermodynamic characteristics of the $Fe(AL)_x$ complex formed, defines the analytical window of the analyses. This analytical window is described as $\alpha_{Fe(AL)_x}$, where $\alpha_{Fe(AL)_x} = \beta^{cond}_{Fe(AL)_x,Fe'} \bullet [AL]^x$. The analytical window applied constrains the measured ligand concentrations and conditional stability constants such that the end result is best described as averages of the different ligand classes identified within an analytical window. These parameters produce an α_{FeL_i}, where $\alpha_{FeL_i} = K^{cond}_{FeL_i,Fe'} \bullet [L_i]$. In most cases, only one ligand class is identified in Fe speciation titrations, but in the case of more than one ligand class, $\alpha_{FeL_i} = K^{cond}_{FeL_1,Fe'} \bullet [L_1] + K^{cond}_{FeL_2,Fe'} \bullet [L_2] + \ldots + K^{cond}_{FeL_i,Fe'} \bullet [L_i]$.

While the use of multiple analytical windows has not yet been addressed for Fe speciation, there is some indication from recent GEOTRACES inter calibration efforts that the analytical window applied to Fe speciation may impact calculated results for $[L_i]$ and $K^{cond}_{FeL_i,Fe'}$ (Buck et al., under review). This effect is much less pronounced, however, than has been established previously for dissolved copper (Cu) speciation (Bruland et al., 2000), likely reflecting the very different inorganic side reactions of Cu and Fe, as well as the relative breadth of the ligand pools for these elements.

With respect to ligand classes, it should be noted that analysts commonly apply the notation of "L_1" to the strongest (or only) ligand class detected in their sample, regardless of the associated $K^{cond}_{FeL_i,Fe'}$. Thus, ligand class definitions may vary widely between analysts and sample data sets, complicating comparisons across studies. For example, the range of $\log K'^{cond}_{FeL_1,Fe}$ reported in the literature, for either the single ligand class identified or the designated L_1 in two ligand systems, covers more than four orders of magnitude (from ∼9 to ∼13.5; **Table 1**). Even in field studies distinguishing two ligand classes, the $\log K'^{cond}_{FeL_1,Fe}$ reported for the stronger ligand class range between 11.1 and 13.9, overlapping with the weaker ligand class $\log K'^{cond}_{FeL_2,Fe}$ values of 9.7–11.95 reported (**Table 1**; Rue and Bruland, 1995, 1997; Cullen et al., 2006; Buck and Bruland, 2007; Buck et al., 2007; Ibisanmi et al., 2011). Correspondingly, it would be useful to agree on definitions for ligand classes based on the range of $K'^{cond'}_{FeL_i,Fe}$s reported in natural systems. Along these lines, we would propose using "L_1" for $\log K^{cond}_{FeL_i,Fe'} > 12$, "$L_2$" for $\log \log K^{cond}_{FeL_i,Fe'} = 11$–$12$, and "$L_3$" for $\log K^{cond}_{FeL_i,Fe'} < 11$. Regardless of whether such new definitions are employed, when comparing results between studies we implore analysts to consider making comparisons between $\log K^{cond}_{FeL_i,Fe'}$ instead of designated ligand classes.

LIMITATIONS OF INTERPRETATION

Competitive ligand exchange–ACSV is an indirect approach to determining the organic complexation of dFe. As such, there are some fundamental assumptions and limitations inherent to CLE–ACSV data interpretation, which are worth reviewing in brief before attempting to contextualize published field data. First, raw titration is interpreted assuming that ambient ligands are coordinated with dFe in a 1:1 ratio. In reality, the wide range of dissolved organic matter present in seawater likely includes ligands that may bind dFe in ratios greater than or less than 1:1. Thus, the reported ligand concentrations measured from CLE–ACSV represent the binding capacity for organic ligand classes present in the sample, not necessarily an absolute concentration of ligand molecules. As a consequence, some analysts report their measured ligand concentrations in terms of nanoequivalents (nEq; e.g., Nolting et al., 1998; Gerringa et al., 2008) or nanomolar Fe equivalents (e.g., Croot et al., 2004) instead of simply nanomolar concentrations to highlight this distinction.

A second, and more problematic, assumption in the interpretation of CLE–ACSV data is that all of the dFe in a given sample is in an exchangeable form with respect to the added competitive ligand (AL). Arising from this assumption, any dFe that does not bind to the AL to form $Fe(AL)_x$ is then assumed in the data interpretation to be complexed by an organic ligand class with a larger α_{FeL_i} than the $\alpha_{Fe(AL)_x}$ applied. This is clearly problematic in natural samples, where much of the dFe, especially in high dFe environments, may exist as stable inorganic or organically associated colloids, or as other phases of dFe not exchangeable with AL (e.g., Fe_{inert}). It has

Table 1 | Compilation of published field data on the organic complexation of dFe in marine environments, as measured by CLE–ACSV techniques.

Region	Depth, m	Filter	[Fe], nM	$[L_1]$, nM $[L_2]$, nM	$Log K^{cond}_{FeL_1,Fe'}$ $Log K^{cond}_{FeL_2,Fe'}$	eL_1, nM eL_T, nM	Reference
NE Atlantic	2–1002	<0.45 μm	0.8–8.5	3–10.1	10.4–13.1[1]	1.6–4.1	Gledhill and van den Berg (1994)
Central N Pacific	20–2000	<0.4 μm	0.09–0.77	0.37–1 1.3–2.8	12.7–13.2 11.3–11.8	0.13–2.13 1.63–4.93	Rue and Bruland (1995)
Mediterranean	20–2586	<0.4 μm	∼2.5–6*	4.21–12.65	12.0–13.6	∼1.2–9.1*	van den Berg (1995)
NW Atlantic	5–15	<0.4 μm	0.6–3.7	0.45–6.4	> 15[1]	n.d.	Wu and Luther (1995)
Equatorial Pacific	15	<0.4 μm	0.009–2.8	0.31–1.75 0.19–2	11.2–13 10.6–11.91	−1.4 to 1.73 −0.63 to 2.98	Rue and Bruland (1997)
N Atlantic	0–70	Unfiltered	1.3–35.9	1.3–39.2	10.3–12.1[1]	−0.4 to 4.1	Gledhill et al. (1998)
Southern Ocean, Pacific Sector	25–800	Unfiltered	0.14–0.72	1.08–13.27	10.93–11.93	0.87–13	Nolting et al. (1998)
NW Atlantic	11–2874	<0.2 μm	0.36–1.9	1.67–4.62	12.2–12.9	0.71–2.72	Witter and Luther (1998)
Southern Ocean, Atlantic Sector	5–110	<0.4 μm	7–14.3	2.4–17.6	10.7–11.1	−4.6 to 5.6	Croot and Johansson (2000)
Arabian Sea	25–600	<0.4 μm	1.25–2.63	1.47–6.33	11.6–12.5	0.19–4.62	Witter et al. (2000)
Southern Ocean, Atlantic Sector	20–4500	<0.2 μm	0.05–0.65	0.37–1.39	10.92–13	0.01–1.01	Boye et al. (2001)
Peconic Estuary, NW Atlantic	5	<0.2 μm	28.6–237	17–209	12.9–13.5	−39 to −3.4	Gobler et al. (2002)
NE Atlantic	2	<0.2 μm	0.56–2.46	1.68–3.87	10.5–11.4	0.84–2.1	Boye et al. (2003)
Mississippi River	2	<0.2 μm	1.4–29.9	4.3–64.1	10.4–12.3	−0.2 to 60.3	Powell and Wilson-Finelli (2003a)
Southern Ocean, Atlantic Sector	10–1500	<0.4 μm	0.04–0.6	0.9–3	11.4–13.4	0.64–2.58	Croot et al. (2004)
Southern Ocean, Atlantic Sector	20–100	<0.2 μm	0.06–5.5	0.6–3.52	11.05–13	−2.05 to 1.15	Boye et al. (2005)
		<200 kDa	0.03–1.62	0.5–1.58	11.15–12.76	−0.04 to 0.66	
NE Atlantic	10–2000	<0.2 μm	0.48–1.57	1.17–3.52	10.36–12.25	0.1–2.73	Boye et al. (2006)
NW Atlantic	5–5256	<0.4 μm	0.23–0.66	0.81–1.14 1.11–2.11	12.69–13.14 11.50–11.93	−0.43 to 0.58 0.69–2.50	Cullen et al. (2006)
		<0.02 μm	0.04–0.28	0.56–0.63 0.83–2.08	12.38–13 11.38–11.94	−0.28 to 0.59 0.57–2.67	
NE Atlantic	9.8–152.2	<0.2 μm	0.06–0.67	0.83–4.78	9.68–12.67	0.4–4.65	Gerringa et al. (2006)
SW Pacific	2	<0.2 μm	0.07–0.84	0.66–1.72	12.23–13.05	0.39–1.56	Tian et al. (2006)
Central N Pacific	3–1000	<0.1 μm	0.08–1.6	0.86–2.45	11.42–12.3	0.11–1.48	van den Berg (2006)
NE Pacific, Columbia River	2–31	<0.4 μm	0.6–22.4	1–55.8 nd-9	11.8–13.9 10.7–11.8	−0.4 to 39 0–39	Buck et al. (2007)
NW Pacific	10–3941	<0.22 μm	0.25–1.83	0.43–1.46	12.2–13.8	−0.64 to 0.48	Kondo et al. (2007)
Scheldt Estuary, NE Atlantic	2	<0.2 μm <1 kDa	12–536	40–526	9.6	0–27	Gerringa et al. (2007)
Bering Sea	2–57	<0.4 μm	0.01–13	0.43–18 1.2–15	11.1–12 9.7–10.8	−0.4 to 5.4 1.61–19	Buck and Bruland (2007)
Eastern Tropical N Pacific	10–190	<0.4 μm	0.06–1.12	0.44–1.63	11.11–12.77	0–1.17	Hopkinson and Barbeau (2007)
Southern Ocean, Indian Sector	20–620	<0.2 μm	0.046–0.385	0.082–1.61	11.01–12.79	0–1.48	Gerringa et al. (2008)
NW Pacific	2	<0.22 μm <200 kDa	0.3–1.4 0.1–0.39	0.29–2.02 0.31–1.78	11.9–12.5 10.9–12.3	0.12–0.94 0.21–1.63	Kondo et al. (2008)
NE Atlantic	3	<0.2 μm	0.088–0.332	0.822–1.463	11.94–13.41	0.67–1.34	Rijkenberg et al. (2008b)
Humic-rich coastal water, NE Atlantic	1	<0.4 μm	23.1–573.2	46.5–604.4	10.23–11.97	−52.1 to 49.3	Batchelli et al. (2010)

(Continued)

Table 1 | Continued

Region	Depth, m	Filter	[Fe], nM	[L_1], nM [L_2], nM	Log$K^{cond}_{FeL_1,Fe'}$ Log$K^{cond}_{FeL_2,Fe'}$	eL_1, nM eL_T, nM	Reference
Southern Ocean, Atlantic Sector	20–1000	<0.2 μm	0.04–0.41	0.58–0.86	11–12.86	0.31–0.75	Boye et al. (2010)
		<200 kDa	0.03–0.21	0.42–0.76	11.25–12.9	0.27–0.69	
NE Atlantic	26–3998	<0.2 μm	0.13–0.7	0.65–1.76	11.68–13	0.23–1.09	Thuroczy et al. (2010)
		<1000 kDa	0.019–0.22	0.42–1.35	11.98–12.47	0.4–1.32	
		Unfiltered	0.91–4.1	1.74–4.56	12.23–13.4	0.46–1.18	
Southern Ocean, Indian and Pacific Sector	15–1000	<0.2 μm	0.2–0.39	0.26–0.61	12.28–13.72	−0.37 to 0.25	Ibisanmi et al. (2011)
				0.2–1.51	11–11.95	−0.11 to 1.28	
High latitude N Atlantic	5–2237	<0.2 μm	0.04–0.34	0.2–3.2	11.5–13.9	0.1–1.8	Mohamed et al. (2011)

**Estimated concentrations from figures, as data were not available from publications in table format. Values originally reported as log$K^{cond}_{FeL_i,Fe^{3+}}$ were converted to log log$K^{cond}_{FeL_i,Fe'}$ using an $\alpha_{Fe'}$ of 10^{10}. [1] $K^{cond}_{FeL_i,Fe'}$ calculated using $\alpha_{Fe'} = 8.4$.*

been noted previously that inclusion of Fe_{inert} in calculations of ligand concentrations results in an overestimation of $[L_i]$ and a shift in the log$K^{cond}_{FeL_i,Fe'}$ toward higher stabilities (Bruland and Rue, 2001). This becomes particularly critical if ligand titrations are carried out in unfiltered samples (Gledhill et al., 1998; Thuroczy et al., 2010), but given the evidence for an inert colloidal fraction (see below), is also likely to affect determination of ligands in dissolved samples. Determinations of $[L_i]$ and log$K^{cond}_{FeL_i,Fe'}$ in the ocean are, thus, potentially subject to systematic errors when using the total dFe concentration in the interpretation of CLE–ACSV titration data.

To further explore the implications of overestimating exchangeable Fe, we consider the data in Thuroczy et al. (2010) and data on titrations in unfiltered samples from Gledhill et al. (1998), recalculated using the reactive Fe concentration (Fe_R) determined in the unfiltered samples (Gledhill et al., 1998). Although the datasets used were both obtained for unfiltered samples, the same systematic errors with respect to Fe_{inert} and exchangeable Fe will occur within the dFe pool, albeit to a lesser degree.

Plots of $[L_i]$ and log$K^{cond}_{FeL_i,Fe'}$, determined using Fe_T (unfiltered), against $[L_i]$ and log$K^{cond}_{FeL_i,Fe'}$ determined using either dissolved or reactive Fe concentration (dFe or Fe_R), are presented in **Figures 2A,B**. In these studies, Fe_T was determined in unfiltered samples either by flow injection analysis (FIA) after acidification (pH 1.8, samples analyzed after 1 year; Thuroczy et al., 2010) or by ACSV after acidification (pH 2) and UV irradiation (Gledhill et al., 1998). Dissolved Fe was determined by FIA after filtration (<0.2 μm) and acidification (pH 1.8, samples analyzed after 12 h, Thuroczy et al., 2010) and Fe_R was determined in unfiltered samples by ACSV and defined as the amount of Fe freely complexed by 20 μM 1-nitroso-2-napthol at pH 6.9 (Gledhill et al., 1998).

From these plots, it is clear that both $[L_i]$ and log log$K^{cond}_{FeL_i,Fe'}$ are overestimated if the Fe concentration used in data transformation includes Fe_{inert} (**Figures 2A,B**). An overestimation of $[L_i]$ and log$K^{cond}_{FeL_i,Fe'}$ is not desirable as this will result in an overestimation of the degree to which L can stabilize Fe in solution, and can thus underestimate the potential for competing biogeochemical processes such as colloidal aggregation, scavenging, and uptake. Calculation of the excess ligand (eL_i) for each case confirms results shown previously (Thuroczy et al., 2010), that this parameter is more or less independent of the Fe concentration used in the transformation, at least at low excess ligand concentrations (**Figure 2C**).

Figure 2D shows that overestimation of log $K^{cond}_{FeL_i,Fe'}$ is likely to be important only in areas where the Fe_{inert} concentration is high. Such areas will include coastal regions as observed in Gledhill et al. (1998), hydrothermal vents, and the edge of the ice shelf (Bennett et al., 2008; van der Merwe et al., 2009; Batchelli et al., 2010; Stolpe and Hassellov, 2010; Stolpe et al., 2010). In these regions a good distinction between the dissolved Fe_{inert} and exchangeable Fe could be very informative, and may strongly influence our interpretation of the role of ligands in stabilizing Fe in solution (e.g., Sander and Koschinsky, 2011). Further work is therefore required in order to identify a practical method which can distinguish between Fe_{inert} and dFe. One approach may simply be the standard addition of dFe with over-competition with a higher concentration of AL, although this may be complicated by limits in the concentration of AL that may be used before saturation of the HMDE becomes problematic.

Clearly, the fractionation of Fe, particularly within the dissolved phase, between Fe_{inert} and exchangeable Fe deserves further attention. In the meantime, analysts may qualify ligand concentrations by reporting excess L ($[eL] = [L] - [dFe]$) as a proxy for ligand under saturation (Wu and Luther, 1995; Witter and Luther, 1998; Witter et al., 2000; Boye et al., 2001; Tian et al., 2006; Rijkenberg et al., 2008b; Thuroczy et al., 2010; Ibisanmi et al., 2011).

DISTRIBUTIONS OF Fe-BINDING LIGANDS IN THE MARINE ENVIRONMENT

The organic complexation of Fe, with typically >99.9% of dFe complexed by ligands in the marine environment, is a nearly ubiquitous feature of dFe speciation in seawater. While these Fe-binding ligands are present seemingly everywhere, from surface to deep waters of the coastal and open ocean, there are some distinguishable trends in their distributions and thermodynamic characteristics. Previous reviews have highlighted the predominant feature of higher ligand concentrations in surface waters of depth profiles, often with stronger stability constants, compared

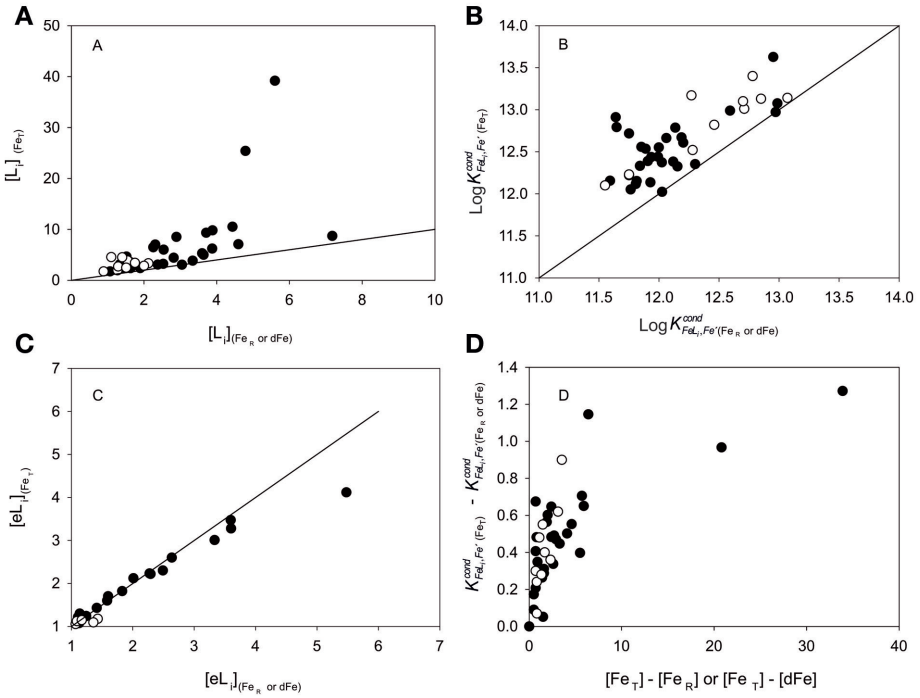

FIGURE 2 | Comparison of data obtained for (A) the ligand concentration [L_i], (B) conditional stability constant log$K^{cond}_{FeL_i,Fe'}$, and (C) excess ligand concentration [eL_i] determined using either total Fe concentrations or the lower dissolved or reactive Fe concentrations. Closed symbols represent data from Gledhill et al. (1998), where Fe_R was used in the comparison, and open symbols represent data from Thuroczy et al. (2010), where dFe was used in the comparison. **(D)** Plot of the dependence of the change in log$K^{cond}_{FeL_i,Fe'}$ on the difference between Fe_T and the lower Fe concentration. Solid lines represent a 1:1 relationship.

to deep waters (Bruland and Rue, 2001; Hunter and Boyd, 2007). Here we review trends of organic complexation of Fe in terms of excess ligand concentrations ($[eL_i] = [L_i] - [dFe]$), since total ligand concentrations ($[L_i]$) determined by CLE–ACSV will include stable inorganic colloidal Fe or other Fe_{inert} components (see above).

In most waters, Fe-binding ligand concentrations exceed dFe (**Table 1**). Excess ligand concentrations are commonly highest and most variable in the upper water column (Rue and Bruland, 1995; van den Berg, 1995, 2006; Witter and Luther, 1998; Boye et al., 2001, 2006, 2010; Croot et al., 2004; Gerringa et al., 2006; Hopkinson and Barbeau, 2007; Kondo et al., 2007; Rijkenberg et al., 2008b; Thuroczy et al., 2010; Ibisanmi et al., 2011; Mohamed et al., 2011), and relatively static at depth within individual profiles (Rue and Bruland, 1995; van den Berg, 1995; Nolting et al., 1998; Boye et al., 2001, 2006, 2010; Ibisanmi et al., 2011). The highest excess ligand concentrations are often associated with the fluorescence or chlorophyll biomass maxima (Rue and Bruland, 1995; van den Berg, 1995, 2006; Boye et al., 2001, 2006; Croot et al., 2004; Gerringa et al., 2006, 2008; Tian et al., 2006; Buck and Bruland, 2007; Wagener et al., 2008; Ibisanmi et al., 2011). The uptake of dFe associated with fluorescence or biomass maxima results in elevated and variable excess ligand concentrations at low dFe (e.g., Buck and Bruland, 2007).

An atmospheric source has been hypothesized for surface waters of the NE Atlantic with low chlorophyll (Gerringa et al., 2006), though a reduction in excess ligand after dust deposition was observed by Rijkenberg et al. (2008b). Excess ligands in low chlorophyll surface waters may alternatively be the remnants of a previous bloom, as excess ligands have been shown in incubation experiments to increase in proportion to chlorophyll consumption by grazers (Sato et al., 2007). In some cases, a minimum in excess ligands within the upper water column is attributed to photochemical ligand destruction at the surface (Boye et al., 2001; Croot et al., 2004), although the photochemical lability of ambient Fe-binding ligands has also been shown to be rather unpredictable (Powell and Wilson-Finelli, 2003b; Rijkenberg et al., 2006b).

Anomalously high excess ligand concentrations have been reported in shelf and bottom boundary layers (Croot and Johansson, 2000; Gobler et al., 2002; Boye et al., 2003; Buck et al., 2007; Kondo et al., 2007; Gerringa et al., 2008; Batchelli et al., 2010), as well as in river plumes (Powell and Wilson-Finelli, 2003a; Buck et al., 2007; Kondo et al., 2007). The excess Fe-binding ligands measured in these coastal waters may be humic substances (HS), which have been suggested to be an important component of the ligand pool for dFe in margin environments (Laglera et al., 2007; Laglera and van den Berg, 2009). Regardless of chemical nature, river plumes and sediment resuspension on shelves appears to be a source of both dFe and Fe-binding ligands to the marine water column (Croot and Johansson, 2000; Powell and Wilson-Finelli, 2003a; Buck

et al., 2007; Gerringa et al., 2008; Batchelli et al., 2010). As with dFe, total dissolved ligand concentrations also typically decrease from shore to sea (Boye et al., 2003; Buck and Bruland, 2007).

When two ligand classes are detected, a particularly strong ligand class (log $K^{cond}_{FeL_1,Fe'} > 12$) is reported primarily in the upper water column, and the weaker ligand class (log $K^{cond}_{FeL_2,Fe'} = 11$–12) exists throughout the water column (Rue and Bruland, 1995, 1997; Cullen et al., 2006; Ibisanmi et al., 2011). When only one ligand class is measured, no trend in log$K^{cond}_{FeL_i,Fe'}$ values (∼11–12) is reported with depth in profiles, with similar log log $K^{cond}_{FeL_i,Fe'}$ values through the entire water column (van den Berg, 1995, 2006; Witter and Luther, 1998; Boye et al., 2001, 2006, 2010; Croot et al., 2004; Gerringa et al., 2006, 2008; Thuroczy et al., 2010). Log $K^{cond}_{FeL_i,Fe'}$ values reported for coastal and open ocean samples are within the same range (∼9–14; **Table 1**), as are values from river plumes (10.4–13.9; Powell and Wilson-Finelli, 2003b; Buck et al., 2007; **Table 1**). Transects conducted between the shore and sea found no significant trends in log $K^{cond}_{FeL_i,Fe'}$ values with distance from shore (Boye et al., 2003; Buck and Bruland, 2007; Hopkinson and Barbeau, 2007).

Recent size fractionation studies of the dissolved ligand pool have shown that the excess ligand is observed predominantly in the soluble size fraction throughout the water column (Cullen et al., 2006; Boye et al., 2010; Thuroczy et al., 2010), but particularly in upper waters (Cullen et al., 2006; Kondo et al., 2008; Boye et al., 2010; Thuroczy et al., 2010). Colloidal ligands, on the other hand, approach Fe saturation (Gobler et al., 2002; Boye et al., 2005, 2010; Cullen et al., 2006; Gerringa et al., 2007; Kondo et al., 2008; Batchelli et al., 2010; Thuroczy et al., 2010), with the colloidal fraction of Fe, and presumably L, increasing with depth (Thuroczy et al., 2010).

The conditional stability constants of Fe-binding ligands in the soluble (<1–1000 kDa) size fraction are largely within 1 SD of the values reported in the total dissolved (<0.2–0.4 μm) size fraction (Boye et al., 2005, 2010; Cullen et al., 2006; Gerringa et al., 2007; Kondo et al., 2008; Thuroczy et al., 2010; **Table 1**). When two ligand classes were detected within the soluble and dissolved size fractions (Cullen et al., 2006), most of the ligands of both classes were present in the soluble (<0.02 μm) fraction, and excess ligand concentrations of both L_1 and L_2 were higher in the soluble fraction. The conditional stability constants of these ligand classes were similar in both size fractions (Cullen et al., 2006; **Table 1**). In mesoscale Fe fertilization experiments, Fe additions were observed primarily in the colloidal fraction (Boye et al., 2005; Kondo et al., 2008), and both Fe and ligand concentrations increased in response to Fe-enrichment (Rue and Bruland, 1997; Boye et al., 2005; Kondo et al., 2008). Excess ligand concentrations in these experiments, however, typically decreased as Fe additions saturated ligands, and some of the increase in $[L_i]$ may reflect an artifact in interpretation. At the conclusion of the SEEDS II experiment in the NW Pacific, excess ligand concentrations increased, predominantly in the soluble fraction, as the stimulated bloom declined (Kondo et al., 2008). Shipboard microzooplankton grazing experiments conducted during the SEEDS II experiment demonstrated an increase in ligand concentrations proportional to the chlorophyll consumed by added grazers (Sato et al., 2007).

In environments high in Fe, dFe concentrations may meet or exceed measured ligand concentrations. Examples of this, where $[dFe] > [L_T]$, have been reported in hydrothermal vent plumes (Bennett et al., 2008), artificial Fe-enrichment experiments (Rue and Bruland, 1997; Boye et al., 2005; Kondo et al., 2008), and Fe-rich coastal shelf environments (Croot and Johansson, 2000; Gobler et al., 2002; Powell and Wilson-Finelli, 2003a; Buck and Bruland, 2007; Buck et al., 2007; Kondo et al., 2007; Batchelli et al., 2010). In the Eastern Tropical North Pacific suboxic zone, dFe concentrations also approach dissolved ligand concentrations, resulting in diminished excess ligand concentrations compared to surrounding oxygenated waters (Hopkinson and Barbeau, 2007). The conditional stability constant of the ligand measured in the suboxic zone was also slightly stronger than the ligands measured in the oxic waters above (Hopkinson and Barbeau, 2007). In the suboxic zone of the Arabian sea, on the other hand, excess ligand concentrations were much greater than in the oxic waters, with a similar or slightly lower conditional stability constant of these suboxic zone ligands (Witter et al., 2000).

LINKS BETWEEN BIOLOGICAL ACTIVITY AND LIGAND CONCENTRATIONS

Previous reviews have emphasized the important interplay between biological activity and Fe-binding ligand cycling (Bruland and Rue, 2001; Hirose, 2006, 2007; Hunter and Boyd, 2007; Boyd and Ellwood, 2010). There are multiple lines of evidence in support of a biological source of Fe-binding ligands in the marine environment. As mentioned above, field studies have commonly found highest excess ligand concentrations within and around the biomass maximum in the water column (Rue and Bruland, 1995; van den Berg, 1995, 2006; Boye et al., 2001, 2006; Croot et al., 2004; Gerringa et al., 2006, 2008; Tian et al., 2006; Buck and Bruland, 2007; Wagener et al., 2008; Ibisanmi et al., 2011; Mohamed et al., 2011). Excess ligand concentrations have been observed to show an annual cycle (Wagener et al., 2008), with increases in excess ligand concentrations observed during the most productive periods. Surface transects also show elevated excess ligand concentrations with high productivity in Fe-depleted waters (Boye et al., 2003; Gerringa et al., 2006; Tian et al., 2006; Buck and Bruland, 2007). The particularly strong Fe-binding ligand class, detected only in the upper water column (Rue and Bruland, 1995, 1997; Cullen et al., 2006; Ibisanmi et al., 2011), presents the same class of log K values (log $K > 12$) as siderophore-type ligands measured by CLE–ACSV (Rue and Bruland, 1995; Witter et al., 2000; Buck et al., 2010; Poorvin et al., 2011).

Recent incubations of natural surface seawater have shown active production of Fe-binding ligands concomitant with diatom growth under Fe-limiting conditions (Buck et al., 2010; King et al., 2012). In these incubations, ligand production was only observed in the unamended bottles, Fe-amended bottles presented much higher growth but no ligand production, suggesting that the Fe-limitation status of the diatoms in the unamended bottles was related to the ligand production observed (Buck et al., 2010; King et al., 2012). In the field, Gerringa et al. (2006) found that 63% of the variability in ligand concentrations in profiles from the Canary

Basin was explained by changes in phytoplankton biomass and silicic acid concentrations, indicating a correlation between diatom growth and Fe-binding ligand concentrations. Recent incubation studies have furthermore shown an increase in Fe bioavailability due to redox speciation changes specifically in diatom cultures (Rijkenberg et al., 2008a). In combination, these studies suggest a connection between Fe-stressed diatom communities and Fe-binding ligand concentrations that deserves further attention.

The passive production of Fe-binding ligands from grazing and bacterial remineralization of organic matter is another important biological source of ligands. HS, degradation products of terrestrial and marine organic matter, may be a substantial component of the Fe-binding ligand pool in some coastal and deep ocean waters (Laglera and van den Berg, 2009). A recent study of coastal estuarine waters found that Fe was strongly ($\log K^{\mathrm{cond}}_{\mathrm{FeL}_i,\mathrm{Fe}'} = 11$–$12$) but reversibly complexed with HS, predominantly in the colloidal fraction (Batchelli et al., 2010).

Increased excess ligand concentrations, largely in the soluble size fraction, were reported during the bloom decline of the SEEDS II experiment (Kondo et al., 2008). Shipboard grazer experiments, also conducted during SEEDS II, showed that dFe and ligand concentrations increased as chlorophyll biomass was consumed (Sato et al., 2007). The highest increases in ligand concentrations, normalized to biomass consumption, were measured in the copepod grazing experiments (Sato et al., 2007). The ligands produced in these grazer experiments were similar to the L_1 type ligands ($\log K^{\mathrm{cond}}_{\mathrm{FeL}_i,\mathrm{Fe}'} > 12$), and were found to be more bioavailable to diatom species than to picoplankton in the incubations (Sato et al., 2007).

The ability of ligands to solubilize natural Fe sources may also be linked to biological productivity. An annual cycle in the dissolution of Fe from Saharan dust has been observed in water sampled at different times of the year from the Mediterranean (Wagener et al., 2008), with dust derived Fe being less soluble in water sampled during the winter period (Dec–Feb). This was linked to a change in excess ligand concentration, and a potential change in ligand characteristics (although stability constants were not reported in the study), as Fe dissolution could not be determined in the winter, despite the presence of excess ligands (Wagener et al., 2008).

Bacterial remineralization of sinking biogenic particles, on the other hand, produces weaker Fe-binding ligands ($\log K^{\mathrm{cond}}_{\mathrm{FeL}_i,\mathrm{Fe}'} =$ 11–12, or lower) concomitant with dFe release (Boyd et al., 2010). Viral lysis of cells in grazing experiments has also recently been shown to produce similarly weak Fe-binding ligands (Poorvin et al., 2011). The weakly complexed Fe released by these passive grazing processes (Boyd et al., 2010; Poorvin et al., 2011) may be more biologically available to the phytoplankton community than the strongly complexed siderophore-bound Fe (Poorvin et al., 2011).

THE CHEMICAL CHARACTERIZATION OF THE DISSOLVED IRON LIGAND POOL

Since the first evidence for Fe complexation by natural organic ligands in seawater was presented (Gledhill and van den Berg, 1994; Rue and Bruland, 1995; van den Berg, 1995; Wu and Luther, 1995), the question of the identity, chemical structure, and source of Fe-binding organic ligands in the oceans has fueled research across disciplines. While we have learned a great deal about Fe-binding ligands, it is still not possible to give definitive answers to these questions some 17 years later. Initially, the strength and concentration of the ligands measured by competitive equilibrium techniques indicated that ambient ligands had a high affinity for Fe (Gledhill and van den Berg, 1994; Rue and Bruland, 1995; van den Berg, 1995; Wu and Luther, 1995), while, as had been highlighted above, many profiles of ligand distributions in the ocean point to an autochthonous biological source. Determination of the conditional stability constants of potential ligand types produced by phytoplankton and bacteria indicated that some of these ligand types had very similar binding strengths in seawater to the detected natural ligands (Rue and Bruland, 1995; Witter et al., 2000; Macrellis et al., 2001). Hence these biologically produced ligand types, which may include compounds like siderophores and porphyrins, were hypothesized to make up a major part of the ligand pool. However, characterization of Fe ligands in seawater is a considerable challenge because the ligands are of unknown composition, are likely complex in chemical nature and are present at very low concentrations in a matrix of high ionic strength. The recent progress made in this field has been greatly facilitated by improvements in the sensitivity, mass accuracy and robustness of both inorganic and organic mass spectrometers. Such improvements have resulted in the detection of specific iron organic complexes such as siderophores by HPLC–ESI-MS (McCormack et al., 2003; Gledhill et al., 2004; Mawji et al., 2008a, 2011; Velasquez et al., 2011) and the detection of Fe associated with more complex organic fractions by FFFF–ICP-MS (Stolpe and Hassellov, 2010; Stolpe et al., 2010; Baalousha et al., 2011).

SMALL, DEFINED ORGANIC LIGANDS

Siderophores are compounds produced by bacteria in order to sequester Fe from their environment (Hider and Kong, 2010). Siderophores are known to be produced by a wide variety of bacteria, including marine bacteria (Amin et al., 2009; Cabaj and Kosakowska, 2009; Vraspir and Butler, 2009). Bacteria appear to be able to produce families of different but related siderophores (Martinez et al., 2000, 2003; Ito and Butler, 2005; Martinez and Butler, 2007; Homann et al., 2009a,b), but uptake of siderophores by bacteria is not necessarily specific (Stintzi et al., 2000), so that a bacterial species may be able to acquire siderophores produced by other species. There has been much progress in the characterization of specific siderophores produced by marine bacteria (Amin et al., 2009; Vraspir and Butler, 2009), in particular by the A. Butler research group at the University of California in Santa Barbara.

Relatively large quantities of isolated siderophore are currently required for a complete description of chemical structure so that it is only possible to fully characterize siderophores in bacteria that can be cultured in the laboratory. In addition, the time and effort required also imposes restrictions on the number of siderophores that can be fully characterized. Characterized siderophores are, thus, likely to represent only a fraction of the potential siderophore pool. Marine siderophores produced in laboratory cultures have been found to contain all the major siderophore chelating groups of hydroxamate, catecholate, and carboxylate functional groups (Vraspir and Butler, 2009). To date, the majority of marine siderophores characterized contain mixed

ligand carboxylate groups, and many of these characterized marine siderophores have fatty acid tails attached to the chelating head (Martinez et al., 2000, 2003; Xu et al., 2002; Owen et al., 2005; Martin et al., 2006; Martinez and Butler, 2007; Homann et al., 2009a,b). Such fatty acid tails are likely to strongly influence siderophore biogeochemistry, affecting siderophore partitioning between dissolved and particulate phases and perhaps mitigating against diffusive losses of siderophores from the bacterial cell (Xu et al., 2002; Martinez and Butler, 2007).

Progress has also been made in the detection and characterization of siderophores in natural seawater itself (Gledhill et al., 2004; Mawji et al., 2008a, 2011; Velasquez et al., 2011; **Table 2**; **Figure 3**). The first reports of dissolved siderophores in seawater were made by Kosakowska et al. (Kosakowska et al., 1999; Mucha et al., 1999) using capillary electrophoresis to detect hydroxamate siderophores in the Baltic Sea. Macrellis et al. (2001) used siderophore assays to report the presence of siderophore like functional groups in coastal NE Pacific upwelling waters. More recently, chromatographic techniques have been coupled to ESI or ICP-MS in order to either characterize or quantify specific siderophores in seawater (Mawji et al., 2008a; Velasquez et al., 2011; **Table 2**). Separation techniques coupled to mass spectrometry show much promise for both the identification and quantification of specific metal complexes like with siderophores, largely as a result of the high sensitivity of these techniques, which are capable of detecting in the picomolar–nanomolar range. Mass spectrometry has been used to detect unknown and known siderophores in the Southern Ocean and in the Atlantic Ocean (Mawji et al., 2008a; Velasquez et al., 2011). In the Southern Ocean, unidentified siderophore-type complexes were detected with the molecular masses varying from station to station (Velasquez et al., 2011). In the Atlantic Ocean, ferrioxamine type siderophores were detected ubiquitously and were found to be present at concentrations of upto 20 pM, and to make up between 0.5 and 5% of the total dissolved Fe pool (Mawji et al., 2008a). The somewhat sparse data so far obtained indicates that siderophore distributions may be linked to bacterial abundance, but otherwise gives little clue as to how siderophore concentrations might vary with, for example, depth. It is clear, however, that the presence of marine siderophores is not limited to low dFe waters.

It is notable that, while the available data is limited, the siderophores detected in seawater to date are all hydroxamates, with no reports of any identifiable siderophores containing carboxylate or catecholate functional groups being recovered from the dissolved phase in seawater. The lack of detected carboxylate or catecholate type siderophores indicates that either these siderophore types are not present in the dissolved phase, or more likely, that the analytical techniques used to detect these compounds are biased toward the detection of hydroxamate siderophores. Current methods to detect siderophores in seawater rely on a preconcentration step, necessary in order to both remove interfering matrices, and to increase siderophore concentrations to detectable ranges (Mucha et al., 1999; Mawji et al., 2008a; Velasquez et al., 2011). Such preconcentration techniques introduce bias and probably restrict the types of siderophores that can be detected. For example, at the natural pH of seawater (~8), both carboxylate and catecholate type Fe–siderophore complexes will be deprotonated and negatively charged (Harris et al., 1979a; Loomis and Raymond, 1991). Thus, the preconcentration efficiency of catecholate and carboxylate siderophore types onto the commonly used hydrophobic resins (e.g., C18, polystyrene divinyl benzene, XAD) will be reduced. Acidification of the sample prior to preconcentration (Mucha et al., 1999; Velasquez et al., 2011), in order to neutralize negatively charged complexed siderophores and thus make them more hydrophobic may also result in siderophore hydrolysis or precipitation (Harris et al., 1979b; Loomis and Raymond, 1991). Changes in sample pH during analysis are also common, with chromatographic separations performed at low pH (McCormack et al., 2003; Velasquez et al., 2011). However, catecholate type siderophore–Fe complexes undergo hydrolysis at low pH and are not detectable when either the sample pH is low or the chromatographic conditions employ low pH eluants (Loomis and Raymond, 1991; Gledhill, unpublished data). Consequently, further work is necessary in order to develop robust preconcentration and analysis techniques applicable to a wider variety of siderophore types.

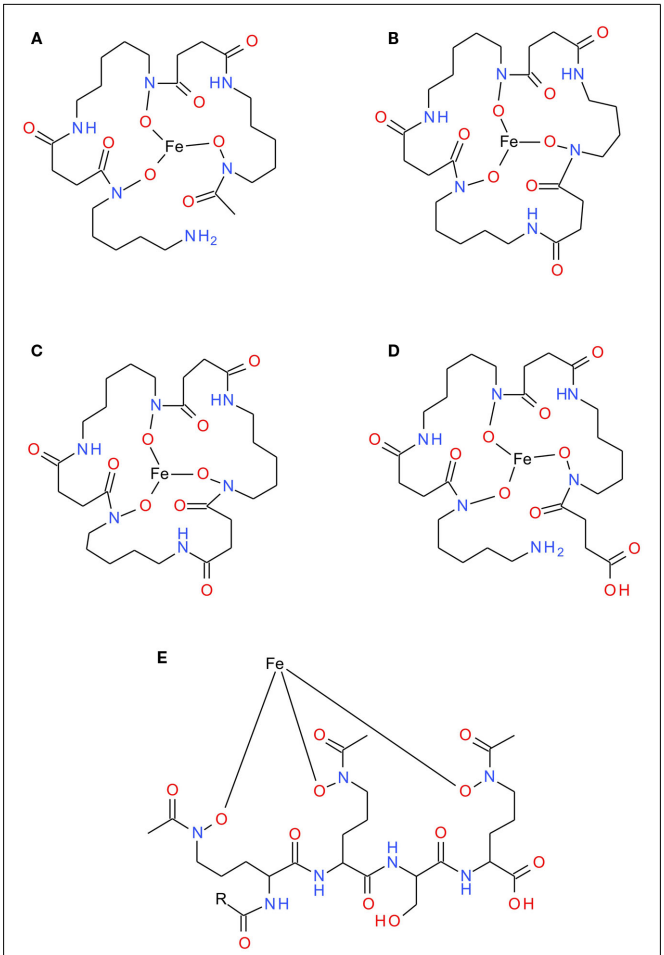

FIGURE 3 | Structures of fully characterized siderophores that have been identified in seawater or natural seawater incubations. (A) Ferrioxamine B, **(B)** Ferrioxamine D_2, **(C)** Ferrioxamine E, **(D)** Ferrioxamine G, and **(E)** Amphibactins D ($R = C_{13}H_{27}$) and E ($R = C_{15}H_{29}$).

Table 2 | Siderophores identified in seawater or natural seawater incubations by high performance liquid chromatography – electrospray ionization mass spectrometry.

Molecular ion mass (m/z, H^+ ion)	Compound identity	Sample location	Reference
494	Cyclic ferrioxamine	Neritic Otago Shelf waters	Velasquez et al. (2011)
501	Linear hydroxamate siderophore	Sub-Antarctic surface waters	Velasquez et al. (2011)
620, 603, 559	Cyclic ferrioxamine and fragments	Sub-Antarctic surface waters	Velasquez et al. (2011)
605	Cyclic hydroxamate siderophore	Sub-Antarctic surface waters	Velasquez et al. (2011)
614	Ferrioxamine B	Atlantic Ocean, British coastal waters	Gledhill et al. (2004), Mawji et al. (2008a), Mawji et al. (2011)
622	Unknown	North Atlantic subtropical gyre	Mawji et al. (2011)
640	Ferrioxamine D_2	North Atlantic subtropical gyre	Mawji et al., 2011
654	Ferrioxamine E	Atlantic Ocean	Mawji et al. (2008a), Mawji et al. (2011)
658	Unknown ferrioxamine	British coastal waters	Gledhill et al. (2004)
672	Ferrioxamine G	Atlantic Ocean, British coastal waters	Gledhill et al. (2004), Mawji et al. (2008a), Mawji et al. (2011)
675	Unknown hydrophilic siderophore	South Atlantic subtropical gyre	Mawji et al. (2011)
857	Amphibactin	British coastal waters	Gledhill et al. (2004)
883	Amphibactin	South Atlantic subtropical gyre	Gledhill et al. (2004), Mawji et al. (2011)
885	Amphibactin D	South Atlantic subtropical gyre	Gledhill et al. (2004), Mawji et al. (2011)
911	Amphibactin E	South Atlantic subtropical gyre	Gledhill et al. (2004), Mawji et al. (2011)
1044	Unknown	South Atlantic subtropical gyre	Mawji et al. (2011)

Identification of siderophore complexes in mass spectra takes place via the utilization of distinctive isotopic ratios endowed upon the complex by the metal ion (McCormack et al., 2003; Velasquez et al., 2011). Two strategies are currently employed; the first involves complexation of the siderophore with gallium, which has a very identifiable isotopic ratio for ^{69}Ga:^{71}Ga of 3:2 and allows for several mechanisms of checking against false positives, increasing the robustness of the analysis (McCormack et al., 2003; Mawji et al., 2011). Such checks include analysis of the original sample for the presence of the Fe-complexed or apo- (metal free) siderophore and analysis by ICP-MS in order to check that gallium is indeed present at the expected relative retention time (Mawji et al., 2011). The gallium exchange method suffers from disadvantages in that it involves reduction of the sample pH in order to keep gallium in solution and, thus, is likely to result in losses of chemically unstable siderophores (see above).

A second promising technique recently applied to the identification of siderophores in seawater is based on the distinctive isotopic ratio endowed on a molecule by Fe (Velasquez et al., 2011). The natural abundance of the ^{54}Fe isotope is approximately 5.6% of the ^{56}Fe isotope. When incorporated into an organic complex, the combination of the Fe and carbon isotopic abundances increases the abundance of the lighter molecular ion so that ferrioxamine B will have expected isotopic ratios of 6.4:100:32.4 for m/z ($M + H^+$) 612, 614, and 617. A key component of this technique is the ability to detect the putative ^{54}Fe containing molecular ion and then confirm it otherwise has the same structure as the ^{56}Fe containing molecular ion. This has been shown to be possible with a nano-HPLC coupled to a high resolution mass spectrometer (Velasquez et al., 2011). Unfortunately, the background noise in lower resolution instruments working with higher flow rates may make it difficult to identify the ^{54}Fe isotope, as it is present at quite a low relative abundance in MS spectra. However, even in lower resolution instruments fragment ions obtained on collision induced dissociation of pseudo molecular ions can be used to provide evidence for Fe complexes (Velasquez et al., 2011) as Fe is strongly retained in fragment ions (Mawji et al., 2008b; Velasquez et al., 2011). In theory, Fe could also be determined in parallel by ICP-MS in analogy to the gallium technique in order to confirm the presence of the metal at the expected retention time, although more care would have to be taken with respect to contamination. Furthermore the determination of Fe by ICP-MS can be more difficult due to isobaric interferences (Mawji et al., 2008a, 2011).

The limited number of reports on siderophore concentrations in the dissolved phase in the ocean indicates that the concentrations of individual siderophores are likely to be quite low, in the picomolar range (Mawji et al., 2008a). However, as has been pointed out above, while the pool of potential siderophores is apparently quite large (e.g., Amin et al., 2009; Cabaj and Kosakowska, 2009; Vraspir and Butler, 2009), it is likely that only a limited number of siderophores in seawater are detectable using the currently applied methods. Thus, although it is now clear that siderophores can be present in the open ocean, it is not possible at this stage to say what proportion of the dissolved ligand pool is made up of siderophores.

Porphyrins (molecular weight 600–1000 Da) are another biologically produced class of compounds that have been suggested as potential Fe ligands (Witter et al., 2000; Hunter and Boyd, 2007). Porphyrins function as prosthetic groups in proteins and are useful for their ability to absorb light, transfer electrons, and bind oxygen (Mochizuki et al., 2010). Porphyrins, which include chlorophylls, chlorophyll breakdown products like phaeophytin, hemes, and

vitamin B12, are produced by almost all living organisms via a well conserved tetrapyrrole biosynthesis pathway (Mochizuki et al., 2010). The biological production of these compounds is tightly controlled, as they cause oxidative stress if present in excess of their proteins (Mochizuki et al., 2010). Hemes have been detected at picomolar concentrations in particulate material (Gledhill et al., under review) and heme like compounds have been detected in the dissolved fraction at nanomolar concentrations in river and estuarine waters (Vong et al., 2007). However, given that porphyrins have a very low solubility in water at pH 8 and more recent work has found little evidence to show that Fe(III) spontaneously complexes with porphyrins in solution (Rijkenberg et al., 2006a; Schlosser and Croot, 2008) it remains questionable as to whether porphyrins form a part of the dissolved ligand pool.

Domoic acid (DA), an algal toxin produced by *Pseudo-nitzschia* spp., has also been shown to complex Fe (Rue and Bruland, 2001), although with a weak stability constant (log $K'_{FeDA} = 8.7$) that is unlikely to make it an effective competitor in the ocean. However, there is evidence that DA, through its ability to complex dissolved Cu, may facilitate the high affinity Fe uptake from strongly complexed Fe by diatoms in Fe-limited environments (Wells et al., 2005), regions where DA levels can be elevated (Silver et al., 2010). Thus, while possibly not a significant component of the Fe-binding ligand pool, DA may nonetheless play an important role in the biogeochemical cycling of Fe, particularly in Fe-limited environments.

LARGER, LESS WELL-DEFINED ORGANIC LIGANDS

Recent evidence has indicated that more diffuse, less well-defined organic compounds such as HS and exopolysaccharides (EPS) may contribute to the Fe ligand pool (Batchelli et al., 2009, 2010; Laglera and van den Berg, 2009; Stolpe and Hassellov, 2010; Stolpe et al., 2010; Hassler et al., 2011a,b). Laglera and van den Berg recently reported an electrochemical technique that allows for the direct detection of humic like substances in seawater by ACSV (Laglera et al., 2007; Laglera and van den Berg, 2009). The technique determines the catalytically enhanced reduction current produced by Fe bound to HS, and is standardized using the Suwannee River fulvic acid (SRFA) standard (Laglera et al., 2007). Determination of the conditional stability constants and binding capacities of these putative humic like substances by competition with ethylenediaminetetraacetic acid (EDTA) has shown that these ligands have similar stability constants to the natural organic ligands measured by CLE–ACSV (Laglera and van den Berg, 2009). Apparent binding capacities for these humic like substances in seawater are also similar to those determined by CLE–ACSV (Laglera and van den Berg, 2009), and it has been suggested that HS can account for the majority of the total ligand pool in coastal and deep waters (Batchelli et al., 2009, 2010; Laglera and van den Berg, 2009). The coincidence of similar reduction potentials and binding capacities for the detected ambient Fe ligand, SRFA, and Suwannee River humic acid (SRHA) make it tempting to identify the ambient ligand detected using the technique as a humic like substance (Laglera et al., 2007). However, the technique is not specific to HS, as EPS will also become electrochemically active upon addition of Fe and are, thus, indistinguishable from HS by ACSV (Hassler et al., 2011b). Further support for identification of a ligand fraction as HS is, however, provided by FFFF. Studies in coastal waters using FFF–ICP-MS and FFFF coupled to UV and fluorescence detectors have indicated that dFe in coastal waters is associated with fluorescent, colored, dissolved humic like organic matter (Stolpe and Hassellov, 2010; Stolpe et al., 2010), and that, furthermore, freshly added Fe readily associates with this fraction (Stolpe et al., 2010).

By their very nature, both HS and EPS are challenging to chemically characterize. Both HS and EPS are oxygen rich – the SRFA used in Laglera and van den Berg (2009) consists of 44% oxygen (% w/w, http://www.ihss.gatech.edu/elements.html), while EPS are predominantly composed of neutral sugars and contain a significant fraction of acidic polysaccharides like uronic acids (Mancuso Nichols et al., 2004). Uronic acids are known to complex Fe (Gyurcsik and Nagy, 2000), with complexes being more stable at high pH (Gyurcsik and Nagy, 2000), as observed for Fe–HS complexes (Laglera et al., 2007). Classical pH-metric determinations of stability constants for simple acidic polysaccharide-Fe complexes show that they are low (log β 3–4; Gyurcsik and Nagy, 2000) and Fe complexation of model polysaccharides carrageenan, laminarin, and alginic acid in seawater has been found to be undetectable by CLE–ACSV (Strmecki et al., 2010), although this may have been an artifact of the selected AL (Laglera et al., 2011). In other studies, EPS from bacteria have been observed to be associated with Fe (Hassler et al., 2011a,b) and EPS has been shown to reduce the lability of Fe to other Fe ligands while enhancing Fe availability to phytoplankton when compared to Fe–siderophore complexes (Hassler et al., 2011b).

In addition to an Fe–HS fraction, Stolpe and Hassellov (2010) also observed an association of Fe with a higher molecular weight organic fraction described as nanofibrils, particularly at a time of enhanced productivity (Stolpe and Hassellov, 2010). The nanofibrils were consistent in size and appearance to transparent exopolymer (TEP) like compounds (Stolpe and Hassellov, 2010). However, although Fe present in the samples was found to co-elute with the nanofibril fraction, freshly added Fe did not associate with the nanofibrils. Stolpe and Hassellov (2010) suggested that this behavior could be explained as an inorganic Fe-nanoparticle association (Stolpe and Hassellov, 2010), although it could also be a reflection of under saturation of binding sites in the HS fraction, coupled to a weaker affinity between Fe and the larger nanofibrils.

APPROACHING AN OVERVIEW OF IRON COMPLEXATION AND PHYSICO-CHEMICAL SPECIATION IN SEAWATER

Several types of Fe organic complexes and associations have now been shown to exist in seawater, ranging from high affinity siderophores present at low concentrations, to weaker but more abundant HS and EPS associations, and likely also including associations between inorganic Fe nanoparticles and larger TEP like organic macromolecules (**Figure 4**). These organic complexes and associations are currently best distinguished by size fractionation, as they generally fall along an increasing size spectrum from siderophores to macromolecules. Often coupled to this increasing size spectrum is a decreasing thermodynamic stability of the complexes as measured by CLE–ACSV, but increasing kinetic inertness, leading to an overall potential decrease in biological availability. It is, therefore, becoming possible to unravel

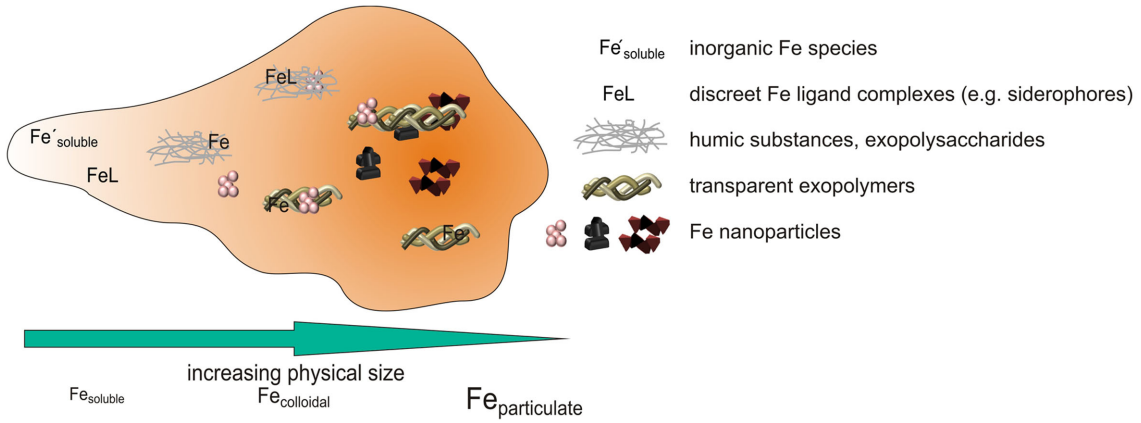

FIGURE 4 | Schematic figure illustrating potential components of the dFe pool so far identified in seawater. Decreasing kinetic lability of Fe within the components is represented by deeper orange background shading.

the different biogeochemical behaviors of the many components of the dFe pool.

Siderophores are associated with bacterial productivity and may only be produced in significant quantities when readily available carbon is abundant (Mawji et al., 2011). Siderophores maybe important in regions where organic carbon concentrations are high enough to support significant bacterial productivity, but where dFe is not readily available. The photochemical lability of siderophores suggests that many siderophore types will not persist in the water column, although their breakdown products may be more stable and form weaker, more bioavailable, Fe complexes (Barbeau et al., 2001, 2003). Siderophores may play an important role in increasing the availability of Fe for particular types of bacteria, influencing bacterial diversity and productivity in the ocean. Siderophores may also play a role in the solubilization of particulate and colloidal Fe. Given their origin, function and reactivity, siderophores are anticipated to contribute to Fe-binding ligand pools primarily in the upper water column, and especially in the truly soluble size fraction of ligands, although siderophores may also be associated with colloidal and particulate fractions as well.

Field studies of Fe-binding ligand distributions consistently report higher excess ligand concentrations in the upper water column, and these maxima in eL_i are often, though not always, associated with elevated fluorescence and phytoplankton biomass. When size fractionation is assessed, these excess ligand concentrations also appear to be predominantly in the soluble size fraction. In combination, field studies support a siderophore-type origin of ambient Fe-binding ligands in the upper oceans. However, siderophores extracted from natural waters to date have been found in only the picomolar range, while ambient strong Fe-binding ligands are measured by CLE–ACSV in the nanomolar range. Recent incubation studies of natural surface seawater have shown strong Fe-binding ligand production, also measured by CLE–ACSV in the nanomolar range, under conditions of both Fe-limited phytoplankton growth and stimulated bloom decay (Sato et al., 2007; Buck et al., 2010). Furthermore, the thermodynamic stability constants (log K') of some known Fe–siderophore complexes are too high to detect with usual CLE–ACSV approaches. Altogether, this would suggest that, in addition to siderophores, other strong Fe-binding ligand types are also likely to contribute to the Fe-binding ligand pool measured by CLE–ACSV in surface waters.

Humic substances and EPS may be either terrestrial or autochthonous in nature, and are typically found in the colloidal fraction. It appears that the HS fraction is quite refractory and persists into the deep ocean while EPS is likely to be produced in surface waters as it is, by definition, associated with phytoplankton productivity. Fe bound to model humic acids and Fe bound to EPS have been shown to be as available to phytoplankton as inorganic Fe (Chen and Wang, 2008; Hassler et al., 2011b). However, both EPS and HS are complex molecules that remain poorly defined; greater effort is required in order to characterize the association between Fe, HS, and EPS, and the contribution of HS and EPS to the ambient ligand pool in the open ocean. It is apparent that current techniques may not distinguish particularly well between HS and EPS, yet the biogeochemistry of these two organic fractions is potentially quite different.

The biological availability of colloidal Fe is rather hard to define as it is probably highly dependent on the chemical nature of the colloids (Kuma and Matsunaga, 1995; Yoshida et al., 2006), as well as the capabilities of organisms present to extract Fe from the colloids, whether by reduction (Maldonado and Price, 2001; Rijkenberg et al., 2008a) or by dissolution via a high affinity uptake mechanism (Vraspir and Butler, 2009). The biological availability of some colloids, like Fe nanoparticles, is poorly understood. Colloidal Fe biogeochemistry is also likely to be strongly influenced by temperature, another consideration that has yet to be investigated fully. However, it is becoming apparent that Fe biogeochemistry in the open ocean may be strongly influenced by the stability of the colloidal fraction. While it has been suggested that organic Fe colloids formed in surface waters are scavenged quite rapidly through the water column (Wu and Luther, 1994; Nishioka et al., 2001; Wu et al., 2001; Cullen et al., 2006; Bergquist et al., 2007; Hurst and Bruland, 2008; Kondo et al., 2008; Schlosser and Croot, 2008; Boye et al., 2010; Thuroczy et al., 2010), stable Fe colloids from continental shelves have also been implicated in the long range

transport of Fe to the open ocean (Elrod et al., 2004; Lam and Bishop, 2008). More information is, thus, needed on the nature of Fe colloids in open ocean surface and continental shelf waters in order to understand more fully these potentially contrasting behaviors. Investigation of an organic Fe colloid-like fraction in future global ocean models incorporating Fe speciation would also allow the role of this fraction in the Fe biogeochemical cycle to be further examined.

Taken together, the evidence described above points toward the existence of a spectrum of Fe ligands in seawater, and we found that the different experimental approaches employed by Fe biogeochemists appear to be converging toward a consistent overview. Increases in the size and complexity of the Fe species appear to be accompanied by a weakening of the thermodynamic stability of the Fe complex. The weaker complexation between Fe′ and the larger sized organic macromolecules is, however, potentially mitigated by the existence of associations between inert Fe nanoparticles and nanofibrils like TEP, resulting in an apparently Fe saturated inert colloidal ligand pool. Substantial progress has been made in trace metal clean size fractionation, CLE–ACSV, and HPLC–ESI-MS techniques over the last decade. We anticipate that future studies will increasingly couple these techniques, along with incubations and other biological process studies, providing much needed insight on the nature and cycling of Fe-binding ligands in the oceans. Finally, we conclude that the biogeochemical role of each of the organic ligand fractions appears to be very different and deserves further investigation, as this spectrum of organic Fe-binding ligands overwhelmingly complexes dFe in the marine environment.

ACKNOWLEDGMENTS

Gledhill was supported by UK – NERC Advanced Fellowship (NE/E013546/1) and contributed to the manuscript whilst a visiting scientist at the Royal Netherlands Institute of Sea Research, Texel, The Netherlands. Buck was supported by institutional funding from the G. Unger Vetlesen Foundation at the Bermuda Institute of Ocean Sciences (BIOS). This manuscript constitutes BIOS contribution number 2017 for co-author Buck.

REFERENCES

Amin, S. A., Green, D. H., Hart, M. C., Kupper, F. C., Sunda, W. G., and Carrano, C. J. (2009). Photolysis of iron-siderophore chelates promotes bacterial-algal mutualism. *Proc. Natl. Acad. Sci. U.S.A.* 106, 17071–17076.

Archer, D. E., and Johnson, K. (2000). A model of the iron cycle in the ocean. *Global Biogeochem. Cycles* 14, 269–279.

Baalousha, M., Stolpe, B., and Lead, J. R. (2011). Flow field-flow fractionation for the analysis and characterization of natural colloids and manufactured nanoparticles in environmental systems: a critical review. *J. Chromatogr. A* 1218, 4078–4103.

Barbeau, K., Rue, E. L., Trick, C. G., Bruland, K. T., and Butler, A. (2003). Photochemical reactivity of siderophores produced by marine heterotrophic bacteria and cyanobacteria based on characteristic Fe(III) binding groups. *Limnol. Oceanogr.* 48, 1069–1078.

Barbeau, K. A., Rue, E. L., Bruland, K., W,, and Butler, A. (2001). Photochemical cycling of iron in the surface ocean mediated by microbial iron(III)-binding ligands. *Nature* 413, 409–413.

Batchelli, S., Muller, F. L. L., Baalousha, M., and Lead, J. R. (2009). Size fractionation and optical properties of colloids in an organic-rich estuary (Thurso, UK). *Mar. Chem.* 113, 227–237.

Batchelli, S., Muller, F. L. L., Chang, K. C., and Lee, C. L. (2010). Evidence for strong but dynamic iron-humic colloidal associations in humic-rich coastal waters. *Environ. Sci. Technol.* 44, 8485–8490.

Bennett, S. A., Achterberg, E. P., Connelly, D. P., Statharn, P. J., Fones, G. R., and Gernian, C. R. (2008). The distribution and stabilisation of dissolved Fe in deep-sea hydrothermal plumes. *Earth Planet. Sci. Lett.* 270, 157–167.

Bergquist, B. A., Wu, J., and Boyle, E. A. (2007). Variability in oceanic dissolved iron is dominated by the colloidal fraction. *Geochim. Cosmochim. Acta* 71, 2960–2974.

Bligh, M. W., and Waite, T. D. (2010). Role of heterogeneous precipitation in determining the nature of products formed on oxidation of Fe(II) in seawater containing natural organic matter. *Environ. Sci. Technol.* 44, 6667–6673.

Boyd, P. W., and Ellwood, M. J. (2010). The biogeochemical cycle of iron in the ocean. *Nat. Geosci.* 3, 675–682.

Boyd, P. W., Ibisanmi, E., Sander, S. G., Hunter, K. A., and Jackson, G. A. (2010). Remineralization of upper ocean particles: implications for iron biogeochemistry. *Limnol. Oceanogr.* 55, 1271–1288.

Boyd, P. W., Jickells, T., Law, C. S., Blain, S., Boyle, E. A., Buesseler, K. O., Coale, K. H., Cullen, J. J., De Baar, H. J. W., Follows, M., Harvey, M., Lancelot, C., Levasseur, M., Owens, N. P. J., Pollard, R., Rivkin, R. B., Sarmiento, J., Schoemann, V., Smetacek, V., Takeda, S., Tsuda, A., Turner, S., and Watson, A. J. (2007). Mesoscale iron enrichment experiments 1993-2005: synthesis and future directions. *Science* 315, 612–617.

Boye, M., Aldrich, A., Van Den Berg, C. M. G., De Jong, J. T. M., Nirmaier, H., Veldhuis, M., Timmermans, K. R., and De Baar, H. J. W. (2006). The chemical speciation of iron in the north-east Atlantic Ocean. *Deep Sea Res. Part I Oceanogr. Res. Pap.* 53, 667–683.

Boye, M., Nishioka, J., Croot, P., Laan, P., Timmermans, K. R., Strass, V. H., Takeda, S., and De Baar, H. J. W. (2010). Significant portion of dissolved organic Fe complexes in fact is Fe colloids. *Mar. Chem.* 122, 20–27.

Boye, M., Nishioka, J., Croot, P. L., Laan, P., Timmermans, K. R., and De Baar, H. J. W. (2005). Major deviations of iron complexation during 22 days of a mesoscale iron enrichment in the open Southern Ocean. *Mar. Chem.* 96, 257–271.

Boye, M., Van Den Berg, C. M. G., De Jong, J. T. M., Leach, H., Croot, P., and De Baar, H. J. W. (2001). Organic complexation of iron in the Southern Ocean. *Deep Sea Res. Part I Oceanogr. Res. Pap.* 48, 1477–1497.

Boye, M. B., Aldrich, A. P., Van Den Berg, C. M. G., De Jong, J. T. M., Veldhuis, M. J. W., and De Baar, H. J. W. (2003). Horizontal gradient of the chemical speciation of iron in surface waters of N.E. Atlantic Ocean. *Mar. Chem.* 80, 129–143.

Bruland, K. W., Rue, E. L., Donat, J. R., Skrabal, S. A., and Moffett, J. W. (2000). Intercomparison of voltammetric techniques to determine the chemical speciation of dissolved copper in a coastal seawater sample. *Anal. Chim. Acta* 405, 99–113.

Bruland, K. W., and Rue, E. L. (2001). "Analytical methods for the determination of concentrations and speciation of iron," in *The Biogeochemistry of Iron in Seawater*, eds D. R. Turner and K. A. Hunter (Chichester: Wiley), 255–290.

Buck, K. N., and Bruland, K. W. (2007). The physicochemical speciation of dissolved iron in the Bering Sea, Alaska. *Limnol. Oceanogr.* 52, 1800–1808.

Buck, K. N., Lohan, M. C., Berger, C. J. M., and Bruland, K. W. (2007). Dissolved iron speciation in two distinct river plumes and an estuary: implications for riverine iron supply. *Limnol. Oceanogr.* 52, 843–855.

Buck, K. N., Selph, K. E., and Barbeau, K. A. (2010). Iron-binding ligand production and copper speciation in an incubation experiment of Antarctic Peninsula shelf waters from the Bransfield Strait, Southern Ocean. *Mar. Chem.* 122, 148–159.

Byrne, R. H., Kump, L. R., and Cantrell, K. J. (1988). The influence of temperature and pH on trace metal speciation in seawater. *Mar. Chem.* 25, 163–181.

Cabaj, A., and Kosakowska, A. (2009). Iron-dependent growth of and siderophore production by two heterotrophic bacteria isolated from brackish water of the southern Baltic Sea. *Microbiol. Res.* 164, 570–577.

Chen, M., and Wang, W. X. (2008). Accelerated uptake by phytoplankton of iron bound to humic acids. *Aquat. Biol.* 3, 155–166.

Croot, P. L., Andersson, K., Öztürk, M., and Turner, D. R. (2004). The distribution and speciation of iron along 6°E in the Southern Ocean. *Deep Sea Res. Part II Top. Stud. Oceanogr.* 51, 2857–2879.

Croot, P. L., and Johansson, M. (2000). Determination of iron speciation by cathodic stripping voltammetry in seawater using the competing ligand 2-(2-thiazolylazo)-*p*-cresol (TAC). *Electroanalysis* 12, 565–576.

Croot, P. L., Laan, P., Nishioka, J., Strass, V., Cisewski, B., Boye, M., Timmermans, K. R., Bellerby, R. G., Goldson, L., Nightingale, P., and De Baar, H. J. W. (2005). Spatial and temporal distribution of Fe(II) and H_2O_2 during EisenEx, an open ocean mescoscale iron enrichment. *Mar. Chem.* 95, 65–88.

Cullen, J. T., Bergquist, B. A., and Moffett, J. W. (2006). Thermodynamic characterization of the partitioning of iron between soluble and colloidal species in the Atlantic Ocean. *Mar. Chem.* 98, 295–303.

Cutter, G., Andersson, P., Codispoti, L., Croot, P., Francois, R., Lohan, M., Obata, H., and Rutgers Van Der Loeff, M. (eds). (2010). *Sampling and Sample-Handling Protocols for GEOTRACES Cruises.* GEOTRACES. Available at: http://www.geotraces.org/library/geotraces-policies/170-sampling-and-sample-handling-protocols-for-geotraces-cruises

De Baar, H. J. W., and De Jong, J. T. M. (2001). "Distribution, sources and sinks of iron in seawater," in *The Biogeochemistry of Iron in Seawater*, eds D. R. Turner and K. A. Hunter (Chichester: Wiley), 123–253.

Elrod, V. A., Berelson, W. M., Coale, K. H., and Johnson, K. S. (2004). The flux of iron from continental shelf sediments: a missing source for global budgets. *Geophys. Res. Lett.* 31, L12307.

Fan, S. M. (2008). Photochemical and biochemical controls on reactive oxygen and iron speciation in the pelagic surface ocean. *Mar. Chem.* 109, 152–164.

Fan, S. M., and Dunne, J. P. (2011). Models of iron speciation and concentration in the stratified epipelagic ocean. *Geophys. Res. Lett.* 38, L15611.

Garnier, C., Pizeta, I., Mounier, S., Benaim, J. Y., and Branica, M. (2004). Influence of the type of titration and of data treatment methods on metal complexing parameters determination of single and multi-ligand systems measured by stripping voltammetry. *Anal. Chim. Acta* 505, 263–275.

Gerringa, L. J. A., Herman, P. M. J., and Poortvliet, T. C. W. (1995). Comparison of the linear Van den Berg/RuziC transformation and the non-linear fit of the Langmuir isotherm applied to Cu speciation data in the estuarine environ ment. *Mar. Chem.* 48, 131–142.

Gerringa, L. J. A., Blain, S., Laan, P., Sarthou, G., Veldhuis, M. J. W., Brussaard, C. P. D., Viollier, E., and Timmermans, K. R. (2008). Fe-binding dissolved organic ligands near the Kerguelen Archipelago in the Southern Ocean (Indian Sector). *Deep Sea Res. Part I Oceanogr. Res. Pap.* 55, 606–621.

Gerringa, L. J. A., Rijkenberg, M. J. A., Wolterbeek, H. T., Verburg, T. G., Boye, M., and De Baar, H. J. W. (2007). Kinetic study reveals weak Fe-binding ligand, which affects the solubility of Fe in the Scheldt estuary. *Mar. Chem.* 103, 30–45.

Gerringa, L. J. A., Veldhuis, M. J. W., Timmermans, K. R., Sarthou, G., and De Baar, H. J. W. (2006). Covariance of dissolved Fe-binding ligands with phytoplankton characteristics in the Canary Basin. *Mar. Chem.* 102, 276–290.

Gledhill, M., Mccormack, P., Ussher, S., Achterberg, E. P., Mantoura, R. F. C., and Worsfold, P. J. (2004). Production of siderophore type chelates by mixed bacterioplankton populations in nutrient enriched seawater incubations. *Mar. Chem.* 88, 75–83.

Gledhill, M., and van den Berg, C. M. G. (1994). Determination of complexation of iron (III) with natural organic complexing ligands in sea water using cathodic stripping voltammetry. *Mar. Chem.* 47, 41–54.

Gledhill, M., and van den Berg, C. M. G. (1995). Measurement of the redox speciation of iron in seawater by catalytic cathodic stripping voltammetry. *Mar. Chem.* 50, 51–61.

Gledhill, M., Van Den Berg, C. M. G., Nolting, R. F., and Timmermans, K. R. (1998). Variability in the speciation of iron in the northern North Sea. *Mar. Chem.* 59, 283–300.

Gobler, C. J., Donat, J. R., Consolvo, J. A. III, and Sanudo-Whilhelmy, S. A. (2002). Physicochemical speciation of iron during coastal algal blooms. *Mar. Chem.* 77, 71–89.

Gyurcsik, B., and Nagy, L. (2000). Carbohydrates as ligands: coordination equilibria and structure of the metal complexes. *Coord. Chem. Rev.* 203, 81–149.

Hansard, S. P., Landing, W. M., Measures, C. I., and Voelkar, B. M. (2009). Dissolved iron(II) in the Pacific Ocean: measurements from PO_2 and P16N Clivar/CO_2 repeat hydrography expeditions. *Deep Sea Res. Part I Oceanogr. Res. Pap.* 56, 1117–1129.

Harris, W. R., Carrano, C. J., and Raymond, K. N. (1979a). Coordination chemistry of microbial iron transport compounds.16. Isolation, characterization, and formation-constants of ferric aerobactin. *J. Am. Chem. Soc.* 101, 2722–2727.

Harris, W. R., Carrano, C. J., and Raymond, K. N. (1979b). Spectrophotometric determination of the proton-dependent stability constant of ferric enterobactin. *J. Am. Chem. Soc.* 101, 2213–2214.

Hassler, C. S., Alasonati, E., Nichols, C. A. M., and Slaveykova, V. I. (2011a). Exopolysaccharides produced by bacteria isolated from the pelagic Southern Ocean – role in Fe binding, chemical reactivity, and bioavailability. *Mar. Chem.* 123, 88–98.

Hassler, C. S., Schoemann, V., Nichols, C. M., Butler, E. C. V., and Boyd, P. W. (2011b). Saccharides enhance iron bioavailability to Southern Ocean phytoplankton. *Proc. Natl. Acad. Sci. U.S.A.* 108, 1076–1081.

Hider, R. C., and Kong, X. L. (2010). Chemistry and biology of siderophores. *Nat. Prod. Rep.* 27, 637–657.

Hirose, K. (2006). Chemical speciation of trace metals in seawater: a review. *Anal. Sci.* 22, 1055–1063.

Hirose, K. (2007). Metal-organic matter interaction: ecological roles of ligands in oceanic DOM. *Appl. Geochem.* 22, 1636–1645.

Homann, V. V., Edwards, K. J., Webb, E. A., and Butler, A. (2009a). Siderophores of *Marinobacter aquaeolei*: petrobactin and its sulfonated derivatives. *Biometals* 22, 565–571.

Homann, V. V., Sandy, M., Tincu, J. A., Templeton, A. S., Tebo, B. M., and Butler, A. (2009b). Loihichelins A-F, a suite of amphiphilic siderophores produced by the marine bacterium *Halomonas* LOB-5. *J. Nat. Prod.* 72, 884–888.

Hong, H., and Kester, D. R. (1986). Redox state of iron in the offshore waters of Peru. *Limnol. Oceanogr.* 31, 512–524.

Hopkinson, B. M., and Barbeau, K. A. (2007). Organic and redox speciation of iron in the eastern tropical North Pacific suboxic zone. *Mar. Chem.* 106, 2–17.

Hudson, R. J. M., Covault, D. T., and Morel, F. M. M. (1992). Investigations of iron coordination and redox reactions in seawater using ^{59}Fe radiometry and ion-pair solvent extraction of amphiphilic iron complexes. *Mar. Chem.* 38, 209–235.

Hunter, K. A., and Boyd, P. W. (2007). Iron-binding ligands and their role in the ocean biogeochemistry of iron. *Environ. Chem.* 4, 221–232.

Hurst, M. P., and Bruland, K. W. (2008). The effects of the San Francisco Bay plume on trace metal and nutrient distributions in the Gulf of the Farallones. *Geochim. Cosmochim. Acta* 72, 395–411.

Hutchins, D. A., Witter, A. E., Butler, A., and Luther, G. W. III. (1999). Competition among marine phytoplankton for different chelated iron species. *Nature* 400, 858–861.

Ibisanmi, E., Sander, S. G., Boyd, P. W., Bowie, A. R., and Hunter, K. A. (2011). Vertical distributions of iron-(III) complexing ligands in the Southern Ocean. *Deep Sea Res. Part II Top. Stud. Oceanogr.* 58, 2113–2125.

Ito, Y., and Butler, A. (2005). Structure of synechobactins, new siderophores of the marine cyanobacterium *Synechococcus* sp PCC 7002. *Limnol. Oceanogr.* 50, 1918–1923.

Johnson, K. S., Coale, K. H., Elrod, V. A., and Tindale, N. W. (1994). Iron photochemistry in waters from the equatorial Pacific. *Mar. Chem.* 46, 319–334.

King, A. L., Buck, K. N., and Barbeau, K. A. (2012). Quasi-Lagrangian drifter studies of iron speciation and cycling off Point Conception, California. *Mar. Chem.* 128-129, 1–12.

Kitayama, S., Kuma, K., Manabe, E., Sugie, K., Takata, H., Isoda, Y., Toya, K., Saitoh, S. I., Takagi, S., Kamei, Y., and Sakaoka, K. (2009). Controls on iron distributions in the deep water column of the North Pacific Ocean: iron(III) hydroxide solubility and marine humic-type dissolved organic matter. *J. Geophys. Res.* 114, C08019.

Kondo, Y., Takeda, S., and Furuya, K. (2007). Distribution and speciation of dissolved iron in the Sulu Sea and its adjacent waters. *Deep Sea Res. Part II Top. Stud. Oceanogr.* 54, 60–80.

Kondo, Y., Takeda, S., Nishioka, J., Obata, H., Furuya, K., Johnson, W. K., and Wong, C. S. (2008). Organic iron(III) complexing ligands during an iron enrichment experiment in the western subarctic North Pacific. *Geophys. Res. Lett.* 35, L12601.

Kosakowska, A., Kupryszewski, G., Mucha, P., Rekowski, P., Lewandowska, J., and Pazdro, K. (1999). Identification of selected siderophores in the Baltic Sea environment by the use of capillary electrophoresis. *Oceanologia* 41, 573–587.

Kuma, K., and Matsunaga, K. (1995). Availability of colloidal ferric oxides to coastal marine-phytoplankton. *Mar. Biol.* 122, 1–11.

Kuma, K., Nakabayashi, S., Suzuki, Y., Kudo, I., and Matsunaga, K. (1992). Photo-reduction of Fe(III) by dissolved organic substances and existence of Fe(II) in seawater during spring blooms. *Mar. Chem.* 37, 15–27.

Kuma, K., Nishioka, J., and Matsunaga, K. (1996). Controls on iron(III) hydroxide solubility in seawater: the influence of pH and natural organic chelators. *Limnol. Oceanogr.* 41, 396–407.

Laglera, L. M., Battaglia, G., and Van Den Berg, C. M. G. (2007). Determination of humic substances in natural waters by cathodic stripping voltammetry of their complexes with iron. *Anal. Chim. Acta* 599, 58–66.

Laglera, L. M., Battaglia, G., and Van Den Berg, C. M. G. (2011). Effect of humic substances on the iron speciation in natural waters by CLE/CSV. *Mar. Chem.* 127, 134–143.

Laglera, L. M., and van den Berg, C. M. G. (2009). Evidence for geochemical control of iron by humic substances in seawater. *Limnol. Oceanogr.* 54, 610–619.

Lam, P. J., and Bishop, J. K. B. (2008). The continental margin is a key source of iron to the HNLC North Pacific Ocean. *Geophys. Res. Lett.* 35, L07608.

Liu, X., and Millero, F. J. (2002). The solubility of iron in seawater. *Mar. Chem.* 77, 43–54.

Loomis, L. D., and Raymond, K. N. (1991). Solution equilibria of enterobactin and metal enterobactin complexes. *Inorg. Chem.* 30, 906–911.

Macrellis, H. M., Trick, C. G., Rue, E. L., Smith, G., and Bruland, K. (2001). Collection and detection of natural iron-binding ligands from seawater. *Mar. Chem.* 76, 175–187.

Maldonado, M. T., and Price, N. M. (2001). Reduction and transport of organically bound iron by *Thalassiosira oceanica* (Bacillariophyceae). *J. Phycol.* 37, 298–309.

Maldonado, M. T., Strzepek, R. F., Sander, S., and Boyd, P. W. (2005). Acquisition of iron bound to strong organic complexes, with different Fe binding groups and photochemical reactivities, by plankton communities in Fe-limited subantarctic waters. *Global Biogeochem. Cycles* 19, GB4S23.

Mancuso Nichols, C. A., Garon, S., Bowman, J. P., Raguenes, G., and Guezennec, J. (2004). Production of exopolysaccharides by Antarctic marine bacterial isolates. *J. Appl. Microbiol.* 96, 1057–1066.

Martin, J. D., Ito, Y., Homann, V. V., Haygood, M. G., and Butler, A. (2006). Structure and membrane affinity of new amphiphilic siderophores produced by *Ochrobactrum* sp SP18. *J. Biol. Inorg. Chem.* 11, 633–641.

Martin, J. H., and Fitzwater, S. (1988). Iron deficiency limits phytoplankton growth in the north-east Pacific subarctic. *Nature* 331, 341–343.

Martinez, J. S., and Butler, A. (2007). Marine amphiphilic siderophores: marinobactin structure, uptake, and microbial partitioning. *J. Inorg. Biochem.* 101, 1692–1698.

Martinez, J. S., Carter-Franklin, J. N., Mann, E. L., Martin, J. D., Haygood, M. G., and Butler, A. (2003). Structure and membrane affinity of a suite of amphiphilic siderophores produced by a marine bacterium. *Proc. Natl. Acad. Sci. U.S.A.* 100, 3754–3759.

Martinez, J. S., Zhang, G. P., Holt, P. D., Jung, H.-T., Carrano, C. J., Haygood, M. G., and Butler, A. (2000). Self-assembling amphiphilic siderophores from marine bacteria. *Science* 287, 1245–1247.

Mawji, E., Gledhill, M., Milton, J. A., Tarran, G. A., Ussher, S., Thompson, A., Wolff, G. A., Worsfold, P. J., and Achterberg, E. P. (2008a). Hydroxamate siderophores: occurrence and importance in the Atlantic Ocean. *Environ. Sci. Technol.* 42, 8675–8680.

Mawji, E., Gledhill, M., Worsfold, P. J., and Achterberg, E. P. (2008b). Collision-induced dissociation of three groups of hydroxamate siderophores: ferrioxamines, ferrichromes and coprogens/fusigens. *Rapid Commun. Mass Spectrom.* 22, 2195–2202.

Mawji, E., Gledhill, M., Milton, J. A., Zubkov, M. V., Thompson, A., Wolff, G. A., and Achterberg, E. P. (2011). Production of siderophore type chelates in Atlantic Ocean waters enriched with different carbon and nitrogen sources. *Mar. Chem.* 124, 90–99.

McCormack, P., Worsfold, P. J., and Gledhill, M. (2003). Separation and detection of siderophores produced by marine bacterioplankton using high-performance liquid chromatography with electrospray ionization mass spectrometry. *Anal. Chem.* 75, 2647–2652.

Mochizuki, N., Tanaka, R., Grimm, B., Masuda, T., Moulin, M., Smith, A. G., Tanaka, A., and Terry, M. J. (2010). The cell biology of tetrapyrroles: a life and death struggle. *Trends Plant Sci.* 15, 488–498.

Mohamed, K. N., Steigenberger, S., Nielsdottir, M. C., Gledhill, M., and Achterberg, E. P. (2011). Dissolved iron(III) speciation in the high latitude North Atlantic Ocean. *Deep Sea Res. Part I Oceanogr. Res. Pap.* 58, 1049–1059.

Moore, J. K., and Braucher, O. (2008). Sedimentary and mineral dust sources of dissolved iron to the world ocean. *Biogeosciences* 5, 631–656.

Moore, J. K., Doney, S. C., and Lindsay, K. (2004). Upper ocean ecosystem dynamics and iron cycling in a global three-dimensional model. *Global Biogeochem. Cycles* 18, GB4028.

Mucha, P., Rekowski, P., Kosakowska, A., and Kupryszewski, G. (1999). Separation of siderophores by capillary electrophoresis. *J. Chromatogr. A* 830, 183–189.

Nishioka, J., Takeda, S., Wong, C. S., and Johnson, W. K. (2001). Size-fractionated iron concentrations in the northeast Pacific Ocean: distribution of soluble and small colloidal iron. *Mar. Chem.* 74, 157–179.

Nolting, R. F., Gerringa, L. J. A., Swagerman, M. J. W., Timmermans, K. R., and De Baar, H. J. W. (1998). Fe (III) speciation in the high nutrient, low chlorophyll Pacific region of the Southern Ocean. *Mar. Chem.* 62, 335–352.

Owen, T., Pynn, R., Martinez, J. S., and Butler, A. (2005). Micelle-to-vesicle transition of an iron-chelating microbial surfactant, marinobactin E. *Langmuir* 21, 12109–12114.

Parekh, P., Follows, M. J., and Boyle, E. A. (2005). Decoupling of iron and phosphate in the global ocean. *Global Biogeochem. Cycles* 19, GB2020.

Poorvin, L., Sander, S. G., Velasquez, I., Ibisanmi, E., Lecleir, G. R., and Wilhelm, S. W. (2011). A comparison of Fe bioavailability and binding of a catecholate siderophore with virus-mediated lysates from the marine bacterium *Vibrio alginolyticus* PWH3a. *J. Exp. Mar. Biol. Ecol.* 399, 43–47.

Powell, R. T., and Wilson-Finelli, A. (2003a). Importance of organic Fe complexing ligands in the Mississippi River plume. *Estuar Coast Shelf Sci* 58, 757–763.

Powell, R. T., and Wilson-Finelli, A. (2003b). Photochemical degradation of organic iron complexing ligands in seawater. *Aquat Sci* 65, 367–374.

Raven, J. A., Evans, M. C. W., and Korb, R. E. (1999). The role of trace metals in photosynthetic electron transport in O_2-evolving organisms. *Photosyn. Res.* 60, 111–149.

Rijkenberg, M. J. A., Gerringa, L. J. A., Carolus, V. E., Velzeboer, I., and De Baar, H. J. W. (2006a). Enhancement and inhibition of iron photoreduction by individual ligands in open ocean seawater. *Geochim. Cosmochim. Acta* 70, 2790–2805.

Rijkenberg, M. J. A., Gerringa, L. J. A., Velzeboer, I., Timmermans, K. R., Buma, A. G. J., and De Baar, H. J. W. (2006b). Iron-binding ligands in Dutch estuaries are not affected by UV induced photochemical degradation. *Mar. Chem.* 100, 11–23.

Rijkenberg, M. J. A., Gerringa, L. J. A., Timmermans, K. R., Fischer, A. C., Kroon, K. J., Buma, A. G. J., Wolterbeek, B. T., and De Baar, H. J. W. (2008a). Enhancement of the reactive iron pool by marine diatoms. *Mar. Chem.* 109, 29–44.

Rijkenberg, M. J. A., Powell, C. F., Dall'osto, M., Nielsdottir, M. C., Patey, M. D., Hill, P. G., Baker, A. R., Jickells, T. D., Harrison, R. M., and Achterberg, E. P. (2008b). Changes in iron speciation following a Saharan dust event in the tropical North Atlantic Ocean. *Mar. Chem.* 110, 56–67.

Rue, E., and Bruland, K. (2001). Domoic acid binds iron and copper: a possible role for the toxin produced by the marine diatom *Pseudo-nitzschia*. *Mar. Chem.* 76, 127–134.

Rue, E. L., and Bruland, K. W. (1995). Complexation of iron(III) by natural organic ligands as determined by a new competitive equilibration/adsorptive cathodic stripping voltammetry method. *Mar. Chem.* 50, 117–139.

Rue, E. L., and Bruland, K. W. (1997). The role of organic complexation on ambient iron chemistry in the Equatorial Pacific Ocean and the response of a mesoscale iron addition experiment. *Limnol. Oceanogr.* 42, 901–910.

Ružic, I. (1982). Theoretical aspects of the direct titration of natural-waters and its information yield for trace-metal speciation. *Anal. Chim. Acta* 140, 99–113.

Sander, S. G., Hunter, K. A., Harms, H., and Wells, M. (2011). Numerical approach to speciation and estimation of parameters used in modeling trace metal bioavailability. *Environ. Sci. Technol.* 45, 6388–6395.

Sander, S. G., and Koschinsky, A. (2011). Metal flux from hydrothermal vents

increased by organic complexation. *Nat. Geosci.* 4, 145–150.

Sarthou, G., Bucciarelli, E., Chever, F., Hansard, S. P., Gonzalez-Davila, M., Santana-Casiano, J. M., Planchon, F., and Speich, S. (2011). Labile Fe(II) concentrations in the Atlantic sector of the Southern Ocean along a transect from the subtropical domain to the Weddell Sea Gyre. *Biogeosciences* 8, 2461–2479.

Sato, M., Takeda, S., and Furuya, K. (2007). Iron regeneration and organic iron(III)-binding ligand production during in situ zooplankton grazing experiment. *Mar. Chem.* 106, 471–488.

Scatchard, G. (1949). The attractions of proteins for small molecules and ions. *Ann. N.Y. Acad. Sci.* 51, 606–672.

Schlosser, C., and Croot, P. L. (2008). Application of cross-flow filtration for determining the solubility of iron species in open ocean seawater. *Limnol. Oceanogr.* 6, 630–642.

Silver, M. W., Bargu, S., Coale, S. L., Benitez-Nelson, C. R., Garcia, A. C., Roberts, K. J., Sekula-Wood, E., Bruland, K. W., and Coale, K. H. (2010). Toxic diatoms and domoic acid in natural and iron enriched waters of the oceanic Pacific. *Proc. Natl. Acad. Sci. U.S.A.* 107, 20762–20767.

Stintzi, A., Barnes, C., Xu, L., and Raymond, K. N. (2000). Microbial iron transport via a siderophore shuttle: a membrane ion transport paradigm. *Proc. Natl. Acad. Sci. U.S.A.* 97, 10691–10696.

Stolpe, B., Guo, L., Shiller, A. M., and Hassellov, M. (2010). Size and composition of colloidal organic matter and trace elements in the Mississippi River, Pearl River and the northern Gulf of Mexico, as characterized by flow field-flow fractionation. *Mar. Chem.* 118, 119–128.

Stolpe, B., and Hassellov, M. (2010). Nanofibrils and other colloidal biopolymers binding trace elements in coastal seawater: significance for variations in element size distributions. *Limnol. Oceanogr.* 55, 187–202.

Strmecki, S., Plavsic, M., Steigenberger, S., and Passow, U. (2010). Characterization of phytoplankton exudates and carbohydrates in relation to their complexation of copper, cadmium and iron. *Mar. Ecol.* 408, 33–46.

Sunda, W., and Huntsman, S. (2003). Effect of pH, light, and temperature on Fe-EDTA chelation and Fe hydrolysis in seawater. *Mar. Chem.* 84, 35–47.

Tagliabue, A., Bopp, L., Aumont, O., and Arrigo, K. R. (2009). Influence of light and temperature on the marine iron cycle: from theoretical to global modeling. *Global Biogeochem. Cycles* 23, 2017.

Tagliabue, A., and Voelker, C. (2011). Towards accounting for dissolved iron speciation in global ocean models. *Biogeosciences* 8, 3025–3039.

Thuroczy, C. E., Gerringa, L. J. A., Klunder, M. B., Middag, R., Laan, P., Timmermans, K. R., and De Baar, H. J. W. (2010). Speciation of Fe in the Eastern North Atlantic Ocean. *Deep Sea Res. Part I Oceanogr. Res. Pap.* 57, 1444–1453.

Tian, F., Frew, R. D., Sander, S., Hunter, K. A., and Ellwood, M. J. (2006). Organic iron(III) speciation in surface transects across a frontal zone: the Chatham Rise, New Zealand. *Mar. Freshw. Res.* 57, 533–544.

Toner, B. M., Fakra, S. C., Manganini, S. J., Santelli, C. M., Marcus, M. A., Moffett, J., Rouxel, O., German, C. R., and Edwards, K. J. (2009). Preservation of iron(II) by carbon-rich matrices in a hydrothermal plume. *Nat. Geosci.* 2, 197–201.

Ussher, S. J., Worsfold, P. J., Achterberg, E. P., Laes, A., Blain, S., Laan, P., and De Baar, H. J. W. (2007). Distribution and redox speciation of dissolved iron on the European continental margin. *Limnol. Oceanogr.* 52, 2530–2539.

Van Den Berg, C. M. G. (1982). Determination of copper complexation with natural organic ligands in seawater by equilibration with MnO_2. I. theory. *Mar. Chem.* 11, 307–322.

van den Berg, C. M. G. (1995). Evidence for organic complexation of iron in seawater. *Mar. Chem.* 50, 139–157.

van den Berg, C. M. G. (2006). Chemical speciation of iron in seawater by cathodic stripping voltammetry with dihydroxynaphthalene. *Anal. Chem.* 78, 156–163.

van der Merwe, P., Lannuzel, D., Nichols, C. A. M., Meiners, K., Heil, P., Norman, L., Thomas, D. N., and Bowie, A. R. (2009). Biogeochemical observations during the winter-spring transition in East Antarctic sea ice: evidence of iron and exopolysaccharide controls. *Mar. Chem.* 115, 163–175.

Velasquez, I., Nunn, B. L., Ibisanmi, E., Goodlet, D. R., Hunter, K. A., and Sander, S. G. (2011). Detection of hydroxamate siderophores in coastal and sub-Antarctic waters off the South Eastern coast of New Zealand. *Mar. Chem.* 126, 97–107.

Vong, L., Laes, A., and Blain, S. (2007). Determination of iron-porphyrin-like complexes at nanomolar levels in seawater. *Anal. Chim. Acta* 588, 237–244.

Vraspir, J., and Butler, A. (2009). Chemistry of marine ligands and siderophores. *Ann. Rev. Mar. Sci.* 1, 43–63.

Wagener, T., Pulido-Villena, E., and Guieu, C. (2008). Dust iron dissolution in seawater: results from a one-year time-series in the Mediterranean Sea. *Geophys. Res. Lett.* 35, L16601.

Weber, L., Volker, C., Schartau, M., and Wolf-Gladrow, D. A. (2005). Modeling the speciation and biogeochemistry of iron at the Bermuda Atlantic Time-series Study site. *Global Biogeochem. Cycles* 19, GB1019.

Wells, M. L., Trick, C. G., Cochlan, W. P., Hughes, M. P., and Trainer, V. L. (2005). Domoic acid: the synergy of iron, copper, and the toxicity of diatoms. *Limnol. Oceanogr.* 50, 1908–1917.

Witter, A. E., Hutchins, D. A., Butler, A., and Luther, G. W. III. (2000). Determination of conditional stability constants and kinetic constants for strong model Fe-binding ligands in seawater. *Mar. Chem.* 69, 1–17.

Witter, A. E., and Luther, G. W. III. (1998). Variation in Fe-organic complexation with depth in the Northwestern Atlantic Ocean as determined using a kinetic approach. *Mar. Chem.* 62, 241–258.

Wu, J., and Luther, G. W. III. (1994). Size fractionated iron concentrations in the water column of the Northwest Atlantic Ocean. *Limnol. Oceanogr.* 39, 1119–1129.

Wu, J., and Luther, G. W. III. (1995). Complexation of iron(III) by natural organic ligands in the Northwest Atlantic Ocean by a competitive ligand equilibration method and a kinetic approach. *Mar. Chem.* 50, 159–179.

Wu, J. F., Boyle, E., Sunda, W., and Wen, L. S. (2001). Soluble and colloidal iron in the oligotrophic North Atlantic and North Pacific. *Science* 293, 847–849.

Xu, G. F., Martinez, J. S., Groves, J. T., and Butler, A. (2002). Membrane affinity of the amphiphilic marinobactin siderophores. *J. Am. Chem. Soc.* 124, 13408–13415.

Ye, Y., Voelker, C., and Wolf-Gladrow, D. A. (2009). A model of Fe speciation and biogeochemistry at the Tropical Eastern North Atlantic Time-Series Observatory site. *Biogeosciences* 6, 2041–2061.

Yoshida, M., Kuma, K., Iwade, S., Isoda, Y., Takata, H., and Yamada, M. (2006). Effect of aging time on the availability of freshly precipitated ferric hydroxide to coastal marine diatoms. *Mar. Biol.* 149, 379–392.

Conflict of Interest Statement: The authors declare that the research was conducted in the absence of any commercial or financial relationships that could be construed as a potential conflict of interest.

Received: 14 November 2011; accepted: 09 February 2012; published online: 28 February 2012.

Citation: Gledhill M and Buck KN (2012) The organic complexation of iron in the marine environment: a review. Front. Microbio. ***3****:69. doi: 10.3389/fmicb.2012.00069*

This article was submitted to Frontiers in Microbiological Chemistry, a specialty of Frontiers in Microbiology.

Copyright © 2012 Gledhill and Buck. This is an open-access article distributed under the terms of the Creative Commons Attribution Non Commercial License, which permits non-commercial use, distribution, and reproduction in other forums, provided the original authors and source are credited.

frontiers in
MICROBIOLOGY

REVIEW ARTICLE
published: 15 February 2012
doi: 10.3389/fmicb.2012.00050

Molecular underpinnings of Fe(III) oxide reduction by *Shewanella oneidensis* MR-1

***Liang Shi*[1]*, *Kevin M. Rosso*[1], *Tomas A. Clarke*[2], *David J. Richardson*[2], *John M. Zachara*[1] and *James K. Fredrickson*[1]**

[1] *Pacific Northwest National Laboratory, Richland, WA, USA*
[2] *University of East Anglia, Norwich, UK*

Edited by:
David Emerson, Bigelow Laboratory for Ocean Sciences, USA

Reviewed by:
Jeffrey A. Gralnick, University of Minnesota, USA
Joel Weiner, University of Alberta, Canada

***Correspondence:**
Liang Shi, Microbiology Group, Pacific Northwest National Laboratory, 902 Battelle Blvd., P.O. Box 999, Richland, WA, USA.
e-mail: liang.shi@pnnl.gov

In the absence of O_2 and other electron acceptors, the Gram-negative bacterium *Shewanella oneidensis* MR-1 can use ferric [Fe(III)] (oxy)(hydr)oxide minerals as the terminal electron acceptors for anaerobic respiration. At circumneutral pH and in the absence of strong complexing ligands, Fe(III) oxides are relatively insoluble and thus are external to the bacterial cells. *S. oneidensis* MR-1 and related strains of metal-reducing *Shewanella* have evolved machinery (i.e., metal-reducing or Mtr pathway) for transferring electrons from the inner-membrane, through the periplasm and across the outer-membrane to the surface of extracellular Fe(III) oxides. The protein components identified to date for the Mtr pathway include CymA, MtrA, MtrB, MtrC, and OmcA. CymA is an inner-membrane tetraheme *c*-type cytochrome (*c*-Cyt) that belongs to the NapC/NrfH family of quinol dehydrogenases. It is proposed that CymA oxidizes the quinol in the inner-membrane and transfers the released electrons to MtrA either directly or indirectly through other periplasmic proteins. A decaheme *c*-Cyt, MtrA is thought to be embedded in the trans outer-membrane and porin-like protein MtrB. Together, MtrAB deliver the electrons through the outer-membrane to the MtrC and OmcA on the outmost bacterial surface. MtrC and OmcA are the outer-membrane decaheme *c*-Cyts that are translocated across the outer-membrane by the bacterial type II secretion system. Functioning as terminal reductases, MtrC and OmcA can bind the surface of Fe(III) oxides and transfer electrons directly to these minerals via their solvent-exposed hemes. To increase their reaction rates, MtrC and OmcA can use the flavins secreted by *S. oneidensis* MR-1 cells as diffusible co-factors for reduction of Fe(III) oxides. Because of their extracellular location and broad redox potentials, MtrC and OmcA can also serve as the terminal reductases for soluble forms of Fe(III). In addition to Fe(III) oxides, Mtr pathway is also involved in reduction of manganese oxides and other metals. Although our understanding of the Mtr pathway is still far from complete, it is the best characterized microbial pathway used for extracellular electron exchange. Characterizations of the Mtr pathway have made significant contributions to the molecular understanding of microbial reduction of Fe(III) oxides.

Keywords: dissimilatory Fe(III) oxide reduction, *Shewanella oneidensis* MR-1, extracellular electron transfer pathway, *c*-type cytochromes with multiple hemes, molecular biology

INTRODUCTION

The Gram-negative bacterium *Shewanella oneidensis* MR-1 can use ferric [Fe(III)] (oxy)(hydr)oxide minerals as the terminal electron acceptors for anaerobic respiration [i.e., dissimilatory Fe(III) reduction] (Myers and Nealson, 1990). Dissimilatory reduction of Fe(III) oxides by microorganisms plays a critical role in the biogeochemical cycle of Fe (Weber et al., 2006). At circumneutral pH and in the absence of strong complexing ligands, Fe(III) oxides are usually sparingly soluble in water and their redox potentials vary, which depend on their phases and range from −300 to 0 mV (Thamdrup, 2000). Because of their insolubility in water, Fe(III) oxides are unable to cross the bacterial outer-membrane to the periplasm and the cytoplasmic or inner-membrane where the bacterial terminal reductases are usually located. To overcome this physical barrier, *S. oneidensis* MR-1 and other metal-reducing *Shewanella* have developed the ability to transfer electrons from the inner-membrane where electrons are accumulated from bacterial metabolic activity to the bacterial cell surface where reduction of Fe(III) oxides occurs. Gene inactivation and subsequent phenotypic analyses of *S. oneidensis* MR-1 mutants have identified several proteins directly involved in this electron transfer system. These include four *c*-type cytochromes (*c*-Cyts) CymA, MtrA, MtrC, and OmcA and a trans outer-membrane and porin-like protein MtrB (**Table 1**; Myers and Myers, 1997a,b, 2002; Beliaev and Saffarini, 1998; Beliaev et al., 2001; Lies et al., 2005; Gorby et al., 2006; Bretschger et al., 2007; Coursolle and Gralnick, 2010; Reardon et al., 2010). Together, they form a pathway (i.e., Mtr pathway) through which electrons move from the quinone/quinol

Table 1 | Identified protein components of Mtr pathway.

Name	Locus tag	Number of heme	Location
CymA	SO_4591	4	Inner-membrane
MtrA	SO_1777	10	Outer-membrane
MtrB	SO_1776	0	Outer-membrane
MtrC	SO_1778	10	Outer-membrane
OmcA	SO_1779	10	Outer-membrane

pool in the inner-membrane, through the periplasm and across the outer-membrane to the surface of Fe(III) oxides (for recent reviews, see Richardson, 2000; Shi et al., 2007, 2009; Fredrickson and Zachara, 2008; Fredrickson et al., 2008). Investigation of the Mtr pathway not only has advanced our understanding of molecular mechanisms by which microbial cells transfer electrons to the external environment, such as for the reduction of Fe(III) minerals, but also will enable improved applications of *S. oneidensis* MR-1 and other metal-reducing *Shewanella* in microbial fuel cells and for electrobiosynthesis of valuable bio-materials (Hau and Gralnick, 2007; Fredrickson et al., 2008; Ross et al., 2011).

In *S. oneidensis* MR-1, the genes encoding MtrABC and OmcA are clustered in a sequential order of *omcA-mtrC-mtrA-mtrB*. Comparative analysis of the genomes of 19 metal-reducing *Shewanella* strains reveals that *mtrC-mtrA-mtrB* genes are well conserved, while *omcA* is sometimes replaced by *undA* or *undA1*, the genes predicted to encode 11-heme *c*-Cyts (Fredrickson et al., 2008; Shi et al., 2011). PCR analysis of seven metal-reducing *Shewanella* strains isolated from the Hanford Reach of the Columbia River also indicates that all tested strains possess an *mtrC* homolog, while three strains have an *omcA* homolog, and the remaining four strains contain an *undA1* homolog. Thus, essentially all characterized metal-reducing *Shewanella* strains contain *mtr* and related genes that are originally identified from *S. oneidensis* MR-1 (Shi et al., 2011). *S. oneidensis* MR-1 and other metal-reducing *Shewanella* are key contributors to metal redox cycling in energy-rich gradient environments where electron acceptor type and availability, including Fe(III) and Mn oxides, vary spatially and temporally (Nealson and Scott, 2003). The respiratory versatility enabled by the Mtr pathway allows *Shewanella* to effectively compete with other microorganisms in environments where such solid-phase electron acceptors are common. In addition to Fe(III) oxide reduction, MtrAB homologs are also involved in the electron transfer reactions for extracellular reduction of dimethylsulfoxide (DMSO) by *S. oneidensis* MR-1 and extracellular Fe(II) oxidation by *Rhodopseudomonas palustris* TIE-1 (Gralnick et al., 2006; Jiao and Newman, 2007). A survey of recently finished genomes of the Fe(II)-oxidizing bacteria *Gallionella ferruginea* ES-2 and *Sideroxydans lithotrophicus* ES-1 reveals that each genome has a pair of *mtrAB* homologs that are clustered together, indicating that MtrAB homologs may also be widely employed by the Gram-negative bacteria for extracellular Fe(II) oxidation (L. Shi, personal observation).

Shewanella oneidensis MR-1 secretes water-soluble molecules that function either as electron shuttles or Fe(III) complexing ligands to enhance Fe(III) oxide reduction (Marsili et al., 2008; von Canstein et al., 2008; Jones et al., 2010). Non-biogenic organic shuttle molecules, such as anthraquinone disulfonate, are also well known to accelerate Fe(III) oxide reduction rates (Zachara et al., 1998), in part because of thermodynamically accessible redox potentials, and in part because of intrinsically fast electron transfer kinetics (Rosso et al., 2004). Quinones and molecules bearing quinone moieties have been shown to be particularly efficient electron transfer mediators to Fe(III) oxides (Stack et al., 2004). These molecules exert or are thought to exert their roles in Fe(III) oxide reduction by working in concert with the Mtr pathway (Ross et al., 2009; Shi et al., 2009; Coursolle and Gralnick, 2010; Jones et al., 2010). Extracellular appendages or nanowires are also observed to be associated with *S. oneidensis* MR-1 cells where they are believed to be involved in Fe(III) oxide reduction. Key components of the Mtr pathway, such as MtrC and OmcA, have been implicated as important electron transfer proteins in the *Shewanella* nanowires (Gorby et al., 2006; El-Naggar et al., 2008, 2010). This review focuses on our current understandings of functional roles of the identified protein components of the Mtr pathway in the electron transfer reactions during extracellular Fe(III) oxide reduction by *S. oneidensis* MR-1.

CymA IS THE ENTRY POINT OF THE Mtr PATHWAY

Tetraheme *c*-Cyt CymA is a member of the NapC/NrfH family of quinol dehydrogenases that are critical for quinol oxidation during bacterial anaerobic respiration (Simon and Kern, 2008). In addition to Fe(III) oxide reduction, CymA is also required for reducing DMSO, fumarate, nitrate, and nitrite by *S. oneidensis* MR-1 and for reducing arsenate by *Shewanella* sp. strain ANA-3 and *S. putrefaciens* CN-32 (Myers and Myers, 1997a; Schwalb et al., 2003; Murphy and Saltikov, 2007). The N-terminal region of CymA polypeptide contains a single trans-membrane domain that anchors CymA to the inner-membrane, and the rest of the CymA polypeptide covalently binds four heme groups and protrudes into the periplasm. The periplasmic portion of CymA ($CymA_{sol}$) can reduce DMSO, fumarate, and nitrite *in vivo* (Schwalb et al., 2003). Likewise, purified $CymA_{sol}$ transfers electrons directly to the fumarate reductase FccA of *S. oneidensis* MR-1 with an apparent second-order rate constant of $19\,\mu M^{-1}\,s^{-1}$ (Schwalb et al., 2003). $CymA_{sol}$ has a broad redox potential ranging from ~ -350 to ~ 0 mV vs. the standard hydrogen electrode (SHE), which is similar to the redox potential measured for the membrane-bound CymA of *S. frigidimarina* NCIMB400 (Field et al., 2000; Firer-Sherwood et al., 2008). Like other members of the NapC/NrfH family of quinol dehydrogenases, CymA is believed to oxidize quinol in the inner-membrane and transfer the released electrons to redox proteins located in the periplasm. Purified CymA of *S. frigidimarina* NCIMB400 indeed can be reduced by duroquinol and menaquinol *in vitro* (Field et al., 2000). Structural determination of NrfH of *Desulfovibrio vulgaris*, which is the only available molecular structure for the NapC/NrfH family of quinol dehydrogenases, reveals that quinol binds in a pocket adjacent to the heme 1 of NrfH of *D. vulgaris*, where quinol oxidation occurs (Rodrigues et al., 2006, 2008). Heme 1 of NrfH of *D. vulgaris* is unique in terms of its coordination. Its proximal axial ligand is a methionine residue (Met49) that is two residues downstream from the histidine residue of the CX_2CH motif for binding of heme 1, and an aspartate residue (Asp89) is at the position usually

occupied by the distal axial ligand. However, Asp89 is not used for heme coordination; rather, it binds quinol (Rodrigues et al., 2006, 2008). Consequently, heme 1 of NrfH of *D. vulgaris* is a single methionine-coordinated, high-spin heme (Rodrigues et al., 2006). In contrast to NrfH of *D. vulgaris*, neither Met49 nor Asp89 is conserved in the CymA of *S. oneidensis* MR-1. In fact, purified CymA of *S. frigidimarina* NCIMB400 contains four low-spin hemes each of which is most likely coordinated in the axial positions by two histidine residues (Field et al., 2000). Thus, it is still unclear how CymA binds and oxidizes quinol at the molecular-level.

Unlike NrfH of *D. vulgaris* that forms a stable complex with NrfA, the interactions between CymA and its redox partners in the periplasm appear weak because CymA can be easily purified to homogeneity from *S. frigidimarina* NCIMB400 (Field et al., 2000; Rodrigues et al., 2006, 2008). The apparent transient nature of the protein–protein interactions between CymA and its redox partners in the periplasm may be attributed to the fact that CymA interacts with different periplasmic proteins, such as NrfA and FccA, depending on the nature of the terminal electron acceptors. Weak interactions would permit CymA considerable flexibility with regards to its binding partners in response to electron acceptors. Periplasmic proteins small tetraheme cytochrome (STC, also known as CctA), MtrA, and FccA are all proposed to receive electrons from CymA during Fe(III) oxide reduction (Ross et al., 2007; Shi et al., 2007; Schuetz et al., 2009). *In vivo* chemical cross-linking, however, fails to detect any physical interaction between CymA and STC or MtrA (Ross et al., 2007). *In vitro,* direct electron transfer has been demonstrated between CymA and MtrA, FccA, or STC and between MtrA and FccA, but not between STC and MtrA (Schwalb et al., 2003; Schuetz et al., 2009; Firer-Sherwood et al., 2011b). Investigation of reverse electron transfer reactions from electrode surfaces through the Mtr pathway to the periplasmic FccA suggests that electron transfer between MtrA and FccA is facilitated by CymA, while direct electron transfer from MtrA to FccA is minimal (Ross et al., 2011). Furthermore, deletion of *cctA* or *fccA* has little impact on Fe(III) oxide reduction by *S. oneidensis* MR-1 (Schuetz et al., 2009; Coursolle and Gralnick, 2010). Collectively, all these results suggest that neither STC nor FccA play a major role in mediating electron transfer between CymA and MtrA during extracellular reduction of Fe(III) oxides.

Survey of the genome of the neutrophilic Fe(II)-oxidizing bacterium *S. lithotrophicus* ES-1 identifies a *cymA* homolog located next to a pair of *mtrAB* homologs, *mtoAB*, in a sequential order of *mtoA-mtoB-cymA*. This finding raises a possibility that CymA homolog may also be involved in Fe(II) oxidation, in which it may serve as a quinone reductase.

MtrA AND MtrB TRANSLOCATE THE ELECTRONS ACROSS THE OUTER-MEMBRANE TO THE MtrC AND OmcA LOCATED OUTSIDE OF BACTERIAL CELLS

MtrA can be purified, following overexpression, from either *S. oneidensis* MR-1 or *Escherichia coli*. Purified MtrA contains 10 low-spin hemes with a redox potential ranging from −400 to −100 mV vs. SHE (Pitts et al., 2003; Shi et al., 2005; Firer-Sherwood et al., 2008, 2011b). *In vivo* cross-linking with formaldehyde indicates a physical interaction between MtrA and MtrB (Ross et al., 2007). When Triton X-100 is used as a solubilizing reagent, MtrABC can be isolated as a protein complex with a stoichiometry of 1:1:1 (Ross et al., 2007; Hartshorne et al., 2009). The purified MtrABC complex can transfer electrons across a lipid bilayer following incorporation into proteoliposomes, providing direct evidence that together, MtrABC serve as an electron conduit between the periplasm of *S. oneidensis* MR-1 cells and its extracellular environments (Hartshorne et al., 2009). Consistent with these results, heterologous co-expression of MtrABC enables *E. coli* to reduce solid-phase Fe(III) oxides (Jensen et al., 2010). Furthermore, while MtrAB can form a stable complex in the absence of MtrC, an MtrBC complex cannot be isolated in the absence of MtrA. When MtrB is present, MtrA only associates with the bacterial membrane, presumably with MtrB that spans the outer-membrane. Measurement by sedimentation equilibrium indicates a high binding affinity ($K_d < 0.1\ \mu M$) between MtrAB and MtrC. Based on these findings, it is proposed that MtrB is a trans outer-membrane spanning β-barrel protein that serves as a sheath to embed MtrA in the membrane where MtrAB form a trans outer-membrane delivery module for transferring electrons to MtrC, which functions as an extracellular reductase (Hartshorne et al., 2009). This is the first molecular model of electron transfer across the bacterial outer-membrane, which we hypothesize will apply more broadly to a number of bacterial genera that either gain energy by oxidizing extracellular substrates, such as Fe(II), or reducing compounds such as DMSO as part of anaerobic respiration (Hartshorne et al., 2009).

MtrA contains a signal peptide that targets the synthesized polypeptide to the periplasm via the bacterial Sec system. The MtrA polypeptides can be divided into two pentaheme domains, each of which shares sequence similarity with NrfB of *E. coli* (Beliaev and Saffarini, 1998; Clarke et al., 2007, 2008). When it is expressed in *E. coli*, the truncated MtrA with only one of its pentaheme domains is folded properly and possesses five hemes, providing experimental evidence that MtrA contains two repetitive functional domains (Clarke et al., 2008). The molecular structure of NrfB of *E. coli* has been determined and contains five closely packed hemes (<6 Å between neighboring hemes) with a maximal edge to edge distance of 40 Å. This type of heme arrangement permits rapid electron transfer among the heme groups of NrfB that form a molecular wire (**Figure 1**; Clarke et al., 2007, 2008). The heme groups NrfH of *D. vulgaris* are also closely packed in a nearly linear array with a maximal edge to edge distance of 13 Å (Rodrigues et al., 2006). Based on the structures of NrfB of *E. coli* and NrfH of *D. vulgaris*, one could speculate that the heme groups of MtrA may also form a molecular wire that could be 80 Å long, while those in CymA may form a 13-Å-long molecular wire. Consistent with this idea, measurements with small angle X-ray scattering show that MtrA adapts to a flat elongated shape with overall dimensions of 104 Å × 20 Å × 50 Å (Firer-Sherwood et al., 2011a). Because MtrB is thought to be a porin-like protein with an estimated pore size that is >30 Å × 40 Å, MtrA can, in principle, be embedded at least partially in MtrB (Firer-Sherwood et al., 2011a).

Given that the thickness of the Gram-negative bacterial outer-membrane is ∼70 Å (or 7 nm; Matias et al., 2003), the estimated length of MtrA is sufficient for transferring electrons heme-to-heme across the entire outer-membrane. However, the periplasmic width of *S. oneidensis* MR-1 is 235 ± 37 Å (Dohnalkova et al.,

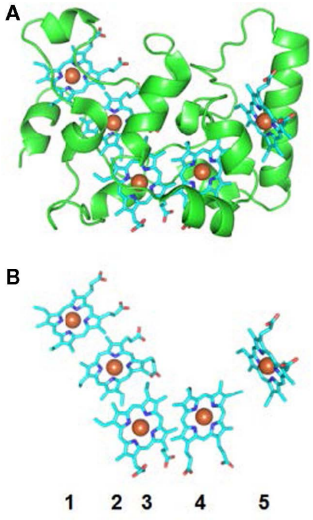

FIGURE 1 | Molecular structure of NrfB of *E. coli*. (A) Crystal structure of NrfB (PDB-ID: 2OZY) showing the peptide chain (green) and hemes (Blue). **(B)** Arrangement of NrfB hemes shown in the same orientation as panel **(A)**. The hemes are numbered according to the position of their corresponding CXXCH binding motif in the NrfB amino acid sequence.

2011), too great a distance for a pair of MtrA and CymA to bridge. Additional periplasmic redox proteins thus appear to be necessary for conducting electrons between CymA in the inner-membrane and MtrA in the outer-membrane. The periplasmic redox protein involved in this aspect of electron transfer chain, however, has not been identified. As discussed in the previous section, STC and FccA, two of the most abundant redox proteins in the periplasm of *S. oneidensis* MR-1, do not appear to mediate electron transfer between CymA and MtrA. Given that NrfH of *D. vulgaris* (i.e., a CymA homolog) and NrfB of *E. coli* (i.e., an MtrA homolog) all physically interact with NrfA, and that heterologously expressed MtrA of *S. oneidensis* MR-1 exchanges electrons with the NrfA in *E. coli* (Pitts et al., 2003), it seems possible that NrfA may conduct the electrons between CymA and MtrA during Fe(III) oxide reduction (Shi et al., 2007). Alternatively, CymA may be localized in the periplasmic regions that are sufficiently close enough for direct electron transfer between CymA and MtrA as demonstrated *in vitro* (Matias et al., 2003; Schuetz et al., 2009; Firer-Sherwood et al., 2011b).

MtrC AND OmcA ARE THE TERMINAL REDUCTASES OF Fe(III) OXIDES

MtrC and OmcA are two outer-membrane *c*-Cyts located on the bacterial surface where they are translocated across the outer-membrane by the bacterial type II secretion system (DiChristina et al., 2002; Myers and Myers, 2003; Donald et al., 2008; Shi et al., 2008; Lower et al., 2009; Reardon et al., 2010). Following expression in *S. oneidensis* MR-1, OmcA is co-isolated with MtrC when they are solubilized with *n*-octyl-β-D-glucopyranoside. *In vitro* characterization shows that purified MtrC and OmcA form a stable complex ($K_d < 500$ nM) with a stoichiometry of 1: 2 (Shi et al., 2006). Subsequent *in vivo* cross-linking with different chemical reagents consistently demonstrates that MtrC and OmcA physically interact with each other on the bacterial cells (Ross et al., 2007; Tang et al., 2007; Zhang et al., 2008, 2009). The physical interaction between MtrC and OmcA synergistically enhances the metal reductase activity of MtrC and OmcA (Shi et al., 2006).

Purified MtrC and OmcA, each of which contains 10 hemes, show broad redox potentials ranging from −400 to 100 mV vs. SHE and −320 to −20 mV vs. SHE, respectively (Shi et al., 2006; Hartshorne et al., 2007; Firer-Sherwood et al., 2008). Both UV–visible spectropotentiometric titrations and electron paramagnetic resonance (EPR) analyses show that MtrC has only low-spin hemes (Hartshorne et al., 2007), while EPR measurement reveals at least one high-spin heme in OmcA, although UV–visible spectropotentiometric titrations fail to detect it (Bodemer et al., 2010). Scanning tunneling microscopy and tunneling spectroscopy show that MtrC and OmcA immobilized on gold surfaces have distinct current–voltage (*I–V*) tunneling spectra at the single-molecule level (Wigginton et al., 2007a,b). Theoretical interpretation of their *I–V* spectra suggest that MtrC and OmcA possess different electron transfer properties, related to apparent participation of MtrC hemes with redox potentials between −81 and −365 mV vs. SHE, whereas for OmcA no heme participation is detectable by single-molecule tunneling spectroscopy. It is proposed that in this measurement, conductance is through the peptide backbone of OmcA (Wigginton et al., 2007a). However, in other measurements, the heme groups of OmcA are involved in electron transfer to metal ions (Shi et al., 2006; Xiong et al., 2006; Borloo et al., 2007; Marshall et al., 2008; Wang et al., 2008; Ross et al., 2009; Reardon et al., 2010). These different results can probably be attributed to the different methods used for the measurements. Nevertheless, all these measurements consistently show that MtrC and OmcA possess different electron transfer properties (Marshall et al., 2006, 2008; Shi et al., 2006; Borloo et al., 2007; Wigginton et al., 2007b; Wang et al., 2008; Reardon et al., 2010; Belchik et al., 2011). The distinct electron transfer properties observed for MtrC and OmcA suggest different physiological roles for these *c*-Cyts during metal reduction (Shi et al., 2006; Wigginton et al., 2007b).

Interactions between purified MtrC or OmcA and Fe(III) oxides have been extensively investigated using a variety of methods. Analyses with co-sedimentation and fluorescence correlation spectroscopy show that OmcA binds hematite (α-Fe_2O_3) directly with a partition coefficient of $\sim 2 \times 10^5$ ($\Delta G^{0'} = -28$ kJ/mol), which corresponds to 10^{14} OmcA molecules per cm^2 of hematite (Xiong et al., 2006). Similar binding affinity to hematite is also observed for OmcA using neutron reflectometry (Johs et al., 2010). Atomic force microscopy measurements reveal that MtrC and OmcA bind hematite with distinct force characteristics. The binding strength of OmcA to hematite is approximately twice that for MtrC, while the binding frequency of MtrC to hematite is twice that for OmcA (Lower et al., 2007). Measured force signatures with purified MtrC and OmcA also correlate well with those measured with intact cells (Lower et al., 2001), a finding that supports the direct electron transfer to Fe(III) oxide by MtrC and OmcA (Lower et al., 2007). Screening with phage-display technology identifies a polypeptide with a conserved hematite-binding motif of Ser/Thr-hydrophobic/aromatic-Ser/Thr-Pro-Ser/Thr. Molecular dynamics simulation with Ser-Pro-Ser polypeptide and hematite suggests

that Ser-Pro-Ser peptide binds hematite via the hydrogen bonds formed between the two serine residues and hydroxylated hematite surface, while the proline residue helps stabilize the binding by limiting the peptide flexibility. The putative hematite-binding motif of Thr-Pro-Ser/Thr is found close to heme 10 of both MtrC and OmcA polypeptides (Lower et al., 2008).

Measurements with spectroscopy and protein film voltammetry consistently show that purified MtrC and OmcA transfer electrons directly to hematite with the rate constants ranging from 0.025 to 63.5 s^{-1} (Xiong et al., 2006; Eggleston et al., 2008; Meitl et al., 2009). Most important, the voltammograms of purified MtrC and OmcA on hematite electrodes are very similar to those of the *S. oneidensis* MR-1 cells expressing only the corresponding outer-membrane *c*-Cyt, suggesting that MtrC and OmcA on the bacterial surface exchange electrons directly with hematite (Meitl et al., 2009). Furthermore, MtrC and OmcA are co-localized with hematite and secondary mineral phases after ferrihydrite reduction by *S. oneidensis* MR-1 and *E. coli* cells with heterologously expressed MtrABC reduce solid-phase Fe(III) oxide in the absence of any mediators such as flavins (Lower et al., 2009; Jensen et al., 2010; Reardon et al., 2010). Taken together, these results demonstrate that MtrC and OmcA are the terminal reductases that bind and reduce Fe(III) oxides directly.

Compared to measurements with intact cells and the total membrane fraction, purified MtrC and OmcA reduce goethite [α-FeO(OH)] at much slower rates. Addition of flavin, however, increases the rates comparable to those measured with intact cells and the total membrane fraction. Further investigations show that OmcA reduces flavins much faster than flavins reduce goethite, suggesting an electron shuttle role for flavins during MtrC- and OmcA-mediated reduction of Fe(III) oxides (Ross et al., 2009). Consistent with this suggestion, the Mtr pathway is required for *in vivo* reduction of flavins by *S. oneidensis* MR-1 cells (Coursolle et al., 2010).

Recent determination of the molecular structure of MtrF, an MtrC homolog, at a resolution of 3.2 Å has provided the unprecedented molecular structural evidence supporting the terminal reductase role for the outer-membrane *c*-Cyts of *S. oneidensis* MR-1 in Fe(III) oxide reduction (Clarke et al., 2011). Results show that MtrF is folded into four distinct domains: domains I (aa 49–186) and III (aa 319–473) each contains seven anti-parallel β-strands folded together to form a split-β barrel structure, while domains II (aa 187–318) and IV (aa 474–641) each bind five tightly packed hemes (**Figure 2A**). The four domains fold together so that the pentaheme domains II and IV are packed to form a central core with the two split-β barrel domains I and III flanking either side. This organizes 10 hemes of MtrF into a unique "wire cross," in which a staggered 65-Å octaheme chain (hemes 10, 9, 8, 6, 1, 3, 4, 5) transects the length of the protein through domains IV and II and is crossed at the middle by a 45-Å tetraheme chain (hemes 2, 1, 6, 7) that connects the two split β-barrel domains I and III. This "wire cross" is made up of a lower order organization of two triads of parallel hemes (hemes 3, 4, 5 and hemes 8, 9, 10) that lie perpendicular to a quartet of parallel hemes. Each heme is within 7 Å of its nearest neighbor(s), permitting rapid electron transfer among the hemes (**Figure 2B**). It is proposed that domain II interacts with solid-phase Fe(III) oxides by transferring electrons directly to the oxides via the solvent-exposed heme 5. Domain I and III are thought to be involved in binding and reduction of flavins and soluble metals such as chelated Fe(III), while domain IV is predicted to physically interact with the MtrDE (MtrAB homologs) complex and exchange electrons with MtrD via heme 10 (Clarke et al., 2011). It should be noted that the functional roles of domain II and IV of MtrF are interchangeable and that the overall shape of MtrF is very similar to that of OmcA (Johs et al., 2010; Clarke et al., 2011); the latter suggests that MtrF and OmcA may fold similarly. Like MtrC and OmcA, MtrF also reduces Fe(III) oxides and flavins (Coursolle and Gralnick, 2010; Clarke et al., 2011). Thus, the structural characteristics of MtrF support the notion that bacterial surface-localized *c*-Cyts MtrC, MtrF, and OmcA transfer electrons directly to the surface of Fe(III) oxides via their solvent-exposed hemes, such as heme 5 or 10 of MtrF. They also support the notion that, in order to enhance their reaction rates, these *c*-Cyts also use flavins secreted by *S. oneidensis* MR-1 cells as diffusible co-factors (i.e., shuttles) for reduction of Fe(III) oxides. Because of the direct binding of the *c*-Cyts to the Fe(III) oxides, the distance that flavins diffuse between the putative flavin-reducing sites in the *c*-Cyts and the surface of Fe(III) oxide can be very short [∼20 Å between MtrF and Fe(III) oxide], which makes the shuttle-mediated electron transfer efficient. Given that they physically interact with each other *in vivo*, MtrC and OmcA may exchange electrons through diffusible flavins. MtrC, MtrF, and OmcA also reduce soluble Fe(III) complexed with different ligands (Shi et al., 2006; Borloo et al., 2007; Wang et al., 2008; Ross et al., 2009; Bucking et al., 2010; Coursolle and Gralnick, 2010; Clarke

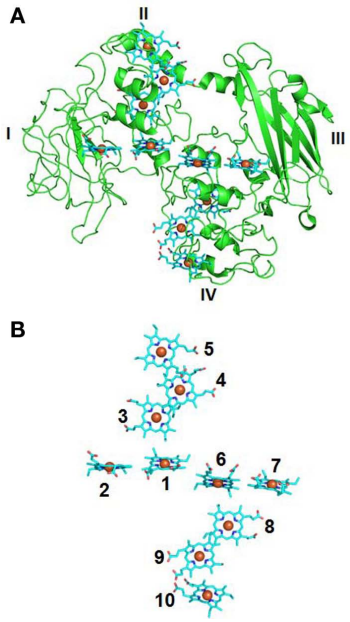

FIGURE 2 | Molecular structure of MtrF of *S. oneidensis* MR-1. (A) Crystal structure of MtrF (PDB-ID: 3PMQ) showing the peptide chain (green) and hemes (Blue). Domains I–IV are labeled. **(B)** Arrangement of MtrF hemes shown in the same orientation as panel **(A)**. The hemes are numbered according to the position of their corresponding CXXCH binding motif in the MtrF amino acid sequence.

et al., 2011). Reduction of chelated Fe(III) by MtrC, MtrF, and OmcA, in principle, also occurs via their solvent-exposed hemes as well as the hemes adjacent to the flavin-binding domains (i.e., hemes 2 and 7 of MtrF).

Despite the detailed structural and electrochemical spectroscopic information becoming available for outer-membrane *c*-Cyts, the electron transfer step from hemes to shuttle molecules, such as flavins, or directly to terminal electron acceptors, such as Fe(III) oxide itself, remains difficult to isolate. Although solvent exposure of hemes is suggestive of a possible role as an interfacial electron transfer mediator (i.e., input or output redox site), many conditions must be met at the molecular scale for this process to be usefully efficient to the organism. Indeed, solvent exposure to an aqueous environment often intrinsically reduces heme electron transfer efficiency compared to that fully embedded within the protein; a higher reorganization energy and thus higher activation energy is associated with repolarizing a high dielectric medium, such as water, to move an electron from water-exposed donor heme to a water-solvated acceptor species (Marcus and Sutin, 1985). Exclusion of water between *c*-Cyts and an Fe(III) oxide surface is demonstrated with computational molecular simulation to be necessary to reduce both the reorganization energy and the interfacial electron transfer distance between heme groups of STC and Fe(III) sites in the oxide surface (Kerisit et al., 2007). It shows that STC docks with a solvent-exposed heme in direct contact to a hematite (001) surface in 89% of the approach simulations, but the frequency of specific heme contact does not correlate with solvent exposure but rather the formation of covalent bonds to the surface via heme proprionate groups. Furthermore, it is shown that heme-surface encounter orientations involving the porphyrin plane at ∼90° with respect to the surface plane, along with heme Fe to surface Fe distances of 9–10 Å, enable interfacial electron transfer rates consistent with overall macroscopic rates measured by protein film voltammetry.

In addition to bacterial cell surfaces, MtrC and OmcA are found to be associated with extracellular polymeric substances (EPS) where they are directly associated with hematite as well as U(IV)O_2 and Fe(II)-containing secondary mineral phases presumably because these are the sites for reducing U(VI) and ferrihydrite, respectively (Marshall et al., 2006; Lower et al., 2009; Reardon et al., 2010). Likewise, MtrC and OmcA are released to the growth medium and are also involved in the formation of chromium [Cr(III)] precipitates that are found in the extracellular matrix following reduction of Cr(VI) by *S. oneidensis* MR-1 (Shi et al., 2008; Belchik et al., 2011). Global proteomic and Western blot analyses show that the homologs of MtrC and OmcA are the key components of the bound and loosely associated EPS isolated from the biofilm of the metal-reducing bacterium *Shewanella* sp HRCR-1 (Cao et al., 2011b). Interestingly, while an MtrB homolog was present in the isolated EPS, no MtrA homolog was detected (Cao et al., 2011b). MtrC and OmcA homologs in these isolated EPS are also implicated in U(VI) reduction (Cao et al., 2011a). These results suggest that after they are released from the bacterial cell surface, MtrB, MtrC, and OmcA may not be in association with MtrA. Although their roles in Fe(III) oxide reduction and their relationship with *Shewanella* nanowires and the outer-membrane vesicles are currently uncharacterized, it is proposed that EPS-associated MtrC, OmcA, and probably MtrB may be part of non-local electron transfer strategy used by *S. oneidensis* MR-1 for reduction of the Fe(III) oxide minerals distant from the bacterial cell surface (Rosso et al., 2003; Gorby et al., 2008; Bose et al., 2009; Lower et al., 2009).

CONCLUDING REMARKS

Recent *in vivo* and especially *in vitro* characterizations of Mtr and related proteins of *S. oneidensis* MR-1 have significantly advanced our understanding of the molecular mechanisms by which bacteria reduce Fe(III) oxides. These proteins, most of which are *c*-Cyts with multiple hemes, are strategically positioned along the width of the bacterial envelope. Through protein–protein interactions, they form a pathway for electron conductance across entire bacterial cell envelope to the surface of Fe(III) oxides. The electron conductance is mediated mainly by the heme groups of the *c*-Cyts. The quinol in the inner-membrane is believed to be oxidized by the heme 1 of CymA. Released electrons most likely

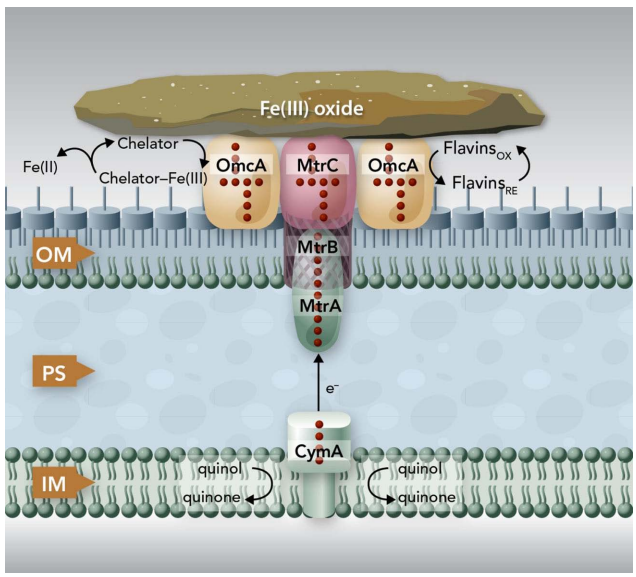

FIGURE 3 | The proposed Mtr extracellular electron transfer pathway of *S. oneidensis* MR-1. The protein components identified to date for the Mtr pathway include CymA, MtrA, MtrB, MtrC, and OmcA. CymA is a tetraheme *c*-Cyt that belongs to the NapC/NrfH family of quinol dehydrogenases. Through its N-terminal region, CymA is anchored in the inner-membrane (IM) where it oxidizes quinol in the IM and transfers the released electrons to MtrA in the outer-membrane (OM) either directly or indirectly via other periplasmic proteins. MtrA is a decaheme *c*-Cyt that is thought to be embedded in MtrB, a trans OM, and porin-like protein. Together, MtrAB facilitate the electron transfer across the OM to the MtrC and OmcA on the bacterial surface. Both MtrC and OmcA are the OM decaheme *c*-Cyts that are translocated across the OM by the bacterial type II secretion system. MtrC and OmcA are the terminal reductases that bind the surface of Fe(III) oxides and transfer electrons directly to the oxides via their solvent-exposed hemes. To increase their reaction rates, MtrC and OmcA use flavins secreted by the *S. oneidensis* MR-1 cells as diffusible co-factors or shuttles for Fe(III) oxide reductions. MtrC and OmcA can also serve as the terminal reductases for the Fe(III) solubilized from the Fe(III) oxides by the Fe(III)-complexing ligands secreted from the *S. oneidensis* MR-1 cells. The sizes of the components depicted are not drawn to the scale.

move along the heme groups of CymA. Through the heme 4, CymA transfers the electrons to MtrA either directly or indirectly via other periplasmic proteins. Inserted into the trans outer-membrane porin formed by MtrB, MtrA transfers electron across the outer-membrane to MtrC and OmcA on the bacterial surface. MtrC and OmcA bind the surface of Fe(III) oxides and transfer electrons directly to Fe(III) via their solvent-exposed hemes. Through direct binding and reduction, MtrC and OmcA also use flavins as diffusible shuttles for Fe(III) oxide reduction. Because of their extracellular location, broad redox potentials, and ability to reduce Fe(III) complexed with different ligands *in vitro*, MtrC and OmcA can also reduce complexed forms of Fe(III) *in vivo* (**Figure 3**).

Despite the advances in understanding the molecular mechanisms of Fe(III) oxide reduction by *S. oneidensis* MR-1, key knowledge gaps still remain regarding the critical steps of the Mtr electron transfer pathway. First, it is still unclear which heme groups of the outer-membrane *c*-Cyts are directly involved in reduction of Fe(III) oxides and flavins. The molecular structure of MtrF predicts that heme 5 and 10 are highly solvent-exposed and thus candidates for interfacial electron transfer from MtrF to Fe(III) oxides, while hemes 2 and 7 are likely involved in flavin reduction. These predictions can be readily tested using site-directed mutagenesis. How the identified heme groups of MtrF interacts with and mediates the interfacial electron transfer to Fe(III) oxides and how MtrF binds and reduces flavins also need to be investigated, preferably using an integrated experiment and molecular modeling approach. Second, how MtrABC interact with each other to facilitate electrons transfer across the bacterial outer-membrane has yet to be determined. Structural determination of the MtrABC complex by X-ray crystallography could provide key insights of the electron conductance mechanism through the bacterial outer-membrane. Given that MtrABC is a trans outer-membrane protein complex, determination of its molecular structure will be challenging. Third, how electrons are transferred from CymA to MtrA remains unclear. Identification of this electron transfer mechanism will help determine how electrons are delivered across the bacterial periplasm. Another major knowledge gap is that the molecular details regarding how CymA interacts with and oxidizes the quinol in the inner-membrane are currently unclear. Determination of CymA structure will enable insights into how it binds and oxidizes quinol at the molecular-level. Finally, what are the functional roles of the MtrC and OmcA associated with EPS? Their relationship to bacterial outer-membrane vesicles and conductive nanowire also needs to be thoroughly characterized. Characterization of their roles will help understand the non-local electron transfer mechanisms by which *S. oneidensis* MR-1 cells reduce the Fe(III) oxide minerals distant from the cell surface. Although these key knowledge gaps persist, Mtr pathway of *S. oneidensis* MR-1 is the best characterized microbial pathway used for extracellular electron transfer. Characterization of the Mtr pathway has enabled unprecedented molecular-level understanding of microbial reduction of Fe(III) oxides.

ACKNOWLEDGMENTS

The authors would like to thank the U.S. Department of Energy (DOE) Office of Biological and Environmental Science's Subsurface Biogeochemical Research Program (SBR) for its support under the Pacific Northwest National Laboratory SBR Scientific Focus Area. The Pacific Northwest National Laboratory is operated for DOE by Battelle Memorial Institute under Contract DE-AC05-76RLO1830.

REFERENCES

Belchik, S. M., Kennedy, D. W., Dohnalkova, A. C., Wang, Y., Sevinc, P. C., Wu, H., Lin, Y., Lu, H. P., Fredrickson, J. K., and Shi, L. (2011). Extracellular reduction of hexavalant chromium by cytochromes MtrC and OmcA of *Shewanella oneidensis* MR-1. *Appl. Environ. Microbiol.* 77, 4035–4041.

Beliaev, A. S., and Saffarini, D. A. (1998). *Shewanella putrefaciens mtrB* encodes an outer membrane protein required for Fe(III) and Mn(IV) reduction. *J. Bacteriol.* 180, 6292–6297.

Beliaev, A. S., Saffarini, D. A., McLaughlin, J. L., and Hunnicutt, D. (2001). MtrC, an outer membrane decahaem c cytochrome required for metal reduction in *Shewanella putrefaciens* MR-1. *Mol. Microbiol.* 39, 722–730.

Bodemer, G. J., Antholine, W. A., Basova, L. V., Saffarini, D., and Pacheco, A. A. (2010). The effect of detergents and lipids on the properties of the outer-membrane protein OmcA from *Shewanella oneidensis*. *J. Biol. Inorg. Chem.* 15, 749–758.

Borloo, J., Vergauwen, B., De Smet, L., Brige, A., Motte, B., Devreese, B., and Van Beeumen, J. (2007). A kinetic approach to the dependence of dissimilatory metal reduction by *Shewanella oneidensis* MR-1 on the outer membrane cytochromes c OmcA and OmcB. *FEBS J.* 274, 3728–3738.

Bose, S., Hochella, M. F., Gorby, Y., Kennedy, D. W., McCready, D. E., Madded, A. S., and Lower, B. H. (2009). Bioreduction of hematite nanoparticles by the dissimilatory iron reducing bacterium *Shewanella oneidensis* MR-1. *Geochim. Cosmochim. Acta* 73, 962–976.

Bretschger, O., Obraztsova, A., Sturm, C. A., Chang, I. S., Gorby, Y. A., Reed, S. B., Culley, D. E., Reardon, C. L., Barua, S., Romine, M. F., Zhou, J., Beliaev, A. S., Bouhenni, R., Saffarini, D., Mansfeld, F., Kim, B. H., Fredrickson, J. K., and Nealson, K. H. (2007). Current production and metal oxide reduction by *Shewanella oneidensis* MR-1 wild type and mutants. *Appl. Environ. Microbiol.* 73, 7003–7012.

Bucking, C., Popp, F., Kerzenmacher, S., and Gescher, J. (2010). Involvement and specificity of *Shewanella oneidensis* outer membrane cytochromes in the reduction of soluble and solid-phase terminal electron acceptors. *FEMS Microbiol. Lett.* 306, 144–151.

Cao, B., Ahmed, B., Kennedy, D. W., Wang, Z., Shi, L., Marshall, M. J., Fredrickson, J. K., Isern, N. G., Majors, P. D., and Beyenal, H. (2011a). Contribution of extracellular polymeric substances from *Shewanella* sp. HRCR-1 biofilms to U(VI) immobilization. *Environ. Sci. Technol.* 45, 5483–5490.

Cao, B., Shi, L., Brown, R. N., Xiong, Y., Fredrickson, J. K., Romine, M. F., Marshall, M. J., Lipton, M. S., and Beyenal, H. (2011b). Extracellular polymeric substances from *Shewanella* sp. HRCR-1 biofilms: characterization by infrared spectroscopy and proteomics. *Environ. Microbiol.* 13, 1018–1031.

Clarke, T. A., Cole, J. A., Richardson, D. J., and Hemmings, A. M. (2007). The crystal structure of the pentahaem *c*-type cytochrome NrfB and characterization of its solution-state interaction with the pentahaem nitrite reductase NrfA. *Biochem. J.* 406, 19–30.

Clarke, T. A., Edwards, M. J., Gates, A. J., Hall, A., White, G. F., Bradley, J., Reardon, C. L., Shi, L., Beliaev, A. S., Marshall, M. J., Wang, Z., Watmough, N. J., Fredrickson, J. K., Zachara, J. M., Butt, J. N., and Richardson, D. J. (2011). Structure of a bacterial cell surface decaheme electron conduit. *Proc. Natl. Acad. Sci. U.S.A.* 108, 9384–9389.

Clarke, T. A., Holley, T., Hartshorne, R. S., Fredrickson, J. K., Zachara, J. M., Shi, L., and Richardson, D. J. (2008). The role of multihaem cytochromes in the respiration of nitrite in *Escherichia coli* and Fe(III) in *Shewanella oneidensis*. *Biochem. Soc. Trans.* 36, 1005–1010.

Coursolle, D., Baron, D. B., Bond, D. R., and Gralnick, J. A. (2010). The Mtr respiratory pathway is essential for reducing flavins and electrodes in *Shewanella oneidensis*. *J. Bacteriol.* 192, 467–474.

Coursolle, D., and Gralnick, J. A. (2010). Modularity of the Mtr respiratory pathway of *Shewanella oneidensis* strain MR-1. *Mol. Microbiol.* 77, 995–1008.

DiChristina, T. J., Moore, C. M., and Haller, C. A. (2002). Dissimilatory Fe(III) and Mn(IV) reduction by *Shewanella putrefaciens* requires *ferE*, a homolog of the *pulE (gspE)* type II protein secretion gene. *J. Bacteriol.* 184, 142–151.

Dohnalkova, A. C., Marshall, M. J., Arey, B. W., Williams, K. H., Buck, E. C., and Fredrickson, J. K. (2011). Imaging hydrated microbial extracellular polymers: comparative analysis by electron microscopy. *Appl. Environ. Microbiol.* 77, 1254–1262.

Donald, J. W., Hicks, M. G., Richardson, D. J., and Palmer, T. (2008). The *c*-type cytochrome OmcA localizes to the outer membrane upon heterologous expression in *Escherichia coli*. *J. Bacteriol.* 190, 5127–5131.

Eggleston, C. M., Vörös, J., Shi, L., Lower, B. H., Droubay, T. C., and Colberg, P. J. S. (2008). Binding and direct electrochemistry of OmcA, an outer-membrane cytochrome from an iron reducing bacterium, with oxide electrode: a candidate biofuel system. *Inorganica Chim. Acta* 361, 769–777.

El-Naggar, M. Y., Gorby, Y. A., Xia, W., and Nealson, K. H. (2008). The molecular density of states in bacterial nanowires. *Biophys. J.* 95, L10–L12.

El-Naggar, M. Y., Wanger, G., Leung, K. M., Yuzvinsky, T. D., Southam, G., Yang, J., Lau, W. M., Nealson, K. H., and Gorby, Y. A. (2010). Electrical transport along bacterial nanowires from *Shewanella oneidensis* MR-1. *Proc. Natl. Acad. Sci. U.S.A.* 107, 18127–18131.

Field, S. J., Dobbin, P. S., Cheesman, M. R., Watmough, N. J., Thomson, A. J., and Richardson, D. J. (2000). Purification and magneto-optical spectroscopic characterization of cytoplasmic membrane and outer membrane multiheme *c*-type cytochromes from *Shewanella frigidimarina* NCIMB400. *J. Biol. Chem.* 275, 8515–8522.

Firer-Sherwood, M., Pulcu, G. S., and Elliott, S. J. (2008). Electrochemical interrogations of the Mtr cytochromes from *Shewanella*: opening a potential window. *J. Biol. Inorg. Chem.* 13, 849–854.

Firer-Sherwood, M. A., Ando, N., Drennan, C. L., and Elliott, S. J. (2011a). Solution-based structural analysis of the decaheme cytochrome, MtrA, by small angle X-ray scattering and analytical ultracentrifugation. *J. Phys. Chem. B* 115, 11208–11214.

Firer-Sherwood, M. A., Bewley, K. D., Mock, J. Y., and Elliott, S. J. (2011b). Tools for resolving complexity in the electron transfer networks of multiheme cytochromes c. *Metallomics* 3, 344–348.

Fredrickson, J. K., Romine, M. F., Beliaev, A. S., Auchtung, J. M., Driscoll, M. E., Gardner, T. S., Nealson, K. H., Osterman, A. L., Pinchuk, G., Reed, J. L., Rodionov, D. A., Rodrigues, J. L., Saffarini, D. A., Serres, M. H., Spormann, A. M., Zhulin, I. B., and Tiedje, J. M. (2008). Towards environmental systems biology of *Shewanella*. *Nat. Rev. Microbiol.* 6, 592–603.

Fredrickson, J. K., and Zachara, J. M. (2008). Electron transfer at the microbe–mineral interface: a grand challenge in biogeochemistry. *Geobiology* 6, 245–243.

Gorby, Y., McLean, J., Korenevsky, A., Rosso, K., El-Naggar, M. Y., and Beveridge, T. J. (2008). Redox-reactive membrane vesicles produced by *Shewanella*. *Geobiology* 6, 232–241.

Gorby, Y. A., Yanina, S., McLean, J. S., Rosso, K. M., Moyles, D., Dohnalkova, A., Beveridge, T. J., Chang, I. S., Kim, B. H., Kim, K. S., Culley, D. E., Reed, S. B., Romine, M. F., Saffarini, D. A., Hill, E. A., Shi, L., Elias, D. A., Kennedy, D. W., Pinchuk, G., Watanabe, K., Ishii, S., Logan, B., Nealson, K. H., and Fredrickson, J. K. (2006). Electrically conductive bacterial nanowires produced by *Shewanella oneidensis* strain MR-1 and other microorganisms. *Proc. Natl. Acad. Sci. U.S.A.* 103, 11358–11363.

Gralnick, J. A., Vali, H., Lies, D. P., and Newman, D. K. (2006). Extracellular respiration of dimethyl sulfoxide by *Shewanella oneidensis* strain MR-1. *Proc. Natl. Acad. Sci. U.S.A.* 103, 4669–4674.

Hartshorne, R. S., Jepson, B. N., Clarke, T. A., Field, S. J., Fredrickson, J., Zachara, J., Shi, L., Butt, J. N., and Richardson, D. J. (2007). Characterization of *Shewanella oneidensis* MtrC: a cell-surface decaheme cytochrome involved in respiratory electron transport to extracellular electron acceptors. *J. Biol. Inorg. Chem.* 12, 1083–1094.

Hartshorne, R. S., Reardon, C. L., Ross, D., Nuester, J., Clarke, T. A., Gates, A. J., Mills, P. C., Fredrickson, J. K., Zachara, J. M., Shi, L., Beliaev, A. S., Marshall, M. J., Tien, M., Brantley, S., Butt, J. N., and Richardson, D. J. (2009). Characterization of an electron conduit between bacteria and the extracellular environment. *Proc. Natl. Acad. Sci. U.S.A.* 106, 22169–22174.

Hau, H. H., and Gralnick, J. A. (2007). Ecology and biotechnology of the genus *Shewanella*. *Annu. Rev. Microbiol.* 61, 237–258.

Jensen, H. M., Albers, A. E., Malley, K. R., Londer, Y. Y., Cohen, B. E., Helms, B. A., Weigele, P., Groves, J. T., and Ajo-Franklin, C. M. (2010). Engineering of a synthetic electron conduit in living cells. *Proc. Natl. Acad. Sci. U.S.A.* 107, 19213–19218.

Jiao, Y., and Newman, D. K. (2007). The *pio* operon is essential for phototrophic Fe(II) oxidation in *Rhodopseudomonas palustris* TIE-1. *J. Bacteriol.* 189, 1765–1773.

Johs, A., Shi, L., Droubay, T., Ankner, J. F., and Liang, L. (2010). Characterization of the decaheme *c*-type cytochrome OmcA in solution and on hematite surfaces by small angle x-ray scattering and neutron reflectometry. *Biophys. J.* 98, 3035–3043.

Jones, M. E., Fennessey, C. M., DiChristina, T. J., and Taillefert, M. (2010). *Shewanella oneidensis* MR-1 mutants selected for their inability to produce soluble organic-Fe(III) complexes are unable to respire Fe(III) as anaerobic electron acceptor. *Environ. Microbiol.* 12, 938–950.

Kerisit, S. N., Rosso, K. M., Dupuis, M., and Valiev, M. (2007). Molecular computational investigation of electron transfer kinetics across cytochrome-iron oxide interfaces. *J. Phys. Chem. C* 111, 11363–11375.

Lies, D. P., Hernandez, M. E., Kappler, A., Mielke, R. E., Gralnick, J. A., and Newman, D. K. (2005). *Shewanella oneidensis* MR-1 uses overlapping pathways for iron reduction at a distance and by direct contact under conditions relevant for biofilms. *Appl. Environ. Microbiol.* 71, 4414–4426.

Lower, B. H., Lins, R. D., Oestreicher, Z., Straatsma, T. P., Hochella, M. F. Jr., Shi, L., and Lower, S. K. (2008). In vitro evolution of a peptide with a hematite binding motif that may constitute a natural metal-oxide binding archetype. *Environ. Sci. Technol.* 42, 3821–3827.

Lower, B. H., Shi, L., Yongsunthon, R., Droubay, T. C., McCready, D. E., and Lower, S. K. (2007). Specific bonds between an iron oxide surface and outer membrane cytochromes MtrC and OmcA from *Shewanella oneidensis* MR-1. *J. Bacteriol.* 189, 4944–4952.

Lower, B. H., Yongsunthon, R., Shi, L., Wildling, L., Gruber, H. J., Wigginton, N. S., Reardon, C. L., Pinchuk, G. E., Droubay, T. C., Boily, J. F., and Lower, S. K. (2009). Antibody recognition force microscopy shows that outer membrane cytochromes OmcA and MtrC are expressed on the exterior surface of *Shewanella oneidensis* MR-1. *Appl. Environ. Microbiol.* 75, 2931–2935.

Lower, S. K., Hochella, M. F. Jr., and Beveridge, T. J. (2001). Bacterial recognition of mineral surfaces: nanoscale interactions between *Shewanella* and alpha-FeOOH. *Science* 292, 1360–1363.

Marcus, R. A., and Sutin, N. (1985). Electron transfers in chemistry and biology. *Biochim. Biophys. Acta* 811, 265–322.

Marshall, M. J., Beliaev, A. S., Dohnalkova, A. C., Kennedy, D. W., Shi, L., Wang, Z., Boyanov, M. I., Lai, B., Kemner, K. M., McLean, J. S., Reed, S. B., Culley, D. E., Bailey, V. L., Simonson, C. J., Saffarini, D. A., Romine, M. F., Zachara, J. M., and Fredrickson, J. K. (2006). *c*-Type cytochrome-dependent formation of U(IV) nanoparticles by *Shewanella oneidensis*. *PLoS Biol.* 4, e268. doi: 10.1371/journal.pbio.0040268

Marshall, M. J., Plymale, A. E., Kennedy, D. W., Shi, L., Wang, Z., Reed, S. B., Dohnalkova, A. C., Simonson, C. J., Liu, C., Saffarini, D. A., Romine, M. F., Zachara, J. M., Beliaev, A. S., and Fredrickson, J. K. (2008). Hydrogenase- and outer membrane *c*-type cytochrome-facilitated reduction of technetium(VII) by *Shewanella oneidensis* MR-1. *Environ. Microbiol.* 10, 125–136.

Marsili, E., Baron, D. B., Shikhare, I. D., Coursolle, D., Gralnick, J. A., and Bond, D. R. (2008). *Shewanella* secretes flavins that mediate extracellular electron transfer. *Proc. Natl. Acad. Sci. U.S.A.* 105, 3968–3973.

Matias, V. R., Al-Amoudi, A., Dubochet, J., and Beveridge, T. J. (2003). Cryotransmission electron microscopy of frozen-hydrated sections of *Escherichia coli* and *Pseudomonas aeruginosa*. *J. Bacteriol.* 185, 6112–6118.

Meitl, L. A., Eggleston, C. M., Colberg, P. J. S., Khare, N., Reardon, C. L., and Shi, L. (2009). Electrochemical interaction of *Shewanella oneidensis* MR-1 and its outer membrane cytochromes OmcA and MtrC with hematite electrodes. *Geochim. Cosmochim. Acta* 2009, 5292–5307.

Murphy, J. N., and Saltikov, C. W. (2007). The *cymA* gene, encoding a tetraheme *c*-type cytochrome, is required for arsenate respiration in *Shewanella* species. *J. Bacteriol.* 189, 2283–2290.

Myers, C. R., and Myers, J. M. (1997a). Cloning and sequence of *cymA*, a gene encoding a tetraheme cytochrome c required for reduction of iron(III), fumarate, and nitrate by *Shewanella putrefaciens* MR-1. *J. Bacteriol.* 179, 1143–1152.

Myers, C. R., and Myers, J. M. (1997b). Outer membrane cytochromes of *Shewanella putrefaciens* MR-1: spectral analysis, and purification of the 83-kDa *c*-type cytochrome. *Biochim. Biophys. Acta* 1326, 307–318.

Myers, C. R., and Myers, J. M. (2002). MtrB is required for proper incorporation of the cytochromes OmcA and OmcB into the outer membrane of *Shewanella putrefaciens* MR-1. *Appl. Environ. Microbiol.* 68, 5585–5594.

Myers, C. R., and Myers, J. M. (2003). Cell surface exposure of the outer membrane cytochromes of *Shewanella oneidensis* MR-1. *Lett. Appl. Microbiol.* 37, 254–258.

Myers, C. R., and Nealson, K. H. (1990). Respiration-linked proton translocation coupled to anaerobic reduction of manganese(IV) and iron(III) in *Shewanella putrefaciens* MR-1. *J. Bacteriol.* 172, 6232–6238.

Nealson, K. H., and Scott, J. (eds). (2003). *Ecophysiology of the genus Shewanella. The Prokaryotes: An Evolving Electronic Resource for the Microbial Community*. New York, NY: Springer, LLC.

Pitts, K. E., Dobbin, P. S., Reyes-Ramirez, F., Thomson, A. J., Richardson, D. J., and Seward, H. E. (2003). Characterization of the *Shewanella oneidensis* MR-1 decaheme cytochrome MtrA: expression in *Escherichia coli* confers the ability to reduce soluble Fe(III) chelates. *J. Biol. Chem.* 278, 27758–27765.

Reardon, C. L., Dohnalkova, A. C., Nachimuthu, P., Kennedy, D. W., Saffarini, D. A., Arey, B. W., Shi, L., Wang, Z., Moore, D., McLean, J. S., Moyles, D., Marshall, M. J., Zachara, J. M., Fredrickson, J. K., and Beliaev, A. S. (2010). Role of outer-membrane cytochromes MtrC and OmcA in the biomineralization of ferrihydrite by *Shewanella oneidensis* MR-1. *Geobiology* 8, 56–68.

Richardson, D. J. (2000). Bacterial respiration: a flexible process for a changing environment. *Microbiology* 146(Pt 3), 551–571.

Rodrigues, M. L., Oliveira, T. F., Pereira, I. A., and Archer, M. (2006). X-ray structure of the membrane-bound cytochrome c quinol dehydrogenase NrfH reveals novel haem coordination. *EMBO J.* 25, 5951–5960.

Rodrigues, M. L., Scott, K. A., Sansom, M. S., Pereira, I. A., and Archer, M. (2008). Quinol oxidation by *c*-type cytochromes: structural characterization of the menaquinol binding site of NrfHA. *J. Mol. Biol.* 381, 341–350.

Ross, D. E., Brantley, S. L., and Tien, M. (2009). Kinetic characterization of OmcA and MtrC, terminal reductases involved in respiratory electron transfer for dissimilatory iron reduction in *Shewanella oneidensis* MR-1. *Appl. Environ. Microbiol.* 75, 5218–5226.

Ross, D. E., Flynn, J. M., Baron, D. B., Gralnick, J. A., and Bond, D. R. (2011). Towards electrosynthesis in *Shewanella*: energetics of reversing the *mtr* pathway for reductive metabolism. *PLoS ONE* 6, e16649. doi:10.1371/journal.pone.0016649

Ross, D. E., Ruebush, S. S., Brantley, S. L., Hartshorne, R. S., Clarke, T. A., Richardson, D. J., and Tien, M. (2007). Characterization of protein-protein interactions involved in iron reduction by *Shewanella oneidensis* MR-1. *Appl. Environ. Microbiol.* 73, 5797–5808.

Rosso, K. M., Smith, D. M. A., Wang, Z., Ainsworth, C. C., and Fredrickson, J. K. (2004). Self-exchange electron transfer kinetics and reduction potentials for anthraquinone disulfonate. *J. Phys. Chem. A* 108, 3292–3303.

Rosso, K. M., Zachara, J. M., Fredrickson, J. K., Gorby, Y. A., and Smith, S. C. (2003). Nonlocal bacterial electron transfer to hematite surface. *Geochim. Cosmochim. Acta* 67, 1081–1087.

Schuetz, B., Schicklberger, M., Kuermann, J., Spormann, A. M., and Gescher, J. (2009). Periplasmic electron transfer via the *c*-type cytochromes MtrA and FccA of *Shewanella oneidensis* MR-1. *Appl. Environ. Microbiol.* 75, 7789–7796.

Schwalb, C., Chapman, S. K., and Reid, G. A. (2003). The tetraheme cytochrome CymA is required for anaerobic respiration with dimethyl sulfoxide and nitrite in *Shewanella oneidensis*. *Biochemistry* 42, 9491–9497.

Shi, L., Belchik, S. M., Wang, Z., Kennedy, D. W., Dohnalkova, A. C., Marshall, M. J., Zachara, J. M., and Fredrickson, J. K. (2011). Identification and characterization of $UndA_{HRCR-6}$, an outer membrane endecaheme *c*-type cytochrome of *Shewanella* sp. strain HRCR-6. *Appl. Environ. Microbiol.* 77, 5521–5523.

Shi, L., Chen, B., Wang, Z., Elias, D. A., Mayer, M. U., Gorby, Y. A., Ni, S., Lower, B. H., Kennedy, D. W., Wunschel, D. S., Mottaz, H. M., Marshall, M. J., Hill, E. A., Beliaev, A. S., Zachara, J. M., Fredrickson, J. K., and Squier, T. C. (2006). Isolation of a high-affinity functional protein complex between OmcA and MtrC: two outer membrane decaheme *c*-type cytochromes of *Shewanella oneidensis* MR-1. *J. Bacteriol.* 188, 4705–4714.

Shi, L., Deng, S., Marshall, M. J., Wang, Z., Kennedy, D. W., Dohnalkova, A. C., Mottaz, H. M., Hill, E. A., Gorby, Y. A., Beliaev, A. S., Richardson, D. J., Zachara, J. M., and Fredrickson, J. K. (2008). Direct involvement of type II secretion system in extracellular translocation of *Shewanella oneidensis* outer membrane cytochromes MtrC and OmcA. *J. Bacteriol.* 190, 5512–5516.

Shi, L., Lin, J. T., Markillie, L. M., Squier, T. C., and Hooker, B. S. (2005). Overexpression of multi-heme C-type cytochromes. *Biotechniques* 38, 297–299.

Shi, L., Richardson, D. J., Wang, Z., Kerisit, S. N., Rosso, K. M., Zachara, J. M., and Fredrickson, J. K. (2009). The roles of outer membrane cytochromes of *Shewanella* and *Geobacter* in extracellular electron transfer. *Environ. Microbiol. Rep.* 1, 220–227.

Shi, L., Squier, T. C., Zachara, J. M., and Fredrickson, J. K. (2007). Respiration of metal (hydr)oxides by *Shewanella* and *Geobacter*: a key role for multihaem *c*-type cytochromes. *Mol. Microbiol.* 65, 12–20.

Simon, J., and Kern, M. (2008). Quinone-reactive proteins devoid of haem b form widespread membrane-bound electron transport modules in bacterial respiration. *Biochem. Soc. Trans.* 36, 1011–1016.

Stack, A. G., Rosso, K. M., Smith, D. M. A., and Eggleston, C. M. (2004). Reaction of hydroquinone with hematite II. Calculated electron transfer rates and comparison to the reductive dissolution rate. *J. Colloid Interface Sci.* 274, 442–450.

Tang, X., Yi, W., Munske, G. R., Adhikari, D. P., Zakharova, N. L., and Bruce, J. E. (2007). Profiling the membrane proteome of *Shewanella oneidensis* MR-1 with new affinity labeling probes. *J. Proteome Res.* 6, 724–734.

Thamdrup, B. (2000). Bacterial manganese and iron reduction in aquatic sediments. *Adv. Microb. Ecol.* 16, 41–84.

von Canstein, H., Ogawa, J., Shimizu, S., and Lloyd, J. R. (2008). Secretion of flavins by *Shewanella* species and their role in extracellular electron transfer. *Appl. Environ. Microbiol.* 74, 615–623.

Wang, Z., Liu, C., Wang, X., Marshall, M. J., Zachara, J. M., Rosso, K. M., Dupuis, M., Fredrickson, J. K., Heald, S., and Shi, L. (2008). Kinetics of reduction of Fe(III) complexes by outer membrane cytochromes MtrC and OmcA of *Shewanella oneidensis* MR-1. *Appl. Environ. Microbiol.* 74, 6746–6755.

Weber, K. A., Achenbach, L. A., and Coates, J. D. (2006). Microorganisms pumping iron: anaerobic microbial iron oxidation and reduction. *Nat. Rev. Microbiol.* 4, 752–764.

Wigginton, N. S., Rosso, K. M., and Hochella, M. F. (2007a). Mechanisms of electron transfer in two decaheme cytochromes from a metal-reducing bacterium. *J. Phys. Chem. B* 111, 12857–12864.

Wigginton, N. S., Rosso, K. M., Lower, B. H., Shi, L., and Hochella, M. F. (2007b). Electron tunneling properties of outer-membrane decaheme cytochromes from *Shewanella oneidensis*. *Geochim. Cosmochim. Acta* 71, 543–555.

Xiong, Y., Shi, L., Chen, B., Mayer, M. U., Lower, B. H., Londer, Y., Bose, S., Hochella, M. F., Fredrickson, J. K., and Squier, T. C. (2006). High-affinity binding and direct electron transfer to solid metals by the *Shewanella oneidensis* MR-1 outer membrane *c*-type cytochrome OmcA. *J. Am. Chem. Soc.* 128, 13978–13979.

Zachara, J. M., Fredrickson, J. K., Li, S. M., Kennedy, D. W., Smith, S. C., and Gassman, P. L. (1998). Bacterial

reduction of crystalline Fe^{3+} oxides in single phase suspensions and subsurface materials. *Am. Mineral.* 83, 1426–1443.

Zhang, H., Tang, X., Munske, G. R., Tolic, N., Anderson, G. A., and Bruce, J. E. (2009). Identification of protein-protein interactions and topologies in living cells with chemical cross-linking and mass spectrometry. *Mol. Cell. Proteomic* 8, 409–420.

Zhang, H., Tang, X., Munske, G. R., Zakharova, N., Yang, L., Zheng, C., Wolff, M. A., Tolic, N., Anderson, G. A., Shi, L., Marshall, M. J., Fredrickson, J. K., and Bruce, J. E. (2008). In vivo identification of the outer membrane protein OmcA-MtrC interaction network in *Shewanella oneidensis* MR-1 cells using novel hydrophobic chemical cross-linkers. *J. Proteome Res.* 7, 1712–1720.

Conflict of Interest Statement: The authors declare that the research was conducted in the absence of any commercial or financial relationships that could be construed as a potential conflict of interest.

Received: 15 October 2011; accepted: 30 January 2012; published online: 15 February 2012.

Citation: Shi L, Rosso KM, Clarke TA, Richardson DJ, Zachara JM and Fredrickson JK (2012) Molecular underpinnings of Fe(III) oxide reduction by Shewanella oneidensis MR-1. Front. Microbio. ***3****:50. doi: 10.3389/fmicb.2012.00050*

This article was submitted to Frontiers in Microbiological Chemistry, a specialty of Frontiers in Microbiology.

Copyright © 2012 Shi, Rosso, Clarke, Richardson, Zachara and Fredrickson. This is an open-access article distributed under the terms of the Creative Commons Attribution Non Commercial License, which permits non-commercial use, distribution, and reproduction in other forums, provided the original authors and source are credited.

frontiers in
MICROBIOLOGY

REVIEW ARTICLE
published: 29 March 2012
doi: 10.3389/fmicb.2012.00112

Abiotic and microbial interactions during anaerobic transformations of Fe(II) and NO_X^-

Flynn Picardal*

School of Public and Environmental Affairs, Indiana University, Bloomington, IN, USA

Edited by:
Eric Roden, University of Wisconsin–Madison, USA

Reviewed by:
John Senko, The University of Akron, USA
Andreas Kappler, University of Tuebingen, Germany
Karrie Weber, University of Nebraska–Lincoln, USA

***Correspondence:**
Flynn Picardal, School of Public and Environmental Affairs, Indiana University, MSBII – Room 418, 702 North Walnut Grove Avenue, Bloomington, IN 47405-2204, USA.
e-mail: picardal@indiana.edu

Microbial Fe(II) oxidation using NO_3^- as the terminal electron acceptor [nitrate-dependent Fe(II) oxidation, NDFO] has been studied for over 15 years. Although there are reports of autotrophic isolates and stable enrichments, many of the bacteria capable of NDFO are known organotrophic NO_3^--reducers that require the presence of an organic, primary substrate, e.g., acetate, for significant amounts of Fe(II) oxidation. Although the thermodynamics of Fe(II) oxidation are favorable when coupled to either NO_3^- or NO_2^- reduction, the kinetics of abiotic Fe(II) oxidation by NO_3^- are relatively slow except under special conditions. NDFO is typically studied in batch cultures containing millimolar concentrations of Fe(II), NO_3^-, and the primary substrate. In such systems, NO_2^- is often observed to accumulate in culture media during Fe(II) oxidation. Compared to NO_3^-, abiotic reactions of biogenic NO_2^- and Fe(II) are relatively rapid. The kinetics and reaction pathways of Fe(II) oxidation by NO_2^- are strongly affected by medium composition and pH, reactant concentration, and the presence of Fe(II)-sorptive surfaces, e.g., Fe(III) oxyhydroxides and cellular surfaces. In batch cultures, the combination of abiotic and microbial Fe(II) oxidation can alter product distribution and, more importantly, results in the formation of intracellular precipitates and extracellular Fe(III) oxyhydroxide encrustations that apparently limit further cell growth and Fe(II) oxidation. Unless steps are taken to minimize or account for potential abiotic reactions, results of microbial NDFO studies can be obfuscated by artifacts of the chosen experimental conditions, the use of inappropriate analytical methods, and the resulting uncertainties about the relative importance of abiotic and microbial reactions. In this manuscript, abiotic reactions of NO_3^- and NO_2^- with aqueous Fe^{2+}, chelated Fe(II), and solid-phase Fe(II) are reviewed along with factors that can influence overall NDFO reaction rates in microbial systems. In addition, the use of low substrate concentrations, continuous-flow systems, and experimental protocols that minimize experimental artifacts and reduce the potential for under- or overestimation of microbial NDFO rates are discussed.

Keywords: nitrate-dependent Fe(II) oxidation, nitrate reduction, anoxic Fe(II) oxidation, abiotic Fe(II) oxidation

INTRODUCTION

To state the obvious, some geomicrobiological systems are easier to work with than others. In the same way that microbial, microaerophilic Fe(II) oxidation at circumneutral pH presents experimental challenges (Emerson and Floyd, 2005) microbial NO_3^--dependent Fe(II) oxidation (NDFO) present a variety of complexities that can complicate experimental design and confuse interpretation of results. Fe(II) is usually initially provided as soluble Fe^{2+}, but can also be introduced as sorbed Fe(II) or Fe(II)-bearing minerals of varying crystallinity and reactivity. The oxidized Fe(III) produced precipitates rapidly at circumneutral pH forming oxyhydroxides, thereby providing highly sorptive and reactive surfaces not initially present and frequently forming extensive cell coatings which can strongly effect microbial metabolism. Although usually not measured, the final product of NO_3^- reduction, based on stoichiometry and lack of NH_4^+ production, is typically assumed to be N_2 or N_2O. One of the reduction intermediates, i.e., NO_2^-, is more reactive with Fe(II) than NO_3^-, can accumulate in the medium, and result in abiotic reaction opportunities not present in abiotic controls.

Rather than present new data, this manuscript will review potential abiotic reactions between either NO_3^- or NO_2^- and homogeneous solutions of Fe^{2+} or heterogeneous systems containing solid-phase Fe(II). Numerous studies have been conducted for more than four decades (e.g., Chao and Kroontje, 1966), often under significantly different experimental conditions and resulting in varying reports of reactivity, reaction rates, and disparate distributions of products. This manuscript will describe previous abiotic studies in the context of microbial NDFO, attempt to provide deeper insights into the potential for simultaneous abiotic and biotic reactions of Fe and N, and assist in interpreting relative contributions of both reaction types in studies of microbial NDFO.

ABIOTIC OXIDATION OF Fe(II) BY NO_3^-

The oxidation of Fe^{2+} to goethite (α-FeOOH) by NO_3^- can be written such that either N_2, N_2O, NH_4^+, or NO_2^- are produced as

final products.

$$5\,Fe^{2+} + NO_3^- + 7H_2O \rightarrow 5\,\alpha\text{-FeOOH} + \frac{1}{2}N_{2\,(g)} + 9\,H^+ \quad \Delta G^{o'} = -127.3\,kJ/mol\,e^- \quad (1)$$

$$4\,Fe^{2+} + NO_3^- + \frac{11}{2}H_2O \rightarrow 4\,\alpha\text{-FeOOH} + \frac{1}{2}N_2O_{(g)} + 7\,H^+ \quad \Delta G^{o'} = -112.6\,kJ/mol\,e^- \quad (2)$$

$$8\,Fe^{2+} + NO_3^- + 13\,H_2O \rightarrow 8\,\alpha\text{-FeOOH} + NH_4^+ + 14\,H^+ \quad \Delta G^{o'} = -90.2\,kJ/mol\,e^- \quad (3)$$

$$2\,Fe^{2+} + NO_3^- + 3\,H_2O \rightarrow 2\,\alpha\text{-FeOOH} + NO_2^- + 4\,H^+ \quad \Delta G^{o'} = -96.7\,kJ/mol\,e^- \quad (4)$$

Calculations based on commonly used thermodynamic data (Stumm and Morgan, 1981) show that the standard free energy change at pH 7 for all reactions is favorable. Even though the thermodynamics are favorable, the kinetics of abiotic aqueous Fe^{2+} oxidation by NO_3^- at circumneutral pH in the absence of catalytic ions or surfaces are relatively slow. With respect to catalysts for abiotic reactions, Cu^{2+} and other metal ions have been shown to increase reaction rates (Buresh and Moraghan, 1976; Ottley et al., 1997). In an oft-cited study, Buresh and Moraghan (1976) described the oxidation of aqueous Fe^{2+} by NO_3^- over a pH range of 6–10 in the presence of 0–160 μM Cu^{2+} as a catalyst. In the presence of 0.0 and 1.6 μM Cu^{2+}, NO_3^- was stable over the 24-h experiment regardless of the pH. In the presence of Cu^{2+} at concentrations of 16 μM or greater, NO_3^- reduction occurred, and the extent of reduction increased with pH, becoming quite significant at pH 8 and above. When Cu-catalyzed NO_3^- reduction occurred, $Fe(OH)_2$ or other solid phases were presumed to be the reducing agents rather than soluble Fe^{2+} due to increased NO_3^- reduction at pH values >7 where extensive production of solid-phase Fe occurred. Ottley et al. (1997) further examined the reduction of NO_3^- by Fe^{2+} in the presence of 7 μM to 7 mM Cu^{2+} and other trace metal ions at pH 7–8.5. Relatively rapid NO_3^- reduction rates in the presence of Cu^{2+} again increased at alkaline pH and the authors determined that solid-phase Cu produced during incubations was catalytically active rather than the soluble Cu^{2+}.

Solid-phase Fe(II), whether adsorbed or crystalline, has been shown to be a more effective reductant than aqueous Fe^{2+} for reactions involving both organic and inorganic compounds (Sung and Morgan, 1980; Tamura et al., 1980; Klausen et al., 1995; Cui and Eriksen, 1996; Kim and Picardal, 1999; Amonette et al., 2000; Williams et al., 2005; Neumann et al., 2009). The importance of solid-phase or adsorbed Fe(II) in the abiotic reduction of NO_3^- appears to be dependent upon the time scale of the studies, pH, and characteristics of the solid phase. Postma (1990) studied reduction of low-micromolar concentrations of NO_3^- by Fe(II)-bearing silicate minerals at pH 2–7 over periods of 1000–2000 h. No aqueous Fe^{2+} was added and reduction relied on slow release of Fe^{2+} during silicate mineral dissolution. Maximal NO_3^- reduction rates were observed at pH 4 where small amounts of nitrite were also measured and reduction rates were thought to be dependent on precipitation of secondary Fe(III) minerals such as goethite. Overall NO_3^- reduction rates were quite low, however, and reduction by Fe(II)-bearing silicate minerals was considered to be important only in groundwater systems with long residence times. Although the Postma study may have significance for microbial NDFO as an environmental process in suitable sediments, the acidic pH regime and low micromolar concentrations of NO_3^- and Fe^{2+} used in his studies make it difficult to extrapolate his findings to laboratory studies of microbial NDFO.

In the work of Ottley et al. (1997), weeklong incubations of NO_3^- and initially aqueous Fe^{2+} in the absence of metal ion catalysts at pH 8 showed a 15% NO_3^- loss. Such losses would be important in microbial experiments where incubations are often conducted over similar or longer time scales. Since such losses of NO_3^- are typically not observed in microbiological experiments with aqueous Fe^{2+} (Straub et al., 1996; Weber et al., 2001; Blothe and Roden, 2009), it is not clear if trace amounts of O_2 caused abiotic Fe^{2+} oxidation and subsequent NO_3^- reduction by sorbed or solid-phase Fe(II). As also described by Ottley et al. addition of goethite to systems containing Fe^{2+} increased rates of NO_3^- reduction. Since goethite is sometimes a product of microbial NDFO (described below), this shows the potential importance of solid phases and suggests that sorption of Fe^{2+} to some Fe(III) oxyhydroxides may increase abiotic NO_3^- reduction rates.

Petersen (1979) described the abiotic oxidation of NO_3^- by Fe^{2+} over a pH range of 4–9. Reaction rates were very slow at pH ≤6 and maximal at pH 8. Petersen suggested that the reductant was a colloidal form of $Fe(OH)_2$ which began to precipitate at pH 6. Although Petersen's experiments were conducted at 70°C and should be carefully considered when working with hyperthermophiles, the applicability of his results to microbial experiments typically done at much lower temperatures is questionable.

Select, crystalline Fe(II)-bearing minerals are also known to reduce NO_3^-. Wüstite (FeO) has been shown to reduce NO_3^- to NH_4^+ at temperature (3–41°C), pH (5.45–7.45), and concentration regimes appropriate to microbial studies (Rakshit et al., 2005). In addition, clear evidence of rapid abiotic reduction of NO_3^- by green rust (GR) minerals has been provided by Hansen and coworkers (Hansen et al., 1994, 1996, 2001) and others (Choi and Batchelor, 2008). The GRs are highly reactive and consist of trioctahedral Fe(II)–Fe(III) hydroxide layers separated by hydrated anionic interlayers. The anions in the GR interlayer are variable, e.g., sulfate in GR_{SO_4} or chloride in GR_{Cl}. Both GR_{SO_4} and GR_{Cl} have been shown to abiotically reduce NO_3^- to NH_4^+ during oxidation of the GR to magnetite (Hansen et al., 1996, 2001). The kinetics of these reactions at circumneutral and slightly alkaline pH are sufficiently rapid to provide a competing pathway for microbial NO_3^- reduction when GR is present at sufficiently high concentrations.

Considering all of the above studies, several generalities are possible. Firstly, Fe^{2+} and NO_3^- are generally stable at circumneutral pH over the time scale used in most microbial NDFO experiments. This is quite apparent in the killed-cell or uninoculated controls typically used in NDFO batch experiments (Straub et al., 1996; Weber et al., 2001, 2006a; Kappler et al., 2005). In addition, both NO_3^- and Fe(II)-EDTA were stable in uninoculated and killed-cell controls in the limited number of experiments using Fe(II)-EDTA

instead of Fe^{2+} (Kumaraswamy et al., 2006; Chakraborty et al., 2011). Although catalysis by Cu^{2+} and other trace metal ions may have importance in some natural, sedimentary environments, such catalyzed reactions will likely be unimportant in the culture media commonly used in laboratory NDFO experiments. Trace metal solutions used in anaerobic studies (Strapoć et al., 2008; Wolfe et al., 2011) typically result in final Cu^{2+} concentrations more than one to two orders-of-magnitude less than the lowest effective catalytic concentration found in the above studies.

Solid-phase or adsorbed Fe(II) may reduce NO_3^- in some cases, but the effectiveness of the reductant is largely determined by the pH and the identity of the solid phase. The ability of the solid phase to function as a catalyst for NO_3^- reduction may also be dependent on the simultaneous presence of Fe^{2+}. In controls without supplemental Fe^{2+} using pasteurized, microbially reduced goethite, and other Fe(II)-bearing solid phases, concomitant losses of NO_3^- and Fe(II) were not observed (Weber et al., 2001; Chakraborty et al., 2011). GR minerals are effective reductants, especially at slightly alkaline pH, and their transient formation in experimental systems used in microbial NDFO experiments should always be considered. The usual method of GR synthesis involves either controlled oxidation of aqueous $FeCl_2$ or $FeSO_4$ (Tamaura et al., 1984b), the same compounds often used to study microbial Fe^{2+} oxidation, or an "induced hydrolysis" method involving reaction of Fe^{2+} with HFO in a pH 7, carbonate-buffered system (Hansen, 1989). In addition, GR-like minerals may also be transiently formed during conversion of other Fe(III) oxyhydroxides, e.g., lepidocrocite, to magnetite during incubation with Fe^{2+} (Tamaura et al., 1984a; Sørensen and Thorling, 1991). Since similar conditions needed for GR synthesis may exist during microbial NDFO studies, transient formation of minor GR-containing phases during microbial experiments must be taken into consideration. Typical uninoculated or killed-cell controls would not be suitable controls for a possible abiotic GR reaction since GR synthesis from aqueous Fe^{2+} requires Fe^{2+} oxidation.

The Fe(III) mineral phases that form as products are often poorly crystalline and their mineralogy can be determined by factors such as pH, phosphate, or bicarbonate concentrations used in the culture media, rates of Fe(II) oxidation, presence of humic compounds or other ligands, and other factors. In cases where mineral identity has been characterized, end-products such as goethite, lepidocrocite, HFO, or Fe(III) phosphates are usually identified (Lack et al., 2002; Kappler et al., 2005; Senko et al., 2005; Miot et al., 2009; Larese-Casanova et al., 2010). Early work included one report of formation of GR and magnetite (Chaudhuri et al., 2001), but later work by the same authors using the same culture and media found formation of HFO with no evidence of GR formation (Lack et al., 2002). The authors attributed the disparate finding to differences in the rate of Fe(II) oxidation by variously treated cultures. Clear evidence of GR formation during Fe(II) oxidation by *Acidovorax* sp. strain BoFeN1 was recently reported (Pantke et al., 2012) and the relative contribution of enzymatic NDFO versus GR-catalyzed NO_3^- reduction cannot yet be determined in most cases. It should be noted that, although NH_4^+ has been produced in some microbial NDFO studies that utilized sediments or sediment inoculum (Weber et al., 2006b; Coby et al., 2011) and with a pure culture of *Geobacter metallireducens* (Weber et al., 2006b), NDFO enrichment cultures and isolates generally reduce NO_3^- to N_2 or N_2O (Straub et al., 1996, 2004; Benz et al., 1998; Straub and Buchholz-Cleven, 1998; Weber et al., 2009). Since the products of abiotic oxidation of wüstite or GR by NO_3^- are magnetite and NH_4^+, the absence of these products in most NDFO studies suggests that the abiotic reduction of NO_3^- by transient amounts of GR minerals formed during Fe^{2+} oxidation may not be a significant contributor in many experiments.

ABIOTIC OXIDATION OF Fe(II) BY NO_2^-

The thermodynamics of Fe^{2+} oxidation to goethite (α-FeOOH) coupled with the reduction of NO_2^- to either N_2, N_2O, or NH_4^+ are also favorable.

$$3\,Fe^{2+} + NO_2^- + 4H_2O \rightarrow 3\,\alpha\text{-FeOOH} + \frac{1}{2}N_{2\,(g)} + 5\,H^+ \qquad \Delta G^{o'} = -147.6\,\text{kJ/mol e}^- \tag{5}$$

$$2\,Fe^{2+} + NO_2^- + \frac{5}{2}H_2O \rightarrow 2\,\alpha\text{-FeOOH} + \frac{1}{2}N_2O_{(g)} + 3\,H^+ \qquad \Delta G^{o'} = -128.5\,\text{kJ/mol e}^- \tag{6}$$

$$6\,Fe^{2+} + NO_2^- + 10\,H_2O \rightarrow 6\,\alpha\text{-FeOOH} + NH_4^+ + 10\,H^+ \qquad \Delta G^{o'} = -88.0\,\text{kJ/mol e}^- \tag{7}$$

Compared to NO_3^-, the kinetics of NO_2^- reduction by Fe(II) are generally more rapid in both homogeneous and heterogeneous reactions. In early work, Nelson and Bremner (1970) showed that only 4% of 3.6 mM NO_2^- remained after 24 h incubation with 25 mM Fe^{2+} at pH 5. It is not clear, however, if air was excluded from their reaction system. Moraghan and Buresh (1977) conducted experiments with 14 mM Fe^{2+} under anoxic conditions and found complete removal of 1.8 mM NO_2^- after 24 h at pH 8 with N_2O as the primary product. At pH 6, only 12% of the NO_2^- was reduced during the same period, although the presence of Cu^{2+} dramatically increased reaction rates. Since Fe(III) oxyhydroxide precipitates formed during their studies, the role of heterogeneous reactions could not be definitively ascertained. Van Cleemput and Baert (1983) examined reduction of NO_2^- by aqueous Fe^{2+} under anoxic conditions over a pH range of 4–6. Rates of NO_2^- reduction were slowest at pH 6 and increased as the solution became more acidic. Fast rates of reaction between Fe^{2+} and NO_2^- at acidic pH were also reported by Wullstein and Gilmour (1966).

In addition to the presence of Cu^{2+} or low pH, abiotic NO_2^- oxidation of Fe^{2+} is enhanced by the presence of solid phases. Van Cleemput and Baert (1983) reported that the addition of amorphous Fe(III) hydroxide (HFO) and, to a lesser extent, magnetite, greatly accelerated rates of reaction compared to systems containing Fe^{2+} alone. The effect of added HFO in heterogeneous systems was especially pronounced at pH 6 and 8 where rates of NO_2^- reduction were relatively slow absent the solid phase. Tai and Dempsey (2009) also showed that NO_2^- reduction rates at pH 6.8 were greatly enhanced in heterogeneous systems containing both HFO and Fe^{2+} compared to systems containing Fe^{2+} alone.

Sorption of Fe(II) to crystalline Fe(III) oxyhydroxides is also known to increase abiotic NO_2^- reduction rates. Sørensen and Thorling (1991) examined the effect of added lepidocrocite (γ-FeOOH) on the rates of abiotic Fe(II)-dependent NO_2^- reduction

over a pH range of 6–8.5 under anoxic conditions. Rates of reduction of NO_2^-, primarily to N_2O, occurred much more rapidly in the presence of lepidocrocite than in its absence and increased progressively from pH 7.5 to 8.5. Fe^{2+} reacted with the solid phase to form magnetite (Fe_3O_4) and the authors suggest that a transient GR phase may have formed at pH 8 and above during magnetite formation. Sorption of Fe^{2+} to goethite was also found by Coby and Picardal (2005) to increase reduction of NO_2^- to N_2O at pH 7 compared to systems lacking goethite.

The ability of GR_{SO_4} to reduce NO_2^- has been shown by Hansen et al. (1994) who proposed that NO_2^- can be both reduced rapidly during GR formation and more slowly by Fe(II) in the GR lattice. In a recent report by Kampschreur et al. (2011), reduction of NO_2^- to NO and N_2O by Fe^{2+} at pH 5.6–7.6 was attributed both to reaction with aqueous Fe^{2+} and the transient formation of GR-like compounds although a characterization was not done of the solid-phase formed during the reaction. With the exception of a recent report (Pantke et al., 2012) as described above, GR minerals are typically not found as final products during microbial NDFO exists in spite of conditions, i.e., presence of Fe^{2+} and freshly precipitated Fe(III) oxyhydroxides (Hansen, 1989), that may favor transient appearance during reaction progress.

In addition to reactions with GR and Fe^{2+} sorbed to Fe(III) oxyhydroxides, other studies have shown abiotic reactions of NO_2^- with various forms of solid-phase Fe(II). Weber et al. (2001) demonstrated that NO_2^- can abiotically oxidize Fe(II) in microbially reduced goethite and subsoils in addition to biogenic magnetite. In their experiments, neither biogenic nor chemically precipitated siderite ($FeCO_3$) was abiotically oxidized by NO_2^-. This contrasts with the subsequent experiments of Rakshit et al. (2008) who demonstrated abiotic reduction of NO_2^- to N_2O by chemically precipitated siderite at increasing rates as the pH was reduced from 7.9 to 5.5. In a separate study, Rakshit et al. (2005) also showed that wüstite (FeO) was able to reduce NO_2^- to NH_4^+ at rates significantly greater than corresponding NO_3^- reduction rates.

NO_2^- may also be reactive with Fe(II)-EDTA although results are equivocal. In 6-day, abiotic experiments with 2.5 mM NO_2^-, 5 mM NO_3^-, and 5 mM Fe(II)-EDTA at pH 7, no losses of any compound were observed (Chakraborty and Picardal, unpublished data). In the experiments of Kumaraswamy et al. (2006) at the same pH, however, 18% of 10 mM Fe(II)-EDTA was oxidized after 24 h. The greater reactivity of NO_2^- has also been highlighted in studies (Cooper et al., 2003; Coby and Picardal, 2005) which described abiotic reactions between NO_2^- and Fe(II) sorbed to microbial cell surfaces. The products of this reaction were N_2O and Fe(III) oxyhydroxide encrustations on cell surfaces that impeded subsequent transport of soluble substrates into cells.

A unified and comprehensive understanding of abiotic reactions between NO_2^- and Fe^{2+} is difficult to develop due to sometimes conflicting results in some of the above studies, likely due to the wide range of reactant concentrations (micromolar to tens of millimolar), different pH regimes, varying experimental conditions, incomplete characterization of aqueous:solid-phase Fe speciation, potential transient formation of reactive species and complexes, and often unspecified final reaction products. It is clear, however, that NO_2^- and soluble Fe^{2+} are reactive at acidic pHs and the Fe^{2+} sorption to amorphous and crystalline Fe(III) oxyhydroxides can increase rates of NO_2^- reduction. Sorption of Fe^{2+} to cell surfaces or transient formation of reactive GR minerals may also create artifacts under certain experimental conditions.

MICROBIAL NO_3^- -DEPENDENT Fe(II) OXIDATION AND POTENTIAL ABIOTIC INTERACTIONS

Nitrate-dependent Fe(II) oxidation was first described by Straub et al. (1996) and is catalyzed by phylogenetically diverse bacteria in a variety of environments (Hafenbradl et al., 1996; Benz et al., 1998; Straub and Buchholz-Cleven, 1998; Straub et al., 2004; Kumaraswamy et al., 2006; Muehe et al., 2009; Weber et al., 2009). NDFO has been demonstrated in a variety of sediment enrichments, microbial consortia, and pure cultures, including both autotrophic and mixotrophic cultures. In addition to the autotrophic enrichment culture originally described by Straub et al. (1996), autotrophic growth has been reported for *Pseudogulbenkiania* sp. Strain 2002 (Weber et al., 2006a, 2009), *Paracoccus ferrooxidans* using organically complexed Fe(II) (Kumaraswamy et al., 2006), and a hyperthermophilic archaeum (Hafenbradl et al., 1996). Most pure cultures capable of NDFO, however, are organotrophic, NO_3^--reducing bacteria that oxidize Fe(II) in the presence of an organic cosubstrate such as acetate, either cometabolically or through a mixotrophic physiology. Examples of such bacteria include *Paracoccus denitrificans* (Muehe et al., 2009), various *Acidovorax* sp. (Straub et al., 2004; Kappler et al., 2005; Muehe et al., 2009; Byrne-Bailey et al., 2010; Chakraborty et al., 2011), *Aquabacterium* sp. Strain BrG2 (Straub et al., 2004), *G. metallireducens* (Finneran et al., 2002; Weber et al., 2006b), *Azospira oryzae* ("*Dechlorosoma suillum*") (Lack et al., 2002), and other members of the α-, β-, γ-, and δ-subgroups of the Proteobacteria in addition to Gram-positive bacteria (Straub and Buchholz-Cleven, 1998; Straub et al., 2004; Kappler and Straub, 2005).

Fe(II) oxidation by mixotrophic organisms may be linked to energy conservation and growth or, in some cases, result from a summation of both enzymatic reactions and abiotic side reactions that occur fortuitously during organotrophic growth. Fe(II)-oxidation-enhanced growth has been clearly shown during mixotrophic growth by some *Acidovorax* sp. In experiments with two different *Acidovorax* isolates (Muehe et al., 2009; Chakraborty et al., 2011), increases in growth yield in batch cultures using 4–10 mM Fe^{2+}, 8–10 mM NO_3^-, and 1.5–5 mM acetate were consistently greater in the presence of Fe^{2+} than in its absence. In the experiments of Chakraborty et al. growth typically ceased after several days, regardless of the presence of remaining substrate, likely as a result of Fe(III) oxyhydroxide coatings that develop on cells. When Fe(II)-EDTA was used instead of Fe^{2+} in their experiments, oxyhydroxide encrustations did not form and further additions of substrate could be utilized. In a continuous-flow system using 50–250 μM Fe^{2+}, 100 μM NO_3^-, and 20 μM acetate, they did not observe formation of cell encrustations and cell growth was sustained over a 14-day period rather than the 3–4 days observed using higher concentrations in batch cultures. Overall, it is clear that NDFO can enhance growth of some mixotrophic Fe(II) oxidizers and that the formation of cell encrustations in batch systems at millimolar substrate concentrations can limit growth and substrate utilization. These cell encrustations are commonly observed

during NDFO in batch culture and their characterization has received detailed scrutiny (Kappler et al., 2005, 2010; Miot et al., 2009; Schädler et al., 2009).

Although it is clear that NDFO is a biological process that can increase growth yields in some bacteria, the possibilities of abiotic reactions between Fe(II) and oxidized N species during the course of batch NDFO studies requires that experimenters consider both biotic and abiotic mechanisms when evaluating results. This is particularly important since typical abiotic controls in such experiments do not effectively mimic the changing aqueous and solid-phase chemical conditions that occur in live-culture replicates. Uninoculated or killed-cell controls in microbiological NDFO experiments typically consist of anoxic bottles containing culture medium components, ferrous iron (usually aqueous Fe^{2+}) and NO_3^- (Straub et al., 1996; Weber et al., 2001). Controls of this type have established that NO_3^- is usually unreactive with Fe^{2+} or the solid-phase Fe(II) initially added over the time period used in typical experiments.

Such controls, however, do not contain the freshly precipitated Fe(III) oxyhydroxides that form in live-culture replicates. These materials likely include a spectrum of metastable oxyhydroxides of unknown mineralogy that are able to sorb Fe^{2+} from the aqueous phase and which are subject to continuing phase changes over the course of the experiment. The final phases formed will be a function of the solution chemistry, buffer choice, Fe^{2+} concentration, and Fe(II) oxidation rate. Although the predominant mineral phases present at the conclusion of the experiment have been characterized in a number of studies (Lack et al., 2002; Kappler et al., 2005; Miot et al., 2009), these identified phases represent a "snapshot" at a particular time and may also not capture highly reactive minor phases. Such reactive phases, especially in the presence of the 5- to 10-mM Fe^{2+} concentrations used in typical batch experiments, may lead to limited abiotic reactions with NO_3^- and, to a greater extent, with biogenic NO_2^-.

The accumulation of NO_2^- in live cultures can potentially be more problematic than NO_3^- in producing abiotic artifacts due to greater possibility of reactions with Fe^{2+} sorbed to cellular materials or biogenic Fe(III) oxyhydroxides.The accumulation of 0.5–1.5 mM NO_2^- in NDFO batch cultures has been noted in several studies (Kappler et al., 2005; Larese-Casanova et al., 2010; Chakraborty et al., 2011). This NO_2^- accumulation did not occur during organotrophic growth with acetate and often coincides with Fe^{2+} oxidation. In some studies, controls have been used to attempt to discount the contribution of abiotic Fe(II) oxidation by NO_2^-. These controls contained NO_2^- and either soluble Fe^{2+} (Kappler et al., 2005) or solid-phase Fe(II) (Weber et al., 2001), but not both. Since the abiotic studies described above have shown that NO_2^- can react with Fe^{2+} sorbed to Fe-containing minerals, controls lacking both a Fe(III) oxyhydroxide and millimolar Fe^{2+} concentrations are not truly representative of conditions present in live cultures and may underestimate abiotic reaction kinetics. It is therefore currently difficult to accurately ascertain the relative contributions of abiotic and biotic reaction pathways in most studies where NO_2^- accumulates in batch culture media.

The reason why NO_2^- accumulates in mixotrophic, Fe(II)-oxidizing batch cultures but not in cultures growing organotrophically is also subject to speculation. One possibility is that electrons from Fe(II) enter the respiratory electron transport chain at a branch point where electron transport is possible to NO_3^- but not to NO_2^-. Alternately, Fe^{2+} could diffuse into the periplasm and sorb to a periplasmic NO_2^- reductase. Since studies have shown that Fe^{2+} sorbed to cellular material can reduce NO_2^- (Coby and Picardal, 2005), abiotic oxidation of the sorbed Fe^{2+} by biogenic NO_2^- could result in accumulation of Fe(III)-mineral precipitates on the NO_2^- reductase and in the periplasm. Periplasmic accumulations of Fe(III) minerals have indeed been observed (Miot et al., 2009, 2011; Schädler et al., 2009). Although it is not clear if these periplasmic mineral accumulations are the result of abiotic or enzymatic Fe^{2+} oxidation, the recent observation (Miot et al., 2011) of mineralized protein globules in the periplasm and outer face of the plasma membrane supports the hypothesis that NO_2^- accumulation in Fe(II)-oxidizing cultures results from inhibition of the nitrite reductase by mineral deposition. Ultimately, very little is definitively known at the current time about mechanisms of microbial NDFO and the location of Fe(II) oxidation. The demonstration of NO_3^--dependent oxidation of solid-phase Fe(II) (Weber et al., 2001), however, strongly suggests that physiological oxidation takes place outside the cell since solid-phase Fe(II) is unlikely to enter cells.

Although alternate mechanisms governing production of mineral cell encrustations during mixotrophic NDFO have been proposed (Kappler and Newman, 2004; Kappler et al., 2005; Schädler et al., 2009), the sorption of Fe^{2+} to cell surfaces in media containing NO_2^- is sufficient for abiotic cell encrustation by Fe(III) oxyhydroxides (Coby and Picardal, 2005). When Fe(II)-EDTA was used in batch cultures instead of Fe^{2+} in the studies of Chakraborty et al. (2011) encrusted cells did not develop and utilization of additional amendments of soluble substrate was not blocked, even though >1 mM NO_2^- accumulated . In continuous-flow systems in which advective transport and low-micromolar Fe^{2+}, acetate, and NO_3^- concentrations prevent NO_2^- accumulation, they observed no significant cell encrustations. Lack of encrustations in continuous-flow systems may also be a result of advective removal of nanoscale Fe(III) oxide precipitates before they have an opportunity to aggregate and accumulate on cells.

The use of such continuous-flow systems may be helpful in establishing whether Fe(II)-oxidation can be coupled to energy conservation and growth in other isolates. Since measurements of substrate conversion are problematic in a continuous-flow system operated at low micromolar substrate concentrations (described in Chakraborty et al., 2011), batch systems are still likely required to examine reaction stoichiometry and achieve a mass balance of reactants and products. In such cases, reducing concentrations of one or all substrates may lower abiotic reaction rates relative to microbial rates, reduce NO_2^- accumulation, and thereby minimize development of cell encrustations. Alternately, it may be possible to develop opposing-gradient culture systems based on those used to study microaerophilic Fe(II) oxidation (Emerson and Floyd, 2005). Additional studies are needed to determine if such approaches are useful alternatives to the use of 5–10 mM concentrations of Fe^{2+} and NO_3^- commonly used in batch NDFO systems.

It is also important to consider abiotic reactions when measuring Fe species in NDFO experiments in which NO_2^- accumulates.

Total Fe(II), i.e., sorbed and aqueous Fe^{2+}, are commonly measured using 0.5 M HCl extraction. As described above, NO_2^- oxidizes Fe^{2+} relatively rapidly in acidic solution and a sequential extraction (Cooper et al., 2000; Weber et al., 2001) is necessary to avoid overestimating the extent of Fe(II) oxidation. A review of the literature reveals that this is not always done, raising doubts about Fe speciation data in such studies whenever NO_2^- is present.

CONCLUSION

Although the focus of this paper has been on potential abiotic reactions between Fe(II) and NO_3^- or NO_2^-, it should be emphasized that the microbial oxidation of Fe(II) can clearly be enzymatically catalyzed by microorganisms and conservation of energy from the reaction can, at least in some cases, be coupled to growth. Microaerobic Fe(II) oxidizers active at circumneutral pH must compete with the abiotic oxidation of Fe(II) by O_2 and potential Fe(III) oxide encrustations by specializing in environments, e.g., at oxic:anoxic boundaries with low substrate concentrations, where abiotic reactions are not overly detrimental (Emerson, 2000). Likely to a lesser extent, NO_3^--dependent Fe(II) oxidizers must similarly exist in natural aquatic systems in a defined environmental milieu or substrate concentration regime where abiotic and biotic reactions can coexist, inhibitory accumulations of mineral encrustations do not form, and NO_2^- accumulations are minimized. These environments certainly differ from the "unnatural" conditions used in most batch studies. As in microaerobic systems, although possibly to a lesser extent, experimenters will need to deal with special challenges that arise from the potential abiotic reactions when designing experiments and interpreting experimental results.

ACKNOWLEDGMENTS

This research was supported by National Science Foundation Biogeosciences Program Grant 0525069 to F. Picardal.

REFERENCES

Amonette, J. E., Workman, D. J., Kennedy, D. W., Fruchter, J. S., and Gorby, Y. A. (2000). Dechlorination of carbon tetrachloride by Fe(II) associated with goethite. *Environ. Sci. Technol.* 34, 4606–4613.

Benz, M., Brune, A., and Schink, B. (1998). Anaerobic and aerobic oxidation of ferrous iron at neutral pH by chemoheterotrophic nitrate-reducing bacteria. *Arch. Microbiol.* 169, 159–165.

Blothe, M., and Roden, E. E. (2009). Composition and activity of an autotrophic Fe(II)-oxidizing, nitrate-reducing enrichment culture. *Appl. Environ. Microbiol.* 75, 6937–6940.

Buresh, R. J., and Moraghan, J. T. (1976). Chemical reduction of nitrate by ferrous iron. *J. Environ. Qual.* 5, 320–325.

Byrne-Bailey, K. G., Weber, K. A., Chair, A. H., Bose, S., Knox, T., Spanbauer, T. L., Chertkov, O., and Coates, J. D. (2010). Completed genome sequence of the anaerobic iron-oxidizing bacterium *Acidovorax ebreus* strain TPSY. *J. Bacteriol.* 192, 1475–1476.

Chakraborty, A., Roden, E. E., Schieber, J., and Picardal, F. (2011). Enhanced growth of *Acidovorax* sp. strain 2AN during nitrate-dependent Fe(II) oxidation in batch and continuous-flow systems. *Appl. Environ. Microbiol.* 77, 8548–8566.

Chao, T.-T., and Kroontje, W. (1966). Inorganic nitrogen transformations through the oxidation and reduction of iron. *Soil Sci. Soc. Am. J.* 30, 193–196.

Chaudhuri, S., Lack, J., and Coates, J. (2001). Biogenic magnetite formation through anaerobic biooxidation of Fe(II). *Appl. Environ. Microbiol.* 67, 2844–2848.

Choi, J., and Batchelor, B. (2008). Nitrate reduction by fluoride green rust modified with copper. *Chemosphere* 70, 1108–1116.

Coby, A. J., Picardal, F., Shelobolina, E., Xu, H. F., and Roden, E. E. (2011). Repeated anaerobic microbial redox cycling of iron. *Appl. Environ. Microbiol.* 77, 6036–6042.

Coby, A. J., and Picardal, F. W. (2005). Inhibition of NO_3^- and NO_2^- reduction by microbial Fe(III) reduction: evidence of a reaction between NO_2^- and cell surface-bound Fe^{2+}. *Appl. Environ. Microbiol.* 71, 5267–5274.

Cooper, D. C., Picardal, F., Rivera, J., and Talbot, C. (2000). Zinc immobilization and magnetite formation via ferric oxide reduction by *Shewanella putrefaciens* 200. *Environ. Sci. Technol.* 34, 100–106.

Cooper, D. C., Picardal, F. W., Schimmelmann, A., and Coby, A. J. (2003). Chemical and biological interactions during nitrate and goethite reduction by *Shewanella putrefaciens* 200. *Appl. Environ. Microbiol.* 69, 3517–3525.

Cui, D., and Eriksen, T. E. (1996). Reduction of pertechnetate by ferrous iron in solution: influence of sorbed and precipitated Fe(II). *Environ. Sci. Technol.* 30, 2259–2262.

Emerson, D. (2000). "Microbial oxidation of Fe(II) and Mn(II) at circumneutral pH," in *Environmental Microbe-Metal Interactions*, ed. D. R. Lovley (Washington, DC: ASM Press), 31–52.

Emerson, D., and Floyd, M. M. (2005). Enrichment and isolation of iron-oxidizing bacteria at neutral pH. *Meth. Enzymol.* 397, 112–123.

Finneran, K. T., Housewright, M. E., and Lovley, D. R. (2002). Multiple influences of nitrate on uranium solubility during bioremediation of uranium-contaminated subsurface sediments. *Environ. Microbiol.* 4, 510–516.

Hafenbradl, D., Keller, M., Dirmeier, R., Rachel, R., Roßnagel, P., Burggraf, S., Huber, H., and Stetter, K. O. (1996). *Ferroglobus placidus* gen. nov., sp. nov., a novel hyperthermophilic archaeum that oxidizes Fe^{2+} at neutral pH under anoxic conditions. *Arch. Microbiol.* 166, 308–314.

Hansen, H. C. B. (1989). Composition, stabilization, and light absorption of Fe(II)Fe(III) hydroxy-carbonate ('green rust'). *Clay Miner.* 24, 663–669.

Hansen, H. C. B., Borggaard, O. K., and Sørensen, J. (1994). Evaluation of the free energy of formation of Fe(II)-Fe(III) hydroxide-sulphate (green rust) and its reduction of nitrite. *Geochim. Cosmochim. Acta* 58, 2599–2608.

Hansen, H. C. B., Guldberg, S., Erbs, M., and Bender Koch, C. (2001). Kinetics of nitrate reduction by green rusts-effects of interlayer anion and Fe(II):Fe(III) ratio. *Appl. Clay Sci.* 18, 81–91.

Hansen, H. C. B., Koch, C. B., Nancke-Krogh, H., Borggaard, O. K., and Sørensen, J. (1996). Abiotic nitrate reduction to ammonium: key role of green rust. *Environ. Sci. Technol.* 30, 2053–2056.

Kampschreur, M. J., Kleerebezem, R., De Vet, W. W. J. M., and Van Loosdrecht, M. C. M. (2011). Reduced iron induced nitric oxide and nitrous oxide emission. *Water Res.* 45, 5945–5952.

Kappler, A., Johnson, C. M., Crosby, H. A., Beard, B. L., and Newman, D. K. (2010). Evidence for equilibrium iron isotope fractionation by nitrate-reducing iron(II)-oxidizing bacteria. *Geochim. Cosmochim. Acta* 74, 2826–2842.

Kappler, A., and Newman, D. K. (2004). Formation of Fe(III)-minerals by Fe(II)-oxidizing photoautotrophic bacteria. *Geochim. Cosmochim. Acta* 68, 1217–1226.

Kappler, A., Schink, B., and Newman, D. K. (2005). Fe(III) mineral formation and cell encrustation by the nitrate-dependent Fe(II)-oxidizer strain BoFeN1. *Geobiology* 3, 235–245.

Kappler, A., and Straub, K. L. (2005). Geomicrobiological cycling of iron. *Rev. Mineral. Geochem.* 59, 85–108.

Kim, S., and Picardal, F. W. (1999). Enhanced anaerobic biodegradation of carbon tetrachloride in the presence of reduced iron oxides. *Environ. Toxicol. Chem.* 18, 2142–2150.

Klausen, J., Tröber, S. P., Haderlein, S. B., and Schwarzenbach, R. (1995). Reduction of substituted nitrobenzenes by Fe(II) in aqueous mineral solutions. *Environ. Sci. Technol.* 29, 2396–2404.

Kumaraswamy, R., Sjollema, K., Kuenen, G., Van Loosdrecht, M., and Muyzer, G. (2006). Nitrate-dependent $[Fe(II)EDTA]^{2-}$ oxidation by *Paracoccus ferrooxidans* sp nov., isolated from a denitrifying bioreactor. *Syst. Appl. Microbiol.* 29, 276–286.

Lack, J. G., Chaudhuri, S. K., Chakraborty, R., Achenbach, L. A., and Coates, J. D. (2002). Anaerobic biooxidation of Fe(II) by *Dechlorosoma suillum*. *Microb. Ecol.* 43, 424–431.

Larese-Casanova, P., Haderlein, S. B., and Kappler, A. (2010). Biomineralization of lepidocrocite and goethite by nitrate-reducing Fe(II)-oxidizing bacteria: effect of pH, bicarbonate, phosphate, and humic acids. *Geochim. Cosmochim. Acta* 74, 3721–3734.

Miot, J., Benzerara, K., Morin, G., Kappler, A., Bernard, S., Obst, M., Férard, C., Skouri-Panet, F., Guigner, J.-M., Posth, N., Galvez, M., Brown, G. E. Jr., and Guyot, F. (2009). Iron biomineralization by anaerobic neutrophilic iron-oxidizing bacteria. *Geochim. Cosmochim. Acta* 73, 696–711.

Miot, J., Maclellan, K., Benzerara, K., and Boisset, N. (2011). Preservation of protein globules and peptidoglycan in the mineralized cell wall of nitrate-reducing, iron(II)-oxidizing bacteria: a cryo-electron microscopy study. *Geobiology* 9, 459–470.

Moraghan, J. T., and Buresh, R. J. (1977). Chemical reduction of nitrite and nitrous oxide by ferrous iron. *Soil Sci. Soc. Am. J.* 41, 47–50.

Muehe, E. M., Gerhardt, S., Schink, B., and Kappler, A. (2009). Ecophysiology and the energetic benefit of mixotrophic Fe(II) oxidation by various strains of nitrate-reducing bacteria. *FEMS Microbiol. Ecol.* 70, 3–11.

Nelson, D. W., and Bremner, J. M. (1970). Role of soil minerals and metallic cations in nitrite decomposition and chemodenitrification in soils. *Soil Biol. Biochem.* 2, 1–8.

Neumann, A., Hofstetter, T. B., Skarpeli-Liati, M., and Schwarzenbach, R. P. (2009). Reduction of polychlorinated ethanes and carbon tetrachloride by structural Fe(II) in smectites. *Environ. Sci. Technol.* 43, 4082–4089.

Ottley, C. J., Davison, W., and Edmunds, W. M. (1997). Chemical catalysis of nitrate reduction by iron (II). *Geochim. Cosmochim. Acta* 61, 1819–1828.

Pantke, C., Obst, M., Benzerara, K., Morin, G., Ona-Nguema, G., Dippon, U., and Kappler, A. (2012). Green rust formation during Fe(II) oxidation by the nitrate-reducing Acidovorax sp. strain BoFeN1. *Environ. Sci. Technol.* 46, 1439–1446.

Petersen, H. J. S. (1979). Reduction of nitrate by iron(II). *Acta Chem. Scand.* 33a, 795–796.

Postma, D. (1990). Kinetics of nitrate reduction by detrital Fe(II)-silicates. *Geochim. Cosmochim. Acta* 54, 903–908.

Rakshit, S., Matocha, C. J., and Coyne, M. S. (2008). Nitrite reduction by siderite. *Soil Sci. Soc. Am. J.* 72, 1070–1077.

Rakshit, S., Matocha, C. J., and Haszler, G. R. (2005). Nitrate reduction in the presence of wüstite. *J. Environ. Qual.* 34, 1286–1292.

Schädler, S., Burkhardt, C., Hegler, F., Straub, K. L., Miot, J., Benzerara, K., and Kappler, A. (2009). Formation of cell-iron-mineral aggregates by phototrophic and nitrate-reducing anaerobic Fe(II)-oxidizing bacteria. *Geomicrobiol. J.* 26, 93–103.

Senko, J. M., Dewers, T. A., and Krumholz, L. R. (2005). Effect of oxidation rate and Fe(II) state on microbial nitrate-dependent Fe(III) mineral formation. *Appl. Environ. Microbiol.* 71, 7172–7177.

Sørensen, J., and Thorling, L. (1991). Stimulation by lepidocrocite (γ-FeOOH) of Fe(II)-dependent nitrite reduction. *Geochim. Cosmoschim. Acta* 55, 1289–1294.

Straub, K., Schonhuber, W., Buchholz-Cleven, B., and Schink, B. (2004). Diversity of ferrous iron-oxidizing nitrate-reducing bacteria and their involvement in oxygen-independent iron cycling. *Geomicrobiol. J.* 21, 371–378.

Straub, K. L., Benz, M., Schink, B., and Widdel, F. (1996). Anaerobic, nitrate-dependent microbial oxidation of ferrous iron. *Appl. Environ. Microbiol.* 62, 1458–1460.

Straub, K. L., and Buchholz-Cleven, B. E. E. (1998). Enumeration and detection of anaerobic ferrous iron-oxidizing, nitrate-reducing bacteria from diverse European sediments. *Appl. Environ. Microbiol.* 64, 4846–4856.

Strąpoć, D., Picardal, F. W., Turich, C., Schaperdoth, I., Macalady, J. L., Lipp, J. S., Lin, Y.-S., Ertefai, T. F., Schubotz, F., Hinrichs, K.-U., Mastalerz, M., and Schimmelmann, A. (2008). Methane-producing microbial community in a coal bed of the Illinois Basin. *Appl. Environ. Microbiol.* 74, 2424–2432.

Stumm, W., and Morgan, J. J. (1981). *Aquatic Chemistry*. New York: John Wiley & Sons.

Sung, W., and Morgan, J. J. (1980). Kinetics and product of ferrous iron oxygenation in aqueous systems. *Environ. Sci. Technol.* 14, 561–568.

Tai, Y.-L., and Dempsey, B. A. (2009). Nitrite reduction with hydrous ferric oxide and Fe(II): stoichiometry, rate, and mechanism. *Water Res.* 43, 546–552.

Tamaura, Y., Saturno, M., Yamada, K., and Katsura, T. (1984a). The transformation of γ-FeO(OH) to Fe_3O_4 and green rust II in an aqueous solution. *Bull. Chem. Soc. Jpn.* 57, 2417–2421.

Tamaura, Y., Yoshida, T., and Katsura, T. (1984b). The synthesis of green rust II(FeIII1-FeII2) and its spontaneous transformation into Fe_3O_4. *Bull. Chem. Soc. Jpn.* 57, 2411–2416.

Tamura, H., Kawamura, S., and Hagayama, M. (1980). Acceleration of the oxidation of Fe^{2+} ions by Fe(III)-oxyhydroxides. *Corros. Sci.* 20, 963–971.

Van Cleemput, O., and Baert, L. (1983). Nitrite stability influenced by iron compounds. *Soil Biol. Biochem.* 15, 137–140.

Weber, K., Pollock, J., Cole, K., O'Conner, S., Achenbach, L., and Coates, J. (2006a). Anaerobic nitrate-dependent iron (II) bio-oxidation by a novel lithoautotrophic betaproteobacterium, strain 2002. *Appl. Environ. Microbiol.* 72, 686–694.

Weber, K. A., Urrutia, M. M., Churchill, P. F., Kukkadapu, R. K., and Roden, E. E. (2006b). Anaerobic redox cycling of iron by freshwater sediment microorganisms. *Environ. Microbiol.* 8, 100–113.

Weber, K. A., Hedrick, D. B., Peacock, A. D., Thrash, J. C., White, D. C., Achenbach, L. A., and Coates, J. D. (2009). Physiological and taxonomic description of the novel autotrophic, metal oxidizing bacterium, *Pseudogulbenkiania* sp strain 2002. *Appl. Microbiol. Biotechnol.* 83, 555–565.

Weber, K. A., Picardal, F. W., and Roden, E. E. (2001). Microbially catalyzed nitrate-dependent oxidation of biogenic solid-phase Fe(II) compounds. *Environ. Sci. Technol.* 35, 1644–1650.

Williams, A. G. B., Gregory, K. B., Parkin, G. F., and Scherer, M. M. (2005). Hexahydro-1,3,5-trinitro-1,3,5-triazine transformation by biologically reduced ferrihydrite: evolution of Fe mineralogy, surface area, and reaction rates. *Environ. Sci. Technol.* 39, 5183–5189.

Wolfe, R. S., Amy, C. R., and Stephen, W. R. (2011). "Techniques for cultivating methanogens," in *Methods in Enzymology*, Vol. 494, eds A. Rosenzweig and S. Ragsdale (Salt Lake: Academic Press), 1–22.

Wullstein, L. H., and Gilmour, C. M. (1966). Non-enzymatic formation of nitrogen gas. *Nature* 210, 1150–1151.

Conflict of Interest Statement: The author declares that the research was conducted in the absence of any commercial or financial relationships that could be construed as a potential conflict of interest.

Received: 22 November 2011; accepted: 09 March 2012; published online: 29 March 2012.

Citation: Picardal F (2012) Abiotic and microbial interactions during anaerobic transformations of Fe(II) and NO_X^-. Front. Microbio. ***3****:112. doi: 10.3389/fmicb.2012.00112*

This article was submitted to Frontiers in Microbiological Chemistry, a specialty of Frontiers in Microbiology.

Copyright © 2012 Picardal. This is an open-access article distributed under the terms of the Creative Commons Attribution Non Commercial License, which permits non-commercial use, distribution, and reproduction in other forums, provided the original authors and source are credited.

frontiers in
MICROBIOLOGY

REVIEW ARTICLE
published: 16 March 2012
doi: 10.3389/fmicb.2012.00096

Redox transformations of iron at extremely low pH: fundamental and applied aspects

D. Barrie Johnson*, Tadayoshi Kanao† and Sabrina Hedrich

School of Biological Sciences, Bangor University, Bangor, UK

Edited by:
David Emerson, Bigelow Laboratory for Ocean Sciences, USA

Reviewed by:
Benjamin Kocar, Stanford University, USA
Kelly Wrighton, University of California Berkeley, USA

****Correspondence:***
D. Barrie Johnson, School of Biological Sciences, University of Wales, LL57 2UW Bangor, UK.
e-mail: d.b.johnson@bangor.ac.uk

†Present address:
Tadayoshi Kanao, Division of Bioscience Graduate School of Natural Science and Technology, Okayama University, 3-1-1, Tsushima-Naka, Okayama 700-8530, Japan.

Many different species of acidophilic prokaryotes, widely distributed within the domains *Bacteria* and *Archaea*, can catalyze the dissimilatory oxidation of ferrous iron or reduction of ferric iron, or can do both. Microbially mediated cycling of iron in extremely acidic environments (pH < 3) is strongly influenced by the enhanced chemical stability of ferrous iron and far greater solubility of ferric iron under such conditions. Cycling of iron has been demonstrated *in vitro* using both pure and mixed cultures of acidophiles, and there is considerable evidence that active cycling of iron occurs in acid mine drainage streams, pit lakes, and iron-rich acidic rivers, such as the Rio Tinto. Measurements of specific rates of iron oxidation and reduction by acidophilic microorganisms show that different species vary in their capacities for iron oxido-reduction, and that this is influenced by the electron donor provided and growth conditions used. These measurements, and comparison with corresponding data for oxidation of reduced sulfur compounds, also help explain why ferrous iron is usually used preferentially as an electron donor by acidophiles that can oxidize both iron and sulfur, even though the energy yield from oxidizing iron is much smaller than that available from sulfur oxidation. Iron-oxidizing acidophiles have been used in biomining (a technology that harness their abilities to accelerate the oxidative dissolution of sulfidic minerals and thereby facilitate the extraction of precious and base metals) for several decades. More recently they have also been used to simultaneously remediate iron-contaminated surface and ground waters and produce a useful mineral by-product (schwertmannite). Bioprocessing of oxidized mineral ores using acidophiles that catalyze the reductive dissolution of ferric iron minerals such as goethite has also recently been demonstrated, and new biomining technologies based on this approach are being developed.

Keywords: acidophiles, iron, oxidation, reduction

ENERGETIC CONSTRAINTS ON THE OXIDO-REDUCTION OF IRON AT LOW pH

Iron is the most abundant transition metal in the lithosphere, as well as the most abundant element (on a weight basis) in planet earth. In contrast, the concentration of soluble, bio-available iron often limits the growth of primary producing organisms in many aquatic (e.g., marine) and terrestrial (e.g., calcareous soils) environments. However, extremely acidic (pH < 3) environments tend to buck this trend, though there are exceptions, such as acidic sites that develop in calcareous substrata due to the microbiological oxidation of hydrogen sulfide (e.g., in the Frasissi cave system, Italy; Macalady et al., 2007). There are two main reasons why iron is more bio-available (often to the point at which it becomes toxic to most life forms) at low pH: (i) extremely acidic environments, both natural and man-made, are often associated with the oxidative dissolution of sulfide minerals, many of which contain iron (including the most abundant of all such minerals, pyrite; FeS_2), and (ii) both ionic forms of (uncomplexed) iron are far more soluble (especially ferric iron) at low pH than at circum-neutral pH. Metallic (zero-valent) iron is rare in the lithosphere, while the dominant non-complexed ionic form of this metal in the environment is mostly dictated by its aeration status, with ferrous iron [iron (II)] being more relatively abundant in anoxic environments and ferric iron [iron (III)] in aerobic sites. This is also the case in extremely acidic environments, though the causative agents of ferrous iron oxidation are often very different in the two situations. At pH 7, the spontaneous (abiotic) rate of oxidation in an oxygen-saturated solution containing 100 mg ferrous iron L^{-1} is 8.4 mg min^{-1}, while at pH 2 the corresponding rate is 8.4×10^{-7} μg min^{-1} (using the equation described in Stumm and Morgan, 1981). Spontaneous chemical oxidation of (uncomplexed) iron can, therefore, be rapid at circum-neutral pH, though it is much slower where oxygen concentrations are low, e.g., the oxidation rate of the same hypothetical solution (pH 7, containing 100 mg ferrous iron L^{-1}) is much slower (0.47 mg min^{-1}) when the dissolved oxygen concentration is 0.5 mg L^{-1}, as opposed to 9 mg L^{-1}. An important consequence of this is that acidophilic iron-oxidizing bacteria and archaea can exploit ferrous iron as a resource in oxygen-saturated waters where, in contrast to their neutrophilic counterparts, abiotic iron oxidation is not competitive.

The greatly enhanced solubility of ferric iron at low pH derives chiefly from the fact that ferric (oxy-)hydroxide phases have very small solubility products. For example, the log K_{sp} of

$Fe(OH)_3$ is −38.6 at 25°C (Monhemius, 1977) so that the theoretical maximum concentrations of non-complexed ferric iron at pH 2 is 140 mg L^{-1}, compared to 140 ng L^{-1} at pH 4 and 0.14 *fg* L^{-1} at pH 7. However, the most significant ferric iron mineral phases that form in sulfate-containing low pH environments are jarosites [e.g., $KFe_3(SO_4)_2(OH)_6$] and schwertmannite [ideal formula $Fe_8O_8(OH)_6SO_4$; Bigham et al., 1996] the solubility products of which have not been determined. Schwertmannite is metastable with respect to goethite (α-FeO.OH) and recrystallizes to the latter in an acid-generating reaction:

$$Fe_8O_8(OH)_6SO_4 + 2\ H_2O \rightarrow 8\ FeO.OH + SO_4^{2-} + 2H^+$$

At very low pH values, and in the presence of monovalent cations, schwertmannite is also metastable with respect to jarosite (Regenspurg et al., 2004). In addition, ferric iron forms complexes with both sulfate and hydroxyl ions, and the dominant soluble forms of this ionic species in acidic, sulfate liquors are $Fe(SO_4)_2^-$ and $Fe(SO_4)^+$ rather than uncomplexed Fe^{3+} (Welham et al., 2000), which influences its solubility.

The standard redox potential of the ferrous/ferric couple at pH 2 is generally quoted as +770 mV. However, the fact that ferric iron is complexed by sulfate ions in most natural and man-made extremely acidic environments influences this value, and the standard redox couples of both the $Fe(SO_4)_2^-$ and $Fe(SO_4)^+/Fe^{2+}$ couples are more electronegative than that of the uncomplexed metal. In sulfate solutions at pH 1, the standard potential of the ferrous/ferric couples has been calculated to be +697 mV (Welham et al., 2000), and it is slightly more electropositive (∼ + 720 mV) at pH 3 (O'Hara and Johnson, unpublished data). Although significant, these more electronegative redox potentials do still not allow the oxidation of iron to be coupled, at low pH, to potential alternative electron acceptors to oxygen, such as nitrate (the redox potential of the nitrate/nitrite couple is +430 mV). This bioenergetic constraint is one of the factors that differentiates the metabolic diversities of acidophilic and neutrophilic iron-oxidizing bacteria (Hedrich et al., 2011). However, the more electronegative redox potential of the ferrous/ferric sulfate complex couple, together with the more electropositive potential of the oxygen/water couple in acidic liquors (1.12 V at pH 2) than at pH 7 (+820 mV), means that the net potential difference between ferrous iron as electron donor and oxygen as electron acceptor is ∼420 mV at pH 2, which is far greater than values (50–350 mV) that are often quoted.

BIODIVERSITY OF PROKARYOTES THAT CATALYZE REDOX TRANSFORMATIONS OF Fe AT LOW pH

Acidophilic microorganisms, as a generic group, have wide metabolic diversities, including the abilities to use solar and chemical (organic and inorganic) sources of energy, a variety of electron acceptors, and to use both inorganic and organic sources of carbon (and, in some cases, both). In phylogenetic terms, iron-metabolizing acidophiles are highly diverse, occurring in the domain *Bacteria* within the *Proteobacteria* (*alpha-*, *beta-*, *and gamma*-classes), *Nitrospirae*, *Firmicutes*, *Actinobacteria*, and *Acidobacteria* phyla, and in the domain *Archaea* within the *Crenarchaeota* and *Euryarchaeota* phyla. They also vary in their response to temperature, and include species that are psychrotolerant (e.g., *Acidithiobacillus ferrivorans*), mesophilic (e.g., *Ferrimicrobium acidiphilum*), thermotolerant/moderately thermophilic (e.g., *Sulfobacillus acidophilus*), and extremely thermophilic (e.g., *Sulfolobus metallicus*).

Chemolithotrophy (using inorganic chemicals as sole or major electron donors) is a particularly widespread and much studied trait among acidophilic bacteria and archaea (Johnson and Hallberg, 2009). Reduced forms of sulfur (including elemental sulfur) are used by diverse genera of acidophilic bacteria (e.g., *Acidithiobacillus* spp.) and archaea (e.g., *Sulfolobus* spp.), and some species of acidophiles can also use hydrogen as an energy source (e.g., Drobner et al., 1990). The first ferrous iron-oxidizing acidophile to be characterized was *Acidithiobacillus* (*At.*) *ferrooxidans* (strains variously named at the time as *Thiobacillus ferrooxidans*, *Ferrobacillus ferrooxidans*, and *Ferrobacillus sulfooxidans*). These were all described as chemo-autotrophic bacteria that appeared to vary in their capacities for oxidizing reduced sulfur. Subsequently, many different species of acidophilic bacteria, though fewer acidophilic archaea, have also been shown to be able to utilize the energy derived from oxidizing ferrous iron to support their growth, including species that are obligate and facultative heterotrophs, as well as other autotrophic species.

In contrast to iron oxidation at low pH, the ability of acidophiles to grow *via* the dissimilatory reduction of ferric iron was only discovered in the late 1980s/early 1990s, with this trait being first reported for an autotrophic bacterium (*At. ferrooxidans*; Pronk et al., 1991) and heterotrophic bacteria (*Acidiphilium* spp.; Johnson and McGinness, 1991). Currently, all acidophiles that are known to use ferric as an electron acceptor to support their growth are facultative reducers, in that all of them can also reduce molecular oxygen. Electron donors that are coupled to iron reduction are inorganic (sulfur or hydrogen) in the case of chemolithotrophic acidophiles such as *At. ferrooxidans*, and organic (e.g., glucose or glycerol) in the case of heterotrophic acidophiles, such as *Acidiphilium* spp.

Table 1 groups acidophiles that catalyze the dissimilatory redox transformations of iron into three categories, based in their abilities to oxidize ferrous iron, to reduce ferric iron or (depending on environmental conditions) to do both. One interesting fact is that the majority of iron-oxidizing bacteria can also reduce ferric iron and, in cases where this has been examined, use the latter to support their growth. Exceptions to this include *Leptospirillum* spp. and "*Ferrovum* (*Fv.*) *myxofaciens*," though this is explained by the fact that these two genera are known to use only ferrous iron as an electron donor, thereby restricting them to an aerobic life-style and negating the possibility that they can grow by ferric iron respiration. In the case of the currently mis-named acidophile "*Thiobacillus* (*T.*) *prosperous*" (proposed to be re-classified as "*Acidihalobacter prosperous*"; Nicolle et al., 2009) there are currently no published data showing that this salt-tolerant acidophilic iron- and sulfur-oxidizer can grow anaerobically using sulfur as electron donor and ferric iron as electron acceptor. For all other iron-oxidizing acidophilic bacteria, the co-existence of iron oxidation and iron reduction capabilities suggests that the electron shuttle pathways involved might have some components in common. This, however, is patently not the case for heterotrophic acidophiles, such as *Acidiphilium* spp., that catalyze iron reduction

Table 1 | Acidophilic bacteria and archaea that have been reported to catalyze the dissimilatory oxidation of ferrous iron or reduction of ferric iron.

Iron-oxidizing acidophiles	Iron-reducing acidophiles	Iron-oxidizing/reducing acidophiles
BACTERIA		
Leptospirillum (L.)[1]	*Acidiphilium (A.)*[2/3]	*Acidithiobacillus (At.)*[1]
L. ferrooxidans	*A. cryptum*[2]	*At. ferrooxidans*
L. ferriphilum	*A. acidophilum*[3]	*At. ferrivorans*
"L. ferrodiazotrophum"	*A. angustum/rubrum*[2]	*Acidiferrobacter thiooxydans*[1]
"Ferrovum myxofaciens"[1]	*A. organovorum*[2]	*Ferrimicrobium acidiphilum*[2]
"Thiobacillus prosperous"[1]	*A. multivorum*[2]	*Acidimicrobium ferrooxidans*[3]
	Acidocella (Ac.)[2]	*Ferrithrix thermotolerans*[2]
	Ac. facilis	*Sulfobacillus (Sb.)*[3]
	"Ac aromatica"	*Sb. acidophilus*
	Acidobacterium[2]	*Sb. thermosulfidooxidans*
	Acb. capsulatum	*Sb. benefaciens*
	Acidobacterium spp.	*Alicyclobacillus (Alb.)*
		Alb. tolerans
		Alb. ferrooxydans
		Alb. aeris
		Alb. pohliae
		Alicyclobacillus sp. GSM
ARCHAEA		
Sulfolobus (S.)		*Ferroplasma (Fp.)* spp.
S. metallicus		*Fp. acidiphilum*
S. tokodaii		*"Fp. acidarmanus"*
Metallosphaera sedula		*Acidiplasma (Ap.)*
		Ap. cupricumulans
		Ap. aeolicum

[1] *Obligate autotrophs;* [2] *obligate heterotrophs;* [3] *facultative autotrophs.*

but not iron oxidation. Also, Ohmura et al. (2002) found that *At. ferrooxidans* grown anaerobically using ferric iron as electron donor synthesized large amounts of an acid-stable *c*-type cytochrome whose reduced form was re-oxidized by ferric iron. Interestingly, neither species of *Acidithiobacillus* that oxidizes sulfur but not ferrous iron (*At. thiooxidans* and *At. caldus*) can grow anaerobically by ferric iron respiration. Although Brock and Gustafson (1976) had reported that *At. thiooxidans* can reduce ferric iron, Hallberg et al. (2001) showed that this only occurred in cell suspensions that were incubated aerobically, and that there was no corresponding increase in cell numbers. This suggests that iron reduction may have been mediated abiotically by a metabolite produced during sulfur oxidation and that *At. thiooxidans* cannot grow by ferric iron respiration. Interestingly, the situation with iron-oxidizing archaea is less clear, though it appears that the ability to couple the oxidation of sulfur to the reduction of ferric iron is commonplace among the *Sulfolobales* (Paul Norris, Warwick University, unpublished data). Brock and Gustafson (1976) also reported that a *Sulfolobus* sp. [quoted to be *Sulfolobus* (*S.*) *acidocaldarius*, though this is unlikely as this archaeon does not grow autotrophically as described in the paper] coupled sulfur oxidation to ferric iron reduction. Both classified genera of iron-oxidizing euryarchaeotes (*Ferroplasma* and *Acidiplasma*) can also reduce ferric iron, though the electron donor here is organic (e.g., yeast extract) rather than elemental sulfur (Dopson et al., 2004; Golyshina et al., 2009).

New insights into the nature of iron-oxidizing acidophiles and how they interact with each other and with other acidophilic microorganisms have arisen from the detailed microbiological and molecular studies carried out at the abandoned Richmond mine at Iron Mountain, California (e.g., Denef et al., 2010). Among other things, this research has highlighted the important role of the iron-oxidizing/reducing archaeon "*Ferroplasma* (*Fp.*) *acidarmanus*" in the dissolution of sulfide minerals in extremely acidic (pH < 1) moderately thermal (~40°C) environments, and identified very small (<0.45 μm diameter) pleomorphic cells within acidic biofilms as novel archaeal lineages (designated "ARMAN": Archaeal Richmond Mine Acidophilic Nanoorganisms; Baker et al., 2006).

BIOCHEMICAL MECHANISMS OF DISSIMILATORY OXIDATION AND REDUCTION OF Fe AT LOW pH

The pathway of dissimilatory iron oxidation has been elucidated for *At. ferrooxidans*, and genomic and proteomic studies have provided revealing insights of how this is mediated in other acidophiles (reviewed in Bonnefoy and Holmes, 2011). By maintaining a near-neutral cytoplasmic pH and living in acidic solutions, acidophiles have a "ready-made" trans-membrane pH gradient for generating ATP. However, continued influx of protons would lead to severe acidification of the cytoplasm and cell death if this was not counterbalanced by equivalent amounts of negatively charged ions or particles. Electrons derived from the oxidation of ferrous iron satisfy this requirement, and the reduction of molecular oxygen completes the energy-synthesizing ("downhill electron flow") pathway (**Figure 1**). Electrons derived from ferrous iron are also used to generate reducing equivalents (e.g., NADH) but since the redox potential of the ferrous/ferric couple is far more electropositive than that of NAD^+/NADH (−320 mV), energy is required to fuel this reaction ("uphill electron flow") which is thought to derive from the proton motive force (Bonnefoy and Holmes, 2011). For mixotrophic and heterotrophic iron-oxidizers, the latter appears not to be the case as reducing equivalents can be generated from the oxidation of organic carbon.

The "uphill" and "downhill" electron transport pathways run concurrently in all iron-oxidizing chemoautotrophs, but the molecular complexes involved are often quite different, suggesting that iron oxidation in acidophiles has evolved independently on several occasions (Bonnefoy and Holmes, 2011). For example, the *rus* operon, which contains genes coding for the blue copper protein rusticyanin and several cytochromes, mediates ferrous oxidation in iron-oxidizing acidithiobacilli and, seemingly, in the salt-tolerant gammaproteobacterium "*T. prosperous*" (Nicolle et al., 2009). The role of another high potential iron-sulfur protein found in *At. ferrivorans* (at least one strain of which does not appear to contain rusticyanin) encoded by the *iro* gene, has yet to be resolved (Amouric et al., 2011). Interestingly, *Ferroplasma* spp. also contain a blue copper protein (sulfocyanin) which is also thought to be

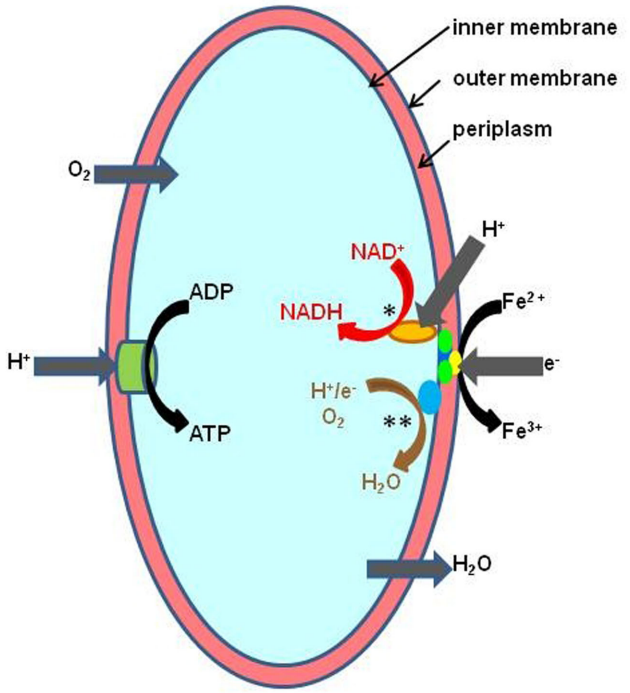

FIGURE 1 | Schematic representation of ferrous iron oxidation by the Gram-negative autotrophic acidophile, *At. ferrooxidans*. Controlled influx of protons is used to generate ATP *via* the membrane-bound ATP synthetase complex (ATPase). Iron oxidation is mediated by a cytochrome located on the outer membrane and electrons transferred *via* periplasmic cytochromes and rusticyanin either to a terminal oxidase ("downhill pathway," indicated in brown text and by **) where they are used to reduce oxygen, or used to reduce NAD^+ ("uphill pathway," indicated red text and by *) in a reaction also driven by the proton motive force across the inner membrane (Bonnefoy and Holmes, 2011).

involved in iron oxidation in this euryarchaeote (Bonnefoy and Holmes, 2011). In contrast, rusticyanin/sulfocyanin has not been detected in *Leptospirillum* spp., where the electron shuttle pathway is thought to involve four or five different cytochromes (Bonnefoy and Holmes, 2011). In the iron-oxidizing crenarchaeotes [*S. metallicus*, *S. tokodaii*, and *Metallosphaera* (*M.*) *sedula*], the *fox* [Fe(II) oxidation] cluster, which houses genes coding for cytochrome *b*, electron transporters, and a terminal oxidase, appears to have an analogous role to the *rus* operon in *At. ferrooxidans*, an hypothesis strengthened by the fact that this cluster has not been found in *Sulfolobus* spp. (e.g., *S. acidocaldarius*) that do not oxidize ferrous iron.

Relatively little is known about how prokaryotes catalyze ferric iron reduction at low pH, for example whether this is mediated enzymatically (via "iron reductases"), indirectly via metabolic intermediates, or both. All *Acidiphilium* spp. are known to reduce ferric iron, though most strains do not grow under strictly anoxic conditions in the presence of ferric iron, (Johnson and McGinness, 1991; Bridge and Johnson, 2000) and growth coupled to ferric iron reduction is most readily observed in cultures inoculated under micro-aerobic conditions (Johnson and McGinness, 1991; Bridge and Johnson, 2000). However, Küsel et al. (2002) reported that one strain [*Acidiphilium* (*A.*) *cryptum* JF-5] could reduce ferric iron in oxygen-saturated media. Johnson and Bridge (2002) showed that ferric iron reduction was constitutive in obligately heterotrophic *Acidiphilium* SJH (also identified as a strain of *A. cryptum*) but was inducible in the facultative autotroph *A. acidophilum*. Low oxygen concentrations, rather than ferric iron, appeared to induce a putative "iron reductase" in *A. acidophilum*. Whole cell protein profiles of *Acidiphilium* SJH were similar for cells grown under oxygen-saturated or micro-aerobic conditions, while in contrast three additional proteins were detected in SDS-PAGE profiles of *A. acidophilum* cells that could reduce ferric iron compared to those where iron reduction had not been induced. *A. organovorum* and *A. multivorum* were also reported to have constitutive iron reduction systems, while iron reduction appeared to be inducible in *A. rubrum*. Interestingly, Küsel et al. (2002) reported that the ferric iron reduction enzyme(s) were not constitutive in *A. cryptum* JF-5, a strain that is closely related to *Acidiphilium* SJH. Recent annotation of the draft genome of another *Acidiphilium* strain (PM) has failed to identify a putative iron reductase gene (San Martin-Uriz et al., 2011). Elsewhere, an outer membrane cytochrome *c* has been implicated as having a role in ferric iron reduction by *A. cryptum* JF-5 (Magnuson et al., 2010), which is intriguing in the light of the induced production of an acid-stable *c*-type cytochrome by *At. ferrooxidans* when respiring on ferric iron (Ohmura et al., 2002). Whether *c*-type cytochromes are also involved in iron reduction by other species of heterotrophic bacteria that are known to reduce ferric iron (e.g., *Acidocella* and *Acidobacterium*; Coupland and Johnson, 2008) is unknown.

MEASUREMENT AND INTERPRETATION OF SPECIFIC RATES OF IRON OXIDATION AND IRON REDUCTION IN ACIDOPHILES

Determining specific rates of iron oxidation and iron reduction by acidophilic microorganisms is a relatively simple procedure. The data obtained illustrate how different species vary in their capacities for iron oxido-reduction, and how this is influenced by growth histories and environmental parameters. Such information is also of fundamental importance for the design of biotechnological processes that utilize microbial iron oxidation or reduction in low pH liquids (see following sections). The technique involves growing biomass under controlled conditions, harvesting and concentrating cells and assaying their abilities to either oxidize ferrous iron or reduce ferric iron (typically 1 mM of either) under suitable conditions, e.g., in the presence of a suitable electron donor, and under anoxic conditions, for iron reduction (**Figure 2**). Biomass measurements are simultaneously carried out on sub-samples of the concentrated cells. Usually, this involves determination of protein contents using, for example, the Bradford assay (Bradford, 1976) but measurements of active biomass (e.g., of ATP; Okibe and Johnson, 2011) are more relevant where the total biomass includes a significant proportion of dead or moribund cells. The time taken to determine rates of iron oxidation and reduction is also important and needs to be much smaller than the culture doubling time of the organism being assayed in order for there to be no significant increase in biomass during the assay period. Typically, 20 min to 2 h provides sufficient time to allow sufficient iron oxidation or reduction by cell suspensions while avoiding significant biomass perturbations (acidophiles generally have culture

doubling times varying between 6 and 12 h). Details of the method used to determine specific rates of ferrous iron oxidation are given in Hallberg et al. (2011a). Specific rates of ferric iron reduction referred to in **Table 2** were measured using a similar protocol, with nitrogen replacing air (to create anoxic conditions in the cell suspensions) and a suitable electron donor (organic or inorganic) supplied in stoichiometric excess to ferric iron.

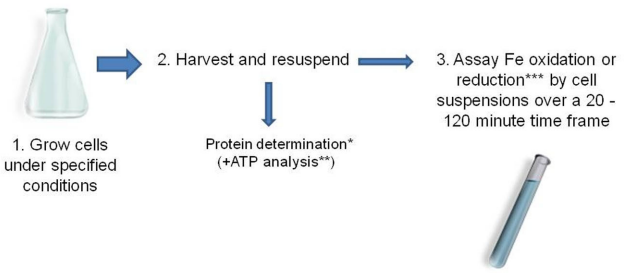

FIGURE 2 | Typical protocol used for determining specific rates of ferrous iron oxidation and ferric iron reduction by acidophilic prokaryotes (*Bradford, 1976; **Okibe and Johnson, 2011; * e.g., using the ferrozine assay, Lovley and Phillips, 1987).**

Table 2 | Specific rates of ferrous iron oxidation determined for different species of acidophilic bacteria and the archaeon *Ferroplasma*.

Acidophile	Fe^{2+} oxidation (mg min^{-1} g $protein^{-1}$)
(I) AUTOTROPHIC SPECIES	
Iron-oxidizing acidithiobacilli	
Group I (*At. ferrooxidans*^{T})	484 ± 3.3
Group II (ATCC 33020)	440 ± 11.5
Group III (*At. ferrivorans*^{T})	192 ± 14
Group IV (JCM 7812)	446 ± 6.8
Leptospirillum spp.	
L. ferrooxidans^T	426 ± 6.5
L. ferriphilum^T*	484 ± 88
Others	
Acd. thiooxidans^T	457 ± 20
"*Fv. myxofaciens*"^{T}	532 ± 23
(II) MIXOTROPHIC/HETEROTROPHIC SPECIES	
Ferrimicrobium acidiphilum	
(25 mM Fe^{2+}/100 μM glycerol)	191 ± 7.5
(100 μM Fe^{2+}/5 mM glycerol)	7.7 ± 0.14
Sulfobacillus spp.*	
Sb. thermosulfidooxidans	449 ± 4.0
Sb. acidophilus	236 ± 11
Sb. benefaciens	341 ± 16
*Ferroplasma acidiphilum**	371 ± 4.0

*(i) All specific iron oxidation rates were determined at 30°C (except those indicated *, which were determined at 37°C); (ii) all prokaryotes were grown in 25 mM ferrous iron medium, supplemented (for mixotrophs and heterotrophs) with 0.02% (w/v) yeast extract (the media used for Fm. acidophilum were as indicated in the Table).*

Table 2 shows specific rates of iron oxidation by different species of autotrophic acidophiles, and facultatively and obligately heterotrophic species, using this approach. Most of the autotrophic species show similar specific rates of oxidation, varying between mean values of 428 and 484 mg ferrous iron oxidized min^{-1} g $protein^{-1}$. The two outliers in **Table 2** are *At. ferrivorans* and the betaproteobacterium "*Fv. myxofaciens*." Two other strains of *At. ferrivorans* (Peru6 and CF27) also displayed lower rates (236 ± 2.4 and 312 ± 6.6 mg ferrous iron oxidized min^{-1} g $protein^{-1}$, respectively) than the other three "Groups" of iron-oxidizing acidithiobacilli (based on the delineation described by Amouric et al., 2011) suggesting that this is a species-specific trait. "*Fv. myxofaciens*" displayed the fastest specific rate of iron oxidation of all bacteria (and the sole archaeon) examined, but since the isolate tested (P3G; the nominated type strain of the species) is the only strain currently available in pure culture, the question of whether this is a genus- or species-specific characteristic remains to be verified. All of the mixotrophic and heterotrophic prokaryotes tested, with the exception of *Sulfobacillus* (*Sb.*) *thermosulfidooxidans*, displayed significantly lower specific rates of iron oxidation than the mean value found with autotrophic species, even though these assays were carried out at 37°C rather than at 30°C [as for all of the autotrophic strains, except *Leptospirillum* (*L.*) *ferriphilum*], since most mixotrophic iron-oxidizing acidophilic bacteria are thermotolerant or moderate thermophiles. In the case of the mesophilic heterotroph *Fm. acidiphilum* which was, like the autotrophic strains, assayed at 30°C, the specific rate of iron oxidation was very much dictated by the growth medium used, in particular the ratio of ferrous iron to organic carbon source (**Table 2**).

Specific rates of ferric iron reduction by the heterotroph *Acidiphilium* SJH and two autotrophic *Acidithiobacillus* spp. (*At. ferrooxidans*^{T}, and *Acidithiobacillus* sp ATCC 33020, the proposed type strain of "Group II" iron-oxidizing acidithiobacilli), again using the approach described above, are shown in **Table 3**. These were much smaller (by about one order of magnitude) than typical rates of iron oxidation found in acidophiles. Data obtained for *Acidiphilium* SJH suggested that the electron donor had little

Table 3 | Specific rates of ferric iron reduction by heterotrophic (*Acidiphilium*) and autotrophic (*Acidithiobacillus* spp.) acidophiles.

Bacterium	Growth conditions (incubation time)	Fe^{3+} reduction (mg min^{-1} g $protein^{-1}$)
A. cryptum SJH	Glycerol/Fe^{3+}	32 ± 3.7
	Galactose/Fe^{3+}	40 ± 8.0
At. ferrooxidans^T	H_2/O_2 (7 days)	46 ± 10
	H_2/O_2 (21 days)	23 ± 5.0
	H_2/Fe^{3+}* (5 days)	84 ± 2.3
Acidithiobacillus sp. ATCC 33020	H_2/O_2 (7 days)	63 ± 7.3
	H_2/O_2 (21 days)	53 ± 1.9
	H_2/Fe^{3+}* (5 days)	76 ± 2.1

**Cultures grown under anoxic conditions; the electron donors used to grow the acidophiles (glycerol, galactose, or hydrogen) were also those used for the measurements of specific rates of ferric iron reduction.*

influence on the specific rate of ferric iron reduction, with the value being similar when either glycerol or galactose was supplied. Ferric iron reduction data shown in **Table 3** for the two iron-oxidizing *Acidithiobacillus* spp. are for hydrogen-grown cultures grown either aerobically, or under anoxic conditions with ferric iron as electron acceptor. There was evidence of suppression of the potential for ferric iron reduction by *At. ferrooxidans*^{T} with protracted aerobic growth on hydrogen, and the reverse when it was grown anaerobically on hydrogen and ferric iron. While similar tends were apparent for *Acidithiobacillus* spp. ATCC 33020, differences in specific rates of iron reduction were far less pronounced.

The effect of growing iron-oxidizing acidithiobacilli on alternative electron donors to ferrous iron on the specific rates of iron oxidation is shown in **Table 4**. Data shown for tetrathionate-grown cultures are of cells harvested at early stationary phase (generally after ∼5 days) from cultures grown in 5 mM $S_4O_6^{2-}$ with varying concentrations of ferrous iron, while for both elemental sulfur and hydrogen more protracted growth was possible by providing excess elemental sulfur or by continuously replenishing the hydrogen supply. These results showed that specific rates of iron oxidation were lower for both *At. ferrooxidans*^{T} and *Acidithiobacillus* sp. ATCC 33020 when grown on electron donors other than ferrous iron, though this varied with the electron donor used and incubation period. In the case of *At. ferrooxidans*^{T}, the specific rate of iron oxidation for sulfur-grown cells was about 10% of that of iron-grown cells after 10 days, and was not detectable after 3 weeks of growth on this electron donor. In contrast, the specific rate of ferrous iron oxidation by cells grown aerobically on hydrogen for 3 weeks was still about 50% of that of ferrous iron-grown cells. Ferrous iron has been reported to induce expression of the *rus* operon in *At. ferrooxidans* (Amouric et al., 2009), and the lack of ferrous oxidation ability in sulfur-grown cultures can be explained by the ferrous iron originally present in the cultures being rapidly oxidized (within 1 day) to ferric. However, the same would have been true for hydrogen-grown biomass grown with excess oxygen, so why the *rus* operon was still apparently being expressed in these cultures is unclear. Similar results were obtained for *Acidithiobacillus* sp. ATCC 33020 (**Table 4**). Both *Acidithiobacillus* spp. displayed significant rates of iron oxidation when grown anaerobically on hydrogen (even after 14 days, in the case of *Acidithiobacillus* sp. ATCC 33020) though this can be explained that ferrous iron would have accumulated in these cultures as a result of dissimilatory reduction of ferric iron, causing the *rus* operon to be expressed.

In natural and man-made (biomining) environments, pyrite is a major energy resource for chemo-autotrophic acidophiles. Ferric iron attack on this mineral releases both ferrous iron and soluble reduced sulfur species (Rohwerder et al., 2003) so that bacteria that can use both as electron donors, such as *At. ferrooxidans*, may use one or the other in preference, or both simultaneously. Comparison of specific rates of iron oxidation of bacteria grown on pyrite with those of the same strain grown on ferrous iron or reduced sulfur can provide insights into what substrate is being utilized. Results for the type strains of *At. ferrooxidans* and *L. ferrooxidans* grown in pure culture in 1% (w/v) pyrite liquid medium, in which planktonic-phase cells and those attached to the mineral were harvested separately using the protocol described by Okibe and Johnson (2004), are shown in **Table 5**. After 1 week of incubation, the specific rates of ferrous iron oxidation by planktonic-phase cells of both acidophiles were actually somewhat greater than those of ferrous iron-grown cells, and much greater than of those of sulfur-grown cells, implying that both

Table 4 | Effects of different electron donors and culture conditions on the specific rates of ferrous iron oxidation by *Acidithiobacillus* spp.

Bacterium and culture medium	Fe^{2+} oxidation ($mg\ min^{-1}\ g\ protein^{-1}$)
***AT. FERROOXIDANS*^{T}**	
(i) $S_4O_6^{2-}$-grown cultures	
+0 Fe^{2+}	69 ± 1.0
+10 μM Fe^{2+}	219 ± 2.0
+100 μM Fe^{2+}	210 ± 4.0
+1000 μM Fe^{2+}	190 ± 7.5
(ii) S^0-grown cultures	
+0 Fe^{2+}; 10 days	44 ± 8.0
+10 μM Fe^{2+}; 10 days	24 ± 0.6
+100 μM Fe^{2+}; 10 days	38 ± 0.95
+1000 μM Fe^{2+}; 10 days	32 ± 1.5
+0 Fe^{2+}; 21 days	<0.01
(iii) H_2-grown cultures	
7 days	149 ± 2.0
21 days	210 ± 3.1
+25 mM Fe^{3+}; 5 days*	178 ± 8.3
***ACIDITHIOBACILLUS* SP. ATCC 33020**	
(i) $S_4O_6^{2-}$-grown culture	
+100 μM Fe^{2+}	45 ± 2.0
(ii) H_2-grown cultures	
7 days	132 ± 4.8
21 days	225 ± 7.5
+25 mM Fe^{3+}; 5 days*	139 ± 12
+25 mM Fe^{3+}; 14 days*	130 ± 7.0

*All cultures were grown aerobically, except those indicated by *, which were grown under anoxic conditions.*

Table 5 | Specific rates of ferrous iron oxidation by the type strains of *L. ferrooxidans* and *At. ferrooxidans* grown on pyrite.

Bacterium	Fe^{2+} oxidation ($mg\ min^{-1}\ g^{-1}$ protein)	RLU* (μg protein^{-1})
***L. FERROOXIDANS* (PYRITE; PLANKTONIC CELLS)**		
Week 1	527 ± 7.8	5,112
Week 2	283 ± 6.1	2,291
***AT. FERROOXIDANS* (PYRITE; PLANKTONIC CELLS)**		
Week 1	562 ± 1.0	5,486
Week 2	240 ± 1.0	2,444
At. ferrooxidans: pyrite		
Planktonic cells	224 ± 1.0	n.d.
Attached cells	307 ± 1.0	n.d.

**Relative light units (measurement of ATP concentration).*

bacteria were oxidizing ferrous iron rather than reduced sulfur species. However, by week 2, corresponding values of both had fallen by about 50%. While this might suggest a switch from iron to sulfur oxidation, this could not be the case for *L. ferrooxidans* which does not use reduced sulfur as an electron donor. Measurements of ATP concentrations in harvested cells showed that these had also fallen by about 50% from week 1 to 2 relative to protein contents, implying that much of the bacterial populations in these cultures had become moribund or had died. Indexed relative to ATP concentrations, specific rates of ferrous iron oxidation were similar on weeks 1 and 2, suggesting that both bacteria were continuing to use ferrous iron as their preferred electron donor. The specific rates of iron oxidation by planktonic-phase and attached cells of *At. ferrooxidans* sampled at the same time were found to be similar, suggestion that bacteria attached to the mineral phase were also using ferrous iron as their major energy source.

The conclusion that bacteria such as *At. ferrooxidans* use ferrous iron in preference to reduced sulfur when oxidizing pyrite correlates with similar observations reported when these bacteria are grown in liquid or on solid media that contain both ferrous iron and a soluble (usually tetrathionate) sulfur oxy-anion (Johnson, 1995; Yarzábal et al., 2004). Using ferrous iron in preference to reduced sulfur would appear not to make thermodynamic sense, given that the free energies (ΔG values) of elemental sulfur and tetrathionate (-507 and $-1225\,\mathrm{kJ\,mol^{-1}}$, respectively) far exceed that of ferrous iron ($-30\,\mathrm{kJ\,mol^{-1}}$; Kelly, 1978). However, the specific rates of tetrathionate oxidation tend to be much slower than ferrous iron oxidation for the acidithiobacilli (**Table 6**; data for *Acidithiobacillus* sp. ATCC 33020) so that the rates at which these bacteria can generate energy by oxidizing ferrous iron or tetrathionate are very similar. In addition, whereas ferrous iron oxidation by *At. ferrooxidans* involves a relatively short electron transport chain (comprising three cytochromes and rusticyanin), tetrathionate metabolism by this acidophile requires the synthesis of several enzymes (tetrathionate hydrolase, sulfur dioxygenase, thiosulfate quinone oxidoreductase, sulfite oxidoreductase, and rhodanese; Kanao et al., 2007), in addition to trans-membrane electron transport proteins. The additional energy expenditure required to synthesize these enzymes coupled with the fact that energy yields in unit time are similar for both tetrathionate and ferrous iron oxidation help explain why ferrous iron is used as a preferential electron donor by *Acidithiobacillus* spp. Additional supporting evidence for ferrous iron being the preferred electron donor for *At. ferrooxidans* comes from the observation that the *rus* operon is not repressed by elemental sulfur when ferrous iron is present (Amouric et al., 2009).

Table 6 | Comparison of the specific rates of ferrous iron and tetrathionate oxidation by *Acidithiobacillus* sp. ATCC 33020, and conversion of these into specific rates of energy generation in unit time.

Electron donor	Oxidation rate (mmol $\mathrm{min^{-1}}$ g $\mathrm{protein^{-1}}$)	Energy generation (J $\mathrm{min^{-1}}$ g $\mathrm{protein^{-1}}$)
Fe^{2+}	7.9 ± 0.21	237 ± 6
$S_4O_6^{2-}$	0.21 ± 0.027	260 ± 33

ENVIRONMENTAL ASPECTS OF OXIDO-REDUCTION OF IRON IN LOW pH ENVIRONMENTS

One of the first reports of active iron cycling in an acidic environment was by Johnson et al. (1993) who noted that 30 cm deep acid streamer growths found within an abandoned pyrite mine were stratified in terms of their color and consistency, and that these correlated with variations in concentrations of dissolved oxygen and redox potentials, the latter reflecting relative concentrations of ferrous and ferric iron (**Table 7**). Later work identified the major iron-oxidizing acidophile in the surface streamers as "*Fv. myxofaciens*," while iron-reducing *Acidiphilium* spp. and novel *Firmicutes* were more abundant in the lower depths of the streamer growths (Kimura et al., 2011). Johnson et al. (1993) also demonstrated that iron cycling by a mixed bioreactor culture of *At. ferrooxidans* and *Acidiphilium* SJH could be controlled by varying concentrations of dissolved oxygen (**Figure 3**). Pure cultures of moderate thermophiles [*Sulfobacillus* spp. and *Acidimicrobium* (*Am.*) *ferrooxidans*] also displayed iron cycling *in vitro* (**Figure 4**). Stratified acid streamer/mat growths have also been reported in an adit draining an abandoned small-scale copper mine (Cantareras) in Spain (**Figure 5**). Fragments of acid streamers from the site were shown to both oxidize and reduce iron *in vitro*, and acidophiles known to catalyze the oxido-reduction of iron were identified by molecular techniques and isolated from the streamer growths (Rowe et al., 2007). The Cantareras streamers have also been materials from which acidophilic sulfate-reducing bacteria have been isolated. The latter can also mediate ferric iron reduction in acidic environments indirectly *via* the hydrogen sulfide they generate as a waste product ($H_2S + 2\,Fe^{3+} \rightarrow S^0 + 2\,Fe^{2+} + 2H^+$) and possibly also directly, using ferric iron as an alternative electron acceptor to sulfate.

The Rio Tinto is a 100 km long river located in south-west Spain, characterized by being extremely acidic (pH 1.5–3.1) throughout its length and containing elevated concentrations of soluble iron (both ferrous and ferric, the latter conferring the characteristic burgundy red color of the river). The microbiology of this extensive extreme environment has been researched in depth by Ricardo Amils and colleagues at the Centro de Astrobiologia/Universidad Autonoma in Madrid. They found that the dominant bacteria in the Tinto river were the iron-metabolizing acidophiles *At. ferrooxidans*, *L. ferrooxidans*, and *Acidiphilium* spp., and that other prokaryotes that also catalyze the oxido-reduction of iron at low pH (*Ferrimicrobium* and *Ferroplasma* spp.) were present in smaller numbers (González-Toril et al., 2003). Iron cycling, involving ferrous iron oxidation mediated primarily by *At. ferrooxidans* and *L. ferrooxidans* in the oxic zones of the river and ferric iron reduction by *Acidiphilium* spp. and *At. ferrooxidans* in the anoxic zones, maintain the iron dynamics of the river from its source at the Peña de Hierro in the Iberian Pyrite Belt to Huelva, where it enters the Atlantic Ocean. Since the oxidation of ferrous to (soluble) ferric iron is a proton-consuming reaction, while the reverse reaction (as well as ferric iron hydrolysis) generates protons, the net effect of ongoing oxido-reduction of iron is to maintain the extremely low pH of the Tinto river throughout its length.

Table 7 | Depth-related chemical changes in acid streamer growths found within the abandoned Cae Coch pyrite mine.

Streamer depth (cm)	pH	DO_2 (% of ambient)	E_h (mV)	Fe^{2+} (g L^{-1})	Fe^{3+} (g L^{-1})	SO_4^{2-} (g L^{-1})
0–10	2.35	82	+734	0.25	1.15	5.9
10–20	2.40	10	+634	1.21	0.39	6.0
20–30	2.45	<0.1	+484	2.16	<0.01	5.2

Johnson et al. (1993), Kimura et al. (2011).

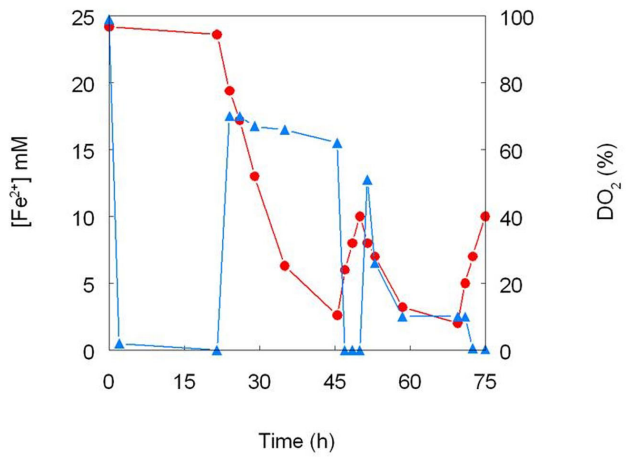

FIGURE 3 | Cycling of iron by a mixed culture of *At. ferrooxidans* and *Acidiphilium* SJH. The culture medium (pH 2.0) contained (initially) 25 mM ferrous sulfate and 10 mM glycerol, and was maintained at 30˚C under controlled aeration. Ferrous iron concentrations are shown in red and concentrations of dissolved oxygen in blue (modified from Johnson et al., 1993).

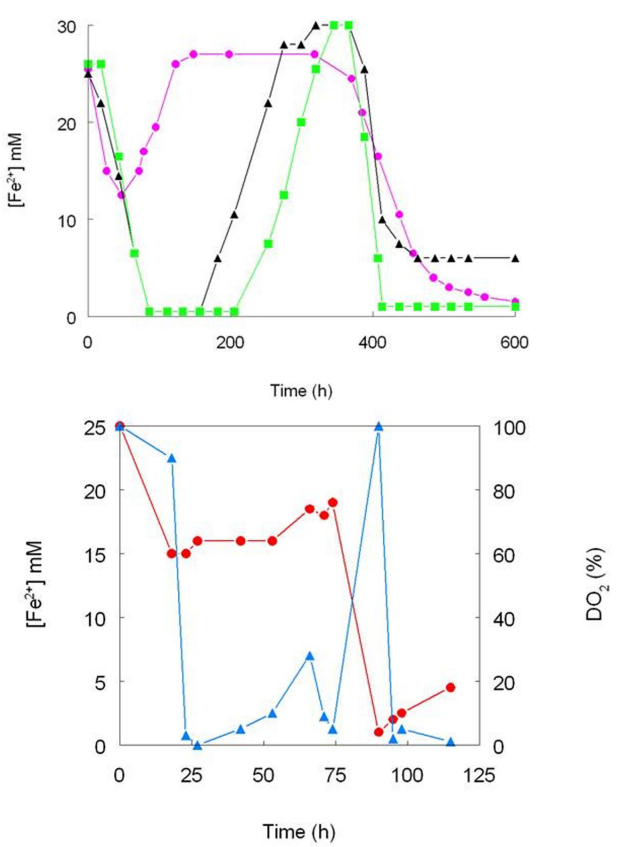

FIGURE 4 | Iron cycling by pure cultures of moderately thermophilic acidophiles. (Top) -▲- *Sb. thermosulfidooxidans* (strain TH1), -■- *Sb. acidophilus* (strain THWX), -●- *Acidimicrobium* sp. (strain HPTH; all cultures grown in pH 2.0 medium containing 25 mM ferrous sulfate, 10 mM glucose and 0.02% yeast extract; no aeration control); (bottom) the effect of controlling concentrations of dissolved oxygen iron cycling by *Sb. acidophilus* (strain THWX) grown at pH 2.0 in a medium containing 25 mM ferrous sulfate, 10 mM glycerol and 0.02% yeast extract; ferrous iron concentrations are shown in red and concentrations of dissolved oxygen in blue (modified from Johnson et al., 1993).

Extensive opencast mining of lignite in Lusatia and other regions of Germany has left a legacy of a large number of abandoned and flooded sites ("pit lakes"), many of which are moderately or extremely acidic and contain elevated concentrations of soluble iron and sulfate, resulting from the oxidation of pyrite and other minerals present in the disturbed substrata (Geller et al., 1998). Microbially mediated cycling of both iron and sulfur has been described in these pit lakes (Küsel, 2003; Meier et al., 2004). Oxidation of reduced sulfur and of ferrous iron (coupled with hydrolysis of ferric iron) in oxic surface waters causes these to be acidic (pH as low as 2.0) whereas the reductive dissolution of schwertmannite and microbial sulfidogenesis in the anoxic lake sediments generates net alkalinity, results in these zones having higher pH values (typically about 5.5; Küsel et al., 1999). The major iron-oxidizing bacteria identified in the lignite pit lakes are the acidophiles *At. ferrooxidans*, *L. ferrooxidans*, and *Ferrimicrobium* (Küsel, 2003; Lu et al., 2010) whereas the neutrophile *Geobacter* as well as acidophilic species (*Acidiphilium*, *Acidobacteria*, *Acidocella*, and *Acidithiobacillus*) have been implicated in mediating ferric iron reduction in these ecosystems (Lu et al., 2010).

Ferrous iron oxidation is an exergonic reaction, but for cycling of iron to perpetuate in acidic streams, rivers and lakes, energy is required to fuel the reduction of ferric iron, which may be microbially mediated or an abiotic process. Both organic and inorganic electron donors can be used by iron-reducing acidophiles. The latter may arise from extraneous sources (e.g., leaf detritus in surface waters) or derive from the indigenous primary producers present. These include chemautotrophic bacteria such as *Leptospirillum* and *Acidithiobacillus* spp., and photoautotrophic acidophiles, which are predominantly eukaryotic micro-algae (Gross, 2000). A proportion of the inorganic carbon fixed by both groups is released into the environments as organic compounds (cell

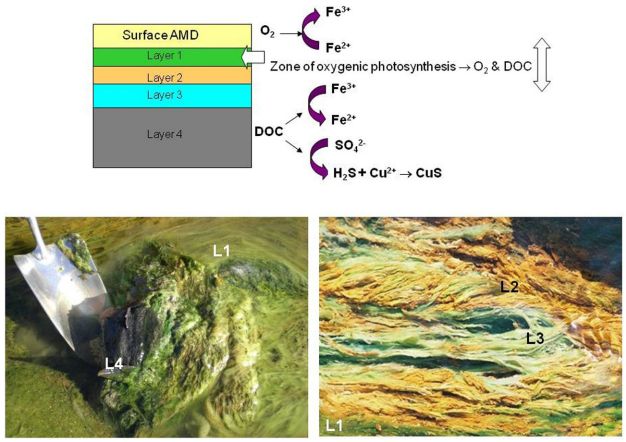

FIGURE 5 | Redox transformations of iron and sulfur in stratified streamer/mat growths found in a channel draining ad abandoned copper mine (Cantareras, Spain). The differently colored streamer/mat layers are indicated in the top diagram, and shown (as L1, L2 etc.) in the lower photographs.

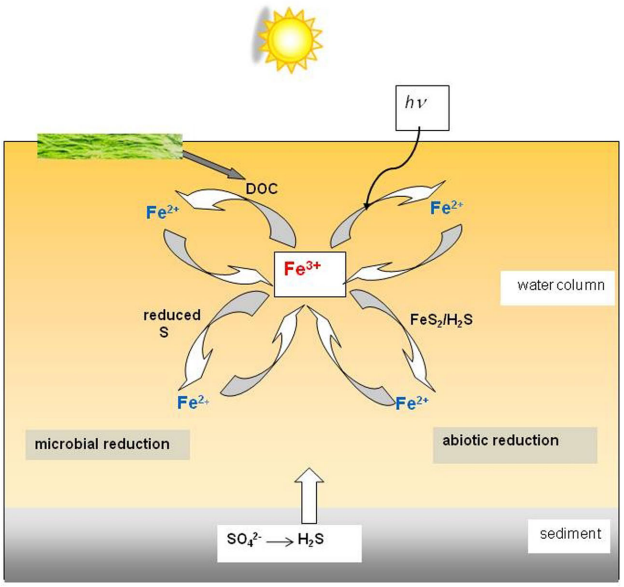

FIGURE 6 | Schematic of the different microbial and abiotic routes of ferric iron reduction in an acidic (pH < 3) stream, river, or pit lake. Abiotic iron oxidation proceeds slowly in these environments, and is primarily mediated by prokaryotic microorganisms.

exudates and lysates) that can be utilized by heterotrophic and mixotrophic iron-reducing prokaryotes. The nature and composition of organic exudates arising from acidophilic primary producers varies from species to species, however, and this impacts their potential utilization by organotrophic acidophiles. For example, glycolic acid was identified by Ňancucheo and Johnson (2010) as a significant exudate (accounting for up to 24% of total dissolved organic carbon) in cultures of iron- and sulfur-oxidizing acidophiles but was shown to be utilized by relatively few species (mostly *Firmicutes*) of organotrophic acidophiles. In contrast, monosaccharides (fructose, glucose and mannitol) identified in exudates of the acidophilic algae *Euglena mutabilis* and *Chlorella protothecoides* var. *acidicola* were found to support the growth of both iron-reducing and sulfate-reducing acidophiles (Ňancucheo and Johnson, 2011). These findings suggest that reduction of both ferric iron and sulfate can be more active processes in surface acidic environments where acidophilic algae are active (such as at Cantareras) than in subterranean sites like the Cae Coch mine. Reduced sulfur and hydrogen can also act as inorganic electron donors for iron reduction by some species of acidophiles (Johnson and Hallberg, 2009). The former can arise by a variety of routes in extremely acidic environments. For example, elemental sulfur and sulfur oxy-anions are formed as by-products of the abiotic oxidation of pyrite and other sulfide minerals by (microbially generated) ferric iron (Rohwerder et al., 2003), and hydrogen sulfide may be generated by sulfur- and sulfate-reducing prokaryotes in anaerobic sediments in acid lakes and streams. However, dissimilatory sulfur- and sulfate-reduction also requires a suitable electron donor, which may again be either organic or inorganic (hydrogen). Hydrogen, therefore, has a potentially important (though currently unknown) role in fueling ferric iron reduction (directly or indirectly) in acidic environments, where it may be formed *via* the acid dissolution of metals (e.g., relics of mining activities) and some minerals.

Ferric iron reduction in acidic waters can also, however, be mediated by solar energy. Diez Ercilla et al. (2009) showed that solar radiation was a major driver of diel changes in ferrous iron concentrations (10–90 μM) recorded in an acidic (pH 2.8) pit lake in the Iberian pyrite belt. The kinetics of photo-reduction of iron were shown to be zero-order and to be a function of temperature and the intensity of solar radiation, but were found to be independent of ferric iron concentration. Wavelengths within the UV-A spectrum and part of the visible spectrum (400–700 nm) were both shown to be active in iron reduction in the acidic lake. This is a particularly significant observation as it explains how iron cycling can perpetuate in acidic waters, such as acid mine drainage streams and pit lakes, in the absence of either inorganic or organic reductants, or of iron-reducing and sulfate-reducing bacteria. In addition, photochemical regeneration of ferrous iron explains why numbers of iron-oxidizing acidophiles can be maintained or even increase when their primary energy source (e.g., pyrite) is exhausted.

Iron cycling in acidic waters, highlighting the various possible routes of ferric iron reduction, is summarized schematically in **Figure 6**.

TECHNOLOGICAL APPLICATIONS OF MICROBIAL IRON OXIDO-REDUCTION AT LOW pH

Acidophilic iron-metabolizing prokaryotes are increasingly used in biotechnologies, the longest established of which is "biomining."

TECHNOLOGIES UTILIZING ACIDOPHILIC IRON-OXIDIZERS

The discovery of the first bacterium (*At. ferrooxidans*) shown, in the late 1940s, to oxidize iron in acidic liquors and, several years

later, demonstrated to accelerate the oxidative dissolution of pyrite and other sulfide minerals, was relatively quickly followed up by the first full-scale industrial application that used this acidophile (a dump copper leaching operation in Utah, in the mid-1960s). In reality, human civilisations had been exploiting the abilities of acidophiles to solubilize metals from ores for many years, recovering bioleached metals (chiefly copper, *via* cementation) from mine waters at the Rio Tinto mine in Spain, Mynydd Parys in Wales, the Song Guo Mountain and other locations in China, and probably elsewhere in the world. Since the 1960s there have been many developments and refinements in both the engineering design and in understanding the mineral bioprocessing. Biomining technologies have also diversified into recovering metals other than copper, including gold, uranium, nickel, cobalt and zinc. More details accounts of biomining can be found in Rawlings (2002); Rawlings and Johnson (2007a); and Johnson (2010).

Ferric iron is a powerful oxidizing agent in aqueous solutions, and can degrade a variety of minerals, including metal sulfides. It follows, therefore, that any prokaryote that can oxidize ferrous iron in an extremely acidic (pH < 3) medium should, in theory, be able to accelerate the dissolution of such minerals. This indeed has proven to be the case, with all of the iron-oxidizing bacteria listed in **Table 1** having been reported to also oxidize pyrite, though some (e.g., *Fm. acidiphilum*) only do this when supplied with organic carbon, which may originate from an extraneous source (e.g., added yeast extract) or from a sulfur-oxidizing autotroph in a mixed culture. The most numerous iron-oxidizing prokaryotes in commercial operations tend, however, to be autotrophs. For example *L. ferriphilum*, has frequently been reported to be the major primary mineral-degrader in stirred tanks that operate between 35° and 45°C. Although iron-oxidizing prokaryotes are the major players in the bioprocessing of sulfide ores and concentrates, these are members of microbial consortia in commercial operations. These consortia include "secondary" sulfur-oxidizing (acid-generating) prokaryotes, and "tertiary" heterotrophic or mixotrophic acidophiles that degrade the small molecular weight organic compounds, such as glycolic acid, that are excreted by autotrophic iron- and sulfur-oxidizers and which could otherwise accumulate to inhibitory concentrations, especially in tank leaching operations, as well as the "primary" iron-oxidizers (Rawlings and Johnson, 2007b). Some acidophiles can assume more than one role in such consortia, for example the heterotrophic iron-oxidizer *Ferroplasma* (**Figure 7**). Although, as also indicated in **Figure 7**, dissolution of sulfide minerals by ferric iron does not involve molecular oxygen, the process does not continue unless the ferrous iron generated by this reaction is re-oxidized to ferric. This microbially catalyzed reaction requires molecular oxygen, and oxygen is also consumed during the oxidation of reduced sulfur intermediates and the catabolism of organic materials, and therefore the process is described as "oxidative mineral dissolution."

The concept of using iron-oxidizing acidophiles to remediate mine waters has a long history, but only recently has such a system been demonstrated at pilot-scale level. Many streams and ground waters associated with the mining of coals and metals are enriched with soluble ferrous iron. The most effective way of removing soluble iron is first to oxidize ferrous iron to ferric, thereby facilitating the formation of ferric minerals such as

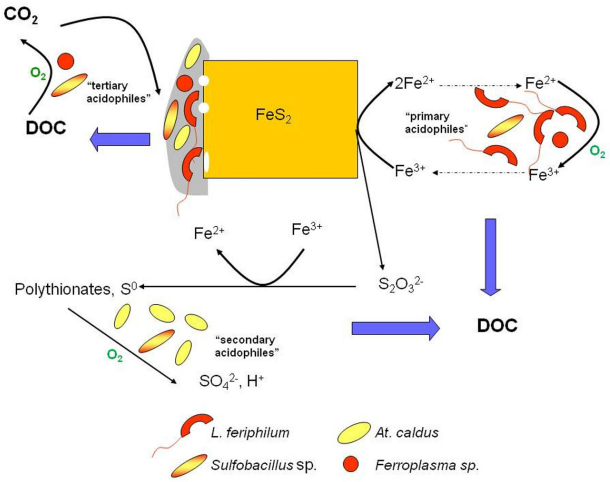

FIGURE 7 | The oxidative dissolution of pyrite in acidic liquors, showing the major microorganisms identified in the biooxidation of refractory gold concentrates and the bioleaching of a cobaltiferous pyrite concentrate processed at *ca.* 40°C. Those reactions that consume oxygen are indicated; "DOC" is dissolved organic carbon.

schwertmannite and ferrihydrite, which may require some additional input of alkaline materials. As noted previously, abiotic rates of ferrous iron oxidation in low pH waters tend to be very slow, but can be greatly accelerated by iron-oxidizing acidophiles. Since autotrophic species use the energy from ferrous iron oxidation to support their growth and have minimal nutritional requirements, the use of these acidophiles to remediate iron-contaminated waters is particularly attractive. Specific rates of iron oxidation (previous section) can provide important fundamental data when determining the size of a reactor required for this purpose. The maximum rate of iron oxidation by a mesophilic bacterium such as *At. ferrooxidans* is $\sim 5 \times 10^{-8}$ μg cell^{-1} min^{-1} (based on data shown in **Table 2**). Acidic mine water discharged at 10 L s^{-1} and containing 500 mg ferrous iron L^{-1} would require a reactor containing $\sim 6 \times 10^{15}$ iron-oxidizing bacteria. Cell numbers of autotrophic iron-oxidizers are typically $\sim 5 \times 10^{7}$ mL^{-1} in media containing 500 mg iron L^{-1}, so that a minimum bioreactor volume of just over 10 m^3 would be required to oxidize all of the iron present. In reality, a much larger reactor would be required as the bacteria would need to be immobilized on a support material to prevent them being washed out, in a continuous flow system.

A pilot-scale (10 m^3 reactor volume) system in Nochten, eastern Germany, is being used to oxidize ferrous iron and precipitate schwertmannite from acidic (pH 5.3) ground water containing, typically, 350 mg ferrous iron L^{-1} with a flow rate of 2,500 L h^{-1} (Janneck et al., 2010). The iron oxidation efficiency is ~70%, which is partly due to the temperature at which the system operates (ranging from 12 to 18°C). In addition, hydrolysis of ferric iron causes the pH of the oxidized groundwater to fall to 3.0, which results in a considerable proportion of the ferric iron being retained in solution. The Nochten plant was originally inoculated with *At. ferrooxidans* and *L. ferrooxidans*, but analysis of the indigenous microbial population several months after the plant was

commissioned revealed that these bacteria were not detectable, but that another iron-oxidizing acidophile ("*Fv. myxofaciens*") and bacteria related to the neutrophilic iron-oxidizer *Gallionella*, were the dominant bacteria present (Heinzel et al., 2009). "*Fv. myxofaciens*" has also been used in laboratory-scale systems to remediate mine waters (Rowe and Johnson, 2008; Hedrich and Johnson, 2012). Besides its fast specific rate of iron oxidation (**Table 2**), "*Fv. myxofaciens*" also has the important advantage of producing copious amounts of extracellular polymeric substances, by which it attaches to a variety of materials (including glass, plastics, metals, and minerals) and causing it to grow as long macroscopic streamers in flowing waters. This obviates the need of an inert support material for these bacteria and maximizes the biovolume of an operating reactor. A modular system for remediating acidic iron-rich mine waters using "*Fv. myxofaciens*" to oxidize ferrous iron and controlled pH adjustment to precipitate schwertmannite has recently been described by Hedrich and Johnson (2012). The system was shown to be highly efficient (an equivalent 10 m^3 primary reactor was calculated to be able to process ~2.7 L pH 2 mine water containing 250 mg L^{-1} ferrous iron s^{-1}) and produced pure-grade schwertmannite from mine water containing elevated concentrations of copper, zinc, aluminum, and manganese, in addition to iron. Concentrations of soluble iron were lowered from 250 g L^{-1} in the untreated water to <1 mg L^{-1} in the processed water.

TECHNOLOGIES UTILIZING ACIDOPHILIC IRON-REDUCERS

Development of technologies that use iron-reducing acidophiles has lagged well behind those that use iron-oxidizers. However, there has been at least one recent report that has demonstrated the potential for utilizing acidophilic iron-reducing bacteria to extract metals from mineral reserves. Not all metals occur exclusively as oxidized ores. Nickel is found within sulfide minerals (such as pentlandite) in, for example, reduced black shales, but is more abundant in the lithosphere in oxidized lateritic ores (~73% of estimated global reserves). In the case of limonitic laterites, nickel is intimately associated with ferric oxyhydroxide minerals such as goethite (FeOOH). Using an oxidative dissolution approach to process such ores is obviously not viable, whereas a reductive approach is feasible. By coupling the oxidation of an organic or an inorganic substrate to the reduction of ferric iron within the goethite lattice, the oxidized mineral is destroyed and the associated nickel liberated. When the reaction occurs in an acidic medium, both the iron and nickel that are solubilized remain in solution.

Bridge and Johnson (2000) showed that a variety of ferric iron minerals, including goethite, could be solubilized by the heterotrophic acidophilic iron-reducer *Acidiphilium* sp. SJH. In terms of an industrial process, however, elemental sulfur has several advantages (including cost) over an organic electron donor, and Hallberg et al. (2011b) elected to use *At. ferrooxidans* to demonstrate the bioleaching of a nickel limonite by reductive dissolution, using the reaction shown in the equation below:

$$S^0 + 6FeOOH + 11H^+ \rightarrow HSO_4^- + 6Fe^{2+} + 8H_2O.$$

Over 80% of the nickel present in a test ore was shown to be recovered when processed in this way, in a bioreactor maintained at 30°C and pH 1.8. Currently, similar ores are processed by high pressure acid leaching at elevated temperatures (in excess of 250°C). The bioreductive technology appears to have generic application for oxidized ores (e.g., of manganese, as well as iron) and bioprocessing of nickel laterites using this approach has been integrated into a full cycle operation (the "*Ferredox*" process; du Plessis et al., 2011). This recent development suggests that harnessing the potential of iron-metabolizing prokaryotes in new and emerging technologies could expand significantly in the near future.

ACKNOWLEDGMENTS

Part of this work was carried out in the frame of ProMinE (European project contract NMP-2008-LARGE-2:# 228559; DBJ and SH acknowledge the financial support given to this project by the European Commission under the Seventh Framework Program for Research and Development. Tadayoshi Kanao would like to thank the Japanese Ministry of Education, Culture, Sports, Science and Technology for providing financial support for his research.

REFERENCES

Amouric, A., Appia-Ayme, C., Yarzabal, A., and Bonnefoy, V. (2009). Regulation of the iron and sulfur oxidation pathways in the acidophilic *Acidithiobacillus ferrooxidans*. *Adv. Mat. Res.* 71–73; 163–166.

Amouric, A., Brochier-Armanet, C., Johnson, D. B., Bonnefoy, V., and Hallberg, K. B. (2011). Phylogenetic and genetic variation among Fe(II)-oxidizing acidithiobacilli supports the view that these comprise multiple species with different ferrous iron oxidation pathways. *Microbiology* 157, 111–122.

Baker, B. J., Tyson, G. W., Webb, R. I., Flanagan, J., Hugenholtz, P., Allen, E. E., and Banfield, J. F. (2006). Lineages of acidophilic archaea revealed by community genomic analysis. *Science* 314, 1933–1935.

Bigham, J. M., Schwertmann, U., Traina, S. J., Winland, R. L., and Wolf, M. (1996). Schwertmannite and the chemical modeling of iron in acid sulfate waters. *Geochim. Cosmochim. Acta* 60, 2111–2121.

Bonnefoy, V., and Holmes, D. S. (2011). Genomic insights into microbial iron oxidation and iron uptake strategies in extremely acidic environments. *Environ. Microbiol.* doi:10.1111/j.1462-2920.2011.02626.x

Bradford, M. M. (1976). A rapid and sensitive method for the quantification of microgram quantities of protein utilizing the principle of protein-dye binding. *Anal. Biochem.* 72, 248–254.

Bridge, T. A. M., and Johnson, D. B. (2000). Reductive dissolution of ferric iron minerals by *Acidiphilium* SJH. *Geomicrobiol. J.* 17, 193–206.

Brock, T. D., and Gustafson, J. (1976). Ferric iron reduction by sulfur- and iron-oxidizing bacteria. *Appl. Environ. Microbiol.* 32, 567–571.

Coupland, K., and Johnson, D. B. (2008). Evidence that the potential for dissimilatory ferric iron reduction is widespread among acidophilic heterotrophic bacteria. *FEMS Microbiol. Lett.* 279, 30–35.

Denef, V. J., Mueller, R. S., and Banfield, J. F. (2010). AMD biofilms: using model communities to study microbial evolution and ecological complexity in nature. *ISME J.* 4, 599–610.

Diez Ercilla, M., López Pamo, E., and Sánchez España, J. (2009). Photoreduction of Fe(III) in the acidic mine pit lake of San Telmo (Iberian Pyrite Belt): field and experimental work. *Aquat. Geochem.* 15, 391–419.

Dopson, M., Baker-Austin, C., Hind, A., Bowman, J. P., and Bond, P. L. (2004). Characterization of Ferroplasma isolates and *Ferroplasma acidarmanus* sp. nov., extreme acidophiles from acid mine drainage and industrial bioleaching environments. *Appl. Environ. Microbiol.* 70, 2079–2088.

Drobner, E., Huber, H., and Stetter, K. O. (1990). *Thiobacillus ferrooxidans*, a facultative hydrogen oxidizer. *Appl. Environ. Microbiol.* 56, 2922–2923.

du Plessis, C. A., Slabbert, W., Hallberg, K. B., and Johnson, D. B. (2011). Ferredox: a biohydrometallurgical processing concept for limonitic nickel laterites. *Hydrometallurgy* 109, 221–229.

Geller, W., Klapper, H., and Salomons, W. (eds). (1998). *Acid Mining Lakes – Acid Mine Drainage, Limnology and Reclamation. Environmental Science Series.* Berlin, Springer.

Golyshina, O. V., Yakimov, M. M., Lünsdorf, H., Ferrer, M., Nimtz, M., Timmis, K. N., Wray, V., Tindall, B. J., and Golyshin, P. N. (2009). *Acidiplasma aeolicum* gen. nov., sp. nov., a euryarchaeon of the family *Ferroplasmaceae* isolated from a hydrothermal pool, and transfer of *Ferroplasma cupricumulans* to *Acidiplasma cupricumulans* comb. nov. *Int. J. Syst. Evol. Microbiol.* 59, 2815–2823.

González-Toril, E., Llobet-Brossa, E., Casamayor, E. O., Amman, R., and Amils, R. (2003). Microbial ecology of an extreme acidic environment, the Tinto river. *Appl. Environ. Microbiol.* 69, 4853–4865.

Gross, W. (2000). Ecophysiology of algae living in highly acidic environments. *Hydrobiology* 433, 31–37.

Hallberg, K. B., Hedrich, S., and Johnson, D. B. (2011a). *Acidiferribacter thiooxydans*, gen. nov. sp. nov.; an acidophilic, thermo-tolerant, facultatively anaerobic iron- and sulfur-oxidizer of the family Ectothiorhodospiraceae. *Extremophiles* 15, 271–279.

Hallberg, K. B., Grail, B. M., du Plessis, C., and Johnson, D. B. (2011b). Reductive dissolution of ferric iron minerals: a new approach for bioprocessing nickel laterites. *Miner. Eng.* 24, 620–624.

Hallberg, K. B., Thomson, H. E. C., Boeselt, I., and Johnson, D. B. (2001). "Aerobic and anaerobic sulfur metabolism by acidophilic bacteria," in *Biohydrometallurgy: Fundamentals, Technology and Sustainable Development, Process Metallurgy 11A*, eds V. S. T. Ciminelli and O. Garcia Jr. (Amsterdam: Elsevier), 423–431.

Hedrich, S., and Johnson, D. B. (2012). A modular continuous flow reactor system for the selective bio-oxidation and precipitation of iron in mine-impacted waters. *Bioresour. Technol.* 106, 44–49.

Hedrich, S., Schlömann, M., and Johnson, D. B. (2011). The iron-oxidizing proteobacteria. *Microbiology* 157, 1551–1564.

Heinzel, E., Hedrich, S., Janneck, E., Glombitza, F., Seifert, J., and Schlömann, M. (2009). Bacterial diversity in a mine water treatment plant. *Appl. Environ. Microbiol.* 75, 858–861.

Janneck, E., Arnold, I., Koch, T., Meyer, J., Burghard, D., Ehinger, S. (2010). "Microbial synthesis of schwertmannite from lignite mine water and its utilization for removal of arsenic from mine waters and for production of iron pigments," in *Proceedings of the International Mine Water Association Symposium 2010: Mine Water and Innovative Thinking*, eds C. Wolkersdorfer and A. Freund (Sydney: Cape Breton University Press), 131–134.

Johnson, D. B. (1995). Selective solid media for isolating and enumerating acidophilic bacteria. *J. Microbiol. Methods* 23, 205–218.

Johnson, D. B. (2010). "The biogeochemistry of biomining," in *Geomicrobiology: Molecular and Environmental Perspective*, eds L. Barton and M. Mandl (Dordrecht: Springer), 401–426.

Johnson, D. B., and Bridge, T. A. M. (2002). Reduction of ferric iron by acidophilic heterotrophic bacteria: evidence for constitutive and inducible enzyme systems in *Acidiphilium* spp. *J. Appl. Microbiol.* 92, 315–321.

Johnson, D. B., and Hallberg, K. B. (2009). Carbon, iron and sulfur metabolism in acidophilic microorganisms. *Adv. Microb. Physiol.* 54, 202–256.

Johnson, D. B., and McGinness, S. (1991). Ferric iron reduction by acidophilic heterotrophic bacteria. *Appl. Environ. Microbiol.* 57, 207–211.

Johnson, D. B., McGinness, S., and Ghauri, M. A. (1993). Biogeochemical cycling of iron and sulfur in leaching environments. *FEMS Microbiol. Rev.*11, 63–70.

Kanao, T., Kamimura, K., and Sugio, T. (2007). Identification of a gene encoding a tetrathionate hydrolase in *Acidithiobacillus ferrooxidans. J. Biotechnol.* 132, 16–22.

Kelly, D. P. (1978). "Bioenergetics of chemolithotrophic bacteria," in *Companion to Microbiology; Selected Topics for Further Discussion*, eds A. T. Bull and P. M. Meadow (London: Longman), 363–386.

Kimura, S., Bryan, C. G., Hallberg, K. B., and Johnson, D. B. (2011). Biodiversity and geochemistry of an extremely acidic, low temperature subterranean environment sustained by chemolithotrophy. *Environ. Microbiol.* 13, 2092–2104.

Küsel, K. (2003). Microbial cycling of iron and sulfur in acidic coal mining lake sediments. *Water Air Soil Pollut.* 3, 67–90.

Küsel, K., Dorsch, T., Acker, G., and Stackebrandt, E. (1999). Microbial reduction of Fe(III) in acidic sediments: isolation of *Acidiphilium* cryptum JF-5 capable of coupling the reduction of Fe(III) to the oxidation of glucose. *Appl. Environ. Microbiol.* 65, 3633–3640.

Küsel, K., Roth, U., and Drake, H. (2002). Microbial reduction of Fe(III) in the presence of oxygen under low pH conditions. *Environ. Microbiol.* 4, 414–421.

Lovley, D. R., and Phillips, E. J. P. (1987). Rapid assay for microbially reducible ferric iron in aquatic sediments. *Appl. Environ. Microbiol.* 53, 1536–1540.

Lu, S., Gischkat, S., Reiche, M., Akob, D. M., Hallberg, K. B., and Küsel, K. (2010). Ecophysiology of Fe-cycling bacteria in acidic sediments. *Appl. Environ. Microbiol.* 76, 8174–8183.

Macalady, J. L., Jones, D. S., and Lyon, E. H. (2007). Extremely acidic, pendulous cave wall biofilms from the Frasassi cave system, Italy. *Environ. Microbiol.* 9, 1402–1414.

Magnuson, T. S., Swenson, M. W., Paszczynski, A. J., Deobald, L. A., Kerk, D., and Cummings, D. E. (2010). Proteogenomic and functional analysis of chromate reduction in *Acidiphilium* cryptum JF-5, an Fe(III)-respiring acidophile. *Biometals* 23, 1129–1138.

Meier, J., Babenzien, H. D., and Wendt-Potthoff, K. (2004). Microbial cycling of iron and sulfur in sediments of acidic and pH-neutral mining lakes in Lusatia (Brandenburg, Germany). *Biogeochemistry* 67, 135–156.

Monhemius, A. J. (1977). Precipitation diagrams for metal hydroxides, sulfides, arsenates and phosphates. *Trans. Inst. Min. Metall.* 86, C202–C206.

Ňancucheo, I., and Johnson, D. B. (2010). Production of glycolic acid by chemolithotrophic iron- and sulfur-oxidizing bacteria and its role in delineating and sustaining acidophilic sulfide mineral-oxidizing consortia. *Appl. Environ. Microbiol.* 76, 461–467.

Ňancucheo, I., and Johnson, D. B. (2011). Safeguarding reactive mine tailings by ecological engineering: the significance of microbial communities and interactions. *Appl. Environ. Microbiol.* 77, 8201–8208.

Nicolle, J. L. C., Simmons, S., Bathe, S., and Norris, P. R. (2009). Ferrous iron oxidation and rusticyanin in halotolerant, acidophilic "Thiobacillus prosperous." *Microbiology* 155, 1302–1309.

Ohmura, N., Sasaki, K., Matsumoto, N., and Saiki, H. (2002). Anaerobic respiration using Fe^{3+}, S^0 and H_2 in the chemolithotrophic bacterium *Acidithiobacillus ferrooxidans. J. Bacteriol.* 184, 2081–2087.

Okibe, N., and Johnson, D. B. (2004). Biooxidation of pyrite by defined mixed cultures of moderately thermophilic acidophiles in pH-controlled bioreactors: the significance of microbial interactions. *Biotechnol. Bioeng.* 87, 574–583.

Okibe, N., and Johnson, D. B. (2011). A rapid ATP-based method for determining active microbial populations in mineral leach liquors. *Hydrometallurgy* 108, 195–198.

Pronk, J. T., Liem, K., Bos, P., and Kuenen, J. G. (1991). Energy transduction by anaerobic ferric iron reduction in *Thiobacillus ferrooxidans. Appl. Environ. Microbiol.* 57, 2063–2068.

Rawlings, D. E. (2002). Heavy metal mining using microbes. *Annu. Rev. Microbiol.* 56, 65–91.

Rawlings, D. E., and Johnson, D. B. (eds). (2007a). *Biomining.* Heidelberg: Springer-Verlag.

Rawlings, D. E., and Johnson, D. B. (2007b). The microbiology of biomining: development and optimization of mineral-oxidizing microbial consortia. *Microbiology* 153, 315–324.

Regenspurg, S., Brand, A., and Peiffer, S. (2004). Formation and stability of schwertmannite in acidic mining lakes. *Geochim. Cosmochim. Acta* 68, 1185–1197.

Rohwerder, T., Gehrke, T., Kinzler, K., and Sand, W. (2003). Bioleaching review part A: progress in bioleaching: fundamentals and mechanisms of bacterial metal sufide oxidation. *Appl. Microbiol. Biotechnol.* 63, 239–248.

Rowe, O. F., and Johnson, D. B. (2008). Comparison of ferric iron generation by different species of

acidophilic bacteria immobilised in packed-bed reactors. *Syst. Appl. Microbiol.* 31, 68–77.

Rowe, O. F., Sánchez-España, J., Hallberg, K. B., and Johnson, D. B. (2007). Microbial communities and geochemical dynamics in an extremely acidic, metal-rich stream at an abandoned sulfide mine (Huelva, Spain) underpinned by two functional primary production systems. *Environ. Microbiol.* 9, 1761–1771.

San Martin-Uriz, P., Gomez, M. J., Arcas, A., Bargiela, R., and Amils, R. (2011). Draft genome Sequence of the electricigen *Acidiphilium* sp. strain PM (DSM 24941). *J. Bacteriol.* 193, 5585–5586.

Stumm, W., and Morgan, J. J. (1981). *Aquatic Chemistry: An Introduction Emphasizing Chemical Equilibria in Natural Waters.* New York: Wiley.

Welham, N. J., Malatt, K. A., and Vukcevic, S. (2000). The effect of solution speciation on iron-sulfur-arsenic-chloride systems at 298 K. *Hydrometallurgy* 57, 209–223.

Yarzábal, A., Appia-Ayme, C., Ratouchniak, J., and Bonnefoy, V. (2004). Regulation of the expression of the *Acidithiobacillus ferrooxidans* rus operon encoding two cytochromes c, a cytochrome oxidase and rusticyanin. *Microbiology* 150, 2113–2123.

Conflict of Interest Statement: The authors declare that the research was conducted in the absence of any commercial or financial relationships that could be construed as a potential conflict of interest.

Received: 31 October 2011; accepted: 27 February 2012; published online: 16 March 2012.

Citation: Johnson DB, Kanao T and Hedrich S (2012) Redox transformations of iron at extremely low pH: fundamental and applied aspects. Front. Microbio. ***3****:96. doi: 10.3389/fmicb.2012.00096*

This article was submitted to Frontiers in Microbiological Chemistry, a specialty of Frontiers in Microbiology.

Copyright © 2012 Johnson, Kanao and Hedrich. This is an open-access article distributed under the terms of the Creative Commons Attribution Non Commercial License, which permits non-commercial use, distribution, and reproduction in other forums, provided the original authors and source are credited.

frontiers in
MICROBIOLOGY

PERSPECTIVE ARTICLE
published: 20 February 2012
doi: 10.3389/fmicb.2012.00057

Toward a mechanistic understanding of anaerobic nitrate-dependent iron oxidation: balancing electron uptake and detoxification

Hans K. Carlson[1], Iain C. Clark[1,2], Ryan A. Melnyk[1] and John D. Coates[1]*

[1] *Department of Plant and Microbial Biology, University of California Berkeley, Berkeley, CA, USA*
[2] *Department of Civil and Environmental Engineering, University of California Berkeley, Berkeley, CA, USA*

Edited by:
Eric Roden, University of Wisconsin–Madison, USA

Reviewed by:
Amy Michele Grunden, North Carolina State University, USA
Flynn Picardal, Indiana University, USA

***Correspondence:**
John D. Coates, Department of Plant and Microbial Biology, University of California Berkeley, Berkeley, CA 94720, USA.
e-mail: jdcoates@berkeley.edu

The anaerobic oxidation of Fe(II) by subsurface microorganisms is an important part of biogeochemical cycling in the environment, but the biochemical mechanisms used to couple iron oxidation to nitrate respiration are not well understood. Based on our own work and the evidence available in the literature, we propose a mechanistic model for anaerobic nitrate-dependent iron oxidation. We suggest that anaerobic iron-oxidizing microorganisms likely exist along a continuum including: (1) bacteria that inadvertently oxidize Fe(II) by abiotic or biotic reactions with enzymes or chemical intermediates in their metabolic pathways (e.g., denitrification) and suffer from toxicity or energetic penalty, (2) Fe(II) tolerant bacteria that gain little or no growth benefit from iron oxidation but can manage the toxic reactions, and (3) bacteria that efficiently accept electrons from Fe(II) to gain a growth advantage while preventing or mitigating the toxic reactions. Predictions of the proposed model are highlighted and experimental approaches are discussed.

Keywords: nitrate dependent ferrous iron oxidation, NDFO, Fe(II) oxidoreductase, electron sparing, *Acidovorax*

INTRODUCTION

In recent years, significant progress has been made toward understanding the biochemical mechanisms used by bacteria to catalyze the aerobic and anaerobic oxidation of Fe(II) in the environment. Recent reviews focus on aerobic/microaerobic iron oxidation (Emerson et al., 2010) and iron oxidation by acidophiles and anoxygenic phototrophs (Bird et al., 2011), however a number of microorganisms have been described which can couple iron oxidation to nitrate reduction (Chaudhuri et al., 2001; Weber et al., 2001, 2006a,b; Finneran et al., 2002; Lack et al., 2002; Muehe et al., 2009) in the absence of oxygen and light. The growth benefit from anaerobic iron oxidation varies widely. In both photosynthetic and nitrate reducing bacteria, oxidation of Fe(II) may represent an important detoxification strategy (Muehe et al., 2009; Poulain and Newman, 2009), and in some cases may have also evolved into a metabolic strategy (Widdel et al., 1993; Croal et al., 2007; Jiao and Newman, 2007; Muehe et al., 2009; Weber et al., 2009; Chakraborty et al., 2011). In this paper, we suggest that the success of an iron-oxidizing microorganism depends on the extent to which electron donation from Fe(II) can be controlled and toxic reactions prevented or managed. We propose working models to analyze the results of experiments aimed at elucidating the mechanisms of iron oxidation by anaerobic nitrate reducing bacteria. We also highlight some of the predictions of the models that future experiments should address. Our intention is not to exhaustively review the literature, but rather to highlight some of the salient features of anaerobic nitrate-dependent iron oxidation and provide insight for new research directions.

RUSTING AWAY IN THE DARK, WITHOUT OXYGEN: EVIDENCE FOR ANAEROBIC NITRATE-DEPENDENT IRON OXIDATION BY ENVIRONMENTAL BACTERIA

Bacterial species that couple the oxidation of Fe(II) to nitrate reduction have been isolated from a wide range of habitats and are phylogenetically diverse (Hafenbradl et al., 1996; Straub et al., 1996; Chaudhuri et al., 2001). Iron-oxidizing microbes have been demonstrated to oxidize both soluble and insoluble Fe(II) (Widdel et al., 1993; Chaudhuri et al., 2001; Weber et al., 2001, 2006c), and to produce a variety of insoluble Fe(III) mineral products (Machulla et al., 1998; Straub and Buchholz-Cleven, 1998; Chaudhuri et al., 2001; Weber et al., 2006c). Although the metabolism is based on thermodynamically favorable redox reactions (Koppenol, 1996; Bartberger et al., 2002; Shafirovich and Lymar, 2002; Dutton et al., 2005; Flores-Santana et al., 2011), little is known about the mechanisms used by anaerobic neutrophilic nitrate-dependent iron oxidizers (Weber et al., 2006a; Bird et al., 2011). However, a few studies do suggest an energetic benefit from this metabolism for the organisms involved (Muehe et al., 2009; Weber et al., 2009). **Figure 1** presents several conceivable mechanisms for obtaining energetic benefit from iron oxidation catalyzed by anaerobic denitrifying bacteria. Some of these mechanisms may be inducible in specialized iron-oxidizing microorganisms, while others may be general to all nitrate reducing bacteria. One of these mechanisms (*electron sparing*) includes both enzymatically mediated components and abiotic interactions between Fe(II) and reactive intermediates resulting in a net energy gain. These mechanisms may be mutually exclusive, but based on reactive species formed during metabolism, it is more likely that hybrid abiotic/biotic

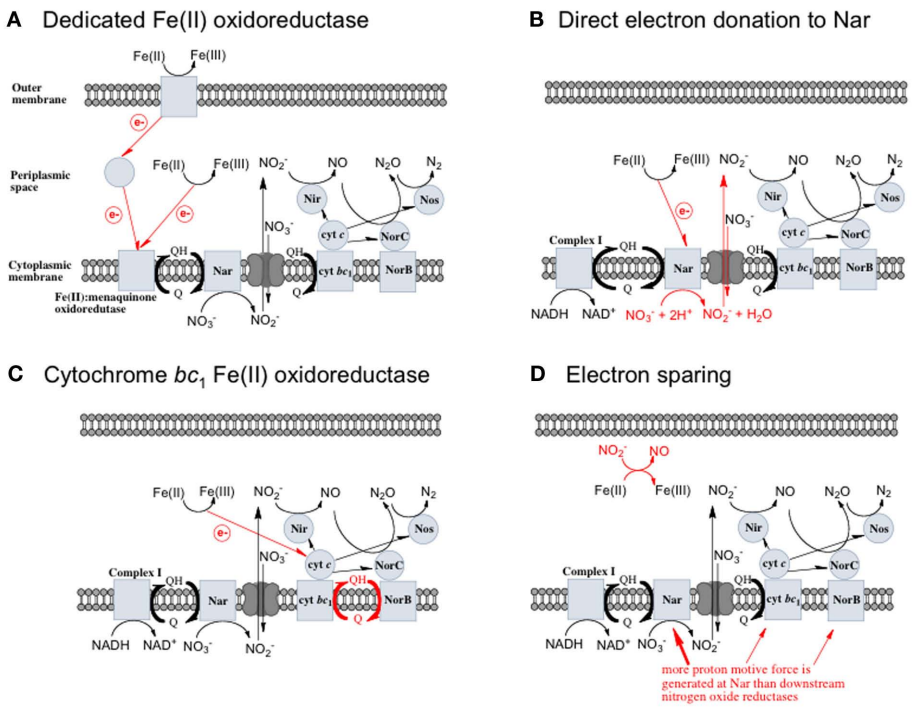

FIGURE 1 | Possible mechanisms for energetic benefit from iron oxidation coupled to nitrate reduction. (A) A true Fe(II):menaquinone oxidoreductase accepts electrons from iron and reduces the quinone pool, **(B)** Nar accepts electrons from Fe(II) and reduces nitrate cytoplasmically, consuming protons to generate a PMF, **(C)** the cytochrome bc_1 complex accepts electrons from Fe(II) and reduces the quinone pool, **(D)** more protons are pumped per electron at Nar than other nitrogen oxide reductases. If abiotic reactions dominate for the reduction of NO_2^-, an energetic benefit is conferred through an electron sparing mechanism. Nar, nitrate reductase; Nir, nitrite reductase; Nor, nitric oxide reductase; Nos, nitrous oxide reductase; QH_2, reduced quinone; Q, oxidized quinone; bc_1, cytochrome bc_1; cyt *c*, cytochrome *c*.

mechanisms are functioning. To the best of our knowledge such hybrid abiotic/biotic mechanisms represent a novel metabolic process in microbiology. Below follows a brief description of these mechanisms and the evidence to support their existence.

A DEDICATED Fe(II) OXIDOREDUCTASE

A dedicated Fe(II): menaquinone oxidoreductase protein, or protein complex, could oxidize iron at the cell surface or in the periplasm and reduce the quinone pool, providing reducing equivalents for downstream nitrogen oxide reductases (**Figure 1A**) allowing for proton motive force (PMF) generation. This mechanism predicts inducibility of iron oxidation and the expression of a specific protein or proteins in response to Fe(II).

DIRECT ELECTRON DONATION TO NITRATE REDUCTASE

In this model a standard membrane bound Nar could serve as the combined Fe(II) oxidase and nitrate reductase. If Nar can accept electrons from Fe(II) to catalyze cytoplasmic NO_3^- reduction to NO_2^- and H_2O, two protons are consumed in the cytoplasm without the need for electrons from NADH resulting in an enhanced PMF (**Figure 1B**). Although, this mechanism may be inducible, it is unlikely as Nar will be expressed during nitrate reducing conditions regardless. As such, it could be an inadvertent mechanism of dissimilatory nitrate reduction using Nar. NO_3^- Transport into the cytoplasm by NO_3^-/NO_2^- antiporters without consumption of periplasmic protons is necessary for this mechanism to generate a PMF. It is important to note that nitrate reductases with periplasmic sites for NO_3^-, such as Nap, consume periplasmic protons to reduce nitrate and no energetic benefit would result from Fe(II) electron donation to catalyze NO_3^- reduction by Nap.

CYTOCHROME bc_1 COMPLEX MEDIATED Fe(II) OXIDATION

A third possibility is that the cytochrome bc_1 complex can accept electrons from Fe(II) and reduce the quinone pool This is similar to the proposed mechanism that *Acidithiobacillus* and anoxygenic phototrophs use to generate NADH from Fe(II) oxidation (**Figure 1C**; Bird et al., 2011). In these metabolisms, the cytochrome bc_1 complex is proposed to be involved in reverse electron transfer to reduce the quinone pool (Bird et al., 2011). The exact mechanism and the net proton translocation associated with reverse electron transfer by bc_1 is not well understood, but is thought to be at the expense of the PMF (Ferguson and Ingledew, 2008). For neutrophilic iron oxidation, the redox potential of Fe(III)/Fe(II) is low enough to reduce menaquinone ($E^{\circ\prime} = -0.074$ V; Wagner et al., 1974; Schoepp-Cothenet et al., 2009). However, for this mechanism to generate a PMF, the quinone pool must obtain protons from the cytoplasm upon reduction by the bc_1 complex, and release those protons into the periplasm upon oxidation. Coupled to a quinol dehydrogenase, this would provide net proton translocation (Note: some NorBC are quinol dehydrogenases; Kraft et al., 2011). We envision that alternating fluxes of acetate and nitrate in the environment could

be harnessed by a bc_1 ferroxidase in this way. When high acetate concentrations are present, electrons flow through cytochrome *c* to sustain denitrification, and iron oxidation by bc_1 is minimal. As acetate becomes scarce, the quinone pool is largely oxidized, and electrons from iron could be used to reduce the quinone pool at bc_1.

ELECTRON SPARING

A fourth mechanism for obtaining an energetic benefit from Fe(II) oxidation involves differential electron flow to the terminal reductases. If more protons are translocated per electron at the nitrate reductase (Nar) than at downstream reductases coupled to bc_1, then a shift in electron flow to Nar would be beneficial (**Figure 1D**). If this is the case, under heterotrophic growth conditions with excess electron acceptor (e.g., NO_3^-), abiotic redox reactions between Fe(II) and NO_2^- and other nitrogen oxides would allow greater net proton translocation per electron from Complex I. We refer to this phenomenon as electron sparing. More nitrate would be consumed in such a mechanism, but an energetic benefit to the organism would be gained per mole of electron donor (i.e., organic co-substrate, H_2). This mechanism only applies to iron oxidizers when a co-substrate is available as an electron donor, and could be more pronounced when abiotically produced nitrogen oxide gases are continuously removed, as in flow through experimental setups. However, when electron acceptor is limiting, such reactions are likely to lead to a growth disadvantage due to a loss of electron accepting capacity. This hypothesis can be tested by looking for differences in growth on Fe(II) under donor or acceptor limiting conditions in batch culture. It is also important to emphasize that the location of the Fe(II) reaction with NO_2^- is potentially very important in determining the consequences for the bacterial cell. If the reaction happens in the periplasm, insoluble Fe(III) crusts may be harmful, but if the reaction happens outside of the cell, the NO_2^- could react with insoluble Fe(II) in minerals without negative consequences for the cell.

THINKING OUTSIDE OF THE CELL: EVIDENCE FOR ABIOTIC REDUCTION OF NITROGEN OXIDES CATALYZED BY SOLUBLE Fe(II) AND INSOLUBLE Fe(II) MINERALS

Regardless of whether abiotic reactions of nitrogen oxides and Fe(II) can lead to an energetic benefit through electron sparing, uncoupling the denitrification pathway is likely to create a significant flux of toxic reactive nitrogen species. The characterization of these products and the mechanisms whereby microorganisms cope with the toxicity will lead to an understanding of the benefit or cost of microbial iron oxidation.

The abiotic reaction of nitrate (NO_3^-) with soluble Fe(II) is slow (Moraghan and Buresh, 1977). However, the reaction between (NO_2^-) and soluble Fe(II) is rapid (Moraghan and Buresh, 1977). The products of the abiotic reactions vary with pH and include NO, N_2O, and NH_4^+ (Chalamet, 1973; Moraghan and Buresh, 1977). Copper (Cu^{2+}) or silver (Ag^+) can catalyze abiotic NO_3^- reduction coupled to Fe(II) oxidation at room temperature and neutral pH (Moraghan and Buresh, 1977; Ottley et al., 1997). Green rusts (GR), mixed Fe(II)/Fe(III) hydroxides, can also catalyze the reduction of nitrogen oxides (**Figure 2A**). As with soluble Fe(II), GR reactions with NO_3^- and NO_2^- produce NO, N_2O, and NH_4 depending on the pH (**Figure 2A**; Summers and Chang, 1993; Hansen et al., 1994, 1996). It has further been observed that the intercalating anion in the GR mineral affects the rate of NO_3^- reduction. GR intercalated with chloride (Cl^-) has a 30- to 40-fold faster rate of NO_3^- reduction compared with GR intercalated with sulfate (SO_4^-) (Hansen et al., 2001). A number of microorganisms produce GR as intermediates or products of nitrate-dependent iron oxidation (Chaudhuri et al., 2001; Lack et al., 2002). Therefore, it is possible that abiotic reactions catalyzed by GR can contribute to nitrate removal in iron-oxidizing microcosms and cultures during the growth phase, after growth has stopped, or in non-growth cultures in which GR has formed.

A WRENCH IN THE GEARS: EVIDENCE FOR UNCOUPLING OF BACTERIAL DENITRIFICATION BY Fe(II)

In *Escherichia coli*, it has been known for some time that the presence of millimolar Fe(II) and NO_3^- leads to an uncoupling of electron transport and dissimilatory nitrate reduction resulting in the production of high micromolar to millimolar levels of nitric oxide (NO) and nitrous oxide (N_2O; Brons et al., 1991; **Figure 2B**). Further evidence for uncoupling of nitrate reduction electron transport by Fe(II) was observed with *Shewanella putrefaciens* 200 and *Paracoccus denitrificans* (Cooper et al., 2003; Coby and Picardal, 2005). The location and form of Fe(II), the pH, and the nitrogen oxide starting material are all likely to contribute to the products of abiotic uncoupling reactions during microbial nitrate and nitrite reduction (Chalamet, 1973; Moraghan and Buresh, 1977; Hansen et al., 2001).

As the reaction between Fe(II) and NO_3^- is slow, the first likely point of uncoupling is Fe(II) oxidation by NO_2^- to produce NO and Fe(III) as initial products (**Figure 2B**). In previous studies, NO was found to be produced at a higher rate and accumulate in cultures of heterotrophically grown nitrate reducers in the presence of Fe(II) (Brons et al., 1991). NO is a gas, and will partition into the headspace of sealed culture tubes, potentially representing a significant loss of electron accepting equivalents in open systems. However, NO is also toxic, and can react with metalloproteins in the cell and components of the electron transport chain, and in the presence of redox active metals can nitrosate thiols (Beckman and Koppenol, 1996). Fortunately, the respiratory NO reductase (Nor) of denitrifying bacteria can reduce NO to less toxic products, and other enzymes involved in the reduction of nitrogen oxides can play a protective role in addition to their respiratory function (Gardner et al., 2002; Gomes et al., 2002; Mills et al., 2008). Nor is independently regulated from other components of the denitrification pathway and can be upregulated to reduce excess NO (Rodionov et al., 2005).

Little NO_2^- should accumulate in denitrifying cultures as a result of fast abiotic reactions between NO_2^- and Fe(II). Contrary to this prediction, some previous studies have measured nitrite accumulation and attributed this finding to the inhibition of nitrite reductase by Fe(III) precipitation (Straub et al., 1996; Weber et al., 2006b). However, it should be noted that NO (and other nitrogen oxides) will rapidly react with O_2 to form nitrite (Feelisch, 1991; Beckman and Koppenol, 1996). If samples are not kept anaerobic

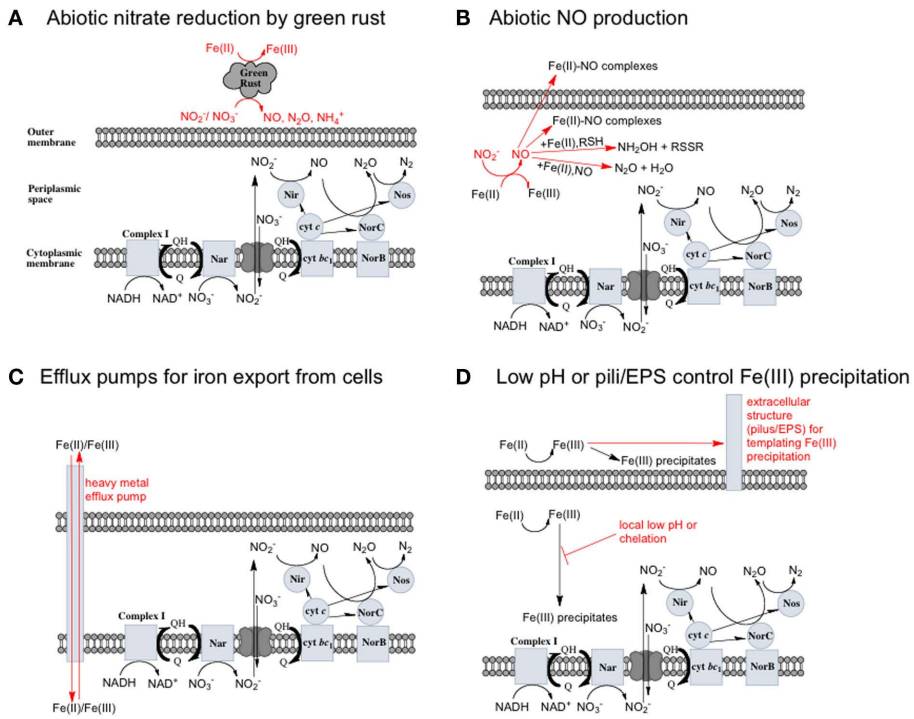

FIGURE 2 | Possible reactions resulting in toxicity and energetic loss during iron oxidation coupled to nitrate reduction and potential microbial responses. (A) Green rusts are capable of catalyzing nitrate reduction coupled to iron oxidation. If they are produced, they will consume NO_3^- and compete with bacteria for electron acceptor. **(B)** NO_2^- will rapidly react with Fe(II) to form NO. NO can be further reduced, but can also bind to metalloproteins and disrupt electron transport chains. Upregulation of Nor or other NO reductase proteins could protect cells from NO. **(C)** Soluble Fe(II) or Fe(III) could be exported from cells by heavy metal efflux pumps before it reacts with cellular components (in the case of Fe(II)) or precipitates to form mineral crusts (in the case of Fe(III)). **(D)** Extracellular polysaccharides or pili may scaffold the precipitation of Fe(III) outside of cells, or a local low pH or chelators may prevent the precipitation of Fe(III) in the periplasm.

during sample preparation for nitrite analysis, the nitrite analyzed may also represent other reactive nitrogen species (Straub et al., 1996; Weber et al., 2006b). Some researchers have suggested that NO_2^- may function as a shuttle to oxidize iron (Miot et al., 2009a; Chakraborty et al., 2011). We find this hypothesis plausible, and have also proposed that abiotic reactions between Fe(II) and NO_2^- could lead to an energetic benefit through an electron sparing mechanism (**Figure 1D**).

Excess NO produced by bacteria can also further react to form other compounds. NO will bind to free Fe(II) outside of the cell to form stable iron–nitrosyl complexes (Brons et al., 1991; **Figure 2B**), but will not bind tightly to Fe(III). Thus, as Fe(II) oxidation continues, bound NO will be released. Further reduction of NO can produce the high energy intermediate nitroxyl (NO^-, HNO) which can react with thiols to form hydroxylamine (Flores-Santana et al., 2011), or with another nitroxyl to form N_2O (Beckman and Koppenol, 1996; Flores-Santana et al., 2011; **Figure 2B**). Some evidence for nitroxyl as an intermediate in denitrification exists (Turk and Hollocher, 1992), and though the redox potential of the NO/NO^- couple is −0.8 V vs. SHE at pH 7 (Bartberger et al., 2002), the evidence for its presence and a role in other biological systems is increasing. It is possible that a nitroxyl-like species is an intermediate in biological and chemical denitrification pathways (Flores-Santana et al., 2011).

IN A METAL CAGE: Fe(II) DIFFUSION INTO CELLS AND CELL ENCRUSTATION BY THE FORMATION OF PERIPLASMIC AND OUTER MEMBRANE IRON OXIDE MINERALS

Iron-oxidizing bacteria produce insoluble Fe(III) minerals as a product. In some cases, these insoluble minerals have been found associated with the periplasm of cells or on the cell surface. Precipitation outside of cell was observed for *Rhodobacter capsulatus* SW2 (Kappler and Newman, 2004), and a local drop in pH around the cells was proposed to be involved in preventing precipitation in the periplasm (Kappler and Newman, 2004). In contrast, precipitates in the periplasm were observed in the nitrate-dependent iron oxidizer *Acidovorax* sp. Strain BoFeN1 (Kappler et al., 2005, 2010; Miot et al., 2009b). More specifically, these precipitates appear to be initially localized to the periplasmic face of the inner membrane (Miot et al., 2011).

The insolubility of Fe(III) creates a serious problem for iron oxidizers. If ferric minerals begin to crystallize in the periplasm or on the surface of cells, damage to membranes, proteins, and other cellular components will likely ensue, and under extreme cases, the permeability of the cells to soluble nutrients may be impaired. If Fe(II) enters the cytoplasm, it can replace other metals in proteins, and participate in damaging redox reactions (Crichton, 2009). Cellular Fe(II) homeostasis is carefully controlled in microbes by the activity of metalloregulatory proteins such as

the ferric uptake regulator, Fur (Crichton, 2009). Efflux pumps are widely used by bacteria for the export of toxic metal ions, and at the expense of ATP, provide a means of exporting metals from the cell (Nies, 2003). Most studies investigating transcriptional responses of microorganisms to iron have focused on iron uptake under iron limiting conditions, but environmental conditions certainly exist where a cell is faced with iron overload. It seems likely that under high iron conditions, efflux pumps would be upregulated (**Figure 2C**). Consumption of ATP by these pumps may attenuate any energy gains as a result of Fe(II) oxidation by the organism. Although significant research effort has focused on these efflux pumps, most studies have looked at their expression in the presence of metals other than Fe(II) (Nies, 2003).

It has been suggested that Fe(II) bound to cell surface minerals can further catalyze denitrification reactions (Coby and Picardal, 2005), and that these mineral deposits may prevent the diffusion of soluble electron acceptors into the cell. It appears that some bacteria are able to avoid periplasmic encrustation, but the mechanism for exporting the Fe(III) before it precipitates is not known. It has been suggested that a local low pH in the periplasm and outside of cells could prevent Fe(III) precipitation, and extracellular polysaccharide fibers or pili may provide a scaffold for mineralization outside of the cell (**Figure 2D**; Miot et al., 2009b).

A BALANCING ACT: HARNESSING ELECTRONS FROM Fe(II) AND AVOIDING TOXICITY

Electrons from the oxidation of Fe(II) are thermodynamically poised to reduce NO_3^- (Koppenol, 1996; Bartberger et al., 2002; Shafirovich and Lymar, 2002; Dutton et al., 2005; Flores-Santana et al., 2011), but the kinetics of the abiotic reactions are slow (Moraghan and Buresh, 1977). Therefore, high rates of nitrate-dependent Fe(II) oxidation observed in many studies indicate that Fe(II) is enzymatically coupled to the reduction of nitrate to at least nitrite. This is further supported by the results of washed cell suspension experiments where nitrate-dependent oxidation occurs rapidly with Fe(II) as the sole electron donor (Chaudhuri et al., 2001; Lack et al., 2002; Weber et al., 2006b). If the reactions were entirely abiotic, the rate of Fe(II) oxidation should not differ from the heat-killed controls.

A number of bacteria are capable of growth in the presence of Fe(II) (Weber et al., 2006a), and in some cases, growth benefit from neutrophilic iron oxidation has been reported (Muehe et al., 2009; Weber et al., 2009; Chakraborty et al., 2011). It is clear from these studies that the culture conditions can greatly affect the growth benefit associated with iron oxidation (Weber et al., 2009; Chakraborty et al., 2011). What is not clear, however, are the exact mechanisms whereby diverse species of bacteria harness Fe(II) electrons in the presence of competing abiotic reactions with nitrogen oxides.

CONCLUSION

Our central hypothesis is that the mechanisms used by neutrophilic anaerobic nitrate-dependent iron-oxidizing bacteria likely exist along a continuum from purely abiotic reactions between microbially produced nitrogen oxides to mixed biotic/abiotic mechanisms involving direct electron donation from iron to cellular components. This fascinating and geochemically important process may also be unique in that the microbial metabolisms themselves might take advantage of abiotic reactions, for example by using NO_2^- as a shuttle (Miot et al., 2009a; Chakraborty et al., 2011), or through the electron sparing hypothesis in **Figure 1D**. With the growing number of pure isolates of robust iron oxidizing microorganisms, we are optimistic that the mechanistic proposals in this paper can be tested in the laboratory.

ACKNOWLEDGMENTS

Research on microbial Fe(II) oxidation in the John D. Coates laboratory is supported by funding from the Energy Biosciences Institute, CA, USA.

REFERENCES

Bartberger, M. D., Liu, W., Ford, E., Miranda, K. M., Switzer, C., Fukuto, J. M., Farmer, P. J., Wink, D. A., and Houk, K. N. (2002). The reduction potential of nitric oxide (NO) and its importance to NO biochemistry. *Proc. Natl. Acad. Sci. U.S.A.* 99, 10958–10963.

Beckman, J. S., and Koppenol, W. H. (1996). Nitric oxide, superoxide, and peroxynitrite: the good, the bad, and ugly. *Am. J. Physiol.* 271, C1424–C1437.

Bird, L. J., Bonnefoy, V., and Newman, D. K. (2011). Bioenergetic challenges of microbial iron metabolisms. *Trends Microbiol.* 19, 330–340.

Brons, H. J., Hagen, W. R., and Zehnder, A. J. (1991). Ferrous iron dependent nitric oxide production in nitrate reducing cultures of *Escherichia coli*. *Arch. Microbiol.* 155, 341–347.

Chakraborty, A., Roden, E. E., Schieber, J., and Picardal, F. (2011). Enhanced growth of *Acidovorax* sp. strain 2AN during nitrate-dependent Fe(II) oxidation in batch and continuous-flow systems. *Appl. Environ. Microbiol.* 77, 8548–8556.

Chalamet, A. (1973). Reduction sous atmosphere inerte de l'acide nitreux par les ions ferreux. *Ann. Chimie* 8, 353–358.

Chaudhuri, S. K., Lack, J. G., and Coates, J. D. (2001). Biogenic magnetite formation through anaerobic biooxidation of Fe(II). *Appl. Environ. Microbiol.* 67, 2844–2848.

Coby, A. J., and Picardal, F. W. (2005). Inhibition of NO_3^- and NO_2^- reduction by microbial Fe(III) reduction: evidence of a reaction between NO_2^- and cell surface-bound Fe^{2+}. *Appl. Environ. Microbiol.* 71, 5267–5274.

Cooper, D. C., Picardal, F. W., Schimmelmann, A., and Coby, A. J. (2003). Chemical and biological interactions during nitrate and goethite reduction by *Shewanella putrefaciens* 200. *Appl. Environ. Microbiol.* 69, 3517–3525.

Crichton, R. R. (2009). *Iron Metabolism: From Molecular Mechanisms to Clinical Consequences*. Chichester: John Wiley & Sons.

Croal, L. R., Jiao, Y. Q., and Newman, D. K. (2007). The *fox* operon from *Rhodobacter* strain SW2 promotes phototrophic Fe(II) oxidation in *Rhodobacter capsulatus* SB1003. *J. Bacteriol.* 189, 1774–1782.

Dutton, A. S., Fukuto, J. M., and Houk, K. N. (2005). Theoretical reduction potentials for nitrogen oxides from CBS-QB3 energetics and (C)PCM solvation calculations. *Inorg. Chem.* 44, 4024–4028.

Emerson, D., Fleming, E. J., and McBeth, J. M. (2010). Iron-oxidizing bacteria: an environmental and genomic perspective. *Annu. Rev. Microbiol.* 64, 561–583.

Feelisch, M. (1991). The biochemical pathways of nitric-oxide formation from nitrovasodilators – appropriate choice of exogenous NO donors and aspects of preparation and handling of aqueous NO solutions. *J. Cardiovasc. Pharmacol.* 17, S25–S33.

Ferguson, S. J., and Ingledew, W. J. (2008). Energetic problems faced by micro-organisms growing or surviving on parsimonious energy sources and at acidic pH: I. *Acidithiobacillus ferrooxidans* as a paradigm. *Biochim. Biophys. Acta* 1777, 1471–1479.

Finneran, K. T., Housewright, M. E., and Lovley, D. R. (2002). Multiple influences of nitrate on uranium solubility during bioremediation of uranium-contaminated subsurface sediments. *Environ. Microbiol.* 4, 510–516.

Flores-Santana, W., Salmon, D. J., Donzelli, S., Switzer, C. H., Basudhar, D., Ridnour, L., Cheng, R., Glynn, S. A., Paolocci, N., Fukuto, J. M., Miranda, K. M., and Wink, D. A. (2011). The specificity of nitroxyl chemistry is unique among nitrogen oxides in biological systems. *Antioxid. Redox Signal.* 14, 1659–1674.

Gardner, A. M., Helmick, R. A., and Gardner, P. R. (2002). Flavorubredoxin, an inducible catalyst for nitric oxide reduction and detoxification in *Escherichia coli*. *J. Biol. Chem.* 277, 8172–8177.

Gomes, C. M., Giuffre, A., Forte, E., Vicente, J. B., Saraiva, L. M., Brunori, M., and Teixeira, M. (2002). A novel type of nitric-oxide reductase. *Escherichia coli* flavorubredoxin. *J. Biol. Chem.* 277, 25273–25276.

Hafenbradl, D., Keller, M., Dirmeier, R., Rachel, R., Robnagel, P., Burggraf, S., Huber, H., and Stetter, K. O. (1996). *Ferroglobus placidus* gen. nov., sp. nov. a novel hyperthermophilic archaeum that oxidizes Fe^{2+} at neutral pH under anoxic conditions. *Arch. Microbiol.* 166, 308–314.

Hansen, H. C. B., Borggaard, O. K., and Sorensen, J. (1994). Evaluation of the free-energy of formation of Fe(II)-Fe(III) hydroxide-sulfate (green rust) and its reduction of nitrite. *Geochim. Cosmochim. Acta* 58, 2599–2608.

Hansen, H. C. B., Guldberg, S., Erbs, M., and Koch, C. B. (2001). Kinetics of nitrate reduction by green rusts – effects of interlayer anion and Fe(II): Fe(III) ratio. *Appl. Clay Sci.* 18, 81–91.

Hansen, H. C. B., Koch, C. B., Nancke-krogh, H., Borggaard, O. K., and Sorensen, J. (1996). Abiotic nitrate reduction to ammonium: key role of green rust. *Environ. Sci. Technol.* 30, 2053–2056.

Jiao, Y., and Newman, D. K. (2007). The pio operon is essential for phototrophic Fe(II) oxidation in *Rhodopseudomonas palustris* TIE-1. *J. Bacteriol.* 189, 1765–1773.

Kappler, A., Johnson, C. M., Crosby, H. A., Beard, B. L., and Newman, D. K. (2010). Evidence for equilibrium iron isotope fractionation by nitrate-reducing iron(II)-oxidizing bacteria. *Geochim. Cosmochim. Acta* 74, 2826–2842.

Kappler, A., and Newman, D. K. (2004). Formation of Fe(III)-minerals by Fe(II)-oxidizing photoautotrophic bacteria. *Geochim. Cosmochim. Acta* 68, 1217–1226.

Kappler, A., Schink, B., and Newman, D. K. (2005). Fe(III)-mineral formation and cell encrustation by the nitrate-dependent Fe(II)-oxidizer strain BoFeN1. *Geobiology* 3, 235–245.

Koppenol, W. H. (1996). Thermodynamics of reactions involving nitrogen-oxygen compounds. *Meth. Enzymol.* 268, 7–12.

Kraft, B., Strous, M., and Tegetmeyer, H. E. (2011). Microbial nitrate respiration – genes, enzymes and environmental distribution. *J. Biotechnol.* 155, 104–117.

Lack, J. G., Chaudhuri, S. K., Chakraborty, R., Achenbach, L. A., and Coates, J. D. (2002). Anaerobic biooxidation of Fe(II) by *Dechlorosoma suillum*. *Microbiol. Ecol.* 43, 424–431.

Machulla, G., Thieme, J., and Niemeyer, J. (1998). "Interaction of microorganisms with soil colloids observed by X-ray microscopy," in *X-Ray Microscopy and Spectroscopy*, eds J. Thieme, G. Schmahl, D. Rudolph, and E. Umbach (Heidelberg: Springer-Verlag), II-21–II-28.

Mills, P. C., Rowley, G., Spiro, S., Hinton, J. C., and Richardson, D. J. (2008). A combination of cytochrome c nitrite reductase (NrfA) and flavorubredoxin (NorV) protects *Salmonella enterica* serovar Typhimurium against killing by NO in anoxic environments. *Microbiology* 154, 1218–1228.

Miot, J., Benzerara, K., Morin, G., Bernard, S., Beyssac, O., Larquet, E., Kappler, A., and Guyot, F. (2009a). Transformation of vivianite by anaerobic nitrate-reducing iron-oxidizing bacteria. *Geobiology* 7, 373–384.

Miot, J., Benzerara, K., Morin, G., Kappler, A., Obst, M., Brown, G. E., and Guyot, F. (2009b). Iron biomineralization by neutrophilic nitrate-reducing iron-oxidizing bacteria. *Geochim. Cosmochim. Acta* 73, A884–A884.

Miot, J., MacLellan, K., Benzerara, K., and Boisset, N. (2011). Preservation of protein globules and peptidoglycan in the mineralized cell wall of nitrate-reducing, iron(II)-oxidizing bacteria: a cryo-electron microscopy study. *Geobiology* 9, 459–470.

Moraghan, J. T., and Buresh, R. J. (1977). Chemical reduction of nitrite and nitrous-oxide by ferrous iron. *Soil Sci. Soc. Am. J.* 41, 47–50.

Muehe, E. M., Gerhardt, S., Schink, B., and Kappler, A. (2009). Ecophysiology and the energetic benefit of mixotrophic Fe(II) oxidation by various strains of nitrate-reducing bacteria. *FEMS Microbiol. Ecol.* 70, 335–343.

Nies, D. H. (2003). Efflux-mediated heavy metal resistance in prokaryotes. *FEMS Microbiol. Rev.* 27, 313–339.

Ottley, C. J., Davison, W., and Edmunds, W. M. (1997). Chemical catalysis of nitrate reduction by iron(II). *Geochim. Cosmochim. Acta* 61, 1819–1828.

Poulain, A. J., and Newman, D. K. (2009). *Rhodobacter capsulatus* catalyzes light-dependent Fe(II) oxidation under anaerobic conditions as a potential detoxification mechanism. *Appl. Environ. Microbiol.* 75, 6639–6646.

Rodionov, D. A., Dubchak, I. L., Arkin, A. P., Alm, E. J., and Gelfand, M. S. (2005). Dissimilatory metabolism of nitrogen oxides in bacteria: comparative reconstruction of transcriptional networks. *PLoS Comput. Biol.* 1, e55. doi:10.1371/journal.pcbi.0010055

Schoepp-Cothenet, B., Lieutaud, C., Baymann, F., Vermeglio, A., Friedrich, T., Kramer, D. M., and Nitschke, W. (2009). Menaquinone as pool quinone in a purple bacterium. *Proc. Natl. Acad. Sci. U.S.A.* 106, 8549–8554.

Shafirovich, V., and Lymar, S. V. (2002). Nitroxyl and its anion in aqueous solutions: spin states, protic equilibria, and reactivities toward oxygen and nitric oxide. *Proc. Natl. Acad. Sci. U.S.A.* 99, 7340–7345.

Straub, K. L., Benz, M., Schink, B., and Widdel, F. (1996). Anaerobic, nitrate-dependent microbial oxidation of ferrous iron. *Appl. Environ. Microbiol.* 62, 1458–1460.

Straub, K. L., and Buchholz-Cleven, B. E. E. (1998). Enumeration and detection of anaerobic ferrous iron-oxidizing, nitrate-reducing bacteria from diverse European sediments. *Appl. Environ. Microbiol.* 64, 4846–4856.

Summers, D. P., and Chang, S. (1993). Prebiotic ammonia from reduction of nitrite by iron (II) on the early Earth. *Nature* 365, 630–633.

Turk, T., and Hollocher, T. C. (1992). Oxidation of dithiothreitol during turnover of nitric oxide reductase: evidence for generation of nitroxyl with the enzyme from *Paracoccus denitrificans*. *Biochem. Biophys. Res. Commun.* 183, 983–988.

Wagner, G. C., Kassner, R. J., and Kamen, M. D. (1974). Redox potentials of certain vitamins K: implications for a role in sulfite reduction by obligately anaerobic bacteria. *Proc. Natl. Acad. Sci. U.S.A.* 71, 253–256.

Weber, K. A., Achenbach, L. A., and Coates, J. D. (2006a). Microorganisms pumping iron: anaerobic microbial iron oxidation and reduction. *Nat. Rev. Microbiol.* 4, 752–764.

Weber, K. A., Pollock, J., Cole, K. A., O'Connor, S. M., Achenbach, L. A., and Coates, J. D. (2006b). Anaerobic nitrate-dependent iron(II) bio-oxidation by a novel lithoautotrophic betaproteobacterium, strain 2002. *Appl. Environ. Microbiol.* 72, 686–694.

Weber, K. A., Urrutia, M. M., Churchill, P. F., Kukkadapu, R. K., and Roden, E. E. (2006c). Anaerobic redox cycling of iron by freshwater sediment microorganisms. *Environ. Microbiol.* 8, 100–113.

Weber, K. A., Hedrick, D. B., Peacock, A. D., Thrash, J. C., White, D. C., Achenbach, L. A., and Coates, J. D. (2009). Physiological and taxonomic description of the novel autotrophic, metal oxidizing bacterium, *Pseudogulbenkiania* sp. strain 2002. *Appl. Microbiol. Biotechnol.* 83, 555–565.

Weber, K. A., Picardal, F. W., and Roden, E. E. (2001). Microbially catalyzed nitrate-dependent oxidation of biogenic solid-phase Fe(II) compounds. *Environ. Sci. Technol.* 35, 1644–1650.

Widdel, F., Schnell, S., Heising, S., Ehrenreich, A., Assmus, B., and Schink, B. (1993). Ferrous iron oxidation by anoxygenic phototrophic bacteria. *Nature* 362, 834–836.

Conflict of Interest Statement: The authors declare that the research was conducted in the absence of any commercial or financial relationships that could be construed as a potential conflict of interest.

Received: 03 November 2011; paper pending published: 07 December 2011; accepted: 02 February 2012; published online: 20 February 2012.

Citation: Carlson HK, Clark IC, Melnyk RA and Coates JD (2012) Toward a mechanistic understanding of anaerobic nitrate-dependent iron oxidation: balancing electron uptake and detoxification. Front. Microbio. ***3****:57. doi: 10.3389/fmicb.2012.00057*

This article was submitted to Frontiers in Microbiological Chemistry, a specialty of Frontiers in Microbiology.

Copyright © 2012 Carlson, Clark, Melnyk and Coates. This is an open-access article distributed under the terms of the Creative Commons Attribution Non Commercial License, which permits non-commercial use, distribution, and reproduction in other forums, provided the original authors and source are credited.

frontiers in
MICROBIOLOGY

ORIGINAL RESEARCH ARTICLE
published: 19 June 2012
doi: 10.3389/fmicb.2012.00219

The importance of kinetics and redox in the biogeochemical cycling of iron in the surface ocean

***Peter L. Croot*†* and *Maija I. Heller†*

FB2: Marine Biogeochemistry, Helmholtz-Zentrum für Ozeanforschung Kiel, Kiel, Germany

Edited by:
Benjamin Twining, Bigelow Laboratory for Ocean Sciences, USA

Reviewed by:
Benjamin Kocar, Stanford University, USA
Jochen Nuester, Bigelow Laboratory for Ocean Sciences, USA

***Correspondence:**
Peter L. Croot, Earth and Ocean Sciences, School of Natural Sciences, National University of Ireland Galway, Galway, Ireland.
e-mail: peter.croot@nuigalway.ie

†***Present address:***
Peter L. Croot, Earth and Ocean Sciences, School of Natural Sciences, National University of Ireland Galway, Galway, Ireland;
Maija I. Heller, University of Southern California, Los Angeles, CA, USA.

It is now well established that Iron (Fe) is a limiting element in many regions of the open ocean. Our current understanding of the key processes which control iron distribution in the open ocean have been largely based on thermodynamic measurements performed under the assumption of equilibrium conditions. Using this equilibrium approach, researchers have been able to detect and quantify organic complexing ligands in seawater and examine their role in increasing the overall solubility of iron. Our current knowledge about iron bioavailability to phytoplankton and bacteria is also based heavily on carefully controlled laboratory studies where it is assumed the chemical species are in equilibrium in line with the free ion association model and/or its successor the biotic ligand model. Similarly most field work on iron biogeochemistry generally consists of a single profile which is in essence a "snap-shot" in time of the system under investigation. However it is well known that the surface ocean is an extremely dynamic environment and it is unlikely if thermodynamic equilibrium between all the iron species present is ever truly achieved. In sunlit waters this is mostly due to the daily passage of the sun across the sky leading to photoredox processes which alter Fe speciation by cycling between redox states and between inorganic and organic species. Episodic deposition events, dry and wet, are also important perturbations to iron cycling as they bring in new iron to the system and alter the equilibrium between iron species and phases. Here we utilize new field data collected in the open ocean on the complexation kinetics of iron in the surface ocean to identify the important role of weak iron binding ligands (i.e., those that cannot maintain iron in solution indefinitely at seawater pH: $\alpha_{FeL} < \alpha_{Fe'}$) in allowing transient increases in iron solubility in response to iron deposition events. Experiments with the thermal O_2^- source SOTS-1 also indicate the short term impact of this species on iron solubility also with relevance to the euphotic zone. This data highlights the roles of kinetics, redox, and weaker iron binding ligands in the biogeochemical cycling of iron in the ocean.

Keywords: iron biogeochemistry, iron solubility, redox kinetics, complexation kinetics

INTRODUCTION

That Iron (Fe) is an important limiting nutrient for primary productivity over large areas of the ocean has been clearly demonstrated in iron enrichment experiments in the open ocean over the last 20 years (Martin et al., 1994; Boyd et al., 2000; de Baar et al., 2005). Since the first proposals that linked low productivity in the open ocean with distance from the coast and iron sources (Gran, 1931; Harvey, 1937), and since the first evidence showing the link between low iron and slow growth in the open ocean (Martin and Fitzwater, 1988), studies on the (geo)chemical aspects of iron biogeochemistry were mainly focused on conditions of thermodynamic equilibrium. The thermodynamically favored redox form of Fe in seawater, Fe(III), is only weakly soluble in seawater (Millero, 1998). The reduced form, Fe(II), is found in oxic waters as a transient species, primarily generated by photochemical processes (Johnson et al., 1994; Croot et al., 2008), and existing at extremely low concentrations (picomolar or less) because of rapid oxidation by O_2 and H_2O_2 in warm surface waters. The oxidation of Fe(II) to the less soluble Fe(III) species, leads to the formation of colloidal oxyhydroxide (Kuma et al., 1996) species which coagulate and form particulate iron (Johnson et al., 1997). Dissolved iron ($<0.4\,\mu m$) has been shown to be strongly organically complexed throughout the water column (Rue and Bruland, 1995; Boye et al., 2001) and is comprised of colloidal material or truly soluble (<100 kDa) complexes (Boye et al., 2010). In the absence of organic ligands iron solubility is extremely low (<80 pM) Fe (Kuma et al., 1996; Liu and Millero, 2002). Iron solubility however varies in the ocean with higher concentrations in coastal waters (Kuma et al., 1998b, 2000; Schlosser and Croot, 2009), than in the Open Ocean (Kuma et al., 1998a; Nakabayashi et al., 2001).

The main supply routes for iron to the open oceans is via upwelling or atmospheric dust deposition (Jickells et al., 2005). Dust deposition is episodic in nature and alters the equilibrium between soluble, colloidal, and particulate iron phases. The daily cycle of the sun also strongly imprints a photo-induced redox iron cycle in the euphotic zone (Johnson et al., 1994) and involves transient Fe(II) species existing (Croot et al., 2001, 2008; Roy et al., 2008) at concentrations far above that predicted by

thermodynamic equilibrium calculations. Indeed it also has been known for some time that iron uptake by phytoplankton is under kinetic rather than thermodynamic control (Hudson and Morel, 1990, 1993). Thus information about the kinetics of exchange between these phases is critically important to our understanding of the biogeochemical cycling of iron in seawater as the system is normally far from any thermodynamic equilibrium state.

A key controlling factor in the kinetics is the rate of water exchange (or loss) for the inner coordination sphere of Fe, as this sets the upper rate at which ligand exchange reactions can occur. The inorganic speciation of Fe(III) in seawater is dominated by hydroxide complexes and measurements of the water exchange rate under seawater conditions for Fe′ (the sum of all the inorganic Fe(III) species) has been measured $k_{ex} = 8 \times 10^6\,M^{-1}\,s^{-1}$ (Hudson et al., 1992). This is consistent with measurements in simple solutions for the individual iron hydroxy species: Fe(III) $1.6 \times 10^2\,M^{-1}\,s^{-1}$ and $Fe(OH)^{2+}$ $1.2 \times 10^5\,M^{-1}\,s^{-1}$ (Grant and Jordan, 1981), $Fe(OH)_2^+ > 10^7 M^{-1}s^{-1}$ and $Fe(OH)_4^- > 10^9 M^{-1}s^{-1}$ (Schneider, 1988). The rate of water exchange for the aquo Fe(II), $k_{ex} \sim 1 \times 10^7\,M^{-1}\,s^{-1}$ (Helm and Merbach, 1999), is considerably faster than that of Fe(III). Once formed an iron organic complex may dissociate via either an adjunctive pathway, involving the direct attack of the incoming species on the initial complex and the formation of a ternary intermediate species, or a disjunctive pathway involving complete dissociation of the initial complex (Hering and Morel, 1990a,b). For a complete description of the mechanisms involved in the different dissociation pathways the reader is referred to Morel and Hering (1993). It has been found for many Fe(III) siderophore complexes that adjunctive pathways are important with the loss of the iron initiated by the formation of a ternary complex with another ligand (inorganic or organic) resulting in either the simple exchange of the iron or a subsequent reduction to Fe(II) via an external reductant or photochemical process followed by release of the iron from the complex (Dhungana and Crumbliss, 2005; Mies et al., 2006).

A small number of studies performed over the last 20 years have indicated that thermodynamically weak iron binding ligands, i.e., those that cannot maintain iron in solution indefinitely at seawater pH (i.e., $\alpha_{FeL} < \alpha_{Fe'}$), may be important as transient species either as short term soluble species (Gerringa et al., 2007) or for their involvement in photochemically induced redox cycling (Kuma et al., 1995). The mesoscale iron enrichment experiments performed over the last 20 years, for a summary see de Baar et al. (2005), are now classic examples of the functioning of the iron biogeochemical cycle to a transient episodic event and how the system responds. Based on these and other recent findings we use **Figure 1** to illustrate the key processes and exchange mechanisms affecting dissolved iron concentrations identified to date. **Figure 1** also highlights the main natural inputs that perturb the system and prevent it from achieving "geochemical" thermodynamic equilibrium. Note that in this context iron in upwelled waters may be considered closer to equilibrium due to the water mass age and so is neglected here. In the present work we focus on the kinetics of processes involving weak ligands with regard to important

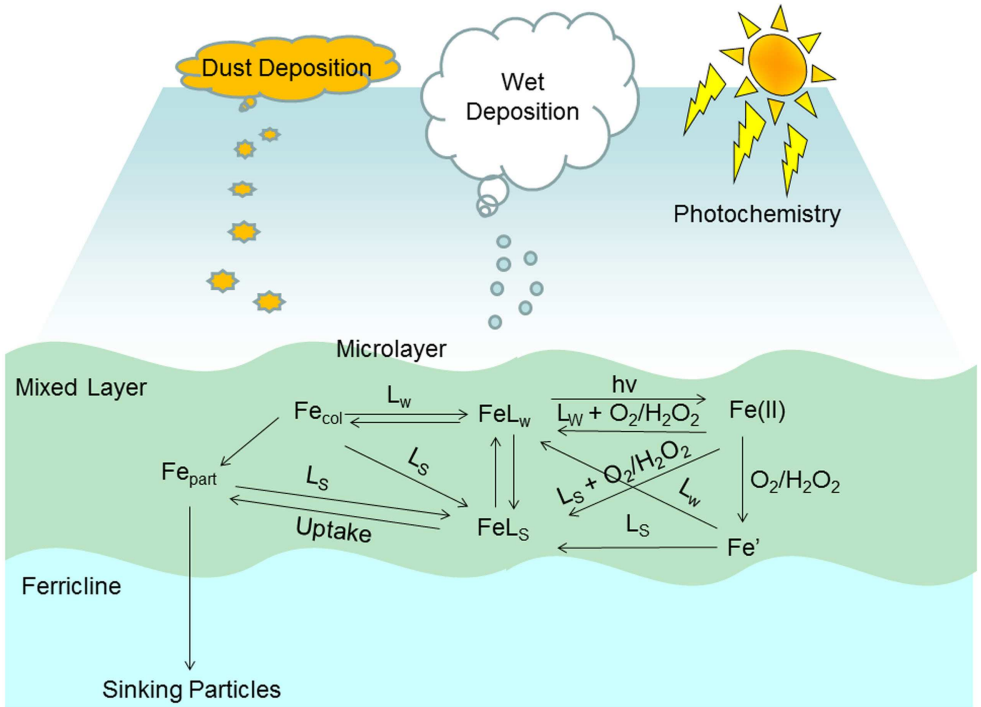

FIGURE 1 | Schematic of key processes in the biogeochemical cycling of dissolved iron in the surface ocean. Abbreviations used in figure (see main text for details): L_S, strong iron binding ligand; L_W, weak iron binding ligand; FeL_S, iron complexed by strong iron binding ligand; FeL_W, iron complexed by weak iron binding ligand; Fe(II), all sum of all Fe(II) species; Fe′, the sum of all inorganic Fe(III) species; Fe_{col}, colloidal iron species; Fe_{part}, iron in the particulate phase; hv, photon flux; O_2, dissolved oxygen; and H_2O_2, dissolved hydrogen peroxide.

iron transformation pathways in the surface ocean. In particular in the here we focus on the role that weak ligands can play in maintaining soluble iron in the surface ocean over short time scales through a series of kinetic experiments employing different analytical approaches (voltammetry and radiotracers). This work highlights the importance of kinetic processes in the temporal evolution of iron speciation and biogeochemistry in dynamic marine systems.

MATERIALS AND METHODS

IRON SPECIATION

Competitive ligand exchange-cathodic stripping voltammetry

In the present work we determined conditional stability constants for natural iron binding ligands using an established cathodic stripping voltammetry (CSV) technique (Croot and Johansson, 2000) utilizing the ligand 2-(2-thiazolylazo)-4-methylphenol (TAC). A brief description of the procedure for TAC is listed here: Sub-samples (20 mL) of seawater were pipetted into a series of precleaned Teflon bottles (125 mL) and 100 μL of 1 M EPPS buffer [*N*-(2-hydroxyethyl)piperazine-*N*′-2-propanesulfonic acid; pKa 8.00; SigmaUltra] added. Iron was added to all but two of the bottles, yielding concentrations from 0 to 12 nM. The added Fe was left to equilibrate with the natural ligands for 1 h at laboratory temperature (21.0 ± 0.1°C). At the end of this equilibration period, 20 μL of 10 mM TAC was added and the sample left to equilibrate for a further 12 h before analysis by voltammetry (Metrohm VA757). The samples were then transferred to a Teflon cell cup, the sample deaerated for 4 min with dry nitrogen gas, subsequently the $Fe(TAC)_2$ complexes in the sample were adsorbed onto a fresh Hg drop at an applied potential of −0.40 V for 10 min, while the sample was stirred. At the completion of the adsorption period, the stirrer was stopped and the potential was scanned using the fast linear sweep mode from −0.40 to −0.90 V at 10.1 V s^{-1} and the stripping current from the adsorbed $Fe(TAC)_2$ recorded. The Teflon cups were rinsed only with MQ between analyses and the samples were run in the order of increasing Fe additions. Two +0 samples were run, as a check for possible contamination of the cell. Each Teflon bottle was consistently used for a constant Fe addition. Full details of the theory behind the CSV approach can be found in Croot and Johansson (2000). Values for the total iron binding ligand concentration (L_T) and conditional stability constant (Log *k*) were determined by non-linear methods (Gerringa et al., 1995).

Kinetic method for Fe speciation (CSV-KIN)

Rate constants for FeL formation (k_f), and FeL dissociation (k_d), were determined at seawater pH using the same kinetic approach as earlier (Wu and Luther, 1995; Witter and Luther, 1998; Witter et al., 2000) with the exception that the CSV ligand used in those works, 1-Nitroso-2-Naphthol (1N2N), was replaced by TAC (Croot and Johansson, 2000). A similar approach using TAC has been made earlier by Gerringa et al. (2007), as the TAC method (Croot and Johansson, 2000) is more sensitive and better suited for Fe determination at seawater pH than 1N2N. As noted by Witter and Luther (1998), for consistency we note that Fe′ indicates all inorganic forms of Fe(III), Fe^{3+} is only the hexaaquo species $[Fe(H_2O)_6]^{3+}$, and FeL is the ligand complex. Note that in the following we also use the commonly used term Fe′L, to represent the iron ligand complex formed from Fe′ and *L* however we are not suggesting the existence of a mixed inorganic and organic ligand complex as there is no information currently available for this with respect to the natural iron binding ligands.

Determination of k_f for FeL formation

The formation rate constant, *k*f, of the Fe^{3+}-organic ligand complex (represented as FeL) was estimated from the initial rate of complexation of an aliquot of Fe′ added to seawater containing natural organic ligands at *ambient pH*.

$$Fe' + L \xrightarrow{k_f} FeL \quad (1)$$

The rate law for formation of FeL used to calculate the formation rate constant, k_f is shown below:

$$\frac{\partial[FeL]}{\partial t} = k_f[Fe'][L] \quad (2)$$

Experimentally this involved the addition of Fe to a seawater sample and at different time intervals, the competing ligand TAC was added and the TAC labile iron measured. Mass balance considerations resulted in the calculation of FeL. For the purposes of Eq. 2, the initial concentration of Fe′ was set to the iron concentration added (in this case typically ∼7 nM) and [*L*] was estimated from the amount of free ligand present at equilibrium ($L = L_T - FeL$) as determined in the Competitive Ligand Exchange-Cathodic Stripping Voltammetry (CSV-CLE) titration.

Calculation of k_d (rate of dissociation for recovery of Fe from FeL)

The dissociation rate constant, k_d, for recovery of added Fe from FeL could be determined after addition of TAC to seawater which had been pre-equilibrated with an aliquot of 7 nM Fe at ambient pH. Reaction between TAC and Fe (from FeL) results in electroactive complexes which are detected at the hanging mercury drop electrode. In the present work we modified the approach of Witter and Luther (1998) to determine the dissociation rate of both weak and strong ligands. Full details can be found in the appendix to this manuscript.

Measurement of iron solubility kinetics (FESOL-KIN)

The experimental design was principally the same as described previously for iron solubility experiments (Kuma et al., 1996; Nakabayashi et al., 2002; Schlosser and Croot, 2009; Schlosser et al., 2011). An adaptation of these studies was required for the filtration of the samples, as the 0.02 μm Anotop syringe filter (Whatman) previously used (Schlosser and Croot, 2009) were not obtainable and the alternative filter material (Millipore MF) was not available in a syringe filter. The change in filter material required a new filtration system to be constructed. All the equipment used was constructed from Teflon components available commercially (Savillex). The collection vessel was a 500 mL standard jar with transfer closure and two tube ports. A 47 mm filter holder, incorporating the 47 mm diameter 0.025 μm filter (Millipore MF), was connected in between the first of the tube ports and a 200 mL reservoir tube. The sample solution was poured into the reservoir tube immediately prior to filtration. To the second tube port of the

jar, vacuum tubing was attached and connected to a trace metal clean Teflon lined vacuum pump (ILMVAC MPR060E) to allow vacuum filtration of the samples.

In this work we used the radioisotope ^{55}Fe (Perkin Elmer) for all experiments: specific activity 1985.42 MBq/mg Fe, concentration 1466.79 MBq/mL. The ^{55}Fe solution was dissolved in 0.1 M HCl and dilution standards were produced with MQ water and acidified with Q-HCl to a pH <2. Seawater (200 mL) collected from different depths throughout the water column using trace metal clean GO-FLO sampling bottles was transferred into Teflon FEP bottles (1 L) and an aliquot of ^{55}Fe was added to the bottles to give an addition of 21 nM. Sub-samples (20 mL) for filtration were taken after 3, 6, 24, and 48 h and were filtered through 47 mm 0.025 μm Millipore MF filters using the above described Teflon filtration unit (Savillex), the filtrate was collected in a Teflon vial. Duplicate samples of both filtered (0.025 μm) and unfiltered seawater (400 μL) were acidified and transferred into 6 mL vials in which 4.5 mL of scintillation fluid (Lumagel Plus®) were added. Sample storage, treatment, and measurement were performed at room temperature (23°C) in the isotopic container located on the *RV Polarstern*. The activity of the ^{55}Fe solutions were determined by scintillation counting (Packard, Tri-Carb 2900TR) and then converted to soluble Fe concentrations, taking into account the activity of the added isotope solution and the *in situ* dissolved Fe concentration of each sample. Quench curves for ^{55}Fe were produced by adding an identical amount of radiotracer and scintillation fluid to a series of samples containing a range of seawater additions.

Kinetic analysis of iron solubility

This approach has recently been described (Croot et al., 2011) however a brief account is given here. Starting from the mass balance for soluble iron in seawater:

$$[\mathrm{Fe_T}] = \left[\mathrm{Fe'}\right] + [\mathrm{FeL_i}] \tag{3}$$

Where [Fe′] represents here the sum of all the inorganic species [predominantly $\mathrm{Fe(OH)}_x^{(3-x)^+}$] and [$\mathrm{FeL_i}$] is the organically bound iron and L_i classes of natural organic ligands. The speciation of Fe(II) is not considered in this case, as due to the long equilibration times used in these experiments almost all Fe(II) should have been oxidized. Reactions between one class of the natural ligands and Fe′ can be expressed as:

$$\mathrm{Fe'} + \mathrm{L'} \rightarrow \mathrm{FeL} \tag{4a}$$

$$\mathrm{FeL} \rightarrow \mathrm{Fe'} + \mathrm{L'} \tag{4b}$$

L' is the Fe binding ligand not already bound to Fe(III). The equilibrium expression is then:

$$\mathrm{K'_{Fe'L}} = \frac{[\mathrm{FeL}]}{\left[\mathrm{Fe'}\right]\left[\mathrm{L'}\right]} \tag{5}$$

$K'_{\mathrm{Fe'L}}$ is the conditional stability constant under the specific conditions in seawater (in this case pH 8.0) with respect to Fe′. To convert $K'_{\mathrm{Fe'L}}$ to K'_{FeL}, the conditional stability constant for FeL with respect to free Fe^{3+}, the relationship between Fe′ and Fe^{3+}, $\alpha_{\mathrm{Fe'}} = [\mathrm{Fe'}]/[\mathrm{Fe^{3+}}]$, can be used (e.g., $K'_{\mathrm{FeL}} = \alpha_{\mathrm{Fe'}}\, K'_{\mathrm{Fe'L}}$).

The approach applied here uses the assumption that the detected decrease in soluble iron with time is due to the exchange of Fe between the weak organic ligands and the colloidal phase which does not pass through the filter. This assumption is supported by the finding that inorganic iron colloids will rapidly form due to oversaturation in the solution (Nowostawska et al., 2008) and be considerably larger (Hove et al., 2007, 2008) than the cutoff of the filter (Millipore MF 0.025 μm). Earlier work by Okumura confirms that in the absence of a strong chelator over 95% of the Fe is found in the >0.025 μm fraction (Okumura et al., 2004).

The formation and dissociation of Fe complexes are thus described by Eqs 4a and 4b from above. We now further assume that the ligands can be divided into two classes, a strong ligand (L_S) that is practically inert to dissociation and a weaker ligand (L_W) that at equilibrium is not able to keep iron in solution. The time dependence of the soluble Fe fraction can then be described by the following equation, assuming that the formation of both weak and strong complexes is equally fast.

$$\mathrm{Fe_{sol}} = \mathrm{FeL}_s + \mathrm{FeL}_W \left(e^{-kt}\right) \tag{6}$$

$\mathrm{Fe_{sol}}$ is the detected soluble iron, $\mathrm{FeL_S}$ is the concentration of the strong ligand and $\mathrm{FeL_W}$ is the concentration of the weaker ligands, which at thermodynamic equilibrium do not prevent the precipitation of iron from solution, and k is the observed dissociation rate of the weaker iron organic complexes. The measured values of $\mathrm{Fe_{sol}}$ are fitted then to Eq. 6 using a non-linear least squares fitting procedure implemented in Labview™ (National Instruments).

Examination of the influence of O_2^- on iron solubility kinetics

For a limited number of iron solubility experiments we also examined the influence of O_2^- on the solubility of iron by additions of SOTS-1 [Di(4-carboxybenzyl)hyponitrite; Molecular weight 330.3 $\mathrm{gmol^{-1}}$; Heller and Croot, 2010a] as a thermal source. SOTS-1 is an azo-compound which can be stored stably at −80°C but at higher temperatures decomposes thermally to yield either directly or indirectly electron rich carbon-centered radicals that react with O_2 to yield carbocations and O_2^- (Ingold et al., 1997). Five hundred micrograms aliquots of SOTS-1 were used as received (Cayman Chemicals) and stored at −80°C until required. Immediately prior to the start of any experiment the 500 μg SOTS-1 aliquots were dissolved in DMSO (Fluka, puriss p.a. ≥99.9%) before further dilution in seawater. The final concentration calculated for O_2^- produced from SOTS-1 in this study was 1.51 μM (500 μg SOTS-1 in 200 μL DMSO, 40 μL in 200 mL). Experiments in which only DMSO was added showed no discernable difference when compared to the controls (no DMSO, no SOTS-1). For the experiments presented in this work, we used paired samples following the same protocol as for the iron solubility kinetics experiments described above. After the addition of the radiotracer (see above) to both samples, SOTS-1 was added immediately to one of the paired samples (experimental) and the other was left unamended (control). The iron solubility was assessed at different time points as described above. In the current work we use the ratio between the experimental (E) and the control (C), ratio = $[\mathrm{Fe_{sol}}]_\mathrm{E}/[\mathrm{Fe_{sol}}]_\mathrm{C}$, to assess the impact of O_2^- on iron solubility.

RESULTS AND DISCUSSION

IRON KINETICS AS DETERMINED BY CSV

Kinetic experiments (**Table 1**) were performed on samples from the chlorophyll maximum along a west to east transect in the Tropical North Atlantic in Oct/Nov 2002 during the Meteor 55 research expedition. Data on the dissolved iron concentrations found along this transect have been published previously (Croot et al., 2004). The results of the five kinetic experiments performed can be found in **Table 1**. **Figure 2** illustrates the time course in TAC labile Fe as a function of the reaction time (here denotes as the TAC exchange time) for two different initial time points; immediately and 14 h after the addition of Fe to the sample. In **Figure 2** it can be clearly seen that the amount of TAC labile iron decreases with the time since iron addition and that much of this iron was recoverable after the addition of TAC. The gradual increase in the TAC labile Fe is interpreted as the exchange of all the weakly complexed Fe with TAC, though it will ultimately include a contribution from strong iron complexes related to the thermodynamic equilibrium finally established between TAC and the natural ligands. **Figure 3** illustrates the decrease in the labile Fe(TAC) concentration with incubation time resulting from the increase in FeL as the natural ligands complex the iron in solution.

Upon addition of TAC the exchange of iron between the natural ligands and TAC begins. **Figure 4** illustrates that this exchange is effectively come to equilibrium within 6 h and the resulting Fe(TAC) concentration is identical to that found in the 12 h equilibration used in the determination of the thermodynamic data (Croot and Johansson, 2000). It is clear though from the data in **Figure 4** that equilibration times less than 6 h would be insufficient to reach equilibrium. Data like this for the other ligands used in the CSV determination of iron organic complexation (Rue and Bruland, 1995; van den Berg, 2006) is urgently needed to address this issue as some studies have incorporated equilibration times as short as 15 min.

Estimates of the formation rate constant for the natural iron complexes were relatively constant throughout the samples measured (**Table 1**) and similar to other open ocean studies (**Table 2**). In our study k_f values were slightly lower than that found for the siderophore desferrioxamine B (DFO-B), $2 \times 10^6\ M^{-1}\ s^{-1}$ (Hudson et al., 1992) but is similar to measurements of other model Fe ligands (Witter et al., 2000). Dissociation rates found in our work were also similar to other published data from the open ocean (**Tables 1** and **2**).

Comparison with the estuarine data of Gerringa et al. (2007) revealed problems with their model based results, as they indicate that the thermodynamically stronger ligands have both faster dissociation and formation kinetics than the weak ligands. It is highly unlikely that the formation rates for the strong ligands are faster than the water exchange for Fe′ in seawater $8 \times 10^6\ M^{-1}\ s^{-1}$ (Hudson et al., 1992). While this is mathematically feasible it does not make chemical sense and indicates that their model was optimizing for the stability constant (K) of the process and that there were insufficient constraints on the kinetic rates. This can easily arise when there are six or more independent variables but only one or two measured components and no other constraints in place.

Recently there have been a number of general speciation models (thermodynamic) that have treated iron complexation in the ocean as a continuum of ligand binding strengths based on humic complexation (Hiemstra and van Riemsdijk, 2006; Stockdale et al., 2011). In these models there is a relationship between the ligand concentration and the binding strength, with weak ligands present in high concentrations and only trace amounts of strong ligands. Criticisms of this approach with regard to iron usually involve the production of siderophores by organisms as they are specific strong binding ligands capable of being produced in high concentrations in response to iron limitation (Vraspir and Butler, 2009; Butler and Theisen, 2010). However in terms of weak ligands this approach may have some validity but is yet to be applied in a kinetic approach and may be important for resolving the underlying processes occurring in the colloidal phase with regard to humic complexation (Batchelli et al., 2010).

IRON SOLUBILITY KINETICS

Experiments on the kinetics of soluble iron formation and loss were performed at five stations (**Table A1** in Appendix) along a Atlantic meridional section during Polarstern expedition ANTXXVI-4 in April/May 2010. In all experiments the concentration of soluble Fe that passed through the Millipore MF filter decreased with time. **Figure 5** shows the vertical distribution of soluble Fe over time after iron addition at station 294. Overall most data fitted the exponential decay model well and suggested the presence of a weaker Fe binding ligand which was exchanged

Table 1 | CSV-KIN: results from the Meteor Expedition (M55) in the Tropical North Atlantic: Formation and Dissociation rates of natural iron ligands as determined by CSV.

Date	Stn	Latitude	Longitude	Depth (m)	[DFe]	$[L_T]$	Log K	Log k_f	Log k_d (w)[a]	Log k_d (s)[b]
18.10.2002	5	10°00.01′N	51°24.68′W	80	0.94	1.7 ± 0.1	11.9 ± 0.1	5.84 ± 0.18	−3.98 ± 0.10	−6.06 ± 0.21
21.10.2002	11	09°59.99′N	41°43.76′W	80	1.29	1.7 ± 0.1	12.0 ± 0.1	5.84 ± 0.01	−3.56 ± 0.09	−6.16 ± 0.10
23.10.2002	15	10°00.02′N	36°13.66′W	80	0.50	1.4 ± 0.1	12.5 ± 0.4	5.51 ± 0.10	−3.73 ± 0.06	−6.99 ± 0.41
31.10.2002	28	01°56.84′N	23°30.01′W	60	0.19	2.5 ± 0.2	12.1 ± 0.1	5.73 ± 0.05	−3.83 ± 0.02	−6.37 ± 0.11
04.11.2002	36	11°00.02′N	21°40.01′W	80	1.43	5.2 ± 0.4	12.2 ± 0.1	5.60 ± 0.07	−4.20 ± 0.06	−6.60 ± 0.11

All concentrations are in nmol L^{-1}. See the appendix for a full description of the experimental methods. [a]Weak ligands, k_d determined by the time dependent loss of Fe from the natural ligand complexes. [b]Strong ligands, k_d determined from the values of Log k and k_f determined independently from the equilibrium (CSV-CLE) and kinetic approaches (CSV-KIN).

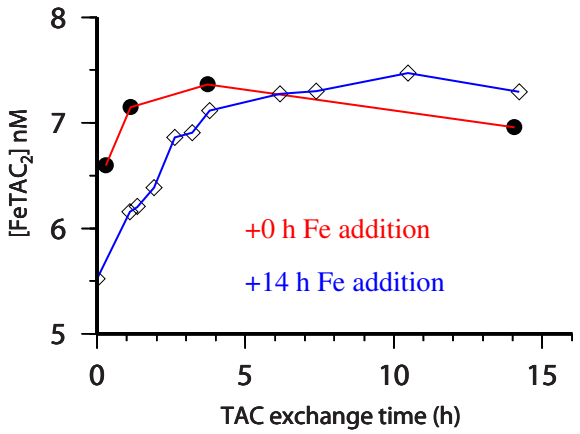

FIGURE 2 | CSV-KIN: time course of recovery of Fe by TAC from natural iron binding ligands. Water sample is from 60 m at Station 28 (see **Table 1** for more details) during the Meteor 55 cruise. Black circles TAC added immediately after Fe addition, open diamonds, TAC added 14 h after iron addition.

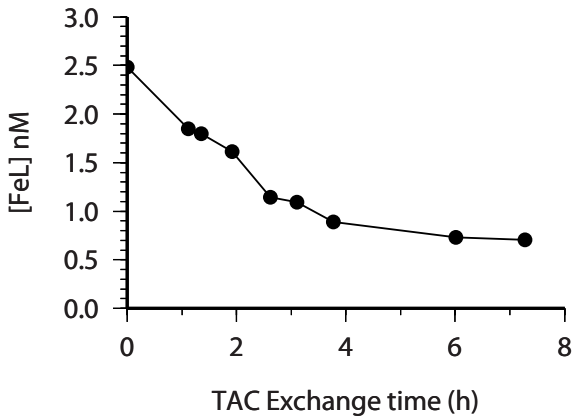

FIGURE 4 | CSV-KIN: time course of FeL (closed circles) concentrations as determined by mass balance from repeated CSV measurements over 8 h. This data is used for the determination of k_d. The samples had been equilibrated with Fe for 14 h prior to the addition of TAC. Water sample is from 60 m at Station 28 (see **Table 1** for more details) during the Meteor 55 cruise.

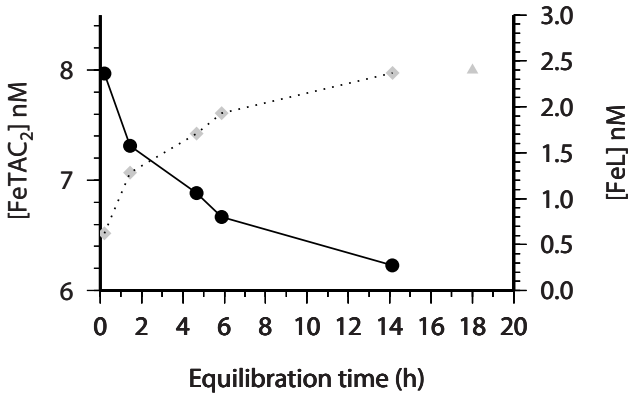

FIGURE 3 | CSV-KIN: time course of initial $Fe(TAC)_2$ (closed circles) concentrations, black circles (solid line) measured over the course of a 14 h incubation experiment (at $t = 0$ Fe was added to the sample, at subsequent time points a subsample was removed, TAC added and the labile Fe measured by CSV). The corresponding FeL concentration, as determined by mass balance, is plotted as gray diamonds (dotted line). The gray triangle represents the [*L*] determined by the conventional thermodynamic CSV titration after 18 h equilibration between the added Fe and TAC. Water sample is from 80 m at Station 36 (see **Table 1** for more details) during the Meteor 55 cruise.

over the course of the experiment into the colloidal/particulate phase and with any remaining strong ligand.

The measured dissociation rates for the weak ligands are slightly slower than the values obtained by CSV (see above and **Table 2**), and this may suggest that the dissociation of the weak iron binding ligands is slightly accelerated in the presence of TAC due to an adjunctive pathway in addition to the disjunctive pathway seen in the radiotracer experiments (see also the electronic appendix to this manuscript). Overall this data indicates the importance of weak ligands in the soluble size range for maintaining iron in solution over short timescales. This finding is particularly relevant to the processes occurring during atmospheric deposition (Baker and Croot, 2010; Duggen et al., 2010) of iron and would help to solubilize iron at the surface and increase the transport of soluble iron throughout the mixed layer and into pycnocline. The estimated lifetime for the retention of iron by weak ligands is from 1 to 2 days, which is significantly shorter than the residence time for dissolved iron in surface waters (weeks to months) of the same region (Croot et al., 2004). This strongly suggests that weakly complexed iron plays an important role in the exchange between soluble and colloidal iron fractions and that colloidal iron is important over longer time scales for maintaining dissolved iron levels (Wu et al., 2001; Bergquist and Boyle, 2006; Bergquist et al., 2007).

Comparison with the CSV data also suggests that TAC can rapidly remove iron from the weaker complexes as solubility measurements with radiotracers indicate that the concentration of soluble iron decreases with time to a constant value while **Figure 3** illustrates that FeL measured by CSV increases with time to a constant value. Thus it appears that the weak ligands that solubilize iron also react within the time scale of the CSV measurement (i.e., minutes) to exchange their iron with TAC suggesting a rapid adjunctive mechanism accelerated by the presence of 10 μM TAC. In the case of the natural ligands this process is considerably slower due to the much lower concentrations of ligands encountered. The rate of exchange between the natural ligands and TAC is slightly faster than that observed with ^{55}Fe and suggests a significant adjunctive reaction is occurring in the presence of TAC (see the appendix to this manuscript for details) but it is assumed that the dissociation kinetics (**Tables 1** and **2**) for the iron complexes in the absence of TAC is of a predominantly disjunctive character.

Our modeling approach is similar to that used recently by Schlosser et al. (2011), with the exception that we focus solely on the soluble Fe and not Fe adsorbed to the bottle walls or retained as

Table 2 | CSV-KIN: summary of FeL kinetic data for natural ligands in seawater from the literature.

Location	Depth (m)	Log k_f	Log k_d	Ligand	Reference
NW Atlantic	Surface	4.6–6.8	−6.0 to −6.5	1N2N	Luther and Wu (1997)
NW Atlantic	11–2874	4.6–6.5	−4.4 to −7.0	1N2N	Witter and Luther (1998)
Arabian Sea	25–600	5.1–6.0	−4.7 to −7.0	1N2N	Witter et al. (2000)
Scheldt Estuary	Surface	8.3–9.4	−0.8 to −2.2 (strong) −3.4 to −4.3 (weak)	TAC	Gerringa et al. (2007)
Tropical Atlantic	60–80	5.5–5.8	−6.0 to −7.0 (strong) −3.6 to −4.2 (weak)	TAC	This study
Tropical Atlantic	20–400	–	−4.1 to −5.3 (weak)	–	This study[a]

Data in the Gerringa et al. work was calculated using a model incorporating at least six kinetic parameters including ferric hydroxide species – see the text for more information. [a]Iron solubility kinetic measurements (see the appendix for full data description).

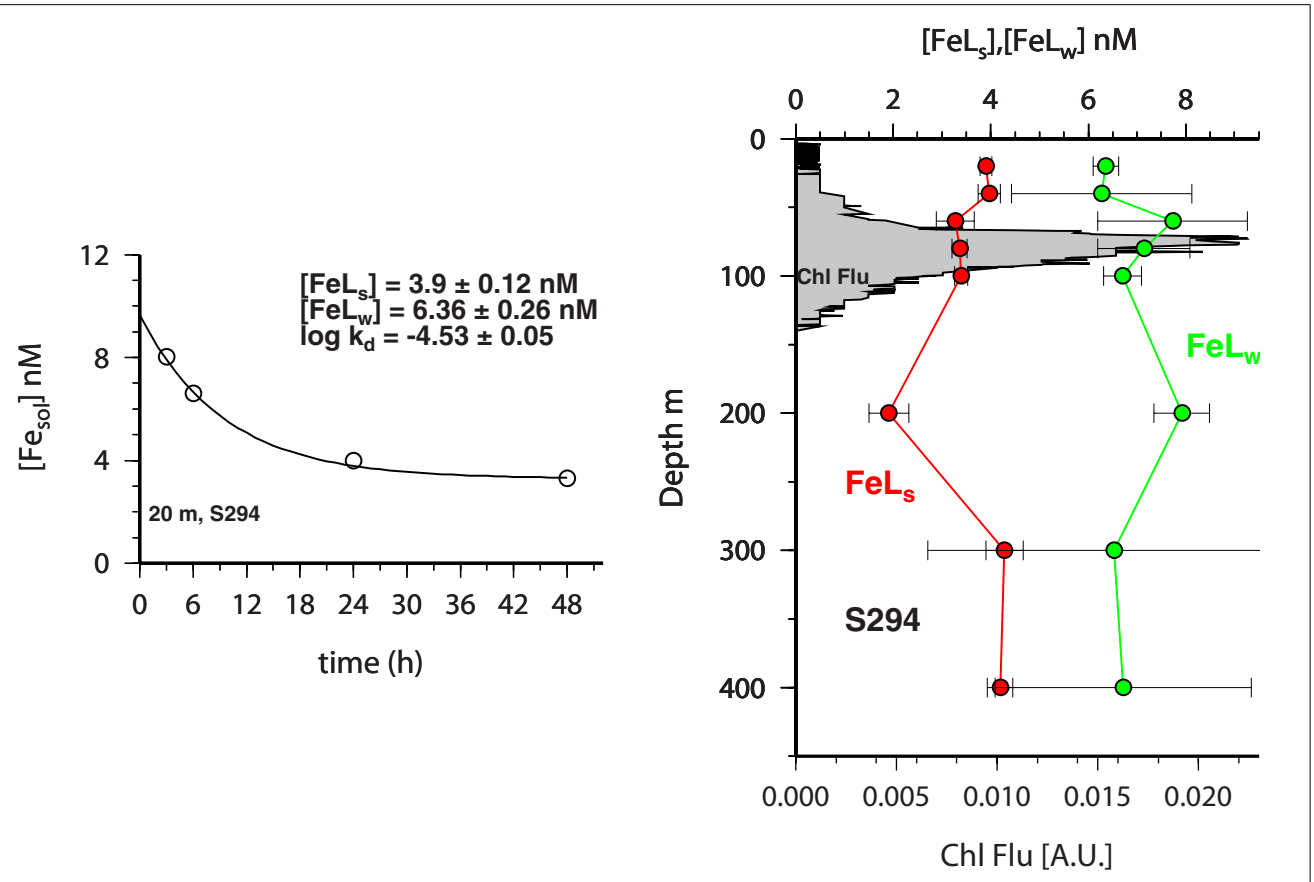

FIGURE 5 | FESOL-KIN: (left) example of fitting equation to Fe solubility (<0.025 μm) data for sample from 20 m depth at S294. (Right) Vertical distribution FeL_s and FeL_w (see text for details of how determined) in the top 400 m of the water column at station 294 during ANTXXVI-4. The chlorophyll fluorescence profile is also shown (gray shading; right).

colloids or particulates on the filter. We also make the assumption that initially most of the added Fe is complexed by soluble weak ligands which slowly exchange with colloidal sized ligands (Schlosser et al., 2011). Wall adsorption however is believed to be a significant sink for added iron in these experiments and is important to consider in the choice of equipment and experimental design (Fischer et al., 2007).

IMPACT OF O_2^- ON IRON SOLUBILITY

The suggestion that O_2^- can dissolve particulate sources of iron, is still very much under debate. Voelker and Sedlak (1995) found in their pulse radiolysis studies that O_2^- did not react with colloidal Fe(III). They observed that at pH values greater than 6 the Fe(II) concentration decreased due to formation of unreactive amorphous $Fe(OH)_3$. More recently Fujii et al. (2006) suggested from

their work that O_2^- can reduce Fe(III) present in amorphous ferric oxides. In our own work, we examined the effect of O_2^- on dissolved Fe formed upon direct addition of Fe to seawater, and found no increase in soluble Fe (Heller and Croot, 2011) or in the loss rate of O_2^- (Heller and Croot, 2010c). We also used a thermal source of O_2^- (Heller and Croot, 2010a) that allows a first order controlled release of O_2^- to follow the O_2^- induced dissolution of iron from atmospheric dust. This work was performed in the presence of 1 mM of the strong Fe(II) chelator Ferrozine (FZ) in order to trap any Fe(II) formed during the experiment. Performed under close to natural conditions our results strongly suggested that O_2^- is not a significant pathway for the dissolution of dust in the ocean (Heller and Croot, 2011). However O_2^- may still play be important for redox cycling between soluble and colloidal phases of iron in dust impacted regions.

In the present work we obtained data for the influence of O_2^- on the solubility of Fe at three stations (279, 287, and 292) along a meridional transect in the Atlantic (ANTXXVI-4). At station 279 a full depth profile in the top 400 m was investigated whereas at station 287 and 292 only one depth was sampled in the mixed layer to address this issue in the surface ocean. In the single samples from station 287 and 292 the solubility of iron increased in the bottles to which O_2^- had been added in the samples which were filtered after 3 and 6 h and showed almost identical values after 24 h, this can be seen in **Figure 6** where we plot the ratio of the experimental sample (i.e., seawater with SOTS-1 added) over the control sample (i.e., seawater without SOTS-1 added). Our results are consistent with the O_2^- flux from SOTS-1 which decays exponentially (Heller and Croot, 2010a) with time (**Figure 6**) to almost negligible fluxes after 24 h. It should be noted that while the production flux of O_2^- is known as a function of time in this case, the pseudo steady state O_2^- concentration will vary proportionally to the decay rate of O_2^- in the sample which is itself dependent on reactivity with Cu, Fe, Mn, and some organic species (e.g., quinones; Heller and Croot, 2010c). Interestingly the apparent maximum for the soluble iron was found at the 6 h time point at both stations indicating that a transient species such as Fe(II) may have been responsible for this result and required time to accumulate in the initial stages but decayed away under lower O_2^- flux conditions. Reactivity with O_2^- appears to be related to the availability of an accessible coordination site on the Fe complex, which is also related to the stability of the complexes (Dhungana and Crumbliss, 2005) thus the weaker FeEDTA complex is significantly more reactive than the stronger complexes ferrioxamine B and FeDTPA (Fisher et al., 2004). This suggests that O_2^- most likely reacts with weakly bound iron and facilitates its release, while strongly bound iron is inert. Once released the Fe(II) may also react with O_2^- leading to a rapid redox cycle between inorganic Fe(II) and Fe(III) whose turn over rate is related to the O_2^- flux. The lag time before achieving the maximum soluble Fe may then be related to a slow reactivity between the weak iron binding ligand relative to Fe′. Further work is needed however to fully elucidate this mechanism.

For the vertical profile collected at station 279 there was no statistically significant variation (paired *t*-test) from unity for the ratio between the soluble iron determined in the SOTS amended treatment and the control for samples below 100 m. However in the upper 100 m (**Figure 7**) there were significant differences observed. Initially all samples in the upper 100 m had ratios lower than 1 and with time the deeper samples (75 and 100 m) converged toward a ratio of 1. Interestingly the sample from 25 m continued to decrease with time to be at 0.46 after 48 h. The sample from 50 m however behaved very differently with the ratio increasing with time to 1.18 after 48 h. The reasons for these differences may be related to vertical differences in redox reactions initiated by the presence of O_2^-; previous work has shown that O_2^- predominantly reacts with Cu in surface waters to form Cu(I) (Heller and Croot, 2010c, 2011), though reactions with CDOM may also be important in Tropical regions(Heller and Croot, 2010b) and as the redox cycling of Mn is also influenced by O_2^- (Hansard et al., 2011) reactions with Mn may also be important in dust impacted regions where Mn is high (Shiller, 1997), such as here at S279. Superoxide reactions with CDOM may create or destroy iron binding ligands while O_2^- reactions with other trace metals will reduce the amount of O_2^- available to react with iron but may

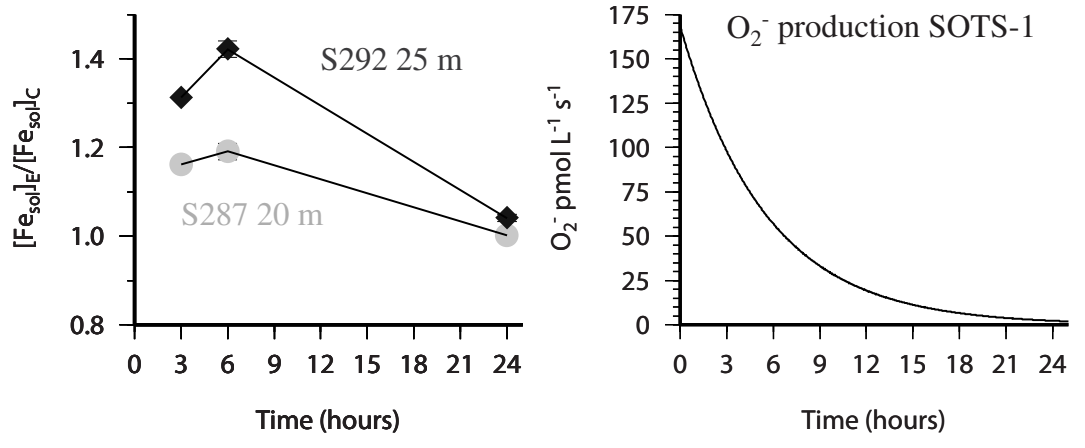

FIGURE 6 | FESOL-KIN: (left) near surface samples from Station 287 (gray circles) and 292 (black diamonds) during ANTXXVI-4 which were spiked with ^{55}Fe and O_2^- (SOTS-1). Shown is the ratio ($[Fe_{sol}]_E/[Fe_{sol}]_C$) of the data obtained from paired bottles where the soluble Fe was measured in both the presence (experimental-E) and absence (control-C) of the thermal O_2^- source SOTS-1. (Right) Time course of the production flux of O_2^- from the thermal decay of SOTS-1 in the experimental treatment (see text for more details).

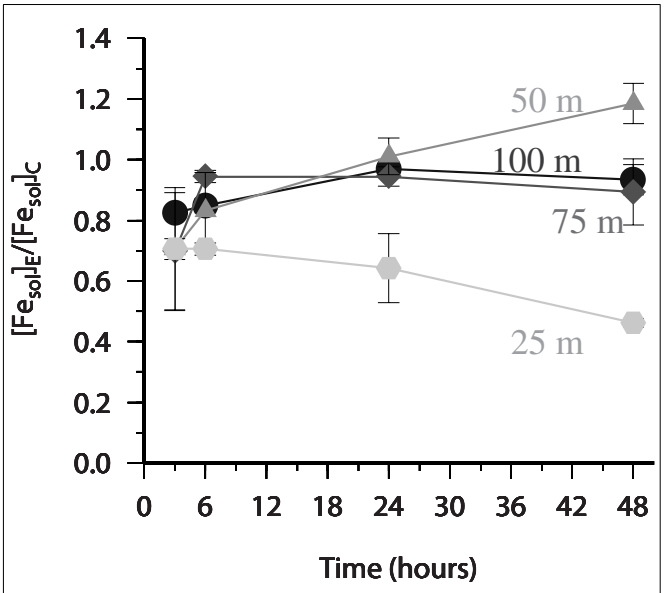

FIGURE 7 | FESOL-KIN: experiment at S279 during ANTXXVI-4 to which a thermal source of O_2^- (SOTS-1) was added. Time variation of the ratio ($[Fe_{sol}]_E/[Fe_{sol}]_C$) of the data obtained from paired bottles where the soluble Fe was measured in both the presence (experimental-E) and absence (control-C) of the thermal O_2^- source SOTS-1 for samples from the upper 100 m (25 m hexagons, 50 m triangles, 75 m diamonds, 100 m circles). There was no statistical significant variation (as assessed by paired *t*-test) in the ratio for samples below 100 m.

additionally provide other oxidants or reductants that react with iron. Further work is on-going to determine the critical processes at work here in the Tropical ocean and at present we lack key data on the cross reactivity between metals and Mn redox cycling in particular.

The initial O_2^- fluxes from the decay of SOTS-1 in the experiments was estimated to be 4 (Experiment at S279) to 10 times (all other experiments) higher than would be found *in situ* based on measured photochemical production rates in the open ocean (Heller and Croot, 2010a). The higher flux of O_2^- may have also influenced the results by altering the balance between redox cycling and complexation reactions so that a more intense redox cycle was initiated. As the O_2^- fluxes decrease exponentially with time typical surface open ocean midday fluxes would have been reached after 6–12 h and continued to decrease with time in essence simulating the decrease in the flux after midday or midday fluxes at deeper depths in the water column. Future experiments with an increased sampling frequency would allow a better estimation of these processes at natural levels, as the first order decay of SOTS allows for a range of O_2^- flux concentrations to be evaluated over the course of a single experiment.

AUTHOR CONTRIBUTIONS

Peter L. Croot performed the voltammetric analysis, and Maija I. Heller undertook the radiotracer work, both authors contributed equally to the writing of this manuscript.

ACKNOWLEDGMENTS

The authors would like to express their deep thanks and appreciation to the crews of the R. V. Polarstern (ANTXXVI-4) and Meteor. This work was in part supported by grants awarded to Peter L. Croot as part of the BMBF Verbundsprojekt SOPRAN2 (IG03) and the DFG project ADIOS-BAO (CR145/18-1). This work is a contribution to German SOLAS (SOPRAN). This work is a contribution of the Sonderforschungsbereich 754 "Climate – Biogeochemistry Interactions in the Tropical Ocean" (www.sfb754.de). Financial support for this work was provided by the Deutsche Forschungsgemeinschaft (DFG) via grants to Peter L. Croot (CR145/2-1, CR145/7-1 CR145/15-1, and SFB754 B5).

REFERENCES

Baker, A. R., and Croot, P. L. (2010). Atmospheric and marine controls on aerosol iron solubility in seawater. *Mar. Chem.* 120, 4–13.

Batchelli, S., Muller, F. O. L. L., Chang, K.-C., and Lee, C.-L. (2010). Evidence for strong but dynamic iron-humic colloidal associations in humic-rich coastal waters. *Environ. Sci. Technol.* 44, 8485–8490.

Bergquist, B. A., and Boyle, E. A. (2006). Dissolved iron in the tropical and subtropical Atlantic Ocean. *Global Biogeochem. Cycles* 20, 247–278.

Bergquist, B. A., Wu, J., and Boyle, E. A. (2007). Variability in oceanic dissolved iron is dominated by the colloidal fraction. *Geochim. Cosmochim. Acta* 71, 2960–2974.

Boyd, P. W., Watson, A., Law, C. S., Abraham, E., Trull, T., Murdoch, R., Bakker, D. C. E., Bowie, A. R., Buesseler, K. O., Chang, H., Charette, M., Croot, P. L., Downing, K., Frew, R., Gall, M., Hadfield, M., Hall, J., Harvey, M., Jameson, G., Laroche, J., Liddicoat, M., Ling, R., Maldonado, M., Mckay, R. M., Nodder, S., Pickmere, S., Pridmore, R., Rintoul, S., Safi, K., Sutton, P., Strzepek, R., Tannenberger, K., Turner, S., Waite, A., and Zeldis, J. (2000). Mesoscale iron fertilisation elevates phytoplankton stocks in the polar Southern Ocean. *Nature* 407, 695–702.

Boye, M., Nishioka, J., Croot, P., Laan, P., Timmermans, K. R., Strass, V. H., Takeda, S., and De Baar, H. J. W. (2010). Significant portion of dissolved organic Fe complexes in fact is Fe colloids. *Mar. Chem.* 122, 20–27.

Boye, M., Van Den Berg, C. M. G., De Jong, J. T. M., Leach, H., Croot, P. L., and De Baar, H. J. W. (2001). Organic complexation of iron in the Southern Ocean. *Deep Sea Res. A* 48, 1477–1497.

Butler, A., and Theisen, R. M. (2010). Iron(III)-siderophore coordination chemistry: reactivity of marine siderophores. *Coord. Chem. Rev.* 254, 288–296.

Croot, P. L., Bluhm, K., Schlosser, C., Streu, P., Breitbarth, E., Frew, R., and Van Ardelan, M. (2008). Regeneration of Fe(II) during EIFeX and SOFeX. *Geophys. Res. Lett.* 35, L19606.

Croot, P. L., Bowie, A. R., Frew, R. D., Maldonado, M., Hall, J. A., Safi, K. A., La Roche, J., Boyd, P. W., and Law, C. S. (2001). Retention of dissolved iron and Fe^{II} in an iron induced Southern Ocean phytoplankton bloom. *Geophys. Res. Lett.* 28, 3425–3428.

Croot, P. L., Heller, M. I., Schlosser, C., and Wuttig, K. (2011). "Utilizing radioisotopes for trace metal speciation measurements in seawater," in *Radioisotopes – Applications in Physical Sciences*, ed. N. Singh (Intech), 247–278.

Croot, P. L., and Johansson, M. (2000). Determination of iron speciation by cathodic stripping voltammetry in seawater using the competing ligand 2-(2-Thiazolylazo)-p-cresol (TAC). *Electroanalysis* 12, 565–576.

Croot, P. L., Streu, P., and Baker, A. R. (2004). Short residence time for iron in surface seawater impacted by atmospheric dry deposition from Saharan dust events. *Geophys. Res. Lett.* 31, L23S08.

de Baar, H. J. W., Boyd, P. W., Coale, K. H., Landry, M. R., Tsuda, A., Assmy, P., Bakker, D. C. E., Bozec, Y., Barber, R. T., Brzezinski, M. A., Buesseler, K. O., Boye, M., Croot, P. L., Gervais, F., Gorbunov, M. Y., Harrison, P. J., Hiscock, W. T., Laan, P., Lancelot, C., Law, C. S., Levasseur, M., Marchetti, A., Millero, F. J., Nishioka, J., Nojiri, Y., Van Oijen, T., Riebesell, U., Rijkenberg, M. J. A., Saito, H., Takeda, S., Timmermans, K. R., Veldhuis, M. J. W., Waite, A. M., and Wong, C.-S. (2005). Synthesis of 8 iron fertilization experiments: from the iron age to the age of enlightenment. *J. Geophys. Res.* 110, C09S16.

Dhungana, S., and Crumbliss, A. (2005). Coordination chemistry and redox

processes in siderophore-mediated iron transport. *Geomicrobiol. J.* 22, 87–98.

Duggen, S., Olgun, N., Croot, P., Hoffmann, L., Dietze, H., Delmelle, P., and Teschner, C. (2010). The role of airborne volcanic ash for the surface ocean biogeochemical iron cycle: a review. *Biogeosciences* 7, 827–844.

Fischer, A. C., Kroon, J. J., Verburg, T. G., Teunissen, T., and Wolterbeek, H. T. (2007). On the relevance of iron adsorption to container materials in small-volume experiments on iron marine chemistry: Fe-55-aided assessment of capacity, affinity and kinetics. *Mar. Chem.* 107, 533–546.

Fisher, A. E. O., Maxwell, S. C., and Naughton, D. P. (2004). Superoxide and hydrogen peroxide suppression by metal ions and their EDTA complexes. *Biochem. Biophys. Res. Commun.* 316, 48–51.

Fujii, M., Rose, A. L., Waite, T. D., and Omura, T. (2006). Superoxide-mediated dissolution of amorphous ferric oxyhydroxide in seawater. *Environ. Sci. Technol.* 40, 880–887.

Gerringa, L. J. A., Herman, P. M. J., and Poortvliet, T. C. W. (1995). Comparison of the linear van den Berg/Ruzic transformation and a non-linear fit of the Langmuir isotherm applied to Cu speciation data in the estuarine environment. *Mar. Chem.* 48, 131–142.

Gerringa, L. J. A., Rijkenberg, M. J. A., Wolterbeek, H. T., Verburg, T. G., Boye, M., and Baar, H. J. W. D. (2007). Kinetic study reveals weak Fe-binding ligand, which affects the solubility of Fe in the Scheldt estuary. *Mar. Chem.* 103, 30–45.

Gran, H. H. (1931). *On the Conditions for Production of Plankton in the Sea.* Rapports et Proces-Verbaux des Reunions Conseil International pour l'Exploration de la Mer, Copenhague, 75, 37–46.

Grant, M., and Jordan, R. B. (1981). Kinetics of solvent water exchange on iron(III). *Inorg. Chem.* 20, 55–60.

Hansard, S. P., Easter, H. D., and Voelker, B. M. (2011). Rapid reaction of nanomolar Mn(II) with superoxide radical in seawater and simulated freshwater. *Environ. Sci. Technol.* 45, 2811–2817.

Harvey, H. W. (1937). The supply of iron to diatoms. *J. Mar. Biol. Assoc.* 22, 205–219.

Heller, M. I., and Croot, P. L. (2010a). Application of a superoxide (O_2^-) thermal source (SOTS-1) for the determination and calibration of O_2^- fluxes in seawater. *Anal. Chim. Acta* 667, 1–13.

Heller, M. I., and Croot, P. L. (2010b). Kinetics of superoxide reactions with dissolved organic matter in tropical Atlantic surface waters near Cape Verde (TENATSO). *J. Geophys. Res.* 115, C12038.

Heller, M. I., and Croot, P. L. (2010c). Superoxide decay kinetics in the southern ocean. *Environ. Sci. Technol.* 44, 191–196.

Heller, M. I., and Croot, P. L. (2011). Superoxide decay as a probe for speciation changes during dust dissolution in tropical Atlantic surface waters near Cape Verde. *Mar. Chem.* 126, 37–55.

Helm, L., and Merbach, A. E. (1999). Water exchange on metal ions: experiments and simulations. *Coord. Chem. Rev.* 187, 151.

Hering, J. G., and Morel, F. M. M. (1990a). "The kinetics of trace metal complexation: implications for metal reactivity in natural waters," in *Aquatic Chemical Kinetics: Reaction Rates of Processes in Natural Waters*, ed. W. Stumm (New York: John-Wiley & Sons).

Hering, J. G., and Morel, F. M. M. (1990b). Kinetics of trace metal complexation: ligand exchange reactions. *Environ. Sci. Technol.* 24, 242–252.

Hiemstra, T., and van Riemsdijk, W. H. (2006). Biogeochemical speciation of Fe in ocean water. *Mar. Chem.* 102, 181–197.

Hove, M., Van Hille, R. P., and Lewis, A. E. (2007). Iron solids formed from oxidation precipitation of ferrous sulfate solutions. *AIChE J.* 53, 2569–2577.

Hove, M., Van Hille, R. P., and Lewis, A. E. (2008). Mechanisms of formation of iron precipitates from ferrous solutions at high and low pH. *Chem. Eng. Sci.* 63, 1626–1635.

Hudson, R. J. M., Covault, D. T., and Morel, F. M. M. (1992). Investigations of iron coordination and redox reactions in seawater using 59Fe radiometry and ion-pair solvent extraction of amphiphilic iron complexes. *Mar. Chem.* 38, 209–235.

Hudson, R. J. M., and Morel, F. M. M. (1990). Iron transport in marine phytoplankton: kinetics of cellular and medium coordination reactions. *Limnol. Oceanogr.* 35, 1002–1020.

Hudson, R. J. M., and Morel, F. M. M. (1993). Trace metal transport by marine microorganisms: implications of metal coordination kinetics. *Deep Sea Res. A* 40, 129–150.

Ingold, K. U., Paul, T., Young, M. J., and Doiron, L. (1997). Invention of the first azo compound to serve as a superoxide thermal source under physiological conditions: concept, synthesis, and chemical properties. *J. Am. Chem. Soc.* 119, 12364–12365.

Jickells, T. D., An, Z. S., Andersen, K. K., Baker, A. R., Bergametti, G., Brooks, N., Cao, J. J., Boyd, P. W., Duce, R. A., Hunter, K. A., Kawahata, H., Kubilay, N., Laroche, J., Liss, P. S., Mahowald, N., Prospero, J. M., Ridgwell, A. J., Tegen, I., and Torres, R. (2005). Global Iron connections between desert dust, ocean biogeochemistry, and climate. *Science* 308, 67–71.

Johnson, K. S., Coale, K. H., Elrod, V. A., and Tindale, N. W. (1994). Iron photochemistry in seawater from the equatorial Pacific. *Mar. Chem.* 46, 319–334.

Johnson, K. S., Gordon, R. M., and Coale, K. H. (1997). What controls dissolved iron concentrations in the world ocean? *Mar. Chem.* 57, 137–161.

Kuma, K., Katsumoto, A., Kawakami, H., Takatori, F., and Matsunaga, K. (1998a). Spatial variability of Fe(III) hydroxide solubility in the water column of the northern north Pacific ocean. *Deep Sea Res.* 45, 91–113.

Kuma, K., Katsumoto, A., Nishioka, J., and Matsunaga, K. (1998b). Size-fractionated iron concentrations and Fe(III) hydroxide solubilities in various coastal waters. *Estuar. Coast. Shelf Sci.* 47, 275–283.

Kuma, K., Katsumoto, A., Shiga, N., Sawabe, T., and Matsunaga, K. (2000). Variation of size-fractionated Fe concentrations and Fe(III) hydroxide solubilities during a spring phytoplankton bloom in Funka Bay (Japan). *Mar. Chem.* 71, 111–123.

Kuma, K., Nakabayashi, S., and Matsunaga, K. (1995). Photoreduction of Fe(III) by Hydroxycarboxylic acids in seawater. *Water Res.* 29, 1559–1569.

Kuma, K., Nishioka, J., and Matsunaga, K. (1996). Controls on iron(III) hydroxide solubility in seawater: the influence of pH and natural organic chelators. *Limnol. Oceanogr.* 41, 396–407.

Liu, X., and Millero, F. J. (2002). The solubility of iron in seawater. *Mar. Chem.* 77, 43–54.

Luther, G. W., and Wu, J. (1997). What controls dissolved iron concentrations in the world ocean? – a comment. *Mar. Chem.* 57, 173–179.

Martin, J. H., Coale, K. H., Johnson, K. S., Fitzwater, S. E., Gordon, R. M., Tanner, S. J., Hunter, C. N., Elrod, V. A., Nowicki, J. L., Coley, T. L., Barber, R. T., Lindley, S., Watson, A. J., Van Scoy, K., Law, C. S., Liddicoat, M. I., Ling, R., Stanton, T., Stockel, J., Collins, C., Anderson, A., Bidigare, R., Ondrusek, M., Latasa, M., Millero, F. J., Lee, K., Yao, W., Zhang, J. Z., Friederich, G., Sakamoto, C., Chavez, F., Buck, K., Kolber, Z., Greene, R., Falkowski, P., Chisholm, S. W., Hoge, F., Swift, R., Yungel, J., Turner, S., Nightingale, P., Hatton, A., Liss, P., and Tindale, N. W. (1994). Testing the iron hypothesis in ecosystems of the equatorial Pacific ocean. *Nature* 371, 123–129.

Martin, J. H., and Fitzwater, S. E. (1988). Iron deficiency limits phytoplankton growth in the north-east Pacific subarctic. *Nature* 331, 341–343.

Mies, K., Wirgau, J., and Crumbliss, A. (2006). Ternary complex formation facilitates a redox mechanism for iron release from a siderophore. *Biometals* 19, 115–126.

Millero, F. J. (1998). Solubility of Fe(III) in seawater. *Earth Planet. Sci. Lett.* 154, 323–329.

Morel, F. M. M., and Hering, J. G. (1993). *Principles and Applications of Aquatic Chemistry*. New York: Wiley-Interscience.

Nakabayashi, S., Kuma, K., Sasaoka, K., Saitoh, S., Mochizuki, M., Shiga, N., and Kusakabe, M. (2002). Variation in iron(III) solubility and iron concentration in the northwestern north Pacific ocean. *Limnol. Oceanogr.* 47, 885–892.

Nakabayashi, S., Kusakabe, M., Kuma, K., and Kudo, I. (2001). Vertical distributions of iron(III) hydroxide solubility and dissolved iron in the northwestern north Pacific ocean. *Geophys. Res. Lett.* 28, 4611–4614.

Nowostawska, U., Kim, J. P., and Hunter, K. A. (2008). Aggregation of riverine colloidal iron in estuaries: a new kinetic study using stopped-flow mixing. *Mar. Chem.* 110, 205.

Okumura, C., Hasegawa, H., Mizumoto, H., Maki, T., and Ueda, K. (2004). Size fractionation of iron compounds in phytoplankton cultures in the presence of chelating ligands. *Bunseki Kagaku* 53, 1215–1221.

Roy, E. G., Wells, M. L., and King, D. W. (2008). Persistence of iron(II) in surface waters of the western subarctic Pacific. *Limnol. Oceanogr.* 53, 89–98.

Rue, E. L., and Bruland, K. W. (1995). Complexation of iron(III) by natural organic ligands in the central north Pacific as determined by a new competitive ligand equilibration/adsorptive cathodic stripping voltammetric method. *Mar. Chem.* 50, 117–138.

Schlosser, C., and Croot, P. (2009). Controls on seawater Fe(III) solubility in the Mauritanian upwelling zone. *Geophys. Res. Lett.* 36, L18606.

Schlosser, C., De La Rocha, C. L., and Croot, P. L. (2011). Effects of iron surface adsorption and sample handling on iron solubility measurements. *Mar. Chem.* 127, 48–55.

Schneider, W. (1988). Iron hydrolysis and the biochemistry of iron – the interplay of hydroxide and biogenic ligands. *Chimia (Aarau)* 42, 9–20.

Shiller, A. M. (1997). Manganese in surface waters of the Atlantic Ocean. *Geophys. Res. Lett.* 24, 1495–1498.

Stockdale, A., Tipping, E., Hamilton-Taylor, J., and Lofts, S. (2011). Trace metals in the open oceans: speciation modelling based on humic-type ligands. *Environ. Chem.* 8, 304–319.

van den Berg, C. M. G. (2006). Chemical speciation of iron in seawater by cathodic stripping voltammetry with dihydroxynaphthalene. *Anal. Chem.* 78, 156–163.

Voelker, B. M., and Sedlak, D. L. (1995). Iron reduction by photoproduced superoxide in seawater. *Mar. Chem.* 50, 93–102.

Vraspir, J. M., and Butler, A. (2009). Chemistry of marine ligands and siderophores. *Annu. Rev. Mar. Sci.* 1, 43–63.

Witter, A., and Luther, G. W. (1998). Variation in Fe-organic complexation with depth in the northwestern Atlantic ocean as determined using a kinetic approach. *Mar. Chem.* 62, 241–258.

Witter, A. E., Hutchins, D. A., Butler, A., and Luther, G. W. (2000). Determination of conditional stability constants and kinetic constants for strong model Fe-binding ligands in seawater. *Mar. Chem.* 69, 1–17.

Wu, J., Boyle, E., Sunda, W., and Wen, L.-S. (2001). Soluble and colloidal iron in the oligotrophic north Atlantic and north Pacific. *Science* 293, 847–849.

Wu, J., and Luther, G. W. (1995). Complexation of Fe(III) by natural organic ligands in the northwest Atlantic ocean by a competitive ligand equilibration method and a kinetic approach. *Mar. Chem.* 50, 159–177.

Conflict of Interest Statement: The authors declare that the research was conducted in the absence of any commercial or financial relationships that could be construed as a potential conflict of interest.

Received: 31 October 2011; accepted: 29 May 2012; published online: 19 June 2012.

Citation: Croot PL and Heller MI (2012) The importance of kinetics and redox in the biogeochemical cycling of iron in the surface ocean. Front. Microbio. ***3****:219. doi: 10.3389/fmicb.2012.00219*

This article was submitted to Frontiers in Microbiological Chemistry, a specialty of Frontiers in Microbiology.

Copyright © 2012 Croot and Heller. This is an open-access article distributed under the terms of the Creative Commons Attribution Non Commercial License, which permits non-commercial use, distribution, and reproduction in other forums, provided the original authors and source are credited.

APPENDIX

METHODS

Kinetic method for Fe speciation

Calculation of k_d (rate of dissociation for recovery of Fe from FeL). Two conditions may result after the recovery period: 100% recovery of added Fe, or <100% recovery of added Fe (i.e., equilibrium is established between Fe, natural ligands and TAC). The solutions described here are adapted from earlier works (Wu and Luther, 1995; Witter and Luther, 1998). For an alternative derivation of the rate laws see the later sections of this appendix.

Weak ligands – all added Fe recovered. The overall reaction for the recovery of Fe^{3+} [as $Fe(TAC)_2$] from $Fe^{3+}L$ (which is abbreviated FeL) is given in A1 as an associative reaction. It was previously assumed (Wu and Luther, 1995; Witter and Luther, 1998) that this process can be described by an *associative reaction* and that Fe^{3+} does not accumulate in solution as Fe′.

$$\mathrm{FeL} + 2\,(\mathrm{TAC}) \xrightarrow{k_{\mathrm{obs}}} \mathrm{Fe(TAC)_2} + \mathrm{L} \tag{A1}$$

The overall reaction rate is pseudo first order in [TAC] due to the large excess of this ligand and can be expressed as:

$$-\frac{\partial\,[\mathrm{FeL}]}{\partial t} = \frac{\partial\,[\mathrm{Fe(TAC)_2}]}{\partial t} = k_{\mathrm{obs}}\,[\mathrm{FeL}]\,[\mathrm{TAC}] \tag{A2}$$

Integrating gives the following solution:

$$\ln\,[\mathrm{FeL}] = -k_{\mathrm{obs}}\,[\mathrm{TAC}]\,t \tag{A3}$$

A1 can be broken into *two elementary reaction steps*; the *dissociation* of the natural organic ligand complex to form Fe′ (A4), where Fe′ represents the inorganic forms of Fe at ambient pH; and the *reaction* of Fe′ with TAC (A5):

$$\mathrm{FeL} \xrightarrow{k_d} \mathrm{Fe'} + \mathrm{L} \tag{A4}$$

$$\mathrm{Fe'} + 2\,(\mathrm{TAC}) \xrightarrow{k_2} \mathrm{Fe(TAC)_2} \tag{A5}$$

The overall reaction A5 is comprised of two sequential steps with the first step ($A5_1$) being the rate limiting step:

$$\mathrm{Fe'} + \mathrm{TAC} \xrightarrow{k_2} \mathrm{Fe\,(TAC)} \tag{$A5_1$}$$

$$\mathrm{Fe\,(TAC)} + \mathrm{TAC} \xrightarrow{k_2} \mathrm{Fe(TAC)_2} \tag{$A5_2$}$$

As [TAC] is greatly in excess over [L] ([TAC] = 1×10^{-5} M compared to [L] ~ $1 - 4.0 \times 10^{-9}$ M), any Fe′ formed will react faster with TAC than with [L], and the product $Fe(TAC)_2$ will not revert to Fe′ and TAC during the timescale of the experiment. The overall reaction rate for A5 will be pseudo first order in [TAC] due to its large excess. Since TAC forms complexes with Fe′ very rapidly ($k_2 \sim 1 \times 10^6\ \mathrm{M\,s^{-1}}$), there will be no accumulation of Fe′ and/or subsequent formation of particulate iron. Therefore, the Fe′ concentration will always be very small (steady state approximation) and we can conclude:

$$\frac{\delta[\mathrm{Fe'}]}{\delta t} \approx 0 \tag{A6}$$

We can write the rate eq. for Fe′ by applying the steady state approximation:

$$0 \approx \frac{\delta\left[\mathrm{Fe'}\right]}{\delta t} = k_d\,[\mathrm{FeL}] - k_f\left[\mathrm{Fe'}\right][\mathrm{L}] - k_2\left[\mathrm{Fe'}\right][\mathrm{TAC}] \tag{A7}$$

Solving for Fe′:

$$\left[\mathrm{Fe'}\right] = \frac{k_d\,[\mathrm{FeL}]}{\left\{k_f\,[\mathrm{L}] + k_2\,[\mathrm{TAC}]\right\}} \tag{A8}$$

A9 is the rate law for the formation of $Fe(TAC)_2$ from Fe′ (A5):

$$\frac{-\delta\,[\mathrm{FeL}]}{\delta t} = \frac{\delta\,[\mathrm{Fe(TAC)_2}]}{\delta t} = k_2\left[\mathrm{Fe'}\right][\mathrm{TAC}] \tag{A9}$$

Substituting A8 into A9 gives A10:

$$\frac{-\delta\,[\mathrm{FeL}]}{\delta t} = \frac{\delta\,[\mathrm{Fe(TAC)_2}]}{\delta t} = \frac{k_2\,[\mathrm{TAC}]\,k_d\,[\mathrm{FeL}]}{\{k_f[\mathrm{L}] + k_2[\mathrm{TAC}]\}} \tag{A10}$$

In Wu and Luther (1995), two possibilities to simplify A10 were discussed. First, assuming $k_f[L] << k_2[\mathrm{TAC}]$ because [TAC] (1×10^{-5} M) is much larger than [L] then A10 reduces to:

$$\frac{-\delta\,[\mathrm{Fel}]}{\delta t} = \frac{\delta\,[\mathrm{Fe(TAC)_2}]}{\delta t} = k_d\,[\mathrm{FeL}] \tag{A11}$$

Integrating A11, and comparing it to A3 gives A12–A13:

$$\ln\,[\mathrm{FeL}] = -k_d t \tag{A12}$$

$$k_d = k_{\mathrm{obs}}\,[\mathrm{TAC}] \tag{A13}$$

The dissociation rate constant, k_d, can be calculated when 100% recovery is achieved using A12. A plot of ln[FeL] (M) versus time (s^{-1}) allows calculation of k_d ($M^{-1}\,s^{-1}$). The conditional stability constant, $K_{\mathrm{Fe3+L}}$, can then be calculated from A 14 to 15.

$$K_{\mathrm{Fe'L}} = \frac{k_f}{k_d} \tag{A14}$$

$$K_{\mathrm{Fe3+L}} = \alpha_{\mathrm{Fe'}} \times K_{\mathrm{Fe'L}} \tag{A15}$$

The inorganic side reaction coefficient for Fe used in this work, $a_{\mathrm{Fe'}} = 10^{10}$, was determined previously by Hudson et al. (1992).

The second possible solution (Wu and Luther, 1995) arises from the observation that the uptake rate of iron by the natural ligands and TAC are indistinguishable:

$$k_f\,[\mathrm{L}] = k_2\,[\mathrm{TAC}] \tag{A16}$$

then A10 simplifies to:

$$\frac{\partial\,[\mathrm{Fe(TAC)_2}]}{\partial} = \frac{k_d\,[\mathrm{FeL}]}{2} \tag{A17}$$

Gerringa et al. (2007) previously estimated the value of k_2 for $Fe(TAC)_2$ formation to vary between 1.14×10^7 and

$34 \times 10^8\ M^{-1}\ s^{-1}$ with the highest values found at lower salinities. These values are higher however than the water loss rate of Fe′ under these conditions (Hudson et al., 1992) and must be considered an artifact of the modeling scheme they employed. Our own estimates (unpublished) indicate a value of k_2 for $Fe(TAC)_2 \sim 1 \times 10^6\ M^{-1}\ s^{-1}$. Using this value in A10, no assumptions are necessary in calculating k_d. The difference in $K_{Fe'L}$ calculated based on A10 with and without assumptions based on the relative magnitude of $k_f[L]$ to $k_2[TAC]$ is $10^{0.3}$, and is not considered as significant.

<100% recovery of added Fe^{3+} (full equilibrium is established). If less than 100% recovery of added Fe occurs, the conditional stability constant for Fe complexation can be determined by considering that the system has reached equilibrium. In seawater with natural organic ligands present, Fe^{3+} shifts from being complexed by organic ligands as $Fe^{3+}L$ to $Fe(TAC)_2$ through an associative type mechanism so Fe′ never forms. A4 can then be expressed in equilibrium form as:

$$K_{rec} = \frac{\left[Fe^{3+}(TAC)_2\right][L]}{\left[Fe^{3+}L\right][TAC]^2} \tag{A18}$$

and a stability constant for the reaction can be calculated. Substituting A19 for $Fe^{3+}L$ in A18 above and rearrangement to A23 allows calculation of K_{Fe3+L}, since K_{rec} is related to the conditional stability constant with respect to Fe^{3+} (K_{Fe3+L}).

$$K_{Fe3+L} = \frac{\left[Fe^{3+}L\right]}{\left[Fe^{3+}\right][L]} \tag{A19}$$

$$K_{Fe3+L} = \frac{K_{Fe(TAC)_2}}{K_{rec}} \tag{A20}$$

The stability constant for $KFe(TAC)_2$ has been determined experimentally at pH 8.0 to be $10^{22.4}$ (Croot and Johansson, 2000). Finally a conditional stability constant with respect to Fe′ can be calculated by considering:

$$K_{Fe'L} = \frac{K_{Fe3+L}}{\alpha_{Fe'}} \tag{A21}$$

In this study, we used an $\alpha_{Fe'}$ at pH 8.0 of 10^{10} (Hudson et al., 1992). The dissociation rate constant, k_d, can then be calculated from A23 using the values for k_f and $K_{Fe'L}$ obtained by experiment (see the methods section in the main text for details).

$$K_{Fe'L} = \frac{k_f}{k_d} \tag{A22}$$

$$k_d = \frac{k_f}{K_{Fe'L}} \tag{A23}$$

Alternative derivation of the kinetic method for iron speciation:
The approach used by Luther and colleagues (Wu and Luther, 1995; Witter and Luther, 1998) considers the overall reaction to be adjunctive (associative) but the rate determining step for the dissociation of FeL is a purely disjunctive mechanism (A4). The dependence on the competing ligand arises from inclusion of a kinetic term incorporating the formation of the electroactive species in solution. This is therefore in many regards not a strictly adjunctive mechanism as no ternary intermediate complex (e.g., M-L-TAC) is postulated. An alternative derivation of the rate equations is developed here which considers that a disjunctive (k_{dis}) and adjunctive (k_{adj}) pathway are occurring simultaneously.

Disjunctive mechanism. Formation and dissociation of FeL

$$Fe' + L \xrightarrow{k_1} FeL \tag{B1a}$$

$$FeL \xrightarrow{k_{-1}} Fe' + L \tag{B1b}$$

The formation of Fe(TAC) and the electroactive complex $Fe(TAC)_2$

$$Fe' + TAC \xrightarrow{k_2} Fe\,(TAC) \tag{B2a}$$

For completeness we include the other reactions that are important in the formation of the assumed electroactive species $Fe(TAC)_2$ (though we neglect the reactions with the individual components that make up Fe′).

$$Fe\,(TAC) \xrightarrow{k_{-2}} Fe' + TAC \tag{B2b}$$

$$Fe\,(TAC) + TAC \xrightarrow{k_3} Fe(TAC)_2 \tag{B3a}$$

$$Fe(TAC)_2 \xrightarrow{k_{-3}} Fe\,(TAC) + TAC \tag{B3b}$$

Adjunctive mechanism. Formation of ternary complex FeL(TAC) from FeL and TAC

$$FeL + TAC \xrightarrow{k_4} FeL\,(TAC) \tag{B4a}$$

$$FeL\,(TAC) \xrightarrow{k_{-4}} FeL + TAC \tag{B4b}$$

Formation of ternary complex FeL(TAC) from Fe(TAC) and L

$$Fe\,(TAC) + L \xrightarrow{k_5} FeL\,(TAC) \tag{B5a}$$

$$FeL\,(TAC) \xrightarrow{k_{-5}} Fe\,(TAC) + L \tag{B5b}$$

In the present case we assume that there is no reaction between $Fe(TAC)_2$ and L. The overall reaction is then the same as that described in A1:

$$FeL + 2\,(TAC) \xrightarrow{k_{obs}} Fe(TAC)_2 + L \tag{B6}$$

The loss rate of FeL can then be described by the following using the equations described above:

$$-\frac{\partial\,[FeL]}{\partial t} = -k_1\left[Fe'\right][L] + k_{-1}\,[FeL] - k_{-4}\,[FeL\,(TAC)] + k_4\,[FeL]\,[TAC] \tag{B7}$$

In the context of the present work, the terms involving k_1 can be omitted as the concentrations of Fe′, L will always be small compared to [FeL] and [TAC]. If it is assumed that [FeL(TAC)] ≪ [FeL] (see below) then B7 reduces to:

$$-\frac{\partial\,[\mathrm{FeL}]}{\partial t} = k_{-1}\,[\mathrm{FeL}] + k_4\,[\mathrm{FeL}]\,[\mathrm{TAC}] \tag{B8}$$

Rearranging leads to:

$$-\frac{\partial\,[\mathrm{FeL}]}{\partial t} = (k_{-1} + k_4\,[\mathrm{TAC}])\,[\mathrm{FeL}] \tag{B9}$$

As above we assume that FeL, $\mathrm{Fe(TAC)_2} \gg \mathrm{Fe'}$, FeL(TAC), and Fe(TAC). A not unreasonable assumption given the stability of these complexes under the analytical conditions, then the following rate law can be postulated from mass balance considerations:

$$-\frac{\partial\,[\mathrm{FeL}]}{\partial t} = \frac{\partial\,[\mathrm{Fe(TAC)_2}]}{\partial t} = (k_{-1} + k_4\,[\mathrm{TAC}])\,[\mathrm{FeL}] \tag{B10}$$

Then the loss rate of formation of the natural ligands can thus be described by the following relationship:

$$-\frac{\partial\,[\mathrm{FeL}]}{\partial t} = k_{\mathrm{obs}}\,[\mathrm{FeL}] \tag{B11}$$

Where

$$k_{\mathrm{obs}} = k_{\mathrm{dis}} + k_{\mathrm{adj}}\,[\mathrm{TAC}] = (k_{-1} + k_4\,[\mathrm{TAC}]) \tag{B12}$$

In this formulation $k_{\mathrm{dis}} = k_{-1}$ and $k_{\mathrm{adj}} = k_4$.

Integrating Eq. B11 and applying the appropriate initial and final conditions results in the following relationship:

$$\ln\frac{[\mathrm{FeL}]_t - [\mathrm{FeL}]_\infty}{[\mathrm{FeL}]_0 - [\mathrm{FeL}]_\infty} = -k_{\mathrm{obs}}t \tag{B13}$$

Where the subscripts 0 and ∞ represent the initial and final time points and the subscript t indicates the time since the experiment started.

Case I: 100% recovery of FeL

In this case B13 reduces to the following:

$$\ln\,[\mathrm{FeL}]_t = -k_{\mathrm{obs}}t + \ln\,[\mathrm{FeL}]_0 \tag{B14}$$

Thus a plot of $\ln[\mathrm{FeL}]_t$ against time has slope k_{obs}. B14 is thus analogous to A12, though in this case k_{obs} includes both an adjunctive and disjunctive term.

Case II: <100% recovery of FeL

In this case B13 rearranges to the relationship:

$$\ln\,([\mathrm{FeL}]_t - [\mathrm{FeL}]_\infty) = -k_{\mathrm{obs}}t + \ln\,([\mathrm{FeL}]_0 - [\mathrm{FeL}]_\infty) \tag{B15}$$

Thus a plot of $\ln([\mathrm{FeL}]_t - [\mathrm{FeL}]_\infty)$ against time has slope k_{obs}. This approach uses kinetic data to determine the value of k_{obs} from which the values of k_{dis} and k_{adj} can be calculated, and is an alternative to the thermodynamic approach employed by Luther and co-workers (see above).

Is there a significant adjunctive mechanism using TAC?

Unfortunately due to logistical constraints we have no data as yet with the following; (i) where different concentrations (multiple detection windows) of TAC have been employed or (ii) simultaneous radiotracer and CSV measurements have been performed on the same water sample. This excludes then a direct assessment of the significance of an adjunctive mechanism in Fe(TAC) formation and this is clearly a goal for future work. However comparison of the maximum and minimum rates measured in the CSV experiments (TAC present) with the radiotracer experiments (TAC absent) gives estimates of $k_{\mathrm{dis}} = 10^{-4.1}$ to $10^{-5.3}\,\mathrm{s}^{-1}$ and $k_{\mathrm{adj}} = 5.8$ to $17.2\,\mathrm{M}^{-1}\,\mathrm{s}^{-1}$. This suggests then that the adjunctive mechanism is a significant reaction (70–90% of the overall rate) even at 10 μM TAC.

Note on Ternary Complex Formation: Central to the derivation above is the premise that the concentration of [FeL(TAC)] is always low, thermodynamically this is likely given that [TAC] ≫ [L] but the kinetics of this reaction have yet to be investigated thoroughly. There is growing evidence for the formation of such ternary iron complexes, with a recent example being the investigation of a series of iron-desferrioxamine B – citric acid complexes (Ito et al., 2011). In the case of TAC, or other ligands used for CSV, it is not yet known if any of the ternary complexes formed might also be electroactive.

Special Case I: When reactions B4a and B4b are in pseudo-equilibrium (steady state approximation) then the following equilibrium applies:

$$K_4 = \frac{k_4}{k_{-4}} = \frac{[\mathrm{FeL\,(TAC)}]}{[\mathrm{FeL}]\,[\mathrm{TAC}]} \tag{B16}$$

B7 then reduces to the following:

$$-\frac{\partial\,[\mathrm{FeL}]}{\partial t} = k_{-1}\,[\mathrm{FeL}] \tag{B17}$$

In this case the reaction is only disjunctive in character. That is the adjunctive mechanism, while occurring, is not rate determining.

RESULTS

Table A1 | Fe_{sol}-KIN: ^{55}Fe kinetic experiment – iron solubility ANTXXVI-4.

Date	Stn	Latitude	Longitude	Depth (m)	[L_s] nM	[L_w] nM	Log k_d (L_w)
17.04.2010	272	31°12.01′S	39°20.53′W	20	1.71 + 1.31	11.2 + 4.79	−4.43 + 0.39
				40	1.83 + 0.24	8.64 + 1.23	−4.19 + 0.08
				60	3.06 + 0.53	4.84 + 1.35	−4.50 + 0.31
				80	3.92 + 0.34	6.98 + 2.35	−4.23 + 0.19
				100	2.46 + 0.41	7.32 + 0.56	−4.63 + 0.15
				200	1.28 + 0.29	5.26 + 0.04	−4.71 + 0.02
				300	2.23 + 0.67	6.12 + 0.58	−4.83 + 0.16
				400	2.08 + 0.84	6.08 + 1.62	−4.71 + 0.35
24.04.2010	279	10°42.47′ S	26°55.75′W	25	5.79 + 0.16	4.79 + 0.36	−4.53 + 0.09
				50	3.86 + 0.12	6.19 + 0.96	−4.88 + 0.03
				75	5.17 + 0.14	5.47 + 1.09	−4.90 + 0.35
				100	4.89 + 0.37	6.67 + 0.53	−4.62 + 0.12
				130	4.84 + 0.29	4.53 + 0.26	−4.77 + 0.10
				200	4.49 + 0.14	3.88 + 0.71	−4.26 + 0.11
				300	6.34 + 0.30	0.76 + 0.27	−5.28 + 0.27
				400	5.06 + 0.91	5.70 + 1.13	−4.66 + 0.32
28.04.2010	283	01°46.47′N	23° 00.07′W	20	2.52 + 0.25	5.96 + 0.25	−5.09 + 0.15
				40	3.51 + 0.08	6.11 + 0.16	−5.13 + 0.15
				60	4.54 + 0.20	6.26 + 0.77	−4.43 + 0.02
				80	5.47 + 0.21	6.78 + 0.42	−4.65 + 0.02
				100	6.36 + 0.01	4.86 + 0.30	−4.67 + 0.15
				200	5.41 + 0.06	7.69 + 0.25	−4.34 + 0.08
				300	5.42 + 0.89	4.80 + 0.25	−4.96 + 0.04
				400	5.47 ± 1.32	8.35 + 1.40	−4.59 + 0.12
04.05.2010	287	17°34.97′N	24°15.18′W	20	2.61 + 0.43	9.23 + 1.19	−4.49 + 0.14
				40	3.83 + 0.32	7.63 + 0.30	−4.39 + 0.13
				60	3.74 + 0.17	6.27 + 0.93	−4.39 + 0.08
				80	4.53 + 0.17	10.46 + 0.30	−4.25 + 0.08
				100	2.94 + 1.19	12.25 + 0.47	−5.07 + 0.03
				200	4.13 + 0.54	8.89 + 1.21	−4.63 + 0.14
				300	5.14 + 0.70	11.65 + 0.69	−4.37 + 0.05
				400	5.80 + 0.21	8.15 + 0.55	−4.38 + 0.01
09.05.2010	294	33°36.03′N	13°51.37′W	20	3.90 + 0.12	6.36 + 0.26	−4.53 + 0.05
				40	3.97 + 0.23	6.27 + 1.85	−4.24 + 0.15
				60	3.27 + 0.39	7.73 + 1.53	−4.41 + 0.17
				80	3.36 + 0.15	7.14 + 0.94	−4.26 + 0.08
				100	3.39 + 0.13	6.70 + 0.39	−4.46 + 0.06
				200	1.91 + 0.41	7.92 + 0.57	−4.64 + 0.11
				300	4.28 + 0.38	6.53 + 3.82	−4.11 ± 0.27a
				400	4.19 + 0.26	6.72 + 2.63	−4.10 + 0.17[a]

The values of L_s, L_w, and k_d (s^{-1}) were obtained by fitting the raw iron solubility data to Eq. 6 in the main article. Notes: [a]The kinetic plots indicated a possible two step process with an initial rapid iron loss from the soluble phase followed by a slower exchange after 6 h. The data presented is calculated using the single kinetic fit described in the text.

REFERENCE

Ito, H., Fujii, M., Masago, Y., Yoshimura, C., Waite, T. D., and Omura, T. (2011). Mechanism and kinetics of ligand exchange between ferric citrate and desferrioxamine B. *J. Phys. Chem. A* 115, 5371–5379.

frontiers in
MICROBIOLOGY

ORIGINAL RESEARCH ARTICLE
published: 21 February 2012
doi: 10.3389/fmicb.2012.00056

Reconstruction of extracellular respiratory pathways for iron(III) reduction in *Shewanella oneidensis* strain MR-1

Dan Coursolle and Jeffrey A. Gralnick*

Department of Microbiology, BioTechnology Institute, University of Minnesota Twin Cities, St. Paul, MN, USA

Edited by:
David Emerson, Bigelow Laboratory for Ocean Sciences, USA

Reviewed by:
Chad Saltikov, University of California Santa Cruz, USA
Tom Clarke, University of East Anglia, UK

****Correspondence:***
Jeffrey A. Gralnick, Department of Microbiology, BioTechnology Institute, University of Minnesota Twin Cities, 140 Gortner Lab, 1479 Gortner Avenue, St. Paul, MN 55108, USA.
e-mail: gralnick@umn.edu

Shewanella oneidensis strain MR-1 is a facultative anaerobic bacterium capable of respiring a multitude of electron acceptors, many of which require the Mtr respiratory pathway. The core Mtr respiratory pathway includes a periplasmic *c*-type cytochrome (MtrA), an integral outer-membrane β-barrel protein (MtrB), and an outer-membrane-anchored *c*-type cytochrome (MtrC). Together, these components facilitate transfer of electrons from the *c*-type cytochrome CymA in the cytoplasmic membrane to electron acceptors at and beyond the outer-membrane. The genes encoding these core proteins have paralogs in the *S. oneidensis* genome (*mtrB* and *mtrA* each have four while *mtrC* has three) and some of the paralogs of *mtrC* and *mtrA* are able to form functional Mtr complexes. We demonstrate that of the additional three *mtrB* paralogs found in the *S. oneidensis* genome, only MtrE can replace MtrB to form a functional respiratory pathway to soluble iron(III) citrate. We also evaluate which *mtrC*/*mtrA* paralog pairs (a total of 12 combinations) are able to form functional complexes with endogenous levels of *mtrB* paralog expression. Finally, we reconstruct all possible functional Mtr complexes and test them in a *S. oneidensis* mutant strain where all paralogs have been eliminated from the genome. We find that each combination tested with the exception of MtrA/MtrE/OmcA is able to reduce iron(III) citrate at a level significantly above background. The results presented here have implications toward the evolution of anaerobic extracellular respiration in *Shewanella* and for future studies looking to increase the rates of substrate reduction for water treatment, bioremediation, or electricity production.

Keywords: iron respiration, anaerobic, Mtr-pathway, extracellular respiration

INTRODUCTION

Shewanella oneidensis strain MR-1 (MR-1) is a facultative anaerobic bacterium capable of respiring a diverse array of compounds. MR-1 respiration can be harnessed for bioremediation of radioactive heavy metals (Wall and Krumholz, 2006), removal of insoluble metal oxides from wastewater (Fredrickson et al., 2008), and generation of electricity in microbial fuel cells (Lloyd et al., 2003; Lovley, 2008). In respiring insoluble metals and electrodes, MR-1 has evolved a mechanism to transfer electrons from the cytoplasmic space to electron acceptors unable to cross the outer-membrane (OM) termed extracellular respiration (Gralnick and Newman, 2007). The respiratory diversity of MR-1 coupled with well-established genetic tools have made this microbe a model organism for understanding mechanisms of anaerobic respiration; most notably extracellular respiration (Marsili et al., 2008; Von Canstein et al., 2008; Coursolle et al., 2010).

The Mtr respiratory pathway of MR-1 contains interchangeable proteins that can form distinct functional modules for the reduction of iron(III) citrate, iron oxide, flavins, and dimethyl sulfoxide (DMSO; Bucking et al., 2010; Coursolle and Gralnick, 2010). A general scheme for how the components of the Mtr respiratory pathway facilitate electron flow in MR-1 is shown in **Figure 1**. Electron transfer from the cytoplasmic membrane (CM) begins with CymA, a CM-anchored tetraheme *c*-type cytochrome capable of receiving electrons from the menaquinone pool (Myers and Myers, 1997). Also contained in each module is a periplasmic electron carrier (PEC), which is a decaheme *c*-type cytochrome. There are three known functional PECs encoded in the MR-1 genome by *mtrA*, *mtrD*, and *dmsE* (Coursolle and Gralnick, 2010). DmsE is primarily used in modules to reduce the terminal electron acceptor DMSO (Gralnick et al., 2006), but has minor activity in modules that reduce iron(III) citrate (Coursolle and Gralnick, 2010). MtrA is the primary periplasmic component used by MR-1 when reducing iron(III) and flavins, but overexpression of MtrD can restore ferric citrate reduction rates to an *mtrA* mutant (Coursolle and Gralnick, 2010). A fourth PEC is encoded in the MR-1 genome (SO4360) but it has no demonstrated function to date. Recently, small-angle X-ray scattering coupled with analytical ultracentrifugation has resolved that MtrA is shaped like a "wire," likely making its purpose to shuttle electrons between CymA and OM proteins (Firer-Sherwood et al., 2011). All functional iron(III)-reducing modules also contain an outer-membrane cytochrome (OMC), a decaheme *c*-type cytochrome which can be MtrC, MtrF, or OmcA (Bucking et al., 2010; Coursolle and Gralnick, 2010). Due to the severely impaired rate of soluble iron reduction in mutants lacking all three OMCs, it has been concluded that all metal reduction occurs outside the cell, even when metal substrates are small enough to penetrate OM porins (Bucking et al., 2010; Coursolle

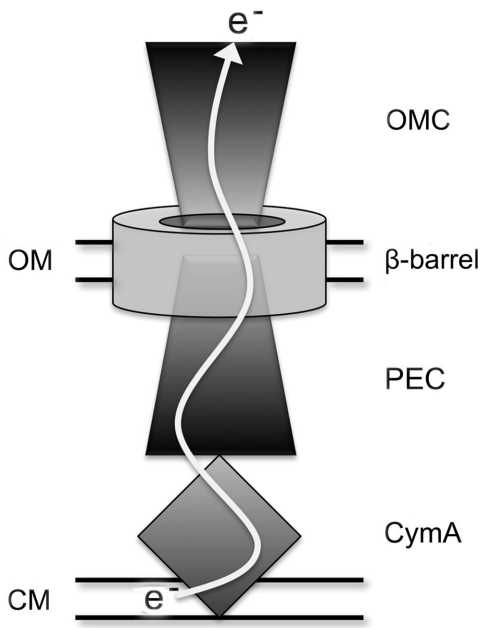

FIGURE 1 | Schematic of extracellular electron transfer pathway in *S. oneidensis*. OMC represents outer-membrane cytochrome paralogs of MtrC, β-barrel represents MtrB paralogs, and PEC represents periplasmic electron carrier paralogs of MtrA. OM and CM represent OM and CM, respectively.

and Gralnick, 2010). A structure of the OMC protein MtrF was recently reported, identifying potential electron transfer pathways directly to insoluble substrates and to soluble flavin electron shuttles (Clarke et al., 2011). The remaining component of a functional Mtr module is an integral membrane β-barrel protein that forms a pore-like structure through the OM that may facilitate direct interaction between PECs and OMCs (Beliaev and Saffarini, 1998; Hartshorne et al., 2009). MtrB is the only protein known to exhibit this function in the Mtr respiratory pathway, though three paralogs (encoding MtrE, DmsF, and SO4359) occur in the genome of *S. oneidensis*.

The biochemical capacities of several Mtr respiratory pathway proteins have been interrogated *in vitro*. Both MtrC and OmcA have been purified and demonstrated to exchange electrons with each other and various forms of iron(III), flavins, and electrodes (Xiong et al., 2006; Shi et al., 2007; Wigginton et al., 2007; Wang et al., 2008; Ross et al., 2009). MtrA has been heterologously expressed in *Escherichia coli* and can be oxidized in the presence of soluble iron(III; Pitts et al., 2003). Likewise, CymA was shown to have soluble iron(III) reduction activity when expressed in *E. coli* (Gescher et al., 2008). Components of the Mtr-pathway have been purified and examined using protein film voltammetry to determine redox windows where electron transfer reactions are favorable as single proteins (Firer-Sherwood et al., 2008) and as complexes (Hartshorne et al., 2009). Three primary constraints complicate comparisons between *in vitro* biochemical analysis and *in vivo* function of Mtr respiratory proteins: first, orientation of the protein cannot effectively be controlled. Orientation is a critical factor in how Mtr respiratory proteins function given that oxidation and reduction is likely to occur in different active sites of an electron transfer proteins. Second, chemical reductants or electrodes rather than a native pathway must provide electrons for purified proteins. Finally, substrate accessibility *in vitro* is unhindered in the absence of cellular structure, therefore allowing reactions to occur that may not reflect activity in a living system. *In vivo* analysis remedies each of these described caveats.

In this study we constructed a *S. oneidensis* strain unable to reduce Fe(III) citrate by first deleting all genes identified in the Mtr-pathway. Then, using a multi-gene complementation strategy we add back various combinations of Mtr paralogs. In doing this, we identify which of the 48 possible *mtrC/mtrA/mtrB* paralog modules (from 4 PEC, 4 β-barrel, and 3 OMC paralogs) can form functional iron(III)-reducing modules *in vivo*. Due to high identity amongst most of these paralogs (**Table 1**), in conjunction with previous studies demonstrating shared functionality between paralogs (Bucking et al., 2010; Coursolle and Gralnick, 2010), we expect many recombinant modules to transfer iron(III) reducing capability to our mutant missing all Mtr genes. We find that in reconstructed modules the PECs SO4360 and DmsE do not exhibit significant activity. We also find that the predicted OM β-barrels DmsF and SO4359 cannot complement an *mtrB* mutant. Lastly, we discover that when functional modules are created, MtrDEF can reduce Fe(III) citrate at approximately half the rate as MtrABC, demonstrating for the first time the functionality of a complete iron-reducing module lacking MtrA, B, and C.

MATERIALS AND METHODS

BACTERIAL STRAINS AND MEDIA USED

MR-1 was originally isolated from Lake Oneida in New York (Myers and Nealson, 1988; Venkateswaran et al., 1999). Strains and plasmids used in this study are found in **Table 2**. Overnight cultures were made from single colonies isolated from a frozen stock inoculated into 2 mL of Luria–Bertani (LB) medium and grown aerobically for 16 h. When necessary, *Shewanella* basal medium (SBM) was used as minimal medium (Baron et al., 2009). Iron(III) citrate was used as indicated as electron acceptor. Kanamycin was used at a concentration of 50 μg/mL and ampicillin was used at a concentration of 100 μg/mL when necessary. Diaminopimelic acid (DAP) was used at a concentration of 360 μM for all growth of *E. coli* strain WM3064. Overnight cultures of *E. coli* were made from single colonies inoculated into 2 mL of LB and grown aerobically for 16 h.

MUTANT CONSTRUCTION

Deletions in the MR-1 genome were made as previously described (Hau et al., 2008; Coursolle et al., 2010). All gene deletions were deigned to be in-frame to minimize polar effects on downstream genes. Briefly, up and downstream fragments flanking the gene targeted for deletion were ligated into the suicide vector pSMV3 and transferred into WM3064. After allowing the plasmid-containing WM3064 strain to conjugate with the parent MR-1 strain, single recombinants were obtained by plating this mixture to LB + kanamycin plates. Double recombinants were obtained by plating single recombinants onto LB + 5% sucrose plates and mutants screened by colony PCR from these plates. All mutants

Table 1 | Amino acid identity between Mtr paralogs.

Gene	PEC (%)				β-Barrel (%)				OMC (%)		
	mtrA	***mtrD***	***dmsE***	***SO4360***	***mtrB***	***mtrE***	***dmsF***	***SO4359***	***mtrC***	***mtrF***	***omcA***
mtrA	100	68	64	53	–	–	–	–	–	–	–
mtrD	68	100	59	48	–	–	–	–	–	–	–
dmsE	64	59	100	51	–	–	–	–	–	–	–
SO4360	53	48	51	100	–	–	–	–	–	–	–
mtrB	–	–	–	–	100	35	35	25	–	–	–
mtrE	–	–	–	–	35	100	30	25	–	–	–
dmsF	–	–	–	–	35	30	100	29	–	–	–
SO4359	–	–	–	–	25	25	29	100	–	–	–
mtrC	–	–	–	–	–	–	–	–	100	34	21
mtrF	–	–	–	–	–	–	–	–	34	100	25
omcA	–	–	–	–	–	–	–	–	21	25	100

were then verified to be kanamycin sensitive and all permanent stocks retested by PCR using primers flanking the targeted gene. Primers used for deletions and complementation can be visualized in **Table A1** in Appendix.

COMPLEMENTATION

Single and multiple genes were complemented into various MR-1 strains using the pBBR/pUC-BioBrick system, pBBR-BB (Vick et al., 2011). Due to prior expression issues (Coursolle and Gralnick, 2010), 38 base pairs of upstream *mtrA* sequence, 53 base pairs of upstream *mtrC* sequence, and 43 base pairs of upstream *mtrB* sequence were included before *mtrA*, *mtrC*, and *mtrB* paralogs, respectively to normalize expression. Each gene is driven by an individual *lac* promoter (Vick et al., 2011). Briefly, each gene was cloned into the pUC-BB vector, digested out, and ligated into pBBR-BB sequentially. Genes cloned in top BBR-BB were verified using PCR, restriction analysis (using *Xba*I and *Spe*I), and sequencing. Primers used for complementation can be seen in **Table A1** in Appendix. When appropriate, heme stains were performed to visualize the presence of *c*-type cytochromes (see below).

IRON(III) CITRATE REDUCTION

Iron(III) citrate was used to test the Mtr-pathway constructs due to the speed and dynamic range of the assay compared to Iron(III) oxide (Coursolle and Gralnick, 2010). MR-1 strains were grown in LB overnight and normalized to an optical density at 600 nm of 0.35 in SBM. Thirty microliters of these cultures was then used to inoculate 270 μL of SBM containing 20 mM lactate and 10 mM iron(III) citrate in a 96-well plate. Iron(II) formation was monitored over time as previously described (Coursolle and Gralnick, 2010) using ferrozine (Stookey, 1970). Between time points 96-well plates were placed in an adapted anaerobic Petri dish holder and flushed with nitrogen for 15 min. Reduction rates were calculated over the linear portion of each curve and normalized to the amount of protein in each well. Protein concentrations were calculated using a BCA protein assay kit (Pierce) according to the manufacturers protocol.

HEME STAINING

Cultures were grown overnight in SBM containing 20 mM lactate and 10 mM iron(III) citrate and sonicated to lyse cells. Supernatants were separated and tested for protein concentration. Ten micrograms protein was loaded into each well of a 4–12% *Bis–Tris* SDS PAGE protein gel (Invitrogen) and run at 110 V for 120 min. The gels were then stained in a 3:7 6.3 mM *tert*-methylbenzadine (TMBZ) in methanol: 0.25 M sodium acetate for 2 h. The gels were visualized upon the addition of 30 mM hydrogen peroxide for 15 min.

RESULTS

FUNCTIONALITY OF MtrB PARALOGS

To determine what *mtrB* paralogs are able to functionally replace MtrB, we placed *mtrB*, *mtrE*, *dmsF*, and *SO4359* under control of a constitutive promoter on the expression vector pBBR1MCS-2 (Kovach et al., 1995) and tested their ability to complement an *mtrB* deletion strain for iron(III) citrate reduction activity. Iron(III) citrate was used as a proxy for all Mtr activity due to its fast reduction rate and electron shuttle independent reduction mechanism (Von Canstein et al., 2008; Coursolle et al., 2010). Both MtrB and MtrE restored activity to levels slightly above wild type with empty vector (**Figure 2**), implying that MtrE can functionally replace MtrB. Neither expression of DmsF or SO4359 in Δ*mtrB* raised iron(III) citrate reduction levels significantly above an empty vector control (**Figure 2**), indicating that these paralogs are not functional in metal reduction modules. Knowing that only two *mtrB* paralogs have functionality during iron(III) citrate reduction limits the number of total possible functional modules to 24 allowing for less downstream plasmid construction.

MtrA/MtrC PAIRED INTERACTIONS

Previous studies have demonstrated that MtrD and DmsE can functionally replace MtrA (Coursolle and Gralnick, 2010), while MtrF and to a smaller extent OmcA can functionally replace MtrC (Bucking et al., 2010; Coursolle and Gralnick, 2010). MtrC and MtrA interact through the pore in the OM created by the β-barrel MtrB protein (Hartshorne et al., 2009), yet remains unknown which OMC/PEC paralog interactions are functional *in vivo*. To

Table 2 | Strains used in this work.

	Relevant genotype; name used in text	Source
STRAIN		
JG274	MR-1, wild type	Myers and Nealson (1988)
JG168	JG274 with empty pBBR1MCS-2, Km^r	Hau et al. (2008)
JG700	Δ*mtrB*	This work
JG1176	Δ*mtrC*/Δ*omcA*/Δ*mtrF*/Δ*mtrA*/Δ*mtrD*/Δ*dmsE*/Δ*SO4360*/Δ*cctA*	This work
JG1194 (ΔMtr)	Δ*mtrC*/Δ*omcA*/Δ*mtrF*/Δ*mtrA*/Δ*mtrD*/Δ*dmsE*/Δ*SO4360*/Δ*cctA*/Δ*recA*	This work
JG1419	Δ*mtrB*/Δ*mtrC*/Δ*omcA*/Δ*mtrF*/Δ*mtrA*/Δ*mtrD*/Δ*dmsE*/Δ*SO4360*/Δ*cctA*/	This work
JG1452	Δ*mtrE*/Δ*mtrC*/Δ*omcA*/Δ*mtrF*/Δ*mtrA*/Δ*mtrD*/Δ*dmsE*/Δ*SO4360*/Δ*cctA*/Δ*recA*	This work
JG1453	Δ*mtrB*/Δ*mtrE*/Δ*mtrC*/Δ*omcA*/Δ*mtrF*/Δ*mtrA*/Δ*mtrD*/Δ*dmsE*/Δ*SO4360*/Δ*cctA*/	This work
JG1485 (ΔMtr/Δ*mtrE)*	Δ*mtrE*/Δ*mtrC*/Δ*omcA*/Δ*mtrF*/Δ*mtrA*/Δ*mtrD*/Δ*dmsE*/Δ*SO4360*/Δ*cctA*/Δ*recA*	This work
JG1486 (ΔMtr/Δ*mtrB*/Δ*mtrE)*	Δ*mtrB*/Δ*mtrE*/Δ*mtrC*/Δ*omcA*/Δ*mtrF*/Δ*mtrA*/Δ*mtrD*/Δ*dmsE*/Δ*SO4360*/Δ*cctA*/Δ*recA*	This work
JG1519 (ΔMtr/Δ*mtrB*)	Δ*mtrB*/Δ*mtrC*/Δ*omcA*/Δ*mtrF*/Δ*mtrA*/Δ*mtrD*/Δ*dmsE*/Δ*SO4360*/Δ*cctA*/Δ*recA*	This work
JG1219	JG700 with p*mtrE*, Km^r	This work
JG1220	JG700 with p*mtrB*, Km^r	This work
JG1221	JG700 with p*dmsF*, Km^r	This work
JG1222	JG700 with p*SO4359*, Km^r	This work
JG1223	JG700 with pBBR1MCS-2, Km^r	This work
JG1280	JG1194 with p*omcA*/*SO4360*, Km^r	This work
JG1281	JG1194 with p*mrF*/*mtrD*, Km^r	This work
JG1282	JG1194 with p*omcA*/*mtrD*, Km^r	This work
JG1283	JG1194 with p*mtrC*/*mtrD*, Km^r	This work
JG1288	JG1194 with p*mtrC*/*dmsE*, Km^r	This work
JG1289	JG1194 with p*mtrF*/*dmsE*, Km^r	This work
JG1290	JG1194 with p*mtrF*/*SO4360*, Km^r	This work
JG1291	JG1194 with p*mtrF*/*mtrA*, Km^r	This work
JG1292	JG1194 with p*omcA*/*dmsE*, Km^r	This work
JG1293	JG1194 with p*mtrC*/*SO4360*, Km^r	This work
JG1294	JG1194 with p*omcA*/*mtrA*, Km^r	This work
JG1295	JG1194 with p*mtrC*/*mtrA*, Km^r	This work
JG1489	JG1485 with p*mtrC*/*mtrD*, Km^r	This work
JG1490	JG1485 with p*mtrF*/*mtrD*, Km^r	This work
JG1491	JG1485 with p*omcA*/*mtrA*, Km^r	This work
JG1492	JG1485 with p*mtrC*/*mtrA*, Km^r	This work
JG1493	JG1485 with p*mtrF*/*mtrA*, Km^r	This work
JG1504	JG1486 with p*mtrC*/*mtrD*, Km^r	This work
JG1505	JG1486 with p*mtrF*/*mtrD*, Km^r	This work
JG1506	JG1486 with p*omcA*/*mtrA*, Km^r	This work
JG1507	JG1486 with p*mtrC*/*mtrA*, Km^r	This work
JG1508	JG1486 with p*mtrF*/*mtrA*, Km^r	This work
JG1525	JG1519 with p*mtrB*/*mtrF*/*mtrD*, Km^r	This work
JG1526	JG1519 with p*mtrB*/*mtrC*/*mtrD*, Km^r	This work
JG1527	JG1519 with p*mtrB*/*mtrC*/*mtrA*, Km^r	This work
JG1528	JG1519 with p*mtrB*/*omcA*/*mtrA*, Km^r	This work
JG1529	JG1519 with p*mtrB*/*mtrF*/*mtrA*, Km^r	This work
JG1530	JG1519 with p*mtrE*/*mtrF*/*mtrD*, Km^r	This work
JG1531	JG1519 with p*mtrE*/*mtrC*/*mtrA*, Km^r	This work
JG1532	JG1519 with p*mtrE*/*mtrF*/*mtrA*, Km^r	This work
JG1533	JG1519 with p*mtrE*/*omcA*/*mtrA*, Km^r	This work
JG1534	JG1519 with p*mtrE*/*mtrC*/*mtrD*, Km^r	This work
JG1535	JG1485 with pBBR-BB, Km^r	This work
JG1536	JG1486 with pBBR-BB, Km^r	This work
JG1537	JG1519 with pBBR-BB, Km^r	This work

(Continued)

Table 2 | Continued

	Relevant genotype; name used in text	Source
PLASMIDS		
pSMV3	Deletion vector, Km^r, *sacB*	Saltikov and Newman (2003)
pBBR1MCS-2	Broad range cloning vector, Km^r	Kovach et al. (1995)
pBBR-BB	Broad range BioBrick vector, Km^r	Vick et al. (2011)
p*mtrB*	*mtrB* and 43 bp upstream in pBBR1MCS-2, Km^r	This work
p*mtrE*	*mtrE* and 43 bp *mtrB* upstream sequence in pBBR1MCS-2, Km^r	This work
p*dmsF*	*dmsF* and 43 bp *mtrB* upstream sequence in pBBR1MCS-2, Km^r	This work
p*SO4359*	*SO4359* and 43 bp *mtrB* upstream sequence in pBBR1MCS-2, Km^r	This work
p*mtrC/mtrA*	*mtrA* and 38 bp upstream, *mtrC* and 53 bp upstream in pBBR-BB, Km^r	This work
p*mtrF/mtrA*	*mtrA* and 38 bp upstream, *mtrF* and 35 bp *mtrC* upstream sequence in pBBR-BB, Km^r	This work
p*omcA/mtrA*	*mtrA* and 38 bp upstream, *omcA* and 53 bp *mtrC* upstream sequence in pBBR-BB, Km^r	This work
p*mtrC/mtrD*	*mtrD* and 38 bp *mtrA* upstream sequence, *mtrC* and 53 bp upstream in pBBR-BB, Km^r	This work
p*mtrF/mtrD*	*mtrD* and 38 bp *mtrA* upstream sequence, *mtrF* and 53 bp *mtrC* upstream sequence in pBBR-BB, Km^r	This work
p*omcA/mtrD*	*mtrD* and 38 bp *mtrA* upstream sequence, *omcA* and 53 bp *mtrC* upstream sequence in pBBR-BB, Km^r	This work
p*mtrC/dmsE*	*dmsE* and 38 bp *mtrA* upstream sequence, *mtrC* and 53 bp upstream in pBBR-BB, Km^r	This work
p*mtrF/dmsE*	*dmsE* and 38 bp *mtrA* upstream sequence *mtrF* and 53 bp *mtrC* upstream sequence in pBBR-BB, Km^r	This work
p*omcA/dmsE*	*dmsE* and 38 bp *mtrA* upstream sequence, *omcA* and 53 bp *mtrC* upstream sequence in pBBR-BB, Km^r	This work
p*mtrC/SO4360*	*SO4360* and 38 bp *mtrA* upstream sequence, *mtrC* and 53 bp upstream in pBBR-BB, Km^r	This work
p*mtrF/SO4360*	*SO4360* and 38 bp *mtrA* upstream sequence, *mtrF* and 53 bp *mtrC* upstream sequence in pBBR-BB, Km^r	This work
p*omcA/SO4360*	*SO4360* and 38 bp *mtrA* upstream sequence, *omcA* and 53 bp *mtrC* upstream sequence in pBBR-BB, Km^r	This work
p*omcA/mtrB/mtrA*	*mtrA* and 38 bp upstream, *omcA* and 53 bp *mtrC* upstream sequence, *mtrB* and 43 bp upstream in pBBR-BB, Km^r	This work
p*mtrF/mtrB/mtrA*	*mtrA* and 38 bp upstream, *mtrF* and 53 bp *mtrC* upstream sequence, *mtrB* and 43 bp upstream in pBBR-BB, Km^r	This work
p*mtrC/mtrB/mtrA*	*mtrA* and 38 bp upstream, *mtrC* and 53 bp upstream, *mtrB* and 43 bp upstream in pBBR-BB, Km^r	This work
p*mtrC/mtrB/mtrD*	*mtrD* and 38 bp *mtrA* upstream sequence, *mtrC* and 53 bp upstream, *mtrB* and 43 bp upstream in pBBR-BB, Km^r	This work
p*mtrF/mtrB/mtrD*	*mtrD* and 38 bp *mtrA* upstream sequence, *mtrF* and 53 bp *mtrC* upstream sequence, *mtrB* and 43 bp upstream in pBBR-BB, Km^r	This work
p*omcA/mtrE/mtrA*	*mtrA* and 38 bp upstream, *omcA* and 53 bp *mtrC* upstream sequence, *mtrE* and 43 bp *mtrB* upstream sequence in pBBR-BB, Km^r	This work
p*mtrF/mtrE/mtrA*	*mtrA* and 38 bp upstream, *mtrF* and 53 bp *mtrC* upstream sequence, *mtrE* and 43 bp *mtrB* upstream sequence in pBBR-BB, Km^r	This work
p*mtrC/mtrE/mtrA*	*mtrA* and 38 bp upstream, *mtrC* and 53 bp upstream, *mtrE* and 43 bp *mtrB* upstream sequence in pBBR-BB, Km^r	This work
p*mtrC/mtrE/mtrD*	*mtrD* and 38 bp *mtrA* upstream sequence, *mtrC* and 53 bp upstream, *mtrE* and 43 bp *mtrB* upstream sequence in pBBR-BB, Km^r	This work
p*mtrF/mtrE/mtrD*	*mtrD* and 38 bp *mtrA* upstream sequence, *mtrF* and 53 bp*mtrC* upstream sequence, *mtrE* and 43 bp *mtrB* upstream sequence in pBBR-BB, Km^r	This work

test which pairs can functionally interact, we constructed a strain of *S. oneidensis* missing all identified OMCs and PECs (*mtrA*, *mtrD*, *dmsE*, *SO4360*, *mtrC*, *mtrF*, *omcA*, and *cctA*). After all genes were individually removed, the *recA* gene was deleted from the strain to nullify recombination between *lac* promoters driving expression of OMCs and PECs tested (see below). The resultant strain was named ΔMtr (**Table 2**). Functional characterization of PEC and OMC pairs (12 total combinations) were cloned into

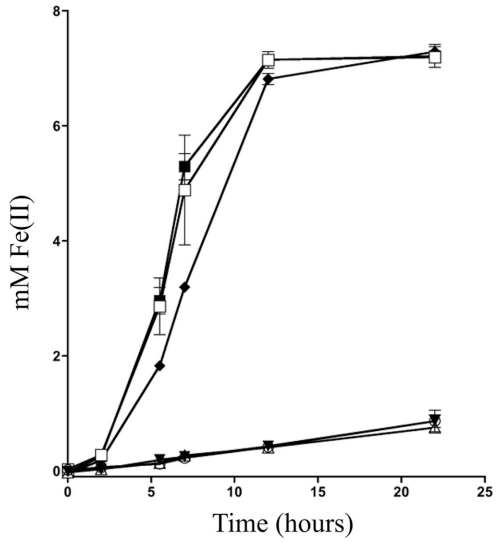

FIGURE 2 | Iron(III) citrate reduction using various *mtrB* paralogs. The reduction of ferric citrate over time was measured for Δ*mtrB* complemented with (□) *mtrB*, (△) *dmsF*, (▼) *SO4359*, (■) *mtrE*, and (◯) empty vector were compared to (♦) MR-1 with empty vector.

the pBBR-BB. Each of the complemented strains was verified via heme staining (Thomas et al., 1976) to express PEC and OMC paralogs. **Figure 3A** demonstrates that each of the 12 strains expressed both a PEC and an OMC with covalently attached heme groups. Interestingly, MtrA and SO4360 appear to be expressed at higher levels than MtrD and DmsE, even though the same promoter and ribosome-binding site drive expression of all four PECs. In the same manner, MtrF appears to be present at lower levels in complemented strains though the genes for all three OMCs share the same promoter, RBS, and 35 base pair upstream sequence. The 12 complemented strains were then evaluated for their ability to reduce iron(III) citrate. Overall, ΔMtr strains expressing MtrC/MtrA, MtrC/MtrD, MtrF/MtrA, MtrF/MtrD, and OmcA/MtrA were able to reduce iron(III) citrate at a rate significantly above an empty vector control (**Figures 3B,C**), while other PEC/OMC pairs did not. ΔMtr strains expressing MtrC/MtrA and MtrF/MtrA reduced iron(III) citrate at rates comparable to MR-1, while the other three functional combinations (MtrC/MtrD, MtrF/MtrD, and OmcA/MtrA) resulted a rate significantly lower than wild type. Though we demonstrated activity of OMC/PEC pairs, we could not yet determine which MtrB homolog was facilitating interactions between the *c*-type cytochromes.

MtrB PARALOGS

Identification of all functional PEC/OMC iron(III) citrate respiratory complexes allowed for evaluation of which *mtrB* paralog(s) can facilitate PEC/OMC interactions. Since only MtrB and MtrE could complement Δ*mtrB* (**Figure 2**), only these two β-barrel proteins were analyzed. To test the involvement of MtrB and MtrE in facilitating electron exchange between PECs and OMCs *mtrB* and *mtrE* were deleted from the *recA*$^+$ ΔMtr parent strain to make ΔMtr/*mtrB* and ΔMtr/*mtrE*, respectively. Once constructed, *recA* was deleted to ensure plasmid stability for testing complementation constructs. When the five functional OMC/PEC paralog combinations were introduced into ΔMtr/*mtrE*, which still expresses *mtrB*, there was no significant difference between when the same combinations were complemented into ΔMtr (**Figure 4**). When the same *mtrA*/*mtrC* paralog combinations were complemented into ΔMtr/*mtrB*, all strains reduced iron(III) citrate at rates comparable to the empty vector control (data not shown). We can therefore conclude that MtrE is not contributing to iron(III) citrate reduction under these conditions and that MtrB is required for the activities observed in **Figure 4**. However, since the relative expression levels of *mtrB* and *mtrE* in these backgrounds are not known, the ability of MtrE to function with OMC/PEC paralog pairs could not be ruled out. To normalize expression levels of MtrE and MtrB, we generated pBBR-BB constructs encoding all three components: PEC, β-barrel, and OMC.

FUNCTIONAL Mtr MODULES

To determine which combinations of *mtrC/mtrA/mtrB* paralogs could form functional iron-reducing complexes, a series of paralog modules were reconstructed. Ten *mtrCAB* paralog modules were chosen because all OMC/PEC paralog combinations capable of forming functional complexes had been identified (**Figure 3C**), and only MtrB and MtrE appear to complement strains lacking *mtrB* (**Figure 2**). To analyze the functionality of complexes, both *mtrB* and *mtrE* were deleted from the ΔMtr parent strain (*recA*$^+$) and plasmids containing each of the 10 complexes to be tested were placed in the resulting strain (ΔMtr/*mtrB/mtrE*) after removal of *recA*. We found that each of these combinations resulted in strains able to reduce iron(III) citrate at variable rates (**Figure 5**). The lowest rates were observed for both constructs producing OmcA, indicating that this protein has very little activity against iron(III) citrate, agreeing with previous observations (Coursolle and Gralnick, 2010; Coursolle et al., 2010). As expected, MtrA/MtrB/MtrC had the highest activity followed by MtrA/MtrB/MtrF. The results are in agreement with recent data demonstrating that MtrF and MtrC share similar activity (Bucking et al., 2010; Coursolle and Gralnick, 2010) and likely a similar structure (Clarke et al., 2011). All complemented strains expressing MtrA had higher reduction rates when co-expressed with MtrB than MtrE. Likewise, complemented strains expressing MtrD reduced iron(III) citrate at the same rate or faster when co-expressed with MtrE. Overall, we observed that all tested MtrA/MtrB/MtrC paralog combinations were able to reduce iron(III) citrate with the exception of MtrA/MtrE/OmcA, suggesting that MtrE is unable to facilitate interaction between MtrA and OmcA.

DISCUSSION

We have reconstructed and identified components from the inventory of *mtrA*, *mtrB*, and *mtrC* paralogs found in the genome of *S. oneidensis* that function together to conduct electrons to soluble iron(III) citrate. Together, the three protein components, a PEC, β-barrel, and OMC form an electron conduit to the outside of the cell (**Figure 1**) where soluble and insoluble substrates are reduced by *S. oneidensis* (Coursolle and Gralnick, 2010). The apparent redundancy of these components is unusual, however the degree of variation in the utility of these components in

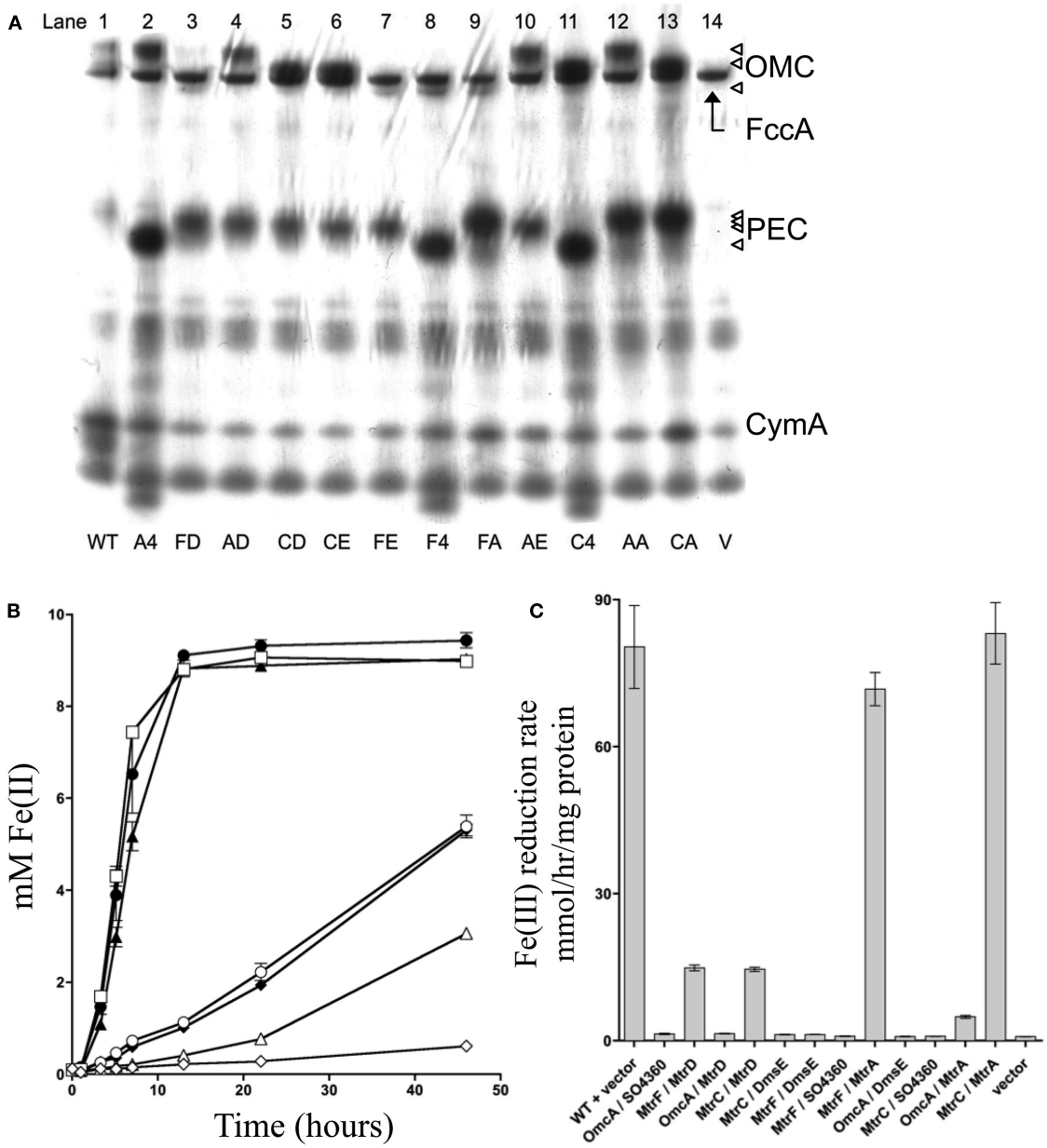

FIGURE 3 | ***mtrC/mtrA*** **paralog interactions. (A)** Heme stain for ΔMtr strains complemented various paralogs. FccA, CymA, and CctA are labeled based on analysis of deletion mutant strains lacking the respective gene (data not shown). Triangles on right represent OmcA, MtrC, and MtrF for outer-membrane cytochromes (OMC) and MtrA, MtrD, DmsE, and 4360 for periplasmic electron carriers (PEC). MR-1 wildtype control (lane 1), OmcA/SO4360 (lane 2), MtrF/MtrD (lane 3), OmcA/MtrD (lane 4), MtrC/MtrD (lane 5), MtrC/DmsE (lane 6), MtrF/DmsE (lane 7), MtrF/SO4360 (lane 8), MtrF/MtrA (lane 9), OmcA/DmsE (lane 10), MtrC/SO4360 (lane 11), OmcA/MtrA (lane 12), MtrC/MtrA (lane 13), and empty pBBR-BB (lane 14). **(B)** Ferric citrate reduction for ΔMtr strains complemented with vectors encoding *mtrF/mtrD* (♦), *mtrC/mtrD* (◯), *mtrF/mtrA* (▲), *omcA/mtrA* (△), *mtrC/mtrA* (□), and empty pBBR-BB (◇). MR-1 with empty pBBR-BB (●) is included for reference. All not shown PEC/OMC combinations did not reduce ferric citrate significantly faster than the ΔMtr+ empty vector control and for the sake of brevity are not depicted. **(C)** Rates of Fe(III) citrate reduction for ΔMtr strain complemented with the indicated proteins. Rates are reported in millimolar per hour per microgram protein.

reducing iron(III) citrate and occurrence in other sequenced *Shewanella* strains (Fredrickson et al., 2008) suggests these paralogs have divergent, but slightly overlapping function. The overlapping functionality may be an artifact of sharing common ancestry or a biochemical constraint on the system from either the source of electrons (the menaquinone pool and CymA) or the destination of the electrons (e.g., an external respiratory substrate) or both. With the exception of *mtrD* up-regulation during oxygen-dependent autoaggregation when exposed to high calcium concentrations (McLean et al., 2008), the conditions under which

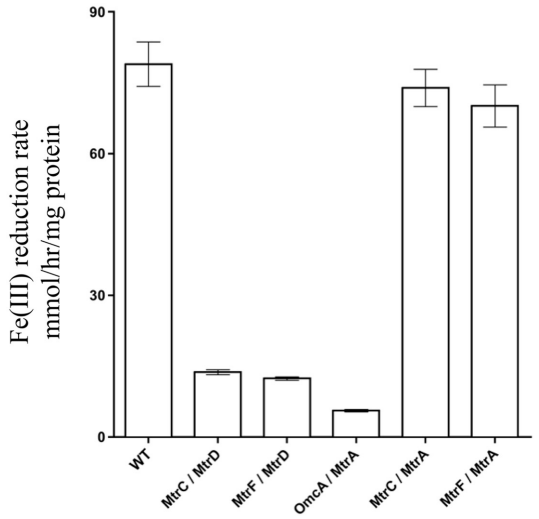

FIGURE 4 | Iron(III) citrate reduction by ΔMtr/Δ*mtrE* complemented strains. Iron(III) citrate reduction rate of ΔMtr/Δ*mtrE* complemented strains. Rates are reported in millimolar per hour per microgram protein.

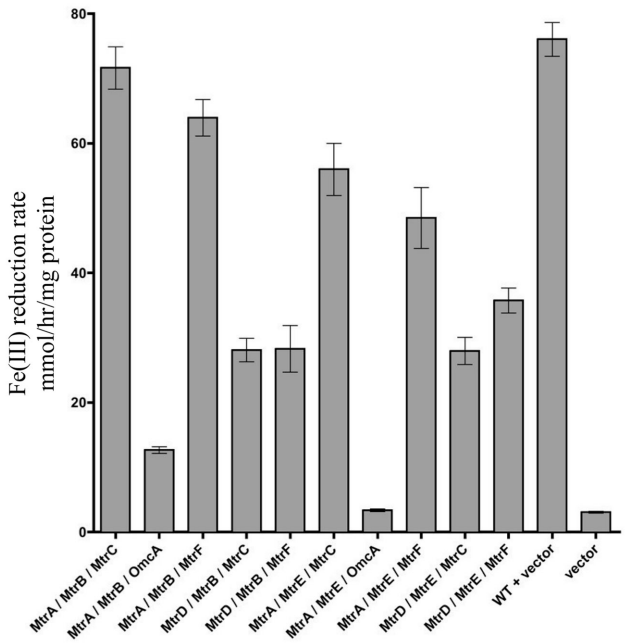

FIGURE 5 | Iron(III) citrate reduction by all possible functional Mtr modules. Iron(III) citrate reduction rate of ΔMtr/Δ*mtrB*/Δ*mtrE* complemented strains. Rates are reported in millimolar per hour per microgram protein.

the *mtrDEF* and *SO4359-62* gene clusters are expressed in MR-1 have not yet been identified, so the specific function of the proteins encoded by these genes remains unknown. The conservation of *mtrDEF* and *SO4359-62* in sequenced *Shewanella* that have copies of *mtrABC* and *dmsABEF* implies that these genes have distinct functions. Moreover, the fact that *SO4360* always clusters with *dmsAB* homologs and *mtrD* with *mtrBC* homologs implies that *SO4359-62* may share overlapping functionality with DMSO reductases and *mtrDEF* with metal reductases. *E. coli*'s DmsAB have shown *in vitro* reduction activity with N-oxides, sulfoxides, hydroxylamine, and chlorate, making these likely substrates for the SO4359-62 module (Bilous et al., 1988).

One unexplained phenomenon is the existence of several parologous pathways that use CymA as the link to CM quinone pools. In fact, all known substrates respired by MR-1, with the exception of oxygen, trimethylamine N-oxide (TMAO), thiosulfate, sulfite, and sulfur require the use of CymA and menaquinone as electron mediators (Myers and Myers, 1997; Schwalb et al., 2003; Shirodkar et al., 2011). In the genome of MR-1, TMAO, sulfite, and elemental sulfur reductases all exist in operons with putative quinone-oxidoreductases, explaining why CymA and in some cases menaquinones are not required for the reduction of these substrates (Kwan and Barrett, 1983; Wissenbach et al., 1992; Gon et al., 2002; Shirodkar et al., 2011). Many of the anaerobic CymA-utilizing pathways present in MR-1 have homologs in other organisms such as *E. coli*. For instance, DmsAB, FrdAB, NrfABC, and NapAB all exist in other organisms and utilize their own quinone-oxidoreductases: DmsC, FrdDC, NrfD, and NapC respectively (Berks et al., 1995; Potter et al., 2001). MR-1 has evolved to integrate the use of these terminal reductases with a single quinone-oxidoreductase, CymA. By using CymA as an electron bottleneck, MR-1 has introduced the ability to regulate multiple anaerobic respiratory pathways with the regulation of a single protein. There is evidence that many anaerobic respiratory pathways are turned on in the absence of oxygen, regardless of electron acceptor availability (Beliaev et al., 2002). The benefit *Shewanella* would experience by turning on several respiratory pathways at once is rapid elimination of electrons from the interior of the cell for redox carrier regeneration to allow energy-generating substrate-level phosphorylation to proceed regardless of which electron acceptor is available (Hunt et al., 2010). Many *Shewanella* species have been isolated at aerobic/anaerobic interfaces in aquatic systems (Nealson and Saffarini, 1994), where they must frequently switch between aerobic and anaerobic respiration. To regulate respiratory pathways individually may prove energetically inefficient, especially if different acceptors are present simultaneously. Therefore, it may be more favorable for MR-1 to up-regulate several anaerobic respiratory pathways at once, especially when oxygen availability may fluctuate often.

One interesting observation made in this study is that neither DmsF nor SO4359 were able to facilitate interactions between PECs and OMCs for the purpose of iron(III) citrate reduction. Both *dmsF* and *SO4359* are located in gene clusters containing predicted homologs to the DMSO reductase subunits *dmsAB*. The putative β-barrel integral OM proteins DmsF and SO4359 each likely interact with PEC proteins encoded in their respective gene clusters. The β-barrel paralogs are similar in predicted size (MtrB – 697aa, MtrE – 712aa, DmsF – 662aa, SO4359 – 656aa), and therefore could have a similar number of transmembrane domains. Consistent with our functional studies, MtrB and MtrF are closer in size when compared to DmsF and SO4359. However, instead of a multiheme *c*-type cytochrome as the terminal

reductase, there are two terminal reductase subunits: DmsB, which contains a 4Fe–4S cluster and DmsA, which contains a molybdopterin cofactor (Weiner et al., 1992). These DmsAB complexes may interface with the MtrB paralogs DmsF and SO4359 differently than with an OMC. Hence, it is more likely that DmsF and SO4359 would be able to functionally replace each other, since the terminal branch of their respiratory chains are also paralogs.

In this study we have identified nine different MtrA/MtrB/MtrC paralog modules of the Mtr respiratory pathway that could be used to move electrons from the CM (CymA) to the outside of the cell (OMC). One could imagine a heterologous expression system where proteins with different redox potentials could be integrated with core Mtr-pathway components. However, though many pathways exist to traffic electrons to the cell surface, the purpose of two of the pathways remain unknown. Their presence in the MR-1 and other *Shewanella* genomes is consistent with their functionality/utility for these bacteria in the environment. Understanding the role of these pathways may help explain the global aquatic presence of *Shewanella* and could lead to new biotechnological applications of these diverse bacteria.

ACKNOWLEDGMENTS

The authors wish to thank the Gralnick and Bond Labs for helpful discussions. This work was funded by the Office of Naval Research (award N000140810166) to Jeffrey A. Gralnick.

REFERENCES

Baron, D., Labelle, E., Coursolle, D., Gralnick, J. A., and Bond, D. R. (2009). Electrochemical measurement of electron transfer kinetics by *Shewanella oneidensis* MR-1. *J. Biol. Chem.* 284, 28865–28873.

Beliaev, A. S., and Saffarini, D. A. (1998). *Shewanella putrefaciens mtrB* encodes an outer membrane protein required for Fe(III) and Mn(IV) reduction. *J. Bacteriol.* 180, 6292–6297.

Beliaev, A. S., Thompson, D. K., Khare, T., Lim, H., Brandt, C. C., Li, G., Murray, A. E., Heidelberg, J. F., Giometti, C. S., Yates, J. III, Nealson, K. H., Tiedje, J. M., and Zhoui, J. (2002). Gene and protein expression profiles of *Shewanella oneidensis* during anaerobic growth with different electron acceptors. *OMICS* 6, 39–60.

Berks, B. C., Ferguson, S. J., Moir, J. W., and Richardson, D. J. (1995). Enzymes and associated electron transport systems that catalyse the respiratory reduction of nitrogen oxides and oxyanions. *Biochim. Biophys. Acta* 1232, 97–173.

Bilous, P. T., Cole, S. T., Anderson, W. F., and Weiner, J. H. (1988). Nucleotide sequence of the dmsABC operon encoding the anaerobic dimethyl sulphoxide reductase of *Escherichia coli*. *Mol. Microbiol.* 2, 785–795.

Bucking, C., Popp, F., Kerzenmacher, S., and Gescher, J. (2010). Involvement and specificity of *Shewanella oneidensis* outer membrane cytochromes in the reduction of soluble and solid-phase terminal electron acceptors. *FEMS Microbiol. Lett.* 306, 144–151.

Clarke, T. A., Edwards, M. J., Gates, A. J., Hall, A., White, G. F., Bradley, J., Reardon, C. L., Shi, L., Beliaev, A. S., Marshall, M. J., Wang, Z., Watmough, N. J., Fredrickson, J. K., Zachara, J. M., Butt, J. N., and Richardson, D. J. (2011). Structure of a bacterial cell surface decaheme electron conduit. *Proc. Natl. Acad. Sci. U.S.A.* 108, 9384–9389.

Coursolle, D., Baron, D. B., Bond, D. R., and Gralnick, J. A. (2010). The Mtr respiratory pathway is essential for reducing flavins and electrodes in *Shewanella oneidensis*. *J. Bacteriol.* 192, 467–474.

Coursolle, D., and Gralnick, J. A. (2010). Modularity of the Mtr respiratory pathway of *Shewanella oneidensis* strain MR-1. *Mol. Microbiol.* 77, 995–1008.

Firer-Sherwood, M., Pulcu, G. S., and Elliott, S. J. (2008). Electrochemical interrogations of the Mtr cytochromes from *Shewanella*: opening a potential window. *J. Biol. Inorg. Chem.* 13, 849–854.

Firer-Sherwood, M. A., Ando, N., Drennan, C. L., and Elliott, S. J. (2011). Solution-based structural analysis of the decaheme cytochrome, MtrA, by small-angle X-ray scattering and analytical ultracentrifugation. *J. Phys. Chem. B* 115, 11208–11214.

Fredrickson, J. K., Romine, M. F., Beliaev, A. S., Auchtung, J. M., Driscoll, M. E., Gardner, T. S., Nealson, K. H., Osterman, A. L., Pinchuk, G., Reed, J. L., Rodionov, D. A., Rodrigues, J. L., Saffarini, D. A., Serres, M. H., Spormann, A. M., Zhulin, I. B., and Tiedje, J. M. (2008). Towards environmental systems biology of *Shewanella*. *Nat. Rev. Microbiol.* 6, 592–603.

Gescher, J. S., Cordova, C. D., and Spormann, A. M. (2008). Dissimilatory iron reduction in *Escherichia coli*: identification of CymA of *Shewanella oneidensis* and NapC of *E. coli* as ferric reductases. *Mol. Microbiol.* 68, 706–719.

Gon, S., Patte, J. C., Dos Santos, J. P., and Mejean, V. (2002). Reconstitution of the trimethylamine oxide reductase regulatory elements of *Shewanella oneidensis* in *Escherichia coli*. *J. Bacteriol.* 184, 1262–1269.

Gralnick, J. A., and Newman, D. K. (2007). Extracellular respiration. *Mol. Microbiol.* 65, 1–11.

Gralnick, J. A., Vali, H., Lies, D. P., and Newman, D. K. (2006). Extracellular respiration of dimethyl sulfoxide by *Shewanella oneidensis* strain MR-1. *Proc. Natl. Acad. Sci. U.S.A.* 103, 4669–4674.

Hartshorne, R. S., Reardon, C. L., Ross, D., Nuester, J., Clarke, T. A., Gates, A. J., Mills, P. C., Fredrickson, J. K., Zachara, J. M., Shi, L., Beliaev, A. S., Marshall, M. J., Tien, M., Brantley, S., Butt, J. N., and Richardson, D. J. (2009). Characterization of an electron conduit between bacteria and the extracellular environment. *Proc. Natl. Acad. Sci. U.S.A.* 106, 22169–22174.

Hau, H. H., Gilbert, A., Coursolle, D., and Gralnick, J. A. (2008). Mechanism and consequences of anaerobic respiration of cobalt by *Shewanella oneidensis* strain MR-1. *Appl. Environ. Microbiol.* 74, 6880–6886.

Hunt, K. A., Flynn, J. M., Naranjo, B., Shikhare, I. D., and Gralnick, J. A. (2010). Substrate-level phosphorylation is the primary source of energy conservation during anaerobic respiration of *Shewanella oneidensis* strain MR-1. *J. Bacteriol.* 192, 3345–3351.

Kovach, M. E., Elzer, P. H., Hill, D. S., Robertson, G. T., Farris, M. A., Roop, R. M. II, and Peterson, K. M. (1995). Four new derivatives of the broad-host-range cloning vector pBBR1MCS, carrying different antibiotic-resistance cassettes. *Gene* 166, 175–176.

Kwan, H. S., and Barrett, E. L. (1983). Roles for menaquinone and the two trimethylamine oxide (TMAO) reductases in TMAO respiration in *Salmonella typhimurium*: Mu d(Apr lac) insertion mutations in *men* and *tor*. *J. Bacteriol.* 155, 1147–1155.

Lloyd, J. R., Lovley, D. R., and MacAskie, L. E. (2003). Biotechnological application of metal-reducing microorganisms. *Adv. Appl. Microbiol.* 53, 85–128.

Lovley, D. R. (2008). The microbe electric: conversion of organic matter to electricity. *Curr. Opin. Biotechnol.* 19, 564–571.

Marsili, E., Baron, D. B., Shikhare, I. D., Coursolle, D., Gralnick, J. A., and Bond, D. R. (2008). *Shewanella* secretes flavins that mediate extracellular electron transfer. *Proc. Natl. Acad. Sci. U.S.A.* 105, 3968–3973.

McLean, J. S., Pinchuk, G. E., Geydebrekht, O. V., Bilskis, C. L., Zakrajsek, B. A., Hill, E. A., Saffarini, D. A., Romine, M. F., Gorby, Y. A., Fredrickson, J. K., and Beliaev, A. S. (2008). Oxygen-dependent autoaggregation in *Shewanella oneidensis* MR-1. *Environ. Microbiol.* 10, 1861–1876.

Myers, C. R., and Myers, J. M. (1997). Cloning and sequence of *cymA*, a gene encoding a tetraheme cytochrome c required for reduction of iron(III), fumarate, and nitrate by *Shewanella putrefaciens* MR-1. *J. Bacteriol.* 179, 1143–1152.

Myers, C. R., and Nealson, K. H. (1988). Bacterial manganese reduction and growth with manganese oxide as the sole electron acceptor. *Science* 240, 1319–1321.

Nealson, K. H., and Saffarini, D. (1994). Iron and manganese in anaerobic respiration: environmental significance, physiology, and regulation. *Annu. Rev. Microbiol.* 48, 311–343.

Pitts, K. E., Dobbin, P. S., Reyes-Ramirez, F., Thomson, A. J., Richardson, D. J., and Seward, H. E. (2003). Characterization of the *Shewanella oneidensis* MR-1 decaheme cytochrome MtrA: expression in *Escherichia coli* confers the ability to reduce soluble Fe(III) chelates. *J. Biol. Chem.* 278, 27758–27765.

Potter, L., Angove, H., Richardson, D., and Cole, J. (2001). Nitrate reduction in the periplasm of gram-negative bacteria. *Adv. Microb. Physiol.* 45, 51–112.

Ross, D. E., Brantley, S. L., and Tien, M. (2009). Kinetic characterization of OmcA and MtrC, terminal reductases involved in respiratory electron transfer for dissimilatory iron reduction in *Shewanella oneidensis* MR-1. *Appl. Environ. Microbiol.* 75, 5218–5226.

Saltikov, C. W., and Newman, D. K. (2003). Genetic identification of a respiratory arsenate reductase. *Proc. Natl. Acad. Sci. U.S.A.* 100, 10983–10988.

Schwalb, C., Chapman, S. K., and Reid, G. A. (2003). The tetraheme cytochrome CymA is required for anaerobic respiration with dimethyl sulfoxide and nitrite in *Shewanella oneidensis*. *Biochemistry* 42, 9491–9497.

Shi, L., Squier, T. C., Zachara, J. M., and Fredrickson, J. K. (2007). Respiration of metal (hydr)oxides by *Shewanella* and *Geobacter*: a key role for multiheme c-type cytochromes. *Mol. Microbiol.* 65, 12–20.

Shirodkar, S., Reed, S., Romine, M., and Saffarini, D. (2011). The octaheam SirA catalyses dissimilatory sulfite reduction in *Shewanella oneidensis* MR-1. *Environ. Microbiol.* 13, 108–115.

Stookey, L. L. (1970). Ferrozine – a new spectrophotometric reagent for iron. *Anal. Chem.* 42, 779–781.

Thomas, P. E., Ryan, D., and Levin, W. (1976). An improved staining procedure for the detection of the peroxidase activity of cytochrome P-450 on sodium dodecyl sulfate polyacrylamide gels. *Anal. Biochem.* 75, 168–176.

Venkateswaran, K., Moser, D. P., Dollhopf, M. E., Lies, D. P., Saffarini, D. A., MacGregor, B. J., Ringelberg, D. B., White, D. C., Nishijima, M., Sano, H., Burghardt, J., Stackebrandt, E., and Nealson, K. H. (1999). Polyphasic taxonomy of the genus *Shewanella* and description of *Shewanella oneidensis* sp. nov. *Int. J. Syst. Bacteriol.* 49(Pt 2), 705–724.

Vick, J. E., Johnson, E. T., Choudhary, S., Bloch, S. E., Lopez-Gallego, F., Tikh, I. B., Wawrzyn, G. T., and Schmidt-Dannert, C. (2011). Optimized compatible set of BioBrick vectors for metabolic pathway engineering. *Appl. Microbiol. Biotechnol.* 92, 1275–1286.

Von Canstein, H., Ogawa, J., Shimizu, S., and Lloyd, J. R. (2008). Secretion of flavins by *Shewanella* species and their role in extracellular electron transfer. *Appl. Environ. Microbiol.* 74, 615–623.

Wall, J. D., and Krumholz, L. R. (2006). Uranium reduction. *Annu. Rev. Microbiol.* 60, 149–166.

Wang, Z., Liu, C., Wang, X., Marshall, M. J., Zachara, J. M., Rosso, K. M., Dupuis, M., Fredrickson, J. K., Heald, S., and Shi, L. (2008). Kinetics of reduction of Fe(III) complexes by outer membrane cytochromes MtrC and OmcA of *Shewanella oneidensis* MR-1. *Appl. Environ. Microbiol.* 74, 6746–6755.

Weiner, J. H., Rothery, R. A., Sambasivarao, D., and Trieber, C. A. (1992). Molecular analysis of dimethylsulfoxide reductase: a complex iron-sulfur molybdoenzyme of *Escherichia coli*. *Biochim. Biophys. Acta* 1102, 1–18.

Wigginton, N. S., Rosso, K. M., and Hochella, M. F. Jr. (2007). Mechanisms of electron transfer in two decaheme cytochromes from a metal-reducing bacterium. *J. Phys. Chem. B* 111, 12857–12864.

Wissenbach, U., Ternes, D., and Unden, G. (1992). An *Escherichia coli* mutant containing only demethylmenaquinone, but no menaquinone: effects on fumarate, dimethylsulfoxide, trimethylamine N-oxide and nitrate respiration. *Arch. Microbiol.* 158, 68–73.

Xiong, Y., Shi, L., Chen, B., Mayer, M. U., Lower, B. H., Londer, Y., Bose, S., Hochella, M. F., Fredrickson, J. K., and Squier, T. C. (2006). High-affinity binding and direct electron transfer to solid metals by the *Shewanella oneidensis* MR-1 outer membrane c-type cytochrome OmcA. *J. Am. Chem. Soc.* 128, 13978–13979.

Conflict of Interest Statement: The authors declare that the research was conducted in the absence of any commercial or financial relationships that could be construed as a potential conflict of interest.

Received: 17 October 2011; accepted: 02 February 2012; published online: 21 February 2012.

Citation: Coursolle D and Gralnick JA (2012) Reconstruction of extracellular respiratory pathways for iron(III) reduction in Shewanella oneidensis strain MR-1. Front. Microbio. ***3****:56. doi: 10.3389/fmicb.2012.00056*

This article was submitted to Frontiers in Microbiological Chemistry, a specialty of Frontiers in Microbiology.

Copyright © 2012 Coursolle and Gralnick. This is an open-access article distributed under the terms of the Creative Commons Attribution Non Commercial License, which permits non-commercial use, distribution, and reproduction in other forums, provided the original authors and source are credited.

APPENDIX

Table A1 | Primers and restriction sites used for cloning and subsequent generation of mutant and complemented strains.

Primer	Restriction site	Sequence
DELETION[a]		
OmcA up 1	*Spe*1	NNACTAGTCAGGTCTCACAGTACCCGCA
MtrB up 1	*Not*I	NNNNNNNNNNNGCGGCCGCCGTTCAACCTCTCGCGCTTA
MtrB up 2	*Bam*HI	NNNGGATCCCTTTACAGCTCCATGCGGAT
MtrB down 1	*Bam*HI	NNNGGATCCATGGCATTTGGAACGTCGTAGG
MtrB down 2	*Spe*I	NNACTAGTTCTGGACGTGGCGGCTTATC
MtrE up 1	*Sac*I	NNNGAGCTCGCAGTAAATCGTAAATACCGG
MtrE up 2	*Bam*HI	NNNGGATCCGTCGATATATTCACTATTTGC
MtrE down 1	*Bam*HI	NNNGGATCCAGGTTTGACCTTAAGCTACC
MtrE down 2	*Not*I	NNNNNNNNGCGGCCGCTATTACAAGTGTCGATCGAGA
COMPLEMENTATION[b]		
OmcA 1	*Bgl*II	NNNAGATCTGTTGGCGCTAGAGCATAGCGGTTAAGCAAT GCCAAACCTATGCAGGGAAAAAAATGATGAAACGGTTCAATTTCA
OmcA 2	*Not*I	NNNNNNNNNNGCGGCCGCAACCACAAGGGAAAAACAAA
MtrC 1	*Bgl*II	NNNAGATCTGTTGGCGCTAGAGCATAG
MtrC 2	*Not*I	NNNNNNNNNNGCGGCCGCTAATAGGCTTCCCAATTTGT
MtrF 1	*Bgl*II	NNNAGATCTGTTGGCGCTAGAGCATAGCGGTTAAGCAA TGCCAAACCTATGCAGGGAAAAAAATGAATAAGTTTGCAAGCT
MtrF 2	*Not*I	NNNNNNNNNNGCGGCCGCTTGGGCCTGCATCATCGAGTTAG
MtrB 1	*Bgl*II	NNNAGATCTCCATCCATCTGGCAAGCTAT
MtrB 2	*Not*I	NNNNNNNNNNGCGGCCGCGGGCTTTTGAGCATATGAGG
MtrE 1	*Bgl*II	NNNAGATCTCCATCCATCTGGCAAGCTATTACAGCGC TAAGGAGACGAGAAAATGCAAATAGTGAATATATCG
MtrE 2	*Not*I	NNNNNNNNNNGCGGCCGCGTGCCTAAGTTACATTTGGTAG CTTAA

[a] *Deletion primers for mtrB, mtrA, mtrD, dmsE, SO4360, cctA, mtrC, mtrF, and omcA were described previously (Coursolle and Gralnick, 2010).*

[b] *Complementation primers for mtrA, mtrD, dmsE, and SO4360 were described previously (Coursolle and Gralnick, 2010).*

frontiers in
MICROBIOLOGY

REVIEW ARTICLE
published: 15 March 2012
doi: 10.3389/fmicb.2012.00089

Iron-based microbial ecosystem on and below the seafloor: a case study of hydrothermal fields of the Southern Mariana Trough

Shingo Kato[1,2], Kentaro Nakamura[3], Tomohiro Toki[4], Jun-ichiro Ishibashi[5], Urumu Tsunogai[6], Akinori Hirota[7], Moriya Ohkuma[1] and Akihiko Yamagishi[2]*

[1] *Japan Collection of Microorganisms, RIKEN BioResource Center, Wako, Saitama, Japan*
[2] *Department of Molecular Biology, Tokyo University of Pharmacy and Life Science, Hachioji, Tokyo, Japan*
[3] *Precambrian Ecosystem Laboratory, Japan Agency for Marine-Earth Science and Technology, Yokosuka, Kanagawa, Japan*
[4] *Department of Chemistry, Biology, and Marine Science, Faculty of Science, University of the Ryukyus, Nishihara, Okinawa, Japan*
[5] *Department of Earth and Planetary Sciences, Faculty of Science, Kyushu University, Higashi-ku, Fukuoka, Japan*
[6] *Department of Natural History Sciences, Graduate School of Science, Hokkaido University, Kita-ku, Sapporo, Japan*
[7] *Volcanic Activity Research Group, Institute of Geology and Geoinformation, National Institute of Advanced Industrial Science and Technology, Tsukuba, Ibaraki, Japan*

Edited by:
David Emerson, Bigelow Laboratory for Ocean Sciences, USA

Reviewed by:
Benjamin Kocar, Stanford University, USA
Craig Lee Moyer, Western Washington University, USA

****Correspondence:***
Akihiko Yamagishi, Department of Molecular Biology, Tokyo University of Pharmacy and Life Science, 1432-1 Horinouchi, Hachioji, Tokyo 192-0392, Japan.
e-mail: yamagish@toyaku.ac.jp

Microbial community structures in deep-sea hydrothermal vents fields are constrained by available energy yields provided by inorganic redox reactions, which are in turn controlled by chemical composition of hydrothermal fluids. In the past two decades, geochemical and microbiological studies have been conducted in deep-sea hydrothermal vents at three geographically different areas of the Southern Mariana Trough (SMT). A variety of geochemical data of hydrothermal fluids and an unparalleled microbiological dataset of various samples (i.e., sulfide structures of active vents, iron-rich mats, borehole fluids, and ambient seawater) are available for comparative analyses. Here, we summarize the geochemical and microbiological characteristics in the SMT and assess the relationship between the microbial community structures and the fluid geochemistry in the SMT by thermodynamic modeling. In the high temperature vent fluids, aerobic sulfide-oxidation has the potential to yield large amounts of bioavailable energy in the vent fluids, which is consistent with the detection of species related to sulfide-oxidizing bacteria (such as *Thiomicrospira* in the Gammaproteobacteria and *Sulfurimonas* in the Epsilonproteobacteria). Conversely, the bioavailable energy yield from aerobic iron-oxidation reactions in the low-temperature fluids collected from man-made boreholes and several natural vents were comparable to or higher than those from sulfide-oxidation. This is also consistent with the detection of species related to iron-oxidizing bacteria (*Mariprofundus* in the Zetaproteobacteria) in such low-temperature samples. The results of combination of microbiological, geochemical, and thermodynamic analyses in the SMT provide novel insights into the presence and significance of iron-based microbial ecosystems in deep-sea hydrothermal fields.

Keywords: deep-sea hydrothermal vent field, shallow sub-seafloor microbial ecosystem, chemolithoautotrophs, iron-oxidizing bacteria, thermodynamic modeling

INTRODUCTION

Microbial ecosystems require energy for maintenance and prosperity. On land and in the sea surface, solar power is the main energy source. In the "photosynthetic ecosystem," photoautotrophs (e.g., plants and cyanobacteria) are the primary producers that fix inorganic carbon and transform it into organic carbon using solar energy. The resulting organic carbon supports the growth of various organisms as carbon and energy sources. In contrast, there are microbial ecosystems that are sustained by chemical energy derived from inorganic redox reactions between electron donors (such as H_2, H_2S, Fe^{2+}, and CH_4) and acceptors (such as O_2, NO_3^-, Fe^{3+}, SO_4^{2-}, and CO_2). Chemolithoautotrophs fix inorganic carbon using the chemical energy, sustaining "Chemosynthetic ecosystems" as primary producers. It is known that chemosynthetic ecosystems are widely distributed on land (e.g., acid mines, hot springs, and deep subsurface) and in oceans (e.g., cold seeps, hydrothermal vents, and potentially enormous sub-seafloor aquifers). Recently, much attention has been paid to deep-sea hydrothermal vents and sub-seafloor aquifers that are potential habitats harboring extensive chemosynthetic ecosystems sustained by a variety of chemolithoautotrophs (reviewed in Orcutt et al., 2011). Although the precise picture of the potentially enormous sub-seafloor biosphere is still not well understood, the elucidation of the distribution, function, activity, and productivity of the deep-sea chemosynthetic ecosystems is important for better understanding not only of the extent and limit of the biosphere on Earth but also the global cycling of elements related to biological activities.

Deep-sea hydrothermal vent fields were initially found in the late 1970s. To date, over 200 deep-sea hydrothermal fields

have been found in various areas, mainly on mid-ocean ridges, arc volcanoes, back-arc basins, and hot-spot volcanoes (http://www.interridge.org/irvents/). The hydrothermal fluids contain a variety of electron donors that serve as energy sources for the life thriving there. The chemical disequilibria, which occur in deep-sea hydrothermal environments by rapid mixing of reduced hydrothermal fluids with oxygenated cold seawater, could provide energy sources for the growth of the chemolithoautotrophs (McCollom and Shock, 1997; Takai and Nakamura, 2010; Amend et al., 2011). In fact, the presence of hydrogen-, sulfide-, and methane-oxidizers was confirmed soon after the discovery of the vent field (Jannasch and Mottl, 1985). Subsequent studies have revealed the ecology of the chemolithoautotrophs inhabiting the deep-sea hydrothermal vent fields, which include mesophiles to hyperthermophiles belonging to the Epsilonproteobacteria, Gammaproteobacteria, and Archaea (Nakagawa and Takai, 2008).

In contrast to hydrogen-, sulfide-, and methane-oxidizers, our knowledge of iron-oxidizers, especially mesophilic and neutrophilic bacteria, in deep-sea hydrothermal fields has been quite limited and was reported only recently. The first neutrophilic, mesophilic, and iron-oxidizing chemolithoautotrophic marine bacterium, *Mariprofundus ferrooxydans*, which belongs to the Zetaproteobacteria, was isolated from iron-rich mats in the hydrothermal fields of the Loihi Seamount (Emerson et al., 2007), and the genome sequence of *M. ferrooxydans* was recently reported (Singer et al., 2011). This isolate produces unique helical-stalks consisting of organic compounds and iron oxides (Chan et al., 2011). It is thus reasonable to consider that the iron-oxidizers play a significant role in the generation of massive iron-rich mats on the seafloor (Emerson and Moyer, 2002). Diverse 16S rRNA gene sequences affiliated in the Zetaproteobacteria have been recovered from iron-rich mats from various marine hydrothermal fields (McAllister et al., 2011). In some cases, members of the Zetaproteobacteria dominate the communities in the iron-rich mats (Kato et al., 2009a) and in the sub-seafloor warm fluids (Kato et al., 2009b), although the physiology of these phylotypes in the Zetaproteobacteria is still unclear because few isolates have been reported. Considering the domination of the Zetaproteobacteria and the abundance of the unique stalk structures in the seafloor massive iron oxide mats, it is very likely that the Zetaproteobacteria contain many iron-oxidizing chemolithoautotrophic species, sustaining the iron-based microbial ecosystem present in the iron-rich mats.

In the deep-sea hydrothermal vent fields, sulfide deposits (like mounds and chimneys) are usually present and sulfide- and hydrogen-oxidizers have been detected in these deposits and venting fluids. The detection of sulfide- and hydrogen-oxidizers in these habitats is consistent with the high potential of bioavailable energy from sulfide- and hydrogen-oxidation reactions in chemical conditions of the habitats (Takai and Nakamura, 2010; Amend et al., 2011). In contrast, iron-rich mats are not always observed in deep-sea hydrothermal vent fields, and the Zetaproteobacterial phylotypes (putative iron-oxidizers) were relatively abundant, compared to the known sulfide- and hydrogen-oxidizers, only in the iron-rich mats and crustal fluids (Kato et al., 2009a,b). A comprehensive and comparative analysis is needed to answer the following question: what is the critical factor(s) for the appearance of iron-based microbial ecosystems. This information is important in order to understand global carbon and iron cycling because iron-based microbial ecosystems are potentially present in enormous sub-seafloor aquifers, which would be the largest chemosynthetic ecosystem on Earth (Bach and Edwards, 2003; Edwards et al., 2003).

The Southern Mariana Trough (SMT; **Figure A1A** in Appendix) is one of the most suitable fields in which assess the factors leading to the appearance of iron-based microbial ecosystems. In the SMT, there are variable temperature habitats, from black and clear smoker sulfide chimneys (up to ∼340°C) to iron-rich mats with shimmering (∼110°C; **Figure 1**), in an area of 5 km × 5 km (**Figure A1B** in Appendix). Furthermore, there are several boreholes that were drilled using a shallow-seafloor drilling instrument, Benthic Multi-coring System (BMS; Marumo et al., 2008). Analysis of the collected fluids from the boreholes can provide valuable information about the geochemical conditions and microbiological activities of the sub-seafloor aquifers. Davis and Moyer (2008) first reported the presence of the Zetaproteobacteria in iron-rich mats in the SMT. Sequentially, comprehensive microbiological analyses of the various samples from the SMT hydrothermal fields have been done (Kato et al., 2009a,b, 2010). Here we summarize the variation of microbial communities in the SMT as shown by culture-independent molecular microbiological analyses, and discuss how these community structures were constructed. In addition, the bioavailable energy yields based on thermodynamic calculations were applied to discuss the geochemical factors leading to the appearance of the iron-based microbial ecosystem.

GEOLOGICAL SETTINGS AND FLUID GEOCHEMISTRY

The SMT is a spreading back-arc basin that is located at the southern extension of the Izu–Bonin arc, western Pacific (**Figure A1A** in Appendix; Fryer, 1995; Ishibashi and Urabe, 1995). Hydrothermal activity hosted by basaltic rocks (Kakegawa et al., 2008) was found on the back-arc spreading ridge (Snail site) and on the off-ridge

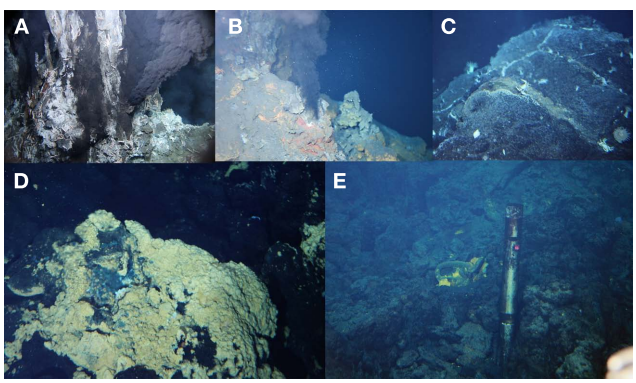

FIGURE 1 | On-site observation of the seafloor in the SMT. Photos were taken by *Shinkai 6500* (JAMSTEC, Japan) in 2010. (A) A black smoker chimney at the Archaean site, **(B)** a black smoker chimney at the Pika site, **(C)** diffuse flows from crack of pillow lavas at the Snail site, **(D)** iron-rich mats at the Snail site, and **(E)** a casing pipe inserted into a borehole at the Snail site.

seamounts (Pika and Archaean sites) in the SMT (**Figure A1B** in Appendix; Wheat et al., 2003; Ishibashi et al., 2004, 2006). In the Pika and Archaean sites, sulfide chimneys venting high temperature fluids (up to >300°C) were found (**Figures 1A,B**). Low-temperature diffusing and shimmering fluids (<150°C) were also observed in both sites. In the Snail site, diffuse flows or shimmering with relatively low-temperature hydrothermal fluids (<120°C) from the fractures of pillow lavas (basalts; **Figure 1C**) and iron-rich mats (containing Fe, Si, and Mn; **Figure 1D**) were also observed (Wheat et al., 2003; Kato et al., 2009a), although chimney-like sulfide structures and associated high temperature hydrothermal venting have not been found.

Boreholes were created on the seafloor at the Snail and Pika sites using BMS (Marumo et al., 2008). These boreholes were cased with titanium pipes (**Figure 1E**). During fluid sampling from the boreholes, the casing pipes minimize the contamination from the seafloor materials into the crustal fluids.

Preliminarily analyses of the geochemical composition of hydrothermal fluids collected in the SMT hydrothermal fields in 2003, 2004, and 2005 have been reported (Wheat et al., 2003; Ishibashi et al., 2004, 2006). Furthermore, we collected hydrothermal fluids from natural vents and boreholes in the SMT in 2010 and analyzed the fluid geochemistry as previously described (Takai et al., 2008; Toki et al., 2008). The geochemistry of the fluids is summarized in **Table A1** in Appendix. Concentrations of O_2, CO_2, CH_4, and H_2 in deep seawater were referred from the previous publication (McCollom, 2007). It should be noted that a significant difference in the ratio of Fe to H_2S was observed among the vent samples collected from the Snail site (**Figure 2**). These samples were divided into Fe-type (high Fe/H_2S) and H_2S-type (low Fe/H_2S) and their geochemical data are shown in separate columns in **Table A1** in Appendix.

The concentrations of Cl, Si, H_2S, and Fe are plotted against its Mg concentration (**Figure 3**). These so-called magnesium diagrams are conventionally used to estimate the hydrothermal end-member composition of a high temperature fluid from the deep-sea hydrothermal system (Von Damm et al., 1985). The collected fluid sample is often conceived to be simple mixture

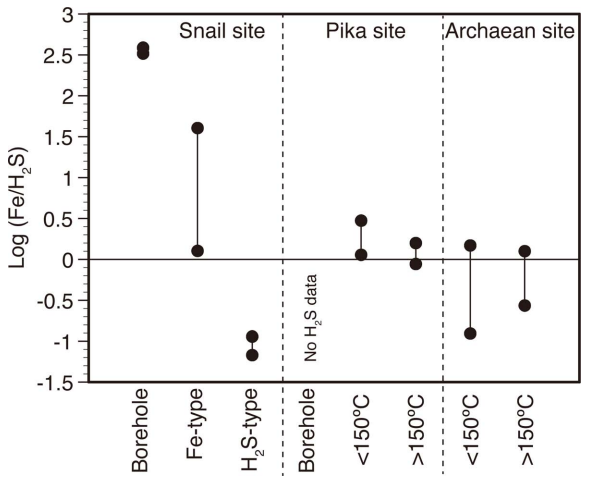

FIGURE 2 | The ratio of Fe to H_2S in fluid samples.

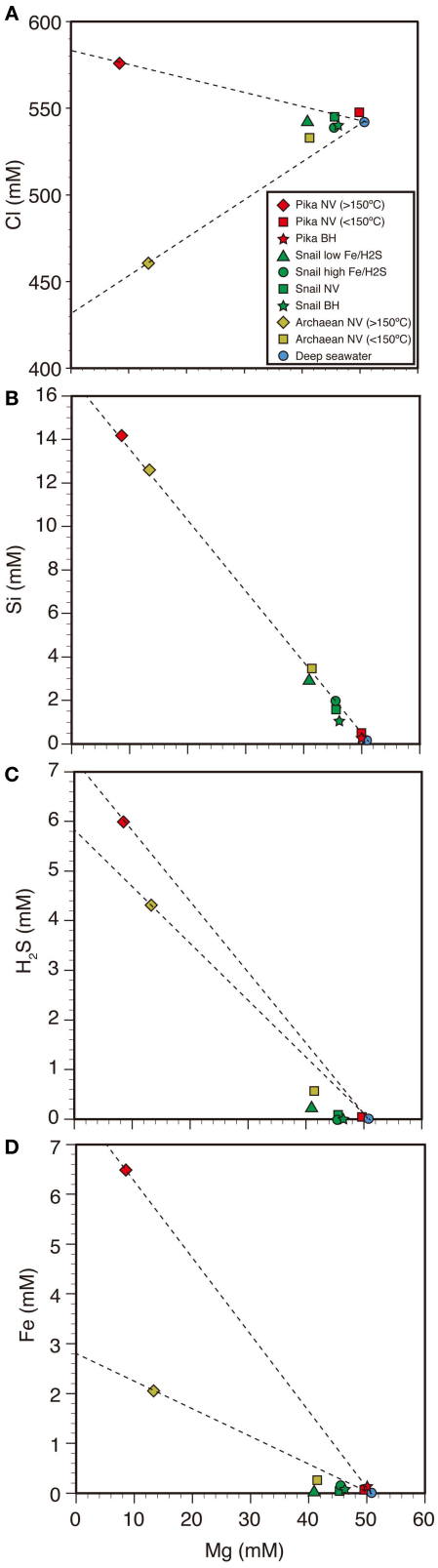

FIGURE 3 | Mg diagrams against Cl, Si, H_2S, and Fe for fluid samples. **(A)** Cl–Mg, **(B)** Si–Mg, **(C)** H_2S–Mg, and **(D)** Fe–Mg diagrams are shown. NV and BH indicate natural vents and borehole fluids, respectively.

between the hydrothermal end-member (completely depleted in Mg) and seawater (Mg concentration is rather high as 50 mM). For conservative chemical species in mixing between the hydrothermal end-member and seawater, plots of the collected samples should be aligned along a simple linear trend.

Chloride is predominant anion of hydrothermal fluid and seawater, which is a representative for such conservative species. In Cl–Mg diagram (**Figure 3A**), plots of the collected samples from the Pika and Archaean sites show clearly different trends. Substantial deviation of Cl concentration of hydrothermal fluid from that of seawater is attributed to sub-seafloor phase separation (e.g., Takai et al., 2008). Based on the data of high temperature (>150°C) fluids, Cl-enriched signature of the Pika fluid can be classified as vapor-lost (i.e., the gases such as H_2, H_2S, and CH_4 are poor) hydrothermal fluid. In contrast, Cl-depleted signature of the Archaean fluid can be classified as vapor-rich (i.e., the gases are enriched) hydrothermal fluid. In the Archaean site, the collected sample of low-temperature (<150°C) shimmering was enriched in H_2 and CH_4 (**Table A1** in Appendix), which is in accordance with occurrence of vapor-rich hydrothermal fluid in this site.

Si concentration of hydrothermal fluid is known as controlled by fluid-mineral equilibrium at the fluid reservoir (Von Damm et al., 1991). The Si–Mg diagram (**Figure 3B**) suggests Si concentrations of the hydrothermal fluid end-members for three sites are commonly as high as 16 mM, which corresponds to equilibrium at high temperature condition above 300°C. This result is reasonable for the Pika and Archaean fluids, since such high temperature fluid vents have been observed in these sites. Similar to these two sites, a high temperature fluid reservoir would exist below the seafloor in the Snail Site. In fact, the first report for the Snail site mentioned that fluid temperature was as high as 250°C (Wheat et al., 2003).

Significantly high H_2S and Fe concentrations were observed for the samples collected from high temperature fluid vents in both Pika and Archaean sites (**Table A1** in Appendix). Based on analogy to the high temperature fluids found at hydrothermal fields in Lau Basin, low pH signature of the fluid could be responsible for enrichment in these species (Takai et al., 2008). In contrast, H_2S and Fe concentrations of the low-temperature fluid samples are noticeably lower than the mixing line between high temperature fluids and seawater (**Figures 3C,D**). It is likely that iron-sulfide mineral precipitation occurred during sub-seafloor mixing, causing the decrease of H_2S and Fe concentrations in the low-temperature fluids. For the Snail site, it is difficult to estimate original H_2S and Fe concentrations in the fluid reservoir, since no high temperature fluid venting was observed. However, it is reasonable to expect similar range to other two sites, since common Si concentration among three sites suggest existence of a high temperature fluid reservoir. If it is the case, the observed Fe and H_2S concentrations of the samples collected from low-temperature shimmering can be interpreted as affected by mineral precipitation during sub-seafloor mixing between the high temperature fluid and seawater.

BACTERIAL COMMUNITY STRUCTURES

The microbial community structures in various habitats (e.g., sulfide structures of active vents, iron-rich mats, borehole fluids, and ambient seawater; **Figure 1**) in the SMT have been investigated using culture-independent molecular microbiological methods (PCR clone library construction and DNA sequencing, fluorescence *in situ* hybridization (FISH) and quantitative real-time PCR; Kato et al., 2009a,b, 2010). The bacterial community structures in the habitats have been determined by 16S rRNA gene clone library analysis as described in our previous reports (Kato et al., 2009a,b, 2010). The microbiological data used in the present paper are originated from the previous reports. The relatively abundant taxonomic groups in the libraries for each habitat are summarized in **Table 1**. It should be noted that the abundance of the phylotypes in the libraries does not indicate their real abundance in the communities but only the relative abundance due to the inherent biases of PCR-based analyses (Wintzingerode et al., 1997).

In the sulfide structures of active vents, phylotypes belonging to the Aquificae or Epsilonproteobacteria were abundant in the libraries. The detection frequencies in the libraries were up to 44% of the total clone numbers. Members of the Aquificae included thermophilic hydrogen-oxidizers, such as *Persephonella hydrogeniphila*. Members of the Epsilonproteobacteria have a variety

Table 1 | Abundant taxonomic groups in the bacterial clone libraries for each habitat.

Habitat	Site	Temp range of venting fluids (°C)	Relative abundant group (potential chemolithoautotrophs)	Potential electron donor*	Growth temperature*
Active sulfide structure	Snail, Pika, Archaean	19–341	Aquificae (e.g., *Persephonella*), Epsilonproteobacteria (e.g., *Hydrogenimonas* and *Sulfurimonas*)	Hydrogen, sulfide	Moderate–Hyperthermophiles
Deep seawater	Snail, Pika, Archaean	2–3	Gammaproteobacteria (SUP05 group)	Sulfide	Psychrophiles (?)
Borehole fluid	Snail, Pika	6–40	Zetaproteobacteria (*Mariprofundus*), Epsilonproteobacteria (e.g., *Sulfurimonas*), Gammaproteobacteria (*Thiomicrospira*)	Iron, sulfide	Mesophiles
Iron-rich mat	Snail	33–116	Zetaproteobacteria (*Mariprofundus*), Gammaproteobacteria (e.g., *Methylomonas* and *Methylobacter*)	Iron, methane	Mesophiles

**Based on the physiological characteristics inferred from the phylogeny of the phylotypes.*

of metabolic and physiological characteristics: hydrogen- and sulfide-oxidation, microaerobic and anaerobic, and mesophilic to thermophilic. However, no iron-utilizing bacteria have been reported in the two taxonomic groups. The microbial community structures of these sulfide structures of active vents in the SMT were similar to those of each habitat in other deep-sea hydrothermal areas including other back-arc basins, arc volcanoes, and mid-ocean ridges (Takai et al., 2006).

The abundant phylotypes in the libraries from the seawater samples were different from those of the sulfide structures of active vents. The phylotypes related to SUP05 group and SAR11 cluster dominated in the libraries from the seawater samples. The SUP05 group belonging to the Gammaproteobacteria predominated in the hydrothermal plume of the Suiyo Seamount (Sunamura et al., 2004) and may include sulfide-oxidizing chemolithoautotrophs as suggested by metagenomic analysis (Walsh et al., 2009). The bottom seawater samples collected in the SMT are likely to be mixed with hydrothermal plumes.

The microbial community structures of the iron-rich mats and borehole fluids were distinguished from those in the chimneys and seawater. The phylotypes belonging to the Zetaproteobacteria were abundant (up to 50% of the total clone numbers) in the libraries from the iron-rich mats and borehole fluids. Quantitative PCR or FISH analysis indicated that the Zetaproteobacteria phylotypes accounted for up to 32% of the total cell numbers in the communities of these samples. In addition, the phylotypes related to sulfide-oxidizers, such as *Thiomicrospira* in the Gammaproteobacteria and *Sulfurimonas* in the Epsilonproteobacteria, were also detected in the libraries from the borehole fluids. However, such phylotypes were not detected in the iron-rich mats. In contrast, the phylotypes related to *Methylomonas* and *Methylophaga* (including methano/methylotrophs) in the Gammaproteobacteria were relatively abundant in the libraries from the iron-rich mats. Davis and Moyer (2008) have also provided 16S rRNA gene data from iron-rich mats in Snail site. They also detected the phylotypes related to Zetaproteobacteria and Gammaproteobacterial methano/methylotrophs, which is consistent with our results.

Based on the microbiological data that we reported previously (Kato et al., 2009a,b, 2010), the bacterial community structures in each habitat (i.e., active sulfide structures, iron-rich mats, borehole fluids and ambient seawater) in the SMT were compared by principal coordination analysis (PCoA) using Fast UniFrac (Hamady et al., 2009). Although Davis and Moyer (2008) have also provided 16S rRNA gene data from iron-rich mats in Snail site, we did not include their data in the comparative analysis to minimize methodological biases accompanied by different experimental procedures (e.g., DNA extraction and PCR). The distribution pattern of the communities for each sample corresponded well to their habitat types (**Figure 4**). The differences in the habitat types resulted in the differences in the abundant phylotypes in the libraries (**Table 1**). The physiology of the phylotypes cannot be determined from their phylogeny, but only inferred from the closest cultured species (**Table 1**). If we assume that the inferred metabolic functions of these phylotypes are correct, the observed differences in the microbial community structures among the habitats can be attributed to the presence/absence of each chemolithoautotroph (i.e., hydrogen-, sulfide-, methane-, or iron-oxidizer). In principle, the distribution pattern in PCoA is greatly influenced by the presence/absence of phylotypes that are phylogenetically distant from one another.

ARCHAEAL COMMUNITY STRUCTURES

In addition to the bacterial communities, diverse archaeal communities were also detected in the habitats in the hydrothermal fields of the SMT (Kato et al., 2009a,b, 2010). The abundant archaeal taxonomic groups were different among the habitats (**Table 2**) like the bacterial communities. A large number of the recovered phylotypes were affiliated with uncultured clone groups, such as the miscellaneous crenarchaeotic group (MCG), terrestrial hot spring crenarchaeota (THSC), pSL12-related group, and Marine Benthic Group E (MBGE). Although the physiologies of these uncultured phylotypes is still unclear, some of them have been inferred from metagenomic and functional gene analyses, and the geochemical characteristics of the environments where they were detected: for example, the MCG includes anaerobic chemoorganotrophs (Teske and Sørensen, 2008), the pSL12-related group includes ammonia-oxidizers (Mincer et al., 2007), and MBGE includes iron-oxidizers (Takai and Nakamura, 2010), respectively.

In the sulfide structures of active vents, phylotypes related to Archaeoglobi, Thermoprotei, and THSC were abundant in the libraries. The total detection frequencies of the three groups in the libraries were over 40%. Members of the Archaeoglobi and Thermoprotei include (hyper)thermophilic hydrogen-oxidizing anaerobes. No isolates of THSC have been reported. Only Marine Group I (MGI) phylotypes were detected in the libraries from the seawater samples. MGI members are common archaeal inhabitants in oceans (Fuhrman et al., 1992) and the group includes an ammonia-oxidizing chemolithoautotrophic isolate (Könneke et al., 2005). Like the bacterial community structures, the archaeal community structures of these sulfide structures and seawater samples were totally similar to those of each habitat in other deep-sea hydrothermal areas including other back-arc basins, arc volcanoes, and mid-ocean ridges (Takai et al., 2006).

All archaeal phylotypes recovered from the iron-rich mats and borehole fluids were classified in uncultured clone groups, such the MBGE, MCG, and pSL12-related group. These uncultured groups have been recovered from other deep-sea environments. For example, the MBGE phylotypes were first reported from deep-sea sediments (Vetriani et al., 1999) and were detected in iron-rich habitats (Suzuki et al., 2004; Takai, 2008). The MCG phylotypes are one of the widely distributed groups of *Archaea* in deep-sea environments (Teske and Sørensen, 2008). Interestingly, a MCG phylotype (NCBI accession number, AB213054) was closely related to those detected in crustal fluids from the IODP borehole 1026B (AY181048; Cowen et al., 2003) and from the inserting pipes at the Baby Bare seamount (AY704375; Huber et al., 2006). This MCG phylotype is potentially an indigenous archaeal member in sub-seafloor crustal aquifers.

Archaeal communities have often been ignored in microbiological analysis of iron-rich mats. However, the archaeal abundance in the communities of the SMT is not so small (over 10%) and should

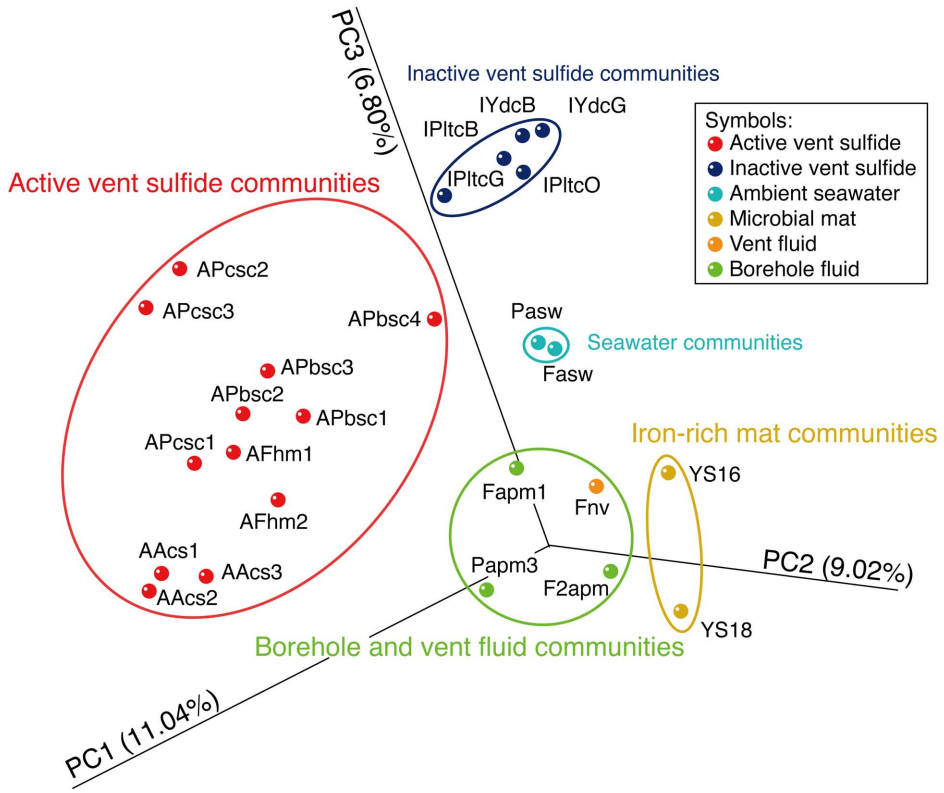

FIGURE 4 | Comparison of the bacterial community structures in the SMT habitats by principal coordination analysis. The used microbiological data are originated from our previous reports (Kato et al., 2009a,b, 2010). The principal coordination analysis was performed using Fast UniFrac (Hamady et al., 2009). Each axis (PC1-3) indicates the first, second, and third principal coordinates. The percentages in the axis labels represent the percentages of variation explained by the principal coordinates. AFhm1 and 2, sulfide mound venting 107°C fluid at the Snail site; AAcs1-3, clear smoker chimney venting 117°C fluid at the Archaean site; APbsc1-4, black smoker chimney venting 270°C fluid at the Pika site; APcsc1-4, clear smoker chimney venting 19°C fluid at the Pika site; IPltcB, G, and O, inactive chimney at Pika site; IYdcB, and G, inactive chimney at the Y site; Pasw, and Fasw, ambient seawater at the Pika and Snail sites, respectively; Fapm1 and F2apm, borehole fluids at the Snail site collected in 2004 and 2005, respectively; Papm3, borehole fluids at the Pika site; Fnv, natural vent fluid at the Snail site; YS16 and YS18, iron-rich mats at the Kaiko and Snail sites, respectively. The data from the Y and Kaiko sites are not mentioned in the present paper (please, see Kato et al., 2009a, 2010 for details).

Table 2 | Abundant taxonomic groups in the archaeal clone libraries for each habitat.

Habitat	Site	Temp range of venting fluids (°C)	Relative abundant group (potential chemolithoautotrophs)	Potential electron donor*	Growth temperature*
Active sulfide structure	Snail, Pika, Archaean	19–341	Archaeoglobi, Thermoprotei	Hydrogen	(Hyper)thermophiles
Deep seawater	Snail, Pika, Archaean	2–3	MGI	Ammonia	Psychrophiles
Borehole fluid	Snail, Pika	6–40	MBGE, MGI, pSL12-related	Iron (?), ammonia	Mesophiles (?)
Iron-rich mat	Snail	33–116	MBGE, MGI, pSL12-related	Iron (?), ammonia	Mesophiles (?)

**Based on the physiological characteristics inferred from the phylogeny of the phylotypes.*

not be ignored (Davis and Moyer, 2008; Kato et al., 2009a). It is possible that archaeal communities play significant role in elemental cycling of Fe, N, and C in iron-rich deep-sea environments, and in the maintenance of the microbial ecosystems. Further cultivation efforts are needed to determine the physiology of these uncultured archaeal groups and to understand their significance in microbial ecosystems and elemental cycling in deep-sea hydrothermal systems.

GEOCHEMICAL CONSTRAINTS SHAPING MICROBIAL COMMUNITY STRUCTURES

It has been proposed that fluid geochemistry constrains microbial community structures in deep-sea hydrothermal fields (McCollom and Shock, 1997). The available chemical energy for chemolithotrophs can be calculated thermodynamically for each metabolic reaction based on the geochemistry of hydrothermal fluids. To assess the relationship between microbial community

structures and geochemical composition of hydrothermal fluids in the SMT, we calculated the bioavailable energy yields of metabolic reactions (aerobic hydrogen-, methane-, sulfide-, ammonia- or iron-oxidation, methanogenesis, sulfate-, iron- or nitrate-reducing hydrogen-oxidation, and anaerobic methane-oxidation) for each type of hydrothermal fluid, and compared them to the inferred metabolic ability for each taxonomic group from their phylogeny (**Tables 1** and **2**).

The procedure for the thermodynamic calculation was previously described in detail (Takai and Nakamura, 2010). In brief, the amounts of chemical energy potentially available for chemolithotrophic metabolisms in hydrothermal fluid were determined by calculating the Gibbs free energy of each of the metabolic reactions. The overall Gibbs free energy of reaction can be calculated using the equation:

$$\Delta \mathrm{Gr} = \Delta \mathrm{Gr}^{\circ} + RT \ln Q \quad (1)$$

where ΔGr is the Gibbs free energy of reaction, $\Delta \mathrm{Gr}^{\circ}$ is the standard state Gibbs free energy of reaction, R is the universal gas constant, T is the temperature in Kelvin, and Q is the activity quotient of the compounds involved in the reaction. The Q term takes into account the contribution of the fluid composition to the Gibbs energy of each reaction. Chemical compositions of the hydrothermal fluids used for the calculation are (i) the measured data of the low-temperature fluids sampled and (ii) the calculated values for low-temperature fluids by mixing between end-member hydrothermal fluids and seawater. The mixing calculations were performed with the aid of the computer program EQ3/6, Version 8.0 (Wolery and Jarek, 2003). The thermodynamic database for the EQ3/6 operations and the values of the standard Gibbs energy for the chemolithotrophic metabolic reactions ($\Delta \mathrm{Gr}^{\circ}$) were generated using the SUPCRT92 code (Johnson et al., 1992) with a customized database.

For reproducing the conditions inside of sulfide structures of active vents, the bioavailable energy yields for the temperature range between 3 and 125°C were calculated (**Figure A2** in Appendix) using the geochemical data of high temperature hydrothermal fluids venting at the Pika and Archaean sites. We could not calculate the bioavailable energy yields for the Snail site because of lack of data for high temperature vent fluids in that site. In the calculation, simple mixing between hydrothermal fluid and seawater without any redox and mineral precipitation reactions was assumed (Takai and Nakamura, 2010). The results of the geochemical model calculations show that aerobic sulfide-oxidation yields the highest bioavailable energy under all temperature conditions (**Figure A2** in Appendix). This suggests that sulfide-oxidizers using O_2 and NO_3^- as electron acceptors can dominate in sulfide structures of active vents at both the Pika and Archaean sites. Indeed, phylotypes related to the Epsilonproteobacteria including aerobic sulfide-oxidizing chemolithoautotrophs (e.g., *Sulfurimonas*) were dominant in the libraries from the active chimneys from the Pika and Archaean sites (**Table 1**). This implies that the high-potentials of the energy availability from sulfide-oxidation reactions affect the relative abundance of these sulfide-oxidizing chemolithoautotrophs in bacterial communities in sulfide structures of active vents. The geochemical modeling results also suggest that iron-oxidation reactions produce the second largest amount of bioavailable energy. In the active chimney samples, however, none of the known iron-oxidizing chemolithoautotrophs was detected. This may suggest that the uncultured phylotypes detected in the sulfide structures contain unknown iron-oxidizers.

To assess the geochemical conditions of the relatively low-temperature (<150°C) fluids for chemolithoautotrophic microorganisms at the Pika, Archaean and Snail sites, the bioavailable energy yields were also calculated using the observed chemical data of the low-temperature shimmering fluids from the vent sites. The calculated bioavailable energy yields show that sulfide-oxidation reactions can produce higher bioavailable energy than other metabolic reactions (**Figures 5A,E,F,H**), except the Archaean site where hydrogen- and methane-oxidizing reactions yield higher bioavailable energy than sulfide-oxidation reactions (**Figure 5G**). The results are generally consistent with those estimated for vent fluids from active sulfide structures (**Figure A2** in Appendix). Regarding the 75–115°C vent fluids of the Archaean site (**Figure 5G**), the bioavailable energy yields from aerobic and anaerobic hydrogen-oxidation reactions are slightly higher than those values estimated for active sulfide structures (**Figure A2** in Appendix) due to relatively high H_2 concentrations of the low-temperature shimmering fluids (comparable to high temperature fluids). Although the hydrogen concentration of the Archaean vent fluids would be variable and fortuitously fluctuating by phase separation and subsequent sub-seafloor mixing, the geochemical modeling result is generally consistent with microbiological observations that putative (hyper)thermophilic hydrogen-oxidizing chemolithoautotrophs belonging to both domains Bacteria (e.g., *Hydrogenimonas*) and Archaea (e.g., Archaeoglobi) were detected in the Archaean site.

It should be noted that the bioavailable energy yields for iron-oxidation in the borehole fluid and high Fe/H_2S vent fluids (i.e., "Fe-type fluids") in the Snail site may be comparable to or higher than those for sulfide-oxidation (**Figures 5B,D**). The result is quite different from those estimated by a simple mixing model of high temperature hydrothermal fluids and seawater (**Figure A2** in Appendix) and those calculated using the observed chemical data of the other low-temperature shimmering fluids (**Figures 5A,C,E–H**). This leads us to propose that there are habitats of iron-oxidizers where bioavailable energy yields from iron-oxidation reactions may be preferable for chemolithoautotrophs compared to those from sulfide-oxidation reactions. Indeed, the phylotypes related to the Zetaproteobacteria including an iron-oxidizing chemolithoautotroph (*M. ferrooxydans*) were abundant in the iron-rich mats accompanied by Fe-type vent fluids and the borehole fluids in the SMT (**Table 1**; Kato et al., 2009a,b). This microbiological result is consistent with the geochemical–thermodynamic result showing the presence of habitats with relatively high bioavailable energy yields for iron-oxidation in the Snail site. The same putative iron-oxidizers were also detected in borehole fluid from the Pika site. Although H_2S and H_2 concentration data for the Pika borehole fluid are not available and thus bioavailable energy yields for hydrogen- and sulfide-oxidation reactions cannot be calculated, Fe-rich, and H_2S-depleted fluids similar to that observed in the Snail site are expected for the Pika

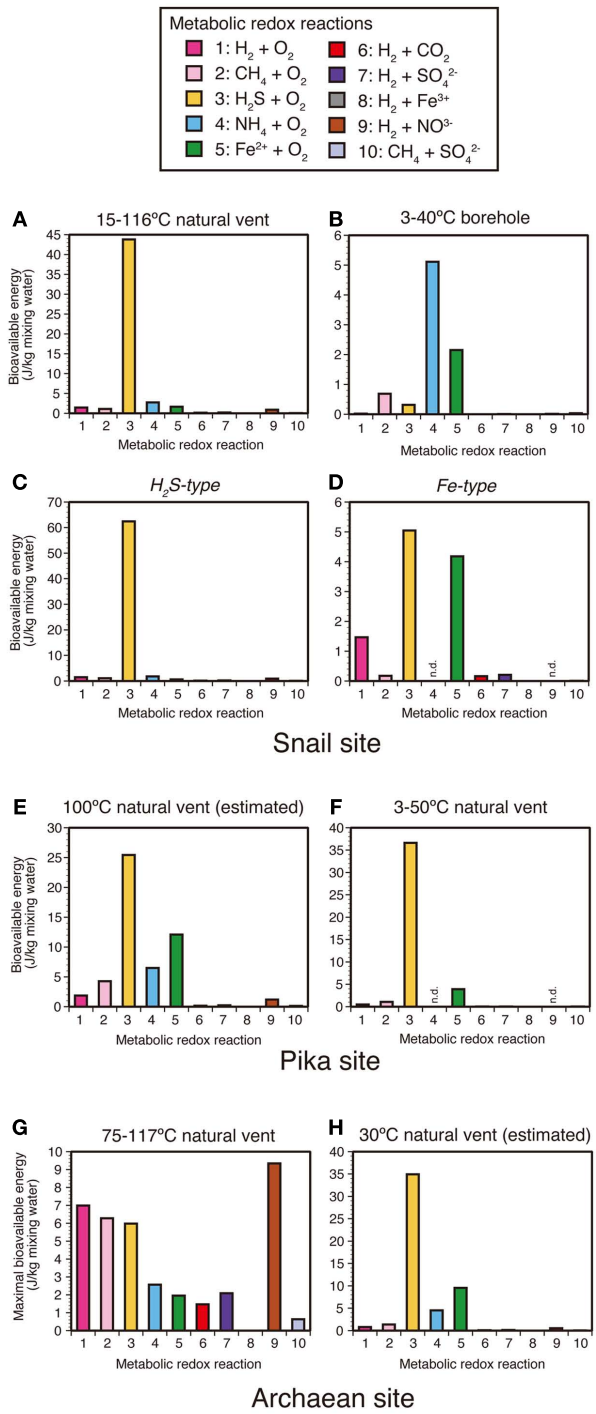

FIGURE 5 | Bioavailable energy yields for metabolic redox reactions for each sample type. For the Snail site, the energy yields result from **(A)** 15–116°C natural vent, **(B)** 3–40°C borehole, **(C)** H_2S-type, and **(D)** Fe-type fluids. For the Pika site, the energy yields result from **(E)** 100°C natural vent and **(F)** 3–50°C natural vent fluids. For the Archaean site, the energy yields result from **(G)** 75–117°C natural vent and **(H)** 30°C natural vent fluids. The bioavailable energy yields for **(E)** 100°C natural vent in the Pika site and for **(H)** 30°C natural vent in the Archaean site were calculated using the geochemical data estimated from a simple mixing model of hydrothermal fluids and seawater.

borehole. Massive iron-rich mats harboring the Zetaproteobacteria were found in other hydrothermal fields, such as on arc volcanoes (Forget et al., 2010), hot-spot volcanoes (Rassa et al., 2009), and mid-ocean ridges (Davis et al., 2009). Furthermore, the phylotypes related to the Zetaproteobacteria were detected in the basaltic oceanic rocks (Santelli et al., 2008). Bach and Edwards (2003) have suggested that oxidation of reduced iron contained in the basaltic oceanic crust can provide energy for chemosynthetic ecosystems, which is corresponding to $\sim 2 \times 10^{11}$ g cellular carbon/year as estimated by thermodynamic calculation. More detailed geochemical–microbiological characterization will provide insight into the relationship between the bioavailable energy yields by iron-oxidation and the abundance and distribution of the Zetaproteobacteria on and below the seafloor.

As shown above, assuming that the vent fluids were simply generated by mixing of end-member hydrothermal fluids with seawater, sulfide-oxidation yields the high energy for chemolithotrophs at all temperature ranges in the SMT hydrothermal fields (**Figure A2** in Appendix). However, in fact, our thermodynamic calculations using the actual geochemical data indicate the presence of habitats in the Snail site where relatively high energy yields are available from iron-oxidation rather than sulfide- and hydrogen-oxidation. This discrepancy between the observation and theoretical expectation may result in part from incomplete modeling of the geochemical composition of the venting fluids as mentioned previously (Amend et al., 2011); for example, residence time, mineral depositions, and/or microbial metabolisms can influence the geochemistry of actual vent fluids, especially for low-temperature shimmering fluids that are likely to migrate in the crust at a slow rate. In the Snail site, many diffuse flows from cracks of the seafloor basalts were observed (**Figure 1C**), while no black smoker chimneys were found. In addition, pyrites (FeS_2) were found in the fractures and vesicles of the sub-seafloor basalts collected by drilling (Kato et al., 2009b). These facts suggest that upwelling hydrothermal fluids are gradually mixed and cooled in the shallow sub-seafloor environments pervaded with the penetrating seawater and then iron and sulfide in the fluids are precipitated as pyrite. Depending on the end-member concentrations of Fe and H_2S, the sub-seafloor mixing, and subsequent pyrite precipitation may result in the presence of high Fe/H_2S low-temperature fluids. However, so far we have not determined the end-member concentrations of iron and sulfide because of lack of high temperature vent fluids in the Snail site. Further investigations are needed to assess the model of the generation of the Fe-type fluids.

It is remarkable that ammonia-oxidation yields the highest bioavailable energy for the borehole fluid in the Snail site followed by iron-oxidation (**Figure 5B**), although the bioavailable energy yields for the borehole fluid in the Pika site could not be calculated due to incomplete geochemical data (**Table A1** in Appendix). Archaea accounted for 27–58% of the total cell number in the borehole fluids (Kato et al., 2009b), and putative ammonia-oxidizers, such as MGI and pSL12-related group, were detected in the borehole fluids (**Table 2**). This may be comparable to or higher than the result that Zetaproteobacteria accounted for 6–32% in the borehole fluids (Kato et al., 2009b) and is consistent with the thermodynamic calculation results: considerable numbers of putative

ammonia-oxidizers as well as putative iron-oxidizers are expected to be present in the borehole fluids.

MODEL OF THE APPEARANCE OF THE MICROBIAL COMMUNITY STRUCTURES IN THE SMT

Considering the inferred metabolic functions of the abundant phylotypes in each library from the samples as described above (**Tables 1** and **2**), it seems that the microbial community structures observed in the SMT hydrothermal fields are constrained by the energy availability of the fluids. We propose a model for the appearance of the microbial community structures in the SMT based on the results of microbiological, geochemical, and thermodynamic analyses (**Figure 6**). Although this model is mainly based on the results from the Snail site, our results from the Pika and Archaean sites can partially fit this model (e.g., the detection of putative sulfide-oxidizers in the active sulfide structures in the Pika and Archaean sites and that of putative iron- and ammonia-oxidizers in the borehole fluids in Pika site).

Upwelling high temperature hydrothermal fluids discharged from vents rapidly react with seawater, and lead to the precipitation of metal sulfides, which results in the formation of the chimney- or mound-like structures on the seafloor. Sequentially, hydrothermal fluids are mixed with seawater within the wall of the sulfide structures, which leads to the occurrence of steep chemical disequilibria. In such environments, hydrogen, and sulfide-oxidation reactions yield high bioavailable energy, and accordingly hydrogen-oxidizers and sulfide-oxidizers may be relatively abundant in the microbial communities.

In contrast, a portion of the upwelling hydrothermal fluids can permeate into porous basaltic pillow lava. The hydrothermal fluids may be gradually mixed and cooled in the shallow sub-seafloor environments pervaded with the penetrating seawater and then iron and sulfide in the fluids may be precipitated as pyrite. This sub-seafloor process would generate "Fe-type fluids." In the Fe-type fluids, iron-oxidation yields high bioavailable energy, and accordingly, iron-oxidizers can dominate in the microbial communities as observed in the borehole fluids and iron-rich mats.

CONCLUSION AND PERSPECTIVE

In this paper, we summarized the microbial community structures in various habitats in the SMT. These findings highlight the uniqueness of the microbial communities in each habitat. On the whole, the results of thermodynamic calculations using the actual geochemical data are consistent with the presence/absence of each chemolithoautotroph in the microbial communities. The high bioavailable energy yield of iron-oxidation in the borehole and several vent fluids may be related to the appearance of microbial communities with abundant Zetaproteobacteria (putative iron-oxidizing chemolithoautotrophs), i.e., the iron-based

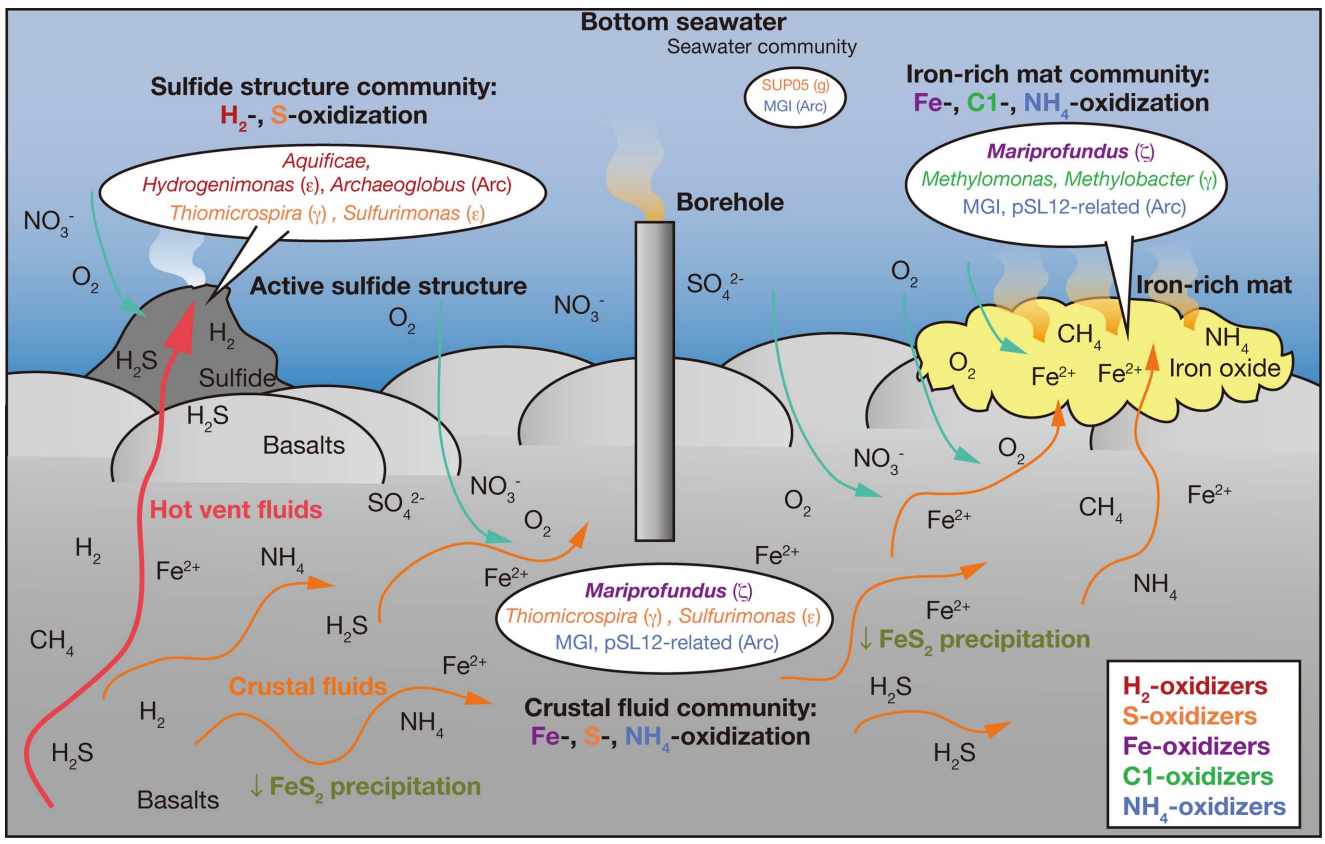

FIGURE 6 | A model for the appearance of the microbial community structures in each habitat in the SMT. This model is based on the microbiological and geochemical characteristics in the Snail site.

ecosystem, in such environments. Based on the microbiological–geochemical–thermodynamic results, a model for the appearance of the microbial community structures in the SMT is proposed. It should be noted that the molecular microbiological methods we used mainly targeted DNA extracted from environmental samples and have some shortcomings (Wintzingerode et al., 1997). Firstly, we cannot determine whether the detected phylotypes are active in the environments or not. RNA-based analysis (such as reverse transcript PCR and FISH) can identify active members thriving in environments. Secondly, the physiologies of the phylotypes cannot be directly determined from the phylogeny. We believe that the diverse phylotypes in the Zetaproteobacteria include iron-oxidizing chemolithoautotrophs, although this must be verified by culture-dependent analyses. As shown here, the thermodynamic modeling by simple mixing of hydrothermal fluids with seawater is a powerful tool for predicting the microbial community structures in active chimneys where the mixing of hydrothermal fluids with seawater occurs immediately (Takai and Nakamura, 2010; Amend et al., 2011). Further careful calculations accompanied by other factors such as mineral precipitation will provide more helpful information for understanding the mechanisms shaping the microbial community structures in global deep-sea hydrothermal systems.

ACKNOWLEDGMENTS

We thank all of the crew, the operation team and scientists joining the YK03-05, TN167A, YK05-09, YK10-10, and YK10-13 cruises for their cooperation. This research was funded by the Ministry of Education, Culture, Science, and Technology (MEXT), Japan, through a special coordination fund (Project TAIGA: Trans-crustal Advection and *In situ* biogeochemical processes of Global subseafloor Aquifer) and partly by the RIKEN Special Postdoctoral Researchers Program.

REFERENCES

Amend, J. P., McCollom, T. M., Hentscher, M., and Bach, W. (2011). Catabolic and anabolic energy for chemolithoautotrophs in deep-sea hydrothermal systems hosted in different rock types. *Geochim. Cosmochim. Acta* 75, 5736–5748.

Bach, W., and Edwards, K. J. (2003). Iron and sulfide oxidation within the basaltic ocean crust: implications for chemolithoautotrophic microbial biomass production. *Geochim. Cosmochim. Acta* 67, 3871–3887.

Chan, C. S., Fakra, S. C., Emerson, D., Fleming, E. J., and Edwards, K. J. (2011). Lithotrophic iron-oxidizing bacteria produce organic stalks to control mineral growth: implications for biosignature formation. *ISME J.* 5, 717–727.

Cowen, J., Giovannoni, S., Kenig, F., Johnson, H., Butterfield, D., Rappé, M., Hutnak, M., and Lam, P. (2003). Fluids from aging ocean crust that support microbial life. *Science* 299, 120–123.

Davis, R., and Moyer, C. (2008). Extreme spatial and temporal variability of hydrothermal microbial mat communities along the Mariana island arc and Southern Mariana back-arc system. *J. Geophys. Res.* 113, B08S15.

Davis, R. E., Stakes, D. S., Wheat, C. G., and Moyer, C. L. (2009). Bacterial variability within an iron-silica-manganese-rich hydrothermal mound located off-axis at the Cleft Segment, Juan de Fuca Ridge. *Geomicrobiol. J.* 26, 570–580.

Edwards, K. J., Bach, W., and Rogers, D. R. (2003). Geomicrobiology of the ocean crust: a role for chemoautotrophic Fe-bacteria. *Biol. Bull.* 204, 180–185.

Emerson, D., and Moyer, C. L. (2002). Neutrophilic Fe-oxidizing bacteria are abundant at the Loihi seamount hydrothermal vents and play a major role in Fe oxide deposition. *Appl. Environ. Microbiol.* 68, 3085–3093.

Emerson, D., Rentz, J. A., Lilburn, T. G., Davis, R. E., Aldrich, H., Chan, C., and Moyer, C. L. (2007). A novel lineage of proteobacteria involved in formation of marine Fe-oxidizing microbial mat communities. *PLoS ONE* 2, e667. doi:610.1371/journal.pone.0000667

Forget, N. L., Murdock, S. A., and Juniper, S. K. (2010). Bacterial diversity in Fe-rich hydrothermal sediments at two South Tonga Arc submarine volcanoes. *Geobiology* 8, 417–432.

Fryer, P. (1995). "Geology of the Mariana Trough," in *Backarc Basins: Tectonics and Magmatism*, ed. B. Taylor (New York: Plenum Press), 237–279.

Fuhrman, M., McCallum, K., Davis, A. A. (1992). Novel major archaebacterial group from marine plankton. *Nature* 356, 148–149.

Hamady, M., Lozupone, C., and Knight, R. (2009). Fast Unifrac: facilitating high-throughput phylogenetic analyses of microbial communities including analysis of pyrosequencing and phylochip data. *ISME J.* 4, 17–27.

Huber, J. A., Johnson, H. P., Butterfield, D. A., and Baross, J. A. (2006). Microbial life in ridge flank crustal fluids. *Environ. Microbiol.* 8, 88–99.

Ishibashi, J., Suzuki, R., Yamanaka, T., Toki, T., Kimura, H., Noguchi, T., and Urabe, T. (2006). Seafloor hydrothermal activity at off-axial seamounts of backarc spreading in Southern Mariana Trough. *Geochim. Cosmochim. Acta* 70, A279.

Ishibashi, J., and Urabe, T. (1995). "Hydrothermal activity related to arc-backarc magmatism in the western Pacific," in *Backarc Basins: Tectonics and Magmatism*, ed. B. Taylor (New York: Plenum Press), 451–495.

Ishibashi, J., Yamanaka, T., Kimura, H., Hirota, A., Toki, T., Tsunogai, U., Gamo, T., Utsumi, M., Roe, K., and Miyabe, S. (2004). "Geochemistry of hydrothermal fluids in South Mariana backarc spreading center," in *American Geophysical Union, Fall Meeting 2004*, San Francisco, abstr. #V44A-05.

Jannasch, H. W., and Mottl, M. J. (1985). Geomicrobiology of deep-sea hydrothermal vents. *Science* 229, 717–725.

Johnson, J. W., Oelkers, E. H., and Helgeson, H. C. (1992). SUPCRT92: a software package for calculating the standard molal thermodynamic properties of minerals, gases, aqueous species, and reactions from 1 to 5000 bar and 0 to 1000°C. *Comput. Geosci.* 18, 899–947.

Kakegawa, T., Utsumi, M., and Marumo, K. (2008). Geochemistry of sulfide chimneys and basement pillow lavas at the Southern Mariana Trough (12.55°N-12.58°N). *Resour. Geol.* 58, 249–266.

Kato, S., Kobayashi, C., Kakegawa, T., and Yamagishi, A. (2009a). Microbial communities in iron-silica-rich microbial mats at deep-sea hydrothermal fields of the Southern Mariana Trough. *Environ. Microbiol.* 11, 2094–2111.

Kato, S., Yanagawa, K., Sunamura, M., Takano, Y., Ishibashi, J., Kakegawa, T., Utsumi, M., Yamanaka, T., Toki, T., Noguchi, T., Kobayashi, K., Moroi, A., Kimura, H., Kawarabayasi, Y., Marumo, K., Urabe, T., and Yamagishi, A. (2009b). Abundance of Zetaproteobacteria within crustal fluids in back-arc hydrothermal fields of the Southern Mariana Trough. *Environ. Microbiol.* 11, 3210–3222.

Kato, S., Takano, Y., Kakegawa, T., Oba, H., Inoue, K., Kobayashi, C., Utsumi, M., Marumo, K., Kobayashi, K., Ito, Y., Ishibashi, J., and Yamagishi, A. (2010). Biogeography and biodiversity in sulfide structures of active and inactive vents at deep-sea hydrothermal fields of the Southern Mariana Trough. *Appl. Environ. Microbiol.* 76, 2968–2979.

Könneke, M., Bernhard, A. E., De La Torre, J. R., Walker, C. B., Waterbury, J. B., and Stahl, D. A. (2005). Isolation of an autotrophic ammonia-oxidizing marine archaeon. *Nature* 437, 543–546.

Marumo, K., Urabe, T., Goto, A., Takano, Y., and Nakaseama, M. (2008). Mineralogy and isotope geochemistry of active submarine hydrothermal field at Suiyo Seamount, Izu–Bonin Arc, west Pacific Ocean. *Resour. Geol.* 58, 220–248.

McAllister, S. M., Davis, R. E., McBeth, J. M., Tebo, B. M., Emerson, D., and Moyer, C. L. (2011). Biodiversity and emerging biogeography of the neutrophilic iron-oxidizing Zetaproteobacteria. *Appl. Environ. Microbiol.* 77, 5445–5457.

McCollom, T. M. (2007). Geochemical constraints on sources of metabolic energy for chemolithoautotrophy in ultramafic-hosted deep-sea hydrothermal systems. *Astrobiology* 7, 933–950.

McCollom, T. M., and Shock, E. L. (1997). Geochemical constraints on chemolithoautotrophic metabolism by microorganisms in seafloor hydrothermal systems. *Geochim. Cosmochim. Acta* 61, 4375–4391.

Mincer, T. J., Church, M. J., Taylor, L. T., Preston, C., Karl, D. M., and Delong, E. F. (2007). Quantitative distribution of presumptive archaeal and bacterial nitrifiers in Monterey Bay and the North Pacific

Subtropical Gyre. *Environ. Microbiol.* 9, 1162–1175.

Nakagawa, S., and Takai, K. (2008). Deep-sea vent chemoautotrophs: diversity, biochemistry and ecological significance. *FEMS Microbiol. Ecol.* 65, 1–14.

Orcutt, B. N., Sylvan, J. B., Knab, N. J., and Edwards, K. J. (2011). Microbial ecology of the dark ocean above, at, and below the seafloor. *Microbiol. Mol. Biol. Rev.* 75, 361–422.

Rassa, A. C., McAllister, S. M., Safran, S. A., and Moyer, C. L. (2009). Zeta-proteobacteria dominate the colonization and formation of microbial mats in low-temperature hydrothermal vents at Loihi Seamount, Hawaii. *Geomicrobiol. J.* 26, 623–638.

Santelli, C. M., Orcutt, B. N., Banning, E., Bach, W., Moyer, C. L., Sogin, M. L., Staudigel, H., and Edwards, K. J. (2008). Abundance and diversity of microbial life in ocean crust. *Nature* 453, 653–656.

Singer, E., Emerson, D., Webb, E. A., Barco, R. A., Kuenen, J. G., Nelson, W. C., Chan, C. S., Comolli, L. R., Ferriera, S., Johnson, J., Heidelberg, J. F., and Edwards, K. J. (2011). *Mariprofundus ferrooxydans* PV-1 the first genome of a marine Fe(II) oxidizing zetaproteobacterium. *PLoS ONE* 6, e25386. doi:10.1371/journal.pone.0025386

Sunamura, M., Higashi, Y., Miyako, C., Ishibashi, J., and Maruyama, A. (2004). Two bacteria phylotypes are predominant in the Suiyo Seamount hydrothermal plume. *Appl. Environ. Microbiol.* 70, 1190–1198.

Suzuki, Y., Inagaki, F., Takai, K., Nealson, K. H., and Horikoshi, K. (2004). Microbial diversity in inactive chimney structures from deep-sea hydrothermal systems. *Microb. Ecol.* 47, 186–196.

Takai, K. (2008). Variability in the microbial communities and hydrothermal fluid chemistry at the newly discovered mariner hydrothermal field, Southern Lau Basin. *J. Geophys. Res.* 113.

Takai, K., Nakagawa, S., Reysenbach, A. L., and Hoek, J. (2006). Microbial ecology of mid-ocean ridges and back-arc basins. *Geophys. Monogr.* 166, 185–213.

Takai, K., and Nakamura, K. (2010). "Compositional, physiological and metabolic variability in microbial communities associated with geochemically diverse, deep-sea hydrothermal vent fluids," in *Geomicrobiology: Molecular and Environmental Perspective*, eds L. L. Barton, M. Mandl, and A. Loy (Dordrecht: Springer), 251–283.

Takai, K., Nunoura, T., Ishibashi, J.-I., Lupton, J., Suzuki, R., Hamasaki, H., Ueno, Y., Kawagucci, S., Gamo, T., Suzuki, Y., Hirayama, H., and Horikoshi, K. (2008). Variability in the microbial communities and hydrothermal fluid chemistry at the newly discovered mariner hydrothermal field, Southern Lau Basin. *J. Geophys. Res.* 113, G02031.

Teske, A., and Sørensen, K. B. (2008). Uncultured archaea in deep marine subsurface sediments: have we caught them all? *ISME J.* 2, 3–18.

Toki, T., Tsunogai, U., Ishibashi, J., Utsumi, M., and Gamo, T. (2008). Methane enrichment in low-temperature hydrothermal fluids from the Suiyo Seamount in the Izu-Bonin Arc of the western Pacific Ocean. *J. Geophys. Res.* 113, B08S13.

Vetriani, C., Jannasch, H. W., Macgregor, B. J., Stahl, D. A., and Reysenbach, A.-L. (1999). Population structure and phylogenetic characterization of marine benthic archaea in deep-sea sediments. *Appl. Environ. Microbiol.* 65, 4375–4384.

Von Damm, K. L., Bischoff, J. L., and Rosenbauer, R. J. (1991). Quartz solubility in hydrothermal seawater; an experimental study and equation describing quartz solubility for up to 0.5 m NaCl solutions. *Am. J. Sci.* 291, 977–1007.

Von Damm, K. L., Edmond, J. M., Grant, B., Measures, C. I., Walden, B., and Weiss, R. F. (1985). Chemistry of submarine hydrothermal solutions at 21°N, East Pacific Rise. *Geochim. Cosmochim. Acta* 49, 2197–2220.

Walsh, D. A., Zaikova, E., Howes, C. G., Song, Y. C., Wright, J. J., Tringe, S. G., Tortell, P. D., and Hallam, S. J. (2009). Metagenome of a versatile chemolithoautotroph from expanding oceanic dead zones. *Science* 326, 578–582.

Wheat, C. G., Fryer, P., Hulme, S., Becker, N., Curtis, A., and Moyer, C. (2003). "Hydrothermal venting in the southern most portion of the mariana backarc spreading center at 12.57 degrees N," in *American Geophysical Union, Fall Meeting 2004*, San Francisco, abstr. T32A-0920.

Wintzingerode, F., Gobel, U. B., and Stackebrandt, E. (1997). Determination of microbial diversity in environmental samples: pitfalls of PCR-based rRNA analysis. *FEMS Microbiol. Rev.* 21, 213–229.

Wolery, T. W., and Jarek, R. L. (2003). *Software User's Manual. EQ3/6, Version 8.0.* U.S. Department of Energy Report 10813-UM-8.0-00, Albuquerque, NM: Sandia National Laboratories, 376.

Conflict of Interest Statement: The authors declare that the research was conducted in the absence of any commercial or financial relationships that could be construed as a potential conflict of interest.

Received: 31 October 2011; accepted: 22 February 2012; published online: 15 March 2012.

Citation: Kato S, Nakamura K, Toki T, Ishibashi J-i, Tsunogai U, Hirota A, Ohkuma M and Yamagishi A (2012) Iron-based microbial ecosystem on and below the seafloor: a case study of hydrothermal fields of the Southern Mariana Trough. Front. Microbio. ***3****:89. doi: 10.3389/fmicb.2012.00089*

This article was submitted to Frontiers in Microbiological Chemistry, a specialty of Frontiers in Microbiology.

Copyright © 2012 Kato, Nakamura, Toki, Ishibashi, Tsunogai, Hirota, Ohkuma and Yamagishi. This is an open-access article distributed under the terms of the Creative Commons Attribution Non Commercial License, which permits non-commercial use, distribution, and reproduction in other forums, provided the original authors and source are credited.

APPENDIX

Table A1 | Summary of the geochemical characteristics of fluid samples collected in the SMT.

Sampling site	Snail (2861 m)					Pika (2773 m)		Archaean (2986 m)		Deep seawater
Sample type	Borehole	Natural vent	*Fe–H_2S available**		Borehole	Natural vent		Natural vent		
			H_2S-type	***Fe-type***		**<150°C**	**>150°C**	**<150°C**	**>150°C**	
T ave.	25	55	*54*	*41*	10	28	265	101	251	3
(Range; °C)	(3–40)	(15–116)	*(15–81)*	*(18–59)*		(3–50)	(230–330)	(75–117)	(153–343)	
pH	6.69	6.65	*5.85*	*6.38*	7.57	6.59	3.33	5.61	3.60	7.73
Alk. (meq)	2.22	2.09	*2.16*	*1.94*	2.37	2.28	−0.95	0.95	−0.63	2.48
Mg (mM)	46.2	45.6	*40.9*	*45.5*	50.0	49.8	8.5	41.3	13.3	50.8
Ca (mM)	10.7	11.2	*12.9*	*11.1*	9.7	10.2	34.4	10.7	16.0	9.6
Sr (μM)	85.0	89.7	*82.4*	*91.6*	83.5	87.5	123	100	102	84.8
Na (mM)	460	455	*450*	*463*	469	460	457	424	370	457
K (mM)	10.8	11.4	*13.0*	*11.7*	9.7	9.7	24.9	13.5	25.6	9.6
Li (mM)	0.046	0.076	*0.118*	*0.081*	0.028	0.044	0.530	0.158	0.391	0.033
B (μM)	388	401	*353*	*481*	n.d.	362	695	524	984	375
C1 (mM)	540	545	*542*	*539*	n.d.	548	576	533	461	542
Br (mM)	0.85	0.85	*0.83*	*0.85*	0.84	0.84	0.93	n.d.	0.77	0.86
SO_4 (mM)	25.3	25.0	*22.9*	*23.9*	25.7	26.9	3.5	23.0	7.6	27.4
Si (mM)	1.05	1.60	*2.98*	*1.97*	0.21	0.49	14.2	3.47	12.6	0.17
NH_4 (μM)	14.3	7.9	*5.2*	*7.3*	n.d.	3.5	36.3	8.4	31.1	11.0
NO_3 (μM)	4.4	13.2	*2.8*	*0.0*	n.d.	25.1	6.8	20.7	8.3	33.8
H_2S (μM)	0.41	57.1	*229*	*6.6*	n.d.	34.6	6001	572	4313	0.04
Mn (mM)	0.15	0.23	*0.32*	*0.20*	0.12	0.02	0.99	0.23	0.89	0.0018
Fe (μM)	62.4	57.0	*19.5*	*119*	115	82.8	6494	244	2056	8.9
Ba (μM)	1.67	22.1	*n.d.*	*33.4*	n.d.	4.60	46.2	44.7	40.2	1.66
O_2 (μM)	286	164	*n.d. (164)*		n.d.	98	18	16	18	100**
N_2 (μM)	1630	1771	*n.d.*	*n.d.*	n.d.	n.d.	1099	1358	967	n.d.
CO_2 (mM)	7.20	7.76	*n.d. (7.76)*	*3.11*	n.d.	8.42	36.2	16.8	16.6	2.3**
CH_4 (μM)	0.86	1.37	*n.d. (1.37)*	*0.22*	n.d.	1.46	14.9	20.9	15.8	0.0003**
H_2 (μM)	0.10	6.62	*n.d. (6.62)*		n.d.	0.69	23.8	67.8	33.2	0.0004**

*Average values for each sample type at each sampling site, i.e., boreholes, low-temperature (<150°C) natural vents and high temperature (>150°C) natural vents are shown. These data were obtained from the samples collected in 2003, 2004, 2005, and 2010. *The chemical data for the samples of the Snail site with iron and sulfide concentrations, which are shown in italic, were divided into H_2S-type (high H_2S/Fe) and Fe-type (high Fe/H_2S). For thermodynamic calculation, the average values in parentheses were used. **Concentrations of O_2, CO_2, CH_4, and H_2 in deep seawater were obtained previously (McCollom, 2007).*

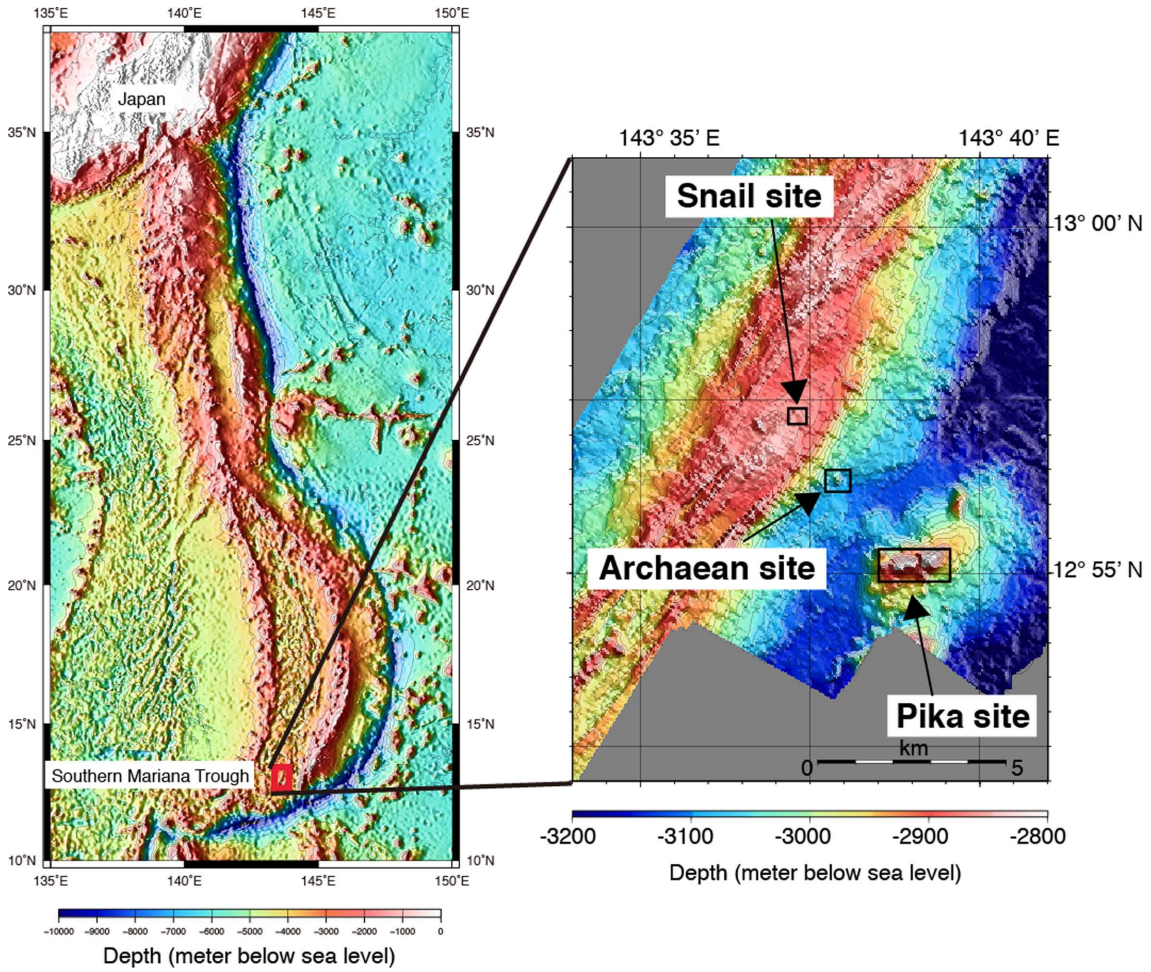

FIGURE A1 | (A) Topographic map of the Southern Mariana Trough with **(B)** an enlarged view of the hydrothermal areas.

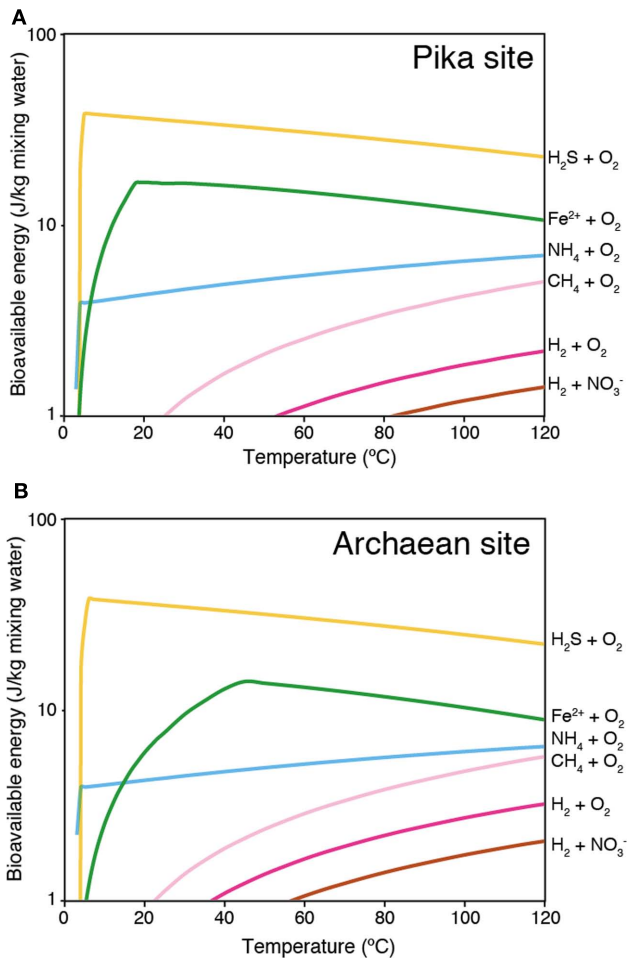

FIGURE A2 | Thermodynamic model calculation of bioavailable energy. Simple mixing between hydrothermal fluid and seawater without any redox and mineral precipitation reactions are assumed in the calculation. The results of **(A)** Pika and **(B)** Archaean sites are shown.

frontiers in
MICROBIOLOGY

ORIGINAL RESEARCH ARTICLE
published: 04 April 2012
doi: 10.3389/fmicb.2012.00134

Isolation of phyllosilicate–iron redox cycling microorganisms from an illite–smectite rich hydromorphic soil

Evgenya Shelobolina*, Hiromi Konishi, Huifang Xu, Jason Benzine, Mai Yia Xiong, Tao Wu, Marco Blöthe and Eric Roden

Department of Geoscience, University of Wisconsin–Madison, Madison, WI, USA

Edited by:
David Emerson, Bigelow Laboratory for Ocean Sciences, USA

Reviewed by:
Kirsten Küsel, Friedrich-Schiller-University Jena, Germany
Nicole Posth, University of Southern Denmark, Denmark

****Correspondence:***
Evgenya Shelobolina, Department of Geoscience, University of Wisconsin–Madison, 1215 West Dayton Street, Madison, WI 53706, USA.
e-mail: shelobolina@wisc.edu

The biogeochemistry of phyllosilicate–Fe redox cycling was studied in a *Phalaris arundinacea* (reed canary grass) dominated redoximorphic soil from Shovelers Sink, a small glacial depression near Madison, WI. The clay size fraction of Shovelers Sink soil accounts for 16% of the dry weight of the soil, yet contributes 74% of total Fe. The dominant mineral in the clay size fraction is mixed layer illite–smectite, and in contrast to many other soils and sediments, Fe(III) oxides are present in low abundance. We examined the Fe biogeochemistry of Shovelers Sink soils, estimated the abundance of Fe redox cycling microorganisms, and isolated in pure culture representative phyllosilicate–Fe oxidizing and reducing organisms. The abundance of phyllosilicate–Fe reducing and oxidizing organisms was low compared to culturable aerobic heterotrophs. Both direct isolation and dilution-to-extinction approaches using structural Fe(II) in Bancroft biotite as a Fe(II) source, and O_2 as the electron acceptor, resulted in recovery of common rhizosphere organisms including *Bradyrhizobium* spp. and strains of *Cupriavidus necator* and *Ralstonia solanacearum*. In addition to oxidizing biotite and soluble Fe(II) with O_2, each of these isolates was able to oxidize Fe(II) in reduced NAu-2 smectite with NO_3^- as the electron acceptor. Oxidized NAu-2 smectite or amorphous Fe(III) oxide served as electron acceptors for enrichment and isolation of Fe(III)-reducing microorganisms, resulting in recovery of a strain related to *Geobacter toluenoxydans*. The ability of the recovered microorganisms to cycle phyllosilicate–Fe was verified in an experiment with native Shovelers Sink clay. This study confirms that Fe in the native Shovelers Sink clay is readily available for microbial redox transformation and can be cycled by the Fe(III)-reducing and Fe(II)-oxidizing microorganisms recovered from the soil.

Keywords: smectite, phyllosilicate, Fe(III) reducing microorganisms, Fe(II) oxidizing microorganisms, neutrophilic, soil, hydromorphic, Shovelers Sink

INTRODUCTION

Clay size Fe-bearing phyllosilicate phases, along with Fe(III) hydroxides, play a central role in the Fe redox biogeochemistry in natural environments (Amonette, 2002). These two groups of Fe-bearing minerals have contrasting geochemical behavior. Reduction of Fe(III) hydroxides typically results in Fe(II) mobilization, with the potential for redistribution of Fe via diffusion/dispersion and pore fluid advection. In contrast, structural Fe in clay minerals can undergo multiple redox cycles without being mobilized, because Fe remains within the mineral structure and within the system (Dong et al., 2009; Stucki, 2011). Multiple Fe(III) hydroxide reducing and soluble Fe(II)-oxidizing organisms are available as model microbial agents (Lovley et al., 2004; Weber et al., 2006; Emerson et al., 2010; Schmidt et al., 2010; Konhauser et al., 2011). Much less is known about microorganisms involved in phyllosilicate–Fe redox cycling. When 10 Fe(III)-reducing organisms [enriched and isolated with Fe(III) hydroxide as the sole electron acceptor] were tested for growth on a model ferruginous smectite, only eight could reduce structural Fe(III) in the smectite (Kashefi et al., 2008). These findings suggest that phyllosilicate–Fe(III)-reducing and Fe(III) (hydr)oxide-reducing microbial populations may not always overlap. Even less is known about organisms capable of oxidizing structural Fe(II) in smectite. The only culture known to catalyze this reaction is a strain of *Desulfitobacterium hafniense* (formerly *D. frappieri*) isolated from a subsurface smectite bedding, which is capable of NO_3^--dependent structural Fe(II) oxidation (Shelobolina et al., 2003).

The coexistence and aggregation of Fe-bearing phyllosilicates and Fe(III) hydroxides makes it challenging to study the redox cycling of phyllosilicate–Fe in many soils and sediments. Certain non-highly weathered soils, however, may be enriched in phyllosilicates relative to Fe and Al oxides (Brady and Weil, 2008). The loess-derived silty clay loam deposits at Shovelers Sink, near Madison, WI, USA (Clayton and Attig, 1997; Bradbury, 2001) provide an excellent example of this type of soil environment. Shovelers Sink is a small, permanent, remnant glacial depression which originated as a proglacial lake fed by water draining off ice when glaciers covered the Madison area about 15,000 years ago (Clayton and Attig, 1997; Bradbury, 2001). At present Shovelers Sink is a wetland managed as a wildlife conservancy area. The dominant

plant species at Shovelers Sink is *Phalaris arundinacea* (reed canary grass, RCG), which forms a dense, up to 1 m deep root system that is tolerant to prolonged anoxia during times of soil saturation (Barclay and Crawford, 1983). The redoximorphic conditions and high abundance of Fe-bearing phyllosilicates relative to Fe(III) oxides makes Shovelers Sink an ideal setting to study the biogeochemistry of phyllosilicate–Fe redox cycling. The aim of this study was to characterize the biogeochemistry and mineralogy of Shovelers Sink soil, and to enumerate and isolate microorganisms capable of reducing or oxidizing phyllosilicate–Fe.

MATERIALS AND METHODS

STUDY SITE AND SAMPLE COLLECTION

Soil and groundwater samples were collected from Shovelers Sink site located in the Cross Plains unit of the Ice Age National Scientific Reserve, c.a. 50 m from Mineral Point Road and 17 m from the pond. Soils were collected (January 2007, July 2007, June 2008, and September 2009) with a stainless steel coring device. Fluid from below the water table was collected in 50-ml plastic tubes. Core sections were placed in sterile sample collection plastic bags and immediately delivered to the laboratory. All core sections were placed into an anaerobic chamber filled with N_2:H_2 mix (95:5), homogenized, and dispensed into serum bottles or pressure tubes for immediate experimentation, or into large Pyrex bottles with thick rubber stoppers for storage and/or later use. After removal from the anaerobic chamber, all bottles were flushed with O_2-free N_2 (passed over reduced, hot copper filings) to remove H_2 from the headspace. Soil water was filtered through a 0.2-μm syringe filter and frozen prior to analysis by ion chromatography.

SEPARATION AND ANALYSIS OF GRAIN SIZE FRACTIONS

Soils were size fractionated by wet-sieving and centrifugation (Jackson, 1969; Gee and Bauder, 1986). Wet-sieving was performed in the anaerobic chamber using water made anoxic by bubbling with N_2. 1000 ml Pyrex bottles containing 900 ml water each were bubbled for 2 h. No gravel size particles (>2 mm) were found in the materials. Sand (50 μm–2 mm) size materials were removed by sieving (USA Standard Testing Sieves, VWR Scientific). The remaining silt (2 μm–50 μm) and clay (<2 μm) grain size fractions were separated by centrifugation in sealed plastic bottles under N_2. The settling time for the clay size fraction was calculated for a particle density of 2.6 g/cm^3 using Stokes' Law. A small portion of each size fraction was used to determine the dry weight per unit volume of soil suspension. These subsamples were dried at 105°C and wet/dry sample weight factors were calculated from weight differences before and after drying.

Total Fe(II) and Fe(III) in the size fractions was determined by the hydrofluoric acid (HF) extraction followed by the 1,10-Phenanthroline assay as described by Stucki (1981) and modified by Komadel and Stucki (1988). Fe(III) oxyhydroxide contents were determined by citrate–bicarbonate–dithionite (CDB) extraction (Mehra and Jackson, 1980) and ferrozine analysis (Stookey, 1970). All Fe measurements were performed in triplicate. Organic carbon was measured with a Leco CHN analyzer at the UW–Madison Soil and Plant Analysis Laboratory.

DETERMINATION OF STEADY STATE H_2 CONCENTRATIONS

To determine steady state dissolved H_2 concentration in the porewater within representative soil samples, c.a. 30 g of each sample were placed into 60 ml serum bottles under an N_2 atmosphere. H_2 concentration in the headspace was monitored over time with a reduction gas analyzer (ta3000 Gas Analyzer, Trace Analytical, Ametek) until stability was reached.

TRANSMISSION ELECTRON MICROSCOPY

Transition electron microscopy (TEM) analyses were carried out using a FEI Titan 80–200 aberration corrected scanning/transmission electron microscope associated with an EDAX AMETEK high resolution energy-dispersive X-ray spectroscopy (EDS) detector and Gatan image filtering system, and operated at 200 kV. The samples were mixed with distilled water and ultrasonicated for ∼3 min. A drop of the resulting suspension was placed on a lacey-carbon coated Cu grid and air-dried.

X-RAY DIFFRACTION

X-ray diffraction (XRD) analyses were done using a Scintag Pad V Diffractometer with CuKα radiation. The instrument used an accelerating voltage of 45 kV, a current of 40 mA, a 2-mm divergence slit, 4-mm incident scatter slit, 1-mm diffracted beam scatter slit, and 0.5-mm receiving slit. Scan parameters used were a step size of 0.02° and a dwelling time of 2 s. Oriented aggregate mounts were prepared by pasting clay-DI water suspension on glass slides and air drying. A drop of ethylene glycol was added directly to the surface of the oriented clay mount with a glass rod for ethylene glycol treatment. Oriented aggregate mounts were heated at 550°C for 3 h in the furnace for heat treatment.

MOST PROBABLE NUMBER ANALYSIS

Microorganisms were enumerated by the most probable number (MPN) method (Woomer, 1994). Strict anaerobic laboratory technique (Miller and Wolin, 1974) was used to quantify anaerobic Fe(III)-reducing bacteria. An anaerobic basal bicarbonate-buffered freshwater (FW) medium (Lovley and Phillips, 1988) was dispensed into 27 ml anaerobic pressure tubes (Bellco Glass, Inc.) under N_2/CO_2 (80:20%). The tubes were capped with butyl rubber stoppers and sterilized by autoclaving. The medium for Fe(III)-reducing bacteria contained either 100 mM hydrous ferric oxide (HFO) or 0.8 weight% of the Fe(III)-bearing smectite NAu-2 [$M^+_{0.72}(Si_{7.55}Al_{0.45})Fe_{3.83}Mg_{0.05})O_{20}(OH)_4$ where M is the interlayer cation; Keeling et al., 2000] as a terminal electron acceptor, H_2 (3 ml filtered H_2 was added to the headspace) and acetate (10 mM) as the combined electron donor, and 1.3 mM $FeCl_2$ as a reducing agent. The medium for Fe(II)-oxidizing bacteria contained O_2 as the terminal electron acceptor (3 ml filtered air added to the headspace) and 1.1% Bancroft (Ward Scientific) biotite [$(K_{0.980}, Na_{0.025}; Fe^{2+}_{0.996}, Fe^{3+}_{0.222}Mg_{1.663}, Ti_{0.117}; Si_{3.048}, Al_{0.812}, Ti_{0.140})O_{10}(OH_{1.02}, F_{0.98})$] as a source of structural Fe(II). Aerobic heterotrophic bacteria were enumerated in medium containing (gram per liter) PIPES (piperazine-*N*,*N*′-bis-2-ethanesulfonic acid) buffer (3.0), NH_4Cl (0.25), $NaH_2PO_4{\cdot}H_2O$ (0.06), KCl (0.1), yeast extract (0.5), and acetate (0.41).

ISOLATION OF Fe(III)-REDUCING ORGANISMS

Smectite-containing MPN cultures were diluted in agarized medium containing 20 mM fumarate and 20 mM acetate with a roll-tube method (Hungate, 1968). An inoculum (1 ml) from the 10-fold serial dilutions of the enrichment culture in a liquid FW

medium was added to 27 ml pressure tubes containing 7 ml melted medium. The contents were mixed gently and the pressure tubes were rolled with a tube spinner. The roll-tubes were incubated vertically at room temperature. Individual colonies were transferred to the pressure tubes with 2 ml liquid FW medium containing 0.8% NAu-2 smectite as the electron acceptor and 10 mM acetate as the electron donor.

ISOLATION OF Fe(II)-OXIDIZING ORGANISMS

Freshly collected samples and highest positive MPN dilution cultures were serially diluted in biotite/O_2-containing roll-tubes. After orange and red colored individual colonies formed, they were transferred to the pressure tubes with 2 ml liquid FW medium containing 1.1% biotite and 3 ml filtered air. Biotite oxidizing cultures were serially diluted and plated on aerobic heterotrophic medium using 1.5% agar as the solidifying agent.

Biotite oxidizing cultures were tested for their ability to grow via microaerophilic $FeCl_2$ oxidation. The cultures were grown on a heterotrophic low-organic medium (0.01% yeast extract and 1 mM acetate, with 3 ml of filtered air in the headspace), and then transferred (5% vol/vol inoculum) to anoxic FW medium, to which 1.3 mM $FeCl_2$ and 1 ml filtered air were added via syringe and needle every other day. After 12 days of cultivation, cell numbers were determined. The aliquots of the culture were fixed with glutaraldehyde. The fixed culture was reacted with ammonium oxalate (28 g/l ammonium oxalate and 15 g/l oxalic acid) in the presence of ca. 1 mM $FeCl_2$ to dissolve Fe(III) hydroxides. Cells were counted by acridine orange staining and epifluorescence microscopy (Hobbie et al., 1977).

MOLECULAR BIOLOGICAL METHODS

The16S rRNA gene sequences of the isolates and enrichment cultures were obtained using standard methodologies as previously described (Shelobolina et al., 2007). 16S rRNA genes were amplified using GM3 and GM4 primer set (Muyzer et al., 1995). For enrichment cultures 16S rRNA genes were cloned using the pGEM-T vector (Promega). The 16S rRNA gene fragments were compared to the GenBank nucleotide database using BLASTN and BLASTX algorithms (Altschul et al., 1990).

Fe CYCLING EXPERIMENT

An iron cycling experiment was performed in FW medium supplemented with natural Shovelers Sink clay. The clay suspension was bubbled with air for 1 day to oxidize structural Fe(II), after which the clay was dried and mixed with FW medium prior to bubbling with N_2:CO_2 mix and autoclaving. XRD analysis of the clay before and after autoclaving showed no difference suggesting no change in the mineralogy of the clay (data not shown). A small amount of acetate (0.25 mM) was provided as a limited source of electron donor. Eighteen culture tubes were inoculated with *G. toluenoxidans* strain sa2 isolated from Shovelers Sink soil, and three tubes served as abiotic controls. Fe(III) reduction was allowed to proceed for 10 days. Five millimolar NO_3^- was then added to 12 tubes, and of these tubes nine were inoculated with Fe(II)-oxidizing isolates with three uninoculated tubes serving as controls. No nitrate or Fe(II)-oxidizing culture were added to three tubes in which Fe(III) reduction was allowed to proceed for the rest of the experiment. To evaluate the reaction of structural Fe(II) oxidation with nitrite, three remaining tubes with reduced Shovelers Sink clay were reacted with ca 2.0 mM nitrite.

Concentrations of 0.5 N HCl-extractable Fe(II), NO_3^-, and NO_2^- were monitored over time. One milliliter of the culture was centrifuged in the anaerobic chamber at 14 K rpm for 5 min. The supernatant was collected for NO_3^-/NO_2^- and dissolved Fe analysis. Samples for Fe analysis were acidified with HCl. The remaining solids were mixed with 0.5 N HCl and extracted for 24 h. Fe(II) in the HCl extracts was quantified using the ferrozine assay as previously described (Lovley and Phillips, 1986). Preliminary studies demonstrated that a 24-h 0.5 N HCl extraction released the same amount of Fe(II) from Shovelers Sink clay as HF extraction (Stucki, 1981). Note that this equivalence applies only to Fe(II), as only a small portion of structural Fe(III) is extracted by 0.5 N HCl (Shelobolina et al., 2004). NO_3^- and NO_2^- concentrations were measured with a Dionex DX-100 ion chromatograph equipped with a AS4-SC IonPac column. Dissolved Fe concentrations were determined by inductively coupled plasma-optical emission spectroscopy (ICP-OES).

RESULTS AND DISCUSSION

BIOGEOCHEMISTRY OF SHOVELERS SINK SOIL

The soil at Shovelers Sink represents a silt loam interspersed with RCG roots down to the depth of 105 cm (**Figure 1**). The depth of the water table ranged from 60 to 80 cm. Soils collected in July 2007 were characterized in detail, at which time the water table was located at c.a. 65 cm depth (**Figure 2**).

Organic carbon concentrations were highest within the main root zone above 55 cm (1.7–2.5%), intermediate in the vicinity of the water table (1.0–1.2%), and lowest below 80 cm (0.32–0.41%) where few, if any, RCG roots were present (**Figure 2B**). Total HF-extractable iron (**Figure 2C**) concentrations ranged between 196 and 333 mmol/kg and showed a trend opposite of that for organic carbon, with Fe concentrations being lowest (166–190 mmol/kg) above a depth of 55 cm, intermediate from the water table down to 105 cm (230–249 mmol/kg), and highest below 105 cm (333–337 mmol/kg). The fraction of total Fe present as Fe(II) was highly

FIGURE 1 | Photograph of Shovelers Sink soil collected in the vicinity of the water table in July 2007, revealing reduced (gray color), and oxidized (bright yellowish-brown colors) regions indicative of redoximorphic conditions. The bar is 1 cm.

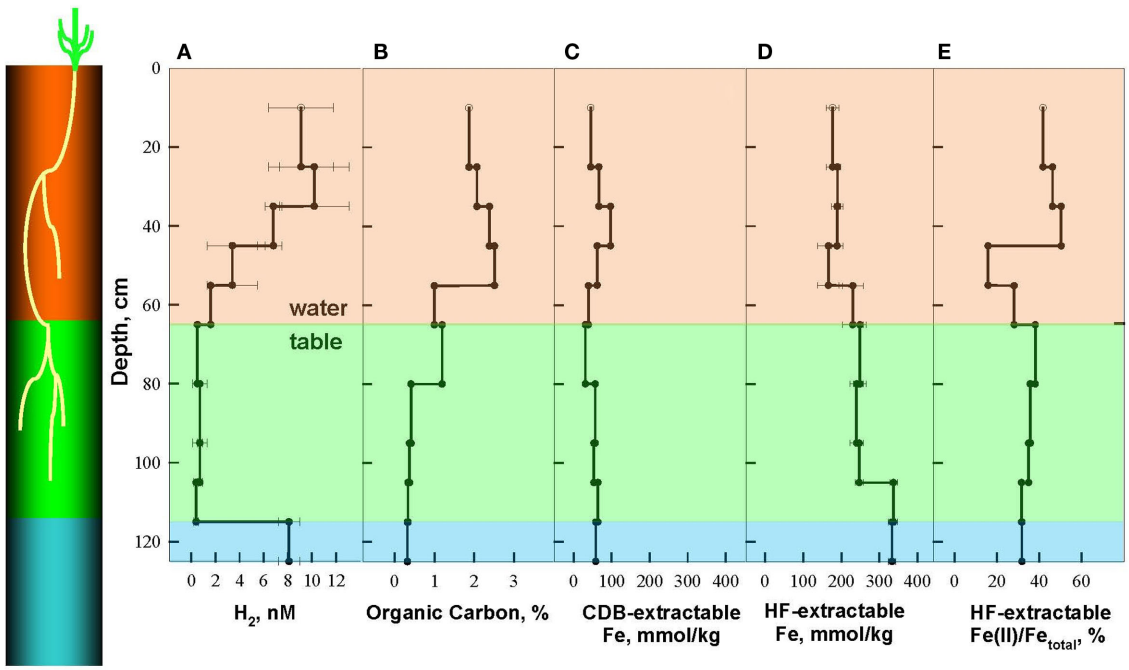

FIGURE 2 | Depth distribution of dissolved H_2 (A), Organic Carbon (B), and Fe phases, including citrate–bicarbonate –dithionite (CDB) extractable Fe (C), and hydrofluoric acid (HF) extractable Fe (D) and Fe(II)/Fe_{total} (E) in Shovelers Sink soil, July 2007. A cartoon on the left shows relative depth of root zone and terminal electron accepting processes (TEAPs): brown for mixed metabolism, green for Fe(III)-reducing zone, and blue for methanogenic zone.

variable above the water table (16–50%) and gradually decreased from 38 to 32% below the water table (**Figure 2D**).

The spatial segregation of terminal electron accepting processes in Shovelers Sink soil was assessed by measuring steady state concentration of dissolved H_2 in incubated soil samples from different depths, according to published criteria (Lovley and Goodwin, 1988; Lovley et al., 1994) and as described in a previous study of clay-rich subsurface sediments (Shelobolina et al., 2004; **Figure 2A**). Three TEAP zones could be distinguished: a mixed metabolism zone above the water table (0–65 cm depth) characterized by a range of H_2 concentrations from 1.6 to 10.2 nM; a dissimilatory Fe(III)-reducing zone between 65 and 115 cm characterized by H_2 concentrations of 0.4–0.7 nM; and a methanogenic zone below 115 cm with steady state H_2 concentration of 8.1 ± 0.9 nM.

Shovelers Sink is a depression in which water balance is maintained through direct precipitation and runoff from the surrounding landscape. Runoff from nearby farms and households could serve as an additional source of both organic carbon and electron acceptors, e.g., NO_3^-, to the system. However, no NO_3^- was detected in fluid from below the water table on any of the sampling events. These results suggest that the localized zones of oxidation observed in the soil (see **Figure 1**) are driven by release of O_2 from RGC roots, as is well-known for a variety of plants that proliferate in water-logged soils (Armstrong, 1978). The observed redoximorphic features (**Figure 1**) and porewater steady state H_2 concentrations (**Figure 2A**) suggest ongoing Fe redox cycling at two scales: (1) at the centimeter-to-decimeter scale within the transition from saturated/anoxic to unsaturated/partially oxic conditions in the vicinity of the water table; and (2) at the microscale around RCG roots both above and below the water table. Soil from the vicinity of the water table (c.a. 65 depth depth in July 2007) was chosen to study microbial Fe redox cycling as it likely contained both Fe(III)-reducing and Fe(II)-oxidizing microorganisms.

SOIL MINERALOGY

Soil collected from the vicinity of the water table in July 2007 was used to study the abundance and mineralogy of Fe in different grain size fractions. The contribution of silt and clay size materials to total dry weight differed dramatically from their contributions to total HF-extractable iron [Fe(II) + Fe(III)] content (**Table 1**). Although the silt size fraction dominated Shovelers Sink soil by weight (83% of total dry weight), it contributed only 26% total HF-extractable iron. In contrast, the clay size fraction, which accounted only for 16% of the dry weight of soil, contributed 74% of the total HF-extractable iron. These results demonstrate that the majority of the Fe content of Shovelers Sink soil is contained within the clay size fraction.

The mineralogy of silt and clay size fractions was characterized by conventional TEM, high resolution TEM (HRTEM), and XRD (**Figures 3–5**). The following mineral phases were identified (by TEM) in the silt size fraction: potassium feldspar, plagioclase, quartz, and mixed layered illite–smectite aggregates (**Figure 3**). Based on TEM and XRD analyses, the dominant mineral in the clay size fraction was illite–smectite mixed layers (**Figures 4** and **5**). Clay size materials also contained kaolinite and illite as minor components. No Fe(III) hydroxides were detected in either the

Table 1 | Characterization of silt and clay size fractions of Shovelers Sink soil.

Parameter	Size fraction	
	Clay	**Silt**
% Dry weight[a]	16	83
Dominant minerals[b]	illite–smectite mixed layers, kaolinite, quartz, illite, and TiO_2	potassium feldspar, plagioclase, quartz, and illite–smectite aggregates
HF-extractable Fe, mmol/kg	1360.5 ± 10.7	95.7 ± 3.3
% Total Fe[c]	74	26
CDB-extractable Fe, mmol/kg	32.7 ± 1.1	47.4 ± 2.0

[a] *Percent of total bulk soil dry weight accounted for by the clay or silt size fractions; in addition to silt and clay, Shovelers Sink soil also contains 1% sand.*
[b] *Minerals were identified by TEM and XRD analyses and are listed in decreasing order based on their detected content in corresponding size fractions.*
[c] *Percent of the total Fe content of bulk soil accounted for by the clay or silt size fractions.*

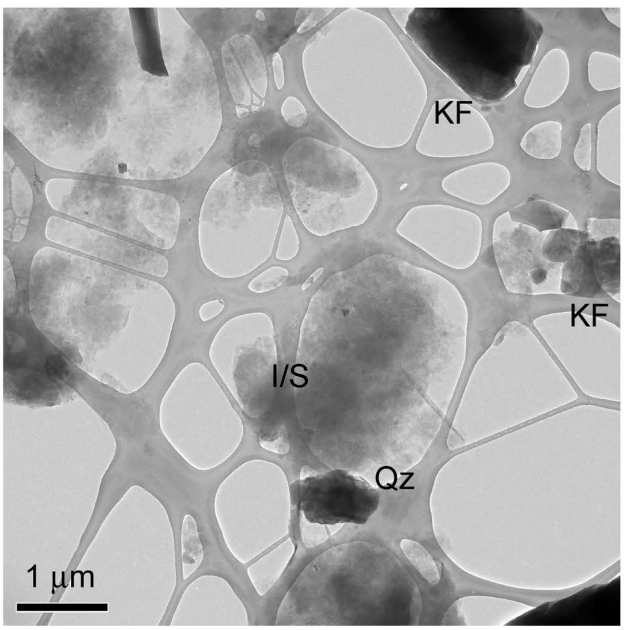

FIGURE 3 | TEM image of Shovelers Sink silt size fraction showing flakes of illite–smectite (I/S), quartz (Qz), and potassium feldspar (KF) grains.

silt or clay size fractions during TEM observations. These results are consistent with CDB extractions, which showed that the abundance of Fe(III) oxides was ca. less than 5% of total HF-extractable Fe in the bulk soil (**Figure 2**) and less than 2.5% in the clay size fraction (**Table 1**). In summary, gravimetric, chemical, and mineralogical analyses collectively suggest that mixed layer illite–smectite is the geochemically dominant Fe-containing phase in Shovelers Sink soil.

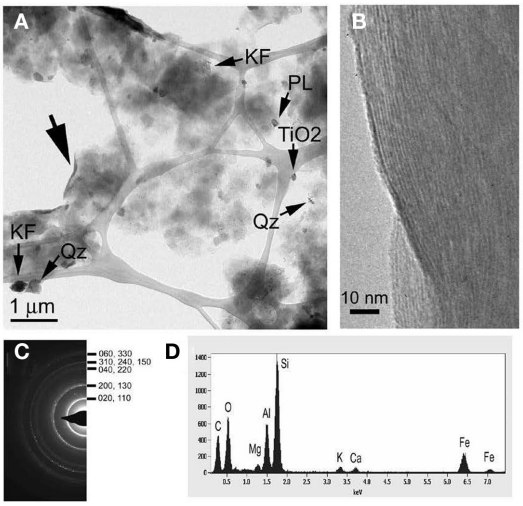

FIGURE 4 | Mineralogy of Shovelers Sink clay size fraction. (A) TEM image showing flakes of smectite-dominated clay minerals (I/S), quartz (Qz), potassium feldspar (KF), plagioclase, and titania (TiO_2) grains. **(B,C)** HRTEM image and selected area diffraction pattern taken from the area indicated by the large arrow in **(A)**, showing the curled edge of a clay aggregate with lattice fringes corresponding to (001) smectite with ca. 10-Å layer spacing; the size of this spacing was likely reduced in the vacuum of the TEM. **(D)** EDAX results for an I/S aggregate. A small amount of potassium is detected, indicating that the smectite contains an illite component.

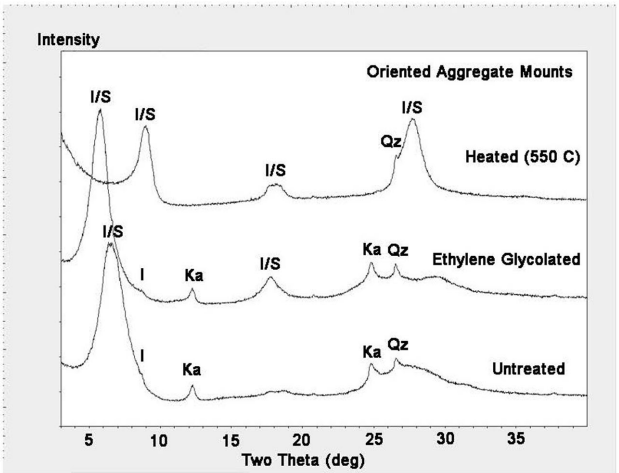

FIGURE 5 | X-ray diffraction analyses of clay size fraction from Shovelers Sink soil showing illite–smectite (I/S) as dominant mineral. Small amounts of illite (I), kaolinite (Ka), and quartz (Qz) also exist. The 13.6-Å [I/S (001)] peak in the untreated sample expanded to 15.2 Å by ethylene glycol treatment, and collapsed to 9.9 Å by heat treatment. The 7.2-Å [kaolinite (001)] and 3.6-A [kaolinite (002)] peaks in the untreated sample disappeared by heating at 550°C.

MPN ENUMERATIONS

Both Fe(III)-reducing and Fe(II)-oxidizing microorganisms were detected in MPN enumerations conducted with soil samples from near the water table in July 2007 and in September 2009.

The abundance of Fe(III)-reducing organisms (2.4×10^1 cells/g wet soil in 2007 and 2.3×10^0 cells/g wet soil in 2009) and Fe(II)-oxidizing organisms (2.9×10^2 cells/g wet soil in 2007 and 2.4×10^3 cells/g wet soil in 2009) was modest compared to the abundance of total culturable aerobic heterotrophs (1.1×10^6 cells/g wet soil in 2007 and 4.2×10^5 cells/g wet soil in 2009). Analogous results have been reported for groundwater seep environments supporting active Fe redox cycling (Blöthe and Roden, 2009; Roden et al., submitted). Although the much larger densities of culturable aerobic heterotrophs compared to Fe(III)-reducers in these environments could suggest intense competition between the two physiological groups (e.g., for utilization of plant-derived organic materials), it is important to note that previous studies have shown the persistence of large numbers of aerobic bacteria in permanently anoxic environments (Jorgensen and Tiedje, 1993). Thus, the presence of high densities of culturable aerobes in the Shoveler's sink soil does not necessarily mean that they contribute extensively to *in situ* carbon metabolism.

Fe(II)-OXIDIZING ISOLATES

Fe(II)-oxidizing organisms were isolated from (1) soil samples collected in July 2007, June 2008, and September 2009, and (2) the highest positive dilutions from MPN studies set up in 2007 and 2009. Biotite was utilized as a solid phase form of Fe(II) for these studies. Unlike reduced smectite, structural Fe(II) in biotite is not subject to spontaneous reaction with O_2, thus permitting the use of O_2 as the electron acceptor for lithotrophic Fe(II) oxidation. Recent studies have demonstrated that the Fe(II)-oxidizing, NO_3^- reducing culture described by Straub et al. (1996) can utilize Fe(II) in biotite as a sole electron donor for chemolithotrophic growth (Shelobolina et al., submitted). Samples and last positive MPN dilution cultures were serially diluted in biotite-containing roll-tubes. After solidification 3 ml of filter sterilized air were added to the headspace. Roll-tubes were incubated vertically at 20–22°C (room temperature). Over a period of 4–8 months, small (0.2–0.5 mm) orange, or in some cases red, colonies formed between the layer of biotite and the layer of agarized medium in a roll-tube. Each colony was transferred to 2 ml liquid medium with biotite provided as the electron donor and O_2 as the electron acceptor. A protracted (4 years) isolation effort (2007–2010) resulted in recovery of 73 biotite oxidizing cultures, which were maintained on liquid medium with biotite and O_2. Eleven cultures capable of oxidizing at least 5% of the structural Fe(II) content in biotite were selected for further study. Culture subsamples were streaked onto aerobic, low carbon medium culture plates. The resulting isolated colonies could be either mixotrophic Fe(II)-oxidizing microorganisms or heterotrophic contaminants. The numerically dominant colony types were tested for microaerophilic growth with $FeCl_2$ as a soluble Fe(II) sources. Cultures capable of growing to a density of at least 10^8 cells/ml with a total of c.a. 8 mM $FeCl_2$ added over time (see Materials and Methods) were identified by 16S rRNA gene sequencing and selected for further study. The isolates so obtained included *Bradyrhizobium* spp., and strains of *Ralstonia solanacearum*, and *Cupriavidus necator*. One strain each was chosen for further study (**Table 2**). Each of the cultures oxidized 3–4% of structural Fe(II) in biotite with O_2 as the electron acceptor, and each was found to be capable of oxidizing chemically reduced smectite with NO_3^- as the electron acceptor (data not shown).

Fe(III)-REDUCING ISOLATE

Ferruginous NAu-2 smectite and hydrous ferric oxide (HFO) were used to enrich Fe(III)-reducing microorganisms from Shovelers Sink soil collected in July 2007 with acetate and H_2 as combined electron donors. Acetate and H_2 were used as these represent the two major sources of electron donor for microbial Fe(III) reduction in anoxic soils and sediments (Lovley et al., 2004). After ca. 2 months of room temperature incubation, small (25 clones each) 16S rRNA gene clone libraries were constructed from 1% enrichment cultures. Both enrichment cultures were dominated by an operational taxonomic unit (OTU) 99% similar to *Geobacter toluenoxydans* (Kunapuli et al., 2010). *G. toluenoxydans* strain sa2 was recovered using the roll-tube method with acetate as the electron donor and fumarate as the electron acceptor. Strain sa2 can conserve energy from dissimilatory Fe(III) reduction concomitant with acetate oxidation using a variety of solid phase Fe(III) sources, including Fe(III) hydroxide and ferruginous smectite, but does not utilize nitrate as the electron acceptor.

MICROBIAL REDOX CYCLING OF Fe IN SHOVELERS SINK CLAY

A Fe redox cycling experiment was conducted with clay size materials isolated from Shovelers Sink soil collected from ca. 65 cm depth in July 2007 (see **Table 1**). Although O_2 is a likely electron acceptor for microbial Fe(II) oxidation at Shovelers Sink (see above), NO_3^- was utilized in this model experiment since it does

Table 2 | Fe redox cycling microorganisms isolated from Shovelers Sink soil.

Strain	GenBank accession #	Identification (closest cultured bacterium,% identity)	Role in Fe cycle
wssl4	JQ655459	*Bradyrhizobium liaoningense* 2281^T, 99.6% *Bradyrhizobium japonicum* USDA 6^T, 99.4%	Fe(II) oxidation
ss1-6-6	JQ655461	*Cupriavidus necator* ATCC 43291^T, 99.5% "*Ralstonia eutropha*" H16, 99.6%	Fe(II) oxidation
in4ss52	JQ655458	*Ralstonia solanacearum* LMG 2299^T, 98.7%	Fe(II) oxidation
sa2	JQ655460	*Geobacter toluenoxydans* TMJ1^T, 98.9% *Geobacter uraniireducens* RF4^T, 97.6%	Fe(III) reduction

The % values indicate the degree of similarity in 16S rRNA gene sequence.

not react spontaneously with phyllosilicate-associated Fe(II). *G. toluenoxidans* strain sa2 (5% vol/vol inoculum from a culture grown previously for three transfers on limiting acetate/Shovelers Sink clay medium, providing c.a. 10^6 cells/ml) reduced 2.1 mmol/l Fe(II) over 7 days (**Figure 6A**). A small increase in aqueous Fe concentration was detected in both abiotic control and the Fe(III)-reducing cultures (35.4 and 50.6 μM, respectively). The source of dissolved Fe cannot be determined with available data. Shovelers Sink clay is a mix of minerals. And although illite–smectite is the main Fe-bearing mineral controlling Fe biogeochemistry in Shovelers Sink soil, the clay size fraction could contain organics-bound or sorbed Fe, as well as small amounts of Fe(III) hydroxide coatings. All of these Fe forms could contribute to aqueous Fe.

After 10 days, an inoculum of each of the three Fe(II)-oxidizing isolates (**Table 2**) were added to replicate microbially reduced clay suspensions. The Fe(II)-oxidizing inocula (1–5% vol/vol) were grown heterotrophically on organics limited NO_3^- reducing medium until the optical density of the culture at 600 nm stabilized, at which point all organic carbon had presumably been utilized. The inoculum volume was adjusted to provide ca 10^6 cells/ml. The cultures reoxidized 60–65% (c.a. 1.2 mmol/l) of the Fe(II) generated by *G. toluenoxidans* strain sa2 (**Figure 6A**) while consuming 0.82–1.15 mM NO_3^- (**Figure 6B**).

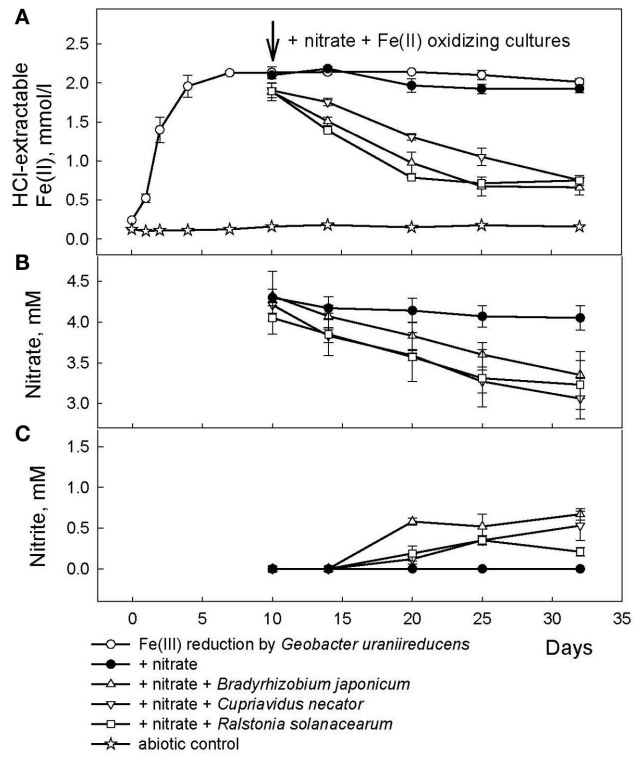

FIGURE 6 | Reduction of native Fe(III) phyllosilicate in Shovelers Sink soil (clay size fraction) by *G. toluenoxidans* strain sa2, followed by oxidation of reduced phyllosilicate by the three Fe(II)-oxidizing isolates with NO_3^- as the electron acceptor. (A) 0.5 N HCl-extractable Fe(II); **(B)** nitrate; **(C)** nitrite.

The incomplete reversibility of structural Fe redox cycle has been observed before (Shen and Stucki, 1994) and a possible explanation for this phenomenon is that the collapsing of smectite layers as the result of Fe(III) reduction makes a portion of structural Fe(II) inaccessible (Stucki, 2011).

No Fe(II) oxidation or NO_3^- consumption took place in absence of Fe(II)-oxidizing organisms. Although all of the Fe(II)-oxidizing isolates are denitrifying bacteria, substantial amounts of NO_2^- (0.35–0.67 mM) were produced during Fe(II) oxidation (**Figure 6C**). The Shovelers Sink soil used in the Fe cycling experiment contained 1–2% associated organic carbon (see **Figure 2**). The possibility therefore existed that NO_2^- produced during organotrophic oxidation of associated organic carbon could have reacted chemically (abiotically) with Fe(II) in the reduced clay, thereby contributing to the Fe(II) oxidation activity shown in **Figure 6A**. We deemed this pathway unlikely given that each of the isolated strains reduced nitrate directly to N_2 with no significant NO_2^- accumulation in organotrophic medium (data not shown). Nevertheless, a separate experiment was conducted to evaluate the extent to which reaction of Fe(II) with NO_2^- may have been responsible for the observed Fe(II) oxidation. Nitrite (2 mM) was added to a suspension of microbially reduced Shovelers Sink clay, and the concentrations of Fe(II) and NO_2^- were followed over time (**Figure 7**). The rate of chemical Fe(II) oxidation by nitrite (c.a. 0.018 mmol/l/day; **Figure 7**) was three to six times less than the rate of oxidation in the microbial Fe cycling experiment (0.058–0.118 mmol/l/day; **Figure 6A**). This result indicates that enzymatic activity was primarily responsible for nitrate-dependent

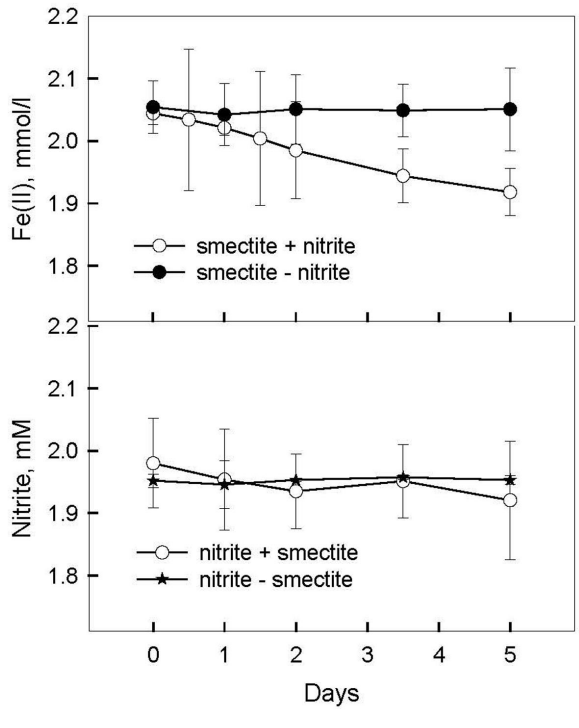

FIGURE 7 | Chemical oxidation of microbially reduced Shovelers Sink soil (clay size fraction) by nitrite.

oxidation of reduced Shovelers Sink clay. Similar conclusions were reached in a prior study of microbial nitrate-dependent oxidation of other types of solid phase Fe(II) compounds in which significant accumulation of NO_2^- took place (Weber et al., 2001). Thus, although the organic matter associated with Shovelers Sink clay brings uncertainty into the exact stoichiometry of Fe/N interactions, the results of this experiment clearly confirm that Fe in the native Shovelers Sink clay is readily available for microbial redox transformation and can be cycled by the Fe(III)-reducing and Fe(II)-oxidizing microorganisms recovered from the soil.

IMPLICATIONS FOR PHYLLOSILICATE–Fe BIOGEOCHEMISTRY

Our studies confirm the presence of both phyllosilicate–Fe(III)-reducing and phyllosilicate–Fe(II)-oxidizing organisms in a redoximorphic soil, the biogeochemical conditions of which are consistent with ongoing phyllosilicate–Fe redox cycling in the vicinity of the water table and O_2-releasing plant roots. Several solid phase Fe redox cycling isolates were recovered from this soil using model Fe(II) and Fe(III) containing phyllosilicates as the electron donor or acceptor, including the Alphaproteobacterium *Bradyrhizobium* sp, Betaproteobacteria *C. necator* and *R. solanacearum*, and Deltaproteobacterium *G. toluenoxydans*. The recovery of a *Geobacter* species as an agent of Fe(III) reduction at Shovelers Sink is not surprising, as members of the Geobacteraceae often dominate soil and sediment Fe(III)-reducing microbial populations (Lovley et al., 2004), and multiple species in this family are known to reduce structural Fe(III) in phyllosilicates (Lovley et al., 1998; Kostka et al., 1999; Kashefi et al., 2008; Shelobolina et al., 2008). *Geobacter* sp. dominated both, smectite and HFO containing enrichment cultures and therefore was well adjusted to using both Fe(III)-bearing phases as the electron acceptor. Although a previous study (Kashefi et al., 2008) suggested that phyllosilicate–Fe(III)-reducing and Fe(III) (hydr)oxide-reducing microbial populations may not always overlap, no specific agents adjusted to using one or another solid phase Fe(III) were recovered at Shovelers Sink.

The microorganisms recovered as potential agents of phyllosilicate–Fe(II) oxidation are all common rhizosphere bacteria. *Bradyrhizobium* spp. are well-known as N_2 fixing bacteria that form a symbiotic relationship with plants, especially soybeans, and are widely utilized in agriculture (Hume and Blair, 1992). In contrast, *R. solanacearum* is a soil-born plant pathogen causing leaf wilting in tomato, pepper, and potato plants as well as many other plant species (Denny, 2005). *C. necator* (including former *Ralstonia eutropha* strains) is a versatile soil bacterium known as an aromatic and chloroaromatic compounds degrader and a non-obligate bacterial predator of the bacteria and fungi (Makkar and Casida, 1987; Lykidis et al., 2010).

Various strains of *Bradyrhizobium* spp. and *C. necator* (*R. eutropha*) can grow autotrophically with H_2 as the electron donor (Bowien and Kusian, 2002; Schwartz et al., 2003; Franck et al., 2008). In addition, a *B. japonicum* strain USDA110 is capable of thiosulfate-based chemolithotrophy (Masuda et al., 2010). None of phytopathogenic *R. solanacearum* strains were reported to grow autotrophically (Palleroni and Doudoroff, 1971). However, a recently recovered *Ralstonia* sp. strain HM08-01, 98% similar to *R. solanacearum*, can oxidize soluble Fe(II) under microaerophilic conditions (Swanner et al., 2011). Our studies suggest a new role for these common rhizosphere bacteria, i.e., oxidation of structural Fe(II) in phyllosilicates. Further research with chemically defined substrates, such as $FeCl_2$ and Fe(II)-NTA, is required to determine exact stoichiometry of Fe(II) oxidation by Shovelers Sink isolates.

The importance of native Fe(III) phyllosilicates as an electron acceptor for organic matter oxidation coupled to dissimilatory Fe(III) reduction in soils and sediments has been increasingly recognized (Kukkadapu et al., 2006; Stucki and Kostka, 2006; Komlos et al., 2008; Dong et al., 2009). In contrast, the role of microbial catalysis in phyllosilicate–Fe(II) oxidation has not received much attention, and to date only one organism is known to carry-out this reaction (Shelobolina et al., 2003). Our work thus significantly expands the range of organisms known to participate in phyllosilicate–Fe(II) oxidation. The ability of common rhizosphere bacteria to carry-out this process has significant implications not only for phyllosilicate–Fe redox geochemistry, but also for phyllosilicates diagenesis, e.g., low-temperature microbially driven smectite-to-illite transition, that may accompany Fe cycling in smectite and affect plant nutrition (Shen and Stucki, 1994; Stucki, 2011).

ACKNOWLEDGMENTS

With thank Cynthia A. Stiles and Matilde M. Urrutia from UW–Madison Soil Science Department for introducing us to the Shovelers Sink site. This research was supported by the U.S. Department of Energy (DOE), Office of Biological and Environmental Research (BER) Subsurface Biogeochemical Research (SBR) Program through grant ER64172-1027487-001191; and the SBR Scientific Focus Area (SFA) at the Pacific Northwest National Laboratory (PNNL).

REFERENCES

Altschul, S. F., Gish, W., Miller, W., Myers, E. W., and Lipman, D. J. (1990). Basic local alignment search tool. *J. Mol. Biol.* 215, 403–410.

Amonette, J. E. (2002). "Iron redox chemistry of clays and oxides: environmental applications," in *Electrochemical Properties of Clays*, ed. A. Fitch (Aurora, CO: The Clay Minerals Society), 90–147.

Armstrong, W. (1978). "Root aeration in the wetland condition," in *Plant Life in Anaerobic Environments*, eds D. Hook and R. Crawford (Ann Arbor, MI: Ann Arbor Science Publishers Inc.), 269–297.

Barclay, A. M., and Crawford, R. (1983). The effect of anaerobiosis on carbohydrate-levels in storage tissues of wetlands plants. *Ann. Bot.* 51, 255–259.

Blöthe, M., and Roden, E. E. (2009). Microbial iron redox cycling in a circumneutral-pH groundwater seep. *Appl. Environ. Microbiol.* 75, 468–473.

Bowien, B., and Kusian, B. (2002). Genetics and control of CO_2 assimilation in the chemoautotroph *Ralstonia eutropha*. *Arch. Microbiol.* 178, 85–93.

Bradbury, K. R. (ed.). (2001). Springs, sinks, and flowing wells: hydrogeology at the urban fringe. *Midwest Ground Water Conference, 46th Annual Meeting, Field Trip Guide*, Madison, WI.

Brady, N., and Weil, R. (2008). *The Nature and Properties of Soils*. Upper Saddle River, NJ: Prentice Hall.

Clayton, L., and Attig, J. W. (eds). (1997). *Pleistocene Geology of Dane County, Wisconsin*. Madison, WI: Wisconsin Geological and Natural History Survey.

Denny, T. P. (2005). "A short history of the biochemical and genetic research on *Ralstonia solanacearum*

pathogenesis," in *Bacterial Wilt Disease and the Ralstonia solanacearum Species Complex*, eds P. P. C. Allen, and A. C. Hayward (St. Paul, MN: APS Press), 323–334.

Dong, H., Jaisi, D. P., Kim, J., and Zhang, G. (2009). Microbe-clay mineral interactions. *Am. Mineral.* 94, 1505–1519.

Emerson, D., Fleming, E. J., and Mcbeth, J. M. (2010). Iron-oxidizing bacteria: an environmental and genomic perspective. *Annu. Rev. Microbiol.* 64, 561–583.

Franck, W. L., Chang, W. S., Qiu, J., Sugawara, M., Sadowsky, M. J., Smith, S. A., and Stacey, G. (2008). Whole-genome transcriptional profiling of *Bradyrhizobium japonicum* during chemoautotrophic growth. *J. Bacteriol.* 190, 6697–6705.

Gee, G. W., and Bauder, J. W. (1986). "Particle-size analysis," in *Methods of Soil Analyses. Physical and Mineralogical Methods*, ed. A. Klute (Madison: American Society of Agronomy; Soil Science Society of America), 386–411.

Hobbie, J. E., Daley, R. J., and Jasper, S. (1977). Use of nuclepore filters for counting bacteria by fluorescence microscopy. *Appl. Environ. Microbiol.* 33, 1225–1228.

Hume, D. J., and Blair, D. H. (1992). Effect of numbers of *Bradyrhizobium japonicum* applied in commercial inoculants on soybean seed yield in Ontario. *Can. J. Microbiol.* 38, 588–593.

Hungate, R. E. (1968). A roll tube method for cultivation of strict anaerobes. *Methods Microbiol.* 3B, 117–132.

Jackson, M. L. (1969). *Soil Chemical Analysis – Advanced Course*, 2nd Edn. Madison: University of Wisconsin.

Jorgensen, K. S., and Tiedje, J. M. (1993). Survival of denitrifiers in nitrate-free, anaerobic environments. *Appl. Environ. Microbiol.* 59, 3297–3305.

Kashefi, K., Shelobolina, E., Elliott, W. C., and Lovley, D. R. (2008). Growth of thermophilic and hyperthermophilic Fe (III)-reducing microorganisms on a ferruginous smectite as the sole electron acceptor. *Appl. Environ. Microbiol.* 74, 251–258.

Keeling, J. L., Raven, M. D., and Gates, W. P. (2000). Geology and characterization of two hydrothermal nontronites from weathered metamorphic rocks at the Uley graphite mine, South Australia. *Clays Clay Miner.* 48, 537–548.

Komadel, P., and Stucki, J. W. (1988). Quantitative assay of minerals for Fe^{2+} and Fe^{3+} using 1,10-phenanthroline: III. A rapid photochemical method. *Clays Clay Miner.* 36, 379–381.

Komlos, J., Peacock, A., Kukkadapu, R. K., and Jaffé, P. R. (2008). Long-term dynamics of uranium reduction/reoxidation under low sulfate conditions. *Geochim. Cosmochim. Acta* 72, 3603–3615.

Konhauser, K. O., Kappler, A., and Roden, E. E. (2011). Iron in microbial metabolisms. *Elements* 7, 89–93.

Kostka, J. E., Wu, J., Nealson, K. H., and Stucki, J. W. (1999). The impact of structural Fe(III) reduction by bacteria on the surface chemistry of smectite clay minerals. *Geochim. Cosmochim. Acta* 63, 3705–3713.

Kukkadapu, R. K., Zachara, J. M., Fredrickson, J. K., Mckinley, J. P., Kennedy, D. W., Smith, S. C., and Dong, H. (2006). Reductive biotransformation of Fe in shale-limestone saprolite containing Fe(III) oxides and Fe(II)/Fe(III) phyllosilicates. *Geochim. Cosmochim. Acta* 70, 3662–3676.

Kunapuli, U., Jahn, M. K., Lueders, T., Geyer, R., Heipieper, H. J., and Meckenstock, R. U. (2010). Desulfitobacterium aromaticivorans sp nov and *Geobacter toluenoxydans* sp. nov., iron-reducing bacteria capable of anaerobic degradation of monoaromatic hydrocarbons. *Int. J. Syst. Evol. Microbiol.* 60, 686–695.

Lovley, D. R., Chapelle, F. H., and Woodward, J. C. (1994). Use of dissolved H_2 concentrations to determine distribution of microbially catalyzed redox reactions in anoxic groundwater. *Environ. Sci. Technol.* 28, 1205–1210.

Lovley, D. R., Fraga, J. L., Blunt-Harris, E. L., Hayes, L. A., Philips, E. J. P., and Coates, J. D. (1998). Humic substances as a mediator for microbially catalyzed metal reduction. *Acta Hydrochim. Hydrobiol.* 26, 152–157.

Lovley, D. R., and Goodwin, S. (1988). Hydrogen concentrations as an indicator or the predominant terminal electron-accepting reactions in aquatic sediments. *Geochim. Cosmochim. Acta* 52, 2993–3003.

Lovley, D. R., Holmes, D. E., and Nevin, K. P. (2004). Dissimilatory Fe(III) and Mn(IV) reduction. *Adv. Microb. Physiol.* 49, 219–286.

Lovley, D. R., and Phillips, E. J. P. (1986). Organic matter mineralization with reduction of ferric iron in anaerobic sediments. *Appl. Environ. Microbiol.* 51, 683–689.

Lovley, D. R., and Phillips, E. J. P. (1988). Novel mode of microbial energy metabolism: organic carbon oxidation coupled to dissimilatory reduction of iron or manganese. *Appl. Environ. Microbiol.* 54, 1472–1480.

Lykidis, A., Perez-Pantoja, D., Ledger, T., Mavromatis, K., Anderson, I. J., Ivanova, N. N., Hooper, S. D., Lapidus, A., Lucas, S., Gonzalez, B., and Kyrpides, N. C. (2010). The complete multipartite genome sequence of *Cupriavidus necator* JMP134, a versatile pollutant degrader. *PLoS ONE* 5, e9729. doi:10.1371/journal.pone.0009729

Makkar, N. S., and Casida, L. E. (1987). *Cupriavidus necator* gen. nov., sp. nov: a nonobligate bacterial predator of bacteria in soil. *Int. J. Syst. Bacteriol.* 37, 323–326.

Masuda, S., Eda, S., Ikeda, S., Mitsui, H., and Minamisawa, K. (2010). Thiosulfate-dependent chemolithoautotrophic growth of *Bradyrhizobium japonicum*. *Appl. Environ. Microbiol.* 76, 2402–2409.

Mehra, O. P., and Jackson, M. L. (1980). Iron oxide removal from soils and clays by a dithionite-citrate system buffered with sodium bicarbonate. *Clays Clay Miner.* 7, 317–327.

Miller, T. L., and Wolin, M. J. (1974). A serum bottle modification of the Hungate technique for cultivating obligate anaerobes. *Appl. Microbiol.* 27, 985–987.

Muyzer, G., Teske, A., Wirsen, C. O., and Jannasch, H. W. (1995). Phylogenetic relationships of *Thiomicrospira* species and their identification in deep-sea hydrothermal vent samples by denaturing gradient gel electrophoresis of 16S rDNA fragments. *Arch. Microbiol.* 164, 165–172.

Palleroni, N. J., and Doudoroff, M. (1971). Phenotypic characterization and deoxyribonucleic acid homologies of *Pseudomonas solanacearum*. *J. Bacteriol.* 107, 690–696.

Schmidt, C., Behrens, S., and Kappler, A. (2010). Ecosystem functioning from a geomicrobiological perspective – a conceptual framework for biogeochemical iron cycling. *Environ. Chem.* 7, 399–405.

Schwartz, E., Henne, A., Cramm, R., Eitinger, T., Friedrich, B., and Gottschalk, G. (2003). Complete nucleotide sequence of pHG1: a *Ralstonia eutropha* H16 megaplasmid encoding key enzymes of H2-based lithoautotrophy and anaerobiosis. *J. Mol. Biol.* 332, 369–383.

Shelobolina, E. C., Vrionis, H., Findlay, R. H., and Lovley, D. R. (2008). *Geobacter uraniireducens* sp. nov., isolated from subsurface sediment undergoing uranium bioremediation. *Int. J. Syst. Evol. Microbiol.* 58, 1075–1079.

Shelobolina, E. S., Anderson, R. T., Vodyanitskii, Y. N., Sivtsov, A. M., Yuretich, R., and Lovley, D. R. (2004). Importance of clays size minerals for Fe(III) respiration in a petroleum-contaminated aquifer. *Geobiology* 2, 67–76.

Shelobolina, E. S., Gaw Vanpraagh, C., and Lovley, D. R. (2003). Use of ferric and ferrous iron containing minerals for respiration by *Desulfitobacterium frappieri*. *Geomicrobiol. J.* 20, 143–156.

Shelobolina, E. S., Nevin, K. P., Blakeney-Hayward, J. D., Johnsen, C. V., Plaia, T. W., Krader, P., Woodward, T., Holmes, D. E., Vanpraagh, C. G., and Lovley, D. R. (2007). *Geobacter pickeringii* sp. nov., *Geobacter argillaceus* sp. nov. and *Pelosinus fermentans* gen. nov., sp. nov., isolated from subsurface kaolin lenses. *Int. J. Syst. Evol. Microbiol.* 56, 126–135.

Shen, S., and Stucki, J. W. (1994). "Effects of iron oxidation state on the fate and behavior of potassium in soils," in *Soil Testing: Prospects for Improving Nutrient Recommendations*, eds J. L. Havlin and J. Jacobsen (Madison, WI: Soil Science Society of America), 173–185.

Stookey, L. L. (1970). Ferrozine – a new spectrophotometric reagent for iron. *Anal. Chem.* 42, 779–781.

Straub, K. L., Benz, M., Schink, B., and Widdel, F. (1996). Anaerobic, nitrate-dependent microbial oxidation of ferrous iron. *Appl. Environ. Microbiol.* 62, 1458–1460.

Stucki, J. (2011). A review of the effects of iron redox cycles on smectite properties. *C. R. Geosci.* 343, 199–209.

Stucki, J. W. (1981). The quantitative assay of minerals for Fe^{2+} and Fe^{3+} using 1,10-phenanthroline: II. A photochemical method. *Soil Sci. Soc. Am. J.* 45, 638–641.

Stucki, J. W., and Kostka, J. E. (2006). Microbial reduction of iron in smectite. *C. R. Geosci.* 338, 468–475.

Swanner, E. D., Nell, R. M., and Templeton, A. S. (2011). *Ralstonia* species mediate Fe-oxidation in circumneutral, metal-rich subsurface fluids of Henderson mine, CO. *Chem. Geol.* 284, 339–350.

Weber, K. A., Achenbach, L. A., and Coates, J. D. (2006). Microorganisms pumping iron: anaerobic microbial iron oxidation and reduction. *Nat. Rev. Microbiol.* 8, 100–113.

Weber, K. A., Picardal, F. W., and Roden, E. E. (2001). Microbially-

catalyzed nitrate-dependent oxidation of biogenic solid-phase Fe(II) compounds. *Environ. Sci. Technol.* 35, 1644–1650.

Woomer, P. L. (1994). "Microbiological and biochemical properties," in *Methods of Soil Analysis. Part 2*, ed. J. M. Bigham (Madison, WI: Soil Science Society of America), 59–79.

Conflict of Interest Statement: The authors declare that the research was conducted in the absence of any commercial or financial relationships that could be construed as a potential conflict of interest.

Received: 09 December 2011; accepted: 21 March 2012; published online: 04 April 2012.

Citation: Shelobolina E, Konishi H, Xu H, Benzine J, Xiong MY, Wu T, Blöthe M and Roden E (2012) Isolation of phyllosilicate–iron redox cycling microorganisms from an illite–smectite rich hydromorphic soil. Front. Microbio. ***3****:134. doi: 10.3389/fmicb.2012.00134*
This article was submitted to Frontiers in Microbiological Chemistry, a specialty of Frontiers in Microbiology.

Copyright © 2012 Shelobolina, Konishi, Xu, Benzine, Xiong, Wu, Blöthe and Roden. This is an open-access article distributed under the terms of the Creative Commons Attribution Non Commercial License, which permits non-commercial use, distribution, and reproduction in other forums, provided the original authors and source are credited.

frontiers in
MICROBIOLOGY

ORIGINAL RESEARCH ARTICLE
published: 31 May 2012
doi: 10.3389/fmicb.2012.00197

Microbial iron(II) oxidation in littoral freshwater lake sediment: the potential for competition between phototrophic vs. nitrate-reducing iron(II)-oxidizers

E. D. Melton, C. Schmidt and A. Kappler*

Geomicrobiology, Centre for Applied Geosciences, University of Tübingen, Tübingen, Germany

Edited by:
David Emerson, Bigelow Laboratory for Ocean Sciences, USA

Reviewed by:
Evgenya Shelobolina, University of Wisconsin–Madison, USA
Sean Crowe, University of Southern Denmark, Denmark

****Correspondence:***
A. Kappler, Geomicrobiology, Center for Applied Geosciences, University of Tübingen, Sigwartstraße 10, D-72076 Tübingen, Germany.
e-mail: andreas.kappler@uni-tuebingen.de

The distribution of neutrophilic microbial iron oxidation is mainly determined by local gradients of oxygen, light, nitrate and ferrous iron. In the anoxic top part of littoral freshwater lake sediment, nitrate-reducing and phototrophic Fe(II)-oxidizers compete for the same e^- donor; reduced iron. It is not yet understood how these microbes co-exist in the sediment and what role they play in the Fe cycle. We show that both metabolic types of anaerobic Fe(II)-oxidizing microorganisms are present in the same sediment layer directly beneath the oxic-anoxic sediment interface. The photoferrotrophic most probable number counted $3.4{\cdot}10^5$ cells$\cdot g^{-1}$ and the autotrophic and mixotrophic nitrate-reducing Fe(II)-oxidizers totaled $1.8{\cdot}10^4$ and $4.5{\cdot}10^4$ cells$\cdot g^{-1}$ dry weight sediment, respectively. To distinguish between the two microbial Fe(II) oxidation processes and assess their individual contribution to the sedimentary Fe cycle, littoral lake sediment was incubated in microcosm experiments. Nitrate-reducing Fe(II)-oxidizing bacteria exhibited a higher maximum Fe(II) oxidation rate per cell, in both pure cultures and microcosms, than photoferrotrophs. In microcosms, photoferrotrophs instantly started oxidizing Fe(II), whilst nitrate-reducing Fe(II)-oxidizers showed a significant lag-phase during which they probably use organics as e^- donor before initiating Fe(II) oxidation. This suggests that they will be outcompeted by phototrophic Fe(II)-oxidizers during optimal light conditions; as phototrophs deplete Fe(II) before nitrate-reducing Fe(II)-oxidizers start Fe(II) oxidation. Thus, the co-existence of the two anaerobic Fe(II)-oxidizers may be possible due to a niche space separation in time by the day-night cycle, where nitrate-reducing Fe(II)-oxidizers oxidize Fe(II) during darkness and phototrophs play a dominant role in Fe(II) oxidation during daylight. Furthermore, metabolic flexibility of Fe(II)-oxidizing microbes may play a paramount role in the conservation of the sedimentary Fe cycle.

Keywords: photoferrotrophs, nitrate-reducing Fe(II)-oxidizers, freshwater littoral sediment, microcosms, competition

INTRODUCTION

Iron is a ubiquitously abundant redox active transition metal in sedimentary systems (Froelich et al., 1979; Canfield et al., 1993). Not only is it required for integral components in cellular processes in many eukaryotic and prokaryotic organisms, but it can also serve as an electron donor or acceptor to many prokaryotes (Kappler and Straub, 2005; Weber et al., 2006a; Konhauser et al., 2011). Particularly, in freshwater lakes with low sulfate concentrations, microbial Fe(III) reduction is an important process in the anaerobic degradation of organic matter (Thamdrup, 2000; Lovley et al., 2004). Freshwater lakes cover approximately 0.8% of the Earth's surface (Dudgeon et al., 2006) and their iron rich redox stratified sediment provides the ideal habitat for Fe-metabolizing bacteria.

Fe(III) and other oxidants in the pore water of the sediment are consumed by bacterial processes in a hierarchical order of decreasing energy production per mole of organic carbon oxidized (Froelich et al., 1979; Canfield and Thamdrup, 2009). This creates a chemical gradient within the sediment column, which describes a defined sequence of redox zones in these sediments that are individually characterized by the dominantly consumed electron acceptor. The dominant electron acceptor in the first layer is oxygen, which is defined as the oxic zone (Froelich et al., 1979; Canfield and Thamdrup, 2009). Once oxygen is depleted, and the redox potential is driven low enough, the next most advantageous oxidants will take over. Following the depth profile: nitrate is followed by manganese, next by ferric iron, then sulfate, and finally by carbon dioxide (Froelich et al., 1979). This sequence remains unchanged throughout profundal and littoral lake sediment. However, exposure to light of the littoral sediment stimulates photosynthesis and O_2 production and thus creates a downward shift, or broadening, in the spatial positioning of the redox zones (Gerhardt et al., 2005, 2010).

In contrast to electron acceptors such as oxygen, nitrate, or sulfate, ferric iron is poorly soluble, and swiftly precipitates into iron(III) (oxyhydr)oxides (Cornell and Schwertmann, 2003) which can subsequently either be reduced through chemical

reactions (Canfield, 1989) or by microbes through organic matter or dihydrogen oxidation (Lovley and Phillips, 1988; Bonneville et al., 2004; Macdonald et al., 2011). The produced ferrous iron is more soluble (Cornell and Schwertmann, 2003) and diffuses upward through the pore water toward the oxic zone, serving as a profitable electron donor to Fe(II)-oxidizing microbial communities.

Iron(II)-oxidizing bacteria have been found in high numbers in many freshwater lakes and sediments (Straub and Buchholz-Cleven, 1998; Diez et al., 2007). Three types of neutrophilic bacteria complete the oxidation part of the freshwater sedimentary iron redox cycle: microaerophiles (Emerson and Moyer, 1997), nitrate-reducing Fe(II)-oxidizers (Straub et al., 1996), and photoferrotrophs (Widdel et al., 1993; Ehrenreich and Widdel, 1994). As microbial iron oxidation products have been found to suitably serve as substrate for iron(III)-reducing bacteria (Emerson and Moyer, 1997; Straub and Buchholz-Cleven, 1998; Bloethe and Roden, 2009a), it is feasible that these oxidizing and reducing communities successfully support a sedimentary iron redox cycle. Their close physical proximity and co-existence in the redox zones of the sediment further supports the presence of a microbial iron redox cycle (Sobolev and Roden, 2002; Bruun et al., 2010), which has also evoked the formulation of a conceptual model for the spatial niche separation for iron metabolizers in the iron cycle (Schmidt et al., 2010). Furthermore, artificial Fe redox cycles in laboratory settings have been successfully achieved at neutral pH through co-cultures of Fe(III)-reducing and Fe(II)-oxidizing bacteria (Straub et al., 2004; Coby et al., 2011).

Neutrophilic nitrate-reducing Fe(II)-oxidizers have been found in high numbers in many freshwater lakes and sediments (Hauck et al., 2001; Muehe et al., 2009) and produce poorly crystalline Fe(III) hydroxides (ferrihydrite) or more crystalline Fe(III) oxyhydroxides (goethite, lepidocrocite) as their Fe(II) oxidation product (Straub et al., 2004; Kappler et al., 2005b; Larese-Casanova et al., 2010). Their metabolism adheres to the following stoichiometric equation: $10Fe^{2+} + 2NO_3^- + 24H_2O \rightarrow 10Fe(OH)_3 + N_2 + 18H^+$ (Straub et al., 1996). Whilst the existence of autotrophic nitrate-reducing Fe(II)-oxidizers has been suggested, to date, a true autotrophic nitrate-reducing Fe(II)-oxidizer that can be successfully transferred without an organic co-substrate over many generations has not been isolated. The enrichment of a co-culture named KS has been achieved (Straub et al., 1996; Bloethe and Roden, 2009b) but so far, all pure nitrate-reducing Fe(II)-oxidizing isolates adhere to a mixotrophic metabolism, requiring the need of an organic co-substrate for Fe(II) oxidation (Straub et al., 1996; Kappler et al., 2005b; Muehe et al., 2009; Chakraborty et al., 2011). This metabolism is widespread within the denitrifying proteobacteria (Straub et al., 1996, 2004). In fact, addition of iron(II) to a denitrifying population enhances their cell growth, implying that iron(II) oxidation is truly a beneficial metabolism and Fe(III) is not simply a byproduct from another minor reaction mechanism (Muehe et al., 2009; Chakraborty et al., 2011). Moreover, in addition to Fe(II) oxidation, many denitrifying bacteria are also capable of switching to microaerophilic Fe(II) oxidation (Benz et al., 1998; Edwards et al., 2003). It is thus conceivable that although nitrate-reducing Fe(II) oxidation is an anaerobic metabolism, the organisms catalyzing this process may also be able to oxidize Fe(II) at oxygen levels up to 50 μM, like other known microaerophilic Fe(II)-oxidizers (Druschel et al., 2008).

Photosynthetic Fe(II) oxidation can only take place during daylight hours, as starlight and even a full moon fail to provide adequate light to support photosynthetic microbial growth (Raven and Cockell, 2006). During daylight hours, light has been shown to penetrate through sediment up until a depth of at least 5–6 mm (Kuehl et al., 1994). As well as being reflected by reflective particles, light is scavenged in the sediment, dramatically decreasing its intensity with depth toward an asymptotic value, posing a potential problem for photoferrotrophs living beneath the oxygen penetration depth (Kuehl et al., 1994). Nevertheless, photoferrotrophs are reasonably widespread in freshwater systems, having been found in freshwater lakes (Straub and Buchholz-Cleven, 1998), and isolated from numerous freshwater sediments (Widdel et al., 1993; Ehrenreich and Widdel, 1994; Heising et al., 1999). Photoferrotrophy is an anaerobic process which requires both light and bicarbonate: $HCO_3^- + 4Fe^{2+} + 10H_2O \xrightarrow{h\nu} CH_2O + 4Fe(OH)_3 + 7H^+$ (Widdel et al., 1993). Thus, photoferrotrophs are most probably spatially restricted by the sedimentary chemocline, the light penetration depth and upward Fe(II) diffusion from the deeper sediment layers. Only dissolved ferrous iron is susceptible to phototrophic Fe(II) oxidation and the oxidation products are poorly crystalline Fe(III) oxides (Kappler and Newman, 2004). The genetic heritage of anoxygenic phototrophs has been traced back to the oldest photosynthetic lineage (Xiong et al., 2000), and photoferrotrophs are able to thrive in archaean ocean analogs (Crowe et al., 2008). Thus, it has been proposed that anoxygenic photoferrotrophy played a paramount role in the deposition of Precambrian banded iron formations (Konhauser et al., 2002; Kappler et al., 2005a; Crowe et al., 2008; Posth et al., 2008).

As both photoferrotrophic and nitrate-reducing Fe(II) oxidation are anaerobic metabolisms, the habitat of the microorganisms catalyzing these processes is likely to be restricted to the same top anoxic part of the sediment where incidentally the local geochemical gradients of Fe(II), oxygen, nitrate and sunlight provide optimal living conditions for both. This means that their growth, and co-existence, depends on their successful competition for reduced iron. Many previous studies focus either solely on one of the iron(II)-oxidizing processes (Straub and Buchholz-Cleven, 1998; Jiao et al., 2005; Muehe et al., 2009; Poulain and Newman, 2009) or on the co-existence of Fe(II)-oxidizers and Fe(III)-reducers in cycling systems (Straub et al., 2004; Coby et al., 2011). So far, the spatial distribution and positioning in relation to each other specifically of phototrophic and nitrate-reducing Fe(II)-oxidizers has not yet been studied. As their habitats probably overlap significantly, they are expected to exhibit fierce competition for Fe(II). However, the individual contributions of photoferrotrophs and nitrate-reducing Fe(II)-oxidizers to iron(II) oxidation, and hence their competition for ferrous iron has also not been previously studied. Therefore, the objectives of this study were firstly: to determine whether both phototrophic and nitrate-reducing anaerobic Fe(II)-oxidizing bacteria are present in the same sediment layer directly beneath the oxic-anoxic boundary, and secondly: what their individual contribution is to sedimentary Fe(III) formation. We also explored geochemical factors that could limit iron(II) oxidation by the two anaerobic Fe(II)-oxidizing groups,

and how they compete with one another for ferrous iron. These experiments combine microbial and geochemical techniques to provide key information needed not only to determine the contribution of microbial activity to the overall iron oxidation budget and their spatial distribution, but also to define the role of geo-/photochemical iron conversion rates and its general importance in littoral freshwater lake sediment.

MATERIALS AND METHODS

SAMPLING SITE AND INITIAL SAMPLE TREATMENT

Littoral sediment and water samples were taken in February 2011 from Lake Constance, a freshwater lake in southern Germany, at a location in the north-western arm known as the Überlingersee, near the island of Mainau at 47°41′42.63″N and 9°11′40.29″E. The samples were transported to the laboratory at 4°C and the sediment was processed immediately for microelectrode analysis, most probable number (MPN) studies and microcosm incubations.

A high-resolution oxygen microelectrode profile was taken from an intact push-core immediately upon arrival in the laboratory (within 2 h of sampling during which time it was stored under darkness) with a Unisense Clark-type oxygen microelectrode with a tip diameter of 100 μm. The electrode was two-point calibrated in air-saturated water and anoxic water. The detection limit was 0.3 $\mu mol \cdot L^{-1}$. Measurements were taken with a micromanipulator at depth intervals of 500 μm.

The water content of littoral sediment was determined in triplicate by weighing portions of wet sediment, drying them for 4 days at 95°C, and subsequently determining the dry weight. Dried samples were pulverized to fine powder from which the percentage of iron by weight was determined using X-ray fluorescence analysis (XRF) employing a Bruker AXS S4 Pioneer X-ray fluorescence spectrometer. The dissolved organic carbon (DOC) and total inorganic carbon (TIC) content of the pore water were determined from a centrifuged portion of wet sediment, of which the supernatant was subsequently filtered with a 0.45 μm filter (mixed esters of cellulose nitrate and acetate membrane). DOC and TIC of the water overlying the surface of the sediment was determined from filtrated water (0.45 μm, mixed esters of cellulose nitrate and acetate membrane). Samples were then analyzed in a High TOC Elementar instrument. The aqueous ferrous iron concentration ($\mu moles \cdot L^{-1}$) was measured from the pore water by the spectrophotometric ferrozine assay (Stookey, 1970) in a Flashscan 550 microplate reader, Analytik Jena AG, Germany with a 5% error.

SET-UP OF MICROCOSM INCUBATIONS

Lake water for the microcosm experiments was purged with N_2 gas for 1 h and buffered with 20 mM 3-(*N*-morpholino)propanesulfonic acid (MOPS) buffer, with the exception of set-ups with bicarbonate amendment which were buffered with 10 mM bicarbonate buffer, and filtered sterilely (0.22 μm, mixed ester cellulose membrane) under a N_2 atmosphere in a glovebox. The pH of the water was adjusted with sterile anoxic 1 M HCl to 7.20, which was the pH measured in the natural lake water before purging.

Hundred milliliter serum bottles were filled with 1 g of wet sediment and 50 mL lake water (natural water, not medium, to stay as close as possible to *in situ* conditions), sealed with a butyl rubber stopper and crimped. The headspace was replaced by N_2/CO_2 (90:10) gas. One set-up contained only pure sediment and water, whilst the other set-ups contained an amendment including: 4 mM NO_3^- or 10 mM Fe^{2+} or 10 mM Fe^{2+} and 10 mM HCO_3^-. Additionally, each set-up included a sterile set of duplicates by anoxic NaN_3 addition (the final concentration was 160 mM). All microcosms were set-up in duplicate at 23°C, of which one set was incubated under constant light (True Light 15 W/5500 K) and the other in constant darkness, for 30 days. The light incubations facilitated both phototrophic and nitrate-reducing iron(II)-oxidizers whilst the dark incubation only permitted nitrate-reducing iron(II)-oxidizers to oxidize Fe(II). This allows a distinction between the two microbial anaerobic iron(II) oxidation processes.

ANALYSIS OF MICROCOSM INCUBATIONS

Two milliliters were sampled from each microcosm at each sampling point under a constant N_2 atmosphere in an anoxic glovebox, without opening the bottles, with a sterile anoxic syringe and needle (inner diameter of 0.80 mm). These 2 mL samples were centrifuged for 5 min at 15.4 g. Part of the supernatant was stabilized in 1 M HCl and used for the spectrophotometric ferrozine assay (Stookey, 1970) to quantify dissolved Fe(II)/Fe(total) in $\mu moles \cdot L^{-1}$ which was then recalculated to the absolute amount per microcosm; another part was frozen anoxically at −20°C and preserved for dissolved NO_3^-/NO_2^- measurement by a flow injection analysis (FIA) system (3-QuAAtro, Bran&Lübbe, Norderstedt, Germany) which exhibited an error of $3.6 \cdot 10^{-3}$ $mol \cdot N \cdot L^{-1}$. The sediment pellet was further incubated anoxically for 1 h on a horizontal shaker at 150 rpm with 0.5 M HCl in order to extract the poorly crystalline Fe(II)/Fe(total) fraction, which was quantified from the supernatant by the spectrophotometric ferrozine assay (Stookey, 1970) in $\mu moles \cdot L^{-1}$ which was then recalculated to the absolute amount per microcosm.

MOST PROBABLE NUMBER QUANTIFICATION OF Fe(II)-OXIDIZING MICROORGANISMS

The 3 mm sediment layer right below the oxic/anoxic boundary, defined by microelectrode measurements, was sampled under air using a subcore slicer (Gerhardt et al., 2005) and homogenized inside an anoxic glovebox. The subcore slicer allows sampling at a resolution of 1 mm by pushing the sediment out of the plexiglass core in 1-mm steps. From this homogenized wet sediment 1 mL was inoculated anoxically into a tube containing 9 mL of 22 mM bicarbonate buffered non-amended freshwater medium with a pH of 7.17 (modified from Hegler et al., 2008; Ehrenreich and Widdel, 1994 containing 0.6 $g \cdot L^{-1}$ KH_2PO_4, 0.3 $g \cdot L^{-1}$ NH_3Cl, 0.5 $g \cdot L^{-1}$ $MgSO_4 \cdot H_2O$, 0.1 $g \cdot L^{-1}$ $CaCl_2 \cdot 2H_2O$). From this a 10-fold dilution series into subsequent medium tubes was prepared anoxically (10^{-1} to 10^{-12}) and inoculated into deep well plates containing medium targeting specifically: photoferrotrophic (22 mM bicarbonate buffered 10 mM Fe^{2+} (before filtration) filtered freshwater medium), mixotrophic nitrate-reducing iron-oxidizing (22 mM bicarbonate buffered freshwater medium with 10 mM Fe^{2+}, 4 mM NO_3^- and 0.5 mM acetate) and autotrophic nitrate-reducing iron-oxidizing (22 mM bicarbonate buffered freshwater medium with 10 mM Fe^{2+} and 4 mM NO_3^-) bacterial groups. Deep well plates were incubated anoxically at 23°C for 8 weeks. Positive wells were

significantly optically darker than negative wells. Results were analyzed using the KLEE software program (Klee, 1993). Three portions from the remaining sediment were weighed and dried for 4 days at 95°C and weighed again for pore water determination.

Fe(II) OXIDATION RATE CALCULATIONS

The maximum Fe(II) oxidation rates (ν_{max}) in pure cultures were determined from different literature studies (Jiao et al., 2005; Hegler et al., 2008; Muehe et al., 2009) by subtracting the minimum Fe(II) concentration at the end of Fe(II) oxidation, from the maximum Fe(II) concentration, i.e., the concentration of iron before the initiation of Fe(II) oxidation, thus obtaining the total amount of Fe(II) that was oxidized [ΔFe(II)]. This was divided by the number of days during which maximum Fe(II) oxidation took place (Δt) and then further divided by the number of cells present at the inflection point of maximum Fe(II) oxidation:

$$\nu_{max} = \frac{\frac{\Delta Fe(II)}{\Delta t}}{\text{cells inflection point}}$$

The maximum Fe(II) oxidation rates per cell in the microcosm studies were determined by dividing the fastest initial Fe(II) oxidation rate by the cell numbers determined from the MPN studies. The number of cells present at the inflection point were not determined, thus for simplicity the MPN values of the cell numbers in the original sediment were used, probably slightly overestimating the oxidation rate per cell at the inflection point.

$$\nu_{max} = \frac{\frac{\Delta Fe(II)}{\Delta t}}{\text{MPN value}}$$

RESULTS

SEDIMENT CHARACTERISTICS

Lake Constance littoral sediment was of a sandy nature without any coarse clumps or large organic material. The DOC content of the water overlying the sediment was 0.15 mM, and the TIC content was 2.45 mM. The pore water content of the sediment at a depth of 6–9 mm was 41% and had a circumneutral pH ranging between 7.17–7.20. The DOC of the pore water was 0.39 mM and the TIC was 6.26 mM. The dissolved nitrate concentration in the pore water was 0.10 μM, and the nitrite concentration was 0.056 μM. The total iron content of the dry weight sediment was 1.19%, as measured by XRF. The sediment pore water contained 9.8 μM Fe(II). A summary of all the measured geochemical parameters of the sediment can be found in **Table 1**.

Table 1 | Geochemical parameters of littoral Lake Constance sediment (6–9 mm).

Sediment characteristics		
Porewater pH	7.17–7.20	
Pore water content	41%	(±1%)
Total $Fe_{(solid\ phase)}$	1.19%	
$Fe(II)_{(aq)}$	9.8 μM	(±2.8 μM)
$DOC_{sediment\ porewater}$	0.39 mM	($\pm 4.2 \cdot 10^{-3}$ mM)
$DOC_{water\ overlying\ the\ sediment}$	0.15 mM	($\pm 3.3 \cdot 10^{-3}$ mM)
$TIC_{sediment\ porewater}$	6.26 mM	($\pm 2.3 \cdot 10^{-2}$ mM)
$TIC_{water\ overlying\ the\ sediment}$	2.45 mM	($\pm 3.3 \cdot 10^{-3}$ mM)
$NO^-_{3(aq),\ porewater + overlying\ water}$	0.10 μM	(±0.008 μM)
$NO^-_{2(aq),\ porewater + overlying\ water}$	0.056 μM	(±0.001 μM)

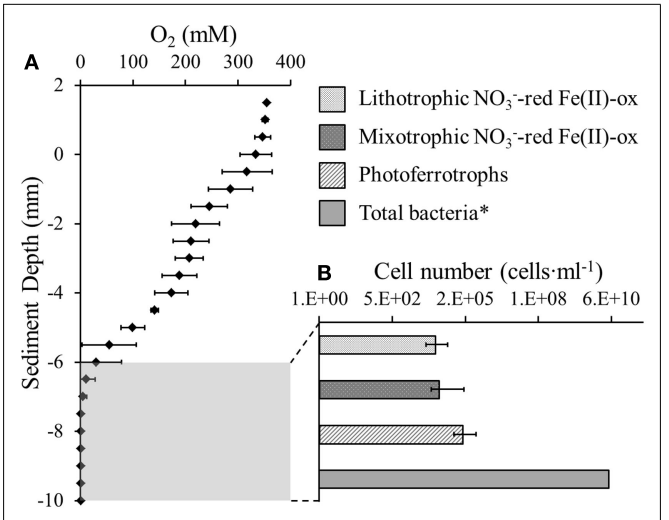

FIGURE 1 | Anaerobic Fe(II)-oxidizing bacteria were quantified beneath the oxic-anoxic boundary zone in littoral Lake Constance sediments. **(A)** An oxygen microelectrode profile indicating the oxygen penetration depth in the littoral sediment. **(B)** Most probable number (MPN) study quantifying phototrophic and nitrate-reducing Fe(II)-oxidizers in the anoxic part of the littoral sediment. Total bacterial cells were quantified by qPCR (Rahalkar et al., 2009).

MICROSENSOR OXYGEN PROFILE AND THE DISTRIBUTION OF Fe(II)-OXIDIZING MICROORGANISMS

The oxygen distribution in the top 6 mm of the littoral Lake Constance sediment showed a stepwise decrease in 2 mm increments until it reached the maximum penetration depth at 6 mm (**Figure 1A**). As anaerobic iron(II)-oxidizing bacteria depend on anoxic conditions, their habitat may be restricted by the overlaying oxygen boundary zone. Therefore, the 3 mm of sediment directly beneath the oxygen penetration depth was inoculated in a MPN study. We found that both nitrate-reducing iron(II)-oxidizers and photoferrotrophs were present in the same 3 mm segment of anoxic sediment (**Figure 1B**). The photoferrotrophs were slightly more abundant than the nitrate-reducing iron(II)-oxidizers at $2.0 \cdot 10^5$ cells·mL^{-1} sediment. As the sediment had a pore water concentration of 41% (**Table 1**), this cell number corresponds to $3.4 \cdot 10^5$ cells·g^{-1} dry weight sediment. The mixotrophic nitrate-reducing iron(II)-oxidizers were slightly more abundant than the autotrophic nitrate-reducing iron(II)-oxidizers at $2.7 \cdot 10^4$ and $1.9 \cdot 10^4$ cells·mL^{-1}, respectively, which corresponds to $4.5 \cdot 10^4$ and $1.8 \cdot 10^4$ cells·g^{-1} dry weight sediment.

MICROBIAL Fe(II) OXIDATION IN LITTORAL LAKE CONSTANCE SEDIMENT

No detectable iron(II) oxidation took place in non-amended sediment microcosms incubated in the dark, neither in the microbially active nor in the sterilized set-up (**Figure 2A**). However, when the

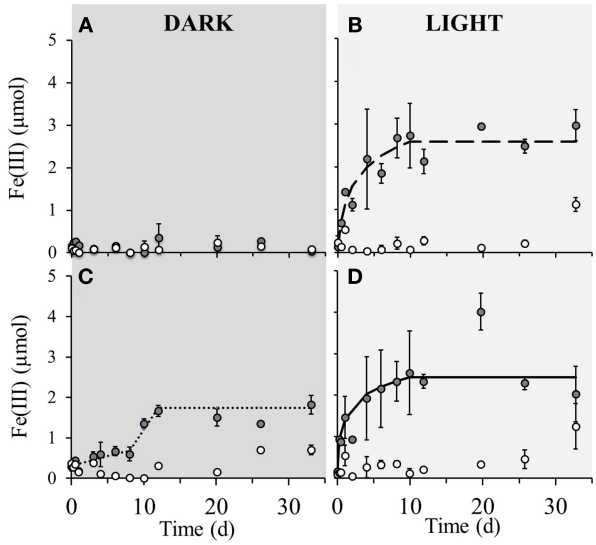

FIGURE 2 | Poorly crystalline Fe(III) formation in microcosm incubations (*y*-axis shows total Fe(III) content per microcosm set-up) over a period of 33 days in dark and light set-ups at 23˚C. Closed circles (●) represent biotic set-ups whilst open circles (○) signify sterile set-ups (160 mM NaN_3 addition). **(A)** Non-amended sediment incubated in the dark, **(B)** Non-amended sediment incubated in the light. **(C)** 4 mM nitrate amended sediment incubated in the dark, **(D)** 4 mM nitrate amended sediment incubated in the light. The dashed and solid lines indicate modeled trendlines. Error bars indicate minimum and maximum Fe(III) values from duplicates.

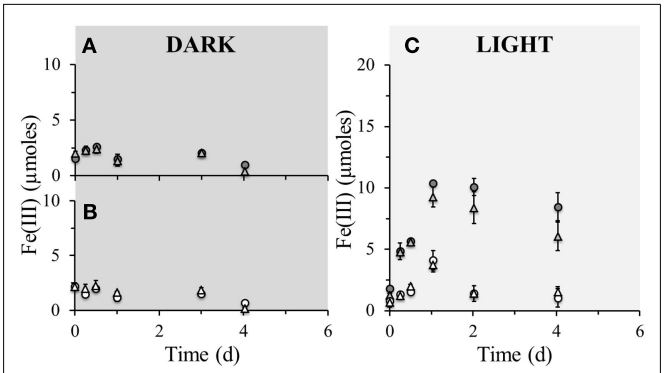

FIGURE 3 | Poorly crystalline Fe(III) formation in microcosm incubations (*y*-axis shows total Fe(III) content per microcosm set-up) over a period of 4 days at 23˚C. Closed circles (●) represent biotic set-ups with 10 mM Fe(II) amendment whilst open circles (○) represent parallel sterile set-ups (160 mM NaN_3 addition) with the same amendment. Closed triangles (▲) represent biotic set-ups with 10 mM Fe(II) and 10 mM HCO_3^- amendment and open triangles (△) represent parallel sterile set-ups (160 mM NaN_3 addition) with the same amendments. **(A)** Comparison of microbially active dark set-up of solely Fe(II) amendment with Fe(II) and supplementary HCO_3^- amendments. **(B)** Comparison of sterile dark set-up of solely Fe(II) amendment with Fe(II) and supplementary HCO_3^- amendments. **(C)** Comparison of microbially active and sterile light set-ups of solely Fe(II) amendment with Fe(II) and supplementary HCO_3^- amendments. Error bars indicate minimum and maximum Fe(III) values from duplicates.

same set-up was incubated under light conditions, instant oxidation occurred in non-sterile microcosms with an initial oxidation rate of $5.4{\cdot}10^{-6}$ µmol Fe(II)/cell·day^{-1} which leveled off after approximately 8 days (**Figure 2B**). Sterile set-ups with light did not exhibit significant Fe(II) oxidation. When nitrate was added to the non-sterile sediment followed by incubation in the dark, iron(II) oxidation occurred after 8 days of incubation and ceased after around the 12th day of incubation (**Figure 2C**). The maximum iron(II) oxidation rate in these set-ups between days 8 and 12 was $7.1{\cdot}10^{-6}$ µmol Fe(II)/cell·day^{-1}. Nitrate addition to the sediment and incubation under light conditions resulted in an instant onset of Fe(II) oxidation at a rate of $3.7{\cdot}10^{-6}$ µmol Fe(II)/cell·day^{-1} which plateaued after approximately 8 days (**Figure 2D**). Fe(II) oxidation in dark microcosms with addition of Fe(II) or Fe(II) and bicarbonate (but without nitrate addition) resulted in no significant Fe(II) oxidation in neither the microbially active nor in the sterilized set-up (**Figures 3A,B**). In light set-ups amended exclusively with ferrous iron, the initial Fe(II)-oxidation rate and extent were practically equivalent to that amended with ferrous iron and supplementary bicarbonate addition (**Figure 3C**).

MAXIMUM Fe(II) OXIDATION RATES CALCULATED FROM PURE CULTURES AND MICROCOSMS

Several growth experiments in the literature with different pure culture strains were investigated to calculate the maximum Fe(II) oxidation rate of several pure strains of anaerobic Fe(II)-oxidizers. Strain BoFeN1 is a nitrate-reducing Fe(II)-oxidizing β-proteobacterium from the *Acidovorax* genus isolated from littoral Lake Constance sediment (Kappler et al., 2005b). Growth experiments with this strain in which cell numbers and Fe(II) concentration were monitored over time (Muehe et al., 2009) provided data that allowed the maximum rate calculation for this species. Two individual photoferrotrophic strains were investigated for their maximum iron oxidation rate. The first was isolated from School Street Marsh in Woods Hole Massachusetts; *Rhodopseudomonas palustris*, or strain TIE-1 (Jiao et al., 2005). The second, *Rhodobacter ferrooxidans* sp. SW2 (Ehrenreich and Widdel, 1994) was isolated from a pond near Hanover, Germany. Growth experiments with this strain (Hegler et al., 2008) allowed the rate calculations to be made. The results are summarized in **Table 2** and show an Fe(II) oxidation rate of $1.0{\cdot}10^{-8}$ µmol Fe(II)/cell·day^{-1} for the nitrate-reducing Fe(II)-oxidizing strain BoFeN1 and $4.4{\cdot}10^{-10}$ and $6.6{\cdot}10^{-9}$ µmol Fe(II)/cell·day^{-1} for the photoferrotrophs SW2 and TIE-1, respectively.

DISCUSSION

SPATIAL DISTRIBUTION OF ANAEROBIC Fe(II)-OXIDIZERS IN FRESHWATER LAKE SEDIMENT

In the littoral zone, where water levels fluctuate according to waves and wind shearing, the top layer of the sediment is subjected to irregular mechanical mixing and light irradiation (Chubarenko et al., 2003). This causes the oxygen penetration depth to vary according to these external forces exerted on the sediment and overlying water (Gerhardt et al., 2005). The oxygen penetration depth is also influenced by the ambient temperature, as the dissolution of oxygen in pore water is facilitated at lower temperatures.

Table 2 | Maximum Fe(II) oxidation rates per cell measured in pure cultures and in littoral freshwater lake sediment from microcosm experiments.

Species/group	Maximum Fe(II) oxidation rate (μmol Fe(II)/cell·day^{-1})
Acidovorax strain BoFeN1[1]	$1.0 \cdot 10^{-8}$
Rhodobacter ferrooxidans sp. SW2[2]	$4.4 \cdot 10^{-10}$
Rhodopseudomonas palustris, strain TIE-1[3]	$6.6 \cdot 10^{-9}$
Microcosm photoferrotrophs[4]	$5.4 \cdot 10^{-6}$
Microcosm NO_3^--reducing Fe(II)-oxidizers[4]	$7.1 \cdot 10^{-6}$

[1] *Kappler et al. (2005b).*

[2] *Hegler et al. (2008).*

[3] *Jiao et al. (2005).*

[4] *This study, the maximum Fe(II) oxidation rate was determined from the microcosm incubations; the cell numbers used for the calculation stem from the MPN quantification.*

Additionally, phototrophic oxygen production causes day/night fluctuations to the littoral oxygen penetration depth (Gerhardt et al., 2005) and to the nitrate-reducing redox zone (Gerhardt et al., 2010). As ferrous iron is readily oxidized to ferric iron by molecular oxygen (Davison and Seed, 1983), the variable intensity of the oxygen concentration indubitably causes a variation in the ferrous iron concentration, which diffuses upward from deeper sediment layers. During daylight hours, light has been shown to penetrate through sediment up unto a depth of at least 5–6 mm (Kuehl et al., 1994). However, the sediment investigated in that study exhibited a grain size toward the lower range of that of the Lake Constance sediment. As light penetration depends on the grain size, it is conceivable that light could reach a depth beyond 6 mm in Lake Constance littoral sediment. This is confirmed by the observation that light exposure of the Lake Constance littoral sediment causes an increase in ferrous iron oxidation up until an approximate depth of 7.5 mm (Gerhardt et al., 2005). Thus, the light penetration depth intersects both the oxic and the denitrification zone. In this case, the denitrification zone provides ideal conditions for both anaerobic photoferrotrophs and nitrate-reducing iron-oxidizing bacteria. Indeed, the geochemical oxygen profile in combination with the MPN data in a littoral sediment core clearly demonstrated that the photoferrotrophic and nitrate-reducing Fe(II)-oxidizers co-exist below the sedimentary chemocline in the topmost anoxic segment of the sediment (**Figure 1**). Although this method is restricted in the sense that it cannot directly assess their activity, their presence is an indication that they could be active in this sediment layer. Sharing a habitat poses some serious constraints on their shared substrate requirement and creates a situation where the potential exists for these two groups of bacteria to individually adapt to compete for the limited ferrous iron supply. Considering the variability of the oxygen penetration depth in littoral lake sediment, the microbes catalyzing these anaerobic processes must have developed a way to overcome the spatial changeability of their anoxic habitat beneath the sedimentary chemocline. This can mean a number of things, for instance they could be more tolerant to oxygen than previously considered and possibly even switch to a metabolism that employs O_2 as electron acceptor, or have developed a way to move together with the oxygen penetration depth, thus avoiding exposure to oxygen.

Abundance of anaerobic Fe(II)-oxidizing bacteria

Phototrophic Fe(II)-oxidizing bacteria have not previously been enumerated in freshwater lake sediments at circumneutral pH. There are many variables that could influence the degree of photoferrotrophic abundance, such as Fe(II) supply and light irradiation. Previously published data only include an MPN study of Fe(II)-oxidizing phototrophic bacteria in a freshwater town ditch and a freshwater pond. They report numbers between $1.1 \cdot 10^2$ and $3.9 \cdot 10^3$ cells·g^{-1} dry weight sediment (Straub and Buchholz-Cleven, 1998), which are lower than the results from this study (**Figure 1**) by approximately two orders of magnitude. An explanation for this discrepancy could simply be that Lake Constance is a more suitable environment for the photoferrotrophs to thrive in, since it is a more stable environment than the small ditch or pond investigated in the other studies and therefore allows the photoferrotrophs to establish themselves more successfully.

Multiple studies have been conducted on quantifying nitrate-reducing Fe(II)-oxidizing bacteria in environmental samples (Straub and Buchholz-Cleven, 1998; Hauck et al., 2001; Weber et al., 2006a; Muehe et al., 2009). In Lake Constance, their abundance was quantified in both profundal ($1.0 \cdot 10^4$–$5.8 \cdot 10^5$ cells/mL; Hauck et al., 2001) and littoral sediment (at 5 mm depth; $8 \cdot 10^3$ cells/mL; Muehe et al., 2009). In the current study we counted $2.7 \cdot 10^4$ cells/mL which lies neatly within range of the previous studies.

Thus, though the littoral Lake Constance photoferrotrophic abundance is slightly higher than measured in previous studies of other environments, nitrate-reducing Fe(II)-oxidizing microorganisms fall within the range of previously quantified cell numbers. To our knowledge, this is the first study which has detected and quantified both groups of bacterial iron oxidation metabolisms in the same sediment layer.

LIMITATIONS OF ANAEROBIC Fe(II) OXIDATION IN ANOXIC SEDIMENTS

Phototrophic and nitrate-reducing Fe(II)-oxidizing microorganisms have been formerly studied and cultured in pure cultures (Ehrenreich and Widdel, 1994; Muehe et al., 2009) and enrichments (Straub and Buchholz-Cleven, 1998) but their collective *in situ* behavior has not previously been monitored in the context of microcosms. Microcosm studies are well suited to investigate substrate limitations imposed on Fe(II)-oxidizers and thereby the environmental competition pressure for their substrate requirements which control the abundance and activity of the different groups of Fe(II)-oxidizers. Such studies have so far not yet been performed for Fe(II)-oxidizers. Consequently, there is little known about the limitations the natural environment imposes on their habitat and diet.

Nitrate limitations

The DOC and aqueous Fe(II) concentration in the pore water of littoral Lake Constance sediment (**Table 1**) were used to calculate their electron donating capacity, and thus the amount of nitrate that could in theory be reduced. Following this, conclusions were

drawn on the excess or limitation of nitrate in the natural sediment assuming the following equation applies to all nitrate-reducing iron(II)-oxidizing bacteria:

$$10Fe^{2+} + 2NO_3^- + 24H_2O \rightarrow 10Fe(OH)_3 + N_2 + 18H^+$$

(Straub et al., 1996)

The measured dissolved ferrous iron concentration in the pore water of the sediment was 9.8 μM (**Table 1**). As 10 mol of iron can reduce 2 mol of nitrate, this amount of iron can reduce 1.96 μM nitrate in the sediment. Additional to Fe(II) oxidation, heterotrophic denitrification is a common process in sedimentary systems which adheres to the following equation:

$$2NO_3^- + 10\,e^- + 12H^+ \rightarrow N_2 + 6H_2O$$

A concentration of 0.39 mM DOC (**Table 1**) was measured in the pore water of the lake sediment. As each carbon atom in organic matter/biomass has the capacity to donate approximately four electrons in reduction reactions, the DOC has a theoretical electron donating capacity of 1.56 mM electrons. These electrons can reduce 0.31 mM nitrate to dinitrogen through the process of denitrification. Adding the amount of nitrate that can be reduced through Fe(II) oxidation and denitrification, $1.96{\cdot}10^{-3} + 0.31$ mM respectively, a total amount of $3.12{\cdot}10^{-1}$ mM nitrate could be reduced. As the dissolved nitrate concentration in the sediment pore water is 0.1 μM (**Table 1**), this suggests that the littoral Lake Constance sediment is severely nitrate limited. Considering that probably only a fraction of the DOC is bioavailable, the more than 100-fold excess of electrons from DOC compared to electrons available from Fe(II) suggests that the reduction of nitrate using electrons from organic matter oxidation is more important in this environment than the oxidation of Fe(II) coupled to nitrate reduction.

If the sediment is indeed limited in nitrate, the metabolism of the nitrate-reducing Fe(II)-oxidizers might be compromised, which would mean they might not be able to optimally oxidize ferrous iron in natural non-amended sediment. In fact, natural sediment incubated in the dark did not reveal any detectable Fe(II) oxidation over time (**Figure 2A**), however, when the sediment was amended with 4 mM nitrate the cells did start to oxidize iron, but only after a lag-phase period of 8 days (**Figure 2C**). This lack of oxidation in absence of supplementary nitrate addition endorses the hypothesis that the sediment is nitrate limited, as predicted from the previous calculations. This gives phototrophic Fe(II)-oxidizers a substantial advantage during daylight hours, as adding light to natural sediment evoked an immediate instigation of microbial Fe(II) oxidation (**Figure 2B**).

It has previously been reported that most nitrate-reducing Fe(II)-oxidizers are capable of pure denitrification (Straub et al., 1996, 2004; Muehe et al., 2009), utilizing organic carbon as electron donor. It is possible that the nitrate-reducing Fe(II)-oxidizers employ this system of denitrification in non-amended sediment, thus explaining the lack of Fe(II) oxidation (**Figure 2A**). In nitrate amended sediment microcosms incubated under darkness, Fe(II) oxidation was only initiated after an 8 day lag-phase (**Figure 2C**). This suggests that initially denitrification is coupled to the oxidation of organic matter before switching to the oxidation of ferrous iron. It has been shown that the model nitrate-reducing Fe(II)-oxidizing strain BoFeN1 oxidizes acetate before it utilizes ferrous iron (Kappler et al., 2005b; Chakraborty et al., 2011). When coupling this observation to the results from this study, this suggests that the reduction of nitrate is controlled by a sequential depletion of preferential substrates led by the oxidation of DOC. Furthermore, DOC may be harvested from the environment and stored in internal storage compartments for use during periods of substrate limitation. Such storage compartments have recently been described in the cytoplasm of model organism BoFeN1 (Miot et al., 2011).

Though mixotrophic iron(II)-oxidizers are known to favor a denitrifying metabolism which couples nitrate reduction to organic matter oxidation, addition of ferrous iron to their environment increases their growth yield (Muehe et al., 2009; Chakraborty et al., 2011), thus making mixotrophic iron(II) oxidation a beneficial lifestyle. Apart from mixotrophic iron(II) oxidation, it has been suggested that autotrophic iron(II) oxidation may also be a feasible metabolism. So far, only an autotrophic nitrate-reducing Fe(II)-oxidizing co-culture has been successfully enriched (Straub et al., 1996; Bloethe and Roden, 2009b) and an isolate is yet to be obtained. As these autotrophic Fe(II)-oxidizers do not require an organic co-substrate for Fe(II)-oxidation, they theoretically should be able to initiate Fe(II) oxidation immediately upon incubation for their growth and survival in nitrate amended sediment (**Figure 2C**). As this did not occur and an isolate has so far not yet been attained and cultured for several generations, this begs the question whether they truly play a significant role in Fe(II) oxidation at all.

Additionally to being capable of denitrification, some nitrate-reducing Fe(II)-oxidizing strains are also capable of switching to a microaerophilic metabolism (Benz et al., 1998; Edwards et al., 2003). Though it is still speculative, it is feasible that the nitrate-reducing Fe(II)-oxidizing bacteria in littoral lake sediments are able to adapt to a microaerophilic Fe(II) oxidation metabolism during daylight hours in order to successfully compete with the phototrophic Fe(II)-oxidizers for ferrous iron. However, as the microcosm incubation experiments in our study were set-up anoxically, microaerophilic Fe(II) oxidation could not occur. Studying the competition between microaerophilic, nitrate-reducing, and phototrophic Fe(II)-oxidizers in a stratified system during the day-night cycle will be an interesting topic of research in future studies.

The capability to switch to an alternative metabolism is also known for other strains instrumental to the Fe cycle. For instance, *Geobacter* strains are capable of switching between nitrate-reducing Fe(II) oxidation and Fe(III) reduction (Weber et al., 2006b; Coby et al., 2011) though a lag-phase resulting from the necessity to synthesize proteins for an alternative metabolism has not yet been described in Fe(II)-oxidizing bacteria and it is hitherto unknown if and how this lag-phase manifests itself in the natural environment. The ability to switch between metabolisms may be more widespread and more frequently engaged than previously thought, to maintain a dynamic Fe cycle in environments subjected to constantly changing geochemical parameters.

Co-substrate limitations

Many nitrate-reducing Fe(II)-oxidizers require an organic co-substrate to maintain optimum iron(II) oxidation rates and for continuous growth over several generations (Straub et al., 1996). Many growth experiments necessitate acetate addition to Fe(II) saturated systems ranging between 0.5 and 2.0 mM acetate per 4–8 mM Fe(II) (Straub et al., 1996, 2004; Kappler et al., 2005b; Muehe et al., 2009). The littoral Lake Constance sediments contain 0.39 mM DOC and 9.8 μM Fe(II) (**Table 1**). Hence, the sediment contains more organic carbon than Fe(II), which means nitrate-reducing Fe(II)-oxidizing bacteria are most probably not limited in the availability of an organic co-substrate required for Fe(II) oxidation. Consequentially, there is no objection for denitrification to be coupled to organic carbon oxidation which explains why there is a lack of Fe(II) oxidation in non-amended sediments incubated under darkness (**Figure 2A**) and why there is an initial lag-phase before Fe(II) oxidation in dark nitrate amended sediments (**Figure 2C**). Photoferrotrophs do not require an organic co-substrate since they use CO_2 as electron acceptor, therefore they would not be affected by an organic carbon limitation.

Bicarbonate limitations

To investigate whether phototrophic Fe(II)-oxidizers are subjected to inorganic carbon limitations, set-ups containing either only 10 mM ferrous iron, or 10 mM ferrous iron and 10 mM bicarbonate amendments were set-up (**Figure 3**). Using the TIC concentration measured in the pore water (**Table 1**) the amount of bicarbonate in the sediments could be estimated to be 6.26 mM. This means that the bicarbonate amended sediments contain roughly three times more bicarbonate than the non-amended sediments. In light set-ups containing ferrous iron amendment, the Fe(II) oxidation extent was independent from bicarbonate addition. This suggests that photoferrotrophic Fe(II) oxidation is not restricted by the supply of bicarbonate in the sediments, which further suggests that as soon as there is Fe(II) and light available, phototrophic Fe(II) oxidation will commence immediately, giving them a seemingly unprecedented advantage over the nitrate-reducing iron(II)-oxidizers. Consequently, phototrophic iron oxidation may be of paramount importance to the iron cycle in these littoral freshwater sediments.

THE POTENTIAL FOR COMPETITION BETWEEN NITRATE-REDUCING AND PHOTOTROPHIC Fe(II)-OXIDIZERS

By quantifying the Fe(II) oxidation rate per cell per day from pure culture studies and environmentally relevant microcosms, the relative contribution efficiency of the two different metabolic groups of anaerobic Fe(II)-oxidizing bacteria to overall environmental Fe(III) formation could be assessed. Additionally, by comparing these oxidation rates and extent of Fe(III) formation, conclusions on the competition between these two co-existing groups could be evaluated, which has hitherto remained an un-investigated research topic.

Maximum Fe(II) oxidation rates

It can be expected that the Fe(II) oxidation rate attained by bacteria cultivated in pure cultures is higher than the rate obtained in environmental systems. In a controlled and optimized laboratory setting they have unlimited access to the nutrients and living space they require to thrive. However, the maximum Fe(II) oxidation rates calculated from pure culture studies were significantly lower, by two to four orders of magnitude, than those observed in the microcosms with littoral sediments (**Table 2**). This may be due to an underestimation of the environmental cell numbers owing to limitations affiliated with the MPN method (Cochran, 1950). As a consequence, the Fe(II) oxidation rate would have been calculated with too few cells, thus obtaining a higher Fe(II)-oxidation rate per cell than is actually achieved. Also, the broader microbial community in the sediment may have a beneficial effect on the Fe(II) oxidation rates which cannot be obtained by a pure culture; as the littoral sediment has a pore water concentration of 41% (**Table 1**), it is conceivable that the cells may achieve interspecies communication networks via quorum sensing. The sediments contain mixed interspecies colonies and biofilms of associated microbes that can interact and thus potentially lead to higher Fe(II) oxidation rates than single species can obtain in pure cultures. Moreover, the natural sediment may provide additional micronutrients and vitamins that are central to their growth and survival that are not mimicked in the artificial medium in laboratory experiments with pure cultures. Overall, the nitrate-reducing Fe(II)-oxidizing bacteria seem to exhibit a faster oxidation rate than the photoferrotrophic bacteria in both the pure cultures and the microcosms (**Table 2**).

Competition dynamics

Assuming that the light set-up with the original sediment specifically selects the phototrophic Fe(II)-oxidizers (**Figure 2B**), whilst the nitrate amended dark sediment set-up solely selects the nitrate-reducing Fe(II)-oxidizers (**Figure 2C**), the two curves, modeled based on trendlines, in these separate set-ups exclusively represent these particular anaerobic Fe(II)-oxidizing groups. The set-up that contains both light and nitrate hosts a combination of both the phototrophic and nitrate-reducing Fe(II)-oxidizing groups (**Figure 2D**). Thus, the superposition of the modeled iron(II) oxidation curves from each individual bacterial group on the Fe(II) oxidation in this particular coupled set-up allows us to draw conclusions on the contribution of each group to the total iron(III) formation (**Figure 4**). This overlay of the separate roles anaerobic phototrophic and nitrate-reducing Fe(II)-oxidizing bacteria play in Fe(III) formation, shows that the phototrophic model corresponds closely to the Fe(III) formation over time when both processes can simultaneously take place. The Fe(II) oxidation capacity of the photoferrotrophic microorganisms in littoral freshwater lake sediment is 1.08 μmol Fe(II) per day. This could be calculated from the photoferrotrophic Fe(II) oxidation rate in littoral sediments (**Table 2**), and the number of photoferrotrophs in the sediment (**Figure 1**). As the Fe(II) concentration in the sediment is 9.8 μM (**Table 1**), the photoferrotrophs will deplete the dissolved Fe(II) supply in the sediment within 1 day. Set-ups containing 10 mM Fe(II) as well as 4 mM supplementary nitrate exhibited the same 8 day lag-phase before initiating Fe(II) oxidation in dark set-ups (data not shown), and they demonstrated the same instant photoferrotrophic Fe(II) oxidation trend as in sediments only containing additional nitrate in light set-ups. This suggests that independent from the supply of Fe(II) from deeper sediment

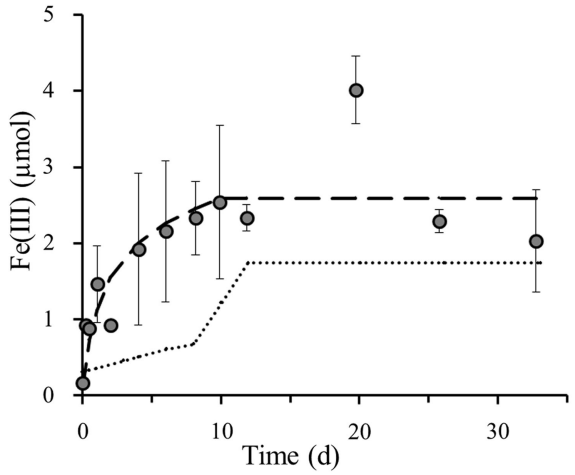

FIGURE 4 | Superposition of poorly crystalline Fe(III) formation (*y*-axis shows total Fe(III) content per microcosm set-up) in littoral lake sediments by photoferrotrophs (– – –) and nitrate-reducing Fe(II)-oxidizing bacteria (·····) onto measured poorly crystalline Fe(III) formation (●) in 4 mM nitrate amended sediments incubated under constant light at 23˚C. Error bars indicate minimum and maximum Fe(III) values from duplicates.

layers and dissolution of Fe(II)-minerals, even though nitrate-reducing Fe(II)-oxidizing bacteria can start actively respiring iron after 8 days, there will not be sufficient Fe(II) left for them to respire as the photoferrotrophs will have depleted the Fe(II) supply by then. So even though nitrate-reducing Fe(II)-oxidizers are able to oxidize iron at a higher rate than their phototrophic competitors (**Table 2**), they are still outcompeted during optimal light and temperature conditions due to substrate limitation. However, even though it is feasible that they should compete with one another for ferrous iron, denitrifiers essentially favor the available organic carbon as electron donor before switching to Fe(II) oxidation. Therefore, they do not necessarily need to compete with the photoferrotrophs for ferrous iron, because they can also survive on organic carbon. This suggests that the dynamics of nitrate dependent Fe(II) oxidation, at least in this sediment, are likely regulated by the relative availability of organic matter rather than by the competition with photoferrotrophs for ferrous iron.

Day-night cycle

Despite the fact that nitrate-reducing Fe(II)-oxidizers are outcompeted by photoferrotrophs during optimum light conditions, and the nitrate-reducers are limited in nitrate, they are still both found in the upper anoxic sediment layer. Although presence does not necessarily indicate activity, it provides an indication that they could be active, in which case they must have developed a mechanism to cope with the substrate limitations they are subjected to. One possibility is that they are able to co-exist due to the occurrence of the day-night cycle. The oxygen penetration depth in the sediments is heavily influenced by light (Gerhardt et al., 2005), thus the upper anoxic sediment layer shifts according to a day-night rhythm. Additionally, the photoferrotrophs are not able to oxidize ferrous iron at night, simply due to the lack of light. Furthermore, the light penetration depth of the incident light must penetrate beyond the oxygen penetration depth for the anaerobic photoferrotrophs to harvest the light for energy, which has previously been shown to occur in similar sediments (Kuehl et al., 1994). When cloud cover and twilight prevent maximum light irradiation, the photoferrotrophs could possibly survive by converting to chemoheterotrophic growth when organics are present in excess, which has been reported to be possible for at least one photoferrotrophic strain (Jiao et al., 2005). This provides nitrate-reducing Fe(II)-oxidizers with the upper hand, as they have the opportunity to utilize all the available Fe(II) after they have consumed the bioavailable carbon, provided this period of heterotrophic nitrate reduction does not take longer than the night and that they are not limited in nitrate. When the sun comes up, the photoferrotrophs immediately take over the dominant role in Fe(II) oxidation. As many nitrate-reducing Fe(II) oxidizers are able to switch to a pure denitrifying metabolism (Straub et al., 1996, 2004; Muehe et al., 2009) this leaves the nitrate-reducing Fe(II)-oxidizers to survive on pure denitrification, as long as organic matter and nitrate are simultaneously available. This means that although there is potential for the two Fe(II)-oxidizing groups to directly compete for ferrous iron during optimal light conditions, they are prevented from doing so because their functions are not separated in space as in conventional niche separation, but in time by the day-night cycle. This means that they still fulfill the same function: oxidizing reduced iron(II) beneath the sedimentary oxic-anoxic interface, but the photoferrotrophs perform this function exclusively during the day, whilst nitrate-reducing Fe(II)-oxidizers mostly have the opportunity to execute this at night. Alternatively, the nitrate-reducing Fe(II)-oxidizing bacteria may compete with the photoferrotrophs during daylight hours by adopting a microaerophilic Fe(II)-oxidizing metabolism once they have exhausted the organic carbon and nitrate supply. By eliminating their nitrate requirement this would allow them to overcome the nitrate limitation imposed on their habitat, thus increasing the probability of success when directly competing with the photoferrotrophs for reduced iron.

When considering all scenarios, a niche separation in time rather than space and the switching from a nitrate-reducing Fe(II)-oxidizing metabolism to a microaerophilic one and the substrate limitations to which the sediment is subjected and combining them altogether, we can speculate on the distribution of the different metabolisms by the two Fe(II)-oxidizing groups of bacteria during daylight and night-time hours (**Figure 5**). Photoferrotrophs outcompete the nitrate-reducing Fe(II)-oxidizers during daylight hours (**Figure 4**). Therefore, it is conceivable that the nitrate-reducing Fe(II)-oxidizers abandon this unfruitful method of energy sequestration for either denitrification or microaerophilia. However, as the sediments are severely limited in nitrate (**Table 1**), it is unlikely that denitrification based on either organic carbon or Fe(II) oxidation will provide sufficient energy to sustain a bacterial population. Therefore, it is more likely that they are able to compete with photoferrotrophs for Fe(II) by using oxygen as electron acceptor in a microaerophilic metabolism. At night photoferrotrophic bacteria are unable to metabolize using a photosynthetic based energy source and the oxygen penetration depth lies nearer to the surface in the sediments. The shallowing of the oxygen penetration depth causes an

upward shift in all the subsequent redox zones. Therefore, the denitrification zone essentially migrates into what was previously the micro-oxic zone (Gerhardt et al., 2010). This provides nitrate to the microaerophilic bacteria, and deprives them of oxygen, providing them with the option to switch back to a nitrate-reducing Fe(II)-oxidizing metabolism as they no longer suffer competition pressure from the photoferrotrophs for ferrous iron. Nevertheless, if they are able to harbor motility, it is also possible for them to maintain microaerophilic Fe(II) oxidation as there is still oxygen present in the sediment at night, albeit less and higher up in the sediment than during the day. During the night the photoferrotrophs will probably switch to a chemoheterotrophic metabolism due to the lack of light, requiring organic carbon as substrate. Denitrification coupled to organic carbon oxidation then becomes an unfavorable option for the nitrate-reducing Fe(II)-oxidizers as they would need to compete for organic carbon with the photoferrotrophs. When the sun comes up, the photoferrotrophs are immediately able to oxidize any Fe(II) present (**Figure 2B**) and other oxygen-producing phototrophic processes are able to proceed, deepening the oxygen penetration depth. This exposes the nitrate-reducing Fe(II)-oxidizers to substrate competitors and oxygen, forcing them to switch back to a microaerophilic metabolism in order to sustain Fe(II)-based growth. Moreover, as the daytime microaerophilic oxidation zone during the day coincides with that of nitrate reduction during the night (**Figure 5**) due to the shifting redox zones, it would be unnecessary for the bacteria to physically move to a different redox zone if they switch their anaerobic metabolism to a microaerophilic one. In fact, bacteria are unable to swim great distances due to buffeting by Brownian motion and their motion path is not straight but curved resulting from a rotating flagellum (Armitage, 1999), reinforcing the hypothesis that switching between metabolisms is a feasible option. Alternatively, they can adopt a denitrifying metabolism, oxidizing organic carbon. This implies that not only their niche for Fe(II) oxidation is organized in a day-night rhythm, their metabolisms are staggered to alternate between organic carbon and ferrous iron oxidation as a strategy to overcome direct competition pressure. Hence, our results suggest that the two iron(II) oxidation processes indeed probably do not need to compete directly with each other, as they are temporally separated by the day-night cycle and due to the fact that the nitrate-reducers preferentially use organic carbon before Fe(II) as their electron donor.

Seasonal dynamics

If these two metabolic groups of anaerobic Fe(II)-oxidizers indeed rely on the day-night cycle, then they are also influenced by seasonal oscillations which create longer days as summer progresses, and shorter ones as the winter comes around. Additionally, the light intensity affects the primary productivity of the overall sedimentary microbial community (Overmann and Tilzer, 1989). Previous studies have reported that the ferrous iron concentration also varied throughout the year, being lowest in winter and highest at the end of the summer (Gerhardt et al., 2005). Moreover, Lake Constance hosts an annual spring phytoplankton bloom which generates a large influx of organic carbon into the sediments (Peeters et al., 2007), possibly facilitating the nitrate-reducing Fe(II)-oxidizing communities in the sediments by blocking direct

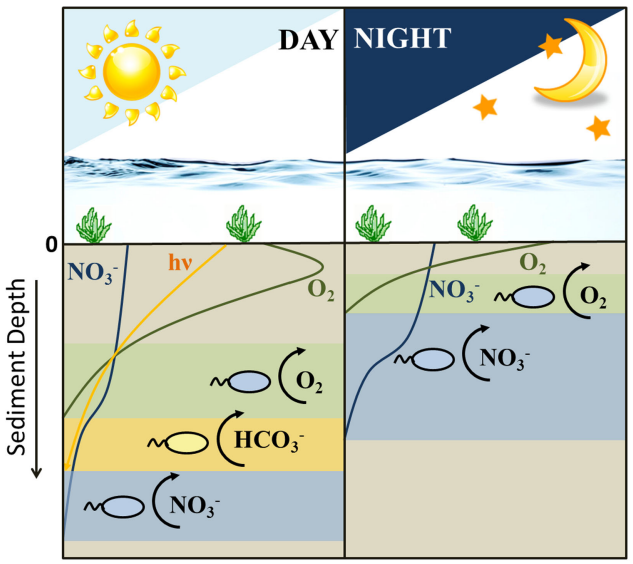

FIGURE 5 | Schematic diagram illustrating the shifting distribution of Fe(II)-oxidizing metabolisms (i.e., varying electron acceptors for ferrous iron oxidation) and the typical depth distribution of oxygen, nitrate, and light during the day/night cycle in littoral freshwater lake sediments. Sediment depth is typically on a mm scale. During the daytime there are three possible Fe(II)-oxidizing metabolisms active in the sediment column: microaerophiles, photoferrotrophs, and nitrate-reducing Fe(II)-oxidizing bacteria. During the night, Fe(II) can only be oxidized through microaerophilic and nitrate-reducing Fe(II) oxidation.

sunlight in the water column, and providing organic co-substrates to the sediment. Another central variable is temperature, which not only affects biotic activity, but also geochemical parameters such as the solubility of oxygen. It has been reported that photoferrotrophic cultures of KoFox and SW2 are able to oxidize ferrous iron over a wide temperature scale ranging from 5°C to 30°C, with their optimum lying around the 25°C (Hegler et al., 2008). This suggests that they might be able to oxidize iron more efficiently during summer when the temperature is higher. As the sediment used in the present study was sampled in winter, it is conceivable that the nitrate and carbon limitations may only be of significant importance during winter. The fact that the variables affecting substrate availability for anaerobic Fe(II) oxidation are controlled by seasonal forcing suggests that seasonal dynamics may play a large role in the co-existence of the microorganisms catalyzing these processes.

CONCLUSION

Anaerobic nitrate-reducing Fe(II)-oxidizers and photoferrotrophs co-exist in littoral freshwater lake sediments in the topmost anoxic sediment layer directly below the oxygen penetration depth. They share a common ferrous iron substrate requirement that is only present in limited supply, thus creating a situation in which they ought to compete for Fe(II). However, the results showed that this is not necessarily the case and their ability to co-exist may be attributed to the day-night cycle. Lake Constance's littoral sediments are limited in nitrate, which poses a challenge for nitrate-reducing

iron(II)-oxidizing bacteria. Nevertheless, nitrate-reducing Fe(II)-oxidizers exhibit a faster Fe(II) oxidation rate both in pure cultures and in the environmental systems (microcosms) than photoferrotrophs. However, during optimal light and substrate conditions they are outcompeted by photoferrotrophic bacteria. Thus, their co-existence may be possible due to a niche separation in time by the day-night cycle, where nitrate-reducing Fe(II)-oxidizers oxidize ferrous iron during darkness and phototrophs play a dominant role in ferrous iron oxidation during daylight. Furthermore, metabolic flexibility of Fe(II)-oxidizing microbes may play a paramount role in the conservation of the sedimentary iron cycle, as the dynamics of nitrate dependent Fe(II) oxidation, at least in this sediment, are likely regulated by the relative availability of organic matter rather than by the competition with photoferrotrophs for ferrous iron.

Many open questions remain that invite the opportunity to explore the previously un-investigated co-existence of these two groups of anaerobic Fe(II)-oxidizers. Future studies will monitor nitrate fluctuations in the sediments and elucidate the role of microaerophilic Fe(II) oxidation in the sedimentary Fe(II) acquisition simultaneous with photoferrotrophy and nitrate-reducing Fe(II) oxidation during light conditions. The possibility and associated lag-phases of the interchanging nitrate-reducing Fe(II)-oxidizing or organic carbon-oxidizing and microaerophilic Fe(II)-oxidizing metabolisms will also be investigated by surveying and comparing Fe(II) and DOC oxidation rates. Additionally, knowledge on Fe (II) oxidation in microcosms which are switched between day and night conditions will pose a valuable contribution to getting closer to *in situ* environmental conditions. Further studies, including seasonality and light iridescence effects, will certainly shed more light on these unknown factors in this fascinating sedimentary system.

ACKNOWLEDGMENTS

This study was funded by a DFG grant to A. Kappler (KA1736/16-1), a Marie Curie ERG grant to C. Schmidt (PERF04-GA-2008-239252), and a Landesgraduiertenförderung fellowship to E. D. Melton (Gz l 1.2_7631.2/Melton). Many thanks to Ellen Struve for the TIC and DOC measurements. Thanks to Dr. Heinrich Taubald (University of Tübingen) for XRF analysis of the sediment and Dr. Reiner Ruser (University of Hohenheim) for measuring dissolved NO_3^- and NO_2^- concentrations. Last, but not least, we would like to thank the two reviewers for improving the manuscript.

REFERENCES

Armitage, J. P. (1999). Bacterial tactic responses. *Adv. Microb. Physiol.* 41, 229–289.

Benz, M., Brune, A., and Schink, B. (1998). Anaerobic and aerobic oxidation of ferrous iron at neutral pH by chemoheterotrophic nitrate-reducing bacteria. *Arch. Microbiol.* 169, 159–165.

Bloethe, M., and Roden, E. E. (2009a). Microbial iron redox cycling in a circumneutral-pH groundwater seep. *Appl. Environ. Microbiol.* 75, 468–473.

Bloethe, M., and Roden, E. E. (2009b). Composition and activity of an autotrophic Fe(II)-oxidizing, nitrate-reducing enrichment culture. *Appl. Environ. Microbiol.* 75, 6937–6940.

Bonneville, S., Van Cappellen, P., and Behrends, T. (2004). Microbial reduction of iron(III) oxyhydroxides: effects of mineral solubility and availability. *Chem. Geol.* 212, 255–268.

Bruun, A. M., Finster, K., Gunnlaugsson, H. P., Nornberg, P., and Friedrich, M. W. (2010). A comprehensive investigation on iron cycling in a freshwater seep including microscopy, cultivation and molecular community analysis. *Geomicrobiol. J.* 27, 15–34.

Canfield, D. E. (1989). Reactive iron in marine sediments. *Geochim. Cosmochim. Acta* 53, 619–632.

Canfield, D. E., and Thamdrup, B. (2009). Towards a consistent classification scheme for geochemical environments, or, why we wish the term "suboxic" would go away. *Geobiology* 7, 385–392.

Canfield, D. E., Thamdrup, B., and Hansen, J. W. (1993). The anaerobic degradation of organic-matter in danish coastal sediments – iron reduction, manganese reduction, and sulfate reduction. *Geochim. Cosmochim. Acta* 57, 3867–3883.

Chakraborty, A., Roden, E. E., Schieber, J., and Picardal, F. (2011). Enhanced growth of *Acidovorax* sp. strain 2AN during nitrate-dependent Fe(II) oxidation in batch and continuous-flow systems. *Appl. Enviorn. Microbiol.* 77, 8548–8556.

Chubarenko, I., Chubarenko, B., Bauerle, E., Wang, Y., and Hutter, K. (2003). Autumn physical limnological experimental campaign in the Island Mainau littoral zone of Lake Constance. *J. Limnol.* 62, 115–119.

Coby, A. J., Picardal, F., Shelobolina, E., Xu, H., and Roden, E. E. (2011). Repeated anaerobic microbial redox cycling of iron. *Appl. Environ. Microbiol.* 77, 6036–6042.

Cochran, W. G. (1950). Estimation of bacterial densities by means of the "most probable number." *Biometrics* 6, 105–116.

Cornell, R. M., and Schwertmann, U. (2003). *The Iron Oxides, Structure, Properties, Reactions, Occurrences and Uses.* Weinheim: Wiley-VCH.

Crowe, S. A., Jones, C., Katsev, S., Magen, C., O'Neill, A. H., Sturm, A., Canfield, D. E., Haffner, G. D., Mucci, A., Sundby, B., and Fowle, D. A. (2008). Photoferrotrophs thrive in an Archean Ocean analogue. *Proc. Natl. Acad. Sci. U.S.A.* 105, 15938–15943.

Davison, W., and Seed, G. (1983). The kinetics of the oxidation of ferrous iron in synthetic and natural waters. *Geochim. Cosmochim. Acta* 47, 67–79.

Diez, S., Noonan, G. O., Macfarlane, J. K., and Gschwend, P. M. (2007). Ferrous iron oxidation rates in the pycnocline of a permanently stratified lake. *Chemosphere* 66, 1561–1570.

Druschel, G. K., Emerson, D., Sutka, R., Suchecki, P., and Luther, G. W. (2008). Low-oxygen and chemical kinetic constraints on the geochemical niche of neutrophilic iron(II) oxidizing microorganisms. *Geochim. Cosmochim. Acta* 72, 3358–3370.

Dudgeon, D., Arthington, A. H., Gessner, M. O., Kawabata, Z. I., Knowler, D. J., Leveque, C., Naiman, R. J., Prieur-Richard, A.-H., Soto, D., Stiassny, M. L. J., and Sullivan, C. A. (2006). Freshwater biodiversity: importance, threats, status and conservation challenges. *Biol. Rev. Camb. Philos. Soc.* 81, 163–182.

Edwards, K. J., Rogers, D. R., Wirsen, C. O., and McCollom, T. M. (2003). Isolation and characterization of novel psychrophilic, neutrophilic, Fe-oxidizing, chemolithoautotrophic alpha- and, gamma-Proteobacteria from the deep sea. *Appl. Environ. Microbiol.* 69, 2906–2913.

Ehrenreich, A., and Widdel, F. (1994). Anaerobic oxidation of ferrous iron by purple bacteria, a new-type of phototrophic metabolism. *Appl. Environ. Microbiol.* 60, 4517–4526.

Emerson, D., and Moyer, C. (1997). Isolation and characterization of novel iron-oxidizing bacteria that grow at circumneutral pH. *Appl. Environ. Microbiol.* 63, 4784–4792.

Froelich, P. N., Klinkhammer, G. P., Bender, M. L., Luedtke, N. A., Heath, G. R., Cullen, D., Dauphin, P., Hammond, D., Hartman, B., and Maynard, V. (1979). Early oxidation of organic matter in pleagic sediments of the eastern equatorial atlantic suboxic diagenesis. *Geochim. Cosmochim. Acta* 43, 1075–1090.

Gerhardt, S., Boos, K., and Schink, B. (2010). Uptake and release of phosphate by littoral sediment of a freshwater lake under the influence of light or mechanical perturbation. *J. Limnol.* 69, 54–63.

Gerhardt, S., Brune, A., and Schink, B. (2005). Dynamics of redox changes of iron caused by light-dark variations in littoral sediment of a freshwater lake. *Biogeochemistry* 74, 323–339.

Hauck, S., Benz, M., Brune, A., and Schink, B. (2001). Ferrous iron oxidation by denitrifying bacteria in profundal sediments of a deep lake (Lake Constance). *FEMS Microbiol. Ecol.* 37, 127–134.

Hegler, F., Kappler, A., Posth, N. R., and Jiang, J. (2008). Physiology of phototrophic iron(II)-oxidizing bacteria: implications for modern and ancient environments. *FEMS Microbiol. Ecol.* 66, 250–260.

Heising, S., Richter, L., Ludwig, W., and Schink, B. (1999). *Chlorobium ferrooxidans* sp nov., a phototrophic green sulfur bacterium that oxidizes ferrous iron in coculture with a "*Geospirillum*" sp strain. *Arch. Microbiol.* 172, 116–124.

Jiao, Y., Kappler, A., Croal, L. R., and Newman, D. K. (2005). Isolation and characterization of a genetically traceable photoautotrophic Fe(II)-oxidizing bacterium, *Rhodopseudomonas palustris* strain TIE-1. *Appl. Environ. Microbiol.* 71, 4487–4496.

Kappler, A., and Newman, D. K. (2004). Formation of Fe(III)-minerals by Fe(II)-oxidizing photoautotrophic bacteria. *Geochim. Cosmochim. Acta* 68, 1217–1226.

Kappler, A., Pasquero, C., Konhauser, K. O., and Newman, D. K. (2005a). Deposition of banded iron formations by anoxygenic phototrophic Fe(II)-oxidizing bacteria. *Geology* 33, 865–868.

Kappler, A., Schink, B., and Newman, D. K. (2005b). Fe(III) mineral formation and cell encrustation by the nitrate-dependent Fe(II)-oxidizer strain BoFeN1. *Geobiology* 3, 235–245.

Kappler, A., and Straub, K. L. (2005). Geomicrobiological cycling of iron. *Rev. Mineral. Geochem.* 59, 85–108.

Klee, A. J. (1993). A computer-program for the determination of most probable number and its confidence-limits. *J. Microbiol. Methods* 18, 91–98.

Konhauser, K. O., Hamade, T., Raiswell, R., Morris, R. C., Ferris, F. G., Southam, G., and Canfield, D. E. (2002). Could bacteria have formed the Precambrian banded iron formations? *Geology* 30, 1079–1082.

Konhauser, K. O., Kappler, A., and Roden, E. E. (2011). Iron in microbial metabolisms. *Elements* 7, 89–93.

Kuehl, M., Lassen, C., and Jorgensen, B. B. (1994). Light penetration and light intensity in sandy marine sediments measured with irradiance and scalar irradiance fiber-optic microprobes. *Mar. Ecol. Prog. Ser.* 105, 139–148.

Larese-Casanova, P., Haderlein, S. B., and Kappler, A. (2010). Biomineralization of lepidocrocite and goethite by nitrate-reducing Fe(II)-oxidizing bacteria: effect of pH, bicarbonate, phosphate, and humic acids. *Geochim. Cosmochim. Acta* 74, 3721–3734.

Lovley, D. R., Holmes, D. E., and Nevin, K. P. (2004). Dissimilatory Fe(III) and Mn(IV) reduction. *Adv. Microb. Physiol.* 49, 219–286.

Lovley, D. R., and Phillips, E. J. P. (1988). Novel mode of microbial energy-metabolism – organic-carbon oxidation coupled to dissimilatory reduction of Iron or Manganese. *Appl. Environ. Microbiol.* 54, 1472–1480.

Macdonald, L. H., Moon, H. S., and Jaffe, P. R. (2011). The role of biomass, electron shuttles, and ferrous iron in the kinetics of *Geobacter sulfurreducens*-mediated ferrihydrite reduction. *Water Res.* 45, 1049–1062.

Miot, J., Maclellan, K., Benzerera, K., and Boisset, N. (2011). Preservation of protein globules and peptidoglycan in the mineralized cell wall of nitrate-reducing, iron(II)-oxidizing bacteria: a cryo-electron microscopy study. *Geobiology* 9, 459–470.

Muehe, E. M., Gerhardt, S., and Kappler, A., and Schink, B. (2009). Ecophysiology and the energetic benefit of mixotrophic Fe(II) oxidation by various strains of nitrate-reducing bacteria. *FEMS Microbiol. Ecol.* 70, 335–343.

Overmann, J., and Tilzer, M. M. (1989). Control of primary and the significance of photosynthetic bacteria in a meromictic kettle lake Mittlerer Buchensee, West-Germany. *Aquat. Sci.* 51, 261–278.

Peeters, F., Straile, D., Lorke, A., and Ollinger, D. (2007). Turbulent mixing and phytoplankton spring bloom development in a deep lake. *Limnol. Oceanogr.* 52, 286–298.

Posth, N. R., Hegler, F., Konhauser, K. O., and Kappler, A. (2008). Alternating Si and Fe deposition caused by temperature fluctuations in Precambrian oceans. *Nat. Geosci.* 1, 703–708.

Poulain, A. J., and Newman, D. K. (2009). Rhodobacter capsulatus catalyzes light-dependent Fe(II) oxidation under anaerobic conditions as a potential detoxification mechanism. *Appl. Environ. Microbiol.* 75, 6639–6646.

Rahalkar, M., Deutzmann, J., Schink, B., and Bussmann, I. (2009). Abundance and activity of methanotrophic bacteria in littoral and profundal sediments of Lake Constance (Germany). *Appl. Environ. Microbiol.* 75, 119–126.

Raven, J. A., and Cockell, C. S. (2006). Influence on photosynthesis of starlight, moonlight, planetlight, and light pollution (reflections on photosynthetically active radiation in the universe). *Astrobiology* 6, 668–675.

Schmidt, C., Behrens, S., and Kappler, A. (2010). Ecosystem functioning from a geomicrobiological perspective – a conceptual framework for biogeochemical iron cycling. *Environ. Chem.* 7, 399–405.

Sobolev, D., and Roden, E. E. (2002). Evidence for rapid microscale bacterial redox cycling of iron in circumneutral environments. *Antonie Van Leeuwenhoek* 81, 587–597.

Stookey, L. L. (1970). Ferrozine-a new spectrophotometric reagent for iron. *Anal. Chem.* 42, 779–781.

Straub, K. L., Benz, M., Schink, B., and Widdel, F. (1996). Anaerobic, nitrate-dependent microbial oxidation of ferrous iron. *Appl. Environ. Microbiol.* 62, 1458–1460.

Straub, K. L., and Buchholz-Cleven, B. E. E. (1998). Enumeration and detection of anaerobic ferrous iron-oxidizing, nitrate-reducing bacteria from diverse European sediments. *Appl. Environ. Microbiol.* 64, 4846–4856.

Straub, K. L., Schoenhuber, W. A., Buchholz-Cleven, B. E. E., and Schink, B. (2004). Diversity of ferrous iron-oxidizing, nitrate-reducing bacteria and their involvement in oxygen-independent iron cycling. *Geomicrobiol. J.* 21, 371–378.

Thamdrup, B. (2000). Bacterial manganese and iron reduction in aquatic sediments. *Adv. Microb. Ecol.* 16, 41–84.

Weber, K. A., Pollock, J., Cole, K. A., O'Connor, S. M., Achenbach, L. A., and Coates, J. D. (2006a). Anaerobic nitrate-dependent iron(II) bio-oxidation by a novel lithoautotrophic betaproteobacterium, strain 2002. *Appl. Environ. Microbiol.* 72, 686–694.

Weber, K. A., Urrutia, M. M., Churchill, P. F., Kukkadapu, R. K., and Roden, E. E. (2006b). Anaerobic redox cycling of iron by freshwater sediment microorganisms. *Environ. Microbiol.* 8, 100–113.

Widdel, F., Schnell, S., Heising, S., Ehrenreich, A., Assmus, B., and Schink, B. (1993). Ferrous iron oxidation by anoxygenic phototrophic bacteria. *Nature* 362, 834–836.

Xiong, J., Fischer, W. M., Inoue, K., Nakahara, M., and Bauer, C. E. (2000). Molecular evidence for the early evolution of photosynthesis. *Science* 289, 1724–1730.

Conflict of Interest Statement: The authors declare that the research was conducted in the absence of any commercial or financial relationships that could be construed as a potential conflict of interest.

Received: 14 November 2011; accepted: 14 May 2012; published online: 31 May 2012.

Citation: Melton ED, Schmidt C and Kappler A (2012) Microbial iron(II) oxidation in littoral freshwater lake sediment: the potential for competition between phototrophic vs. nitrate-reducing iron(II)-oxidizers. Front. Microbio. ***3****:197. doi: 10.3389/fmicb.2012.00197*

This article was submitted to Frontiers in Microbiological Chemistry, a specialty of Frontiers in Microbiology.

Copyright © 2012 Melton, Schmidt and Kappler. This is an open-access article distributed under the terms of the Creative Commons Attribution Non Commercial License, which permits non-commercial use, distribution, and reproduction in other forums, provided the original authors and source are credited.

frontiers in
MICROBIOLOGY

ORIGINAL RESEARCH ARTICLE
published: 12 April 2012
doi: 10.3389/fmicb.2012.00136

In situ spectroscopy on intact *Leptospirillum ferrooxidans* reveals that reduced cytochrome 579 is an obligatory intermediate in the aerobic iron respiratory chain

Robert C. Blake II* and Megan N. Griff

College of Pharmacy, Xavier University of Louisiana, New Orleans, LA, USA

Edited by:
David Emerson, Bigelow Laboratory for Ocean Sciences, USA

Reviewed by:
James Hemp, University of Illinois at Urbana-Champaign, USA
David Emerson, Bigelow Laboratory for Ocean Sciences, USA

****Correspondence:***
Robert C. Blake II, College of Pharmacy, Xavier University of Louisiana, 1 Drexel Drive, New Orleans, LA 70125, USA.
e-mail: rblake@xula.edu

Electron transfer reactions among colored cytochromes in intact bacterial cells were monitored using an integrating cavity absorption meter that permitted the acquisition of accurate absorbance data in suspensions of cells that scatter light. The aerobic iron respiratory chain of *Leptospirillum ferrooxidans* was dominated by the redox status of an abundant cellular cytochrome that had an absorbance peak at 579 nm in the reduced state. Intracellular cytochrome 579 was reduced within the time that it took to mix a suspension of the bacteria with soluble ferrous iron at pH 1.7. Steady state turnover experiments were conducted where the initial concentrations of ferrous iron were less than or equal to that of the oxygen concentration. Under these conditions, the initial absorbance spectrum of the bacterium observed under air-oxidized conditions was always regenerated from that of the bacterium observed in the presence of Fe(II). The kinetics of aerobic respiration on soluble iron by intact *L. ferrooxidans* conformed to the Michaelis–Menten formalism, where the reduced intracellular cytochrome 579 represented the Michaelis complex whose subsequent oxidation appeared to be the rate-limiting step in the overall aerobic respiratory process. The velocity of formation of ferric iron at any time point was directly proportional to the concentration of the reduced cytochrome 579. Further, the integral over time of the concentration of the reduced cytochrome was directly proportional to the total concentration of ferrous iron in each reaction mixture. These kinetic data obtained using whole cells were consistent with the hypothesis that reduced cytochrome 579 is an obligatory steady state intermediate in the iron respiratory chain of this bacterium. The capability of conducting visible spectroscopy in suspensions of intact cells comprises a powerful post-reductionist means to study cellular respiration *in situ* under physiological conditions for the organism.

Keywords: *Leptospirillum ferrooxidans*, electron transfer, aerobic respiration, chemolithotroph, acidophile, cytochrome 579, *in situ* spectroscopy, integrating sphere

INTRODUCTION

Certain chemolithotrophic bacteria inhabit ore-bearing geological formations exposed to the atmosphere and obtain all of their energy for growth from the oxidation and dissolution of minerals within the ore. Energy is derived from oxidative phosphorylation coupled to respiratory electron transfer. The ability to respire aerobically on soluble ferrous ions under strongly acidic conditions is currently known to be expressed by at least 34 species in 14 genera distributed throughout the Gram-negative (Markosyan, 1972; Huber and Stetter, 1989; Kelly and Wood, 2000; Hallberg et al., 2010), Gram-positive (Clark and Norris, 1996; Norris et al., 1996; Johnson et al., 2008, 2009; Guo et al., 2009; Jiang et al., 2009), and Archaea bacteria (Segerer et al., 1986; Huber et al., 1989; Huber and Stetter, 1991; Karavaiko et al., 1994; Golyshina et al., 2000, 2009). Given the genetic diversity within this collection of phenotypically related bacteria, it would not be surprising to learn that phylogenetically distinct groups of bacteria express different electron transfer biomolecules and pathways to accomplish aerobic respiration on soluble iron.

Classic reductionist studies that involve the structural and functional characterization of highly purified proteins in dilute solution have described a bewildering variety of different redox-active electron transport proteins in cell-free extracts derived from iron-grown Gram-negative (Cox and Boxer, 1978; Hart et al., 1991; Blake et al., 1992; Yarzábal et al., 2002, 2004), Gram-positive (Blake et al., 1993; Takai et al., 2001; Dinarieva et al., 2010), and Archaea (Hettmann et al., 1998; Dopson et al., 2005; Auernik and Kelly, 2008) bacteria. The most promising efforts to date have focused on the iron respiratory chain of *Acidithiobacillus ferrooxidans*, where an iron "respirasome" super complex has been defined that is comprised of 2 *c*-type cytochromes, a blue copper protein called rusticyanin, and an aa_3-type terminal oxidase (Castelle et al., 2008). The proteins in the aerobic iron respiratory pathway of *At. ferrooxidans* do not appear to be expressed in many of the phylogenetically distinct bacteria that also respire on iron. Similarly, redox-active proteins expressed in other iron-grown bacteria do not appear to be expressed in iron-grown *At. ferrooxidans*. Comparative analyses conducted using those relevant bacterial genomes where partial or complete DNA sequence data is available

(Chen et al., 2005; Ram et al., 2005; Valdes et al., 2008; Clum et al., 2009; Siezen and Wilson, 2009) have not yet provided significant insight into other iron respiratory proteins or pathways. There is little information in the DNA databases to compare with because the proteins in the aerobic iron respiratory pathway of *At. ferrooxidans* do not appear to be universal among those bacteria that respire on iron. In either case, actual respiratory electron transfer in the intact organism is not directly observed. Rather, the functional properties of the intact electron transfer chain are inferred from observations on isolated molecules.

This paper introduces a new means to study respiratory electron transfer reactions *in situ* in intact bacteria under physiological conditions. The premise is that accurate UV-visible spectroscopy of electron transfer reactions among colored cytochromes can be conducted in highly turbid suspensions if the live bacteria are irradiated in an isotropic homogeneous field of incident measuring light. Under those conditions, the absorbed radiant power is independent of scattering effects (Elterman, 1970; Fry et al., 1992; Javorfi et al., 2006; Hodgkinson et al., 2009). We conducted equilibrium and kinetic studies on the Fe(II)-dependent reduction and O_2-dependent oxidation of cytochromes in intact *Leptospirillum ferrooxidans* at pH 1.7. We used a commercial integrating cavity absorption meter (ICAM) where the cuvette comprised a reflecting cavity completely filled with the absorbing suspension. *L. ferrooxidans* was selected because it is only known to respire on one substrate, reduced iron (Harrison, 1984). We observed that a cytochrome with a reduced spectral peak at 579 nm is an obligatory intermediate in the aerobic iron respiratory chain of *L. ferrooxidans*.

MATERIALS AND METHODS

CELL CULTURE

Leptospirillum ferrooxidans DSMZ 2705 was cultured autotrophically on soluble ferrous ions at 30°C in the medium described elsewhere (Tuovinen and Kelly, 1973), adjusted to pH 1.5 and amended with 44 g/l of $FeSO_4{\cdot}7H_2O$. Cells grown to stationary phase were harvested by centrifugation, washed three times with 0.02 M H_2SO_4, pH 1.7, and resuspended in sufficient 0.02 M H_2SO_4 to achieve a stock suspension of 1.5×10^{10} cells/ml. The stock suspension was stored at 4°C for up to 2 weeks while spectroscopic experiments were conducted on aliquots of the cells. Previous stock suspensions of this organism have been stored in dilute sulfuric acid at 4°C for over 6 weeks before changes in the bacterium's energy metabolism could be detected.

QUANTIFICATION OF BACTERIA

Absolute numbers of *L. ferrooxidans* cells were determined by electrical impedance measurements in a Multisizer 4 particle counter (Beckman Coulter, Inc., Brea, CA, USA) fitted with a 30-μm aperture. The instrument was programmed to siphon 50 μl of sample that contained Isoton II as the electrolyte. The current applied across the aperture was 600 μA. Voltage pulses attendant with impedance changes as particles passed through the aperture were monitored with an instrument gain of four.

Relative numbers of *L. ferrooxidans* cells were determined by photon correlation scattering spectroscopy with a DelsaNano C particle size analyzer, also from Beckman Coulter, Inc. Cell densities were adjusted to 8.3×10^6 cells/ml in 0.02 M sulfuric acid to give an attenuator obscuration of 47%. Determination of the relative numbers of light scattering species as a function of particle diameter was accomplished by the time domain method with operating and analysis software provided by Beckman Coulter, Inc.

ABSORBANCE MEASUREMENTS WITH CELL SUSPENSIONS

Absorbance measurements on intact cells in suspension were conducted in an Olis CLARiTY 1000 A spectrophotometer (On Line Instrument Systems, Inc., Bogart, GA, USA) that employed a novel ICAM. In a typical experiment, identical 4.2 ml solutions that contained ferrous sulfate in 0.02 M sulfuric acid, pH 1.7, were added to both the sample and reference observation cavities of the spectrophotometer. After recording a stable baseline from 350 to 650 nm, 140 μl were withdrawn from the sample cavity and replaced with 140 μl of the stock cell suspension of *L. ferrooxidans*. Apparent absorbance spectra (typically 6.2 s^{-1}) were then collected until any visible absorbance changes had ceased. Raw apparent absorbance values were converted to absorbance values per cm using Fry's method (Fry et al., 2010) as described in the text.

RESULTS

THE REDOX STATE OF ELECTRON TRANSFER PROTEINS CAN BE MONITORED *IN SITU* IN INTACT BACTERIA UNDER PHYSIOLOGICAL CONDITIONS

The principal features of the novel CLARiTY spectrophotometer used to conduct absorbance measurements in turbid solutions are included in the schematic diagram shown in **Figure 1**. The sample and reference observation cells of this dual beam spectrophotometer were each comprised of a 4.2-ml spherical quartz cuvette fused with a 6-mm ID quartz tube. Each quartz chamber was surrounded by a tightly packed proprietary white powder that served to maximize diffuse reflectance of light on the exterior walls of the spherical flask. The apertures in the reflecting sphere through which the measuring light entered and the transmitted/scattered light exited to the photomultiplier tube were positioned at a 90° angle such that the light had to undergo many reflections and cell transversals before it was quantified using the photomultiplier tube. A white Teflon plug with a 6-mm OD was inserted into the quartz tube to minimize the loss of light out of the neck. A 1.0-cm white stir bar was included in the sample chamber to facilitate sample mixing and suspension of any particulate matter.

The data shown in **Figure 2** illustrate how the intact cells of *L. ferrooxidans* were quantified. The solid line in **Figure 2** shows the absolute counts as a function of particle size as determined with a suspension of *L. ferrooxidans* in the Multisizer 4. The Multisizer determined the number and size of intact bacteria suspended in an electrically conductive liquid by forcing a measured volume of the suspension to flow through a small aperture with an immersed electrode on either side. A current passing through the aperture between the two electrodes enabled the bacteria to be detected by the momentary changes in the electrical impedance as they passed through the aperture, since each bacterium displaced its own volume of electrolyte solution within the aperture itself. These changes in impedance were detected as a series of voltage pulses, for which the height and duration of each pulse were proportional to the volume of the bacterium that produced

it. Each pulse was counted and allocated to 1 of 400 arbitrary size categories, or channels. Each channel encompassed a narrow range of volumes that were converted to spherical equivalents and represented by the corresponding spherical diameters on the abscissa of **Figure 2**. The solid line in **Figure 2** shows the number of counts in each size range for spherical equivalents with diameters from 0.6 to 2.0 μm.

The dashed line in **Figure 2** shows the relative number of *L. ferrooxidans* cells as a function of particle size as determined by laser light diffraction. Light scattered by the bacterial suspension produced a diffraction pattern from which the relative numbers of the scattering species at each particle size were calculated. Like the Multisizer, the particle sizes determined by laser light diffraction are expressed as spherical equivalents and are also represented by the corresponding spherical diameters on the abscissa of **Figure 2**.

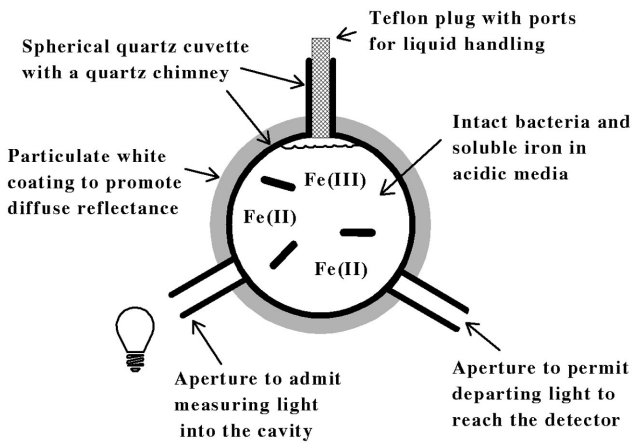

FIGURE 1 | Simplified model of an integrating cavity absorption meter designed to permit accurate absorbance measurements in media that scatter light.

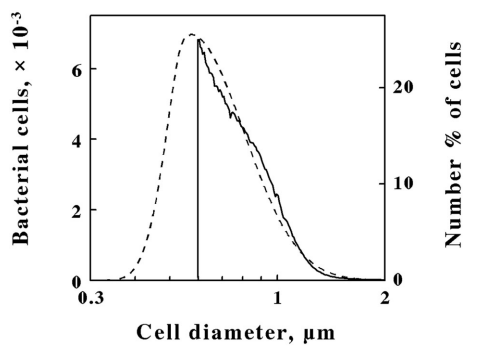

FIGURE 2 | Comparison of *L. ferrooxidans* cell populations by electrical impedance (solid line) and static light diffraction methods (dashed line). Electrical impedance measurements yielded absolute numbers of cells (left ordinate) as a function of size; light diffraction measurements yielded relative numbers of cells (right ordinate) as a function of size. The scale of each ordinate was chosen to facilitate comparison of the curves. The area under the electrical impedance curve was 81.2% of that under the light diffraction curve.

Close correspondence between the electrical impedance and the light diffraction curves was observed down to 0.6 μm, indicating that the two instruments were monitoring the same population of particles. Bacteria with effective diameters less than 0.6 μm were underrepresented by the electrical impedance method, by which observations were limited to particles with effective diameters between 2 and 60% of the 30-μm aperture employed, while the light diffraction method was capable of resolving particles with effective diameters smaller than 0.1 μm. On the basis of comparisons such as that illustrated in **Figure 2**, it was determined that 19.8% of the bacterial cell counts were below the limit of resolution of the electrical impedance method with the 30-μm aperture. Accordingly, absolute counts of *L. ferrooxidans* cells obtained by the electrical impedance method were multiplied by 1.23 to correct for the percentage of bacterial counts that were below the limit of resolution of the instrument.

Cell pellets of *L. ferrooxidans*, which were a pinkish tan color, were obtained by centrifugation of batch cultures grown to stationary phase on soluble ferrous iron. Curve **a** in **Figure 3** shows the absorbance spectrum of oxidized *L. ferrooxidans* that was obtained in the CLARiTY spectrophotometer in sulfuric acid, pH 1.7. Even though the cell suspension contained 5×10^8 cells/ml and was roughly as turbid as non-fat milk, the resulting absorbance spectrum contained no evidence of the light scattering artifacts that one would observe by conducting the same absorbance measurements using a conventional linear spectrophotometer. The spectrum in curve **a** showed a clearly defined Soret peak at 422 nm and a broad α,β band at around 520 nm.

The goal of the initial spectroscopic experiments was simply to determine whether the pink protein(s) in the cells changed color when the cells were suspended in sulfuric acid and subsequently exposed to excess concentrations of soluble ferrous ions under physiological conditions. Curve **b** in **Figure 3** shows the absorbance spectrum that was obtained when the cells of oxidized *L. ferrooxidans* were exposed to 100 mM ferrous sulfate in sulfuric acid, pH 1.7. Exposure to excess soluble iron caused the apparent

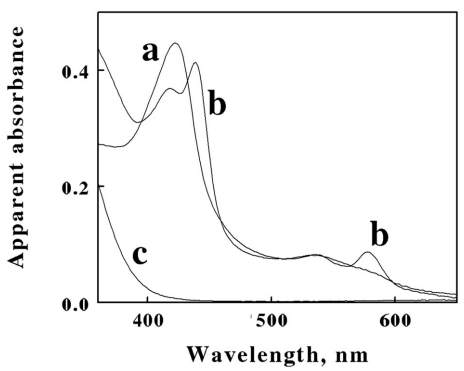

FIGURE 3 | Apparent absorbance spectra of intact *L. ferrooxidans* collected in the CLARiTY in the absence (*a*) and presence (*b*) of 100 mM ferrous sulfate in aerobic sulfuric acid, pH 1.7. The final bacterial suspension contained 2.1×10^9 cells of *L. ferrooxidans* in 4.2 ml. Curve *c* shows the apparent absorbance spectrum of 50 μM ferric ions under the same solution conditions in the absence of bacteria.

Soret peak to split into two peaks with maxima at 418 and 439 nm. In addition, a new absorbance peak appeared with a maximum absorbance at 579 nm. The absorbance spectrum represented by curve **b** appeared immediately after mixing the bacterial suspension in the observation cell that contained the 100-mM soluble iron ($\leq$0.5 s). This observation indicated that the iron-dependent reduction of the cytochrome(s) in intact *L. ferrooxidans* was essentially complete within the 0.5-s mixing time in the observation cell of the spectrophotometer. The resulting spectrum was very stable and did not vary for at least an hour after mixing. Although the live cells could respire aerobically on the soluble iron, the great molar excess of iron over molecular oxygen in the observation cell dictated that the cytochromes in the cells would remain predominantly reduced as the oxygen in the chamber was consumed. Evidence for aerobic respiration was taken from the increase in absorbance at wavelengths below 400 nm in curve **b**. Curve **c** in **Figure 3** shows the absorbance spectrum of 50 μM ferric sulfate in sulfuric acid, pH 1.7. The increase in the absorbance observed at low wavelengths in curve **b** was assumed to be due to ferric ions produced as a consequence of aerobic respiration on iron by the bacteria.

The goal of subsequent spectroscopic experiments was to lower the concentration of soluble iron and determine whether time-dependent changes in the cellular absorbance could be detected. Fe(II) concentrations were chosen such that the total number of electrons available for aerobic respiration was lower than the electron-accepting capacity of the >200 μM O_2 in the air-saturated suspension. The data in **Figure 4A** show selected absorbance spectra that were obtained when cells of *L. ferrooxidans* were exposed to 100 μM ferrous sulfate in sulfuric acid, pH 1.7. The seven absorbance spectra shown in the figure were selected from a data set where 6.2 complete scans from 350 to 650 nm were collected every second for 400 s. Once again, the spectrum of the bacteria produced in the presence of Fe(II) was generated within the operational dead time of mixing, roughly 0.5 s. In this case, however, subsequent aerobic respiration under the conditions of excess molecular oxygen produced time-dependent changes in the observed spectra of whole cells. The reduced peaks at 439 and 579 nm disappeared over a period of 400 s, while the oxidized Soret peak at 422 nm gradually reappeared. In addition, there was a concomitant increase in absorbance at wavelengths below 400 nm. These spectral changes were consistent with the hypothesis that the cells respired aerobically on the soluble iron until the ferrous iron was completely oxidized.

The primary absorbance spectra shown in **Figures 3** and **4A** are presented as "apparent absorbance" because of prior reports that spectra obtained using integrated cavity absorption meters appear distorted when compared with corresponding spectra of the same

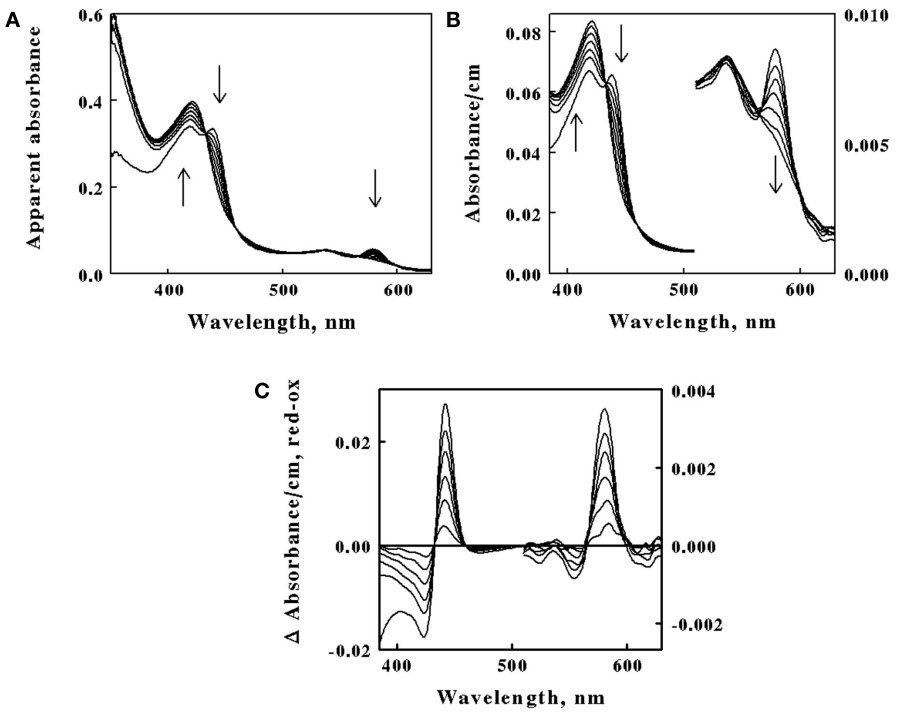

FIGURE 4 | Absorbance spectra obtained at different time points after 2.1 × 10^9 cells of intact *L. ferrooxidans* were introduced into 4.2 ml of 100 μM ferrous sulfate in sulfuric acid, pH 1.7. (A) Apparent absorbance spectra collected in the CLARiTY at seven time points after mixing, ranging from 1.0 to 400 s. Each *arrow* indicates whether the apparent absorbance at that wavelength increased or decreased with time. **(B)** Absorbance spectra obtained when the apparent absorbance values in **(A)** were converted to equivalent absorbance values per cm using the Fry equation (see text) to adjust for mean path length differences at different wavelengths. The absorbances at the longer wavelengths correspond to the more sensitive scale shown on the right ordinate. **(C)** Difference spectra, representing the absolute spectrum of the iron-reduced *L. ferrooxidans* minus those obtained at selected time points following the initial reduction of the bacteria.

materials obtained using a conventional linear spectrophotometer (Elterman, 1970; Fry et al., 1992; Javorfi et al., 2006; Hodgkinson et al., 2009). Unlike single path length spectrophotometers where the Beer–Lambert law governs non-linearity in the measured light intensity as a function of analyte concentration, the measuring light in an integrating sphere makes multiple random passes with different path lengths that exacerbate the apparent non-linearity with analyte concentration. While others have used semi-empirical methods to provide distortion-free spectra (Javorfi et al., 2006), we utilized the approach suggested by Fry because it is based on derivations from first principles (Fry et al., 1992, 2010). Fry arrived at the following exact expression for fractional absorption in an ICAM:

$$1 - T = \frac{1 - \exp\left[-\alpha(\nu) L_{\mathrm{G}}\right]}{1 - \rho(1 - h)\exp\left[-\alpha(\nu) L_{\mathrm{G}}\right]} \tag{1}$$

where T equals the observed transmittance in the ICAM, $\alpha(\nu)$ equals the corresponding absorbance that would be observed in a single path length spectrophotometer, L_{G} represents the mean geometric path length which for a sphere equals 2/3 of the sphere's diameter, ρ represents the reflectance at the walls of the cavity and is a number between 0 and 1, and h is the fraction of the cavity wall that is open for ports. Equation 1 was rearranged to

$$\alpha(\nu) = -\ln\left[\frac{10^{-A}}{1 - \rho\,(1 - h)\left(1 - 10^{-A}\right)}\right] \Big/ L_{\mathrm{G}} \tag{2}$$

where A is the absorbance value observed in the CLARiTY and $\rho(1 - h)$ was determined in separate experiments to be equal to 0.92 (data not shown).

The spectra shown in **Figure 4B** were obtained when the absorbance values in **Figure 4A** were converted to equivalent absorbance values per cm using Eq. 2. The converted absorbance values in **Figure 4B** illustrate the enhanced sensitivity achieved in the CLARiTY where the mean path length of the measuring light is increased by multiple reflections around the interior of the cavity. The conversion also eliminated the apparent distortion in the raw absorbance values wherein the Soret peak appeared to be attenuated compared to the heme absorbance at longer wavelengths. Thus those wavelengths where greater absorption occurred received relatively higher values in the converted data than did those wavelengths where lower absorption occurred.

Figure 4C shows difference spectra representing the absolute absorbance spectrum of the iron-reduced *L. ferrooxidans* minus those obtained at various time points following the rapid reduction of the bacteria. The two prominent peaks of the difference spectrum occur at 443 and 579 nm. The observation of at least four relatively well-defined isosbestic points is extraordinary considering that the spectra were acquired in a highly turbid suspension of bacteria. An isosbestic point is a specific wavelength at which two or more absorbing species have the same molar absorptivity. The existence of those four well-defined isosbestic points suggests that there is only one principal iron-responsive cytochrome that is visible in the aerobic iron respiratory chain of *L. ferrooxidans*.

REDUCED CYTOCHROME 579 IS AN OBLIGATORY INTERMEDIATE DURING AEROBIC RESPIRATION ON SOLUBLE IRON BY INTACT *L. FERROOXIDANS*

The next goal was to determine whether the time-dependent absorbance changes observed when intact *L. ferrooxidans* was exposed to soluble ferrous ions could be correlated with the appearance of product ferric ions as the bacterium respired aerobically on reduced iron. The kinetic data shown in **Figure 5A** were extracted from the data set that yielded the selected spectra shown in **Figure 4A**. The change in absorbance at 355 nm, which represented predominantly the absorbance due to the time-dependent accumulation of ferric ions, increased in a roughly linear fashion until the limiting concentration of ferrous ions was completely depleted at around 320 s after the start of the bacterial-catalyzed reaction. The changes in absorbance at 443 nm, which represented the peak of the difference spectrum in the Soret region shown in **Figure 4C**, slowly decreased over the time course of the reaction until about 300 s, when the absorbance then decreased rapidly back to the initial absorbance observed in the bacterium under air-oxidized conditions. It was evident that the cellular cytochrome returned to the oxidized state at about the same time that the product formation ceased.

The close correspondence between the change in product formation and the transient changes in the redox state of cytochrome 579 in intact *L. ferrooxidans* was consistent with the minimal kinetic mechanism shown in **Figure 5B**. Briefly, the iron-dependent reduction of cytochrome 579 in the intact bacterium is depicted as a relatively rapid reaction, which is consistent with the observation that it is complete within the 0.5-s dead time of the mixing even when the concentration of soluble ferrous ions is only 100 μM. The bacterium with its reduced cellular cytochrome is then shown as reacting with molecular oxygen to regenerate oxidized cytochrome/bacterium in a slower reaction that constitutes the rate-limiting catalytic step. The exchange of electrons between the bacterium and soluble iron is depicted as a reversible reaction until or if experimental observations indicate otherwise.

The kinetic mechanism shown in **Figure 5B** is readily modeled by the Michaelis–Menten formalism where the intact bacterium that contains the reduced cytochrome 579 represents the Michaelis complex. It follows that the velocity of product formation should be a hyperbolic function of the concentration of the substrate ferrous ions, as shown below:

$$-\frac{\mathrm{d}\,[\mathrm{Fe(II)}]}{\mathrm{dt}} = \frac{\mathrm{d}\,[\mathrm{Fe(III)}]}{\mathrm{dt}} = \frac{V_{\max}\,[\mathrm{Fe(II)}]}{K_{\mathrm{M}} + [\mathrm{Fe(II)}]} \tag{3}$$

where $V_{\max}$ is the maximum velocity of the bacterial-catalyzed aerobic oxidation of ferrous ions and K_{M} is the Michaelis constant for soluble iron. **Figure 5C** shows the dependence of the velocity of the absorbance changes at 355 nm on the concentration of ferrous ions that remained in solution when intact cells were mixed with 100 μM ferrous ions. The data points in **Figure 5C** represent the tangents to the 355-nm curve in **Figure 5A** that correspond to the same time points as those at the different concentrations of ferrous ion shown on the abscissa of **Figure 5C**. The values for the rectangular hyperbola drawn through the data points in **Figure 5C**

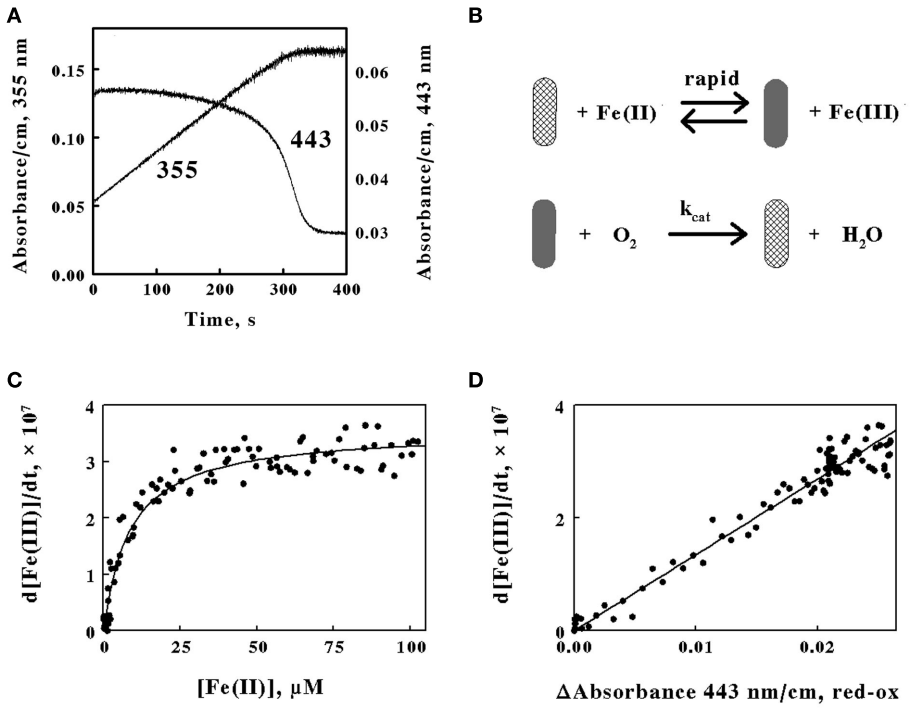

FIGURE 5 | The absorbance of the reduced cytochrome in intact *L. ferrooxidans* correlates with the absorbance of ferric ions produced during aerobic respiration on soluble iron. (A) Time courses of the absorbance changes at 355 and 443 nm obtained when 2.1×10^9 cells of *L. ferrooxidans* were mixed with 100 μM ferrous sulfate in sulfuric acid, pH 1.7. **(B)** Schematic representation of the kinetic mechanism for aerobic respiration on soluble iron as catalyzed by intact *L. ferrooxidans*. The *cross-hatched* and *solid* rods represent bacteria that contain oxidized and iron-reduced cytochromes, respectively. **(C)** Dependence of the velocity of the absorbance change at 355 nm on the concentration of ferrous ions that remain in solution. **(D)** Dependence of the velocity of the absorbance changes at 355 nm on the difference in absorbance values at 443 nm, representing the value at 1.0 s minus the value at time *t*.

were derived from a non-linear least-squares fit of Eq. 3 to the data with an apparent V_{max} of 3.6×10^{-7} Ms^{-1} and a K_M of 8.7 μM.

Another prediction that follows from the application of the Michaelis–Menten formalism to the kinetic mechanism shown in **Figure 5B** is that the rate of appearance of ferric ions should be directly proportional to the concentration of the reduced cytochrome 579 as shown in Eq. 4:

$$-\frac{d\,[Fe(II)]}{dt} = \frac{d\,[Fe(III)]}{dt} = k_{cat}\left[\text{reduced cytochrome 579}\right] \quad (4)$$

Figure 5D shows the dependence of the velocity of the absorbance changes at 355 nm on the concentration of reduced cytochrome 579. The velocities, or tangents to the 355-nm curve in **Figure 5A**, are the same values as those used in **Figure 5C**. In **Figure 5D**, the relative concentrations of reduced cytochrome 579 are represented on the abscissa by the differences in absorbance between those observed at 443 nm at corresponding time points in **Figure 5A** minus the stable absorbance observed at 443 nm at the end of the reaction. The direct proportionality predicted by Eq. 4 is evident, and the slope of the least-squares line in **Figure 5D** yielded a value for k_{cat} of $1.4\ s^{-1}$.

A third prediction that follows from the application of the Michaelis–Menten formalism to the kinetic mechanism shown in **Figure 5B** is shown in **Figure 6**. Equation 4 may be integrated to yield the following:

$$[Fe(II)]_{Total} = k_{cat}\int\left[\text{reduced cytochrome 579}\right]dt \quad (5)$$

where the integral on the right side of the equality represents the total area swept out by the absorbance of the reduced cytochrome over time as illustrated by the 443-nm time course shown in **Figure 5A**. The kinetic curves in **Figure 6A** show the time courses of the absorbance changes at 443 nm that were obtained when constant concentrations of *L. ferrooxidans* were mixed with different total concentrations of ferrous ions from 25 to 125 μM. Although the duplicate curves in **Figure 6A** appeared to differ slightly, the total areas under each pair of curves were remarkably similar, as shown by the five pairs of closely matched data points in **Figure 6B**. The direct proportionality predicted by Eq. 5 is evident, and the slope of the least-squares line in **Figure 6B** yielded a value for k_{cat} of $1.3\ s^{-1}$.

DISCUSSION

Three things can happen to the measuring light in a conventional linear spectrophotometer equipped with a standard 1-cm cuvette: it can be transmitted; it can be absorbed; or it can be scattered without absorption. When the sample is not optically clear, the apparent attenuation of the measuring light reflects losses due

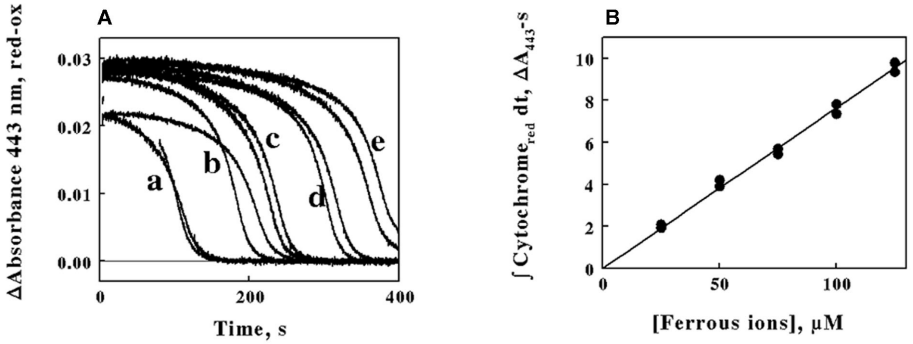

FIGURE 6 | The time integral of the absorbance of the reduced cytochrome in intact *L. ferrooxidans* correlates with the initial concentration of ferrous ions in the solution. (A) Time courses of the differences in the absorbance changes at 443 nm on the initial concentration of ferrous ions. Cells of *L. ferrooxidans* (2.1×10^9) were introduced into sulfuric acid, pH 1.7, that contained 25, 50, 75, 100, and 125 μM ferrous sulfate in curves *a* through *e*, respectively; each curve was obtained in duplicate. **(B)** Dependence of the area swept out under the absorbance versus time curves in **(A)** on the initial concentrations of ferrous ions.

both to true molecular absorption and light lost to scattering by the particulate matter in the turbid suspension (Shibata et al., 1954; Merzlyak and Naqvi, 2000). Efforts to recover and quantify the scattered light have included placing the cuvette inside an integrating sphere with a reflective surface (Nelson and Prezelin, 1993) and positioning the cuvette outside the sphere (Merzlyak and Naqvi, 2000). In either case data interpretation required cumbersome and arcane methods to identify and separate the scattered light from the truly absorbed light. Other investigators have described ICAMs where a spherical cavity created and bounded by a reflective surface was completely filled with the absorbing material (Elterman, 1970; Fry et al., 1992; Javorfi et al., 2006; Hodgkinson et al., 2009). The principle behind the ICAM is that the apparent absorbance recorded by the photodetector will be independent of scattering effects if the sample is in an isotropic homogeneous field of light, like that provided by illuminating the interior of an ICAM surrounded by a surface that maximizes diffuse reflectance. The commercial integrating spectrophotometer utilized herein was loosely based on those described by others (Elterman, 1970; Fry et al., 1992; Javorfi et al., 2006; Hodgkinson et al., 2009) with two notable improvements: it was a dual beam instrument with both sample and reference compartments equipped with matching ICAMs; and it permitted the rapid acquisition of up to 100 absorbance scans per second over a wavelength range of 300 nm. Another notable feature of this and all other ICAMs is that the effective path length of the observation chamber must be considerably longer than the diameter of the cavity due to multiple reflections at the cavity wall, a feature that provides much greater sensitivity.

Prior reductionist studies reported that cell-free extracts derived from iron-grown *L. ferrooxidans* (Hart et al., 1991; Blake and Shute, 1997), the closely related *L. ferriphilum* (Ram et al., 2005), or a microbial community with a low diversity of microbes that was dominated by *Leptospirillum* group II bacteria (Singer et al., 2008) all contained readily discernible quantities of an acid-soluble, acid-stable cytochrome with an unusual absorbance maximum at 579 nm in the reduced state. The probable participation of this novel cytochrome 579 in the aerobic iron respiratory chain of the *Leptospirillum* species is implied because the only known reducing substrates for aerobic respiration that are utilized by these organisms are soluble and insoluble ferrous iron. The same logic applies to the observations that the gene product of the DNA that encodes for cytochrome 579 was expressed in the microbial communities dominated by *Leptospirillum* group II bacteria. In either case, the participation of the expressed cytochrome was inferred from its existence and its cell-free behavior, but no direct observations of its function *in situ* were reported.

It is very difficult to reconstitute functional electron transport chains using partially purified components from cell-free extracts when the organism is an obligate acidophile like *L. ferrooxidans*. If the cell-free extracts are prepared at strongly acidic pH values, one must be concerned about altering or even precipitating those terminal components of the chain that face inward toward the cytoplasm, which is generally agreed to be neutral or only mildly acidic at the worst (Cobley and Cox, 1983; Michels and Bakker, 1985). If the cell-free extracts are prepared at near neutral pH values, one must be concerned about altering the functional behavior of those initial components of the chain that normally exchange electrons in their strongly acidic milieu. In addition, ionic iron is not sufficiently soluble at near neutral pH to permit functional studies on ferrous reduction of purified proteins or components within cell-free extracts. The surest way to study the details and principal features of respiratory electron transfer in obligate acidophiles is to conduct direct observations on the intact chain as it functions *in situ* under physiological conditions. That type of direct observation now appears to be possible using the ICAM that effectively negates the effects of light scattering by the turbid suspensions of intact bacteria.

Any kinetic mechanism that is described by the Michaelis–Menten formalism generates at least three hypotheses (Chance, 1943; Bright and Porter, 1975): (i) the velocity of product formation must be a hyperbolic function of the substrate concentration; (ii) the velocity of product formation must be directly proportional to the concentration of the catalyst–substrate complex from which product formation occurs in a rate-limiting reaction; and (iii) the total amount of product formed (or substrate utilized) must be directly proportional to the integral

over time of the concentration of the limiting catalyst complex. The behavior of the intact *L. ferrooxidans* and its reduced cytochrome 579 fulfilled the predictions of all three hypotheses. The V_{max} obtained from the non-linear fit of Eq. 3 to the data in **Figure 5C** was 3.6×10^{-7} mol of iron oxidized/s/liter. This rate equals 2.6×10^{-15} mol of iron oxidized/hour/cell, because there were 5×10^{8} cells/ml in the observation cavity. If one assumes that there are roughly 6×10^{-14} g of carbon per cell of *L. ferrooxidans* (Blake et al., 1994), then the maximum rate of iron oxidation becomes approximately 0.5 mol of iron oxidized/hour/mole of cellular carbon. This value is slightly lower than those reported elsewhere for *L. ferrooxidans* at temperatures from 30 to 40°C and slightly different pH values (Eccleston et al., 1985). Similarly, the value of K_M of 8.7 μM that was derived from the data in **Figure 5C** is quite a bit lower than those ranging from 250 to 500 μM as reported by others for the same strain of *L. ferrooxidans* (Eccleston et al., 1985). The origins of these differences are unknown.

It must be noted that direct observations on electron transport reactions in intact bacteria also have their limitations if one or more of the colored components has a small absorption coefficient or is present in considerably lower concentrations than those of the other components. The studies described above offer a case in point. If cytochrome 579 participates in the aerobic iron respiratory chain of *L. ferrooxidans*, then what are the other components and why are they not equally prominent in the visible absorbance spectra collected using the intact bacteria? The remarkably clear isosbestic points observed in **Figures 4B,C** indicate that cytochrome 579 is by far and away the principal absorbing species that undergoes changes in its redox state during the reaction. Given the extreme acid stability of the cytochrome 579 that was purified from cell-free extracts of *L. ferriphilum* (Ram et al., 2005), one can hypothesize that the cytochrome 579 functions outside of the plasma membrane and is perhaps the initial cellular electron acceptor from ferrous ions in the acidic milieu. It is unlikely that a single acid-stable, acid-soluble cytochrome is both the initial iron oxidase in the acid milieu and the terminal oxidase that reduces molecular oxygen. There must be subsequent electron transfer reactions across the plasma membrane to one or more components on the cytosolic side to be consistent with the Mitchell hypothesis as it is applied to oxidative phosphorylation in obligate acidophiles (Ingledew, 1982). Perhaps these putative components either possess lower absorption coefficients or they are present at much lower concentrations than the prominent cytochrome 579. In addition to the exergonic transfer of electrons from Fe(II) to molecular oxygen, *L. ferrooxidans* must also accomplish the "uphill" transfer of electrons from Fe(II) to NAD^+ or $NADP^+$. Presumably the formation of reduced pyridine dinucleotides for anabolic metabolism must also require electron transport proteins that, in principle, could be observed as they function in the intact bacterium. There were no indications of additional electron transport proteins in the spectra shown above.

Attempts to identify other electron transfer cytochromes in the aerobic iron respiratory chain of intact *L. ferrooxidans* using classical respiratory inhibitors were unsuccessful. Sodium cyanide complexes spontaneously with ferrous ions to form ferrocyanide (Blake et al., 1991). Similarly, when 100 μM sodium azide was mixed with 1.0 mM ferrous ions at pH 1.7, a new absorbance band with a peak at 380 nm formed rapidly and spontaneously in the spectrophotometer (data not shown). This spectrum was identical to that published previously for a aqueous complex of Fe(II) with azide (Chacarolli et al., 2000). Interestingly, when 100 μM sodium azide was mixed with intact bacteria in the absence of Fe(II) at pH 1.7, the cytochrome 579 was reduced to the same extent as that shown in **Figure 3** or **Figure 4** (data not shown). When *L. ferrooxidans* was heat-inactivated by incubating a suspension at 90°C for 30 min, the cytochromes that were still visible in the intact cell did not show any change when exposed to 100 mM Fe(II).

Despite the limitations discussed above, the direct and accurate observation of absorbance changes *in situ* in intact organisms is a useful complement to traditional reductionist approaches and recent advances in proteomic and transcriptomic studies. The colored prosthetic groups of most electron transport proteins comprise intrinsic spectrophotometric probes whereby transient changes in the oxidation–reduction state of the proteins may be monitored with great sensitivity. There is no better means to establish physiological relevance in a metabolic function than to directly observe it as it occurs in the intact bacterium. The movement of electrons through electron transfer complexes is central to energy production in all living cells. The ability to conduct direct spectrophotometric studies under non-invasive physiological conditions represents a new and powerful approach to examine the extents and rates of biological events *in situ* without disrupting the complexity of the live cellular environment. Studies such as these should increase our fundamental understanding of biological energy transduction.

ACKNOWLEDGMENTS

This research was supported by grants DE-SC0007229 from the United States Department of Energy, 1G12RR026260 from the National Institutes of Health, and W911NF-07-1-001 from the United States Department of Defense through its Army Research Office.

REFERENCES

Auernik, K. S., and Kelly, R. M. (2008). Identification of components of electron transport chains in the extremely thermoacidophilic crenarchaeon *Metallosphaera sedula* through iron and sulfur compound oxidation transcriptomes. *Appl. Environ. Microbiol.* 74, 7723–7732.

Blake, R. C. II, Howard, G. T., and McGinness, S. (1994). Enhanced yield of iron-oxidizing bacteria by in situ electrochemical reduction of soluble iron in the growth medium. *Appl. Environ. Microbiol.* 60, 2704–2710.

Blake, R. C. II, and Shute, E. A. (1997). "Purification and characterization of a novel cytochrome from *Leptospirillum ferrooxidans*," in *International Biohydrometallurgy Symposium '97 – BIOMINE97* (Glenside: Australian Mineral Foundation), PB3.1–PB3.10.

Blake, R. C. II, Schute, E. A., Greenwood, M. M., Spencer, G. M., and Ingeldew, W. J. (1993). Enzymes of aerobic respiration on iron. *FEMS Microbiol. Rev.* 11, 9–18.

Blake, R. C. II, Schute, E. A., Waskovsky, J., and Harrison, A. P. Jr. (1992). Respiratory components in acidophilic bacteria that respire on iron. *Geomicrobiol. J.* 10, 173–192.

Blake, R. C. II, White, K. J., and Shute, E. A. (1991). Mixed ligand complexes of iron with cyanide and phenanthroline as new probes of metalloprotein electron transfer reactivity. *J. Biol. Chem.* 266, 19203–19211.

Bright, H. J., and Porter, D. J. T. (1975). "Flavoprotein oxidases," in *The Enzymes XII: Oxidation Reduction Part B*, ed. P. D. Boyer (New York, NY: Academic Press), 421–505.

Castelle, C., Guiral, M., Malarte, G., Ledgham, F., Leroy, G., Brugna, M., and Giudici-Orticoni, M. T. (2008). A new iron-oxidizing/O_2-reducing supercomplex spanning both inner and outer membranes, isolated from the extreme acidophile *Acidithiobacillus ferrooxidans*. *J. Biol. Chem.* 283, 25803–25811.

Chacarolli, C. J., Andrade, J. F., Guimarales, O. M., Balbo, V. R., Venezuela, C. S., and Teruel, F. S. (2000). Spectrophotometric study of iron oxidation in the iron(II)/azide/tetrahyrofuran system and some analytical applications. *Anal. Chim. Acta* 411, 217–222.

Chance, B. (1943). The kinetics of the enzyme-substrate compound of peroxidase. *J. Biol. Chem.* 151, 553–577.

Chen, L., Brugger, K., Skovgaard, M, Redder, P., She, Q., Torarinsson, E., Greve, B., Awayez, M., Zibat, A., Klenk, H. P., and Garrett, R. A. (2005). The genome of *Sulfolobus acidocaldarius*, a model organism of the Crenarchaeota. *J. Bacteriol.* 187, 4992–4999.

Clark, D. A., and Norris, P. R. (1996). *Acidimicrobium ferrooxidans* gen. nov., sp. nov.: mixed-culture ferrous iron oxidation with *Sulfobacillus* species. *Microbiology* 142, 785–790.

Clum, A., Nolan, M., Lang, E., Del Rio, T. G., Tice, H., Copeland, A., Cheng, J. F., Lucas, S., Chen, F., Bruce, D., Goodwin, L., Pitluck, S., Ivanova, N., Mavromatis, K., Mikhailova, N., Pati, A., Chen, A., Palaniappan, K., Göker, M., Spring, S., Land, M., Hauser, L., Chang, Y. J., Jeffries, C. C., Chain, P., Bristow, J., Eisen, J. A., Markowitz, V., Hugenholtz, P., Kyrpides, N. C., Klenk, H. P., and Lapidus, A. (2009). Complete genome sequence of *Acidimicrobium ferrooxidans* type strain. *Stand. Genomic Sci.* 1, 38–45.

Cobley, J. G., and Cox, J. C. (1983). Energy conservation in acidophilic bacteria. *Microbiol. Rev.* 47, 579–595.

Cox, J. C., and Boxer, D. H. (1978). The purification and some properties of rusticyanin, a blue copper protein involved in iron (II) oxidation from *Thiobacillus ferroxidans*. *Biochem. J.* 174, 497–502.

Dinarieva, T. Y., Zhuravleva, A. E., Pavlenko, O. A., Tsaplina, I. A., and Netrusov, A. I. (2010). Ferrous iron oxidation in moderately thermophilic acidophile *Sulfobacillus sibiricus* N1T. *Can. J. Microbiol.* 56, 803–808.

Dopson, M., Baker-Austin, C., and Bond, P. L. (2005). Analysis of differential protein expression during growth states of *Ferroplasma* strains and insights into electron transport for iron oxidation. *Microbiology* 151, 4127–4137.

Eccleston, M., Kelly, D. P., and Wood, A. P. (1985). "Autotrophic growth and iron oxidation and inhibition kinetics of *Leptospirillum ferrooxidans*," in *Planetary Ecology*, eds D. E. Caldwell, J. A. Brierley, and C. L. Brierley (New York, NY: Van Nostrand Reinhold), 263–272.

Elterman, P. (1970). Integrating cavity spectroscopy. *Appl. Opt.* 9, 2140–2142.

Fry, E. S., Kattawar, G. W., and Pope, R. M. (1992). Integrating cavity absorption meter. *Appl. Opt.* 31, 2055–2065.

Fry, E. S., Kattawar, G. W., Strycker, B. D., and Zhai, P. W. (2010). Equivalent path lengths in an integrating cavity: comment. *Appl. Opt.* 49, 575–577.

Golyshina, O. V., Pivovarova, T. A., Karavaiko, G. I., Kondrateva, T. F., Moore, E. R., Abraham, W. R., Lunsdorf, H., Timmis, K. N., Yakimov, M. M., and Golyshin, P. N. (2000). *Ferroplasma acidiphilum* gen. nov., sp. nov., an acidophilic, autotrophic, ferrous-iron-oxidizing, cell-wall-lacking, mesophilic member of the Ferroplasmaceae fam. nov., comprising a distinct lineage of the Archaea. *Int. J. Syst. Evol. Microbiol.* 50, 997–1006.

Golyshina, O. V., Yakimov, M. M., Lunsdorf, H., Ferrer, M., Nimtz, M., Timmis, K. N., Wray, V., Tindall, B. J., and Golyshin, P. N. (2009). *Acidiplasma aeolicum* gen. nov., sp. nov., a novel euryarchaeon of the family Ferroplasmaceae isolated from a hydrothermal pool, and transfer of *Ferroplasma cupricumulans* to *Acidiplasma cupricumulans* comb. nov. *Int. J. Syst. Evol. Microbiol.* 59, 2815–2823.

Guo, X., You, X. Y., Liu, L. J., Zhang, J. Y., Liu, S. J., and Jiang, C. Y. (2009). *Alicyclobacillus aeris* sp. nov., a novel ferrous iron- and sulfur-oxidizing bacterium isolated from a copper mine. *Int. J. Syst. Evol. Microbiol.* 59, 2415–2420.

Hallberg, K. B., Gonzalez-Toril, E., and Johnson, D. B. (2010). *Acidithiobacillus ferrivorans*, sp. nov.; facultatively anaerobic, psychrotolerant iron- and sulfur-oxidizing acidophiles isolated from metal mine-impacted environments. *Extremophiles* 14, 9–19.

Harrison, A. P. Jr. (1984). The acidic thiobacilli and other acidophilic bacteria that share their habitat. *Annu. Rev. Microbiol.* 38, 265–292.

Hart, A. J., Murrell, J. C., Poole, R. K., and Norris, P. R. (1991). An acid-stable cytochrome in iron-oxidizing *Leptospirillum ferrooxidans*. *FEMS Microbiol. Lett.* 81, 89–94.

Hettmann, T., Schmidt, C. L., Anemuller, S., Zahringer, U., Moll, H., Petersen, A., and Schafer, G. (1998). Cytochrome b558/566 from the archaeon *Sulfolobus acidocaldarius*. *J. Biol. Chem.* 273, 12032–12040.

Hodgkinson, J., Masiyano, D., and Tatam, R. P. (2009). Using integrating spheres as absorption cells: path-length distribution and application of Beer's law. *Appl. Opt.* 48, 5748–5758.

Huber, G., Spinnler, C., Gambacorta, A., and Stetter, K. O. (1989). *Metallosphaera sedula* gen. and sp. nov. represents a new genus of aerobic, metal-mobilizing, thermoacidophilic archaebacteria. *Syst. Appl. Microbiol.* 12, 38–47.

Huber, G., and Stetter, K. O. (1991). *Sulfolobus metallicus*, sp. nov., a novel strictly chemolithoautotrophic thermophilic archaeal species of metal-mobilizers. *Syst. Appl. Microbiol.* 14, 372–378.

Huber, H., and Stetter, K. O. (1989). *Thiobacillus prosperous* sp. nov., represents a new group of halotolerant metal-mobilizing bacteria isolated from a marine geothermal field. *Arch. Microbiol.* 151, 479–485.

Ingledew, W. J. (1982). The bioenergetics of an acidophilic chemolithotroph. *Biochim. Biophys. Acta* 683, 89–117.

Javorfi, T., Erostyak, J., Gal, J., Buzady, A., Menczel, L., Grab, G., and Naqvi, K. R. (2006). Quantitative spectrophotometry using integrating cavities. *J. Photochem. Photobiol. B Biol.* 82, 127–131.

Jiang, C. Y., Liu, Y., Liu, Y. Y., You, X. Y., Guo, X., and Liu, S. J. (2009). *Alicyclobacillus ferrooxydans* sp. nov., a ferrous-oxidizing bacterium from solfataric soil. *Int. J. Syst. Evol. Microbiol.* 58, 2898–2903.

Johnson, D. B., Bacelar-Nicolau, P., Okibe, N., Thomas, A., and Hallberg, K. B. (2009). *Ferrimicrobium acidiphilum* gen. nov., sp. nov. and *Ferrithrix thermotolerans* gen. nov., sp. nov.: heterotrophic, iron-oxidizing, extremely acidophilic actinobacteria. *Int. J. Syst. Evol. Microbiol.* 59, 1082–1089.

Johnson, D. B., Joulian, C., d'Hugues, P., and Hallberg, K. B. (2008). *Sulfobacillus benefaciens* sp. nov., an acidophilic facultative anaerobic Firmicute isolated from mineral bioleaching operations. *Extremophiles* 12, 789–798.

Karavaiko, G. I., Golyshina, O. V., Troitskii, A. V., Valieho-Roman, K. M., Golovacheva, R. S., and Pivovarova, T. A. (1994). *Sulfurococcus yellowstonii* sp. nov., a new species of iron- and sulfur-oxidizing thermoacidophilic archaebacteria. *Mikrobiologiya* 63, 668–682.

Kelly, D. P., and Wood, A. P. (2000). Reclassification of some species of *Thiobacillus* to the newly designated genera *Acidithiobacillus* gen. nov., *Halothiobacillus* gen. nov. and *Thermithiobacillus* gen. nov. *Int. J. Syst. Evol. Microbiol.* 50, 511–516.

Markosyan, G. E. (1972). A new acidophilic iron bacterium *Leptospirillum ferrooxidans*. *Biol. Zh. Arm.* 25, 26–33.

Merzlyak, M. N., and Naqvi, K. R. (2000). On recording the true absorption spectrum and the scattering spectrum of a turbid sample: application to cell suspensions of the cyanobacterium *Anabaena variabilis*. *J. Photochem. Photobiol. B Biol.* 58, 123–129.

Michels, M., and Bakker, E. P. (1985). Generation of a large, protonophore-sensitive proton motive force and pH difference in the acidophilic bacteria *Thermoplasma acidophilum* and *Bacillus acidocaldarius*. *J. Bacteriol.* 161, 231–237.

Nelson, N. B., and Prezelin, B. B. (1993). Calibration of an integrating sphere for determining the absorption coefficient of scattering suspensions. *Appl. Opt.* 32, 6710–6717.

Norris, P. R., Clark, D. A., Owen, J. P., and Waterhouse, S. (1996). Characteristics of *Sulfobacillus acidophilus* sp. nov. and other moderately thermophilic mineral-sulphide-oxidizing bacteria. *Microbiology* 142, 775–783.

Ram, R. J., VerBerkmoes, N., Thelen, M. P., Tyson, G. W., Baker, B. J., Blake, R. C. II, Shah, M., Hettich, R., and Banfield, J. F. (2005). Community proteomics of a natural microbial biofilm. *Science* 308, 1915–1920.

Segerer, A., Neuner, A., Kristjansson, J. K., and Stetter, K. O. (1986). *Acidianus infernus* gen. nov., sp. nov., and *Acidianus brierleyi comb.* nov.: facultatively aerobic, extremely acidophilic, thermophilic sulfur-metabolizing archaebacteria. *Int. J. Syst. Bacteriol.* 36, 559–564.

Shibata, K., Benson, A. A., and Calvin, M. (1954). The absorption

spectra of suspensions of living microorganisms. *Biochim. Biophys. Acta* 15,461–470.

Siezen, R. J., and Wilson, G. (2009). Bioleaching genomics. *Microb. Biotechnol.* 2, 297–303.

Singer, S. W., Chan, C. S., Zemla, A., VerBerkmoes, N. C., Hwang, M., Hettlich, R. L., Banfield, J. L., and Thelen, M. P. (2008). Characterization of cytochrome 579, an unusual cytochrome isolated from an iron-oxidizing microbial community. *Appl. Environ. Microbiol.* 74, 4454–4462.

Takai, M., Kamimura, K., and Sugio, T. (2001). A new iron oxidase from a moderately thermophilic iron oxidizing bacterium strain TI-1. *Eur. J. Biochem.* 268, 1653–1658.

Tuovinen, O. H., and Kelly, D. P. (1973). Studies on the growth of *Thiobacillus ferrooxidans*. I. Use of membrane filters and ferrous iron agar to determine viable numbers, and comparison with $14CO_2$-fixation and iron oxidation as measures of growth. *Arch. Microbiol.* 22, 285–296.

Valdes, J., Pedroso, I., Quatrini, R., Tettelin, H., Blake, R. C. II, Malek, J., Eisen, J. A., and Holmes, D. S. (2008). Modeling *Acidithiobacillus ferrooxidans* metabolism: from genome sequence to industrial applications. *BMC Genomics* 9, 597. doi:10.1186/1471-2164-9-597

Yarzábal, A., Appia-Ayme, C., Ratouchniak, J., and Bonnefoy, V. (2004). Regulation of the expression of the *Acidithiobacillus ferrooxidans rus* operon encoding two cytochromes *c*, a cytochrome oxidase and rusticyanin. *Microbiology* 150, 2113–2123.

Yarzábal, A., Brasseur, G., Appia-Ayme, C., Ratchouchniak, J., Lund, K., Lemesle-Meunier, D., DeMoss, J. A., and Bonnefoy, V. (2002). The high molecular weight cytochrome *c* Cyc2 of *Acidithiobacillus ferrooxidans* is an outer membrane protein. *J. Bacteriol.* 184, 313–317.

Conflict of Interest Statement: The authors declare that the research was conducted in the absence of any commercial or financial relationships that could be construed as a potential conflict of interest.

Received: 22 November 2011; accepted: 21 March 2012; published online: 12 April 2012.

Citation: Blake II RC and Griff MN (2012) In situ spectroscopy on intact Leptospirillum ferrooxidans reveals that reduced cytochrome 579 is an obligatory intermediate in the aerobic iron respiratory chain. Front. Microbio. ***3****:136. doi: 10.3389/fmicb.2012.00136*

This article was submitted to Frontiers in Microbiological Chemistry, a specialty of Frontiers in Microbiology.

Copyright © 2012 Blake II and Griff. This is an open-access article distributed under the terms of the Creative Commons Attribution Non Commercial License, which permits non-commercial use, distribution, and reproduction in other forums, provided the original authors and source are credited.

frontiers in
MICROBIOLOGY

ORIGINAL RESEARCH ARTICLE
published: 26 March 2012
doi: 10.3389/fmicb.2012.00109

Microbial iron cycling in acidic geothermal springs of Yellowstone National Park: integrating molecular surveys, geochemical processes, and isolation of novel Fe-active microorganisms

Mark A. Kozubal[1,2], Richard E. Macur[1,2], Zackary J. Jay[1,2], Jacob P. Beam[1,2], Stephanie A. Malfatti[3], Susannah G. Tringe[3], Benjamin D. Kocar[4], Thomas Borch[5] and William P. Inskeep[1,2]*

[1] *Thermal Biology Institute, Montana State University, Bozeman, MT, USA*
[2] *Department of Land Resources and Environmental Sciences, Montana State University, Bozeman, MT, USA*
[3] *Department of Energy–Joint Genome Institute, Walnut Creek, CA, USA*
[4] *Stanford Synchrotron Radiation Lightsource, Stanford, CA, USA*
[5] *Department of Soil and Crop Sciences, Colorado State University, Fort Collins, CO, USA*

Edited by:
Eric Roden, University of Wisconsin–Madison, USA

Reviewed by:
Vernon Phoenix, University of Glasgow, UK
Johannes Gescher, Karlsruhe Institute of Technology, Germany
David Barrie Johnson, Bangor University, UK

****Correspondence:***
William P. Inskeep, Department of Land Resources and Environmental Sciences, Montana State University, P.O. Box 173120, Bozeman, MT 59717, USA.
e-mail: binskeep@montana.edu

Geochemical, molecular, and physiological analyses of microbial isolates were combined to study the geomicrobiology of acidic iron oxide mats in Yellowstone National Park. Nineteen sampling locations from 11 geothermal springs were studied ranging in temperature from 53 to 88˚C and pH 2.4 to 3.6. All iron oxide mats exhibited high diversity of crenarchaeal sequences from the Sulfolobales, Thermoproteales, and Desulfurococcales. The predominant Sulfolobales sequences were highly similar to *Metallosphaera yellowstonensis* str. MK1, previously isolated from one of these sites. Other groups of archaea were consistently associated with different types of iron oxide mats, including undescribed members of the phyla Thaumarchaeota and Euryarchaeota. Bacterial sequences were dominated by relatives of *Hydrogenobaculum* spp. above 65–70˚C, but increased in diversity below 60˚C. Cultivation of relevant iron-oxidizing and iron-reducing microbial isolates included *Sulfolobus* str. MK3, *Sulfobacillus* str. MK2, *Acidicaldus* str. MK6, and a new candidate genus in the Sulfolobales referred to as Sulfolobales str. MK5. Strains MK3 and MK5 are capable of oxidizing ferrous iron autotrophically, while strain MK2 oxidizes iron mixotrophically. Similar rates of iron oxidation were measured for *M. yellowstonensis* str. MK1 and Sulfolobales str. MK5. Biomineralized phases of ferric iron varied among cultures and field sites, and included ferric oxyhydroxides, K-jarosite, goethite, hematite, and scorodite depending on geochemical conditions. Strains MK5 and MK6 are capable of reducing ferric iron under anaerobic conditions with complex carbon sources. The combination of geochemical and molecular data as well as physiological observations of isolates suggests that the community structure of acidic Fe mats is linked with Fe cycling across temperatures ranging from 53 to 88˚C.

Keywords: iron oxidation, iron reduction, ferric iron mat, geothermal, archaea, Sulfolobales, exobiology, jarosite

INTRODUCTION

Ferric iron oxyhydroxide and jarositic microbial mats are found in numerous environments and have been well studied in acid-mine-drainage systems such as Iron Mountain, CA, USA (Edwards et al., 1999; Singer et al., 2008) where Fe(II) and H_2SO_4 are produced during the oxidation of sulfide minerals such as pyrite and chalcopyrite (Nordstrom and Southam, 1997; Rohwerder et al., 2003). The phylogenetic diversity of microbial populations in acidic systems has been reviewed and acidophiles that respire on Fe(III) have been identified in various mesophilic systems (Blake and Johnson, 2000; Hallberg and Johnson, 2001; Baker and Banfield, 2003; Johnson and Hallberg, 2009). Microbial populations and description of novel species from thermo-acidophilic, iron-rich environments have also been studied (Johnson et al., 2003, 2006; Macur et al., 2004; Inskeep et al., 2005, 2010; Kozubal et al., 2008). Ferric iron mats from acidic geothermal springs in Yellowstone National Park (YNP) provide an outstanding natural laboratory to study thermophilic microorganisms that utilize ferrous iron for energy acquisition coupled to CO_2 fixation as their primary carbon source. Their ability to thrive in high-temperature environments with minimal requirements other than CO_2 and inorganic constituents suggests that these organisms are important primary producers in acidic high-temperature environments. However, the limited energy available from the oxidation of Fe(II) results in the formation of copious amounts of iron oxides. It has been estimated that at pH 2, ∼120 mol of Fe(II) must be oxidized for the formation of 1 mol of glucose (Konhauser, 2007). Thus, low cell numbers can result in the oxidation of large amounts of iron,

which has implications in understanding the biomineralization of iron in many environments outside YNP, as well as throughout Earth's evolutionary history (e.g., banded iron formations; Konhauser, 1998; Kappler and Straub, 2005).

Rates of abiotic Fe(II)-oxidation are slow at pH values less than 4.5 [1×10^{-7} mol Fe(II) min^{-1}; Singer and Stumm, 1970]; therefore, acidophilic microbes have an advantage over neutrophiles by not having to compete for rapid abiotic oxidation of Fe(II). Biologically oxidized Fe(II) often accumulates as ferric oxide minerals, which range in thickness and hardness depending on the geochemistry, flow rate, and microbial populations present (Konhauser, 1998; Inskeep et al., 2004). Solid phase geochemical analyses have been conducted on several ferric iron mats in YNP including 2–4 cm thick amorphous Fe-oxide mats from an acid-sulfate-chloride (ASC) spring (pH ∼3) in the Norris Geyser Basin (NGB) region as well as more crystalline ferric oxides (i.e., goethite, hematite) and jarosite from an acid-sulfate (AS) system located at the Rainbow Springs region (Inskeep et al., 2005). However, new results from synchrotron Fe-extended-X-ray absorption fine-structure spectroscopy (EXAFS) and X-ray diffraction (XRD) analyses across a greater number of Fe-oxide mats are presented in the current study and integrated with aqueous geochemical data and microbial community structure to understand factors controlling Fe-biomineralization across different acidic high-temperature environments.

Previous work has also described the microbial diversity in several low pH, iron-rich geothermal springs in the NGB, Joseph's Coat Hot Springs, and Rainbow Hot Springs regions of YNP (Jackson et al., 2001; Inskeep et al., 2004, 2005; Macur et al., 2004). However, these studies were based primarily on a relatively small number of shorter-length 16S rRNA gene sequences from a few sampling locations. Therefore, a primary aim of this study is to present more comprehensive data on the microbial diversity from numerous acidophilic ferric mats in YNP over a wide variety of environmental conditions ($T = 53$–$88^{\circ}C$; pH = 2.4–3.6), including a larger library of 16S rRNA gene sequences obtained from "next-generation" pyrotag and community shotgun sequencing efforts.

Phylogenetic similarity of observed sequences from molecular studies to cultivated microorganisms (16S rRNA gene) is not sufficient to definitively link microbial metabolism(s) to specific geochemical cycles especially when 16S rRNA gene sequences are highly divergent from those of cultured organisms (e.g., <90% similarity). Therefore, the cultivation of relevant organisms from these habitats is also critical for implicating specific microorganisms and their corresponding metabolic pathways in biogeochemical processes. For example, we recently reported the isolation of a new Sulfolobales isolate from YNP ferric iron mats, *Metallosphaera yellowstonensis* str. MK1, an iron and sulfur-oxidizing chemolithoautotroph (Kozubal et al., 2008). Quantitative analysis of *Metallosphaera*-like 16S rRNA sequences demonstrated that organisms highly similar (>99%) to strain MK1 comprised up to 80% of the total archaeal community in various YNP ferric iron habitats.

The geothermal springs discussed in this study are highly reduced at the source and Fe(II)-oxidizing microbial communities do not occur until the springs have sufficient dissolved oxygen from atmospheric mixing, after dissolved sulfide has degassed. Previous quantitative expression results show that the *M. yellowstonensis foxA-J* gene cluster is important for Fe(II) oxidation in pure culture and *in situ* (Kozubal et al., 2011). The *fox* gene cluster is found in all iron-oxidizing Crenarchaeota (i.e., *Sulfolobus metallicus, Sulfolobus tokodaii,* and *Metallosphaera* spp.) and potential mechanisms for Fe(II) oxidation via Fox proteins have been hypothesized (Kozubal et al., 2011). It is not currently known how widespread this gene complex may be in other members of the Sulfolobales found in Fe-oxide mats, and/or in other archaea.

The primary goal of this study was to couple geochemical processes with microbial community analysis to understand mechanisms of Fe(II)-oxidation and secondary solid phase formation in acidic outflow channels of YNP geothermal springs. The specific objectives were to (i) determine *in situ* Fe(II) oxidation rates and identify predominant secondary minerals formed across a range of environmental conditions ($T = 53$–$88^{\circ}C$; pH = 2.4–3.6), (ii) identify the predominant community members of different high-temperature ferric iron microbial mats, (iii) characterize novel Fe-active isolates determined to be relevant *in situ* populations using molecular surveys, and (iv) present genomic evidence for iron and sulfur oxidation in a novel Sulfolobales isolate (strain MK5), as well as from site metagenomes.

MATERIALS AND METHODS

DESCRIPTION OF SITES

Eleven geothermal springs in Yellowstone National Park were chosen for this study and include eight acid-sulfate-chloride springs (ASC) in NGB, and three acid-sulfate springs (AS) springs from Joseph's Coat and Rainbow Springs (**Figure 1**). Each spring was sampled at multiple locations based on transects established within the main flow channel as a function of distance (temperature) from the outflow source (selected sites shown in **Figure 2**). The ASC springs sampled include "*OSP Spring*" (NGB-OSP), "*Beowulf Spring*" (NGB-BE, NGB-BW), "*Gap Spring*" (NGB-GAP), *Echinus Geyser* (NGB-EG), *Whirligig Geyser* (NGB-WG), "*Grendel Spring*" (NGB-GRN), and "*Porcelain Basin*" (NGB-PB; names in quotations are not official YNP names). Acid-sulfate springs included an unnamed spring at Joseph's Coat Hot Springs (JC2) and two unnamed springs at Rainbow Springs (RS2 and RS3).

DNA EXTRACTION AND 16S rRNA SEQUENCING

The distribution and relative abundance of total archaeal and bacterial 16S rRNA gene sequences were examined using microbial mat samples obtained with sterile tools and collection tubes and immediately placed on dry ice for transport to a −80°C freezer. Samples were obtained over a 5-year period from July 2003 to July 2008. Total DNA was extracted from field samples (or pure cultures) using a FastDNA SPIN kit for soil (Q-Biogene, Irvine, CA, USA). The nearly full-length 16S rRNA gene PCR primers included the *Bacteria*-specific primer Bac8f (5′-AGAGTTTGATCCTGGCTCAG-3′) coupled with the universal primerUniv1392r (5′-ACGGGCGGTGTGTAC-3′) and the *Archaea*-specific primer Arc2f (5′-TTCCGGTTGATCCYGCCGGA-3′) also coupled with the universal primer Univ1392r. Briefly, each

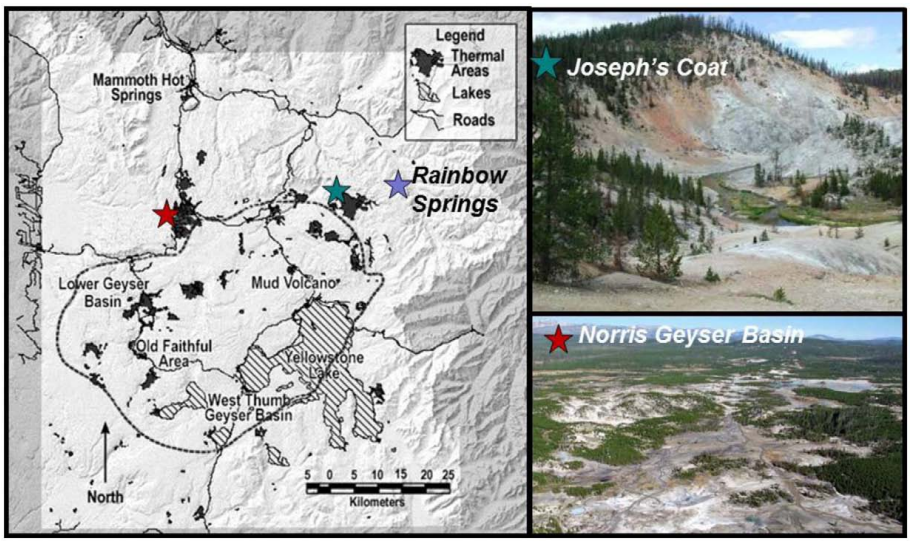

FIGURE 1 | Map of Yellowstone National Park indicating sampling locations at Rainbow Springs, Joseph's Coat Hot Springs, and Norris Geyser Basin (NGB).

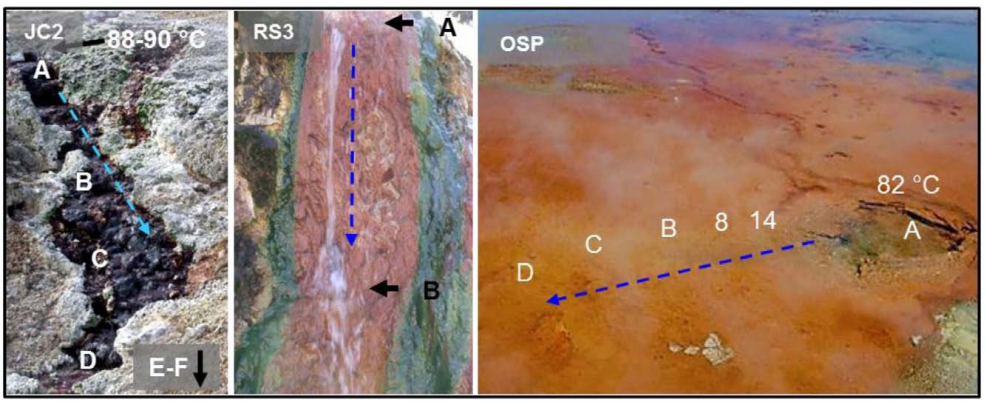

FIGURE 2 | Representative springs (JC2, RS3, and OSP) from Yellowstone National Park showing sampling points within the main flow channels, source water temperatures, and direction of flow channel (blue arrow).

50-μL PCR mixture contained 10 mM Tris–HCl (pH 8), 50 mM KCl, 0.1% Triton X-100, 4.0 mM $MgCl_2$, each deoxynucleoside triphosphate at a concentration of 800 μM, 0.5 μL of each primer, 1.25 U of *Taq* DNA polymerase (Promega, Madison, WI, USA), and 1–5 μL of template DNA (2–20 ng). The thermal cycler protocol was 94°C for 6 min, 25–35 cycles of 94°C for 45 s, 54°C for45 s, and 72°C for 110 s, and a final 7-min extension at 72°C. Negative control reactions (no template) were routinely performed to ensure purity. The purified PCR products were cloned using the pGEM-T vector system from Promega Corp. (Madison, WI, USA), and the inserts were amplified and sequenced (TGEN, Phoenix, AZ, USA, and the Ohio State Plant Genomics Facility, Columbus, OH, USA).

In addition to clone sequences obtained from the method described above, a total of 1348 near full-length 16S rRNA gene sequences were obtained from the Joint Genome Institute (JGI) for two Fe samples from OSP springs as part of a different metagenome study (Community Sequencing Project 787081). The primers used by JGI were *Bacteria* specific 27F (5′-AGAGTTTGATCCTGGCTCAG-3′) and 1391R (5′-GACGGGCRGTGWGTRCA-3′), and *Archaea*-specific 4aF (5′-TCCGGTTGATCCTGCCRG-3′) and 1391R (for details see http://www.jgi.doe.gov/sequencing/protocols/index.html). Finally, samples from several Fe mats (obtained in 2009) were used for 454 "pyrotag" sequencing (16S rRNA amplified template) at the DOE–JGI, including sampling locations at OSPB ($n = 31{,}237$), OSPC ($n = 8719$), OSPD ($n = 146$), BEE ($n = 3574$), and GRN ($n = 21{,}401$). The V6–V8 region of 16S rRNA was amplified using primers 926F (5′-cctatcccctgtgtgccttgg cag tct cag AAA CTY AAA KGA ATT GRC GG-3′) and 1392R (5′-ccatct cat ccc tgcgtgtctccg act cag ACG GGC GGT GTG TRC-3′). Primer sequences were modified by the addition of 454 A or B adapter sequences (lower

case). In addition, the reverse primer included a 5-bp barcode for multiplexing of samples during sequencing. Twenty-microliter PCR reactions were performed in duplicate and pooled to minimize PCR bias using 0.4 μL Advantage GC 2 Polymerase Mix (Advantage-2 GC PCR Kit, Clonetech), 4 μL 5X GC PCR buffer, 2 μL 5 M GC Melt Solution, 0.4 μL 10 mM dNTP mix (MBI Fermentas), 1.0 μL of each 25 nM primer, and 10 ng sample DNA. The thermal cycler protocol was 95°C for 3 min, 25 cycles of 95°C for 30 s, 50°C for45 s, and 68°C for 90 s, and a final 10-min extension at 68°C. PCR Amplicons were purified using SPRI Beads and quantified using a Qubit fluorometer (Invitrogen). Samples were diluted to 10 ng/μL and mixed in equal concentrations. Emulsion PCR and sequencing of the PCR amplicons were performed following the Roche 454 GS FLX Titanium technology manufacturer's instructions. Sequencing tags were analyzed using the software tool PyroTagger (http://pyrotagger.jgi-psf.org) using a 180-bp sequence length threshold as described in Engelbrektson et al. (2010). The 97% operational taxonomic units (OTUs) were also taxonomically classified by Blastn against a curated database of >1500 full-length 16S rRNA sequences from the actual sites that exhibited high nucleotide similarity (>96% of reads were 99.5% similar to prior long-fragment sequences).

CULTIVATION OF MICROORGANISMS FROM Fe MICROBIAL MATS

Approximately 2 g of Fe-oxide microbial mat from NGB-BE, NGB-GAPA, and NB-OSPB was placed into 60 mL serum bottles with synthetic growth medium as described by Kozubal et al. (2008) at sampling times between August 2003 and August 2008. Isolation of *Sulfobacillus* str. MK2 colonies was obtained by streaking ∼0.5 mL of NGB-BE slurry on 1.5% agar plates in synthetic media with 0.5% yeast extract and 10 mM $FeSO_4$. Plates were incubated at 58°C for up to 12 days. Colonies were transferred to serum bottle cultures with 10 mM $FeSO_4$, 0.2% YE in synthetic media for further study. Pure cultures of *Acidicaldus* str. MK6 and Sulfolobales sp. strain MK5 were obtained by streaking ∼0.5 mL of OSPB slurry on 1.2% Gelrite® plates in media described by Itoh et al. (2001) with 2 mM $FeSO_4$. Plates were incubated at 65°C for up to 15 days. Pure colonies of *Acidicaldus* str. MK6 were transferred to serum bottle cultures with synthetic media and 0.05% YE for further studies. *Sulfolobus* str. MK3 was obtained by dilution to extinction with 2% pyrite in synthetic media by the method described for *Metallosphaera* str. MK1 (Kozubal et al., 2008), except inoculum was obtained from GAPA and cultures were incubated at 75°C. The progress of all cultures was monitored by extracting DNA from the serum bottles, followed by PCR amplification of 16S rRNA genes using universal bacterial and archaeal primers and separation and visualization of the PCR products using denaturing gradient gel electrophoresis (DGGE; Macur et al., 2004). The purity of cultures was also confirmed by cloning and sequencing of near full-length16S rRNA gene fragments.

PHYLOGENETIC ANALYSES

Near full-length 16S rRNA gene sequences obtained from cloning were compared to sequences in public databases using the "Blastn" algorithm. Sequence alignments were performed using ClustalX (Version 1.83) and phylogenetic trees were constructed using the Maximum Likelihood method (MEGA 5.0) with 1000 boot straps (Tamura et al., 2011). Accession numbers for all 16S rRNA gene sequences discussed in the current study were deposited with NCBI [*Sulfobacillus* str. MK2 (DQ350778), *Sulfolobus* str. MK3 (JN944177), Sulfolobales str. MK5 (JN971012), and *Acidicaldus* str. MK6 (JQ247723)].

ISOLATE GROWTH CHARACTERISTICS

Temperature and pH optima were determined for all isolates in 20 mL serum bottles with 5 mL headspace composed of 30% O_2, 50% CO_2, and 20% N_2. Heterotrophic growth was determined with the addition of 0.5% yeast extract (YE); autotrophic growth with either 2% pyrite, 2% S^0, or 5 mM Fe(II)SO_4 without added carbon; and mixotrophic growth with 5 mM Fe(II)SO_4 and 0.5% YE. Anaerobic growth was evaluated using Fe(III) as a primary electron acceptor in 20 mL serum bottles with 15 mL of synthetic media, 0.5 g of dried, double-autoclaved NGB-BE mat (120°C), 10 mM glucose, and 0.5% YE. Serum bottle cultures were sealed and purged with N_2 gas for 20 min to obtain sub-oxic conditions.

IRON OXIDATION AND REDUCTION RATES

Iron oxidation rates were determined for *Metallosphaera* str. MK1 and Sulfolobales str. MK5 in 120 mL serum bottles with 1 g of crushed and dried, triple autoclaved NGB-BE HFO mat and 60 mL of BED synthetic media with 10 mM $FeSO_4$ without added carbon and a headspace composed of 50% O_2 and 50% CO_2. Oxidation rates of Fe(II) were determined with an initial cell culture of $\sim 10^6$ cells/mL added at exponential growth phase. Abiotic Fe(II)-oxidation rates were determined with un-inoculated controls. Fe(II) was measured on 1 mL filtered (0.2 micron filters) samples using the ferrozine method (To et al., 1999) on late exponential/lag phase cultures after the addition of 10 mM Fe(II). Samples were taken every 10 min for four hours after cell culture density reached 10^8 cells/mL. Culture density was measured by counting SYBR gold staining. Rates were reported as femtomoles Fe(II) per liter per second per cell after correcting for abiotic oxidation [0.025 μmol Fe(II) L^{-1} s^{-1}].

Iron reduction rates were determined for *Acidicaldus* str. MK6 and Sulfolobales str. MK5 in 120 mL serum bottles with 80 mL of synthetic medium, 10 mM glucose as the electron donor and 1-g triple autoclaved Fe(III)-oxide mat from NGB-BE, which has been previously characterized (Inskeep et al., 2004). Serum bottles were purged with N_2(g) for 20 min prior to inoculation. Samples were inoculated to an initial concentration of 10^5 cells/mL and 1 mL filtered samples were taken twice daily for 10 days and analyzed for Fe(II) as stated above. Cell concentrations were determined by SYBR gold staining and reduction rates were calculated on late exponential/lag phase cultures after cell culture densities reached 10^8 cells/mL and reported as femtomoles Fe(III) per liter per second per cell [abiotic Fe(III)-reduction rates were negligible].

SOLID PHASE CHEMICAL ANALYSIS

Solid phase analysis was performed on field samples and secondary phases obtained from *Metallosphaera* str. MK1 and Sulfolobales str. MK5 culture vessels after 11 days of incubation in *Beowulf* spring water and 2% ground pyrite at 65°C and pH 3.0. Strain MK1

culture vessels contained two distinct iron oxide phases including a dark-red phase around the glass vessel at the air/water interface and an off-yellow phase forming just below the air-water interface. Approximately 0.5–1 g of each phase was scraped from the bottles and analyzed by XRD or X-ray absorption spectroscopy (XAS).

Iron EXAFS spectra were collected at beamline 11-2 at the Stanford Synchrotron Radiation Lightsource. A double crystal Si(220) monochromator was used for energy selection. Scans were conducted from 100 eV below to 1000 eV above the Fe-K-edge at 7111 eV. Iron fluorescence spectra were averaged and normalized to unity using the XAS data reduction software SIXPACK (Webb, 2011). SIXPACK/IFEFFIT algorithms were used to isolate backscattering contributions by subtracting a spline function from the EXAFS data region. The resulting function was then converted from units of eV to $Å^{-1}$, weighted by k3, and windowed from 3 to 14 $Å^{-1}$ Linear combination of model compounds was performed to reconstruct unknown spectra; no more than four standards were varied at a time. Model compound (standards) contributions were deemed significant if their mole percentage was greater than 10%. Model compounds used for linear combination Fe-EXAFS fitting included two-line ferrihydrite sorbed to quartz sand, Si-substituted ferrihydrite, six-line ferrihydrite, lepidocrocite, goethite, hematite, potassium-jarosite, scorodite, synthetic and natural siderite, vivianite, magnetite, green rust phases (chloride, sulfate, carbonate), and amorphous FeS. Synchrotron X-ray powder diffraction was performed at 12,735 eV at beamline 11-3 (SSRL), with an energy resolution ($\Delta E/E$) of $\sim 5 \times 10^{-4}$ equipped with a Si(311) monochromator and a MAR345 CCD detector. Finely crushed samples were placed between two polycarbonate windows to a nominal thickness of 100 μm and mounted in an aluminum sample holder. Patterns were energy calibrated using a lanthanum hexaboride standard. Resulting powder diffraction images were radially integrated, converted to d-space vs. relative intensity, and analyzed for mineral phases using JADE 6.0 (Materials Data, Inc.).

MICROSCOPY

Optical images were obtained utilizing a Zeiss epifluorescence microscope (Zeiss Axioskop 2 plus; Zeiss, Oberkochen, Germany). Samples were stained with 10X SYBR-green for fluorescent images. Environmental samples for scanning electron microscopy (SEM) images were stored at 4°C prior to analysis. Samples were analyzed with either a SEM with cryostage or a field emission-scanning electron microscope (FE-SEM), both equipped with an energy-dispersive X-ray spectrometer (EDS) for elemental analysis.

RESULTS

GEOCHEMISTRY OF ACIDIC Fe-OXIDIZING SPRINGS IN YNP

The major electron donors, pH, oxygen concentration, temperature, and solid phase geochemistry of three acid-sulfate (AS; JC2, RS2, RS3) and eight acid-sulfate-chloride (ASC) geothermal springs (NGB-OSP, NGB-BE, NGB-BW, NGB-GAP, NGB-WG, NGB-EG, NGB-PB, NGB-GRN) are summarized across a total of 19 sampling positions (**Table 1**). The common geochemical properties across this group of thermophilic sites include pH (2.4–3.6), ferrous Fe (~30–240 μM), and dissolved oxygen (20–100 μM). The concentrations of other reduced constituents including arsenite, ammonium, dissolved hydrogen, and dissolved methane can be significant; however, the dissolved sulfide levels of Fe-oxide depositional zones are generally <5–10 μM. Although the concentrations of ammonium (NH_4^+) are ~20–30 times higher in AS springs compared to ASC springs, no consistent changes in NH_4^+ were observed as a function of distance from the spring source, regardless of total NH_4 concentration. Ferrous Fe represents the majority of total dissolved Fe at the point of discharge for nearly all springs sampled. Moreover, total soluble Fe did not decline significantly with distance (in some cases Fe_{TS} can decrease by 10–20%), indicating that the deposition rates of secondary Fe(III) phases are considerably slower than the total flux of Fe(II). However, the amount of ferrous Fe decreased substantially in acid-sulfate springs [JC2, RS2; e.g., levels of Fe(II) decline from 81 to 34 μM in RS2] matching the production of soluble ferric Fe (**Figure 3**), whereas ferric Fe remained low in ASC springs containing high concentrations of arsenic (e.g., >20 μM).

The short residence times between sampling positions in JC2 and RS2 (e.g., JC2A to JC2D is 35 s), combined with the amount of Fe(II)-oxidized results in very high rate constants for the oxidation of Fe(II) (**Figure 3**). A second spring source emerges at sampling position JC2E where Fe(II) is reset to near 100% of the total dissolved iron, and ~43% is oxidized to Fe(III) by sampling point JC2F, a 32-s residence time. Measurements of channel velocities and estimates of total flow rate were used to approximate *in situ* iron oxidation rates in outflow channels of JC2 and RS2. The average rates of Fe(II) oxidized within JC2, RS2, and BE Springs ranged from 0.5 to 1.3, 0.2 to 2, and 0.1 to 0.2 μM Fe(II) oxidized/second, respectively (**Figure 3**).

Solid phase analysis was completed for iron oxide mat samples from all sites discussed in the current study except *Grendel* Spring (**Table 1**; **Figure 4**). XRD and SEM/EDAX data from *OSP* Spring and *Whirligig* Geyser in NGB are similar to those found previously from *Beowulf* Spring (Inskeep et al., 2004) and show high levels of arsenate sorbed to amorphous ferrihydrite-like phases (As:Fe = 0.6–0.7). Solid phases from *Echinus* Geyser (**Figure 4**) are characterized by more crystalline ferrihydrite phase with lower sorbed arsenate, which is not surprising given the lower arsenic concentrations (**Table 1**). Scorodite ($Fe^{III}AsO_4 \cdot 2H_2O$) was the dominant phase detected using XRD in the higher temperature (85°C) Fe mats of *Porcelain Basin* and to a lesser extent in *GAP* Spring.

The lower pH acid-sulfate systems (e.g., JC2, RS2) contain higher concentrations of Fe(II), but lower levels of arsenic (**Table 1**). Solid phase analyses (XRD, XAS) indicate more crystalline phases including jarosite [$KFe_3(OH)_6(SO_4)_2$], goethite, and hematite within the outflow channels of RS2 and JC2, respectively (**Table 1**; **Figure 4**). These systems contain higher concentrations of sulfate, potassium, and total soluble Fe than sites in NGB and as a result, jarosite is an important phase formed in these environments. Jarosite contains Fe(III), and requires that Fe(II) be oxidized (Kappler and Straub, 2005). The abiotic rate of Fe oxidation is quite slow at low pH (Singer and Stumm, 1970), so biological mechanisms are likely responsible for the majority of

Table 1 | A geochemical summary of acid-sulfate-chloride springs (Norris Geyser Basin) and acid-sulfate springs (Joseph's Coat and Rainbow Springs) showing concentrations of major electron donors, O_2 and solid phase analysis using synchrotron X-ray diffraction.

Spring ID[1]	Sampling Point (m)[2]	T (C°)	pH	H_2S μM	O_2 μM	Fe^{II} μM	As^{III} μM	NH_4^+ mM	SO_4^{2-} mM	H_2 (aq) nM	Summary of SEM/EDAX and XRD analysis[3]
NGB-BE	A (0)	75	3.1	120	<3	36	26	0.066	1.5	60	Positions A–C: S^0
	D (6)	66	3	8	55	34	22	0.067	1.6	14	Positions D, E: ∼1–3 cm, soft
	E (7.5)	62	3	3	77	31	19	0.068	1.6	14	Amorphous Fe-oxyhydroxide; 0.7 mol As^V/mole Fe*
NGB-BW	A (0)	72	3	130	<3	33	24	0.067	1.6	40	Positions: A–C: S^0
	D(8.4)	60	3	2	87	30	18	0.068	1.6	11	Position D: ∼0.2–0.4 cm soft, Amorphous Fe-oxyhydroxide; 0.7 molAs^V/mole Fe*
NGB-OSP	A (0)	82	3.6	11	7	28	20	0.08	1.1	46	Positions B, C: ∼1–2 cm, soft
	B (2–3)[4]	73	3.5	2	31	27	21	0.079	1	46	amorphous Fe-oxyhydroxide; 0.6 molAs^V/mole Fe
	C (3.5)	65	3.5	<0.3	46	22	19	0.07	1	18	
	D (4)	57	3.5	<0.3	90	20	nd	0.08	1.1	nd	
NGB-GAP	A (0)	84	3.3	8	<3	63	25	0.065	1	148	Position B: 1–3 cm, soft
	B (0.3)	77	3.3	2	35	58	22	0.067	1	18	Scorodite
NGB-WG	A (0)	64	3.3	<0.3	nd	7	29	0.074	1.2	37	Edge of source pool: 1 cm, soft Amorphous Fe-oxyhydroxide
NGB-PB	A (0)	85	3.4	1.3	nd	13	29	0.068	1.1	12	Edge of source pool: 2–3 cm, soft Scorodite
NGB-EG	A (0)	76	3.5	3.5	44	37	3	0.066	3.2	120	Position C: 1–2 cm, soft
	C (10)	70	3.4	<0.3	56	35.5	2	0.069	3.2	99	Ferrihydrite
JC2	A (0)	88	2.6	4	<3	91	0.25	1.93	5.6	166	Position B, C, D: 0.2–0.4 cm, hard
	B (2.7)	75	2.5	<0.3	6	86	0.13	2.22	6	132	Goethite, hematite, quartz
	C (7.1)	65	2.4	<0.3	48	66	0.09	2.44	6.4	126	
	D (12)	59	2.4	<0.3	78	50	0.03	2.37	6.6	43	
	E (18.5)[5]	75	2.5	230	<3	88	0.33	2.42	5.9	126	Position E: S^0
	F (22.0)	56	2.4	30	48	72	0.19	2.47	6.3	41	
RS2	A (0)	77	2.6	7	<3	91	3.1	1.72	7.3	53	Position B, C, D: 0.2–0.4 cm, hard
	B (2.2)	73	2.5	2	22	81	2.5	1.74	7.3	32	K-jarosite, goethite, quartz
	C (2.3)[5]	77	2.7	6	<3	86	3	1.72	7.3	52	
	D (8.3)	69	2.6	1	44	76	2.5	1.76	7.5	37	
	F (12.6)	54	2.5	<0.3	99	34	0.9	1.75	7.4	28	
RS3	A (0)	54	3.2	<0.3	<3	220	1.1	1.47	6.3	27	Position A, B: 2–4 cm, soft
	B (0.9)	53	3.2	<0.3	14	200	1.2	1.47	6.3	17	Goethite, ferrihydrite

Mineralogy data from Beowulf Spring from Inskeep et al. (2004); all other sites from this study.

[1] *Spring abbreviations: NGB, Norris Geyser Basin, JC, Joseph's Coat Hot Springs; RS, Rainbow Springs (also see materials and Methods for different springs).*

[2] *Letters correspond to different sampling positions within the primary flow channel.*

[3] *SEM/EDAX, scanning electron microscopy–energy-dispersive analysis of X-rays: predominant locations and mat characteristics are provided.*

[4] *Sampling location of metagenome sample "OSP_8."*

nd, Not determined.

iron oxides and jarosite deposited in these systems. Furthermore, the log saturation indices for jarosite were calculated for RS2A, RS2C, and RS3A at −2.9, −1.2, and 0.3, respectively. Negative values indicate under-saturation of aqueous chemical species with respect to K-jarosite, indicating that these solutions would not be expected to precipitate jarosite, except perhaps in spring RS3. In contrast, saturation indices were greater than 10 for NGB-BE and NGB-OSP(owing primarily to the higher pH), which do not contain jarosite as a solid phase.

Solid phases of ferric iron observed using synchrotron XRD (major phases identified in **Table 1**) were used to constrain least squares fitting procedures of Fe-K-edge EXAFS spectra for all field samples. Least squares fits to experimental k3 weighted Fe-EXAFS spectra are shown for each of the major spring types studied here (**Figure 5**) and these fits provide further support for the predominant solid phases observed using XRD. Specifically, the ferric iron mats included in this study can be grouped into these main four categories based on mineralogy: high arsenate-amorphous Fe oxyhydroxides (sites BE, WG, OSP), ferrihydrite and/or scorodite (e.g., GAP, EG, PB), goethite and hematite (e.g., JC2), and jarositic systems containing less Fe oxide (e.g., RS2). The different phases of ferric Fe formed in these systems relate to differences in spring geochemistry and hydrodynamic properties. For example, arsenic concentrations are one to two orders of magnitude higher in NGB springs relative to RS2 and JC2, respectively, and may play an important role

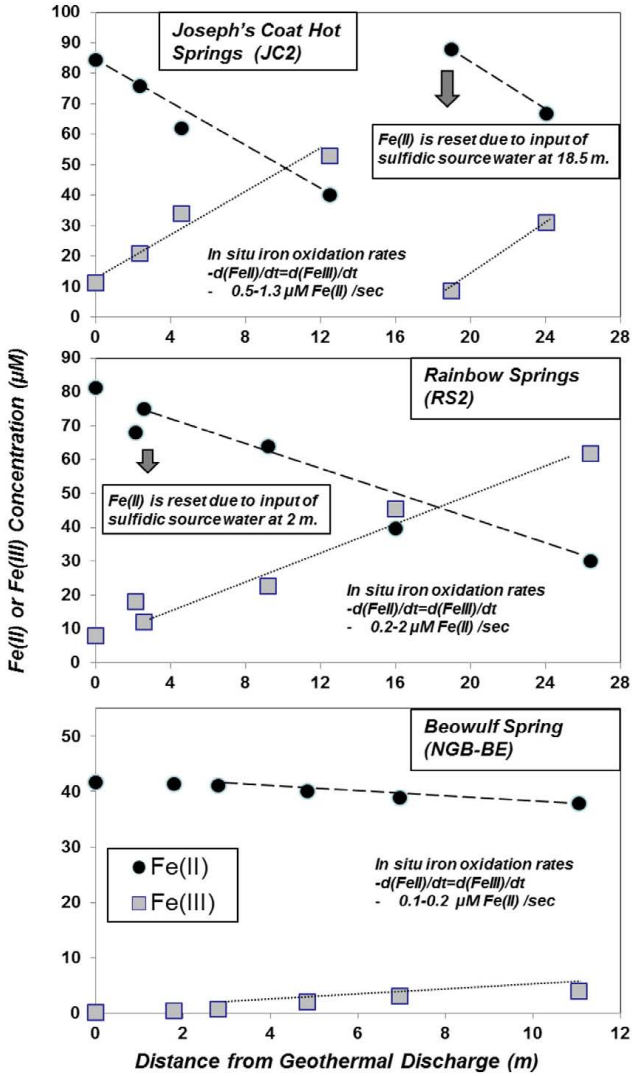

FIGURE 3 | Profile of Fe(II) oxidation in acidic geothermal springs at Joseph's Coat Hot Springs (JC2), Rainbow Springs (RS2) and Norris Geyser Basin (*Beowulf* Spring) plotted as the disappearance of Fe(II) or the production of Fe(III) as a function of time (or distance) within the outflow channel. The total soluble Fe at any position is the sum of Fe(II) and Fe(III), which agreed favorably (<10% difference) with total Fe determined using inductively coupled plasma spectrometry [ICP; total Fe values of JC2A, RS2A, and BEA are ∼100, 90, and 40 μM, respectively]. In JC2, ∼45% of the total ferrous Fe is oxidized to Fe(III) at sampling position D, corresponding to a 35-s travel time [sampling positions JC2E and RSC correspond to a second spring discharge, which resets the concentration of Fe(II)].

in the inhibition of jarosite precipitation and the subsequent formation of amorphous ferrihydrite phases containing significant amounts of sorbed arsenate (Inskeep et al., 2004). Also, the rate of amorphous ferrihydrite precipitation is faster than crystalline phases such as goethite, hematite and jarosite, and is consistent with the increase in dissolved Fe(III) from microbial ferrous iron oxidation in JC2 and RS2 relative to NGB-BE (**Figure 3**).

MICROBIAL COMMUNITY STRUCTURE

Molecular surveys of near full-length 16S rRNA genes present in acidic Fe mats reveal numerous different novel archaea, especially within the Crenarchaeota (i.e., orders Sulfolobales, Desulfurococcales, and Thermoproteales) as well as two deeply rooted novel lineages with no cultured relatives (referred to as "Novel Archaeal Groups" I and II; NAG1 and NAG2). All acidic Fe-oxide mats contained significant numbers of different Sulfolobales-like sequences, which clade with three of the known Sulfolobales genera; however, numerous entries cluster together within a previously undescribed lineage. Sequences related to the novel Sulfolobales clade are particularly well represented in NGB-WG and Joseph's Coat (Spring 2; **Figure 6**). An Fe(II)-oxidizing isolate was obtained representing this novel lineage (strain MK5), and is discussed in more detail below. The other Sulfolobales-like 16S rRNA gene sequences present across the acidic Fe mats include members of the *Metallosphaera* and *Sulfolobus* genera (**Figure 6**), and isolation of *M. yellowstonensis* from these sites was described in previous reports (Kozubal et al., 2008, 2011).

Sequences related to members of the candidate phylum Thaumarchaeota and Euryarchaeota were also observed in acidic Fe mats (**Figure 6**). Many of the thaumarchaeal sequences belong to a separate lineage compared to previously cultivated mesophilic isolates and the metagenome sequence from NGB-BE contains one scaffold over 1 Mb in length, which is discussed in detail elsewhere (Beam et al., 2011). The novel euryarchaeal sequences were observed in BE, OSP, and JC2, and are distantly related to *Thermoplasma volcanium* (∼89–90% similarity to 16S rRNA gene sequences in GenBank).

A significant majority (>99%) of bacterial 16S rRNA gene sequences obtained from acidic Fe mats above ∼70°C were related to *Hydrogenobaculum* spp., a deeply rooted member of the order Aquificales (**Figure 7**). However, bacterial diversity increased when temperatures decreased below 60–65°C. For example, bacteria distantly related to *Acidimicrobium*, *Acidovorax*, *Acidicaldus*, *Methylacidiphilum*, *Meiothermus*, *Geothermobacterium*, and *Sulfobacillus* spp. were found in greater abundance in down-gradient positions, depending on the specific spring. *Acidovorax*, *Acidicaldus*, and *Methylacidiphilum* spp. were more common in acid-sulfate springs (e.g., RS2EF), while *Meiothermus* and *Acidimicrobium*-like populations were observed with greater frequency in the acid-sulfate-chloride springs of NGB. Sequences related to *Acidicaldus*, *Geobacter*, and *Methylacidiphilum* spp. were especially important in Rainbow and Joseph's Coat channel positions below 55°C (e.g., 60–70% of PCR amplified long-fragment bacterial clones observed at RS3A, RS3B, and JC2C). Many of these bacterial sequences are highly divergent from cultivated relatives (<91% similarity, 16S rRNA gene), and include a novel clade related to *Geobacter* spp. (represented by sequences RS2F-SK964 and RS2F–SK975; **Figure 7**). The *Geobacter*-like sequences are only ∼83% (16S rRNA sequence similarity) related to the nearest cultivated delta-proteobacterium, *Geobacter uraniireducens*. Other noteworthy novel bacterial groups observed in these sites include sequences related to *Acidimicrobium ferrooxidans* (clone RS2F-SK971, 90%), *Sulfobacillus acidophilus* (RS2F-SK266, 89%), and finally, a distant relative of Heliobacteriaceae bacterium SLH (clone RS3B-SK292, 83%), representing a highly divergent sequence in the Firmicutes.

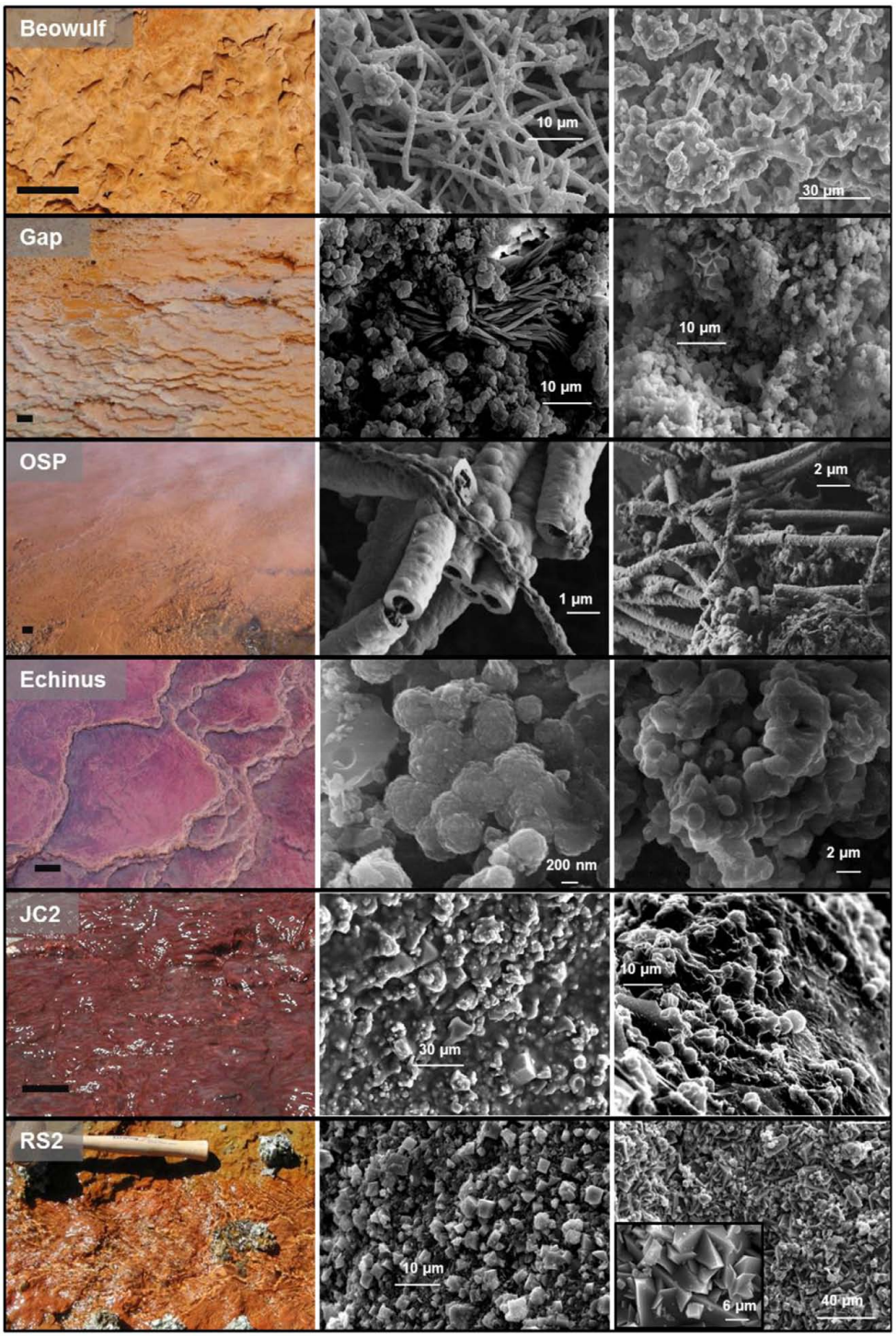

FIGURE 4 | Ferric iron phases from select ferric iron mats in Yellowstone National Park with corresponding scanning electron micrographs of solid phases found within each spring (results also presented in Table 1). Scale bar on site photographs is ∼5 cm.

DEEPER 16S rRNA GENE SURVEYS WITHIN OSP SPRING

Additional full-length 16S rRNA gene sequences (PCR clone libraries) were obtained at two locations within the outflow channel (pH 3.5) of OSP Spring (NGB) as part of a JGI ribosomal panel study of YNP geothermal systems (CSP 787081). The distribution of long-fragment 16S rRNA gene sequences observed in this dataset ($n \sim 1200$) shows extensive archaeal diversity in moderately oxygenated Fe mats NGB-OSP8 (72°C Fe mat) as well as 74°C

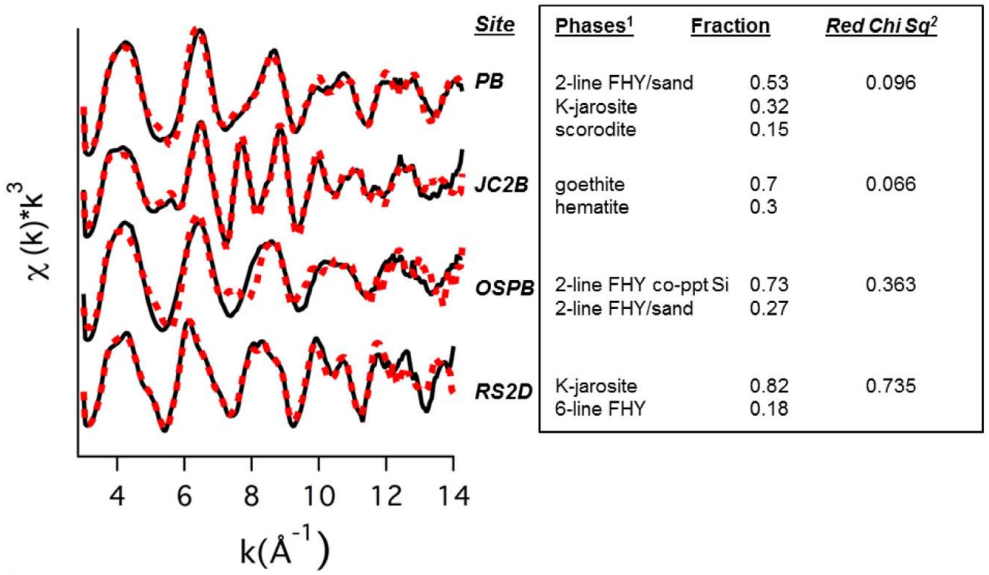

Site	Phases[1]	Fraction	Red Chi Sq[2]
PB	2-line FHY/sand	0.53	0.096
	K-jarosite	0.32	
	scorodite	0.15	
JC2B	goethite	0.7	0.066
	hematite	0.3	
OSPB	2-line FHY co-ppt Si	0.73	0.363
	2-line FHY/sand	0.27	
RS2D	K-jarosite	0.82	0.735
	6-line FHY	0.18	

FIGURE 5 | Least squares fits (dotted lines) to experimental k3 weighted Fe-EXAFS spectra (solid lines) obtained for solids from hot springs representing (bio)geochemical end-members. Predicted fractions of major solid phases (Fe standards 1) included in the fits are shown along with the reduced Chi square value.

filamentous-streamer communities dominated by *Hydrogenobaculum* sp. (NGB-OSP14). Gene sequences observed in OSP8 reveal extensive diversity from all orders of the Crenarchaeota (e.g., 13% *M. yellowstonensis* str. MK1) as well as novel groups (62%). In contrast, the filamentous "streamer" community (OSP14) archaeal clone library was dominated by *M. yellowstonensis* (67%), and less than 2% were related to novel archaeal groups (Thaumarchaeota as well as novel members of the Euryarchaeota). All bacterial clones ($n = 600$) amplified from these two sites in OSP Spring belong to the genus *Hydrogenobaculum*.

Deeper 16S rRNA gene sequence analysis using pyrotag sequencing (average nucleotide length = 180 bp) was also performed in several Fe-oxide microbial mats in NGB, including *OSP* Spring (OSPB, OSPC, OSPD), *Beowulf* Spring (BEE), and *Grendel* Spring (GRN_L). In addition, 16S rRNA sequences were obtained from assemblies of random shotgun metagenome sequence obtained from OSPB, OSPC, BED, and BEE. Given that several locations within OSP received random metagenome and pyrotag sequencing, comparison of phylogenetic signatures observed using the different methods was possible (**Table 2**), including reference to long-fragment 16S rRNA gene sequences from the above mentioned ribosomal panel obtained for OSP8 (which was sampled at same temperature as OSPB). Excellent agreement among three methods of assessing archaeal diversity was obtained for OSPB (**Table 2**) indicating that the higher temperature locations (i.e., 72–76°C) in this spring are dominated by novel archaeal group I (NAG1, 50–60%), followed by *M. yellowstonensis* ∼12–20%), *Vulcanisaeta* spp. (∼10–15%), *Acidilobus* spp. (6–8%), a novel archaeal group II lineage (NAG2, ∼1–3%), and lower amounts of other novel archaeal groups (including Thaumarchaeota and Sulfolobales). Clustering of shorter pyrotag 16S sequences using long-fragment archaeal clone groups (e.g., those shown in **Figure 6**) from the same spring types (as opposed to only cultivated organisms with reference genomes) proved to be an excellent method of binning pyrotag sequences and estimates of percent abundance of the major taxonomic lineages in OSPB using pyrotag analysis are very close to estimates obtained from either long-fragment PCR analysis or binning of random metagenome sequence reads into the same phylogenetic groups (**Table 2**).

Comparison of pyrotag 16S rRNA gene sequence estimates with binning of random shotgun sequence reads from two additional sites (OSPC and D, 65 and 60°C) also reveal excellent agreement between the two methods of obtaining semi-quantitative estimates of the distribution of archaea in Fe-oxide mats. Results from lower temperatures provide evidence for separation of NAG1 and NAG2 groups by temperature, where NAG2-like sequences increase in abundance as temperature decreases; at OSPD, NAG2-like sequences represent the dominant population (∼32%; **Table 2**). Other community members including *M. yellowstonensis* and NAG1 remain important at lower temperatures, and Sulfolobales strain MK5-like populations were slightly more abundant in OSPD.

Two additional Fe-oxide mat samples evaluated using pyrotag sequencing included locations within *Beowulf* and *Grendel* Springs (**Figure 8**). Although similar to end-member amorphous Fe-oxide mats of NGB including the OSP series discussed above, BEE and GRND_L reveal slightly different community types compared to OSP. Consistent populations observed compared to OSP include *M. yellowstonensis*, NAG1, NAG2, and novel Sulfolobales, however, GRND_L contained a significantly higher percentage of thaumarchaeal and novel Thermoplasmatales-like populations.

DESCRIPTION OF NOVEL ISOLATES

Four novel isolates were obtained from three different Fe-oxidizing springs in NGB and include members of the Sulfolobales

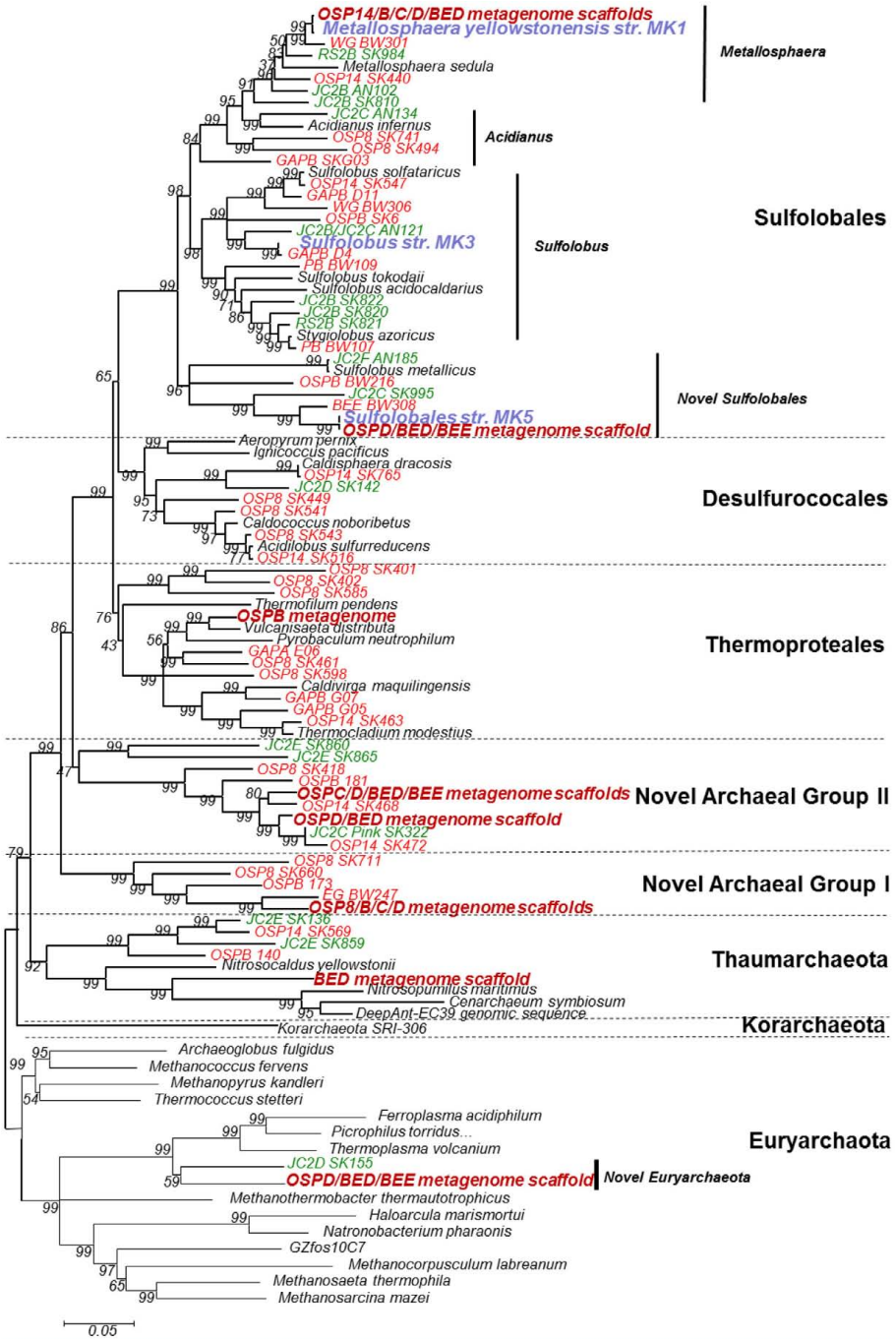

FIGURE 6 | Phylogenetic tree of archaeal 16S rRNA gene sequences (sequence length ∼1400 bp) observed across 19 different acidic iron mat samples from Yellowstone National Park (acid-sulfate-chloride springs are shown in red, acid-sulfate springs shown in green, isolates are highlighted in blue, and metagenome sequence entries are listed in dark red).

(*Sulfolobus* str. MK3, Sulfolobales str. MK5), Bacillales (*Sulfobacillus* str. MK2), and *Acidicaldus* str. MK6. A fifth isolate from *Beowulf* Spring, *M. yellowstonensis* str. MK1, has been described (Kozubal et al., 2008, 2011). The 16S rRNA gene sequences of strains MK2, MK3, and MK6 reveal similarity to previously described isolates ranging from 96 to 98%, and likely represent new species in the *Sulfobacillus*, *Sulfolobus*, and *Acidicaldus* genera, respectively (**Table 3**). However, Sulfolobales str. MK5 is only 88% similar to *Sulfolobus islandicus* (16S rRNA gene), and forms a completely new lineage within the current order Sulfolobales (**Figure 6**). Genome sequencing of strain MK5 is nearly complete and is currently represented as ∼2 Mb of assembled sequence on four scaffolds.

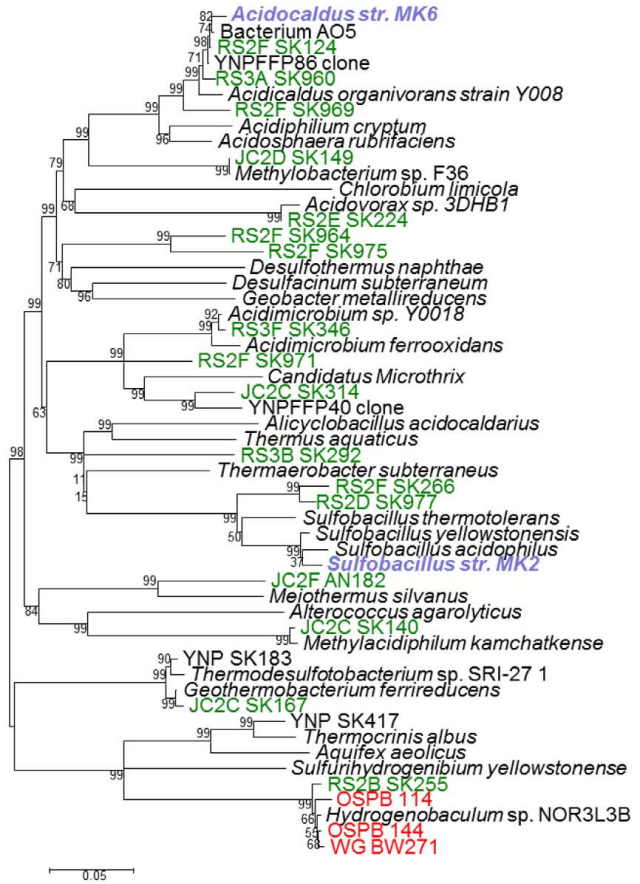

FIGURE 7 | Phylogenetic tree of bacterial 16S rRNA gene sequences (∼1400 bp) observed across 19 different acidic iron mats in Yellowstone National Park (acid-sulfate-chloride springs are shown in red, acid-sulfate springs shown in green, isolates are highlighted in blue, and metagenome sequence entries are listed in dark red).

All isolates were tested for growth using YE, Fe(II), S^0, pyrite, and solid media (**Table 3**). In addition, isolates were tested for their ability to fix carbon dioxide in carbon free media. *Sulfolobus* str. MK3 is capable of autotrophic growth and all isolates are capable of oxidizing Fe(II) except the *Acidicaldus* str. MK6. The Sulfolobales isolates (strains MK3 and MK5) are also capable of oxidizing pyrite (FeS_2). Moreover, strains MK5 and MK6 were shown to both reduce Fe(III) including amorphous Fe oxyhydroxides found in YNP Fe mats and a variety of ferric oxide minerals including hematite, ferrihydrite, and goethite. In fact, strain MK5 was shown to re-reduce Fe oxides (formed during aerobic growth) when grown under anoxic conditions using Gelrite® as a C and energy source. All strains were capable of utilizing complex carbon from yeast extract for heterotrophic growth, consequently, none are obligate autotrophs.

Both *Acidicaldus* str. MK6 and Sulfolobales str. MK5 grew on solid Gelrite® media as round white and cream colored colonies, respectively, whereas *Sulfobacillus* str. MK2 grew on 1.5% agar plates with 0.2% YE and 10 mM $FeSO_4$. Strain MK3 was not successfully grown on Gelrite® or agar plate media supplemented with 10 mM $FeSO_4$ and 0.2% YE and a variety of other plate media. The Sulfolobales isolates (strains MK3 and MK5) had higher temperature optimum (65–75°C) than the two bacterial isolates (55–65°C). All isolates grow optimally between pH 2.0 and 3.0; however, strains MK3 and MK5 exhibited slightly lower pH optima ranging from 2.0 to 2.5 (**Table 2**). Strain MK5 has the lowest pH range for growth and active cells were observed as low as 1.2. The Sulfolobales strains (MK3 and MK5) are ∼1 μm diameter cocci and/or irregular cocci, whereas both bacterial strains (*Sulfobacillus* str. MK2 and *Acidicaldus* str. MK6) are rod-shaped.

IRON OXIDATION AND REDUCTION RATES AND ANALYSIS OF CULTURE Fe SOLID PHASES

Iron oxidation rates were determined for Sulfolobales str. MK5 cultivated at 65°C with 10 mM Fe(II) sorbed to sterile Fe-oxide mat (obtained from NGB-BE). Iron oxidation rates ranged from 15.7 ± 1.2 to 14.5 ± 2.9 fmol Fe(II) L^{-1} s^{-1}cell^{-1} at pH 1.5 and 2.5, respectively, for cultures grown autotrophically (without mixing/exposure to air only). Similar results were shown for *M. yellowstonensis* str. MK1 ranging from 7.4 ± 1.5 to 12.4 ± 3.1 fmol Fe(II) L^{-1} s^{-1}cell^{-1} at pH 3.2 and 2.5, respectively, reflecting slightly different pH optima between strains MK5 (this study) and *M. yellowstonensis* (Kozubal et al., 2008). The secondary phases formed during microbial Fe(II)-oxidation were determined for strain MK5 and *M. yellowstonensis* (not previously reported) grown on pyrite or Fe(II)-ferrihydrite (pyrite cultures shown in **Figure 9**) using both XRD and EXAFS. After 11 days of incubation under these growth conditions, hematite is the primary crystalline phase forming at the water-air interface (XRD analysis), whereas jarosite is found below the water surface. Least squares fitting of Fe-K-edge EXAFS spectra obtained on solid phases formed during microbial oxidation suggest mixed solid phases supported by XRD analyses (∼41% ferrihydrite, 24% jarosite, 16% goethite, and 12% hematite). XRD analysis of strain MK5 cultures revealed both goethite and jarosite in slurry samples from the bottom of the growth vessel (**Figure 9**). Consequently, Fe-oxidation products varied both with the isolate, location in the growth vessel, as well as across different spring compositions (**Table 1**; **Figure 4**). Under field conditions, jarosite was only observed at Rainbow and Joseph's Coat Springs (minor), where higher concentrations of "in channel" Fe(III), SO_4^{2-}, and K^+ all favor the formation of K-jarosite, despite lower saturation indices with respect to jarosite relative to the higher pH (3.1–3.5) systems of NGB (**Table 1**).

Evidence for a complete Fe redox cycle in thermophilic Fe mats was obtained from results of Fe(III)-reducing Sulfolobales strains MK5 and *Acidicaldus* strain MK6. Both isolates were shown to reduce Fe(III)-oxide solid phases, yielding soluble Fe(II). Iron reduction rates of 0.36 fmol Fe(III) L^{-1} s^{-1} cell^{-1} were determined in *Acidicaldus* str. MK6 cultures at pH 3.0 utilizing autoclaved Fe-mat as a source of ferric iron (**Figure 10**) and 10 mM glucose as the electron donor. Rates observed for MK5 were ∼0.5 fmol Fe(III) L^{-1} s^{-1} cell at pH 2.0.

RELEVANT GENES IN THE GENOME OF STRAIN MK5 AND SITE METAGENOMES

Preliminary genome analysis of strain MK5 shows that this organism contains syntenous sequences highly related to the *foxA-F* gene

Table 2 | Comparison of methods to determine phylogenetic distribution of archaeal lineages in Norris Geyser Basin OSP Spring.

Taxonomic lineage	Metagenome read binning (% total Archaea)	JGI ribosomal panel (% total Archaea)	16S rRNA pyro-tag sequences (% total Archaea)	Near full-length metagenome 16S rRNA sequences: Closest cultured relative or environmental sequence (% = nucleotide similarity; length bp)
OSPB				
NAG1	60.7	60.3	49.2	*Thermofilum* sp. 1505; 84% Koz183; 100% (1492)
Metallosphaera	11.7	16.1	21.3	*Metallosphaera yellowstonensis* str. MK1; 100% (1278)
Thermoproteales	15.2	9.9	12.6	*Vulcanisaeta distributa* IC-017; 98.4% SK409; 99.9% (1151)
Acidilobus	5.6	7.9	6.2	None
NAG2	1.1	3.4	2.5	*Staphylothermus* sp. 1633; 85.2% Koz169; 100% (1046)
Sulfolobales str. MK5	nd	0	2.4	None
Thaumarchaeota	nd	0	1.3	None
Other Archaea	5.8% unassigned contigs	2.4	3.7	None
OSPC				
NAG1	56.5		57.1	*Thermofilum* sp. 1505; 84% Clone Koz183; 100% (1334)
NAG2	28.7		17	*Staphylothermus* sp. 1633; 85.7% YNPFFA85; 99.6% (1354)
Metallosphaera	9.9		12	*Metallosphaera yellowstonensis* str. MK1; 99.6% (1354)
Thermoproteales	nd		9.2	None
Sulfolobales str. MK5	nd		1.5	None
Other archaea	5% unassigned contigs		3.1	None
OSPD				
NAG2	31.8		32	Seq1: *Staphylothermus hellenicus*;85.7% YNPFFA4 99.6% (1401) Seq2: *Staphylothermus* sp.1633; 85.7% YNPFFA85; 99.6% (1358)
NAG1	19.8		32	*Thermofilum* sp. 1505; 84% Koz183; 100% (1334)
Metallosphaera	19.2		21.2	*Metallosphaera yellowstonensis* str. MK1; 99.5% (1354)
Sulfolobales str. MK5	13.3		8.5	Sulfolobales str. MK5; 99.8% (1408)
Novel Euryarchaeota	8.1		0	*Aciduliprofundum* sp. EPR07-39; 86.5 BSLdp48 (1297)
Sulfolobus	7.8		4.3	None

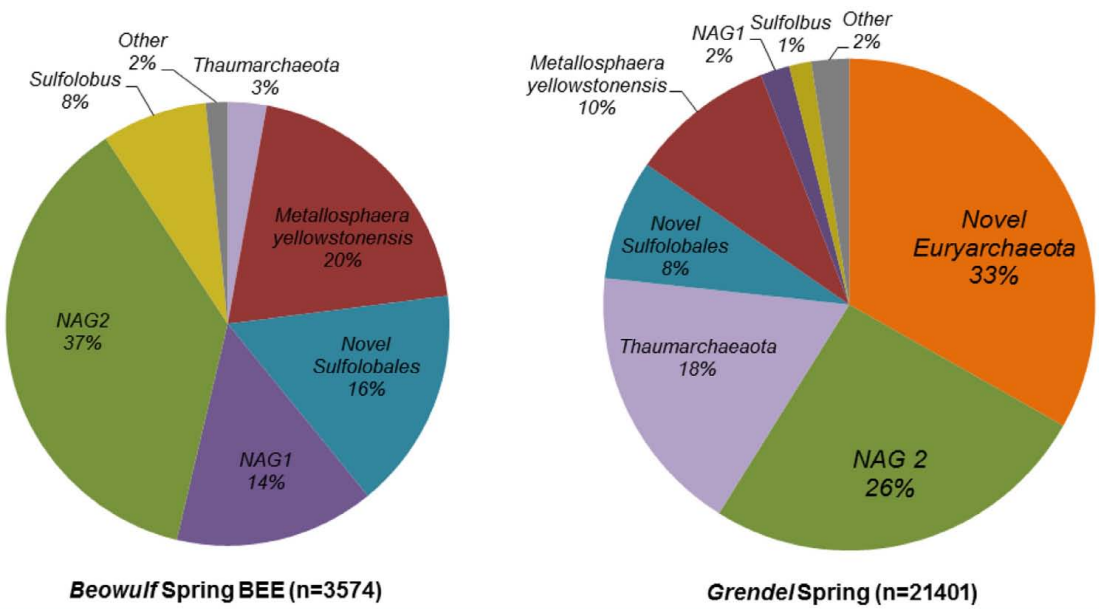

FIGURE 8 | Archaeal microbial community structure in two iron mat samples from Norris Geyser Basin presented as a percentage of total 16S rRNA gene pyrotag sequences that binned to different phylogenetic groups based on libraries of long-fragment sequences specific to these sites.

Table 3 | Novel isolates obtained from acid-sulfate-chloride (ASC) springs and characterization of cell morphology, pH optima, temperature optima, and growth on iron and sulfur substrates as electron donors or Fe(III) as an electron acceptor under anaerobic conditions.

Isolate	Cell morphology	Closest 16S rRNA relative (% similarity)	pH_{optima}	T_{optima} (°C)	Fix CO_2	Plate	H_2	Fe^{2+}	S^0	Pyrite	Fe^{3+}
Sulfolobus str. MK3	~1 μm cocci	*Sulfolobus* sp. T1 (96.6%)	2.0–2.5	75	+	−	−	+	+	+	−
Sulfolobales str. MK5	~1 μm cocci	*Sulfolobus islandicus* HVE10/4 (88%)	2.0–2.5	60–70	−	+	−	+	+	+	+
Sulfobacillus str. MK2	~3–5 μm rods	*Sulfobacillus acidophilus* TPY (98.3%)	2.0–3.0	55–58	−	+	−	+	+	+	−
Acidicaldus str. MK6	~1.2–1.5 μm rods up to 20–30 μm filaments	*Acidicaldus organivorans* str. Y008 (97.6%)	2.5–3.0	55–60	−	+	−	−	−	−	+

The ability to grow on solid media is also indicated. nd, Not determined.

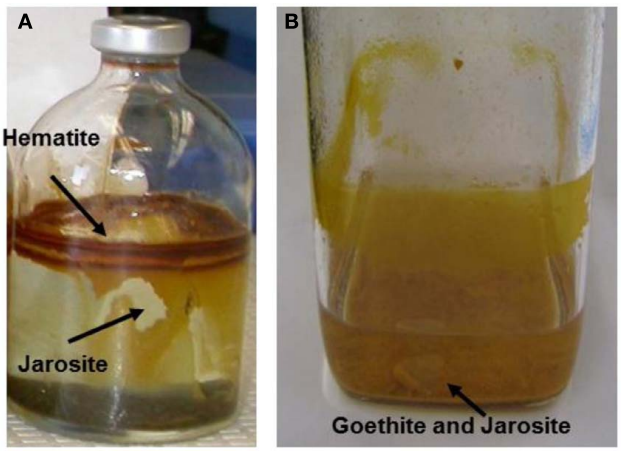

FIGURE 9 | Serum bottle culture of (A) *Metallosphaera yellowstonensis* str. MK1 and (B) Sulfolobales str. MK5 showing location of secondary phases sampled for solid phase analysis (11 days incubation, pyrite used as the electron donor).

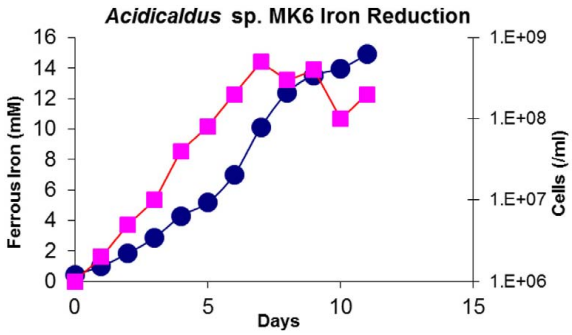

FIGURE 10 | Concentration of ferrous iron (mM) and cell counts (cells/mL) plotted as a function of time in anaerobic serum bottle cultures with *Acidicaldus* sp. strainMK6. Cultures were maintained at pH 3.0 with 10 mM glucose and 0.5 g autoclaved Fe-oxide mat from NGB-BED. Squares = cells/mL; circles = Fe(II)(mM).

cluster in *S. tokodaii* (Bathe and Norris, 2007). Like *S. tokodaii* and *S. metallicus*, strain MK5 has only one copy of *foxA* (the subunit I of the HCO) as compared to two copies in *M. sedula*, and three copies in *M. yellowstonensis* (Auernik et al., 2008; Kozubal et al., 2011). Strain MK5 also has a *cbsAB–soxL2N* gene operon, which has been identified as important in iron-oxidizing Sulfolobales (Kappler et al., 2005). Strain MK5 contains a gene encoding a sulfide quinone oxidoreductase (*sqr*) and a conserved *hdr* gene cluster important in elemental sulfur oxidation (Quatrini et al., 2009). Additionally, the strain has genes for a *tqoAD* thiosulfate oxidase directly upstream to the *cbsAB–soxL2N* gene operon. Strain MK5 does not contain genes for any of the known CO_2 fixation pathways (Berg et al., 2010). However the organism contains a number of genes encoding complex carbon degrading proteins including numerous cellulases, xylanases, and xenobiotic dioxygenases.

Metagenome analysis of NGB-BE and NGB-OSP yielded multiple copies of *fox* genes highly similar to those found in strain MK5 and *M. yellowstonensis*, suggesting these two organisms along with other Sulfolobales strains (e.g., *Sulfolobus* str. MK3) are the dominant populations responsible for Fe(II) oxidation via this mechanism. Genes related to cytochromes linked to Fe(II) oxidation in the well-characterized bacteria *Acidithiobacillus ferrooxidans* and *Leptospirillum* spp. were not found in the OSP and BE metagenomes (Jeans et al., 2008; Singer et al., 2008; Quatrini et al., 2009). Small blue copper proteins have also been associated with Fe(II) oxidation in *A. ferrooxidans* and the Euryarchaeota "*Ferroplasma acidarmanus*" (Dopson et al., 2005) and similar sequences were identified in the YNP metagenomes. However, most of these sequences are homologs of sulfocyanin (*soxE*) from *M. yellowstonensis* – and strain MK5-like species, which are more likely involved in the SoxM-like terminal oxidase complex specific for heterotrophy, and not involved in Fe(II) oxidation (Kozubal et al., 2011).

DISCUSSION

Ferric iron mats of NGB, Joseph's Coat, and Rainbow Springs in YNP exhibit considerable microbial diversity as shown by the extensive compilation of phylogenetic data including 1500 full-length 16S rRNA gene sequences, over ~40,000 pyrotag sequences and five shotgun metagenome sequences from BED, BEE, OSPB, OSPC, and OSPD. The Sulfolobales are important in all 18 spring

sites as indicated by the high percentage of 16S rRNA sequences and binning of metagenome sequence reads. *M. yellowstonensis* str. MK1-like 16S rRNA gene sequences are highly dominant in most sampling points particularly in Joseph's Coat and Rainbow Springs between 60 and 75°C. In addition, metagenome data strongly suggest that *M. yellowstonensis*-like populations are important in NGB-BE and NGB-OSP Springs as evidenced by the number of total reads binning to the *M. yellowstonensis* genome (Inskeep et al., 2010). Detailed community analysis of *M. yellowstonensis* related species along with expression of *fox* genes *in situ* are discussed in more detail elsewhere (Kozubal et al., 2011). Novel Sulfolobales-like MK5-like populations also contribute a high percentage of metagenome reads and 16S rRNA gene sequences, but at slightly lower temperatures (e.g., OSPC and OSPD).

Sequences from members of the Desulfurococcales, Thermoproteales, and novel archaeal lineages are also important in YNP ferric iron mats. In addition, sites below 65°C are characterized by highly divergent 16S rRNA bacterial gene sequences especially at sites RS2F and RS3B. Many of these bacterial sequences are less than 90% similar to cultivated relatives and represent three new taxonomic branches at the order level and higher (**Figure 7**). Above 70°C, bacterial gene sequences are completely dominated by *Hydrogenobaculum* spp. and detailed sequence analysis of NG-OSP and RS2 reveal two distinct sub-clades.

The microbial community structure of acidic iron mats is likely driven by the flux of O_2 required to drive Fe(II) oxidation, as well as the presence of other reduced inorganic electron donors available for growth. However, temperature and pH are also important parameters controlling community structure. For instance, sequences related to *Acidilobus* spp., *Stygiolobus azoricus*, and Thermoproteales spp. (i.e., *Vulcanisaeta distributa*) dominate at higher temperatures, consistent with the range observed for cultivated relatives. Moreover, bacteria such as *Sulfobacillus* and *Acidicaldus* spp. thrive at lower temperatures. *M. yellowstonensis* was found to be prevalent in all sites, and the relative importance of novel populations such as NAG1, NAG2, Thaumarchaeota and Euryarchaeota varies across sites. However, the primary populations involved directly in Fe cycling appear to be aerobic organisms that use the Fox terminal oxidase complex consistent with genome, metagenome, and prior mRNA expression analysis.

The five isolates discussed in this study are highly relevant to our understanding of geomicrobiology and microbial ecology of acidic geothermal ferric iron mats of YNP. All isolates are capable of oxidizing iron and strains MK5 and MK6 are also capable of ferric iron reduction under anaerobic conditions. *M. yellowstonensis* and *Sulfolobus* str. MK3 are capable of autotrophic growth and are likely important primary producers *in situ* linking CO_2 fixation directly with Fe(II) oxidation. These organisms may be a significant source of carbon for other microorganisms such as *Acidicaldus* str. MK6, which may need this carbon source for anaerobic growth on Fe(III). Therefore, the Sulfolobales isolates offer an excellent opportunity to understand mechanisms of CO_2 fixation in model natural systems. Uncharacterized archaeal and bacterial populations in ferric oxide mats may also be linked to other electron donors besides Fe(II) (**Table 1**). For instance, *Methylacidiphilum*-like sequences are found in JC2F and RS3A at 70 and 29% of bacterial sequences, respectively, and may take advantage of the relatively high CH_4 concentrations (2.2 and 3.5 μM) compared to other spring locations. These organisms remain a high priority for isolation.

Analysis of ferric solid phases on serum bottle cultures link observed biomineralized phases found in the springs to cultured organisms. Spring geochemistry [i.e., sulfate and Fe(III) concentrations, pH, presence of arsenate] plays an important role in the formation of mineral phases. However, populations highly similar to strains MK1 and MK5 contribute directly to the observed oxidation of Fe(II) in YNP ferric iron mats and especially MK1-like populations in RS2 and JC2 above 65°C (Kozubal et al., 2008). In culture, *M. yellowstonensis* forms hematite and jarosite on serum bottle surfaces and XRD analysis of strain MK5 identified jarosite and goethite as a slurry on the vessel bottom (**Figure 9**). The different ferric iron phases found in cultures stress that different microbial processes (both "biologically controlled" and "biologically induced") are important in determining the iron phases formed. Moreover, different solution conditions contribute to variation in solid phases observed across field sites.

Strains MK1 and MK5 oxidize Fe(II) at rates similar to those observed in other archaeal species under similar culture conditions (Nemati and Harrison, 2000; Kauppi et al., 2001). Both strains exhibit faster rates of Fe(II)-oxidation at lower pH, which is consistent with observations of other acidophilic Fe(II)-oxidizing microorganisms. The fixation of CO_2 under culture conditions was observed only for strain MK1. In fact, genes for any of the six known CO_2 fixation pathways were not found in strain MK5 (Berg et al., 2010), which is unique compared to other Sulfolobales (all reference Sulfolobales genomes contain genes for the 3-hydroxypropionate/4-hydroxybutyrate pathway). However, strain MK5 has genes that encode for a wide range of proteins known to be involved in the degradation of complex carbon sources. Consequently, these results suggest strain MK1 is a dominant primary producer that links CO_2 fixation to Fe(II) oxidation, whereas strain MK5 is a mixotroph linking Fe(II) oxidation to utilization of complex carbon. Strain MK5 is also capable of Fe(III) reduction by an unknown mechanism and may, alternatively, define its niche *in situ* as an anaerobic complex carbon degrader linked to Fe(III) respiration. Elucidating the mechanism of Fe(III) reduction in strain MK5 will be an important future priority for understanding iron cycling in these systems.

The oxidation of Fe(II) in high-temperature environments may have also been important in Earth's early evolutionary history (>2–3 Ga). The biomineralization of ferric iron phases (e.g., jarosite) and the evolution of key metabolic processes such as aerobic respiration in high-temperature Fe mats has implications for the fields of paleobiology and exobiology, as well as microbiology. The findings presented in this study represent the most detailed analysis of geothermal acidic ferric iron mats reported to date, and will be invaluable for future comparative studies to similar undescribed environments.

ACKNOWLEDGMENTS

This work was supported by the National Science Foundation Microbial Observatory Program (MCB-0132022), the National Aeronautic and Space Administration (NASA) via funds provided to the Thermal Biology Institute at Montana State University

(Project Numbers NAG5-8807, NNG04GR46G), the Stanford Synchrotron Radiation Laboratory (SSRL), the DOE-Pacific Northwest National Laboratory (Subcontract 112443), the NSF IGERT Program (0654336), and the Montana Agricultural Experiment Station (Project 911300). The authors appreciate assistance from, S. Korf, W. P. Taylor, A. Nagy, and G. Ackerman for field work, geochemical analyses, sample collection, and 16S rRNA sequencing, and Drs. Scott Fendorf, S. Webb, and J. Bargar for assistance in collecting and analyzing Fe-edge XANES and EXAFS spectra at SSRL. The authors also appreciate C. Hendrix and T. Olliff for permitting this work in Yellowstone National Park (Permit YELL-2004-2007-SCI-5068). The work conducted by the U.S. Department of Energy Joint Genome Institute is supported by the Office of Science of the U.S. Department of Energy under Contract No. DE-AC02-05CH11231. Portions of this research were carried out at the Stanford Synchrotron Radiation Lightsource (SSRL), a national user facility operated by Stanford University on behalf of the U.S. Department of Energy, Office of Basic Energy Sciences. Thomas Borch was supported by a NSF CAREER Award (EAR 0847683).

REFERENCES

Auernik, K. S., Maezato, Y., Blum, P. H., and Kelly, R. M. (2008). The genome sequence of the metal-mobilizing, extremely thermoacidophilic archaeon *Metallosphaera sedula* provides insights into bioleaching-associated metabolism. *Appl. Environ. Microbiol.* 3, 682–692.

Baker, B. J., and Banfield, J. F. (2003). Microbial communities in acid mine drainage. *FEMS Microbiol. Ecol.* 44, 139–152.

Bathe, S., and Norris, P. R. (2007). Ferrous iron- and sulfur-induced genes in *Sulfolobus metallicus*. *Appl. Environ. Microbiol.* 8, 2491–2497.

Beam J. P., Bernstein, H. C., Kozubal, M., Carlson, R. P., and Inskeep, W. P. (2011). "Distribution and activity of iron-oxidizing microorganisms in acidic geothermal environments," in *Goldschmidt Conference, August 15–19*, Vol. 75 (Prague: Mineralogical Magazine), 503.

Berg, I. A., Kockelkorn, D., Ramos-Vera, W. H., Say, R. F., Zarzycki, J., Hügler, M., Alber, B. E., and Fuchs, G. (2010). Autotrophic carbon fixation in archaea. *Nat. Rev. Microbiol.* 8, 447–460.

Blake, R., and Johnson, D. B. (2000). "Phylogenetic and biochemical diversity among acidophilic bacteria that respire on iron," in *Environmental Microbe–Metal Interactions*, ed. D. R. Lovley (Washington: ASM Press), 53–78.

Dopson, M., Baker-Austin, C., and Bond, P. L. (2005). Analysis of differential protein expression during growth states of *Ferroplasma* strains and insights into electron transport for iron oxidation. *Microbiology* 151, 4127–4137.

Edwards, K. J., Goebel, B. M., Rodgers, T. M., Schrenk, M. O., Gihring, T. M., Cardona, M. M., Hu, B., McGuire, M. M., Hamers, R. J., Pace, N. R., and Banfield, J. F. (1999). Geomicrobiology of pyrite (FeS2) dissolution: case study at Iron Mountain, California. *Geomicrobiol. J.* 16, 155–179.

Engelbrektson, A., Kunin, V., Wrighton, K. C., Zvenigorodsky, N., Chen, F., Ochman, H., and Hugenholtz, P. (2010). Experimental factors affecting PCR-based estimates of microbial species richness and evenness. *ISME J* 5, 642–647.

Hallberg, K. B., and Johnson, D. B. (2001). Biodiversity of acidophilic prokaryotes. *Adv. Appl. Microbiol.* 49, 37–84.

Inskeep, W. P., Ackerman, G. G., Taylor, W. P., Kozubal, M., Korf, S., and Macur, R. E. (2005). On the energetics of chemolithotrophy in nonequilibrium systems: case studies of geothermal springs in Yellowstone National Park. *Geobiology* 3, 297–320.

Inskeep, W. P., Macur, R. E., Harrison, G., Bostick, B. C., and Fendorf, S. (2004). Biomineralization of As(V)-hydrous ferric oxyhydroxide in microbial mats of an acid-sulfate-chloride geothermal spring, Yellowstone National Park. *Geochim. Cosmochim. Acta* 68, 3141–3155.

Inskeep, W. P., Rusch, D., Jay, Z., Herrgard, M. J., Kozubal, M. A., Richardson, T. H., Macur, R. E., Hamamura, N., Fouke, B., Reysenbach, A. L., Roberto, F., Young, M., Jennings, R., Schwartz, A., Korf, S., Boyd, E., Badger, J., Bateson, M., Geesey, G., Mathur, E., and Frazier, M. (2010). Metagenomes from high-temperature chemotrophic systems reveal geochemical controls on microbial community structure and function. *PLoS ONE* 5, e9773. doi:10.1371/journal.pone.0009773

Itoh, Y. H., Kurosawa, N., Uda, I., Sugai, A., Tanoue, S., Itoh, T., Horiuchi, T., and Itoh, T. (2001). *Metallosphaera sedula* TA-2, a calditoglycerocaldarchaeol deletion strain of a thermoacidophilic archaeon. *Extremophiles* 5, 241–245.

Jackson, C. R., Langner, H. W., Donahoe-Christiansen, J., Inskeep, W. P., and McDermott, T. R. (2001). Molecular analysis of microbial community structure in an arsenite-oxidizing acidic thermal spring. *Environ. Microbiol.* 3, 532–542.

Jeans, C., Singer, S. W., Chan, C. S., Verberkmoes, N. C., Shah, M., Hettich, R. L., Banfield, J. F., and Thelen, M. P. (2008). Cytochrome 572 is a conspicuous membrane protein with iron oxidation activity purified directly from a natural acidophilic microbial community. *ISME J* 2, 542–550.

Johnson, D. B., and Hallberg, K. B. (2009). Carbon, iron and sulfur metabolism in acidophilic micro-organisms. *Adv. Microb. Physiol.* 54, 202–256.

Johnson, D. B., Okibe, N., and Roberto, F. F. (2003). Novel thermo-acidophilic bacteria isolated from geothermal sites in Yellowstone National Park: physiological and phylogenetic characteristics. *Arch. Microbiol.* 180, 60–68.

Johnson, D. B., Stallwood, B., Kimura, S., and Hallberg, K. B. (2006). Isolation and characterization of *Acidicaldus organivorus*, gen. nov., sp. nov.: a novel sulfur-oxidizing, ferric iron-reducing thermo-acidophilic heterotrophic *Proteobacterium*. *Arch. Microbiol.* 185, 212–221.

Kappler, A., and Straub, K. L. (2005). Geomicrobiological cycling of iron. *Rev. Mineral. Geochem.* 59, 85–108.

Kappler, U., Sly, L. I., and McEwan, A. G. (2005). Respiratory gene clusters of *Metallosphaera sedula* – differential expression and transcriptional organization. *Microbiology* 151, 35–43.

Kauppi, P. H., Hautakangas, H. J., and Puhakka, J. A. (2001). High rate iron oxidation in fluidized-bed bioreactors. *Proc. Int. Biohydrometal. Symp.* 2001, 385–392

Konhauser, K. O. (1998). Diversity of bacterial iron mineralization. *Earth Sci. Rev.* 43, 91–121.

Konhauser, K. O. (2007). *Introduction to Geomicrobiology*. Oxford: Blackwell Science, 425.

Kozubal, M., Macur, R. E., Korf, S., Taylor, W. P., Ackerman, G. G., Nagy, A., and Inskeep, W. P. (2008). Isolation and distribution of a novel iron-oxidizing crenarchaeon from acidic geothermal springs in Yellowstone National Park. *Appl. Environ. Microbiol.* 74, 942–949.

Kozubal, M. A., Dlakic, M., Macur, R. E., and Inskeep, W. P. (2011). Terminal oxidase diversity and function in "*Metallosphaera yellowstonensis*": gene expression and protein modeling suggest mechanisms of Fe(II) oxidation in the sulfolobales. *Appl. Environ. Microbiol.* 77, 1844–1853.

Macur, R. E., Langner, H. W., Kocar, B. D., and Inskeep, W. P. (2004). Linking geochemical processes with microbial community analysis: successional dynamics in an arsenic-rich, acid-sulfate-chloride geothermal spring. *Geobiology* 2, 163–177.

Nemati, M., and Harrison, S. T. L. (2000). A Comparative Study on thermophilic and mesophilic biooxidation of ferrous iron. *Miner. Eng.* 13, 19–24.

Nordstrom, D. K., and Southam, G. (1997). Geomicrobiology of sulfide mineral oxidation. *Rev. Mineral. Geochem.* 35, 361–390.

Quatrini, R., Appia-Ayme, C., Denis, Y., Jedlicki, E., Holmes, D. S., and Bonnefoy, V. (2009). Extending the models for iron and sulfur oxidation in the extreme acidophile *Acidithiobacillus ferrooxidans*. *BMC Genomics* 10, 394. doi:10.1186/1471-2164-10-394

Rohwerder, T., Gehrke, T., Kinzler, K., and Sand, W. (2003). Bioleaching review part A: progress in bioleaching: fundamentals and mechanisms of bacterial metal sulfide oxidation. *Appl. Microbiol. Biotechnol.* 63, 239–248.

Singer, P. C., and Stumm, M. W. (1970). Acid mine drainage: the rate determining step. *Science* 167, 1121–1123.

Singer, S. W., Chan, C. S., Zemla, A., VerBerkmoes, N. C. M., Hwang, M., Hettich, R. L., Banfield, J. F., and Thelen, M. P. (2008). Characterization of cytochrome 579, an

unusual cytochrome isolated from an iron-oxidizing microbial community. *Appl. Environ. Microbiol.* 74, 4454–4456.

Tamura, K., Peterson, D., Peterson, N., Stecher, G., Nei, M., and Kumar, S. (2011). MEGA5: molecular evolutionary genetics analysis using maximum likelihood, evolutionary distance, and maximum parsimony methods. *Mol. Biol. Evol.* 28, 2731–2739.

To, T. B., Nordstrom, D. K., Cunningham, K. M., Ball, J. W., and McClesky, R. B. (1999). New method for the direct determination of dissolved Fe(III) concentration in acid mine waters. *Environ. Sci. Technol.* 33, 807–813.

Webb, S. (2011). *Sixpack v.0.68; Stanford Synchrotron Radiation Lightsource.* Menlo Park: SLAC National Accelerator Laboratory.

Conflict of Interest Statement: The authors declare that the research was conducted in the absence of any commercial or financial relationships that could be construed as a potential conflict of interest.

Received: 03 November 2011; accepted: 05 March 2012; published online: 26 March 2012.

Citation: Kozubal MA, Macur RE, Jay ZJ, Beam JP, Malfatti SA, Tringe SG, Kocar BD, Borch T and Inskeep WP (2012) Microbial iron cycling in acidic geothermal springs of Yellowstone National Park: integrating molecular surveys, geochemical processes, and isolation of novel Fe-active microorganisms. Front. Microbio. ***3****:109. doi: 10.3389/fmicb.2012.00109*

This article was submitted to Frontiers in Microbiological Chemistry, a specialty of Frontiers in Microbiology.

Copyright © 2012 Kozubal, Macur, Jay, Beam, Malfatti, Tringe, Kocar, Borch and Inskeep. This is an open-access article distributed under the terms of the Creative Commons Attribution Non Commercial License, which permits noncommercial use, distribution, and reproduction in other forums, provided the original authors and source are credited.

frontiers in
MICROBIOLOGY

ORIGINAL RESEARCH ARTICLE
published: 08 February 2012
doi: 10.3389/fmicb.2012.00037

Identification and characterization of MtoA: a decaheme *c*-type cytochrome of the neutrophilic Fe(II)-oxidizing bacterium *Sideroxydans lithotrophicus* ES-1

Juan Liu[1], Zheming Wang[1], Sara M. Belchik[1], Marcus J. Edwards[2], Chongxuan Liu[1], David W. Kennedy[1], Eric D. Merkley[1], Mary S. Lipton[1], Julea N. Butt[2], David J. Richardson[2], John M. Zachara[1], James K. Fredrickson[1], Kevin M. Rosso[1] and Liang Shi[1]*

[1] *Pacific Northwest National Laboratory, Richland, WA, USA*
[2] *Centre for Molecular and Structural Biochemistry, School of Biological Sciences and School of Chemistry, University of East Anglia, Norwich Research Park, Norwich, UK*

Edited by:
David Emerson, Bigelow Laboratory for Ocean Sciences, USA

Reviewed by:
Violaine Bonnefoy, Centre National de la Recherche Scientifique, France
Yongqin Jiao, Lawrence Livermore National Laboratory, USA

***Correspondence:**
Liang Shi, Microbiology Group, Pacific Northwest National Laboratory, 902 Battelle Blvd., P.O. Box 999, Richland, WA 99352, USA.
e-mail: liang.shi@pnnl.gov

The Gram-negative bacterium *Sideroxydans lithotrophicus* ES-1 (ES-1) grows on $FeCO_3$ or FeS at oxic–anoxic interfaces at circumneutral pH, and the ES-1-mediated Fe(II) oxidation occurs extracellularly. However, the molecular mechanisms underlying ES-1's ability to oxidize Fe(II) remain unknown. Survey of the ES-1 genome for candidate genes for microbial extracellular Fe(II) oxidation revealed that it contained a three-gene cluster encoding homologs of *Shewanella oneidensis* MR-1 (MR-1) MtrA, MtrB, and CymA that are involved in extracellular Fe(III) reduction. Homologs of MtrA and MtrB were also previously shown to be involved in extracellular Fe(II) oxidation by *Rhodopseudomonas palustris* TIE-1. To distinguish them from those found in MR-1, the identified homologs were named MtoAB and $CymA_{ES-1}$. Cloned *mtoA* partially complemented an MR-1 mutant without MtrA with regards to ferrihydrite reduction. Characterization of purified MtoA showed that it was a decaheme *c*-type cytochrome and oxidized soluble Fe(II). Oxidation of Fe(II) by MtoA was pH- and Fe(II)-complexing ligand-dependent. Under conditions tested, MtoA oxidized Fe(II) from pH 7 to pH 9 with the optimal rate at pH 9. MtoA oxidized Fe(II) complexed with different ligands at different rates. The reaction rates followed the order $Fe(II)Cl_2$ > Fe(II)–citrate > Fe(II)–NTA > Fe(II)–EDTA with the second-order rate constants ranging from $6.3 \times 10^{-3}\ \mu M^{-1}\ s^{-1}$ for oxidation of $Fe(II)Cl_2$ to $1.0 \times 10^{-3}\ \mu M^{-1}\ s^{-1}$ for oxidation of Fe(II)–EDTA. Thermodynamic modeling showed that redox reaction rates for the different Fe(II)-complexes correlated with their respective estimated reaction-free energies. Collectively, these results demonstrate that MtoA is a functional Fe(II)-oxidizing protein that, by working in concert with MtoB and $CymA_{ES-1}$, may oxidize Fe(II) at the bacterial surface and transfer released electrons across the bacterial cell envelope to the quinone pool in the inner membrane during extracellular Fe(II) oxidation by ES-1.

Keywords: *Sideroxydans lithotrophicus* ES-1, extracellular Fe(II) oxidation, decaheme *c*-type cytochrome MtoA, pH-dependent, ligand complexation

INTRODUCTION

The contribution of Fe(II)-oxidizing bacteria (FeOB) to iron cycling in freshwater, groundwater, and marine environments, as well as in most soils and sediments, has been well recognized (Emerson et al., 2010). A variety of neutrophilic and acidophilic Fe(II)-oxidizing microorganisms have the ability to derive energy for growth from the oxidation of dissolved or structural Fe(II) under either oxic or anoxic conditions. Unlike aerobic acidophilic or anaerobic neutrophilic FeOB, the geologic importance of aerobic neutrophilic FeOB has long been neglected because of the rapid auto-oxidation of Fe(II) by O_2 at circumneutral pH. However, recent studies indicate that aerobic neutrophilic FeOB would play a key role in microoxic niches with low levels of O_2 concentration, where microbial Fe(II)-oxidation can compete with the chemical oxidation of Fe(II). For example, the Gram-negative bacterium *Sideroxydans lithotrophicus* ES-1 (ES-1), originally isolated from the ground water with Fe(II) at neutral pH in MI, USA, grows on $FeCO_3$ or FeS at oxic–anoxic interfaces (Emerson and Moyer, 1997; Emerson et al., 2007). ES-1 does not grow on Mn(II) oxides, sulfide, or organic carbon sources, such as acetate, pyruvate, and glucose, and does not reduce Fe(III) oxides. Fe(III) (oxy)(hydr)oxide precipitates are closely associated with the ES-1 cells, but do not form sheath- or stalk-like structures (Emerson and Moyer, 1997). Recently, the ES-1 genome was sequenced (http://www.ncbi.nlm.nih.gov/sutils/genom_table.cgi). However, the molecular mechanism by which ES-1 oxidizes Fe(II) remains unknown.

Because Fe(III) oxides produced from biotic Fe(II)-oxidation are usually sparingly soluble at circumneutral pH and in the absence of complexing ligands, bacteria oxidize Fe(II)

extracellularly presumably to avoid accumulation of Fe(III) oxides inside their cells. To overcome the physical separation between the bacterial inner membrane where microbial oxidases are located and bacterial cell surface, FeOB have evolved different electron transfer pathways that link the inner membrane to the cell surface. The pathways identified to date include Cyc-2/Rus/Cyc-1 of *Acidithiobacillus ferrooxidans*, PioABC of *Rhodopseudomonas palustris* TIE-1 and FoxEYZ of *Rhodobacter* strain SW2 (Appia-Ayme et al., 1999; Yarzabal et al., 2002; Croal et al., 2007; Jiao and Newman, 2007; Castelle et al., 2008). Although these systems are phylogenetically unrelated, they all have at least one *c*-type cytochrome (*c*-Cyt) as a key electron transfer protein. These *c*-Cyts work in concert with other proteins, often in the form of protein–protein complexes that can span the entire microbial cell envelope to facilitate electron conductance between the inner membrane and Fe(II) external to the bacterial cell.

Notably, PioAB of *R. palustris* TIE-1 are homologs of MtrAB of the Fe(III)-reducing bacterium *Shewanella oneidensis* MR-1 (MR-1; Jiao and Newman, 2007). In MR-1, MtrA is a decaheme *c*-Cyt, while MtrB is a trans-outer membrane (OM), porin-like protein. They form a tight protein complex that transfers electrons across the OM to MtrC and OmcA, two OM decaheme *c*-Cyts that are localized on bacterial outermost surface (Ross et al., 2007; Shi et al., 2008; Hartshorne et al., 2009; Lower et al., 2009; Reardon et al., 2010). MtrABC and OmcA are key components of the MR-1 extracellular electron transfer pathway, which also includes a tetraheme *c*-Cyt CymA in the inner membrane. Together, they facilitate electron transfer from the quinone/quinol pool in the inner membrane across the periplasm, through the OM, to the surface of Fe(III) oxides (Richardson, 2000; Shi et al., 2007, 2009; Fredrickson et al., 2008). In addition to mediating electron transfer to and from Fe, MtrAB homologs are also involved in extracellular reduction of dimethylsulfoxide by MR-1 and are hypothesized to be the prototype of a model system for electron transfer across the bacterial OM (Gralnick et al., 2006; Hartshorne et al., 2009).

To investigate the molecular mechanism used by ES-1 for oxidizing Fe(II), we searched the ES-1 genome for the homologs of Cyc-2/Rus/Cyc-1 of *A. ferrooxidans*, FoxEYZ of *Rhodobacter* strain SW2 and PioAB/MtrAB. This search identified a three-gene cluster that encoded MtrA, MtrB, and CymA homologs. To distinguish them from those found in Fe(III)-reducing bacteria, we named the identified homologs MtoAB and $CymA_{ES-1}$. Cloned *mtoA* partially complemented an MR-1 mutant without MtrA in ferrihydrite (FH) reduction. Recombinant MtoA was purified following overexpression in MR-1 cells and characterized systematically. Purified MtoA was found to be a decaheme *c*-Cyt and able to oxidize soluble Fe(II) *in vitro*. Collectively, these results suggest that MtoA is a Fe(II)-oxidizing protein that works in concert with MtoB and $CymA_{ES-1}$ to mediate electron transfer reactions from the cell surface to the inner membrane during extracellular Fe(II) oxidation by ES-1.

MATERIALS AND METHODS

STANDARD PROCEDURES

Protein concentrations were measured with a bicinchoninic acid (BCA) protein assay kit from Pierce (Rockford, IL, USA). Sodium dodecyl sulfate-polyacrylamide gel electrophoresis (SDS-PAGE) and Western blot analysis were conducted according to the instructions from Invitrogen (Carlsbad, CA, USA). To visualize proteins directly, gels were stained with GelCode blue stain from Pierce. Heme staining was carried out according the protocol described by Thomas et al. (1976). RGS-His antibody was used for detecting the recombinant protein tagged with RGS-His epitope by Western blot analysis (QIAGEN, Valencia, CA, USA). Kanamycin was used at 25 μg/ml.

GENE IDENTIFICATION AND CLONING

The approach used to identify MtoAB from the ES-1 genome was similar to those described previously (Shi et al., 1998; Shi and Zhang, 2004). MR-1 MtrAB and PioAB of *R. palustris* TIE-1 were used as templates to search for open reading frames (ORFs) whose predicted peptide products displayed similarity to the MtrAB/PioAB by BLAST ($E < 0.01$). Following their identification, the polypeptide sequences of MtoA, MtoB, or $CymA_{ES-1}$ and MtrA homologs, MtrB homologs, or CymA homologs of 19 sequenced *Shewanella* strains described by Fredrickson et al. (2008) and PioA or PioB were used to construct phylogenetic trees with the neighbor-joining-based ALGNX program of Vector NTI (Invitrogen). Likewise, the ES-1 genome was also searched for the homologs of Cyc-2/Rus/Cyc-1 of *A. ferrooxidans* and FoxEYZ of *Rhodobacter* strain SW2. The ORF for the identified MtrA homolog was synthesized and then cloned into a protein expression vector pJexpress 401 to create pLS279 by DNA 2.0 (Menlo Park, CA, USA). pLS279 was introduced into MR-1 Δ*mtrB–mtrD* (locus tags SO_1776-SO_1782) or Δ*mtrA* (SO_1777) mutant by electroporation to create LS587 and LS597, respectively (Shi et al., 2005; Hartshorne et al., 2009; Clarke et al., 2011). Δ*mtrA* mutant was also transformed with pJexpress 401 to create LS620.

FERRIHYDRITE REDUCTION

For ferrihydrite (FH) reduction, MR-1, LS597, and LS620 were grown in PIPES-buffered M1 medium with 20 mM sodium lactate aerobically at 30°C for 16 h with agitation (150 rpm) and harvested by centrifugation (5000 × *g*, 5 min). Harvested cells were washed once with the same medium, purged with N_2, and transferred to Balch tubes at final concentration of 1×10^8 cells/ml. FH was added at final concentration of 10 mM. The tubes were incubated horizontally at 30°C with shaking (25 rpm; Shi et al., 2011). At predetermined time points, 0.5 N HCl extractable Fe(II) was determined by the ferrozine assay (Stookey, 1970).

PROTEIN PURIFICATION

MtoA was purified from a mutant without major MR-1 *c*-Cyts, such as MtrA, MtrC, and OmcA. Compared to that in wt, yields of purified *c*-Cyts from this mutant were often two to three times higher. LS587 was grown aerobically in Tryptic Broth at 30°C with agitation (150 rpm) until the culture reached an optical density at 600 nm of 0.6. Isopropyl β-D-1-thiogalactopyranoside (IPTG) was added to a final concentration of 1 mM. The LS587 cells were grown for another 17 h and then harvested by centrifugation at 6000 × *g* for 15 min. The harvested cells were washed once with buffer A (20 mM HEPES, pH 7.8, 150 mM NaCl) and stored at −20°C. Frozen cell pellets were resuspended in buffer

B [buffer A + protease inhibitor (Roche Diagnostic, Indianapolis, IN, USA)] in a ratio of 5 ml/g wet weight cells. The cells were lysed by passage through a French press three times at 8000 lbf/in^2. The unbroken cells and debris were removed by centrifugation at 15,000 × *g* for 30 min. The supernatant was transferred to ultracentrifugation tubes and further centrifuged at 150,000 × *g* for 1 h. The supernatant was loaded onto a Ni^{2+}–nitrilotriacetic acid (NTA) agarose column pre-equilibrated with buffer B. The column was washed with following buffers in sequential order: buffer B, buffer C [buffer B + 10% (v/v) glycerol], and buffer D (buffer C + 40 mM imidazole). MtoA was eluted with buffer E (buffer C + 250 mM imidazole; Shi et al., 2005). The fractions containing MtoA were pooled and concentrated. The concentrated MtoA was loaded on a HiLoad 16/60 column of Superdex 200 and eluted with buffer B by means of an ÄKTA explorer fast protein liquid chromatography system (GE Healthcare, Piscataway, NJ, USA). The MtoA-containing fractions were pooled, concentrated, changed to buffer C, aliquoted, and stored at −20°C. All protein purification steps were performed at 4°C.

MALDI–TOF MASS SPECTROMETRY

MALDI–TOF mass spectra were acquired using a Bruker UltraFlextreme (Billerica, MA, USA) mass spectrometer operated in linear mode. The instrument was calibrated with Protein Standard II (Bruker). MtoA in the final dialysis buffer was either desalted with a C4 OMIX pipette tip (Varian, Palo Alto, CA, USA) before spotting on the MALDI target, or spotted directly. Similar results were obtained with either method. The matrix solution was α-cyano-4-hydroxycinnamic acid in methanol. Laser power and number of lasers shots were adjusted and scans were averaged until the desired signal-to-noise ratio was obtained. Data from four experiments on three different preparations of MtoA were averaged.

LIQUID CHROMATOGRAPHY–MS

Approximately 60 μg of MtoA in a volume of 200 μl was denatured by adding ∼96 mg of solid urea and incubating at room temperature for 1 h. The sample was diluted 12-fold with 100 mM ammonium bicarbonate buffer (pH 8) and then digested with sequencing-grade modified trypsin (Promega, Madison, WI, USA) overnight at 37°C at a protein-to-enzyme ratio of 20:1.The digest was desalted by solid phase extraction with a Supelco Discovery C18 cartridge. The desalted sample was then analyzed by LC–tandem mass spectrometry (MS/MS) on a custom-built LC system coupled to an LTQ Orbitrap mass spectrometer (Thermo Fisher Scientific, San Jose, CA, USA) as previously described (Livesay et al., 2007). The resulting MS/MS data were searched using TurboSequest v27.12 (Eng et al., 1994), with parent mass tolerance, 50 ppm; fragment mass tolerance, 0.5 Da; partially tryptic enzyme rules; a dynamic modification on cysteine (C) residues of 615.1694 (Yang et al., 2005), corresponding to the mass of a heme C group containing ^{56}Fe and accounting for the charge on the heme iron. Because heme C peptides are known to be difficult to identify from database searches, we manually annotated tandem mass spectra of heme C peptides assigned to each observed heme motif.

CYCLIC VOLTAMMETRY

Cyclic voltammetry (CV) was performed inside a Faraday cage housed in a N_2-filled chamber (atmospheric $O_2 < 2$ ppm). The glass electrochemical cell contained three electrodes: a Ag/AgCl (saturated KCl) reference electrode, a basal plane pyrolytic graphite working electrode and a Pt wire counter electrode. The sample chamber was maintained at 4°C. Immediately prior to each experiment the working electrode surface was lightly abraded with "Wet and Dry Abrasive Paper" of fine grade (English Abrasives and Chemicals, Stafford, UK) and polished with an aqueous 0.3-μm Al_2O_3 slurry. After sonication, the electrode was rinsed, dried with a tissue and a few microliters of ice-cold solution containing 100 μM MtoA in 20 mM HEPES pH 7.6 + 100 mM NaCl + 10% (v/v) glycerol were placed on the electrode. After 30–60 s, excess solution was removed from the electrode, which was then immersed in the desired buffer-electrolyte: 25 mM HEPES pH 7.1 with 100 mM NaCl, or 20 mM Tris pH 7.8–9.2 with 100 mM NaCl. Baseline subtraction was carried out as previously described (Hartshorne et al., 2009). Midpoint potentials (E_m) were determined by fitting oxidative and reductive scans to the sum of the theoretical response for 10 centers behaving as isolated $n = 1$ sites (Clarke et al., 2011). Potentials are quoted with respect to the standard hydrogen electrode (SHE) following addition of +0.197 V to the measured values.

SPECTROSCOPIC AND STOPPED-FLOW KINETIC MEASUREMENT

All spectroscopic and kinetic measurements were conducted in an anoxic chamber filled with N_2 from a liquid N_2 boil-off supply (<1 ppm O_2; Innovative Technologies, Port Washington, NY, USA). MtoA stock solution containing 4 μM protein, 150 mM NaCl, and 20 mM HEPES buffer (pH = 7.6) was purged with dry N_2 gas for more than 1 h, then stored at 4°C in serum bottles capped with thick rubber stoppers and crimp sealed. All chemicals, plastic syringes, tubes, vials, and pipette tips were deoxygenated for at least 24 h inside the anoxic chamber prior to use. The UV–visible absorption spectra were collected using Agilent 8452 Diode Array Spectrophotometer (Santa Clara, CA, USA). Purified MtoA was in the oxidized form. To record the spectrum of fully reduced MtoA, 10 mM sodium dithionite solution was gradually added to 0.5 ml of protein stock solution until no changes in the UV–visible spectra were observed. In pH-dependent Fe(II) oxidation experiments, MtoA stock solution was diluted to 0.4 μM in Tris buffer (20 mM buffer with 150 mM NaCl) at the desired pH value. A small volume of $FeCl_2$ stock solution (15 mM) was spiked into the diluted protein solution. Absorption spectra of the resulting solution mixture were observed at ∼5 min after the spiking, allowing the reactions to reach equilibrium.

Electron transfer in the Fe(II) oxidation by MtoA was measured using the reaction between 39.4 μM of $FeCl_2$ and 4 μM of purified MtoA solution at pH 8. The amount of reduced MtoA after reaction was measured using the absorbance at the 552-nm band in the absorption spectrum. The Fe(II) concentration in the solution was measured by ferrozine assay. To minimize the spectral interference of MtoA, the solution was filtered by a 30-kDa centrifuge filter (Amicon Ultra-0.5, Millipore, Billerica, MA, USA) at 13,000 × *g* for 12 min, and then 0.4 ml of the filtrate into 1.6 ml ferrozine (1000 mg/l, pH 7) was added. A control experiment was conducted

without adding MtoA solution, and the Fe(II) concentration after the same filtration process did not change substantially.

Ligand effects on oxidation of Fe(II)-complexes by MtoA were investigated using a stopped-flow system with a BioLogic MOS 250 spectrometer (Knoxville, TN, USA). The method was described in detail by Wang et al. (2008). Briefly, known volumes of MtoA and Fe(II)-complex solutions were rapidly mixed, and then the absorbance at 552 nm was tracked as a function of time. The concentration of oxidized MtoA at time t (C_t) can be calculated from the measured absorbance (A_t) using the following equation (Wang et al., 2008) after baseline correction:

$$C_t = \frac{A_t - C_0\,\varepsilon_{ox}}{\varepsilon_{ox} - \varepsilon_{red}} \quad (1)$$

where C_0 is the initial concentration of oxidized MtoA, ε_{ox}, and ε_{red} are the molar absorption coefficients of the oxidized and reduced MtoA, respectively. All stopped-flow kinetic experiments were conducted in Tris buffer (pH 8) containing 0.4 μM protein and 200 μM Fe(II) complexes. The ferrous iron-to-ligand ratio in Fe–citrate, Fe–NTA, and Fe–EDTA stock solutions was 1:10.

ANALYSIS OF KINETIC DATA

The overall reaction between oxidized MtoA (ox-MtoA) and Fe(II)-complexes can be expressed as:

$$\text{Fe(II)} - ligand + ox - MtoA \rightarrow \text{Fe(III)} - \text{ligand} + \text{re-MtoA} \quad (2)$$

The rate of this reaction can then be expressed as follows:

$$\frac{dC}{dt} = -kCA(1 - Q/K) \quad (3)$$

where k is the rate constant, A and C are the Fe(II) and oxidized MtoA concentrations, respectively. Q is the ion activity product of the redox reaction, and K is the equilibrium constant. The concentration of oxidized MtoA (C) was calculated from the measured absorbance in the stopped-flow system and plotted against time. The residual Fe(II) concentration was calculated from the electron balance between the reacted Fe(II) and reduced MtoA. The calculated MtoA and Fe(II) concentrations as a function of time were then used to estimate rate parameters in Eq. 3. The second-order rate constant (k) and the equilibrium constant (K) were determined by the slope and the ending point of the fitted line, respectively.

RESULTS

IDENTIFICATION OF MtoAB AND CymA$_{ES-1}$

Search of the ES-1 genome did not reveal any homologs for Cyc-2/Rus/Cyc-1 of *A. ferrooxidans* or FoxEYZ of *Rhodobacter* strain SW2, but identified a gene cluster that encoded an MtrA/PioA homolog (Slit_2497) and an MtrB/PioB homolog (Slit_2496). Analysis of the genes adjacent to the *mtrAB* homologs also identified a *cymA* homolog (Slit_2495) that was next to an *mtrB* homolog. To distinguish them from those found in MR-1 and PioAB of *R. palustris* TIE-1, we named these genes and their encoding proteins *mtoAB–cymA* and MtoAB/CymA$_{ES-1}$, respectively (**Figure 1**). No *pioC* homolog was found in the ES-1 genome. The deduced MtoA polypeptide contains 317 amino acids with calculated molecular mass of 33556.2 Da. Ten CXXCH motifs (i.e., putative heme-binding sites) were found within the MtoA polypeptide, suggesting that matured MtoA contains up to 10 heme co-factors. In addition to the 10 histidine residues of the CX_2CH motifs, the MtoA polypeptide contained 14 more histidine residues, most of which were probably used as the distal ligands for the heme Fe. Phylogenetic analysis of the deduced amino acid sequence of MtoA with the MtrA homologs of 19 sequenced *Shewanella* strains (Fredrickson et al., 2008) and PioA of *R. palustris* TIE-1 demonstrated that MtoA was 39% identical to PioA and 42–44% identical to the MtrA sequences analyzed. Furthermore, similar to *Shewanella* MtrA, MtoA lacked the N-terminal extension (~200 amino acids) that was found in PioA polypeptides (Jiao and Newman, 2007). These results show that MtoA is almost equally related to PioA used for Fe(II) oxidation and MtrA for Fe(III) reduction, and the N-terminal extension of PioA is probably used for specific interaction with PioBC, but not directly for Fe(II) oxidation.

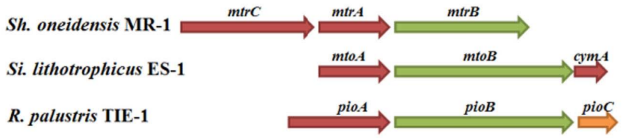

FIGURE 1 | Genetic organization of *mtoA, mtoB,* and *cymA* of *Sideroxydans lithotrophicus* ES-1. Shown are the relative positions of *mtoA, mtoB,* and *cymA* within the complete nucleotide sequence of *S. lithotrophicus* ES-1. The genes are labeled by arrows whose sizes and orientations indicate their relative lengths and directions in which they are presumed to be transcribed. For comparison, *mtrCAB* of *Shewanella oneidensis* MR-1 and *pioABC* of *Rhodopseudomonas palustris* TIE-1 are included. The genes encoding *c*-type cytochromes are labeled in red, while those encoding the β-barrel outer membrane proteins are labeled in green.

Likewise, MtoB was 17% identical to PioB and 19–21% identical to the MtrB sequences analyzed, while CymA$_{ES-1}$ was 56% identical to CymA of *S. baltica* OS223, 34% to MR-1 CymA and 32–36% identical to the other CymA sequences included in the alignment. Like PioB, MtoB is ~110 amino acids longer than the MtrBs of *Shewanella*. Given that in MR-1, MtrAB, and CymA are the key components of the electron transfer pathway used for extracellular reduction of Fe(III) (Richardson, 2000; Shi et al., 2007, 2009), identification of an *mtoAB–cymA* cluster suggests that MtoAB and CymA$_{ES-1}$ may form a pathway for transferring electrons from the bacterial surface to the inner membrane during extracellular Fe(II) oxidation by ES-1.

COMPLEMENTATION OF MR-1 *mtr*A DELETION MUTANT IN FERRIHYDRITE (FH) REDUCTION BY MtoA

MtoA is a homolog of MR-1 MtrA that plays a critical role in FH reduction because deletion of *mtrA* impaired MR-1's ability to reduce FH (Hartshorne et al., 2009). To determine whether MtoA can facilitate trans-membrane electron transfer, pLS279 with *mtoA* was introduced into an MR-1 Δ*mtrA* mutant and

tested for FH reduction. The same mutant was also transformed with an empty vector, and the resulting strain was used as a negative control. Under the conditions tested, the MR-1 wt began to reduce FH within 24 h, while no FH reduction was detected in the reactions mediated by ΔmtrA mutants with either empty vector or *mtoA* at 48 h. After 120 h, FH reduction was detected in the reactions mediated by ΔmtrA mutant with either empty vector or *mtoA*, but no major difference was found between them. After 240 h, wt produced 3.82 ± 0.14 mM Fe(II) ($n = 3$), while mutants with empty vector or MtoA produced 1.56 ± 0.3 and 3.26 ± 0.42 mM Fe(II) ($n = 3$), respectively, which were 40 and 85% of that produced by wt (**Figure 2**). Thus, recombinant MtoA partially complements Δ*mtrA* mutant in FH reduction, demonstrating that it can be inserted into MtrB and transfer electron across the outer membrane to MtrC during FH reduction. Because deletion of *mtrA* up-regulates *mtrD*, an *mtrA* homolog (Coursolle and Gralnick, 2010), the up-regulated MtrD may contribute to the FH reduction observed in the mutant with empty vector.

PURIFICATION OF RECOMBINANT MtoA

Following cell lysis and ultracentrifugation, recombinant MtoA was isolated from the soluble fraction by immobilized metal ion affinity chromatography followed by gel-filtration chromatography. The purified MtoA migrated as two bands on SDS-PAGE with apparent masses of ∼43 and 86 kDa, respectively. Heme staining and Western blot analyses of the same sample showed that both bands were the heme-containing MtoA, indicating that band with ∼86 kDa contained MtoA dimers (**Figure 3**). Measurement of purified MtoA with MALDI–TOF MS revealed that its molecular mass was $42{,}746 \pm 114$ Da ($n = 3$), which was very close to 42,639 Da, the calculated molecular mass for recombinant MtoA matured with 10 heme groups. In addition, liquid chromatography–mass spectrometry (LC–MS)/MS experiments following tryptic digest demonstrated heme modification at 8 out of 10 CXXCH heme-binding motifs in MtoA (all but motifs 9 and 10). Presumably, peptides from motifs 9 and 10 are not observed because of a lack of trypsin cleavage sites in their vicinity. Both motifs 9 and 10 would be in the same 56-residue, 6891-Da tryptic peptide, too large to be readily analyzed by LC–MS (data not shown). All these results clearly demonstrate that purified MtoA is a decaheme *c*-Cyt.

CYCLIC VOLTAMMETRY OF PURIFIED MtoA

Cyclic voltammetry of basal plane graphite electrodes exposed to solutions of MtoA displayed clear peaks describing oxidative and reductive transformations that were not seen in the absence of MtoA (**Figure 4**). The oxidative and reductive peak areas were within error of each other consistent with reversible redox transformation of the adsorbed protein, and typically corresponded to 3×10^{-12} pmol of electroactive MtoA per square centimeter assuming all 10 hemes are redox active. This electroactive population is consistent with monolayer coverage of the electrode by MtoA, and peak currents were found to be directly proportional to the scan rate confirming that the response did indeed arise from an adsorbed protein film. As shown in **Figure 4**, MtoA is redox active over a more positive window of potential than MR-1 MtrA at pH 7.1, suggesting that MtoA is better poised to oxidize Fe(II) than MR-1 MtrA.

The redox properties of MtoA were measured by CV at pH 7.1, 7.8, 8.2, and 9.2. For each pH the protein was redox active

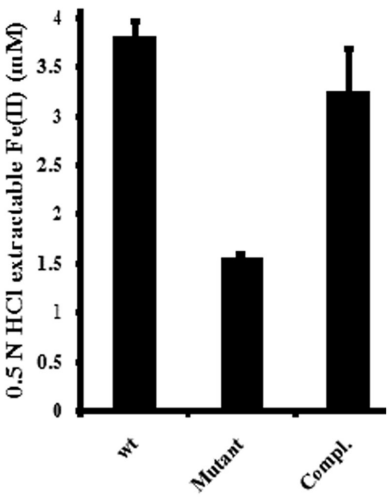

FIGURE 2 | Complementation of *Shewanella oneidensis* MR-1 mutant without MtrA by MtoA. Fe(II) formation after reduction of 10 mM FH by *S. oneidensis* MR-1 wild type (wt), Δ*mtrA* mutant with empty vector, and the mutant complemented with MtoA (Compl.) for 240 h. The values reported are the means and SD of triplicate measurements.

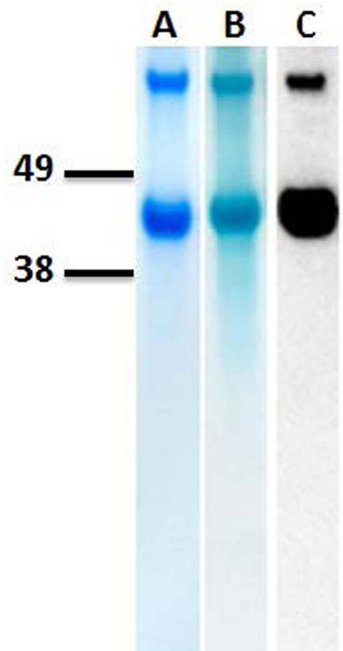

FIGURE 3 | Purification of MtoA. A total of 2 μg of isolated MtoA was run by SDS-PAGE and then visualized by GelCode staining (lane A) and heme staining (lane B) or probed with RGS-His-HRP antibody (lane C). Migration positions of protein standards with different molecular masses (kDa) are indicated at the left.

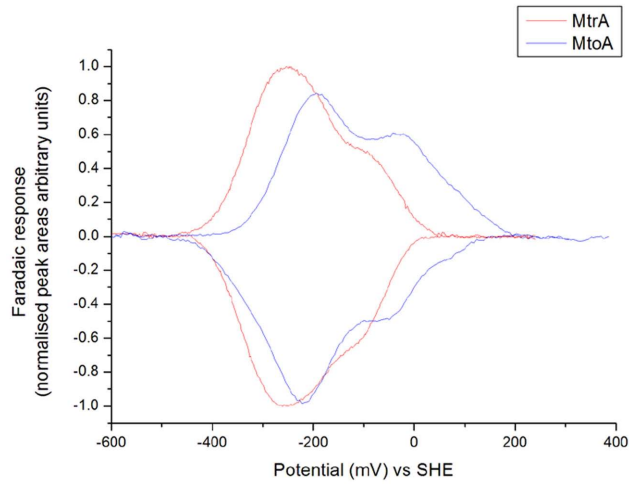

FIGURE 4 | Cyclic voltammograms of MtoA of *Sideroxydans lithotrophicus* ES-1 and MtrA of *Shewanella oneidensis* MR-1 adsorbed on graphite electrodes. Scan rate = 50 mV/s, buffer-electrolyte = 25 mM HEPES pH 7.1 with 100 mM NaCl, $T = 277$ K.

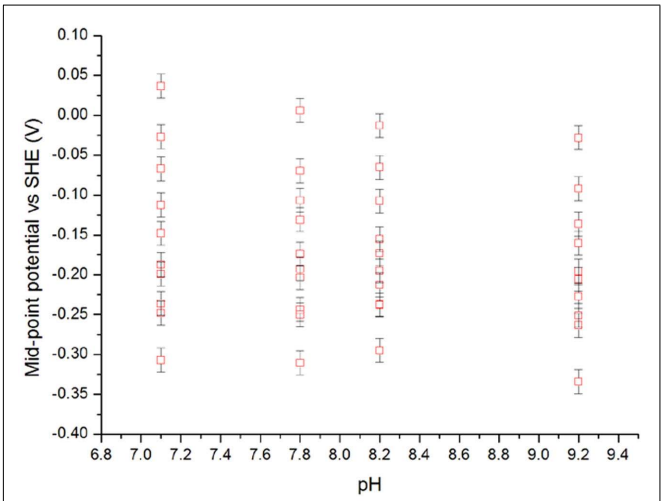

FIGURE 5 | Average E_m values determined from cyclic voltammetry of MtoA at the indicated pH.

between ∼+100 and −400 mV (vs. SHE) with the heme E_m values clustering to define a low potential peak and a higher potential shoulder. The major impact of increased pH was to produce a greater proportion of hemes with lower E_m. A smaller effect was a shift of the higher potential end of redox active window to more negative values. These effects were quantified by assuming that the oxidative and reductive peaks arose from the sum of contributions from 10 independent centers displaying reversible, $n = 1$ electron transfer. This assumption yielded a good fit to the data and averaging the E_m values from oxidative and reductive peaks yielded 10 apparent E_m values for each pH (**Figure 5**).

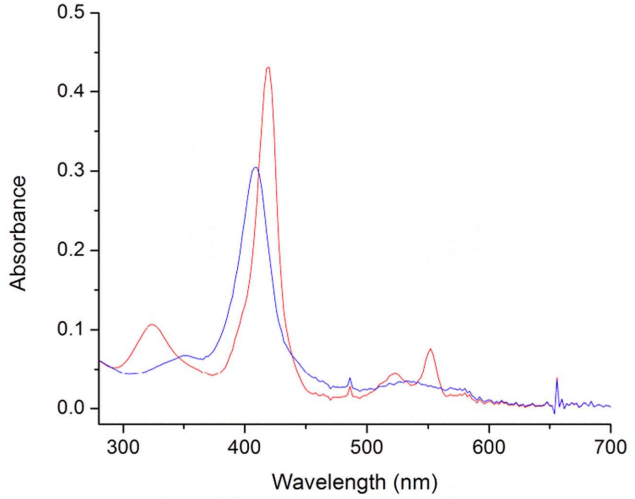

FIGURE 6 | Absorption spectra of MtoA (4 μM) in 50 mM NaCl and 100 mM HEPES buffer (pH = 7) in the oxidized (blue line) and the reduced form (red line).

Fe(II) OXIDATION BY MtoA

The absorption spectrum of purified, oxidized MtoA exhibited a characteristic peak at 408 nm (α peak) with a shoulder at ∼352 nm and a weak absorption band at ∼530 nm. After addition of sodium dithionite solution at pH 7, α peak shifted to 418 nm, and the shoulder shifted to 324 nm to form a distinct peak. In addition, two absorption peaks at 522 nm (β peak) and 552 nm (γ peak) appeared (**Figure 6**). A similar change was observed in absorption spectra of oxidized and reduced MtrC and OmcA (Wang et al., 2008). The fully reduced MtoA could be rapidly re-oxidized by addition of 1 mM of Fe(III)–NTA solution (data not shown), which is consistent with previous results that MR-1 MtrA is a bidirectional protein and can mediate electrons in and out of MR-1 cells as well as proteoliposomes (Hartshorne et al., 2009; Ross et al., 2011). To investigate the mass balance in $FeCl_2$ oxidation by MtoA, the concentration changes of Fe(II) ions (Δ[Fe(II)]) and reduced MtoA ($[MtoA]_{red}$) were investigated with 4 μM of oxidized MtoA reacted with ∼40 μM of $FeCl_2$ at pH 9. At the end of the reaction, the ratio of Δ[Fe(II)] to $[MtoA]_{red}$ was 9.6 ± 1.5 ($n = 3$). Changing the initial concentration of MtoA to 2.3 and 3 μM, respectively, did not significantly change the ratio. Although not all MtoA was reduced by $FeCl_2$ in all experiments, the amount of Fe(II) ions formed was close to 10 times more than the amount of MtoA reduced. It suggests that, under this condition, 10 hemes in MtoA participated in electron transfer, and no other electron acceptor or donor participated in this reaction.

pH-DEPENDENT Fe(II) OXIDATION BY MtoA

Absorption spectra of 0.4 μM MtoA after reaction with 18 μM $FeCl_2$ at pH 7, 7.5, 8, 8.5, and 9, respectively, were compared (**Figure 7**). The comparison showed that, with the same amount of $FeCl_2$, the absorbance at 552 nm increased as pH increased. At pH 7, only $1.0 \pm 1.1\%$ ($n = 3$) of MtoA was reduced by 18 μM $FeCl_2$,

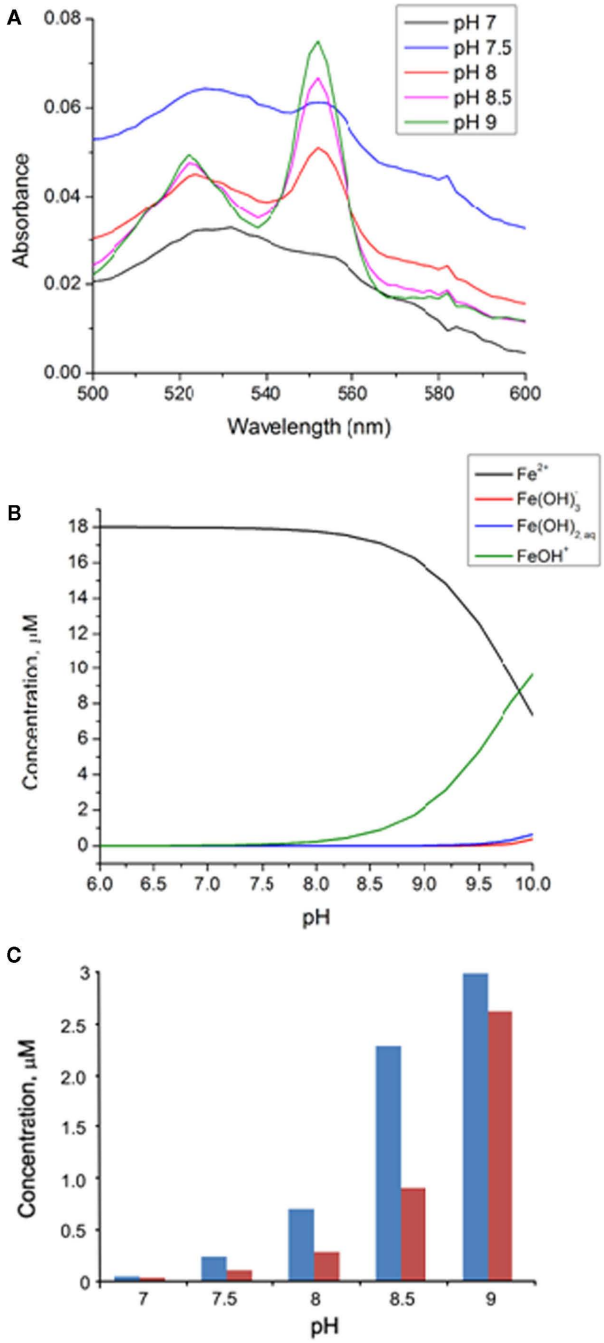

FIGURE 7 | (A) Absorption spectra of MtoA (0.4 μM) after the oxidation of 18 μM $FeCl_2$ at pH 7 (black), pH 7.5 (blue), pH 8 (red), pH 8.5 (pink), and pH 9 (green). **(B)** Speciation of Fe(II; 18 μM) as a function of pH in 150 mM NaCl solution (Allison et al., 1991). **(C)** Variation of Fe(II; blue columns) oxidized by MtoA at the end of reactions and initial $[Fe(OH)^+]$ (red columns) as a function of pH.

but this percentage increased to 4.9 ± 0.3% ($n = 3$) at pH 7.5, 14.7 ± 3.3% ($n = 3$) at pH 8, 48.2 ± 1.7% ($n = 3$) at pH 8.5, and 63.0 ± 9.8% ($n = 3$) at pH 9. The maximum fraction of total MtoA reduced by $FeCl_2$ was therefore systematically larger at higher pH. The same trend was also observed in HEPES buffer at pH 7 and 8 (data not shown). It should be noted that in all of these experiments, MtoA was not totally reduced, even though there was an excess of electron donor, $FeCl_2$. At pH 9, increasing the concentration of $FeCl_2$ up to 400 μM did result in increasingly reduced MtoA. At pH 8, no additional MtoA was reduced as $[FeCl_2]$ was increased to 840 μM. Thus, MtoA has the ability to oxidize $FeCl_2$ in the pH range of 7–9, but reduction of MtoA is incomplete even in the presence of excess $FeCl_2$. Similar incomplete redox reaction was observed in the oxidation of reduced MtrF by flavin mononucleotide (FMN). For that system it was proposed that only a subgroup of the 10 hemes in each MtrF molecule participated in FMN reduction based on reduction potential difference estimated between individual hemes and the midpoint potential of $FMN/FMNH_2$ (Clarke et al., 2011). However, the mass balance experiment in this study showed that the molar ratio of the consumed Fe(II) to reduced MtoA was close to 10:1, consistent in principle with participation of 10 hemes in each MtoA molecule per 10 Fe(II) oxidized. If only a subgroup of MtoA hemes reacted with $FeCl_2$, this ratio should be <10.This suggests that at the end of reaction a subpopulation of MtoA molecules are fully reduced, and incomplete reduction of MtoA is accounted for by a fully oxidized subgroup of MtoA. Hence, in contrast to MtrF, MtoA appears to undergo redox reactions via a cascade whereby once electron transfer into an MtoA molecule begins, it subsequently becomes more energetically favorable to continue reduction of that molecule to completion. This suggests that for any individual MtoA, redox potentials for individual hemes, in CV measurements for example, progressively shift to more oxidizing potentials as reduction proceeds, and vice versa. As Fe(II), Fe(III), and oxidized MtoA concentrations change during the course of reaction, the redox potential difference between ferrous species and MtoA may decrease to zero, at which point the reaction reaches equilibrium. Involvement of all of its 10 hemes during Fe(II) oxidation implies the ability of MtoA for transferring electrons from extracellular Fe(II), across the outer membrane, and into the periplasm, which is consistent with the complementation results described above.

LIGAND-DEPENDENT Fe(II) OXIDATION BY MtoA

Rates of Fe(II)-complex oxidation by MtoA at pH 8 were investigated using a stopped-flow system. In all experiments, the molar ratio of Fe(II) to MtoA was 500. The change of MtoA concentration with time was calculated according to the absorbance change at the γ peak. A control experiment was included by mixing MtoA and Tris buffer (pH 8) in which no significant change was observed in the concentration of oxidized MtoA during the time course of study (**Figure 8**). In all Fe(II)-complex oxidation reactions, the concentration of oxidized MtoA changed in a similar way. It initially decreased very fast, and then the rate of change decreased to reach redox equilibrium. All reactions reached equilibrium within 2 min. The fraction of MtoA reduced by Fe(II)-complexes at the end of each reaction was in the order $Fe(II)Cl_2$ > Fe(II)–citrate > Fe(II)–NTA > Fe(II)–EDTA (**Figure 8**).

The stopped-flow kinetic data were fitted to a second-order rate model using Eq. 3. The rate constant, *k*, was derived from the slope of fitted curves in the fast stage, and the equilibrium constant,

K, was determined from the equilibrium stage (**Table 1**). Rate and equilibrium constants were significantly affected by ligand type. The order for the oxidation rates are similar to the final oxidation fraction, which was $Fe(II)Cl_2$ > Fe(II)–citrate > Fe(II)–NTA > Fe(II)–EDTA. These experiments showed that the type of ligand significantly affected the oxidation kinetics of Fe(II)-complexes by MtoA. Compared to the reduction rates of the analogous Fe(III)-complexes by MtrC and OmcA, which ranged from 0.872 $\mu M^{-1}\,s^{-1}$ for the reaction between MtrC and Fe(III)–EDTA to 0.012 $\mu M^{-1}\,s^{-1}$ for the reaction between OmcA and the Fe(III)–citrate (Wang et al., 2008), the oxidation rates of Fe(II)-complexes by MtoA were two orders of magnitude slower. Moreover, in the Fe(III)-complex reduction reactions by MtrC and OmcA, there was enough free energy driving the redox reaction to consume all heme groups. However, consistent with the discussion above regarding reaction incompleteness, the free energy in the present system was not sufficient for all MtoA to participate in the redox reaction.

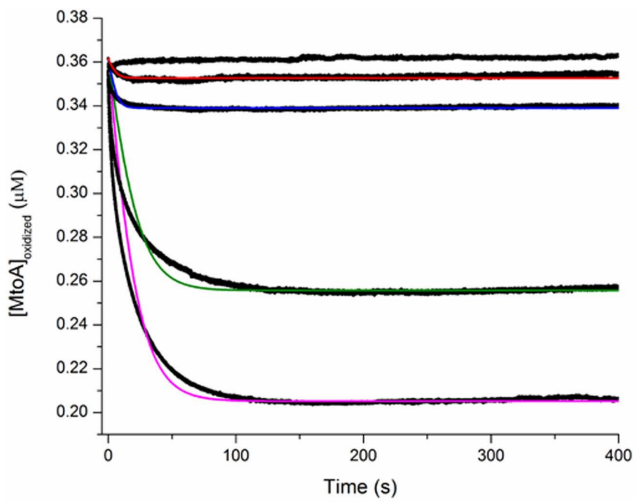

FIGURE 8 | Stopped-flow spectrophotometry results of the oxidation of 0.2 mM Fe(II)-complexes by 0.4 μM MtoA at pH 8 [black dots; from the top to the bottom is MtoA solution without Fe(II)-complexes (control), Fe(II)–EDTA, Fe(II)–NTA, Fe(II)–citrate, and $Fe(II)Cl_2$]. The fitted curves for the kinetic data of MtoA reduction with $Fe(II)Cl_2$ (purple), Fe(II)–citrate (green), Fe(II)–NTA (blue), and Fe(II)–EDTA (red).

DISCUSSION

The increased oxidation of $Fe(II)Cl_2$ by MtoA from pH 7 to pH 9 may be attributed mainly to the expected increased concentration of hydroxylated species of Fe(II), such as $Fe(OH)^+$ and $Fe(OH)_2$. Equilibrium speciation calculations based on Minteqa2 thermodynamic database (Allison et al., 1991) as plotted in **Figure 7B** show the speciation of Fe(II; 18 μM) in 150 mM NaCl solution as a function of pH. Hexaquo ferrous ion is the dominant species in the pH range used in this study, but the amount of $Fe(OH)^+$ increases with increasing pH, especially when pH is greater than 7.5. Both thermodynamic calculations and experimental data indicate that hydroxylated species of Fe(II) have higher reactivity relative to hexaquo Fe(II) (e.g., Wehrli, 1990; Sedlak and Chan, 1997). OH^- ligands in the inner coordination shell of Fe(II) increase its reducing potential and increase its oxidation rate, and therefore could increase reaction to product Fe(III) phases. The concentration change of Fe(II), including hexaquo Fe(II) and $Fe(OH)^+$, at the end of pH-dependent experiments was compared to the initial $Fe(OH)^+$ concentration (**Figure 7C**). It shows that the amount of Fe(II) oxidized by MtoA appears to correlate positively with the initial concentration of $Fe(OH)^+$ from pH 7 to pH 9. Notably, at pH 9, the initial concentration of $Fe(OH)^+$ is expected to be significantly higher than that at pH 8.5, but the amount of Fe(II) oxidized by MtoA only increases slightly. This discrepancy is caused, at least in part, by the fact that the average redox potential of MtoA decreases as pH increases. This decrease is particularly accelerated from pH 8.2 to pH 9.2. The decrease of the redox potential of MtoA from pH 8.2 to pH 9.2 could negatively offset the increase of $Fe(OH)^+$ concentration in the same pH range, which may have the net result of only a slight increase of the Fe(II) oxidized by MtoA at pH 9. These results imply that change of pH in the environments may also have significant influence on Fe(II) speciation, which in turn will strongly affect microorganism-mediated Fe(II) oxidation in their natural settings.

Ligand types impact both reaction rates and equilibrium constants of redox reactions between Fe(II)-complexes and MtoA. The equilibrium speciation calculations showed that the dominant Fe(II) species in the four ligand systems is hexaquo Fe(II), Fe(II)–citrate$^-$, FeOH–NTA$^-$, and Fe–EDTA$^-$, respectively, at a ferrous ion-to-ligand ratio of 1:10. The equilibrium constant for the half electron transfer reactions between Fe(II)–ligand and Fe(III)–ligand (**Table 2**) was calculated using the thermodynamic cycle that involves ligand detachment from Fe(II)–ligand complex,

Table 1 | Kinetic parameters for Fe-complexes oxidation by MtoA at pH 8.

Complex	Rate constants (k, $\mu m^{-1}\,s^{-1}$)	Equilibrium constant (K)	Log K_{ob}[a]	Log K_{calc}[b]
$FeCl_2$	$(6.3 \pm 0.3) \times 10^{-3}$	$(6.5 \pm 0.4) \times 10^{-3}$	−2.22	7.04[c]
Fe–citrate	$(4.1 \pm 0.8) \times 10^{-3}$	$(2.4 \pm 0.4) \times 10^{-3}$	−2.66	−5.46[d]
Fe–NTA	$(2.5 \pm 0.3) \times 10^{-3}$	$(8.3 \pm 1.5) \times 10^{-5}$	−4.125	−0.82
Fe–EDTA	$(1.0 \pm 0.3) \times 10^{-3}$	$(2.1 \pm 1.5) \times 10^{-5}$	−4.959	−1.35

[a] *Log K_{ob} was calculated from the K values estimated from the fitted curve.*

[b] *Log K_{calc} was calculated from theoretical Log K using experimental condition.*

[c] *Calculated assuming in equilibrium with ferrihydrite.*

[d] *Calculated by using thermodynamic data of Fe(III)citrate in Minteqa database.*

Table 2 | Relevant speciation reactions for calculating reaction-free energy at 25°C.

Reaction	Log K ($I = 0$)	Reference
$Fe(III) + e^- \rightarrow Fe(II)$	13.00	Martell and Smith (1995)
$Fe(III) – 3H^+ + 3H_2O = Fe(OH)_3$	−3.96	Cornell and Schwertmann (2003)
$Fe(II) + citrate^{3-} \rightarrow Fe(II)–citrate^-$	5.89	Martell and Smith (1995)
$Fe(III) + citrate^{3-} \rightarrow Fe(III)–citrate$	13.43	Allison et al. (1991), Timberlake (1964)
$Fe(III)OH–NTA^- + e^- \rightarrow Fe(II)OH–NTA^{2-}$	0.82	Wang et al. (2008)
$Fe(III)–EDTA^- + e^- \rightarrow Fe(II)–EDTA^{2-}$	1.35	Wang et al. (2008)

I, ionic strength.

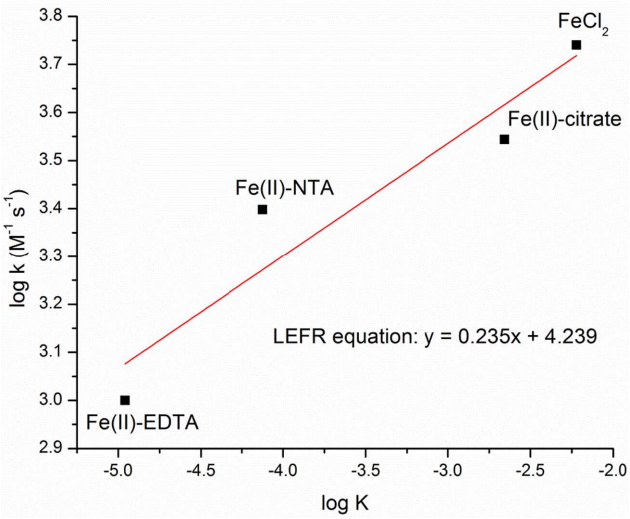

FIGURE 9 | Linear free-energy relationship in Fe(II)-complexes oxidation by MtoA.

Fe(II) oxidation to Fe(III) and Fe(III)–ligand complexation:

$$\begin{array}{ccc} Fe(II)–ligand - e^- & \rightarrow & Fe(III)–ligand \\ \downarrow & & \uparrow \\ - ligand & & + ligand \\ \downarrow & & \uparrow \\ Fe(II) - e^- & \rightarrow & Fe(III) \end{array} \quad (4)$$

Reaction equilibrium constants in this electron transfer pathway are provided in **Table 2**. For the case of $FeCl_2$ at pH 8, it is reasonable to assume that the concentration of produced Fe(III) was controlled by the solubility of FH [$Fe(OH)_3$] because organic ligand was not provided. The equilibrium constant for electron transfer from Fe(II) to FH (log $K = 7.04$; **Table 1**) was then calculated by combining the redox reaction of Fe(II)/Fe(III) and the formation reaction of FH (**Table 2**). The trend of calculated log K is consistent with that of the log K values fitted from the experimental data except for the Fe–citrate case (**Table 1**). The exception is likely because of incomplete understanding of the speciation in the Fe(III)–citrate system; two Fe(III)–citrate speciation models were assembled previously based on literature data (Liu et al., 2001) that involve completely different Fe(III) speciation. In this study, we used the speciation model 1 in Liu et al. (2001), which is also used in the Minteqa2 database (Allison et al., 1991). In this model, the log K for the equation:

$$Fe(III) + citrate^{3-} \rightarrow Fe(III) - citrate \quad (5)$$

is 13.43 Speciation calculations in our Fe(III)–citrate system using Eq. 5, however, suggested that Fe(III)–citrate is not a stable species if Fe(III) is allowed to precipitate as FH. The alternative Fe(III)–citrate speciation model produced the same result. If the FH is used as the end product, then the overall reaction constant (log K) from Fe(II)–citrate to FH at pH 8 is 1.15. With this value, the trend of the calculated equilibrium reaction constants was consistent with the value estimated from the experimental data.

The estimated reaction rate constants (k) and equilibrium constants (K) were positively correlated, establishing a linear free-energy relationship for this system (**Figure 9**). This result implies that it is the reaction-free energy that mainly determined the observed initial reaction rates when it was far away from equilibrium. It is interesting to note that the rate constant order of Fe(II)-complex oxidation, Fe–citrate > Fe–NTA > Fe–EDTA, is the inverse order observed in the reduction of Fe(III) complexes by MtrC and OmcA, where the Fe(III)–ligand reduction rate was Fe(III)–EDTA > Fe(III)–NTA > Fe(III)–citrate (Wang et al., 2008). This is expected from the trend of the activation-free energies for the redox reactions between Fe-complex and proteins (Wang et al., 2008). It is also expected from the relationship of $K = k_f/k_b$, where k_f and k_b are the forward [Fe(II) oxidation] and backward [Fe(III) reduction] reaction rate constants, respectively, and K is the equilibrium constant. Using the estimated K and k, which is k_f here (**Table 1**), the calculated $k_b = k_f/K$, is on the order of Fe–citrate < Fe–NTA < Fe–EDTA, which is consistent with those observed by Wang et al. (2008). These two studies therefore demonstrate the same effect of ligand complexation on the reaction rates for both reduction and oxidation reactions, indicating that complexing ligands will have a significant impact on the reaction rates of microorganism-mediated Fe(II) oxidation in the environments.

In MR-1, MtrAB form a tight protein complex on the OM where MtrB is proposed to serve as a sheath for embedding MtrA and MtrA mediates electron conductance across the OM, while CymA is located in the inner membrane where it recycles quinol back to quinone during extracellular Fe(III) oxide reduction (Hartshorne et al., 2009). In this study, we showed that MtoA was a functional Fe(II)-oxidizing protein with broad redox potential that was more positive than that of MR-1 MtrA, indicating that, like MR-1 MtrA, MtoA is also capable of mediating electron conductance across the OM, but with the direction opposite to that of MR-1 MtrA during

metal-reducing conditions. In addition, ES-1 *mtoAB–cymA* is, to the best of our knowledge, the first example that the genes encoding MtrAB and CymA homologs are clustered together, which suggests that they may belong to the same operon and that their protein products may work together for mediating electron transfer reactions. Based on previous observations and the results from this study, we propose that, similar to MtrAB and CymA in MR-1 cells, MtoAB and $CymA_{ES-1}$ are also located in the OM and inner membrane, respectively, where MtoA is embedded inside MtoB. However, the direction of MtoAB/$CymA_{ES-1}$-mediated electron transfer during Fe(II) oxidation (i.e., outside-in) by ES-1 is opposite to that of MtrABC/CymA-mediated reactions during Fe(III) reduction (i.e., inside-out) by MR-1. We propose that through its heme group(s) exposed to the extracellular environment, MtoA oxidizes Fe(II) directly and then transfers the released electrons across the OM to periplasmic proteins that have yet to be identified, which in turn relay the electrons to $CymA_{ES-1}$. $CymA_{ES-1}$ uses the received electrons to reduce quinone to quinol in the inner membrane (**Figure 10**). Quinol then shuttles the electrons to the redox proteins in the inner membrane for reducing O_2 and/or NAD^+.

PioABC homologs are also found in the Fe(II)-oxidizing bacterium *Gallionella capsiferriformans* (Bonnefoy and Holmes, 2011), indicating the broad involvements of MtoAB/PioAB homologs in microbial Fe(II) oxidation. It should be noted that a group of proteins that show no homologous to MtoAB/CymAES-1 have recently been proposed to be involved in Fe(II) oxidation by the bacterium *Mariprofundus ferrooxydans* PV-1 and homologs of these proteins are also present in ES-1 (Singer et al., 2011). These results emphasize the uncertainty that remains regarding the electron transfer pathway(s) utilized by ES-1 for Fe(II) oxidation and the need for additional research.

In summary, an *mtoAB–cymA* gene cluster is found in the genome of the Fe(II)-oxidizing bacterium *S. lithotrophicus* ES-1. Protein purification and characterization results confirm that MtoA is a decaheme *c*-type cytochrome and oxidizes soluble Fe(II). MtoA-mediated Fe(II) oxidation is pH- and Fe(II)-complexing ligand-dependent. It is proposed that, together, MtoAB and $CymA_{ES-1}$ form a pathway for electron conductance from extracellular Fe(II) to the quinone pool in the bacterial inner membrane.

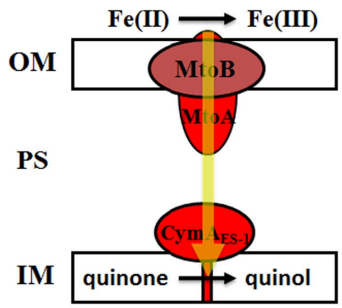

FIGURE 10 | The proposed roles of MtoAB and $CymA_{ES-1}$ in *Sideroxydans lithotrophicus* ES-1-mediated extracellular Fe(II) oxidation. Decaheme *c*-Cyt MtoA, which is inserted into the porin-like, outer membrane (OM) protein MtoB, oxidizes Fe(II) directly on the bacterial surface and transfers the released electrons across the OM to the periplasmic proteins that have yet to be identified. The periplasmic proteins relay the electrons through the periplasm (PS) to the tetraheme *c*-Cyt $CymA_{ES-1}$. $CymA_{ES-1}$, a homolog of NapC/NrfH family of quinol dehydrogenase that is located in the cytoplasmic or inner membrane (IM), reduces quinone to quinol. *c*-Cyts are labeled in red and direction of electron transfer is indicated by a yellow arrow.

ACKNOWLEDGMENTS

This research was supported by the Subsurface Biogeochemical Research program (SBR)/Office of Biological and Environmental Research (BER), U.S. Department of Energy (DOE), and is a contribution of the Pacific Northwest National Laboratory (PNNL) Scientific Focus Area. A portion of the research was performed using EMSL, a national scientific user facility sponsored by DOE-BER and located at PNNL. PNNL is operated for DOE by Battelle under contract DE-AC05-76RLO 1830.

REFERENCES

Allison, J. D., Brown, D. S., and Novo-Gradac, K. J. (1991). *MINITEQ2//PRODEFA2, A Geochemical Assessment Model for Environmental Systems*, 3 Edn. Washington, DC: US Environmental Protection Agency.

Appia-Ayme, C., Guiliani, N., Ratouchniak, J., and Bonnefoy, V. (1999). Characterization of an operon encoding two *c*-type cytochromes, an aa(3)-type cytochrome oxidase, and rusticyanin in *Thiobacillus ferrooxidans* ATCC 33020. *Appl. Environ. Microbiol.* 65, 4781–4787.

Asher, W. B., and Bren, K. L. (2010). A heme fusion tag for protein affinity purification and quantification. *Protein Sci.* 19, 1830–1839.

Bonnefoy, V., and Holmes, D. S. (2011). Genomic insights into microbial iron oxidation and iron uptake strategies in extremely acidic environments. *Environ. Microbiol.* doi:10.1111/j.1462-2920.2011.02626

Castelle, C., Guiral, M., Malarte, G., Ledgham, F., Leroy, G., Brugna, M., and Giudici-Orticoni, M. T. (2008). A new iron-oxidizing/O_2-reducing supercomplex spanning both inner and outer membranes, isolated from the extreme acidophile *Acidithiobacillus ferrooxidans*. *J. Biol. Chem.* 283, 25803–25811.

Clarke, T. A., Edwards, M. J., Gates, A. J., Hall, A., White, G. F., Bradley, J., Reardon, C. L., Shi, L., Beliaev, A. S., Marshall, M. J., Wang, Z. M., Watmough, N. J., Fredrickson, J. K., Zachara, J. M., Butt, J. N., and Richardson, D. J. (2011). Structure of a bacterial cell surface decaheme electron conduit. *Proc. Natl. Acad. Sci. U.S.A.* 108, 9384–9389.

Cornell, R. M., and Schwertmann, U. (2003). *The Iron Oxides: Structure, Properties, Reactions, Occurrences and Uses*. Weinheim: Wiley-VCH.

Coursolle, D., and Gralnick, J. A. (2010). Modularity of the Mtr respiratory pathway of *Shewanella oneidensis* strain MR-1. *Mol. Microbiol.* 77, 995–1008.

Croal, L. R., Jiao, Y., and Newman, D. K. (2007). The *fox* operon from *Rhodobacter* strain SW2 promotes phototrophic Fe(II) oxidation in *Rhodobacter capsulatus* SB1003. *J. Bacteriol.* 189, 1774–1782.

Emerson, D., Fleming, E. J., and Mcbeth, J. M. (2010). Iron-oxidizing bacteria: an environmental and genomic perspective. *Annu. Rev. Microbiol.* 64, 561–583.

Emerson, D., and Moyer, C. (1997). Isolation and characterization of novel iron-oxidizing bacteria that grow at circumneutral pH. *Appl. Environ. Microbiol.* 63, 4784–4792.

Emerson, D., Rentz, J. A., Lilburn, T. G., Davis, R. E., Aldrich, H., Chan, C., and Moyer, C. L. (2007). A novel lineage of proteobacteria involved in formation of marine Fe-oxidizing microbial mat communities. *PLoS ONE* 2, e667. doi:10.1371/journal.pone.0000667

Eng, J. K., McCormack, A. L., and Yates Iii, J. R. (1994). An approach to correlate tandem mass spectral data of peptides with amino acid sequences in a protein database. *J. Am. Soc. Mass Spectrom.* 5, 976–989.

Fredrickson, J. K., Romine, M. F., Beliaev, A. S., Auchtung, J. M., Driscoll, M. E., Gardner, T. S., Nealson, K. H., Osterman, A. L., Pinchuk, G., Reed, J. L., Rodionov, D. A., Rodrigues, J. L., Saffarini, D. A., Serres, M. H., Spormann, A. M., Zhulin, I. B., and Tiedje, J. M. (2008). Towards environmental systems biology of *Shewanella*. *Nat. Rev. Microbiol.* 6, 592–603.

Gralnick, J. A., Vali, H., Lies, D. P., and Newman, D. K. (2006). Extracellular respiration of dimethyl sulfoxide by *Shewanella oneidensis* strain MR-1. *Proc. Natl. Acad. Sci. U.S.A.* 103, 4669–4674.

Hartshorne, R. S., Reardon, C. L., Ross, D., Nuester, J., Clarke, T. A., Gates, A. J., Mills, P. C., Fredrickson, J. K., Zachara, J. M., Shi, L., Beliaev, A. S., Marshall, M. J., Tien, M., Brantley, S., Butt, J. N., and Richardson, D. J. (2009). Characterization of an electron conduit between bacteria and the extracellular environment. *Proc. Natl. Acad. Sci. U.S.A.* 106, 22169–22174.

Jiao, Y., and Newman, D. K. (2007). The *pio* operon is essential for phototrophic Fe(II) oxidation in *Rhodopseudomonas palustris* TIE-1. *J. Bacteriol.* 189, 1765–1773.

Liu, C. G., Zachara, J. M., Gorby, Y. A., Szecsody, J. E., and Brown, C. F. (2001). Microbial reduction of Fe(III) and sorption/precipitation of Fe(II) on *Shewanella putrefaciens* strain CN32. *Environ. Sci. Technol.* 35, 1385–1393.

Livesay, E. A., Tang, K., Taylor, B. K., Buschbach, M. A., Hopkins, D. F., Lamarche, B. L., Zhao, R., Shen, Y., Orton, D. J., Moore, R. J., Kelly, R. T., Udseth, H. R., and Smith, R. D. (2007). Fully automated four-column capillary LC-MS system for maximizing throughput in proteomic analyses. *Anal. Chem.* 80, 294–302.

Lower, B. H., Yongsunthon, R., Shi, L., Wildling, L., Gruber, H. J., Wigginton, N. S., Reardon, C. L., Pinchuk, G. E., Droubay, T. C., Boily, J. F., and Lower, S. K. (2009). Antibody recognition force microscopy shows that outer membrane cytochromes OmcA and MtrC are expressed on the exterior surface of *Shewanella oneidensis* MR-1. *Appl. Environ. Microbiol.* 75, 2931–2935.

Martell, R. E., and Smith, R. M. (1995). *Critical Stability Constants of Metal Complexes Database.* Gaithersburg, MD: NIST Standard Reference Database.

Reardon, C. L., Dohnalkova, A. C., Nachimuthu, P., Kennedy, D. W., Saffarini, D. A., Arey, B. W., Shi, L., Wang, Z., Moore, D., Mclean, J. S., Moyles, D., Marshall, M. J., Zachara, J. M., Fredrickson, J. K., and Beliaev, A. S. (2010). Role of outer-membrane cytochromes MtrC and OmcA in the biomineralization of ferrihydrite by *Shewanella oneidensis* MR-1. *Geobiology* 8, 56–68.

Richardson, D. J. (2000). Bacterial respiration: a flexible process for a changing environment. *Microbiology* 146(Pt 3), 551–571.

Ross, D. E., Flynn, J. M., Baron, D. B., Gralnick, J. A., and Bond, D. R. (2011). Towards electrosynthesis in *Shewanella*: energetics of reversing the mtr pathway for reductive metabolism. *PLoS ONE* 6, e16649. doi:10.1371/journal.pone.0016649

Ross, D. E., Ruebush, S. S., Brantley, S. L., Hartshorne, R. S., Clarke, T. A., Richardson, D. J., and Tien, M. (2007). Characterization of protein-protein interactions involved in iron reduction by *Shewanella oneidensis* MR-1. *Appl. Environ. Microbiol.* 73, 5797–5808.

Sedlak, D. L., and Chan, P. G. (1997). Reduction of hexavalent chromium by ferrous iron. *Geochim. Cosmochim. Acta* 61, 2185–2192.

Shi, L., Belchik, S. M., Wang, Z., Kennedy, D. W., Dohnalkova, A. C., Marshall, M. J., Zachara, J. M., and Fredrickson, J. K. (2011). Identification and characterization of UndAHRCR-6, an outer membrane endecaheme *c*-type cytochrome of *Shewanella* sp. strain HRCR-6. *Appl. Environ. Microbiol.* 77, 5521–5523.

Shi, L., Deng, S., Marshall, M. J., Wang, Z., Kennedy, D. W., Dohnalkova, A. C., Mottaz, H. M., Hill, E. A., Gorby, Y. A., Beliaev, A. S., Richardson, D. J., Zachara, J. M., and Fredrickson, J. K. (2008). Direct involvement of type II secretion system in extracellular translocation of *Shewanella oneidensis* outer membrane cytochromes MtrC and OmcA. *J. Bacteriol.* 190, 5512–5516.

Shi, L., Lin, J. T., Markillie, L. M., Squier, T. C., and Hooker, B. S. (2005). Overexpression of multi-heme C-type cytochromes. *BioTechniques* 38, 297–299.

Shi, L., Potts, M., and Kennelly, P. J. (1998). The serine, threonine, and/or tyrosine-specific protein kinases and protein phosphatases of prokaryotic organisms: a family portrait. *FEMS Microbiol. Rev.* 22, 229–253.

Shi, L., Richardson, D. J., Wang, Z., Kerisit, S. N., Rosso, K. M., Zachara, J. M., and Fredrickson, J. K. (2009). The roles of outer membrane cytochromes of *Shewanella* and *Geobacter* in extracellular electron transfer. *Environ. Microbiol. Rep.* 1, 220–227.

Shi, L., Squier, T. C., Zachara, J. M., and Fredrickson, J. K. (2007). Respiration of metal (hydr)oxides by *Shewanella* and *Geobacter*: a key role for multihaem c-type cytochromes. *Mol. Microbiol.* 65, 12–20.

Shi, L., and Zhang, W. (2004). Comparative analysis of eukaryotic-type protein phosphatases in two streptomycete genomes. *Microbiology* 150, 2247–2256.

Singer, E., Emerson, D., Webb, E. A., Barco, R. A., Kuenen, J. G., Nelson, W. C., Chan, C. S., Comolli, L. R., Ferriera, S., Johnson, J., Heidelberg, J. F., and Edwards, K. J. (2011). *Mariprofundus ferrooxydans* PV-1 the first genome of a marine Fe(II) oxidizing *Zetaproteobacterium*. *PLoS ONE* 6, e25386. doi:10.1371/journal.pone.0025386

Stookey, L. (1970). Ferrozine-a new spectrophotometric reagent for iron. *Anal. Chem.* 42, 779–781.

Thomas, P. E., Ryan, D., and Levin, W. (1976). An improved staining procedure for the detection of the peroxidase activity of cytochrome P-450 on sodium dodecyl sulfate polyacrylamide gels. *Anal. Biochem.* 75, 168–176.

Timberlake, C. F. (1964). Iron-malate + iron-citrate complexes. *J. Chem. Soc.* 5078–5085.

Wang, Z. M., Liu, C. X., Wang, X. L., Marshall, M. J., Zachara, J. M., Rosso, K. M., Dupuis, M., Fredrickson, J. K., Heald, S., and Shi, L. (2008). Kinetics of reduction of Fe(III) complexes by outer membrane cytochromes MtrC and OmcA of *Shewanella oneidensis* MR-1. *Appl. Environ. Microbiol.* 74, 6746–6755.

Wehrli, B. (1990). "Redox reactions of metal ions at mineral surfaces," in *Aquatic Chemcial Kinetics: Reaction Rates of Processes in Natural Waters*, ed. W. Stumm (Wiley), 311–336.

Yang, F., Bogdanov, B., Strittmatter, E. F., Vilkov, A. N., Gritsenko, M., Shi, L., Elias, D. A., Ni, S., Romine, M., Paša-Tolic, L., Lipton, M. S., and Smith, R. D. (2005). Characterization of purified *c*-type heme-containing peptides and identification of *c*-type heme-attachment sites in *Shewanella oneidensis* cytochromes using mass spectrometry. *J. Proteome Res.* 4, 846–854.

Yarzabal, A., Brasseur, G., Ratouchniak, J., Lund, K., Lemesle-Meunier, D., DeMoss, J. A., and Bonnefoy, V. (2002). The high-molecular-weight cytochrome *c* Cyc2 of *Acidithiobacillus ferrooxidans* is an outer membrane protein. *J. Bacteriol.* 184, 313–317.

Conflict of Interest Statement: The authors declare that the research was conducted in the absence of any commercial or financial relationships that could be construed as a potential conflict of interest.

Received: 22 October 2011; accepted: 23 January 2012; published online: 08 February 2012.

Citation: Liu J, Wang Z, Belchik SM, Edwards MJ, Liu C, Kennedy DW, Merkley ED, Lipton MS, Butt JN, Richardson DJ, Zachara JM, Fredrickson JK, Rosso KM and Shi L (2012) Identification and characterization of MtoA: a decaheme c-type cytochrome of the neutrophilic Fe(II)-oxidizing bacterium Sideroxydans lithotrophicus ES-1. Front. Microbio. ***3****:37. doi: 10.3389/fmicb.2012.00037*

This article was submitted to Frontiers in Microbiological Chemistry, a specialty of Frontiers in Microbiology.

Copyright © 2012 Liu, Wang, Belchik, Edwards, Liu, Kennedy, Merkley, Lipton, Butt, Richardson, Zachara, Fredrickson, Rosso and Shi. This is an open-access article distributed under the terms of the Creative Commons Attribution Non Commercial License, which permits non-commercial use, distribution, and reproduction in other forums, provided the original authors and source are credited.

frontiers in
MICROBIOLOGY

ORIGINAL RESEARCH ARTICLE
published: 02 April 2012
doi: 10.3389/fmicb.2012.00118

Mineralogy of iron microbial mats from Loihi Seamount

Brandy M. Toner[1]*, Thelma S. Berquó[2,3], F. Marc Michel[4], Jeffry V. Sorensen[1], Alexis S. Templeton[5] and Katrina J. Edwards[6,7]

[1] *Department of Soil, Water, and Climate, University of Minnesota-Twin Cities, St. Paul, MN, USA*
[2] *Department of Earth Sciences, Institute for Rock Magnetism, University of Minnesota-Twin Cities, Minneapolis, MN, USA*
[3] *Physics Department, Concordia College, Moorhead, MN, USA*
[4] *SLAC National Accelerator Laboratory, Department of Geological and Environmental Sciences, Stanford University, Stanford, CA, USA*
[5] *Department of Geological Sciences, University of Colorado-Boulder, Boulder, CO, USA*
[6] *Department of Biological Sciences, University of Southern California, Los Angeles, CA, USA*
[7] *Department of Earth Sciences, University of Southern California, Los Angeles, CA, USA*

Edited by:
David Emerson, Bigelow Laboratory for Ocean Sciences, USA

Reviewed by:
John Stolz, Duquesne University, USA
Jeffrey G. Catalano, Washington University in St. Louis, USA

****Correspondence:***
Brandy M. Toner, Department of Soil, Water, and Climate, University of Minnesota-Twin Cities, 1991 Upper Buford Circle, 439 Borlaug Hall, St. Paul, MN, USA.
e-mail: toner@umn.edu

Extensive mats of Fe oxyhydroxides and associated Fe-oxidizing microbial organisms form in diverse geochemical settings – freshwater seeps to deep-sea vents – where ever opposing Fe(II)-oxygen gradients prevail. The mineralogy, reactivity, and structural transformations of Fe oxyhydroxides precipitated from submarine hydrothermal fluids within microbial mats remains elusive in active and fossil systems. In response, a study of Fe microbial mat formation at the Loihi Seamount was conducted to describe the physical and chemical characteristics of Fe-phases using extended X-ray absorption fine structure spectroscopy, powder X-ray diffraction, synchrotron radiation X-ray total scattering, low-temperature magnetic measurements, and Mössbauer spectroscopy. Particle sizes of 3.5–4.6 nm were estimated from magnetism data, and coherent scattering domain (CSD) sizes as small as 1.6 nm are indicated by pair distribution function (PDF) analysis. Disorder in the nanostructured Fe-bearing phases results in limited intermediate-range structural order: less than that of standard two-line ferrihydrite (Fh), except for the Pohaku site. The short-range ordered natural Fh (Fh_{SRO}) phases were stable at 4˚C in the presence of oxygen for at least 1 year and during 400˚C treatment. The observed stability of the Fh_{SRO} is consistent with magnetic observations that point to non-interacting nanoparticles. PDF analyses of total scattering data provide further evidence for Fh_{SRO} particles with a poorly ordered silica coating. The presence of coated particles explains the small CSD for the mat minerals, as well as the stability of the minerals over time and against heating. The mineral properties observed here provide a starting point from which progressively older and more extensively altered Fe deposits may be examined, with the ultimate goal of improved interpretation of past biogeochemical conditions and diagenetic processes.

Keywords: EXAFS, total X-ray scattering, Mössbauer, magnetism, microbial mat, Loihi Seamount, biomineral, nanoparticle

INTRODUCTION

Iron (Fe) microbial mats form in opposing iron and oxygen gradients in a wide variety of settings (Emerson and Revsbech, 1994; Chan et al., 2004; Rentz et al., 2007; Druschel et al., 2008; Edwards et al., 2011). The physical and chemical properties of the Fe-bearing phases will determine the biogeochemical reactivity of the minerals within the mats (Ekstrom et al., 2010; Boland et al., 2011; Hansel et al., 2011). Yet the crystallinity, local Fe coordination environment, and available reactive sites of the minerals are difficult to measure, and the structure or continuum of structures that compose one of the most common Fe oxyhydroxides, ferrihydrite (Fh), is an active topic of research and scientific controversy today (Michel et al., 2007a, 2010; Penn, 2007; Manceau, 2009, 2011; Pinney et al., 2009; Maillot et al., 2011), as it has been for more than two decades (Campbell, 1991; Drits et al., 1993; Manceau and Drits, 1993; Waychunas et al., 1996; Jambor and Dutrizac, 1998; Janney et al., 2000; Schwertmann et al., 2004). Poorly crystalline iron oxyhydroxides are often difficult to characterize due to nanometer particle dimensions (Michel et al., 2007a; Hochella Jr. et al., 2008) and a large number of polymorphs (Navrotsky et al., 2008). In addition, structural and compositional variability and complexity is intrinsic to Fe oxyhydroxides formed in settings such as microbial biofilms (Edwards et al., 2003; Chan et al., 2004; Toner et al., 2009) or in the presence of strongly sorbing inorganic and organic ligands (Cornell and Schwertmann, 1979; Waychunas et al., 1996; Rose et al., 1997; Vilge-Ritter et al., 1999; Doelsch et al., 2003; Mikutta, 2011). Considering that the gold standard measurement for mineralogy – powder X-ray diffraction (XSD) – relies on long-range structural order, it is not surprising that Fe mineralogy of microbial mats, often formed in the presence of abundant inorganic ligands and microbial cell surfaces and exudates, remains elusive. One viable strategy for describing Fe microbial mat mineralogy is to measure a suite of fundamental properties: (1) short-range structural order and valence state; (2) degree of structural defects relative to standard synthetic minerals; (3) degree of particle interaction and aggregation;

(4) distribution of particle dimensions and extent of structural coherence; and (5) stability and recrystallization as a function of time and temperature.

In this context, the mineralogy of Loihi Seamount Fe microbial mats was examined as a function of temperature, water depth, and bulk aqueous geochemistry. Loihi Seamount is a seismically active submarine volcano and emerging Hawaiian Island (Klein, 1982; DeCarlo et al., 1983). Hydrothermal venting at Loihi produces opposing Fe and oxygen gradients (Glazer and Rouxel, 2009) and supports abundant microbial life including Fe-oxidizing bacteria (Emerson and Moyer, 2002). Iron mat formation at Loihi is pervasive, occurring at a range of temperatures (0–60°C), in diverse settings (ultra-diffuse regional venting at 5000 m to focused venting as shallow as 1116 m), and microbial activity in the mats has been demonstrated (Moyer et al., 1994, 1995; Emerson and Moyer, 2002; Edwards et al., 2011). Filamentous, non-filamentous, tubular, and branching microbial structures in the mats that form near venting are encrusted with Fe minerals, and biological Fe oxidation contributes approximately 60% of total Fe oxidation (Karl et al., 1988, 1989; Emerson and Moyer, 2002). Vent fluids near the summit of Loihi are enriched in carbon dioxide, ammonium, silicon (Si), Fe, and manganese (Mn) (Sedwick et al., 1992; Wheat et al., 2000). The goal of this research is to describe the physical and chemical properties of the minerals formed in Loihi Fe microbial mats. To accomplish this, we used synchrotron radiation X-ray absorption spectroscopy, X-ray fluorescence microspectroscopy, and X-ray total scattering, as well as Mössbauer spectroscopy and low-temperature magnetic measurements to identify the factors contributing to mat mineralogy. We also examine whether biogeochemical factors that control mineral formation influence only the initial precipitation of Fe oxyhydroxides or their long-term properties and preservation.

MATERIALS AND METHODS

LOIHI MAT COLLECTION AND STORAGE

Iron microbial mats at the Loihi Seamount were collected during research cruises in 2006 (R/V Melville), 2007 (R/V Kilo Moana), and 2008 (R/V Thompson) as part of a National Science Foundation Fe Microbial Observatory (FeMO) project. General characteristics of each site are summarized in **Table 1**. Sites represent the range of naturally occurring characteristics of the vents that occur at Loihi.

The remotely operated vehicle *JASON2* was used to collect mats with scoops and suction samplers. Typically the samples collected by slurp suction sampling experience a vigorous mixing of a large volume (several liters) of mat material, whereas consolidated mats collected in polycarbonate scoops retain some of their structural cohesiveness. Once shipboard, the loosely aggregated, well-mixed mat "flocs" were sub-sampled into 15 mL sterile tubes and either: (1) stored at 4°C and referred to as "fresh" or "aged" mat samples; or (2) frozen at −20°C and referred to as "frozen" mat samples. In the laboratory, a subset of these flocculent mat samples were defrosted, rinsed with purified water to remove sea salts, and dried at 40°C: these samples are referred to as (3) "dry" mat samples. At the deepest, very low-temperature diffuse venting site Ula Nui, approximately the top 5–10 cm of layered Fe–Mn microbial mats were collected in scoop-samplers and were stored fresh and frozen as fully (4) "intact" map samples. All of the mat samples examined for this study are reported in **Table 1**. The term "fresh" mat is applied to samples that were stored at 4°C and analyzed within 1 month of seafloor recovery. The term "aged" mat is applied to samples stored at 4°C and analyzed after 0.5 to greater than 1 year after seafloor recovery.

X-RAY ABSORPTION SPECTROSCOPY

Iron K-edge X-ray absorption microspectroscopy

X-ray microprobe measurements were performed for three types of Loihi mat samples: (a) intact surface crust from Ula Nui; (b) fresh mat flocs; and (c) 4°C aged mat flocs.

One intact surface crust of an Fe–Mn layered mat from Ula Nui was prepared for X-ray microprobe element mapping by slicing a 3-mm thick by 8 cm wide by 4 cm tall section of a sample frozen at −20°C. The slice was then positioned into an anaerobic aluminum sample holder with thin mylar windows that was

Table 1 | Description of the Loihi Seamount vent areas and vent fluid properties.

Area	Description	Depth (m)	T_{max} (°C)[a]		pH_{max}		$[Si]_{max}$[b]		$[P]_{max}$		$[Fe]_{max}$	
			2006	2007	2006	2007	2006	2007	2006	2007	2006	2007
Ula Nui	Ultra-diffuse, cold, base of seamount	4988	1.75	1.75			–	–	–	–	127[c]	–
Naha	Extinct, rim of Pele's Pit	1325	<2.8		–	–	–	–	–	–	–	–
Spillway	Active, warm, rim of Pele's Pit	1272	54.0	55.0	6.37	6.72	4664	2599	9.1	3.1	726.7	354.7
Tower	Active, warm, Pele's Pit	1304	51.0	50.0	6.01	6.29	2966	3092	6.2	4.8	557.8	407.1
Hiolo	Active, warm, Pele's Pit	1302	51.0	52.0	5.94	6.69	3830	4131	6	6.1	568.8	577.8
Lohiau	Active, cool, Pele's Pit site, frequently sampled	1174	22.0	24.5	6.21	6.94	1558	675	2.5	1.2	234.7	68.3
Hiolo Ridge	Active, warm, rim of Pele's Pit	1116	14.6	–	–	–	–	–	–	–	224	–
Pohaku	Active, warm, rim of Pele's pit, not previously sampled	1180	–	26.5	–	7.32	–	2210	–	4.5	–	796.4

[a] *Data from Glazer and Rouxel (2009).*

[b] *All concentrations in micro molar.*

[c] *Data from Edwards et al. (2011).*

continuously purged with helium at room temperature. Three different regions of the slice were then mapped – "R1," a 200-μm × 200-μm region at the very top surface of the mat, "R2," a 1600-μm × 200-μm region located 400 μm below the surface of the mat, and then "R3," a final 200 μm × 200 μm region in the middle of the mat. Each map area was sequentially raster scanned at three energies across the Mn K-edge (6545, 6550, and 6560 eV) and then three energies across the Fe K-edge (7120, 7126, and 7133 eV) at BL 2-3 at the Stanford Synchrotron Radiation Lightsource using a Si 220 phi = 0 monochromator detuned 30% and a focused spot size of 2 μm × 2 μm. Full X-ray fluorescence spectra were collected for each pixel with a 100-ms dwell time using a three-element germanium detector. A matrix of predicted Fe(II) versus Fe(III) and Mn(II) versus Mn(IV) fluorescence yields at each incident energy was generated from the Fe X-ray absorption near-edge structure (XANES) spectra of a reduced basalt glass [88% Fe(II)] versus the 100% Fe(III)-oxide standard, and the Mn XANES spectra of $Mn^{2+}_{(aq)}$ [100% Mn(II)] and δ-MnO_2 [100% Mn(IV)] standards (e.g., Templeton et al., 2009). The resulting I_0-normalized, dead time-corrected element distribution, and oxidation–reduction maps were generated using Microanalysis Toolkit (Webb, 2006). Iron and Mn K-edge XANES spectra were also collected from specific spots in each map and analyzed using SixPack to confirm the oxidation states of Fe and Mn by comparison to our model compound library.

X-ray microprobe measurements were also conducted among a random assortment of disseminated mat particle aggregates (flocs) to determine Fe speciation. These fresh and aged Loihi mat flocs (Lohiau, Pohaku, Naha, and Ula Nui) were deposited on polycarbonate membranes (0.2 μm pore size) and rinsed with purified water using a glass filtration tower (MilliPore) and hand vacuum pump. Mat samples were analyzed at room temperature on the membrane with no further processing using a published method (Toner et al., 2009). Briefly, microprobe Fe extended X-ray absorption fine structure (EXAFS) spectra were collected at the Advanced Light Source on beamline 10.3.2 with a seven-element germanium detector in fluorescence mode (Marcus et al., 2004). The monochromator energy calibration was set with Fe foil at 7110.75 eV. The spectra were collected to a reciprocal space (k) value of 14.4 ($Å^{-1}$) whenever possible. Individual scans collected at the same sample location were examined for changes in line-shape and peak position, and no photon-induced sample damage was observed. Spectra were dead time-corrected, energy calibrated, and averaged using custom beamline software (Marcus et al., 2004) and converted to k-space using SixPack (Webb, 2005). No over-absorption corrections were applied to EXAFS data.

Bulk iron K-edge X-ray absorption spectroscopy

Bulk Fe EXAFS spectra were collected for two types of Loihi mats: (1) frozen samples stored and analyzed under inert gas; and (2) "dry" samples that were frozen shipboard, and defrosted, rinsed, dried, and analyzed in ambient atmosphere.

Synchrotron-based Fe K-edge EXAFS spectra for two bulk mat flocs (Spillway and Hiolo mats) were collected from 7000 to 8000 eV on beamline 11-2 at the Stanford Synchrotron Radiation Lightsource using a Si(220) phi = 0 monochromator crystal detuned 30% for harmonic rejection, and a Lytle detector for fluorescence measurements. All data reduction including averaging, dead time correction, and post-edge normalization was conducted using SixPack to generate background-subtracted, k^3-weighted EXAFS spectra. Spectra were calibrated using the first inflection of a Fe^0 foil at 7112 eV. These three mat samples were analyzed in a hydrated state after being thawed and loaded into a 2-mm × 20-mm slit in a 1-mm mylar holder sealed with kapton tape in an anaerobic chamber. The mylar sample holder was maintained under anaerobic conditions on BL 11-2 by continuously flushing nitrogen through a specialized sample box attached to the fluorescence detector.

Several dry Loihi mat samples (Ula Nui-A, Ula Nui-B, Lohiau A, Spillway A, and BT37) were applied to double-sided adhesive in thin layers. Mat samples were analyzed at room temperature with no further processing. Bulk Fe EXAFS were collected at the Advanced Photon Source on beamline 20-BM in transmission mode. The monochromator energy was set with Fe foil at 7110.75 eV. The spectra were collected to a reciprocal space (k) value of greater than 15 ($Å^{-1}$). Individual scans were examined for changes in line-shape and peak position, and no photon-induced sample damage was observed. Spectra were dead time-corrected, energy calibrated, averaged, and converted to k-space using Athena (Ravel and Newville, 2005). The spectra were compared to reference Fe oxyhydroxides (goethite and two-line Fh) synthesized using published methods (Cornell and Schwertmann, 2003), and sample preparation and data collection were identical to that described for the dry Loihi mat samples.

Reference Fe EXAFS spectra for this data set include goethite, six-line Fh, two-line Fh, lepidocrocite, hematite, siderite, green rust sulfate, jarosite, marcasite, magnetite, vivianite, and Fe(III)–phosphate (Hansel et al., 2003), as well as Fe-smectite (O'Day et al., 2004), additional Fe-silicates such as basalt, olivine, pyroxene, chlorite, Fe-bearing serpentine and talc group minerals (Mayhew et al., 2011), and a biogenic Fe oxyhydroxide formed during a seafloor sulfide incubation study (Toner et al., 2009).

SYNCHROTRON RADIATION X-RAY DIFFRACTION AND TOTAL SCATTERING

High-energy X-ray total scattering experiments were conducted at beamline 11-ID-B of the Advanced Photon Source, Argonne National Laboratory. Selected dry mat samples (Ula Nui-A/B, Lohiau A, Spillway A, and BT37) were packed into ∼1 mm O.D. polyimide (Kapton) capillaries and the scattered intensity from the samples was collected at ambient temperature with an amorphous-silicon-based flat-panel detector system (Perkin Elmer) mounted orthogonal to the incident beam path. For synchrotron radiation X-ray diffraction (XRD; SR-XRD) measurements the X-ray energy was fixed at ∼58 keV (λ = 0.2128 Å) and the sample-to-detector distance was optimized to cover d-spacings ranging from ∼0.5 to 8.5 Å. For pair distribution function (PDF) experiments the X-ray energy was fixed at ∼90.5 keV (λ = 0.13702 Å) and a sample-to-detector distance of ∼21.5 cm was chosen. This experimental geometry yielded scattering data with a maximum usable Q-range of 30 $Å^{-1}$ (where $Q = 4\pi\sin\theta\cdot\lambda^{-1}$ is the magnitude of the scattering vector or momentum transfer). The total exposure time for the blank (i.e., empty capillary) was 3200 s and each sample was 1200 s. Fit2D (Hammersley et al., 1996) was

used to convert two-dimensional data to one-dimensional intensity versus scattering angle (2θ). The experimental total scattering structure function $S(Q)$, reduced structure function $f(Q)$, and PDF were obtained using PDFgetX2 (Qiu et al., 2004). The data were corrected for parasitic background scattering and inelastic contributions (e.g., Compton scattering) as well as those corrections unique to image-plate geometry (Chupas et al., 2003). A Lorch modification function (Lorch, 1969) was applied.

The PDF, or $G(r)$, is the Fourier transform of the reduced structure function and has been described in detail elsewhere (Guinier, 1963; Egami and Billinge, 2003). In general, peaks in the PDF occur at characteristic distances separating pairs of atoms, and thus the PDF is an averaged representation of structure. As discussed below, additional information such as the scattering domain size can be extracted from the attenuation in peak intensities with increasing r (see Gilbert, 2008 for review). In this study, the maximum coherent scattering domain (CSD) size for the samples and references is estimated from the PDFs and is reported with an error of ±3 Å (Hall et al., 2000). Structural information was extracted directly from the experimental PDFs by fitting the features with Gaussian functions (PeakFit v4.12). At shorter length scales (<∼2.5 Å) the peak positions yield actual average bond lengths (e.g., Si-O, Fe-O). At longer length scales the PDF becomes more complicated because peaks from different origins overlap. As such, the full width at half maximum (FWHM) of the Gaussian functions were varied together in order to minimize the number of free parameters. In addition, the positions of peaks at 3.03 and 3.44 Å (representing edge- and corner-sharing Fe polyhedra, respectively, as described below) were fixed during fitting of the natural samples in order to further constrain the number of degrees of freedom. As discussed below, the presence of at least edge-sharing Fe polyhedra is further justified by the EXAFS results for these samples.

Synthetic two-line Fh and amorphous silica were used as references. Ferrihydrite was precipitated at room temperature by the rapid hydrolysis of 0.1 M $Fe(NO_3)_3$ to pH 7 with 2 M NaOH. Amorphous SiO_2 (*am*-SiO_2) was precipitated by hydrolysis of tetraethyl orthosilicate [$Si(OC_2H_5)_4$ (Fisher Scientific)] with 12 M HCl according to the procedure described by Hirata et al. (2003).

MAGNETISM

A commercial SQUID magnetometer (MPMS-XL-Quantum Design) was used to measure induced magnetization curves [zero field cooling (ZFC) and field cooling (FC)], hysteresis loops, room temperature saturation isothermal remanent magnetization (RTSIRM), and AC susceptibility as a function of temperature, and frequency (Institute for Rock Magnetism, University of Minnesota). ZFC induced magnetization curves were obtained by cooling the samples in zero field from 300 to 2 K, then the magnetization was recorded as temperature increases in a small applied field ($B = 5$ mT). For field cooled induced magnetization curves, the sample is cooled to 2 K in a 5-mT applied field, and magnetization is measured as temperature increases. Hysteresis loops were obtained by using maximum applied fields up to 5 T at temperatures from 2 to 300 K. RTSIRM curves were obtained by applying a field of 2.5 T at room temperature, and measuring the remanent magnetization upon cooling to 10 K, and then warming back to 300 K. The AC susceptibility curves are measured for variable frequencies (1–1000 Hz) in the temperature range 2–300 K.

To estimate the particle size using ZFC data, the T_P temperatures were identified directly from ZFC curves and the particle volume was obtained by the Néel–Arrhenius Law:

$$\tau = \tau_0 e^{\frac{KV}{k_B T}}$$

where $T = T_P$, τ is the measuring time, τ_0 is a constant characteristic of the material (10^{-9}–10^{-11} s), V is volume and k_B is Boltzmann's constant. After mathematical manipulation the above equation can be rewritten as

$$V = \frac{25 k_B T}{K}$$

The volume was estimated considering particles with spherical geometry and Fh anisotropy constant of $K = 1.7 \times 10^5$ J/m^3 (Rodmacq, 1984). The values of constant of anisotropy K of Fh available in the literature are still under debate and could be a source of uncertainty in this estimate. The range of K values reported in the literature include: 3.6×10^5 J/m^3 (Gilles et al., 2000); 3.12×10^5 J/m^3 (Duarte et al., 2006); 1.0×10^5 J/m^3 (Berquó et al., 2009); 4.7×10^5–1.5×10^4 J/m^3 (Silva et al., 2008); 1.7×10^5 J/m^3 (Suzdalev et al., 1996). Another source of error is related to the fact that the model used to calculate particle size of natural Fh considered spherical particles. Previous work on synthetic Fh (Erbs et al., 2008) suggests that these particles may have an aspect ratio that is greater than 1. As such, the estimates obtained here are considered *upper limits* and are useful to identify particle size changes associated with the vents temperature.

MÖSSBAUER SPECTROSCOPY

A conventional constant-acceleration spectrometer (Institute for Rock Magnetism, University of Minnesota) was used in transmission geometry with a ^{57}Co/Rh source, using α-Fe at room temperature to calibrate isomer shifts (ISs) and velocity scale. The magnetic hyperfine parameters such as magnetic hyperfine field (B_{HF}), IS, and quadrupole splitting (QS) were fitted using the NORMOS program (Brand, 1987).

HEAT TREATMENT OF HIOLO MAT FLOCS

The Hiolo mat was subjected to heating experiments in an oven to determine the temperature at which the Fh-like minerals transformed to hematite. One mat sample (Hiolo) was dried and divided in five aliquots. One part was kept without thermal treatment and the other four aliquots were used for thermal treatment at different temperatures. The heating procedure started and finished always with samples at room temperature reaching a maximum temperature (T_{max}) of 400, 500, 600, or 800°C. After the oven reached T_{max} the samples were maintained at that temperature for about 20 min, and then samples were cooled inside the oven. Powder XRD measurements were conducted for mat samples using a PANalytical X-Pert PRO MPD X-ray diffractometer equipped with a cobalt source and high speed detector (X-Clerator; Laboratory of R. Lee Penn, Department of Chemistry, University of Minnesota). The data were collected over the range of 10–90 2θ°, with a scan rate

of 0.6°/min, and data are compared to reference powder diffraction patterns. Mössbauer spectra were also collected for the heat treated mat, as described in Section "Mössbauer Spectroscopy."

ELEMENTAL ANALYSES

Thawed Loihi Fe mat samples were prepared for elemental analysis (Aqueous Geochemistry Laboratory, Department of Earth Sciences, University of Minnesota) by 3× centrifugation and rinsing steps (18.2 Ω Milli-Q water), followed by drying for 24 h at 50°C. The dried samples were dissolved in 6 mL of a 50/50 mixture of Trace Grade HCl and HNO_3, and diluted with 18.2 Ω water to a total volume of 30 mL. Major elements (Al, B, Ba, Ca, Co, Cr, Cu, Fe, K, Li, Mg, Mn, Na, Ni, P, Si, Sr, Zn) were measured using a Thermo Scientific iCAP 6500 dual view Inductively Coupled Plasma-Optical Emission Spectrometer. The mat solutions were diluted for analysis with a cesium matrix modifier and yttrium as an internal standard. For trace metal analysis, the dissolved samples were diluted 40×, and 40 ppb of In internal standard was added. Trace elements (Be, Al, Sc, Ti, V, Ga, As, Se, Rb, Y, Zr, Mo, Ag, Cd, Cs, Ba, La, Ce, Pr, Nd, Sm, Eu, Gd, Tb, Dy, Ho, Er, Tm, Yb, Lu, Ta, W, Pb, Th, and U) were measured using a Thermo Scientific XSERIES 2 ICP-MS w/ESI PC3 Peltier cooled spray chamber, SC-FAST injection loop, and SC-4 autosampler. All elements except Li, Be, Al, were analyzed using He/H_2 collision–reaction mode.

To quantify organic carbon contents in several mats, 7–25 mg of material was leached in 0.1 N HCl, dried, reweighed, loaded into tin capsules, and analyzed using a Costech CHN 4010 elemental combustion system.

RESULTS

IRON X-RAY ABSORPTION SPECTROSCOPY

Microprobe Fe EXAFS spectra were collected for fresh and 4°C aged Loihi Fe microbial mats (Ula Nui, Lohiau, Naha, and Pohaku; slurp samples; **Table 1**). The microprobe EXAFS data are presented in **Figure 1** along with bulk EXAFS data and selected reference spectra of Fe oxyhydroxides (goethite, two-line Fh, and Juan de Fuca Ridge biogenic Fe oxyhydroxide). Point measurements from different particle aggregates within the mat samples indicate that Fe speciation was homogeneous at a spatial scale of 10 μm^2. Comparison between the microprobe and bulk Fe EXAFS spectra for these mat flocs shows that the Fe speciation measured at the microscale is also representative of the bulk Fe speciation (**Figure 1**; **Table 2**).

Iron EXAFS spectra (**Figure A1** in Appendix) for the Ula Nui mat were collected on samples with different storage (frozen under N_2, frozen in ambient atmosphere, and aged in ambient seawater at 4°C) and preparation (thawed under N_2, thawed/rinsed in ambient atmosphere, and thawed/rinsed/dried at 40°C) on three different instruments (SSRL 2-3, ALS 10.3.2, and APS 20-BM). These spectra are very similar despite different storage, handling, and instruments. Although there is a perceptible line-shape difference in the EXAFS spectrum for the 4°C aged sample (Ula Nui C) at $k = 7.5$ Å^{-1}, the biggest difference among these Ula Nui spectra is observed in the amplitude of fluorescence versus transmission mode measurements. We interpret the lower amplitude in the fluorescence mode data to be over-absorption effects as the Loihi mats are up to 45.6% by weight Fe (**Table 2**). These observations

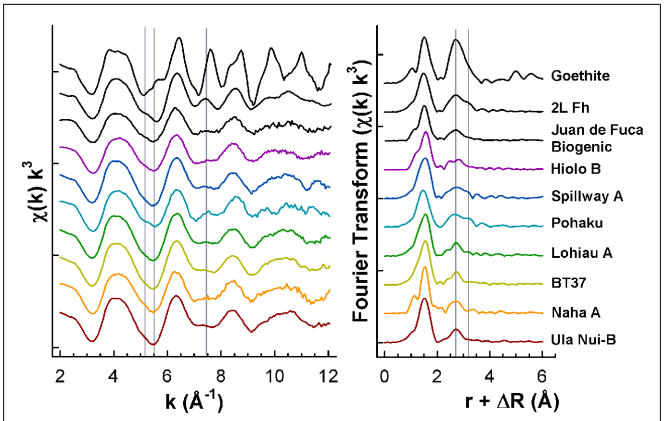

FIGURE 1 | Summary of Fe K-edge EXAFS spectra and Fourier Transform data (magnitude only) for seven Loihi Seamount mats and three reference Fe oxyhydroxides.

hold true for other mats examined by replicate EXAFS measurements. Therefore, in **Figure 1** only representative EXAFS spectra from Loihi mats are displayed while a full summary of spectra are available in **Figure A2** in Appendix.

In **Figure 1**, several spectral features are highlighted for the Loihi mats and reference minerals. The Fe EXAFS spectra collected for the Loihi mats have similarities with two-line Fh in terms of line-shape, amplitude, and phase. In the Fourier transformed data, a corresponding reduction or absence of the longer peak ($R + \Delta R = 3.2$ Å) in the second Fe–Fe shell is observed (except for Pohaku; **Figure 1**). For the Fe oxyhydroxide goethite, the spectral feature observed in k-range = 7–8 Å^{-1} corresponds to corner-sharing Fe-O octahedra and the three-dimensional character of the structure (Toner et al., 2009). The EXAFS data indicate that the mats are composed primarily of Fe(III) oxyhydroxide phases with less three-dimensional ordering than two-line Fh. Therefore, these Fe(III) phases will be referred to as natural short-range ordered Fh (Fh_{SRO}) hereafter.

Iron and Mn oxidation state maps, coupled with total Fe, Mn, Ca, and Ti distributions, were collected for an intact surface crust sample from the Ula Nui site (**Figure 2**). This sample was frozen shipboard under N_2 and analyzed at the synchrotron in the absence of O_2. Noticeable, discontinuous black banding can be observed visually in the laminated mats and these bands are represented in the X-ray fluorescence maps as regions of higher Mn fluorescence intensity [e.g., top of Region I (R1) and II (R2) in **Figure 2**]. XANES fitting of multiple energy maps collected across the Mn K-edge also indicates that these Mn-rich regions are Mn(IV)-oxides. The valence state is confirmed by analysis of Mn K-edge XANES spectra for this sample (data not shown). The majority of the mat profile is then dominated by Fe(III) particles, although a zone dominated by reduced Fe(II) was mapped at the top of R2. Calcium is also enriched by more than an order of magnitude at the top of R2, and these Ca-rich zones envelop the particles in which Fe(II) is present. No micro-EXAFS spectra were collected on this sample and therefore the full speciation of the Fe in discrete regions is unknown, but possible candidate solid-phase Fe species include carbonates, sulfides, or basalt. The Fe(II)-rich particles are

Table 2 | Summary of Loihi Seamount Fe mats examined. Solid-phase% Fe, and Si:Fe and P:Fe mole ratios reported with sample handling and analyses information.

Year	*JASON2* dive#	Marker/ sample type[a]	Area[b]	Mat surface (°C)	% Fe (wt.)	Si:Fe	P:Fe	Sample handling and analysis[d]		
								Aged at 4°C for microprobe Fe EXAFS (months)	Frozen/ rinsed/ dried[c]	Frozen/ no oxygen
2006	J2-241	2–5/a	Lohiau C	–	–	–	–	–	A	–
	J2-241	36/a	Tower	24.9	–	–	–	–	A	–
	J2-242	39/a	Hiolo A	51.0	45.6	0.145	0.041	–	A	–
	J2-242	BT37/a	Hiolo Ridge	11.0	39.8	0.245	0.028	–	A, B, C	–
	J2-244	a	Ula Nui-A	–	29.9	0.289	0.168	–	A, B, C	–
	J2-244	a	Ula Nui-B; C	–	30.7	0.227	0.138	5	A, B, C	–
	J2-245	2–5/a	Lohiau A	–	41.0	0.207	0.035	–	A, B, C	–
	J2-245	34/a	Spillway A	52.0	40.2	0.107	0.046	–	A, B, C	–
2007	J2-308	34/b	Spillway B	53.0–50.0	–	–	–	–	–	B
	J2-308	39/c	Hiolo B	52.0	–	–	–	–	–	B
	J2-309	b, c	Ula Nui Crust	–	–	–	–	–	–	D
	J2-310	55/a	Lohiau B	5.5	–	–	–	<1; 13	–	–
	J2-315	6/a	Naha A; Naha B	–	–	–	–	<1; 13	–	–
	J2-316	57/a	Pohaku	17.3–20.0	–	–	–	13	–	–

[a] *Seafloor sampling type: (a) slurp suction, (b) PVC scoop 1t, (c) PVC scoop 1b.*

[b] *All samples are bulk mats except for the "Ula Nui Crust" which is an intact layered mineral crust sampled by PVC scoop.*

[c] *Splits from slurp suction sampler made shipboard. One set was used for magnetism and Mossbauer, and the second set used for XAS and X-ray scattering.*

[d] *Measurements: A = low-temperature magnetism and Mossbauer spectroscopy; B = bulk Fe EXAFS; C = X-ray scattering; D = microprobe Fe EXAFS.*

likely not basalt given the lack of direct correlation to enrichments in Mn(II) or Ti expected in basaltic glass; there is also no Si as expected for phenocrysts of olivine or feldspar. Instead, carbonates may be forming due to the strong accumulation of Fe(II) and Ca.

SYNCHROTRON X-RAY DIFFRACTION AND PAIR DISTRIBUTION FUNCTION ANALYSIS

Five Loihi mat samples (BT37, Ula Nui-A, Ula Nui-B, Spillway A, and Lohiau A) from the 2006 cruise were analyzed by SR-XRD, and all contain a Fh-like phase based on the presence of diffuse scattering features similar to those observed for the synthetic Fh reference (**Figure 3**). With exception of sample Ula Nui-B, the most significant features occur at *d*-spacings of ∼1.5 and ∼2.55 Å and are indicative of Fh (e.g., Jambor and Dutrizac, 1998; Michel et al., 2007a). The specific crystalline phases attributable to the sharper peaks evident in samples Ula Nui-A, Spillway A, and Lohiau A (**Figure 3**) could not be positively identified due to uncertainty in the relative intensities and possibility of multiple phases. Sample Ula Nui-A contains an additional mineral phase with peaks at *d*-spacings ∼7.2, 3.5, 2.5, 1.4, and 1.2 Å, that can be indexed as Na-rich birnessite (e.g., ICSD 68916). The presence of birnessite in the Ula Nui mat is consistent with Mn EXAFS data for the Ula Nui site (Edwards et al., 2011). Consistent with the SR-XRD results, the total scattering data collected to higher *Q*-space values and presented as the reduced structure functions for these samples (**Figure 4**) are also dominated by features similar to those observed for the synthetic Fh reference.

The Fourier transform of these reduced structure functions results in the PDFs, which contain structural information in real-space for the Loihi mat Fh_{SRO} (**Figure 5**). The first two major features in the PDFs for the BT37, Ula Nui-A, Ula Nui-B, Spillway A, and Lohiau A mats correspond primarily to the average bond lengths for Si and Fe with oxygen. The peaks at ∼1.61 Å correspond to Si-O correlations in the first oxygen shell of Si in tetrahedral coordination. This bond length agrees well with that reported in the literature (e.g., Grimley et al., 1990; Poulsen et al., 1995) and for the *am*-SiO_2 reference compound (**Table 3**). The second major peaks at ∼1.98 Å correspond to Fe-O correlations in the first oxygen shell of Fe. Iron(III) in synthetic Fh is dominantly in octahedral coordination with oxygen (O and/or OH) although recent studies (Michel et al., 2007b, 2010; Maillot et al., 2011; Mikutta, 2011) support the presence of a minor amount (10–25%) of tetrahedrally coordinated Fe(III). As such, the Fe-O correlation for the natural samples may have bond length contributions from both types of coordination environments. The Fe-O peak is slightly asymmetric and also has a small shoulder peak centered at ∼2.13 Å. Similar Fe-O bond lengths were reported for synthetic Fh (Maillot et al., 2011) based on EXAFS spectroscopy data. The fitted Fe-O distances for the Loihi mat samples also correspond well with the Fh reference (**Table 3**), although the distances for the reference were slightly shorter at ∼1.96 and 2.11 Å, respectively. Note that although the Fe-O correlation, particularly in the case of the reference Fh, is expected to have contributions from tetrahedrally coordinated Fe (average bond length ∼1.88 Å) only two Gaussian functions were used to avoid over fitting.

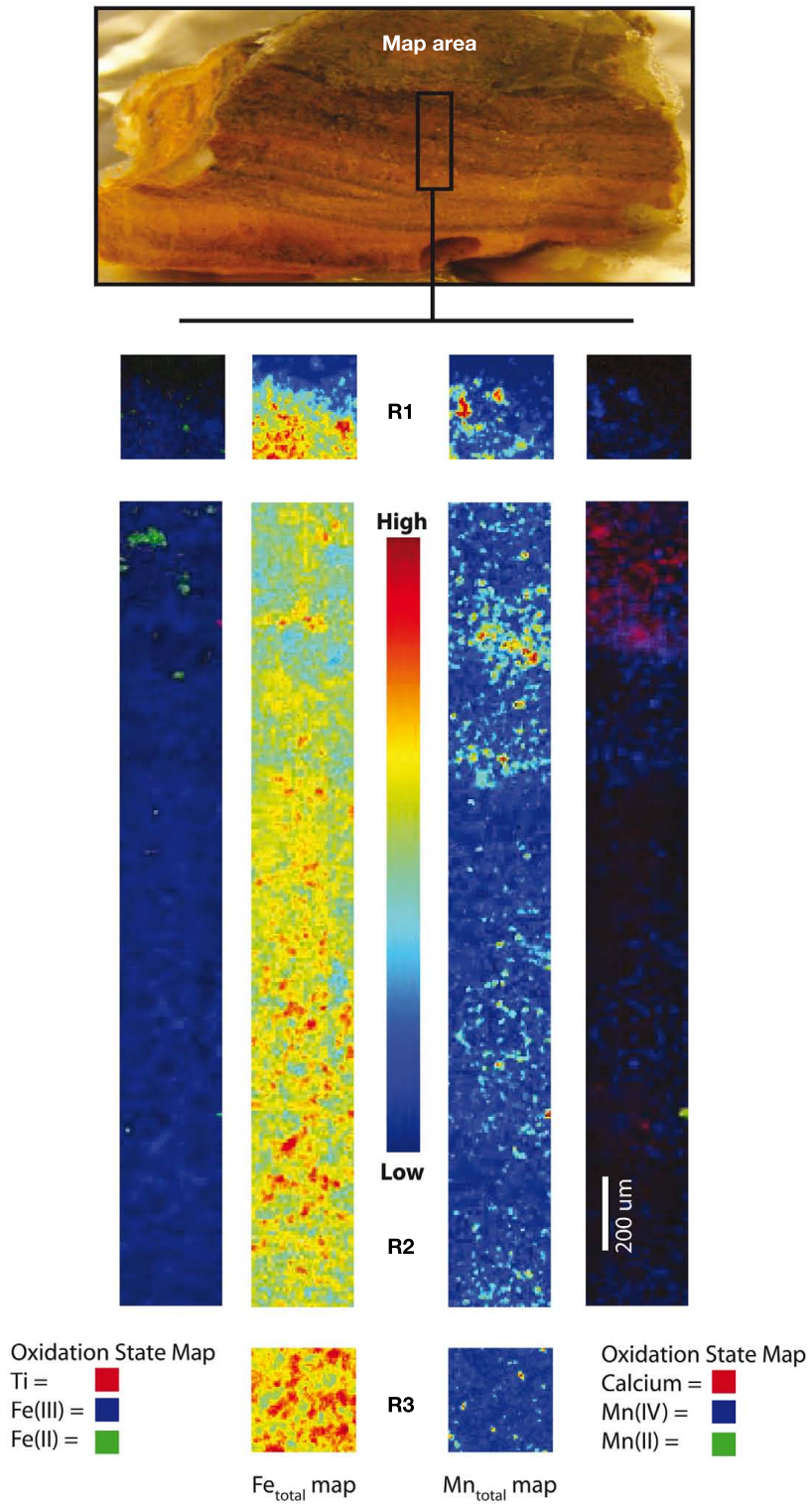

FIGURE 2 | X-ray microprobe fluorescence mapping of an intact Fe/Mn iron microbial mat from Ula Nui. Center maps for Regions 1, 2, and 3 (R1, R2, R3) show total Fe and Mn distributions, while outer maps are tricolor maps that include the redox distribution for Fe(II)/Fe(III), and total Ti (left), as well as Mn(II)/Mn(IV), showing total Ca (right).

Subsequent features in the PDFs correspond to second, third, and higher neighbors around Si and Fe, as well as oxygen pair correlations (i.e., O...O). For example, the small features at ~2.64 Å (**Figure 5**) are due to the O...O distance in tetrahedral

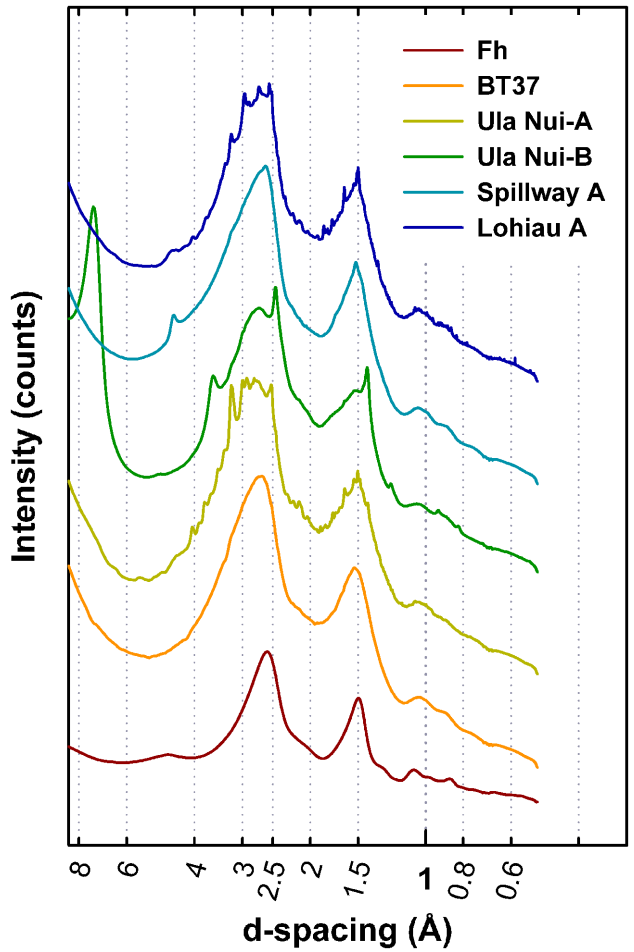

FIGURE 3 | Comparison of the synchrotron radiation X-ray diffraction plotted as *d*-spacing versus intensity. Two broad features characteristic of two-line ferrihydrite (Fh, bottom) occur in all samples at ∼1.5 and 2.55 Å. The most significant impurity phase appears in Ula Nui-B and can be indexed as birnessite, a layered $Mn^{3+/4+}$ (hydr)oxide. Sharp peaks indicating the presence of trace impurities suspected as alumino-silicate phases are also observed in Ula Nui-A, Spillway A, and Lohiau A but could not be positively identified. Increasing background intensity at *d*-spacings greater than ∼6 Å due to effects of small angle scattering.

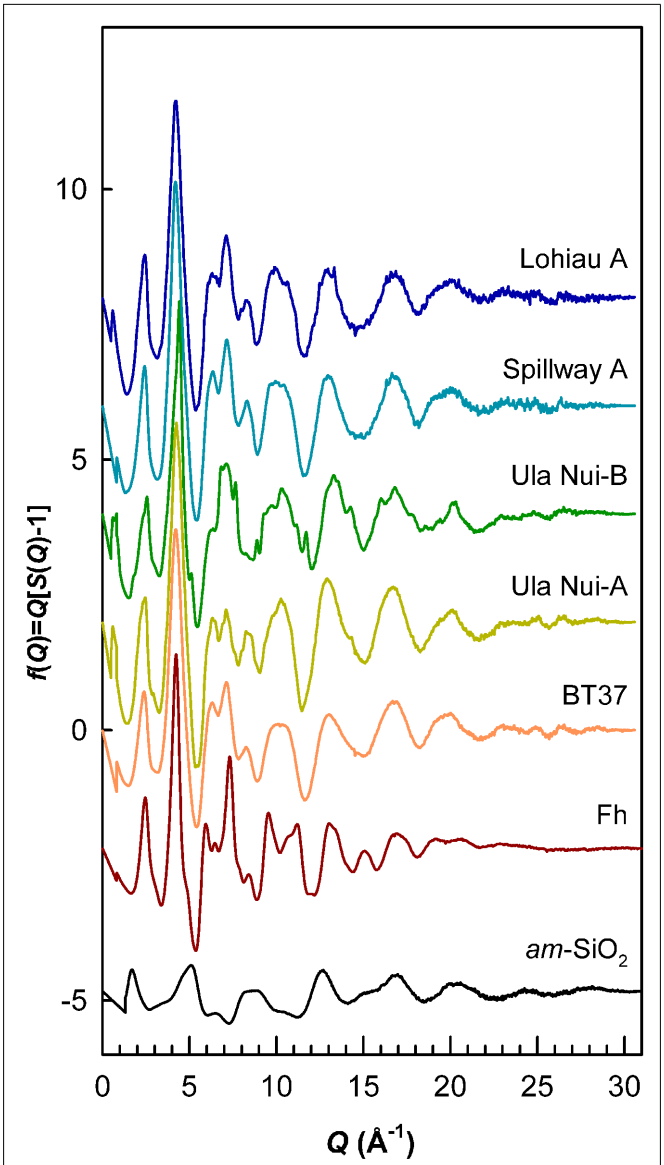

FIGURE 4 | Reduced structure functions for references of Fh and amorphous SiO_2 compared to the five natural samples. Data plotted as $f(Q)$ versus Q ($Q = 4\pi\sin\theta/\lambda$). Overall, the profiles are similar to the Fh reference but differ in terms of peak broadening and the relative intensities of certain features. Sharp features in Ula Nui-B due to birnessite impurity. These data were truncated at maximum Q-range = 30 $Å^{-1}$ and Fourier transformed with a Lorch modification function to obtain PDFs shown in **Figure 5**.

silicate (**Figure 6**) and are consistent with data for the *am*-SiO_2 reference. Also based on the PDF for the reference, a Si. . .Si distance corresponding to corner-sharing silica tetrahedra is expected at ∼3.07 Å (**Figure 6**) but is possibly obscured in the natural samples due, in part, to overlapping correlations resulting from the connectivity of $FeO_{4/6}$ polyhedra. The peak at ∼3.03 Å in synthetic Fh is dominated by Fe. . .Fe and O. . .O correlations for edge-sharing Fe octahedra and the next major peak at ∼3.44 Å has contributions from corner-sharing $FeO_{4/6}$ polyhedra (Michel et al., 2010). These edge- and corner-sharing Fe contributions are not clearly resolved in the mat samples due to the presence of additional features (**Figure 5**) the most significant of which occur at ∼3.14, 3.31, and 3.6 Å (**Table 3**). Previous work (Pokrovski et al., 2003) showed that in varying concentrations of Si solutions, the presence of one to two Si atoms was detected at 3.18 ± 0.03 Å in the second shell around Fe and was ascribed to SiO_4 linked bidentate to two neighboring Fe octahedra via corners (**Figure 6**). Other bonding motifs are also possible (**Figure 6**) and longer Si. . .Fe path lengths could explain the features at distances of ∼3.3 and ∼3.6 Å.

With exception of the degree of PDF decay, the most significant differences between the Loihi mat Fh_{SRO} and Fh reference are in the range $2.5 < r < 4$ Å. As described above, differences in this region of the PDFs appear primarily due to Si. . .Fe pair correlations. Interestingly, the pair correlations beyond $r \approx 4$ Å in BT37,

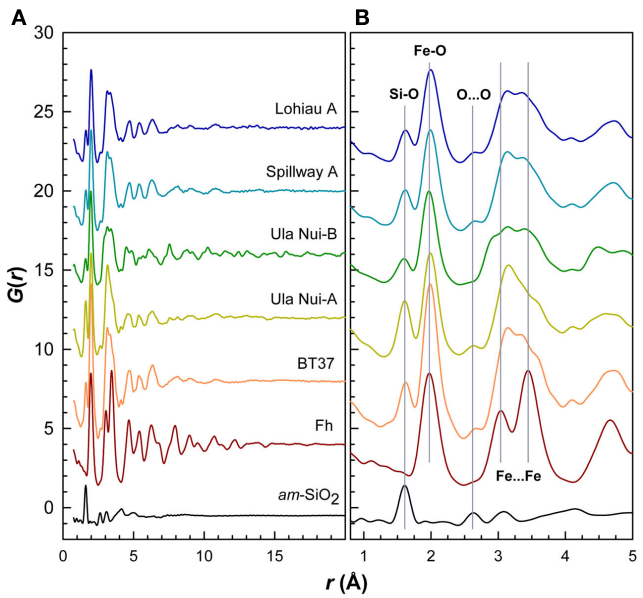

FIGURE 5 | Real-space PDFs or *G*(*r*) for the five natural samples compared to experimental PDFs for Fh and amorphous SiO_2 references. (A) The strong attenuation in the features of the PDFs with increasing *r* for the natural samples indicates smaller coherent scattering domain (CSD) sizes and increased disorder relative to synthetic Fh. Sample Ula Nui-B shows more structure at higher *r* due to birnessite phase impurity. **(B)** Comparison of the short-range order for these samples. Similarities between natural samples and synthetic references for Fh and amorphous silica are highlighted.

Ula Nui-A, Spillway A, and Lohiau A closely resemble synthetic Fh (**Figure A3** in Appendix) suggesting that the intermediate-range order and connectivity of Fe polyhedra are maintained over these length scales. The PDF peaks decay at $r \approx 16$ Å for BT37, Spillway A, and Lohiau A suggesting that these mat samples are more disordered and have smaller CSD sizes compared with synthetic two-line Fh which decays at $r \approx 23$ Å (**Figure A3** in Appendix). Estimated CSD sizes for Ula Nui-A and Ula Nui-B (**Table 3**) are significantly larger (~23 and 37 Å, respectively) however, the presence of relatively crystalline impurities in these samples prevents an accurate estimate for the Fh fractions, which are assumed to be less crystalline than the associated impurity phases. Shifts in peak positions for the natural samples relative to Fh at higher *r* (>4 Å) may be attributable, in part, to increasing strain with decreasing CSD size, and this trend is consistent with previous studies of synthetic Fh in which the size and/or Fe(III) vacancy content varied (Michel et al., 2007a).

LOW-TEMPERATURE MAGNETISM

Representative ZFC/FC curves obtained for Loihi seamount samples are shown in **Figure 7** and **Table 4** summarizes the peak temperature estimated for different samples. Particle size estimates obtained from ZFC curves are also displayed in **Table 4**. A description of the Néel–Arrhenius Law, as well as a discussion of the assumptions used is included in the Section "Magnetism."

Typical hysteresis loops (**Figure 7**), for Loihi Seamount samples, obtained down to 2 K show blocked particles and the presence of coercive force (H_C) and remanent magnetization (M_R). Above T_P value, the hysteresis loops display only the behavior expected for unblocked particles, the loops are closed, and H_C and M_R are zero. For some samples the hysteresis loops are open above T_P as a result of the contribution of trace Ti-magnetite impurity (see also **Figure A4** in Appendix). The particle diameters calculated by this method range from 3.5 to 4.5 nm for the Loihi Seamount natural Fh_{SRO} minerals.

MÖSSBAUER SPECTROSCOPY

Mössbauer spectra were obtained at room temperature and 4.2 K for selected Fe mat samples in order to confirm the valence state of Fe and the magnetic state of the Fh_{SRO}. Detailed chemical, structural, and magnetic information can be obtained with this method (Murad and Cashion, 2004), as the spectra depend on the mineralogy, lattice type, abundance of structural defects, and magnetic properties of the sample. The type of magnetic ordering (ferro-, ferri-, or antiferromagnetic) can be further tested by applying external magnetic fields, and effects related to thermal relaxation in nanoparticles (superparamagnetism) are investigated by obtaining spectra at different temperatures.

The room temperature spectra for the Fe mat samples from the Spillway A, Tower, Hiolo A, Ula Nui-A, Ula Nui-B/C, Lohiau A, and BT37 areas of Loihi Seamount have a Fe^{3+} doublet and magnetic hyperfine parameters corresponding to Fh (**Table 5**; **Figure 8**). The presence of a doublet in a Mössbauer spectrum is a feature associated with paramagnetism and/or superparamagnetism. A superparamagnetic phase has magnetic order below the blocking temperature. The Mössbauer spectra of Fe mats taken at 4.2 K have magnetic order and they exhibit a sextet. The magnetic hyperfine parameters of Loihi mat samples at 4.2 K agree with the ones found in the literature for Fh (Berquó et al., 2009). A decrease was observed in the magnetic hyperfine field (B_{HF}) as compared with synthetic Fh; this feature is associated with structural defects. Ferrihydrite, specifically two-line Fh, has significant defects in both the tetrahedral and octahedral Fe(III) sites (Michel et al., 2010), and these natural Fh_{SRO} samples from Loihi Seamount seem to have extra Fe(III)-site lattice defects due perhaps to Fe substitution and vacancies.

HEAT TREATMENT OF THE HIOLO MAT

A Loihi Seamount mat from the Hiolo area was thermally treated to determine the temperature at which the natural Fh_{SRO} converts to hematite under oxic conditions. The temperature dependent conversion was monitored by powder XRD and room temperature Mössbauer spectroscopy. The XRD pattern obtained for the unheated Hiolo mat sample is presented in **Figure 9**. The pattern has the two broad lines characteristic of Fh and is in agreement with the SR-XRD data for Ula Nui-A, Ula Nui-B/C, BT37, Spillway A, and Lohiau A (**Figure 3**). In addition to the Fh pattern, several sharp diffraction lines are evident for the sample under different conditions: (1) no thermal treatment, halite, and Fh; (2) sample treated at 400°C, halite, Fh, and minor contribution of anhydrite ($CaSO_4$); (3) sample treated at 600°C, halite, hematite (α-Fe_2O_3), and minor contribution of aegirine ($NaFeSi_2O_6$); and (4) sample treated at 800°C, halite, hematite, and minor contribution aegirine. The samples heated at 600 and 800°C have dominant, sharp diffraction lines consistent with the mineral hematite.

Table 3 | Atom pair separations and coherent scattering domain sizes extracted from PDF analysis of references and selected mat samples.

References	Pair assignments										CSD size (Å)
	Si-O	Fe-O[a]	Fe-O[b]	O...O		Fe...Fe_{edge}	Si...Si		Fe...Fe_{crn}		
Fh	–	1.955	2.11	–	–	3.031	–	–	3.437	–	23
am-SiO_2	1.608	–	–	2.626	–	–	3.073	–	–	–	8
Samples	**Correlation no.**										
	1	**2**	**3**	**4**	**5**	**6***	**7**	**8**	**9***	**10**	
BT37	1.616	1.986	2.206	2.653	2.944	3.03	3.147	3.307	3.44	3.605	16
Ula Nui-A	1.604	1.979	2.125	2.624	2.996	3.03	3.140	3.295	3.44	3.605	23
Ula Nui-B	1.594	1.963	2.132	–	2.883	3.03	3.153	3.317	3.44	3.593	37
Spillway A	1.612	1.974	2.121	2.648	2.955	3.03	3.142	3.306	3.44	3.606	16
Lohiau A	1.618	1.977	2.131	2.648	2.898	3.03	3.146	3.309	3.44	3.600	16
					Additional pair assignments						
					Si/O...O		Si...Fe^1	Si...Fe^2		Si...Fe^3	

[a,b]*Two Gaussian functions were used to fit the correlation at ~2 Å.*

[1]*SiO_4 linked bidentate to two neighboring Fe octahedra via corners.*

(–) indicates feature is not applicable (references only) or not present (samples only).

[2]*SiO_4 linked monodentate to O doubly/triply coordinated with Fe.*

**Peak position fixed.*

[3]*SiO_4 linked monodentate to O singly coordinated with Fe (linear Si-O-Fe).*

Average error of ±0.005 Å in fitted peak position.

Estimated error of ±3 Å on CSD size from Hall et al. (2000).

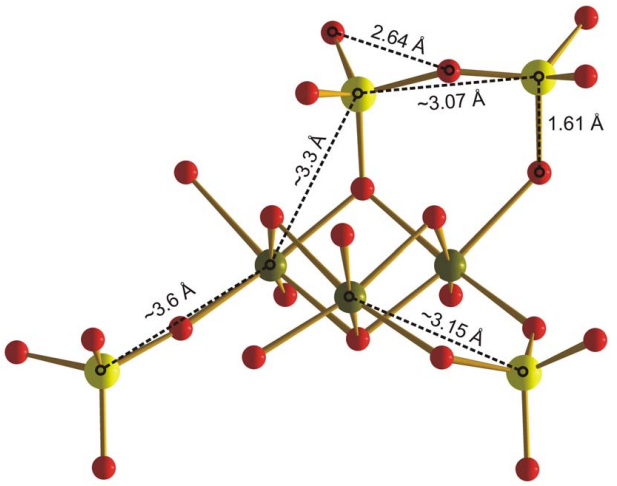

FIGURE 6 | Schematic illustration of three possible silicate surface complexes on an idealized portion of the ferrihydrite structure. Fe(III) (green) is shown in octahedral coordination with O (red). Si (yellow) is tetrahedrally coordinated with O (SiO_4). Approximate Si–Fe distances for SiO_4 linked (1) bidentate to two neighboring Fe octahedra via corners (~3.15 Å), (2) monodentate to a doubly/triply coordinated O (~3.3 Å), and (3) monodentate to a singly coordinated O (~3.6 Å). Si...Si distances (~3.07 Å) indicate formation of silica polymers, possibly also on the ferrihydrite surface.

Mössbauer spectra tell a more detailed story of the mineral conversion (**Figure 10**). The Mössbauer spectra for the Hiolo mat, unheated, and after 400°C treatment, exhibit a doublet indicating a superparamagnetic phase. The Hiolo mat samples heated to 500°C showed the presence of at least two components, a sextet representing magnetic order at room temperature and a Fe^{3+} doublet. The doublet represents the contribution of Fh that was not converted to a more stable phase, while the sextet does not have parameters that correspond to a specific Fe phase. The Fe phase(s) observed at 500°C are intermediates in the conversion process from natural Fh_{SRO} to hematite. In contrast, the spectra at 600 and 800°C suggest the presence of hematite. At 600°C the B_{HF} is reduced as compared with a stoichiometric hematite, indicating the presence of lattice defects in the conversion product. The data at 800°C show magnetic hyperfine parameters similar to stoichiometric hematite and suggest the thermal treatment completely converted Fh_{SRO} to hematite at that temperature.

DISCUSSION

MAT COMPOSITION AND STRUCTURE OF IRON-BEARING PHASES

X-ray fluorescence mapping of major element distributions with depth show that spatial heterogeneity and geochemical zonation occur in layered mats such as at the Ula Nui site. The low-temperature (<2°C) Fe mats at Ula Nui are considered to be modern analogs to ancient umber deposits that form from Fe and Si-rich ultra-diffuse hydrothermal fluids (Edwards et al., 2011). Total cell densities reach values as high as 1.4×10^9 cells/g dry wt. in the Fe/Mn mats, and known Fe-oxidizing bacteria (e.g., Zeta-proteobacteria such as *Mariprofundus ferrooxydans*) that have been identified in these mats are likely supported by the advection of fluids containing 40–150 mM Fe (Glazer and Rouxel, 2009; Edwards et al., 2011). The reductive transformation of the Si-rich Fh_{SRO} would not be predicted to occur substantially

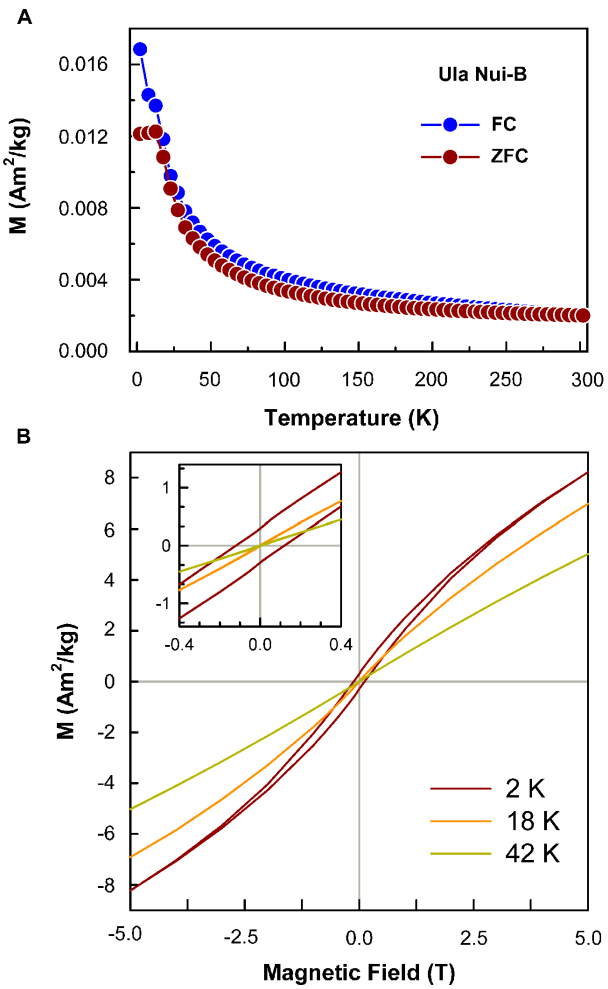

FIGURE 7 | Induced magnetization curves, ZFC/FC and hysteresis loops. (A) ZFC/FC curves typical of Loihi Fe mat samples. Above peak temperature the material behaves as a paramagnetic phase. Below the peak temperature the material has magnetic order. **(B)** The Hysteresis loops at variable temperature show the antiferromagnetic character of ferrihydrite, that is the non-saturation at high fields. At 2 K the coercive force is different of zero (see inset) and indicates the sample has magnetic order. At 18 and 42 K H_c is zero and indicates the sample is in the superparamagnetic state.

Table 4 | Peak temperature obtained from ZFC curves and the corresponding particle size estimate using Néel–Arrhenius law.

Sample	T_P (K)	Particle size (nm)
Ula Nui-A	10	3.5
Ula Nui-B/C	12	3.7
Lohiau A	19	4.3
Spillway A	21	4.4
Lohiau C	22	4.5
Tower	24	4.6
Hiolo A	23	4.6

Table 5 | Magnetic hyperfine parameters fitted at room temperature and 4.2 K.

		B_{HF} (T)	QS (mm/s)	IS (mm/s)
Hiolo A	300 K	–	0.88(1)	0.36(1)
	4.2 K	46.0(2)	−0.02(1)	0.53(1)
Ula Nui-B/C	300 K	–	0.84(1)	0.36(1)
	4.2 K	44.4(4)	−0.02(1)	0.53(1)

Magnetic hyperfine field (B_{HF}), quadrupole splitting (QS), isomer shift (IS), errors are quoted in parenthesis.

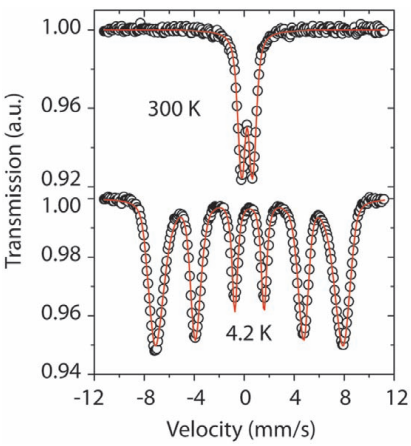

FIGURE 8 | The Mössbauer spectra show the typical behavior of Loihi Fh_{SRO}. At room temperature the spectrum is represented by a doublet and indicates the presence of Fe^{3+}. At 4.2 K the spectrum is a sextet and indicates magnetic order. The sextet has broad lines suggesting the Fe phase is poorly crystallized. The doublet at room temperature represents a phase in a superparamagnetic state.

under these low Fe fluxes, and therefore the EXAFS signature of Fe(III) in the Fh_{SRO} dominates these samples. The Fe(II)-rich zones shown in R2 of **Figure 2** occur several millimeters below the surface of the mat where oxygen concentrations drop to only a few micromolar; the Fe(II)-mineralization may represent regions of localized microbial Fe-reduction using fixed organic carbon (e.g., filaments and extracellular material) resulting in the precipitation of Fe(II)-rich phases such as carbonates or sulfides. Given the strong co-localization between Fe(II) and Ca in this region of the mat, carbonates are the most likely candidate phase, but Fe K-edge XANES were not collected in this region for quantitative analysis. Although 16S rRNA sequences of DNA extracted from Ula Nui mats has not been reported, and enrichments for Fe(III)-reducing bacteria from Ula Nui have been unsuccessful (D. Emerson, personal communication), the potential presence and activity of Fe-reducing bacteria is plausible given the isolation of Fe(III)-reducing bacteria from Fe mats at the Loihi summit (Bailey et al., 2009; Emerson, 2009) and the thermodynamic favorability of coupling organic matter oxidation to Fe(III)-reduction within interior anoxic portions of these mats. Reduction of biogenic Fe oxides has also been demonstrated at the Tonga–Kermadec Arc (Langley et al., 2009).

The local coordination environment of Fe(III) in the Loihi mats was compared to a reference library of Fe oxyhydroxide phases

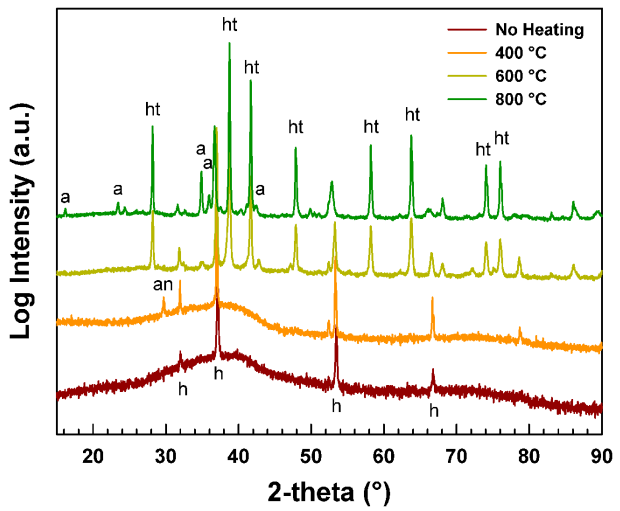

FIGURE 9 | X-ray diffraction pattern of Loihi sample before and after thermal treatment. The pattern obtained with no heat treatment and treatment at 400°C have only two broad lines similar to the pattern of material without treatment. In the 600 and 800°C treatments, the sharp lines correspond to hematite and the broad lines of Fh are no longer present. Aegerine "a," anhydrite "an," hematite "ht," and halite "h."

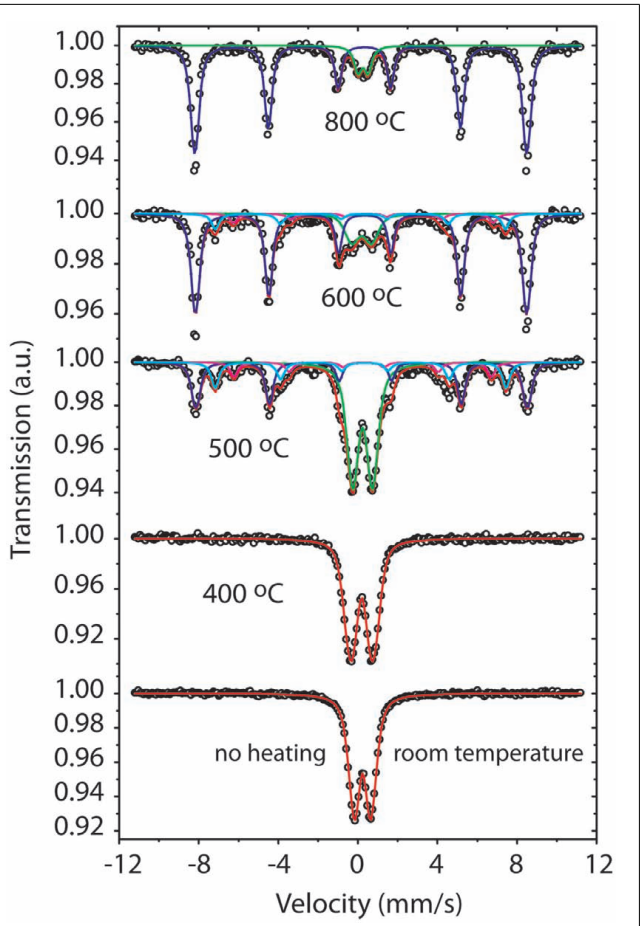

FIGURE 10 | The Mössbauer spectra show that before thermal treatment the sample is represented by a (superparamagnetic) Fe^{3+} doublet. After thermal treatment at 400°C the material still remains a superparamagnetic phase similar to the initial material. The spectra above 500°C have the presence of sextets, they represent the conversion of Fh_{SRO} to a more stable phase, hematite.

(**Figure 1**), and found to be most similar to that of a deep-sea, biogenic Fe oxyhydroxide (seafloor incubation of sulfide minerals at Juan de Fuca Ridge; Toner et al., 2009). Within our dataset, the Fe mat from Pohaku hosts the only phase matching the standard two-line Fh. The most important difference between the Loihi mat spectra and that of the two-line Fh standard is in the k-range = 7–8 $Å^{-1}$, where the peak at $k = 7.5\ Å^{-1}$ is greatly reduced in mat spectra relative to two-line Fh (except for Pohaku). Mikutta (2011) recently reported a similar observation for synthetic Fh formed in the presence of varying amounts of organic ligands and attributed the decrease in intensity of this feature with increasing L/Fe ratio to a reduced number of nearest Fe neighbors. Iron EXAFS spectra with characteristics similar to the Loihi Fh_{SRO} are reported in the presence of Si (Masion et al., 2001; Doelsch et al., 2003; Voegelin et al., 2010; Boland et al., 2011), P (Rose et al., 1997; Voegelin et al., 2010), and organic molecules (Vilge-Ritter et al., 1999; Mikutta, 2011). While the organic C content of the mats is low (~0.3 wt. %), the Si:Fe mole ratio for the Fe-rich mats is 0.107–0.298, and the P:Fe ratio is 0.0280–0.168 (**Table 2**). Based on these EXAFS observations, we hypothesize that Si, and perhaps P, is reducing the degree of structural order in Loihi Seamount natural Fh_{SRO} phases to an extent less than that typically observed for synthetic two-line Fh. In addition, we propose that the natural Fh_{SRO} we detect in all but one Loihi Fe mat is preserved from recrystallization to Fh or other Fe oxyhydroxides such as goethite by the presence of inorganic ligands (Si, P).

Consistent with Fe(III) polymerization in the presence of strongly sorbing ligands, Mössbauer spectroscopy reveals that the Loihi Seamount Fh_{SRO} phases have more structural defects than synthetic Fh. This is observed as a decrease in the magnetic hyperfine field (B_{HF}). Ferrihydrite, specifically two-line Fh, has significant defects in both the tetrahedral and octahedral Fe(III) sites (Michel et al., 2010), and these natural Fh_{SRO} samples from Loihi Seamount seem to have extra Fe(III)-site lattice defects due perhaps to Fe substitution and vacancies.

The SR-XRD (**Figure 3**) and total X-ray scattering data in the form of reduced structure functions (**Figure 4**) reveal that the high-Q (i.e., high angle) scattering maxima for the five natural mat samples are similar, but not identical, to the synthetic two-line Fh reference. In the case of BT37, Spillway A, and Lohiau A (**Tables 1** and **2**), the samples with the most clearly resolvable fraction of natural Fh_{SRO}, the comparison to pure synthetic Fh suggests that these samples bear some structural similarities. Comparison of the PDFs for these samples confirms similarities in short- and intermediate-range structure and provides further insight as to the structural association of Si and Fe in the nanostructured matrix (**Figures 5** and **6**).

The Si:Fe mole ratio measured for the mats by ICP-OES are 0.245, 0.107, and 0.207, respectively. The total measured Si:Fe mole ratios for Ula Nui-A and Ula Nui-B/C mats are 0.289 and 0.227, respectively (**Table 2**). Assuming that these samples are primarily

single-phase, the differences in the region of the PDFs between $2.5 < r < 4$ Å (**Figure 5**) suggest that Si is predominantly associated with the Fh_{SRO} surfaces, perhaps in the form of a poorly ordered silica coating. Alternatively, in the case that these samples are multi-phasic then the observed PDFs could also be explained by at least two phases; one comprised of a Fh-like core, perhaps with a Si-rich coating, and a second comprised of an Fe-bearing amorphous SiO_2 phase, similar to that observed by Pokrovski et al. (2003). Either scenario would also be consistent with the observation that features at higher r (>4 Å) in the PDFs show a return to Fh-like ordering, albeit with smaller CSD sizes. In addition, although the correlations attributable to edge- and corner-sharing Fe polyhedra at ∼3.03 and 3.44 Å, respectively, are not clearly delineated in the PDFs for the mat samples it is possible that they exist but are obscured by other pair correlations involving Si. As discussed above, further evidence for the presence of edge-sharing Fe polyhedra is indicated by the EXAFS for all the Loihi mats. The presence of such polyhedral connectivity would be required in order to produce the intermediate-range Fh-like ordering observed in the region $4 < r < \sim 12$ Å (**Figure A3** in Appendix). Structural information over these longer distances would not be available from previous (and present) EXAFS results since the range of inter-atomic distances measured, particularly in the case of Fh, are typically less than ∼4–5 Å. In summary, the PDFs indicate the presence of limited intermediate-range Fh-like structural ordering, which suggests that silica is not structurally incorporated in ferrihydrite. Differences in short-range ordering of the natural samples relative to Si-free Fh suggest that the Fh particles are coated with Si.

PARTICLE DIMENSIONS AND INTERACTIONS OF IRON-BEARING PHASES

The magnetic behavior of the Loihi Seamount Fh_{SRO} was evaluated since particle coatings such as Si or organic matter are expected to diminish or completely inhibit magnetic interactions of antiferromagnetic Fe oxyhydroxides. In a superparamagnetic system when particles are cooled without an applied field, the magnetic moments are randomly oriented and the resulting induced magnetization is around zero at 0 K. With increasing temperature of the system and in the presence of an external applied field, the magnetic moments begin to fluctuate, then align in the direction of the external field, leading to an increase of the total magnetization (Chantrell et al., 1991; Dormann et al., 1997) and a peak is observed in the ZFC curve (**Figure 7**). Above the peak temperature (T_P) the thermal energy of disorder is higher than the ordering energy and a superparamagnetic behavior results, leading to a decrease of the total magnetization with increasing temperature following the Curie–Weiss law. The presence of a maximum in the ZFC curve is therefore associated with the transition between magnetically relaxing superparamagnetic (unblocked state) and thermally stable magnetization (blocked state). The FC curve represents the superparamagnetic system cooled down in the presence of an external magnetic field.

Current models suggest that particle coatings prevent magnetic interactions for antiferromagnetic systems (Berquó et al., 2009), although this may not prevent magnetic interactions for ferrimagnetic phases such as maghemite and magnetite. Since Fh particles are antiferromagnetic, we apply the antiferromagnetic model to understand Loihi ZFC/FC curves. Berquó et al. (2009) verified that synthetic agglomerated Fh particles, without coating and magnetically interacting, showed a T_P shifted to higher temperatures as compared with the same particles coated, thus considered without magnetic interactions. The T_P estimated from ZFC curves of Loihi samples are similar to the ones obtained by Berquó et al. (2009) for coated synthetic Fh, and this result strongly suggests that the natural Fh_{SRO} particles are also individually wrapped in a way that prevents magnetic interactions. The coating agents that could create this magnetic masking include organic matter or Si in the environment where the particles precipitate. The Loihi Seamount Fe mats are enriched in Si, and Si bonding to the natural Fh_{SRO} is well supported by our X-ray scattering data and analysis. In addition to agreeing with complementary data, this result makes it possible to obtain a better estimate of magnetic particle size (**Table 4**) considering that there is no shift in the peak temperature due to magnetic interaction. The ZFC peak reflects exclusively the changes in particle volume without undesired effects that may contribute to its shift.

Differences in the particle size estimates from low-temperature magnetic data and the CSD sizes from PDF analysis for samples Ula Nui-A, Ula Nui-B, Lohiau A, and Spillway A are evident (**Table 4**) and point toward the presence of structural disorder in the natural Fh_{SRO}. These two types of data can be considered as complementary in the sense that the low-temperature magnetic data indicate an upper limit for the maximum physical dimensions of the particles, while the PDF reveals the average dimensions over which the atoms in the structure scatter coherently. It is possible for the CSD to equal the particle size, but this is not always the case, in particular for Fh (e.g., Michel et al., 2008). In principal, for a monodisperse nanocrystalline material (i.e., with virtually no structural disorder), the PDF peaks decay as r approaches the average maximum dimensions of the particle; therefore, particle size and CSD size are effectively equal. For highly disordered or amorphous structures, the CSD size can be substantially smaller than the physical size of the particles due to the effects of static/dynamic disorder, which attenuate the features in the PDF at higher r. It is worth noting that it becomes increasingly difficult to correlate CSD size with actual particle size, in particular for natural samples, from PDF data alone since the CSD size estimates become increasingly uncertain for polydisperse materials and/or if multiple structural phases are present, as is the case for natural samples Ula Nui-A and -B. However, for Lohiau A and Spillway A, natural samples that are dominantly Fh_{SRO}, the observed discrepancy between average particle size and CSD size suggests strongly that these samples have intrinsic static and dynamic forms of structural disorder. Past studies of pure synthetic Fh (Michel et al., 2010; Cismasu et al., 2011) have suggested that the bulk structure exhibits size-dependent lattice strain and defects in the form of vacancies. In addition, size- and defect-driven restructuring of the Fh surfaces is also possible, although poorly understood at present. Evidence for lattice strain and structural defects in natural Fh_{SRO} is difficult to discern in the present case due, in part, to the presence of minor crystalline impurity phases such as birnessite. Additional complexity due to the presence of compositional impurities and/or adsorbed species such as silica or organic matter are also factors and may account

for the discrepancies between average coherent scattering body size and particle size.

PARTICLE STABILITY OF IRON-BEARING PHASES

The local coordination of Fe in Loihi mats was remarkably insensitive to sample processing, storage, and handling procedures such as freezing, drying, and storage in seawater up to 1 year (**Figure 1**; **Figures A1** and **A2** in Appendix). The short-range order of the Naha and Lohiau Fe mats (**Figure A1** in Appendix; data not shown for Lohiau) did not change after aging for 1 year at 4˚C. Although the Fh_{SRO} phases might be expected to transform to more stable minerals such as goethite (Penn et al., 2006), no recrystallization was observed. The stability of the local structure of the Fh_{SRO} as a function of time and temperature is consistent with non-interacting particles. In addition, the Loihi Seamount Fe mats did not convert to the more stable hematite phase during a 400˚C thermal treatment. Pure Fh is expected to rapidly convert to hematite between 300 and 400˚C (Cornell and Schwertmann, 2003). However, surface coatings on Fh, such as adsorbed Si or organic molecules, are known to slow or inhibit its transformation to crystalline products (Cornell and Schwertmann, 1979; Anderson and Benjamin, 1985; Campbell et al., 2002). Stable Fe minerals such as goethite were not observed at any of the Loihi field sites or under any of the experimental conditions below 400˚C. All EXAFS, PDF, and magnetism data from the present study point to Si particle coatings that limit chemical interactions among natural Fh_{SRO} particles in Loihi mats.

In addition to limited particle–particle interactions, chemical, and biological reactions involving Fe(II) may be limited in Loihi mats and contribute to stability of the Fh_{SRO}. The low activity of Fe-reducing bacteria in Loihi mats suggests that the Fh_{SRO} phases are not subject to intense biological reductive alteration (Emerson, 2009), although some Fe-reducing bacteria are known to solubilize Fe(II) from Si-enriched Fh (Percak-Dennett et al., 2011). Despite the constant source of Fe(II) to all but the "dead" Naha site, Fe(II) induced reduction of Fh_{SRO} may be negligible based on results from synthetic Si-enriched Fh studies (Jones et al., 2009; Boland et al., 2011). For example, Si:Fe ratios of 0.7 have been shown to inhibit Fe(II)-induced recrystallization of Fh to goethite at pH 6.5 (Boland et al., 2011). However, the data presented here does not address the potential for exchange between vent fluid Fe(II) and Fe_{SRO}, and there is evidence that Si-enriched Fh phases retain chemical reactivity. For example, Si:Fe mole ratios up to 0.5 can be achieved without blocking all reactive Fh surface sites due to surface-bound silicate oligomers (Swedlund et al., 2009). In addition, Si-enriched Fh phases are soluble in the presence of organic molecules, such as oxalate and acetate (Carlson and Schwertmann, 1981; Percak-Dennett et al., 2011). We speculate that the low organic carbon content of the Loihi mats may limit both biological and chemical reductive dissolution reactions. These factors combined suggest that the Fe_{SRO} signatures observed at Loihi may be resistant to diagenetic processes and persist over long periods of time.

IRON MICROBIAL MATS AT DIFFUSE HYDROTHERMAL VENTS

Iron and Si-rich microbial mats are observed in shallow and deep marine hydrothermal systems. The number of published observations of Fe microbial mats indicates that these deposits may be common features associated with diffuse venting. Diffuse hydrothermal vents at seamounts and submarine volcanoes associated with island arcs and mid-ocean ridge spreading centers host Fe (and Si) microbial mats, for example: Loihi Seamount (Karl et al., 1988; Edwards et al., 2011), Vailulu'u Seamount (Sudek et al., 2009); Giggenbach Volcano, Kermadec Arc (Jones et al., 2008); Axial Volcano, Juan de Fuca Ridge (Kennedy et al., 2003); South Tonga Arc volcanoes (Langley et al., 2009; Forget et al., 2010); Lilliput vent field, Mid-Atlantic Ridge (Dekov et al., 2010). Among these studies, the Fe mineralogy, when reported, is resoundingly "amorphous" Fe oxyhydroxide, ferrihydrite, and occasionally goethite. A recent review of the microbiology of active seamount Fe microbial mats indicates that Zeta-proteobacteria and/or Epsilonproteobacteria are shared among sites (Emerson and Moyer, 2010), even though inter-site diversity is high (Davis and Moyer, 2008). A cultured representative of the Zeta-proteobacteria from Loihi Seamount (Emerson et al., 2007), *M. ferrooxydans*, is an Fe oxidizer that produces ferrihydrite-like phases in fresh filaments of twisted stalks (Chan et al., 2011). Frequent observations of Fe-encrusted filamentous structures at diffuse vents, and the apparent ubiquity of Zeta-proteobacteria in the mats, suggest that Loihi Seamount mats may represent common depositional environments at the modern seafloor. The present study indicates that the presence of Si and organic templates are both primary geochemical factors in the structure of Fe-bearing phases as well as the preservation of the phases as a function of time and temperature.

CONCLUSION

Certain characteristics of Fe oxyhydroxide phases – particle size, crystallinity – are known to respond to solution conditions such as Si concentration, as well as factors that influence the rate of precipitation, such as temperature and pH (Cornell and Schwertmann, 2003). The overarching goal for this study is to determine whether Fe oxyhydroxide phases can be used to interpret the biogeochemical conditions of past depositional settings. In particular, we are concerned with whether the characteristics of fresh Fe oxyhydroxide phases are preserved over time. As a first step toward this goal, we examined the Fe-rich, flocculant microbial mats hosted by active (and recently active) vents of the Loihi Seamount. The mats are composed of nanoparticulate ferrihydrite (Fh)-like phases with short-range structural order (Fh_{SRO}) at all but one site (Pohaku) irrespective of depth or temperature. The Loihi Fh_{SRO} are primarily Fe(III) with little particle-to-particle variability in the local coordination environment of Fe within a single mat; although careful sampling of the Ula Nui site revealed isolated microzones of solid-phase Fe(II)-enrichment beneath the mat–seawater interface. For our entire sample set, maximum particle diameters of 3.5–4.6 nm (magnetism data) were found to be positively correlated with maximum vent fluid temperature, while CSD sizes (PDF analysis) as small as 1.6 nm were observed, and are inversely correlated with vent fluid temperature. These data indicate that the Loihi Fh_{SRO} phases have intrinsic static and dynamic forms of structural disorder, likely from lattice strain and vacancy or substitutional impurity defects. Magnetic data and PDF analysis both point to Fh_{SRO} particles coated by Si. The Loihi mat Fh_{SRO} phases did not transform to other Fe mineral phases in response to freezing, drying, aging in seawater for up to 1 year, or standard heat treatments under oxic conditions. We hypothesize that Si increases

structural disorder and decreases CSD sizes in Loihi Seamount mats, and propose that the natural Fh_{SRO} we detect is preserved from recrystallization to Fh, or other Fe oxyhydroxides such as goethite, by the presence of Si, although P and organic molecules could potentially contribute.

ACKNOWLEDGMENTS

We thank Clara Chan (University of Delaware) for mat collection during the 2006 cruise, and R. Lee Penn (University of Minnesota) for use of the X-ray diffractometer. We thank Matthew Marcus and Sirine Fakra (Advanced Light Source 10.3.2), Dale Brewe and Steve Heald (Advanced Photon Source 20-BM), and Kevin Beyer (Advanced Photon Source 11-ID-B) for synchrotron support. We thank Sarah Bennett, Cara Santelli, Beth Orcutt, and Amanda Turner Haddad for assistance in synchrotron data collection. F. Marc Michel is supported by the DOE Office of Biological and Environmental Research through the Science Focus Area at the Stanford Synchrotron Radiation Lightsource (SSRL), SLAC National Accelerator Laboratory, Stanford University, and by the National Science Foundation (NSF) and the Environmental Protection Agency (EPA) under NSF Cooperative Agreement EF-0830093 through the Center for Environmental Implications of NanoTechnology (CEINT). The Institute for Rock Magnetism (IRM) is funded by the W. M. Keck Foundation, the Earth Science Division of the US National Science Foundation (NSF/EAR 0732473 and NSF/EAR 1028690), and the University of Minnesota. This is IRM contribution #1109. The Advanced Light Source is supported by the Director, Office of Science, Office of Basic Energy Sciences, of the U.S. Department of Energy under Contract No. DE-AC02-05CH11231. Use of the Advanced Photon Source, an Office of Science User Facility operated for the U.S. Department of Energy (DOE) Office of Science by Argonne National Laboratory, was supported by the U.S. DOE under Contract No. DE-AC02-06CH11357. Alexis S. Templeton also acknowledges SSRL, an Office of Science User Facility operated by the U.S. Department of Energy Office of Science by Stanford University. The SSRL Structural Molecular Biology Program is supported by the DOE Office of Biological and Environmental Research, and by the National Institutes of Health, National Center for Research Resources, Biomedical Technology Program (PR1RR001209).

REFERENCES

Anderson, P. R., and Benjamin, M. M. (1985). Effects of silicon on the crystallization and adsorption properties of ferric oxides. *Environ. Sci. Technol.* 19, 1048–1053.

Bailey, B., Templeton, A. S., Staudigel, H., and Tebo, B. M. (2009). Utilization of substrate components during basaltic glass colonization by *Pseudomonas* and *Shewanella* isolates. *Geomicrobiol. J.* 26, 648–656.

Berquó, T. S., Erbs, J. J., Lindquist, A., Penn, R. L., and Banerjee, S. K. (2009). Effects of magnetic interactions in antiferromagnetic ferrihydrite particles. *J. Phys. Condens. Matter* 21, 176005.

Boland, D. D., Collins, R. N., Payne, T. E., and Waite, T. D. (2011). Effect of amorphous Fe(III) oxide transformation on the Fe(II)-mediated reduction of U(VI). *Environ. Sci. Technol.* 45, 1327–1333.

Brand, R. A. (1987). Improving the validity of hyperfine field distributions from metallic alloys. Part I: unpolarized source. *Nucl. Instrum. Methods Phys. Res. B* 28, 398–405.

Campbell, A. C. (1991). "Mineralogy and chemistry of marine particles by synchrotron X-ray spectroscopy, Mossbauer spectroscopy, and plasma-mass spectrometry," in *Marine Particles: Analysis and Characterization, Vol. 63, Geophysical Monograph Series*, eds D. C. Hurd and D. W. Spencer (Washington: American Geophysical Union), 375–390.

Campbell, A. S., Schwertmann, U., Stanjek, H., Friedl, J., Kyek, A., and Campbell, P. A. (2002). Si incorporation into hematite by hearing Si-ferrihydrite. *Langmuir* 18, 7804–7809.

Carlson, L., and Schwertmann, U. (1981). Natural ferrihydrites in surface deposits from Finland and their association with silica. *Geochim. Cosmochim. Acta* 45, 421–429.

Chan, C. S., Fakra, S. C., Emerson, D., Fleming, E. J., and Edwards, K. J. (2011). Lithotrophic iron-oxidizing bacteria produce organic stalks to control mineral growth: implications for biosignature formation. *ISME J.* 5, 717–727.

Chan, C. S., Stasio, G. D., Welch, S. A., Girasole, M., Frazer, B. H., Nesterova, M. V., Fakra, S., and Banfield, J. F. (2004). Microbial polysaccharides template assembly of nanocrystal fibers. *Science* 303, 1656–1658.

Chantrell, R. W., El-Hilo, M., and O'Grady, K. (1991). Spin-glass behavior in a fine particle system. *IEEE Trans. Magn.* 27, 3570–3578.

Chupas, P. J., Qui, X., Hanson, J. C., Lee, P. L., Grey, C. P., and Billinge, S. J. L. (2003). Rapid-acquisition pair distribution function (RA-PDF) analysis. *J. Appl. Crystallogr.* 36, 1342–1347.

Cismasu, A. C., Michel, F. M., Tcaciuc, A. P., Tyliszczak, T., and Brown, G. E. J. (2011). Composition and structural aspects of naturally occurring ferrihydrite. *C. R. Geosci.* 343, 210–218.

Cornell, R. M., and Schwertmann, U. (1979). Influence of organic anions on the crystallization of ferrihydrite. *Clays Clay Miner.* 27, 402–410.

Cornell, R. M., and Schwertmann, U. (2003). *The Iron Oxides: Structure, Properties, Reactions, Occurrences and Uses*. Darmstadt: Wiley-VCH.

Davis, R. E., and Moyer, C. L. (2008). Extreme spatial and temporal variability of hydrothermal microbial mat communities along the Mariana Island Arc and southern Mariana back-arc system. *J. Geophys. Res.* 113, 1–17.

DeCarlo, E. H., McMurtry, G. M., and Yeh, H.-W. (1983). Geochemistry of hydrothermal deposits from the Loihi submarine volcano, Hawaii. *Earth Planet. Sci. Lett.* 66, 438–449.

Dekov, V. M., Petersen, S., Garbe-Schonberg, C. D., Kamenov, G. D., Perner, M., Kuzmann, E., and Schmidt, M. (2010). Fe-Si-oxyhydroxide deposits at a slow-spreading centre with thickened oceanic crust: the Lilliput hydrothermal field (9 degrees 33' S, Mid-Atlantic Ridge). *Chem. Geol.* 278, 186–200.

Doelsch, E., Masion, A., Rose, J., Stone, W. E. E., Bottero, J. Y., and Bertsch, P. M. (2003). Chemistry and structure of colloids obtained by hydrolysis of Fe(III) in the presence of SiO_4 ligands. *Colloids Surf. A Physicochem. Eng. Asp.* 217, 121–128.

Dormann, J. L., Fiorani, D., and Tronc, E. (1997). "Magnetic relaxation in fine-particle systems," in *Advances in Chemical Physics*, Vol. XCVIII, eds I. Prigogine and S. A. Rice (New York: Wiley), 283–494.

Drits, V. A., Sakharov, B. A., Salyn, A. L., and Manceau, A. (1993). Structural model for ferrihydrite. *Clay Miner.* 28, 185–207.

Druschel, G. K., Emerson, D., Sutka, R., Suchecki, P., and Luther, G. W. III. (2008). Low-oxygen and chemical kinetic constraints on the geochemical niche of neutrophilic iron(II) oxidizing microorganisms. *Geochim. Cosmochim. Acta* 72, 3358–3370.

Duarte, E. L., Itri, R., Lima, E. J., Baptista, M. P., Berquo, T. S., and Goya, G. F. (2006). Large magnetic anisotropy in ferrihydrite nanoparticles synthesized from reverse micelles. *Nanotechnology* 17, 5549–5555.

Edwards, K. J., Glazer, B. T., Rouxel, O. J., Bach, W., Emerson, D., Davis, R. E., Toner, B. M., Chan, C. S., Tebo, B. M., Staudigel, H., and Moyer, C. L. (2011). Ultra-diffuse hydrothermal venting supports Fe-oxidizing bacteria and massive umber deposition at 5000 off Hawaii. *ISME J.* 5, 1–11.

Edwards, K. J., McCollom, T. M., Konishi, H., and Buseck, P. R. (2003). Seafloor bioalteration of sulfide minerals: results from in situ incubation studies. *Geochim. Cosmochim. Acta* 67, 2843–2856.

Egami, T., and Billinge, S. J. L. (2003). *Underneath the Bragg Peaks: Structural Analysis of Complex Materials*. Oxford: Elsevier, 1–404.

Ekstrom, E. B., Learman, D. R., Madden, A. S., and Hansel, C. M. (2010). Contrasting effects of Al substitution on microbial reduction of Fe(III) (hydr)oxides. *Geochim. Cosmochim. Acta* 74, 7086–7099.

Emerson, D. (2009). Potential for iron-reduction and iron-cycling in iron oxyhydroxide-rich microbial mats at Loihi Seamount. *Geomicrobiol. J.* 26, 639–647.

Emerson, D., and Moyer, C. L. (2002). Neutrophilic Fe-oxidizing bacteria are abundant at the Loihi Seamount hydrothermal vents and play a major role in Fe oxide deposition. *Appl. Environ. Microbiol.* 68, 3085–3093.

Emerson, D., and Moyer, C. L. (2010). Microbiology of seamounts: common patterns observed in community structure. *Oceanography* 23, 148–163.

Emerson, D., Rentz, J. A., Lilburn, T. G., Davis, R. E., Aldrich, H., Chan, C., and Moyer, C. L. (2007). A novel lineage of proteobacteria involved in formation of marine Fe-oxidizing microbial mat communities. *PLoS ONE* 2, e667. doi:10.1371/journal.pone.0000667

Emerson, D., and Revsbech, N. P. (1994). Investigation of an iron-oxidizing microbial mat community located near Aarhus, Denmark: field studies. *Appl. Environ. Microbiol.* 60, 4022–4031.

Erbs, J., Gilbert, B., and Penn, R. L. (2008). Influence of size on reductive dissolution of six-line ferrihydrite. *J. Phys. Chem. C* 112, 12127–12133.

Forget, N. L., Murdock, S. A., and Juniper, S. K. (2010). Bacterial diversity in Fe-rich hydrothermal sediments at two South Tonga Arc submarine volcanoes. *Geobiology* 8, 417–432.

Gilbert, B. (2008). Finite size effects on the real-space pair distribution function of nanoparticles. *J. Appl. Crystallogr.* 41, 554–562.

Gilles, C., Bonville, P., Wong, K. K. W., and Mann, S. (2000). Non-Langevin behaviour of the uncompensated magnetization in nanoparticles of artificial ferritin. *Eur. Phys. J. B* 17, 417–427.

Glazer, B. T., and Rouxel, O. J. (2009). Redox speciation and distribution within diverse iron-dominated microbial habitats at Loihi Seamount. *Geomicrobiol. J.* 26, 606–622.

Grimley, D. I., Wright, A. C., and Sinclair, R. N. (1990). Neutron-scattering from vitreous silica.4. Time-of-flight diffraction. *J. Non Cryst. Solids* 119, 49–64.

Guinier, A. (1963). *X-Ray Diffraction in Crystals, Imperfect Crystals, and Amorphous Bodies.* San Francisco: W. H. Freeman.

Hall, B. D., Zanchet, D., and Ugarte, D. (2000). Estimating nanoparticle size from diffraction measurements. *J. Appl. Crystallogr.* 33, 1335–1341.

Hammersley, A. P., Svenson, S. O., Hanfland, M., and Hauserman, D. (1996). Two-dimensional detector software: from real detector to idealised image or two-theta scan. *High Press. Res.* 14, 235–248.

Hansel, C. M., Benner, S. G., Neiss, J., Dohnalkova, A., Kukkadapu, R. K., and Fendorf, S. (2003). Secondary mineralization pathways induced by dissimilatory iron reduction of ferrihydrite under advective flow. *Geochim. Cosmochim. Acta* 67, 2977–2992.

Hansel, C. M., Learman, D. R., Lentini, C. J., and Ekstrom, E. B. (2011). Effect of adsorbed and substituted Al on Fe(II)-induced mineralization pathways of ferrihydrite. *Geochim. Cosmochim. Acta* 75, 4653–4666.

Hirata, Y., Yoshitomi, A., and Sameshima, S. (2003). Reaction, microstructures and mechanical properties of model ceramic ware in the K_2O-Al_2O_3-SiO_2 system. *J. Ceram. Soc. Jpn.* 111, 560–566.

Hochella, M. F. Jr., Lower, S. K., Maurice, P. A., Penn, R. L., Sahai, N., Sparks, D. L., and Twining, B. S. (2008). Nanominerals, mineral nanoparticles, and earth systems. *Science* 319, 1631–1634.

Jambor, J. L., and Dutrizac, J. E. (1998). Occurrence and constitution of natural and synthetic ferrihydrite, a widespread iron oxyhydroxide. *Chem. Rev.* 98, 2549–2585.

Janney, D. E., Cowley, J. M., and Buseck, P. R. (2000). Structure of synthetic 2-line ferrihydrite by electron diffraction. *Am. Mineral.* 85, 1180–1187.

Jones, A. M., Collins, R. N., Rose, J., and Waite, T. D. (2009). The effect of silica and natural organic matter on the Fe(II)-catalysed transformation and reactivity of Fe(III) minerals. *Geochim. Cosmochim. Acta* 73, 4409–4422.

Jones, B., de Ronde, C. E. J., and Renaut, R. W. (2008). Mineralized microbes from Giggenbach submarine volcano. *J. Geophys. Res.* 113, 13.

Karl, D. M., Brittain, A. M., and Tilbrook, B. D. (1989). Hydrothermal and microbial processes at Loihi Seamount, a mid-plate hot-spot volcano. *Deep Sea Res.* 36, 1655–1673.

Karl, D. M., McMurtry, G. M., Malohoff, A., and Garcia, M. O. (1988). Loihi Seamount, Hawaii: a mid-plate volcano with a distinctive hydrothermal system. *Nature* 335, 532–535.

Kennedy, C. B., Scott, S. D., and Ferris, F. G. (2003). Characterization of bacteriogenic iron oxide deposits from Axial Volcano, Juan de Fuca Ridge, Northeast Pacific Ocean. *Geomicrobiol. J.* 20, 199–214.

Klein, F. W. (1982). Earthquakes at Loihi submarine volcano and the Hawaiian hot spot. *J. Geophys. Res.* 87, 7719–7726.

Langley, S., Igric, P., Takahashi, Y., Sakai, Y., Fortin, D., Hannington, M. D., and Schwarz-Schampera, U. (2009). Preliminary characterization and biological reduction of putative biogenic iron oxides (BIOS) from the Tonga-Kermadec Arc, southwest Pacific Ocean. *Geobiology* 7, 35–49.

Lorch, E. (1969). Neutron diffraction by germania silica and radiation-damaged silica glasses. *J. Phys. C Solid State Phys.* 2, 229.

Maillot, F., Morin, G., Wang, Y., Bonnin, D., Ildefonse, P., Chaneac, C., and Calas, G. (2011). New insight into the structure of nanocrystalline ferrihydrite: EXAFS evidence for tetrahedrally coordinated iron (III). *Geochim. Cosmochim. Acta* 75, 2708–2720.

Manceau, A. (2009). Evaluation of the structural model for ferrihydrite derived from real-space modelling of high-energy X-ray diffraction data. *Clay Miner.* 44, 19–34.

Manceau, A. (2011). Critical evaluation of the revised akdalaite model for ferrihydrite. *Am. Mineral.* 96, 521–533.

Manceau, A., and Drits, V. A. (1993). Local structure of ferrihydrite and feroxyhite by EXAFS spectroscopy. *Clay Miner.* 28, 165–184.

Marcus, M. A., MacDowell, A., Celestre, R., Manceau, A., Miller, T., Padmore, H. A., and Sublett, R. E. (2004). Beamline 10.3.2 at ALS: a hard X-ray microprobe for environmental and material sciences. *J. Synchrotron Radiat.* 11, 239–247.

Masion, A., Doelsch, E., Rose, J., Moustier, S., Bottero, J. Y., and Bertsch, P. M. (2001). Speciation and crystal chemistry of iron (III) chloride hydrolyzed in the presence of SiO4 ligands. 3. Semilocal scale structure of the aggregates. *Langmuir* 17, 4753–4757.

Mayhew, L. E., Webb, S. M., and Templeton, A. S. (2011). Microscale imaging and identification of Fe oxidation state, speciation, and distribution in complex geological media. *Environ. Sci. Technol.* 45, 4468–4472.

Michel, F. M., Barrón, V., Torrent, J., Morales, M. P., Serna, C. J., Boily, J. F., Liu, Q. S., Ambrosini, A., Cismasu, A. C., and Brown, G. E. (2010). Ordered ferrimagnetic form of ferrihydrite reveals links among structure, composition, and magnetism. *Proc. Natl. Acad. Sci. U.S.A.* 107, 2787–2792.

Michel, F. M., Ehm, L., Antao, S. M., Lee, P. L., Chupas, P. J., Liu, G., Strongin, D. R., Schoonen, M. A. A., Phillips, B. L., and Parise, J. B. (2007a). The structure of ferrihydrite, a nanocrystalline material. *Science* 316, 1726–1729.

Michel, F. M., Ehm, L., Liu, G., Han, W. Q., Antao, S. M., Chupas, P. J., Lee, P. L., Knorr, K., Eulert, H., Kim, J., Grey, C. P., Celestian, A. J., Gillow, J., Schoonen, M. A. A., Strongin, D. R., and Parise, J. B. (2007b). Similarities in 2- and 6-line ferrihydrite based on pair distribution function analysis of X-ray total scattering. *Chem. Mater.* 19, 1489–1496.

Michel, F. M., MacDonald, J., Feng, J., Phillips, B. L., Ehm, L., Tarabrella, C., Parise, J. B., and Reeder, R. J. (2008). Structural characteristics of synthetic amorphous calcium carbonate. *Chem. Mater.* 20, 4720–4728.

Mikutta, C. (2011). X-ray absorption spectroscopy study on the effect of hydroxybenzoic acids on the formation and structure of ferrihydrite. *Geochim. Cosmochim. Acta* 75, 5122–5139.

Moyer, C. L., Dobbs, F. C., and Karl, D. M. (1994). Estimation of diversity and community structure through restriction fragment length polymorphism distribution analysis of bacterial 16S rRNA genes from a microbial mat at an active hydrothermal vent system, Loihi Seamount, Hawaii. *Appl. Environ. Microbiol.* 60, 871–879.

Moyer, C. L., Dobbs, F. C., and Karl, D. M. (1995). Phylogenetic diversity of the bacterial community from a microbial mat at an active, hydrothermal vent system, Loihi Seamount, Hawaii. *Appl. Environ. Microbiol.* 61, 1555–1562.

Murad, E., and Cashion, J. (2004). *Mössbauer Spectroscopy of Environmental Materials and their Utilization.* Boston: Kluwer.

Navrotsky, A., Mazeina, L., and Majzlan, J. (2008). Size-driven structural and thermodynamic complexity in iron oxides. *Science* 319, 1635–1638.

O'Day, P. A., Rivera, N. Jr., Root, R., and Carroll, S. A. (2004). X-ray absorption spectroscopic study of Fe reference compounds for the analysis of natural sediments. *Am. Mineral.* 89, 572–585.

Penn, L. R. (2007). Resolving an elusive structure. *Science* 316, 1704–1705.

Penn, L. R., Erbs, J., and Gulliver, D. (2006). Controlled growth of alpha-FeOOH nanorods by

exploiting oriented aggregation. *J. Cryst. Growth* 293, 1–4.

Percak-Dennett, E. M., Beard, B. L., Xu, H., Konishi, H., Johnson, C. M., and Roden, E. E. (2011). Iron isotope fractionation during microbial dissimilatory iron oxide reduction in simulated Archaean seawater. *Geobiology* 9, 205–220.

Pinney, N., Kubicki, J. D., Middlemiss, D. S., Grey, C. P., and Morgan, D. (2009). Density functional theory study of ferrihydrite and related Fe-oxyhydroxides. *Chem. Mater.* 21, 5727–5742.

Pokrovski, G. S., Schott, J., Garges, F., and Hazemann, J. L. (2003). Iron (III)-silica interactions in aqueous solution: insights from X-ray absorption fine structure spectroscopy. *Geochim. Cosmochim. Acta* 67, 3559–3573.

Poulsen, H. F., Neuefeind, J., Neumann, H. B., Schneider, J. R., and Zeidler, M. D. (1995). Amorphous silica studied by high-energy X-ray-diffraction. *J. Non Cryst. Solids* 188, 63–74.

Qiu, X., Thompson, J. W., and Billinge, S. J. L. (2004). PDFgetX2: a GUI-driven program to obtain the pair distribution function from X-ray powder diffraction data. *J. Appl. Crystallogr.* 37, 678.

Ravel, B., and Newville, M. (2005). Athena, Artemis, Hephaestus: data analysis for X-ray absorption spectroscopy using IFEFFIT. *J. Synchrotron Radiat.* 12, 537–541.

Rentz, J. A., Kraiya, C., Luther, G. W. III, and Emerson, D. (2007). Control of ferrous iron oxidation within circumneutral microbial iron mats by cellular activity and autocatalysis. *Environ. Sci. Technol.* 41, 6084–6089.

Rodmacq, B. (1984). Superparamagnetic properties of small iron hydroxide precipitates in ion exchange membranes. *J. Phys. Chem. Solids* 45, 1119–1127.

Rose, J., Flank, A.-M., Masion, A., Bottero, J. Y., and Elmerich, P. (1997). Nucleation and growth mechanisms of Fe oxyhydroxide in the presence of PO4 ions. 2. P K-edge EXAFS study. *Langmuir* 13, 1827–1834.

Schwertmann, U., Friedl, J., and Kyek, A. (2004). Formation and properties of a continuous crystallinity series of synthetic ferrihydrites (2- to 6-line) and their relation to FeOOH forms. *Clays Clay Miner.* 52, 221–226.

Sedwick, P. N., McMurtry, G. M., and MacDougall, J. D. (1992). Chemistry of hydrothermal solutions from Pele's Vents, Loihi Seamount, Hawaii. *Geochim. Cosmochim. Acta* 56, 3643–3667.

Silva, N. J. O., Amaral, V. S., Carlos, L. D., Rodríguez-Gonzáles, B., Liz-Marzán, L. M., Berquó, T. S., Banerjee, S. K., de Zea Bermudez, V., Millán, A., and Palacio, F. (2008). Evidence of random magnetic anisotropy in ferrihydrite nanoparticles based on analysis of statistical distributions. *Phys. Rev. B* 77, 1–6.

Sudek, L. A., Templeton, A. S., Tebo, B. M., and Staudigel, H. (2009). Microbial ecology of Fe (hydr)oxide mats and Basaltic Rock from Vailulu'u Seamount, American Samoa. *Geomicrobiol. J.* 26, 581–596.

Suzdalev, I. P., Buravtsev, V. N., Imshennik, V. K., Maksimov, Y. V., Matveev, V. V., Novichikhin, S. V., Trautwein, A. X., and Winkler, H. (1996). Magnetic properties of ultrafine ferrihydrite clusters studied by Mössbauer spectroscopy and by thermodynamical analysis. *Z. Phys. D* 37, 55–61.

Swedlund, P. J., Miskelly, G. M., and McQuillan, A. J. (2009). An attenuated total reflectance IR study of silicic acid adsorbed onto a ferric oxyhydroxide surface. *Geochim. Cosmochim. Acta* 73, 4199–4214.

Templeton, A. S., Knowles, E. J., Eldridge, D. L., Arey, B. W., Dohnalkova, A. C., Webb, S. M., Bailey, J. V., Tebo, B. M., and Staudigel, H. (2009). A seafloor microbial biome hosted within incipient ferromanganese crusts. *Nature Geoscience* 2, 872–876.

Toner, B. M., Santelli, C. M., Marcus, M. A., Wirth, R., Chan, C. S., McCollom, T. M., Bach, W., and Edwards, K. J. (2009). Biogenic iron oxide formation at Mid-Ocean Ridge hydrothermal vents: Juan de Fuca Ridge. *Geochim. Cosmochim. Acta* 73, 388–403.

Vilge-Ritter, A., Rose, J., Masion, A., Bottero, J. Y., and Laine, J. M. (1999). Chemistry and structure of aggregates formed with Fe-salts and natural organic matter. *Colloids Surf. A Physicochem. Eng. Asp.* 147, 297–308.

Voegelin, A., Kaegi, R., Frommer, J., Vantelon, D., and Hug, S. J. (2010). Effect of phosphate, silicate, and Ca on Fe(III)-precipitates formed in aerated Fe(II)- and As(III)-containing water studied by X-ray absorption spectroscopy. *Geochim. Cosmochim. Acta* 74, 164–186.

Waychunas, G. A., Fuller, C. C., Rea, B. A., and Davis, J. A. (1996). Wide angle X-ray scattering (WAXS) study of "two-line" ferrihydrite structure: effect of arsenate sorption and counterion variation and comparison with EXAFS results. *Geochim. Cosmochim. Acta* 60, 1765–1781.

Webb, S. M. (2005). SIXPACK: a graphical user interface for XAS analysis using IFEFFIT. *Phys. Scr.* T115, 1011–1014.

Webb, S. M. (2006). *Sam's Microprobe Analysis Tool Kit.* Available at: http://smak.sams-xrays.com/

Wheat, C. G., Jannasch, H. W., Plant, J. N., Moyer, C. L., Samsone, F. J., and McMurtry, G. M. (2000). Continuous sampling of hydrothermal fluids from Loihi Seamount after the 1996 event. *J. Geophys. Res.* 105, 19353–19367.

Conflict of Interest Statement: The authors declare that the research was conducted in the absence of any commercial or financial relationships that could be construed as a potential conflict of interest.

Received: 22 November 2011; paper pending published: 27 December 2011; accepted: 12 March 2012; published online: 02 April 2012.

Citation: Toner BM, Berquó TS, Michel FM, Sorensen JV, Templeton AS and Edwards KJ (2012) Mineralogy of iron microbial mats from Loihi Seamount. Front. Microbio. ***3****:118. doi: 10.3389/fmicb.2012.00118*

This article was submitted to Frontiers in Microbiological Chemistry, a specialty of Frontiers in Microbiology.

Copyright © 2012 Toner, Berquó, Michel, Sorensen, Templeton and Edwards. This is an open-access article distributed under the terms of the Creative Commons Attribution Non Commercial License, which permits non-commercial use, distribution, and reproduction in other forums, provided the original authors and source are credited.

APPENDIX

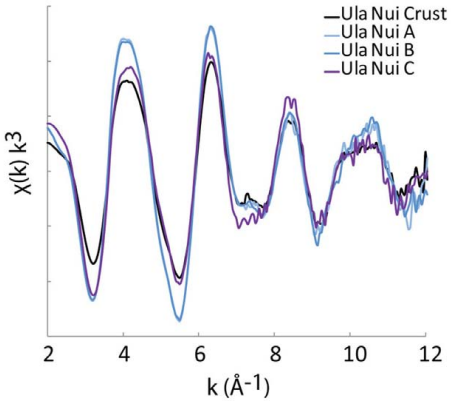

FIGURE A1 | Iron K-edge EXAFS spectra for the Ula Nui mats of Loihi Seamount having different sample handling and data collection conditions. The Ula Nui Crust was stored and analyzed frozen under N_2 at an SSRL microprobe beamline in fluorescence mode. Ula Nui-A/B were stored frozen, thawed, rinsed, and dried at 40˚C with analysis at the APS at a bulk beamline in transmission mode. Ula Nui C was stored in ambient seawater at 4˚C for 6 months, and was analyzed as rinsed/air-dry particles at an ALS microprobe beamline in fluorescence mode.

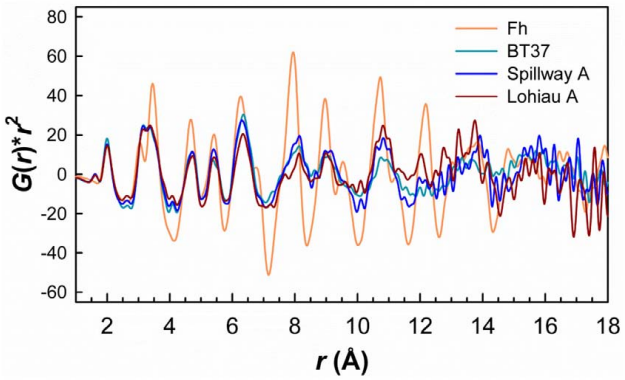

FIGURE A3 | Comparison of PDFs for BT37, Spillway A, and Lohiau A to the Fh reference plotted as $G(r)*r^2$ versus r to amplify the features at higher r values. Although subtle for the natural samples the features >∼4 Å are reasonable similar to those of synthetic Fh. Note that the PDF for Fh was also multiplied by 0.25 for comparison. Ula Nui-A and -B also showed similar features but due to impurities (e.g., birnessite) were excluded for clarity.

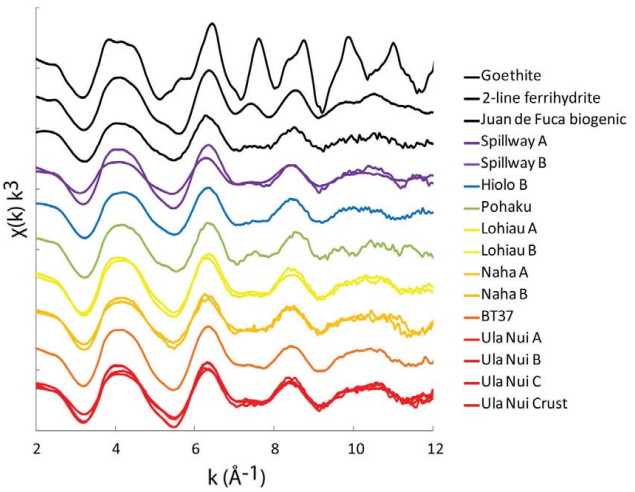

FIGURE A2 | Summary of all Fe K-edge EXAFS data collected for this study. Samples described in **Table 2**.

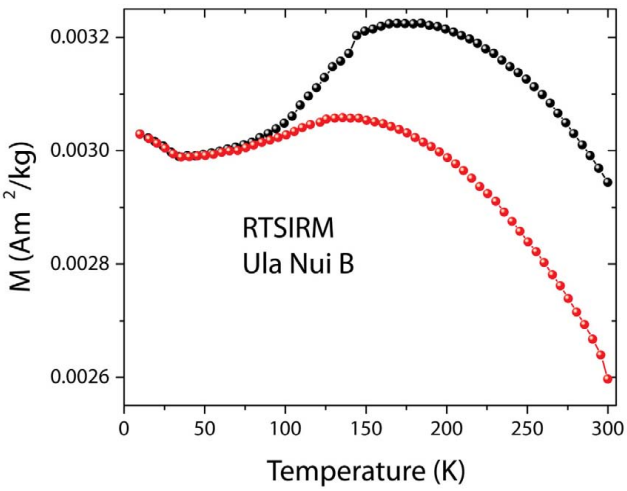

FIGURE A4 | The RTSIM shows the typical behavior associated with the presence of Ti-magnetite. The curves obtained on cooling (black circles) and on warming (red circles) are displayed. Due to its high magnetization, magnetite can be observed in the mats at very low concentrations.

frontiers in
MICROBIOLOGY

ORIGINAL RESEARCH ARTICLE
published: 22 May 2012
doi: 10.3389/fmicb.2012.00172

The microbial ferrous wheel in a neutral pH groundwater seep

Eric E. Roden[1]*, Joyce M. McBeth[2], Marco Blöthe[1,4], Elizabeth M. Percak-Dennett[1], Emily J. Fleming[2], Rebecca R. Holyoke[3], George W. Luther III[3], David Emerson[2] and Juergen Schieber[5]

[1] NASA Astrobiology Institute, Department of Geoscience, University of Wisconsin Madison, Madison, WI, USA
[2] Bigelow Laboratory for Ocean Sciences, East Boothbay, ME, USA
[3] College of Earth, Ocean, and Environment, University of Delaware, Lewes, DE, USA
[4] Federal Institute for Geosciences and Natural Resources, Geozentrum Hannover, Hannover, Germany
[5] Department of Geological Sciences, Indiana University, Bloomington, IN, USA

Edited by:
Benjamin Twining, Bigelow Laboratory for Ocean Sciences, USA

Reviewed by:
John Senko, The University of Akron, USA
Owen Duckworth, North Carolina State University, USA

***Correspondence:**
Eric E. Roden, Department of Geoscience, University of Wisconsin Madison, 1215W Dayton Street, Madison, WI 53706, USA.
e-mail: eroden@geology.wisc.edu

Evidence for microbial Fe redox cycling was documented in a circumneutral pH groundwater seep near Bloomington, Indiana. Geochemical and microbiological analyses were conducted at two sites, a semi-consolidated microbial mat and a floating puffball structure. *In situ* voltammetric microelectrode measurements revealed steep opposing gradients of O_2 and Fe(II) at both sites, similar to other groundwater seep and sedimentary environments known to support microbial Fe redox cycling. The puffball structure showed an abrupt increase in dissolved Fe(II) just at its surface (~5 cm depth), suggesting an internal Fe(II) source coupled to active Fe(III) reduction. Most probable number enumerations detected microaerophilic Fe(II)-oxidizing bacteria (FeOB) and dissimilatory Fe(III)-reducing bacteria (FeRB) at densities of 10^2 to 10^5 cells mL^{-1} in samples from both sites. *In vitro* Fe(III) reduction experiments revealed the potential for immediate reduction (no lag period) of native Fe(III) oxides. Conventional full-length 16S rRNA gene clone libraries were compared with high throughput barcode sequencing of the V1, V4, or V6 variable regions of 16S rRNA genes in order to evaluate the extent to which new sequencing approaches could provide enhanced insight into the composition of Fe redox cycling microbial community structure. The composition of the clone libraries suggested a lithotroph-dominated microbial community centered around taxa related to known FeOB (e.g., *Gallionella*, *Sideroxydans*, *Aquabacterium*). Sequences related to recognized FeRB (e.g., *Rhodoferax*, *Aeromonas*, *Geobacter*, *Desulfovibrio*) were also well-represented. Overall, sequences related to known FeOB and FeRB accounted for 88 and 59% of total clone sequences in the mat and puffball libraries, respectively. Taxa identified in the barcode libraries showed partial overlap with the clone libraries, but were not always consistent across different variable regions and sequencing platforms. However, the barcode libraries provided confirmation of key clone library results (e.g., the predominance of Betaproteobacteria) and an expanded view of lithotrophic microbial community composition.

Keywords: neutral pH, microbial, iron, cycling, microscale, 16S rRNA gene, barcode sequencing

INTRODUCTION

Redox cycling of iron (Fe) is a key process governing carbon and energy flow and the speciation and mobility of a wide variety of aqueous and solid-phase constituents in soils and sediments. Both reduction and oxidation of Fe are microbially catalyzed, and available evidence suggests that microbial Fe redox cycling takes place across a wide range of modern natural environments, including acidic and circumneutral pH soil/sediment (Peine et al., 2000; Sobolev and Roden, 2002; Roden et al., 2004; Wang et al., 2009; Lu et al., 2010; Coby et al., 2011) and groundwater seep systems (Emerson and Revsbech, 1994a; Emerson et al., 1999; Blöthe and Roden, 2009; Duckworth et al., 2009; Emerson, 2009; Bruun et al., 2010). Fe-based microbial ecosystems are hypothesized to be ancient, with both Fe(III)-reducing and Fe(II)-oxidizing microbes deeply rooted in the universal phylogenic tree (Emerson et al., 2010). Fe redox cycling is likely to have played a major role in the global biogeochemistry of Earth during the Archaean and early Proterozoic Eons (Walker, 1984; Konhauser et al., 2002, 2005), when massive deposition of Fe rich sediments (banded iron formations) occurred in association with the slow conversion of the atmosphere and oceans from anoxic to oxic conditions (Holland and Kasting, 1992). In addition, sedimentological, geochemical, and microfossil evidence suggest that Fe redox cycling took place in ancient (ca. two billion year old) layered microbial communities (Planavsky et al., 2009; Schopf et al., 2010).

Although the abiotic oxidation of Fe(II) is very rapid at neutral pH (half-life of ca. 5 min in air-saturated solution at pH 7), various studies have demonstrated that microbial (enzymatic) oxidation can compete effectively with abiotic oxidation under microaerobic (<10% air saturation) conditions (Roden et al., 2004). Microbial Fe(II) oxidation in modern neutral pH freshwater environments is typically dominated by Betaproteobacteria, principally members

of the Gallionellaceae family (genera *Gallionella* and *Sideroxydans*) and the Burkholderiales-related genus *Leptothrix* (James and Ferris, 2004; Duckworth et al., 2009; Bruun et al., 2010; Fleming et al., 2011). Fe(II)-oxidizing bacteria (FeOB) from the Rhodocyclaceae (Sobolev and Roden, 2004) and Comamonadaceae (genus *Comamonas*; Blöthe and Roden, 2009) have also been identified in such environments. At neutral pH, microbial Fe(II) oxidation produces Fe(III) oxides which can be readily used as electron acceptors for dissimilatory Fe(III)-reducing bacteria (FeRB; Emerson and Revsbech, 1994a; Straub et al., 1998; Blöthe and Roden, 2009; Emerson, 2009; Langley et al., 2009). FeRB are a diverse taxa which couple the oxidation of organic carbon or H_2 to the reduction of soluble and solid-phase Fe(III) forms (Lovley et al., 2004). Microbial Fe(III) oxide reduction results in Fe(II) regeneration, thus perpetuating a coupled Fe redox cycle given an input of organic matter to fuel Fe(III) reduction (Roden et al., 2004; Blöthe and Roden, 2009). The close spatial and metabolic coupling of microbial Fe reduction and oxidation has been proposed in various environments where an oxic/anoxic transition zone is observed (Sobolev and Roden, 2002; Roden et al., 2004; Haaijer et al., 2008; Blöthe and Roden, 2009; Bruun et al., 2010). However, details regarding the interaction between FeOB and FeRB and their activities *in situ* are not yet fully understood, e.g., compared to the detailed level of knowledge available on microbial sulfur cycling in microbial mats (Decho et al., 2010).

The spatial/temporal dynamics of Fe oxidation and reduction has critical implications for the abundance and persistence of reactive Fe(III) oxides in soils and sediments. This in turn may have a major influence on the migration of metals (e.g., divalent cations) and radionuclides with a high affinity for Fe(III) oxide surfaces, specifically in situations where Fe(II) and mobilized metals enter more oxidizing environments on the fringes of reducing zones, or where O_2 containing groundwater impinges on reduced zones. Comparatively little information is available on how FeOB and FeRB interact in these situations. Though not direct analogs to sedimentary environments, groundwater Fe seeps provide a convenient natural laboratory for studies of microbial Fe redox cycling. They are typically easily accessible, contain FeOB and FeRB capable of Fe redox cycling, and display spatial and temporal dynamics that are likely to be similar (though not in an absolute way) to those in the subsurface. In particular, mat structures in groundwater seeps tend to display millimeter-to-centimeter scale redox gradients analogous to those present in aquatic surface sediments (e.g., see Roden and Emerson, 2007) and physically/chemically heterogenous aquifer materials (e.g., see Hunter et al., 1998; Jakobsen, 2007). Thus, groundwater Fe seeps are both interesting in their own right and provide a conceptual analog to the myriad of surface and subsurface environments where Fe redox transformations may play a critical role in biogeochemical cycling.

This contribution provides a combined geochemical and microbiological investigation of a circumneutral pH groundwater Fe seep near Bloomington, IN, USA. This seep has been the subject of a limited range of prior work in the context of microbial mat formation (Scheiber, 2004; Schieber and Glamoclija, 2007). Voltammetric microelectrodes were employed to determine the *in situ* distribution of O_2 and soluble Fe species. The potential for native microbial communities to contribute to Fe cycling was assessed through most probable number (MPN) enumerations as well as *in vitro* Fe(III) reduction experiments. The limited microbial diversity within the seep allowed us to investigate several approaches for 16S rRNA gene analysis of microbial communities involved in Fe cycling. Both conventional full-length 16S rRNA gene clone libraries and high throughput barcode sequencing approaches (Illumina and 454) using either the V1, V4, or V6 regions of the 16S rRNA gene were employed to interrogate microbial community composition.

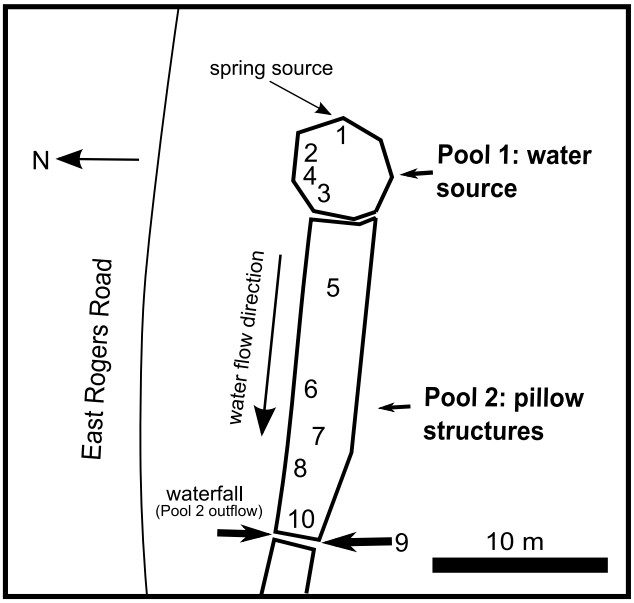

FIGURE 1 | Map of groundwater seep site in Bloomington, IN, USA. Numbers indicate sampling sites.

MATERIALS AND METHODS

FIELD SITE

Samples were collected in September 2008 from a groundwater seep in Jackson Creek near Bloomington, IN, USA (**Figure 1**). Flocculant, reddish brown Fe(III) oxide deposits are prominent at this site (**Figure 2**) due to oxidation of Fe(II) released during weathering of authigenic pyrite in the local subsurface (Schieber and Glamoclija, 2007). Ten locations were used to characterize the geochemistry of the site as a whole. Of these 10 sites, two areas were chosen for sample collection (see **Figures 1** and **2**): site 2, the top few cm of a semi-consolidated microbial mat; and site 7, a floating "puffball" structure that resembled a loose sphere with pillowy morphology. These sites will be referred to hereafter as the "microbial mat" (or "mat") and the "puffball," respectively. While mat-like structures are common to virtually all groundwater Fe seeps, puffball structures are site specific, and typically not present in fast flowing environments. However, they are not uncommon in slow flowing sites like the one studied here, and they provide an interesting contrast to mats in terms of the dimensions and dynamics of Fe redox cycling.

GEOCHEMICAL MEASUREMENTS

Temperature and pH were measured in the field using a portable thermistor and combination electrode. Field voltammetry was performed *in situ* at the 10 sampling sites, as well as on undisturbed materials from the microbial mat and the puffball. The survey measurements were made by placing the electrode several mm below the water surface. At sites 2 and 7, the voltammetric equipment and a micromanipulator were set up on a small wooden platform installed over a selected portion of the seep where lateral flow was minimal (**Figure 3**). Voltammetry allowed direct, *in situ*, measurement of the chemical species present in depth profiles with minimal perturbation during analysis. This system has proven to be very useful for analyzing a wide variety of redox species in a number of environments, including O_2, H_2O_2, Fe^{2+}, Fe^{3+}, $FeS_{(aq)}$, Mn^{2+}, H_2S, S_x^{2-}, S_8, and $S_2O_3^{2-}$ (Brendel and Luther, 1995; Rentz et al., 2007; Druschel et al., 2008; Luther et al., 2008). For analyses in the field, a DLK-100A Potentiostat (Analytical Instrument Systems, Flushing, NJ, USA) was employed with a computer controller and software.

A standard three-electrode system was used for all measurements and two versions were employed. In the first version, the working, reference, and counter electrodes were in separate glass or plastic housings. The working electrode was 0.1 mm diameter gold amalgam (Au/Hg) made by placing Au wire in a 5-mm glass tube drawn out to a 0.2- to 0.3-mm tip. The electrode was constructed, polished, and then plated with Hg after standard practices (Brendel and Luther, 1995; Luther et al., 2008). An Ag/AgCl reference electrode and a Pt counter electrode (both 0.5 mm wires encased in plastic) were placed in the water near the measurement site. The working electrode was mounted on a three-axis micromanipulator (CHPT manufacturing, Georgetown, DE, USA) operated by hand to descend in increments between 0.1 mm or larger increments for each sampling point. A second, more durable type of electrode was made with the Au wire housed in a stainless steel hypodermic needle (1.65 mm diameter by 75 or 125 mm length), which was used as the counter electrode. The working electrode was a 0.125-mm gold wire encased in Teflon (A-M systems, Inc.). Connector wires were attached to the Au wire and the stainless steel needle, and the top part of the working and counter electrodes were encased in rigid Teflon tubing. A non-conductive epoxy was used to stabilize the Au wire, stainless steel needle, and Teflon as one complete two electrode system (working and counter). The tip was polished and plated as above and mounted on the three-axis micromanipulator. The reference electrode was a separate 0.5 mm Ag/AgCl electrode as described above.

Electrochemical measurements began when the working electrode was carefully lowered to the point where the water surface tension was broken and the tip was as close to the surface as possible (defined as 0 depth). Cyclic voltammetry was performed in triplicate at each sampling point in the profile at 1000 mV/s between −0.1 and −1.8 V (vs. Ag/AgCl) with an initial potential of −0.1 V held for 2 s. In order to keep the working electrode surface clean, the electrode was held at −0.9 V between sampling scans.

Calibration of the electrodes was accomplished by standard addition methods using waters collected at the site and filtered through a 0.2-μm nuclepore filter. For O_2 standardization, natural waters were purged with air and then purged with ultra high-purity (UHP) argon to remove O_2; the O_2 detection limit was 3–5 μM. Sample water was also purged with UHP argon and then spiked with stock solutions of $FeCl_2$, $MnCl_2$, and Na_2S (ACS grade reagents). The water for the standards was purged with UHP argon before preparation. Detection limits for Fe(II), Mn(II), thiosulfate, and sulfide are 10, 5, 30, and 0.2 μM respectively.

IN VITRO FE(III) REDUCTION EXPERIMENTS

Fe(III) reduction experiments were conducted with mat and puffball materials to determine the potential for native microbial

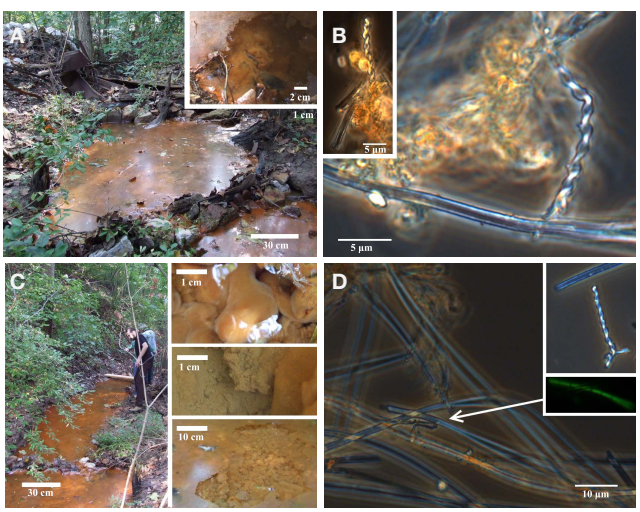

FIGURE 2 | Photos of field site and corresponding light microscopy images. Pool 1 **(A,B)** is the source zone for the seep; note semi-consolidated Fe(III) oxide mats (inset). Pool 2 **(C,D)** is downstream from Pool 1; inset shows images of puffball structures. Light microscopy images show stalk and sheath structures typical of microaerophillic FeOB at both sites.

FIGURE 3 | Photos of voltammetric microelectrode deployment in the microbial mat (left) and the puffball (right). The microbial mat was essentially on the surface, whereas the puffball was overlain by about 10 cm of water.

communities to reduce the Fe(III) phases present, without exogenous electron donor addition. Duplicate sealed, N_2-flushed 60-mL serum bottles were completely filled with a suspension of materials from each site. Small subsamples (0.5 mL) were collected over time (using a N_2-flushed syringe and needle) for 0.5 M HCl extraction (1 h) and Fe(II) determination using the Ferrozine assay (Stookey, 1970).

MPN DETERMINATIONS

A three-tube MPN technique was used to enumerate FeOB and FeRB, as well as aerobic and anaerobic heterotrophic organisms in materials from the mat and puffball. MPN values were calculated from standard MPN tables (Woomer, 1994). Aerobic and anaerobic (fermentative) heterotrophs were grown in tryptic soy broth (0.25% TSB) medium (Difco Laboratories, Detroit, MI, USA); tubes were scored positive by visual turbidity. A carbonate buffered (pH 6.8) freshwater medium (Widdel and Bak, 1992), was used for cultivation of FeRB and aerobic FeOB. For enumeration of FeRB, natural Fe(III) oxide (freeze-dried and autoclaved) from the groundwater Fe seep described in Blöthe and Roden (2009) was utilized at a final concentration of ca. 20 mmol L^{-1}. Either H_2 (10% in headspace) or a mix of 5 mM acetate and 5 mM lactate was used as the electron donor. Tubes for Fe(III) reduction were scored positive by measurement of Fe(II) formation. FeOB were enumerated in Fe(II)-O_2 opposing gradient cultures as described elsewhere (Sobolev and Roden, 2001). Tubes were scored positive by the formation of a compact growth band of cells plus Fe(III) oxide, as compared to the more diffuse band of Fe(III) oxide precipitation that formed in uninoculated controls (Emerson and Moyer, 1997). All MPN tubes were incubated between 1 and 4 weeks at room temperature.

DNA EXTRACTION AND MICROBIAL COMMUNITY ANALYSIS

DNA was extracted from samples collected from sites 2 and 7 using the Mo Bio PowerSoil® (Mo Bio, Carlsbad, CA, USA) DNA Isolation Kit. Near full-length 16S rRNA gene clone libraries were constructed using primers GM3F and GM4R (Muyzer et al., 1995). Clones were constructed using the pGEM-T vector and *Escherichia coli* JM109 competent cells (Promega). 16S rRNA gene sequences of recombinant transformants were obtained from the University of Wisconsin–Madison Biotechnology Center. Assembled clones were screened for chimeras using UCHIME (Edgar et al., 2011) and flagged sequences were subsequently examined in Pintail (Ashelford et al., 2005). Suspicious sequences were excluded from downstream analyses. The resulting sequences were aligned to the SILVA database (Pruesse et al., 2007), filtered using Mothur (Schloss et al., 2009; Schloss, 2010; version 1.22.0), and a distance matrix was generated. The sequences were clustered to identify unique OTUs at the 97% level, and taxonomies were assigned using the Ribosomal Database Project (RDP) classifier (Wang et al., 2007) employing a modified database optimized for detection of neutral pH FeOB. The classifications were bootstrapped 1000 times and taxonomic assignments were only made for bootstrap values of greater than 60%. Unique sequences were submitted to GenBank (accession numbers JQ906267–JQ906408).

High throughput barcode sequencing of PCR-amplified 16S rRNA gene fragments from sites 2 and 7 was completed by Mitch Sogin and colleagues at the Marine Biological Laboratory (MBL) at Woods Hole, MA, and Noah Fierer and colleagues the University of Colorado, Boulder. These sequencing analyses were performed on the same DNA extracts used to construct the clone libraries. Primers 967F and 1046R were used to target the V6 region of the 16S rRNA gene (Kysela et al., 2005; Sogin et al., 2006), and the amplicons were sequenced at MBL using the Roche 454 GS20 platform (∼60 bp reads). Primers 515F and 806R were used to target the V4 region of the 16S rRNA gene (Bates et al., 2011; Caporaso et al., 2010), and the amplicons were sequenced at EnGenCorp (University of South Carolina) using either the Roche 454 GS FLX platform (∼240 bp reads) or the Illumina GAIIx platform (∼100 bp reads). Illumina sequencing was also completed using primers 27F and 338R that targeted the V1 region of the 16S rRNA gene (∼80 bp reads; Hamady et al., 2008). The use of different sequencing platforms and regions of the 16S rRNA gene provided good technical replication for these samples.

Barcoded reads were processed using Mothur: the data were denoised using the Mothur implementation of the AmpliconNoise algorithm (Quince et al., 2011), barcodes and primers were removed, sequences were aligned to the SILVA database and filtered, chimeras were detected using UCHIME and removed, and all sequences were classified using a modified RDP classifier as described above for the clone library sequences.

RESULTS

GEOCHEMICAL MEASUREMENTS

Water temperature and pH showed little variation across the sampling transect (see **Figure 1**; **Table 1**), ranging from 14.9 to 15.9°C, and 6.4–6.6 respectively. Voltammetric measurements revealed O_2 concentrations below the detection limit of ca. 3 μM within a cm of the water–air interface at all but one site. Relatively high concentrations of dissolved Fe(II) (ca. 320–450 μM) were present at all sites; low levels of dissolved Mn(II) were detected at sites 4 (49 μM) and 6 (14 μM). Detectable quantities of dissolved or complexed Fe(III) were observed at all but one site; note that these are qualitative estimates only (expressed in units of nA, 3–50 nA) due to lack of site specific Fe(III) standards (Luther et al., 2008).

Voltammetric depth profiling at sites 2 (microbial mat) and 7 (puffball) revealed a sharp decrease in O_2 within a few mm of the water surface (**Figure 4**). The transition from oxic to very low (<3 μM) O_2 conditions took place at ca. 4 mm depth in the microbial mat, compared to less than 1 mm in water overlying the puffball structure. Dissolved Fe(II) and O_2 coexisted within the upper few mm of the mat, below which Fe(II) concentrations gradually increased. In contrast, dissolved Fe(II) concentrations were nearly uniform within the water column above the puffball, following a sharp increase within the upper ca. 2 mm. A second abrupt increase in dissolved Fe(II) concentration was detected during transection of the upper boundary of the puffball structure at ca. 5 cm depth. Dissolved Fe(III) was present within the upper few mm at the puffball site, but below detection within the mat.

MPN ENUMERATIONS AND *IN VITRO* FE(III) REDUCTION

Most probable number enumerations revealed substantial numbers of culturable FeOB and FeRB (10^2 to 10^5 cells mL^{-1}) in both the mat and puffball materials (**Table 2**). The abundance of these

Table 1 | Results of geochemical survey.

Survey site	Temp (°C)	pH	O_2 (μM)	Fe(II) (μM)	Mn(II) (μM)	Fe(III) (nA)
Site 1	14.9	6.44	BD[a]	322	BD	3.5
Site 2 (microbial mat)	15.1	6.49	BD	355	BD	30
Site 3	15.1	6.45	BD	367	BD	BD
Site 4	15.6	6.50	BD	307	49	22
Site 5	15.4	6.52	BD	406	BD	23
Site 6	15.8	6.54	BD	338	14	11
Site 7 (puffball)	15.7	6.47	BD	394	BD	20
Site 8	15.8	6.53	BD	336	BD	28
Site 10	15.9	6.53	BD	443	BD	15
Site 9	15.9	6.60	BD	328	BD	51

[a] *Below detection.*

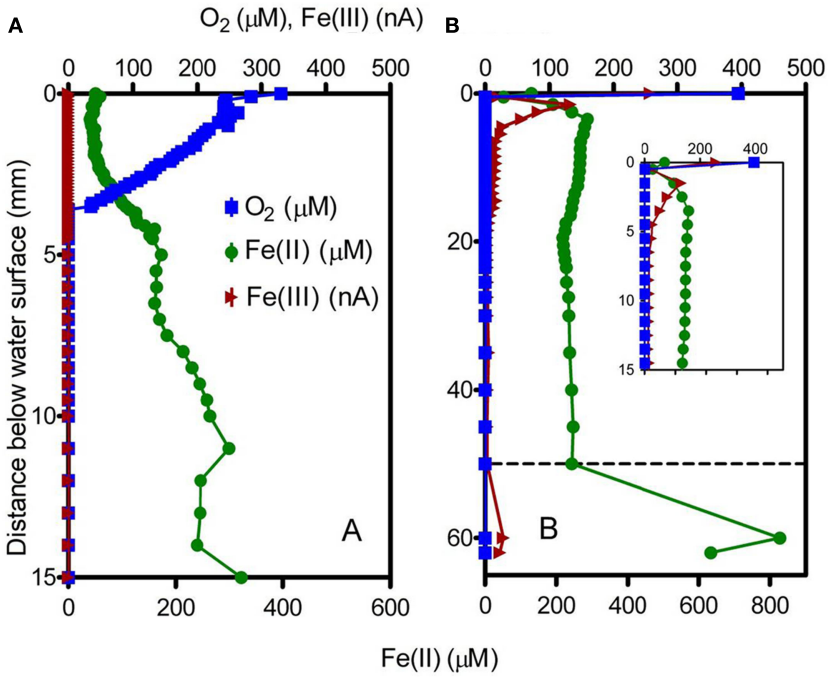

FIGURE 4 | Voltammetric microelectrode profiles for the microbial mat (A) and the puffball structure (B). Dashed line in **(B)** indicates the approximate surface of the flocculant puffball structure; inset shows an expanded scale of the first 15 mm.

organisms was 10- to 1000-fold lower than culturable aerobic and anaerobic heterotrophs. The presence of culturable FeRB was consistent with the results of the *in vitro* Fe(III) reduction experiments, which showed the potential for Fe(III) reduction during anoxic incubation of materials from both sites (**Figure 5**). Fe(II) concentrations leveled off after ca. 25 days, likely due to depletion of electron donors, as no exogenous organic matter was added to the oxide suspensions. Detectable Fe(III) reduction took place within an hour after isolation of the puffball material in sealed, completely filled serum bottles. An initial decline in Fe(II) was observed during the first day of incubation of the mat material, likely due to oxidation of Fe(II) by O_2 entrained during transfer of the flocculant material to the serum bottles. Despite the initial difference in behavior for the two samples, when integrated over the 25-day incubation period, first-order rate constants for Fe(III) reduction were quite similar (ca. 0.085 and 0.083 day^{-1} for the mat and puffball materials, respectively; see **Figure 5**).

MOLECULAR MICROBIAL COMMUNITY ANALYSIS

Clone libraries

The 16S rRNA gene clone libraries revealed modest phylogenetic diversity in the mat and puffball materials (**Figure 6**). A total of 12 families comprising 18 genera were identified (**Table 3**). Proteobacteria were the dominant components of the libraries, accounting for ≥95% of all clones at both sites (**Figure 7**). Betaproteobacteria in turn accounted for ca. 95 and 50% of Proteobacteria

Table 2 | Most probable number values for different types of microorganisms in materials from the microbial mat and puffball.

Physiological group	MPN, cells mL^{-1} (±range)	
	Microbial mat (site 2)	Puffball (site 7)
Aerobic heterotrophs	5.13×10^7 ($\pm 4.69 \times 10^7$)	5.39×10^6 ($\pm 4.92 \times 10^6$)
Anaerobic heterotrophs	2.15×10^7 ($\pm 1.97 \times 10^6$)	9.52×10^3 ($\pm 8.68 \times 10^3$)
Fe(III) reducers with acetate/lactate[a]	6.82×10^5 ($\pm 2.54 \times 10^5$)	9.78×10^3 ($\pm 8.92 \times 10^3$)
Fe(III) reducers with hydrogen[a]	2.20×10^4 ($\pm 2.01 \times 10^4$)	8.57×10^2 ($\pm 7.83 \times 10^2$)
Aerobic Fe(II) oxidizers	1.71×10^3 ($\pm 1.56 \times 10^3$)	7.84×10^3 ($\pm 7.16 \times 10^3$)

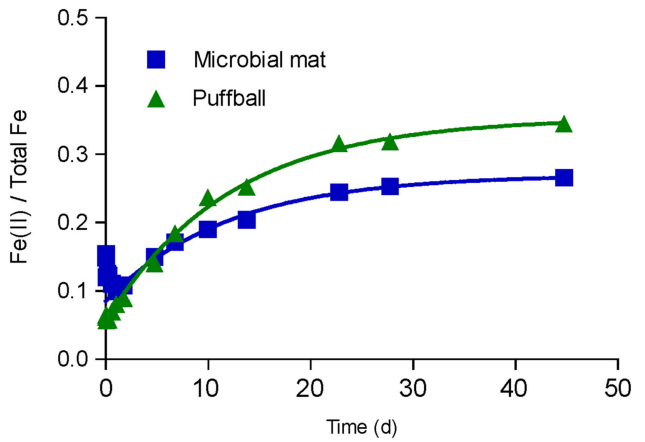

FIGURE 5 | *In vitro* Fe(III) reduction in materials from the microbial mat and puffball. Symbols show the average ratio of Fe(II) to total Fe in 0.5 M HCl extracts from duplicate cultures; lines show results of non-linear least-squares regression fits of the Fe(II) accumulation data to an integrated first-order rate law $Fe(II)_t = Fe(II)_0 + [Fe(II)_{max} - Fe(II)_0] \times [1 - \exp(-k_{red}t)]$. Estimated k_{red} values were 0.085 and 0.083 day^{-1} for the microbial mat and puffball materials, respectively.

in the mat and puffball libraries, respectively, with Gammaproteobacteria and Deltaproteobacteria being much more abundant in the puffball libraries.

Simple inspection of the phylogenetic assignments suggested the presence of recognized Fe(II)-oxidizing and Fe(III)-reducing taxa (see below). A series of BLAST searches was conducted to gain further insight into the potential physiological capacities of the specific taxa detected in the libraries. Although caution must exercised in inferring physiology based on 16S rRNA gene similarity (Achenbach and Coates, 2000), this basic approach, pioneered by Pace (1996, 1997), remains standard practice in microbial ecology. BLAST was used not to exhaustively catalog phylogenetic relatives to the clone sequences, but rather to search for possible evidence of Fe redox metabolic capacity in the identified taxa (see **Table 3**). We focused on pure culture relatives of the clone sequences, for which reasonable physiological inferences could be made. In some cases, the top BLAST matches corresponded to organisms in pure culture that are known to carry out Fe redox metabolism; in other cases, matches to organisms with such physiology were further down in the list of BLAST hits. Only matches with ≥95% sequence similarity (nominal cut-off for assigning genus-level affiliation; Gillis et al., 2001) were considered, except in cases where the top match had a lower degree of similarity.

The most abundant clones in both libraries were closely related to the well known microaerophilic FeOB from the *Gallionella*/*Sideroxydans* group (Emerson et al., 2010). Other abundant FeOB-related phylotypes included ones very similar to Fe(II)-oxidizing denitrifying bacteria from the genus *Aquabacterium* (Buchholz-Cleven et al., 1997), and ones closely related to the microaerophilic Fe(II)-oxidizing *Comamonas* strain IST-3 (Blöthe and Roden, 2009). Both libraries also included sequences related to known Fe(III)-reducing organisms, including *Rhodoferax* at site 2, and *Desulfovibrio*, *Aeromonas*, and *Geobacter* at site 7. Although *Desulfovibrio* is typically known as a sulfate-reducing bacterium, various strains from this genus are known to be capable of coupling organics or H_2 oxidation to Fe(III) reduction (Coleman et al., 1993; Lovley et al., 1993). *Aeromonas* is a facultative anaerobe capable of reducing Fe(III) in complex medium (Knight and Blakemore, 1998), whereas *Rhodoferax* and *Geobacter* are well known organic acid oxidizing FeRB (Lovley et al., 2004). Other sequences present in the libraries were similar to lithotrophic reduced sulfur (*Sulfuricella*, *Ottowia*) and methane (*Methylobacter*, *Methylosarcina*, *Methylomonas*) oxidizing organisms, as well as aerobic and anaerobic heterotrophs.

Barcode sequencing

High throughput barcode sequencing was applied to the same DNA extracts used to construct the clone libraries, resulting in (1) 2400–3000 V4 region sequences and 15,000–16,000 V6 region sequences on the Roche 454 platform; and (2) 20,000–50,000 V1 region sequences and 35,000–120,000 V4 region sequences on the Illumina platform. There was good, though not perfect, overlap among taxa in the different barcode libraries at the phylum level, and at the class level within the Proteobacteria (**Figure 7**). There was also general agreement between the composition of the conventional clone and barcode libraries at these levels of phylogenetic resolution.

Similar relative abundances of Betaproteobacteria sequences within the order Burkholderiales were recorded in all four barcode libraries for the mat and puffball materials (**Tables 4** and **5**), confirming the predominance of these taxa indicated by the clone library results. The significant number of Desulfovibrionales within the Deltaproteobacteria in the puffball clone library was also reflected in each of the barcode libraries. Beyond these overlaps, no broad agreement between the different barcode and the clone library results was evident for taxonomic groupings below the phylum/class level. For example, the predominance of Gallionellaceae in the clone libraries was not evident in the barcode libraries. In addition, Firmicutes from the class Bacilli were well-represented in all mat barcode libraries, but were completely absent from the corresponding clone library. In contrast, Bacilli and other Firmicutes were fairly well-represented (10% of total) in the clone

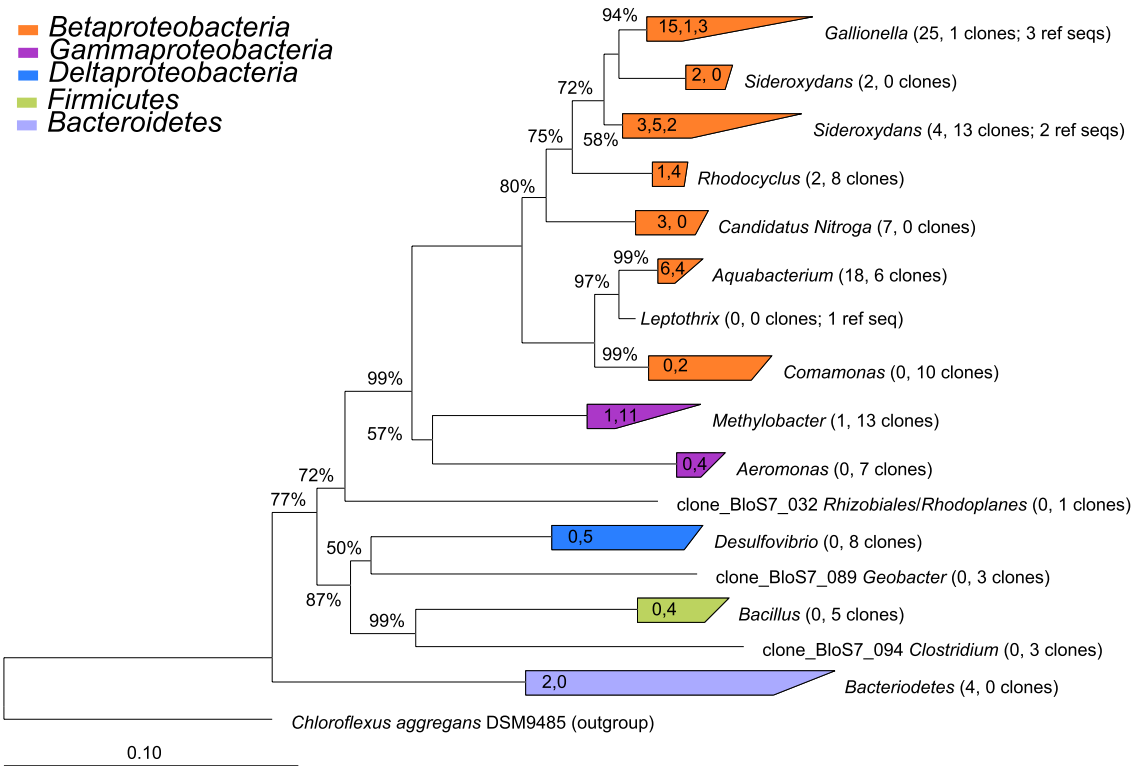

FIGURE 6 | Phylogenetic tree constructed from 16S rRNA gene clones from sites 2 (microbial mat) and 7 (puffball). The number of clones from each of sites 2 and 7 and the number of reference sequences (where used) are indicated beside each taxon in parentheses (number of site 2 clones, number of site 7 number of clones; number of reference sequences). The values in the triangles indicate the number of unique clones from each site and the number of reference sequences used to construct the tree in arb, respectively (values separated by commas). The tree was prepared using neighbor joining analysis with Jukes–Canter correction. Percentages on nodes represent 1000 bootstrap analyses; only values greater than 50% are shown. More details on major taxa identified in each sample are provided in **Table 3**.

library for the puffball, but were completely absent from all four of the barcode libraries. The same was true for Methylococcales related sequences in the puffball, which were abundant in the clone library but absent from the barcode libraries. Finally, the significant number of *Pseudomonas* and *Sphingobacteria* related sequences in some (but not all) of the puffball barcode libraries were absent from the corresponding clone library.

DISCUSSION

GEOCHEMICAL ELUCIDATION OF AN EXTANT MICROBIAL FERROUS WHEEL

The voltammetric microelectrode measurements provided evidence of Fe redox cycling in both the mat and puffball materials. The steep opposing gradients of Fe(II) and O_2 are analogous to those documented previously in circumneutral Fe seep and freshwater sedimentary environments (Emerson and Revsbech, 1994b; Sobolev and Roden, 2002; Druschel et al., 2008; Bruun et al., 2010), as well as *in situ* gradients in Fe rich microbial mats at the Loihi Seamount (Glazer and Rouxel, 2009). These conditions provide an ideal situation for coupled Fe oxidation and reduction, with poorly crystalline Fe(III) oxides generated during Fe(II) oxidation serving as excellent electron acceptors for FeRB (Straub et al., 1998; Roden et al., 2004; Blöthe and Roden, 2009). In addition, soluble or complexed Fe(III) (or very small colloidal phases) formed during Fe(II) oxidation (cf. Sobolev and Roden, 2001) also represents an ideal electron acceptor for FeRB, and it is notable in this regard that almost all of the sampling sites showed the presence of Fe(III) detectable by voltammetry (**Table 1**).

This study did not include determination of the kinetics of Fe(II) oxidation or the contribution of microbial activity to this process. Stirred reactor studies with FeOB pure cultures (Neubauer et al., 2002; Druschel et al., 2008) and native groundwater seep microorganisms (Emerson and Revsbech, 1994a; Rentz et al., 2007) have shown that FeOB activity can accelerate Fe(II) oxidation rates two to fivefold, although competition with abiotic oxidation [including catalysis of abiotic oxidation by amorphous Fe(III) oxide surfaces] is high at neutral pH. Druschel et al. (2008) showed that the relative contribution of microbial activity to Fe(II) oxidation was greatest at O_2 concentrations of less than ca. 50 μM (ca. 18% saturation), whereas biotic and abiotic rates were identical at full O_2 saturation (275 μM). Experiments employing diffusion probes in Fe(II)-O_2 opposing gradient cultures have indicated that microbial activity can account for ≥90% of Fe(II) oxidation under diffusive transport limited conditions (Sobolev and Roden, 2001; Roden et al., 2004) where O_2 concentrations within the zone of Fe(II)-O_2 reaction are typically ca. 20% saturation.

Table 3 | Summary of taxa identified in the 16S rRNA gene clone libraries.

Site	Family	Genus	% Total	Representative pure culture match	Accession No.	Similarity (%)	Physiology	Reference(s)
Microbial mat (61 clones)	Gallionellaceae	*Gallionella*	37.7	*Gallionella capsiferriformans* ES-2	CP002159.1	96–97	**Fe(II) Ox, O_2 red**	Emerson and Moyer (1997)
	Unclassified Burkholderiales	*Aquabacterium*	29.5	Denitrifying Fe(II)-oxidizing bacteria	U51102.1	99	**Fe(II) Ox, NO_3^- red**	Buchholz-Cleven et al. (1997)
	Gallionellaceae	Candidatus Nitroga	11.5	*Sulfuricella denitrificans*	AB506456.1	92	$S^0/S_2O_3^{2-}$ Ox, O_2/NO_3^- red	Kojima and Fukui (2010)
	Comamonadaceae	*Rhodoferax*	8.2	*Rhodoferax ferrireducens* T118	CP000267.1	92	**Fe(III) red**	Finneran et al. (2003)
	Gallionellaceae	*Sideroxydans*	6.6	*Sideroxydans lithotrophicus* ES-1	CP001965.1	94–96	**Fe(II) Ox, O_2 red**	Emerson and Moyer (1997)
	Unclassified Bacteroidetes	Unclassified Bacteroidetes	6.6	Bacteroidetes bacterium RL-C	AB611036.1	84–94	Fermentation	Qiu and Sekiguchi, unpublished
Puffball (80 clones)	Gallionellaceae	*Sideroxydans*	15.0	*Sideroxydans lithotrophicus* ES-1	CP001965.1	97–99	**Fe(II) Ox, O_2 red**	Emerson and Moyer (1997)
	Methylococcaceae	*Methylobacter*	13.8	*Methylobacter* sp. BB5.1	AF016981.1	94–96	CH_4 Ox, O_2 red	Smith et al. (1997)
	Comamonadaceae	*Comamonas*	11.3	*Comamonas* sp. IST-3	DQ386262.1	100	**Fe(II) Ox, O_2 red**	Blöthe and Roden (2009)
	Desulfovibrionaceae	*Desulfovibrio*	10.0	*Desulfovibrio putealis* strain B7-43	NR–029118.1	99	SO_4^{2-} red; **Fe(III) red**	Basso et al. (2005); Lovley et al. (1993)
	Aeromonadaceae	*Aeromonas*	8.8	*Aeromonas hydrophila* strain ATCC 7966	X60404.2	98	**Fe(III) red**	Knight and Blakemore (1998)
	Unclassified Burkholderiales	*Aquabacterium*	7.5	Denitrifying Fe(II)-oxidizing bacteria	U51102.1	99	**Fe(II) Ox, NO_3^- red**	Buchholz-Cleven et al. (1997)
	Rhodocyclaceae	*Propionivibrio*	7.5	*Propionivibrio limicola* strain GolChi1	NR–025455.1	97	Fermentation	Brune et al. (2002)
	Bacillaceae	*Bacillus*	6.3	*Bacillus* sp. MB-5	AF326363.1	99	Ferm; Mn(II) Ox, O_2 red	Francis and Tebo (2002)
	Rhodocyclaceae	*Rhodocyclus*	5.0	*Rhodocyclus tenuis* strain DSM110	D16209.1	97	Anoxygenic Phototroph	Hiraishi (1994)
	Unclassified Clostridiales	*Blautia*	3.8	*Eubacterium plexicaudatum* ASF 492	AF157054.1	94	Fermentation	Dewhirst et al. (1999)
	Geobacteraceae	*Geobacter*	3.8	*Geobacter* sp. strain CdA-2	Y19190.1	96	**Fe(III) red**	Cummings et al. (2000)
	Methylococcaceae	*Methylosarcina*	2.5	*Methylosarcina lacus* strain LW14	NR–042712.1	96	CH_4 Ox, O_2 red	Kalyuzhnaya et al. (2005)
	Hyphomicrobiaceae	*Rhodoplanes*	1.3	*Alphaproteobacterium* Shinshu-th1	AB121772.1	96	Aerobic Heterotroph	Hamaki et al. (2005)
	Comamonadaceae	*Hylemonella*	1.3	*Ottowia thiooxydans* strain K11	NR–029001.1	100	$S_2O_3^{2-}$ Ox, O_2/NO_3^- red	Spring et al. (2004)
	Gallionellaceae	*Gallionella*	1.3	*Gallionella capsiferriformans* ES-2	CP002159.1	96–97	**Fe(II) Ox, O_2 red**	Emerson and Moyer (1997)
	Crenotrichaceae	*Crenothrix*	1.3	*Methylomonas* sp. LW15	AF150794.1	94	CH_4 Ox, O_2 red	Costello and Lidstrom (1999)

Taxa related to known FeOB and Fe(III) reducing organisms are shown in bold in the Physiology column.

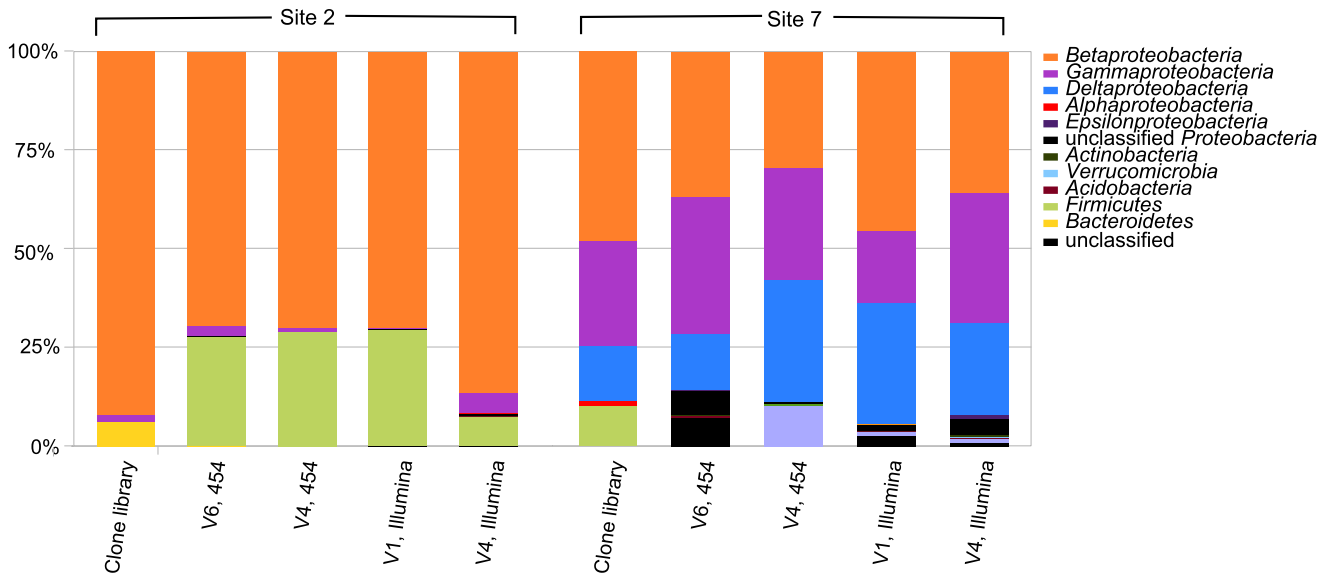

FIGURE 7 | Relative abundance of taxa at the phylum/class level in the 16S rRNA gene clone and barcode libraries from sites 2 (microbial mat) and 7 (puffball). V1, V4, and V6 refer to different variable regions of the 16S rRNA gene; 454 refers to the Roche 454 GS20 (V6) or GS FLX (V4) platform; Illumina refers to the Illumina GAIIx platform. See **Tables 4** and **5** for a more detailed taxonomic breakdown of the components of the different libraries.

The quiescent conditions (no visible water movement or turbulent mixing) at both the mat and puffball sites suggest that Fe(II)-O_2 interactions were likely diffusion limited at the time of sampling. The mat, which was overlain by only a thin layer of water (<1 cm; see **Figure 3**), showed a relatively compact gradient system only a few mm in spatial extent (**Figure 4A**). The observed Fe(II) and O_2 gradients were similar to those in opposing gradient FeOB culture systems in which microbial catalysis dominates Fe(II) oxidation (Sobolev and Roden, 2001), as well as those in diffusion controlled FeOB–FeRB coculture experiments where active Fe redox cycling has been documented (Sobolev and Roden, 2002; Roden et al., 2004).

In contrast, the puffball site, where the water depth was ca. 10 cm, represented a different, less compact type of diffusion limited Fe(II)-O_2 reaction system. Here, low O_2 conditions (<3 μM) were achieved within a mm of the water surface (**Figure 4B**), analogous to other "open water" (i.e., not mat colonized) locations in the seep, where O_2 was undetected just below the water surface and dissolved Fe(II) concentrations were 300–400 μM (**Table 1**). These observations suggest the possibility that the puffballs may originate from conglomerates of bacterial cells and oxides that form at the air–water interface and later coagulate and sink in globular form. Working a few years earlier with samples from the same environment, Schieber and Glamoclija (2007) showed by scanning electron microscopy (SEM) that mat materials are composed of nanometer-sized amorphous Fe(III) oxide particles coordinated with bacterial cells (including stalk and sheath-forming FeOB similar to those shown in **Figure 2**) and extracellular polymeric substances (EPS). In the case of well-consolidated mats, these materials were arranged in a columnar, honeycomb-like matrix. It seems possible that similar structures were present in the puffball materials, although it is not possible to image such structures via SEM as they lose their integrity during sampling. One would expect that such structures, assembled near the water surface, would eventually sink under their own weight, leading to the observed accumulation of fluffy precipitates at depth in the water column.

An alternative explanation for puffball formation is that low levels of dissolved O_2 (below the detection limit in this study) do in fact exist deeper in the water column, leading to Fe(II) oxidation and oxide accumulation at depth. This explanation is consistent with the observation (Schieber, unpublished) that under conditions of water column stagnation, the puffballs appear to form at depth and grow upwards until they intercept the surface. The presence of submicromolar levels of dissolved O_2 at depths below the macroscopic O_2 gradient has been documented in oxygen-minimum-zones in the ocean (Revsbech et al., 2009; Canfield et al., 2010) and in the permanently stratified Black Sea water column (Clement et al., 2009). In the case of the Black Sea, indigenous aerobic bacteria were shown to be capable of efficient oxidation of dissolved Mn(II) at O_2 concentrations well below 1 μM (Clement et al., 2009). It is logical to assume that aerobic FeOB share this same ability, although detailed information on the kinetics of enzymatic Fe(II) oxidation at very low O_2 concentration is not available. Nitrate-dependent Fe(II) oxidation could also contribute to Fe(III) oxide accumulation at depth in the stagnant water column. The presence of dissolved, presumably organic complexed Fe(III) (Taillefert et al., 2000) at depths below which O_2 could be detected (**Table 1**; **Figure 4**) is consistent with ongoing Fe(II) oxidation under very low O_2 or anoxic conditions.

Table 4 | Relative abundance (percentage of total sequences) of different phylogenetic taxa obtained conventional cloning and sequencing (Clone lib) and by pyrosequencing of 16S rRNA genes from site 2 (microbial mat) using different sequencing platforms and primer sets.

Taxa	Percent of sequences				
	Clone lib	V4–454	V6–454	V1-Illumina	V4-Illumina
Bacteria/Firmicutes	0	**29**	**28**	**29**	8
Bacilli	0	**29**	**28**	**29**	7
Bacillales	0	**29**	**28**	**29**	7
Sporolactobacillaceae	0	0	**28**	0	0
Tuberibacillus	0	0	**28**	0	0
Bacillaceae	0	**29**	0	**29**	7
Bacillus	0	**24**	0	**29**	0
Bacteria/Firmicutes	6	0	0	0	0
Bacteria/Proteobacteria	**94**	**71**	**72**	**70**	**92**
Betaproteobacteria	**94**	**70**	**69**	**70**	**86**
Burkholderiales	**38**	**67**	**63**	**62**	**76**
Comamonadaceae	8	**67**	**62**	**61**	**75**
Acidovorax	0	**59**	2	<1	0
Pseudorhodoferax	0	0	**59**	0	0
Rhodoferax	9	0	0	0	0
Unclassified Comamonadaceae	0	5	2	**60**	**75**
Unclassified Burkholderiales	**30**	0	0	0	0
Aquabacterium	**30**	0	0	0	0
Rhodocyclales	0	<1	1	5	6
Rhodocyclaceae	0	<1	1	5	6
Propionivibrio	0	0	0	5	0
Unclassified Rhodocyclaceae	0	<1	1	0	6
Nitrosomonadales	**56**	<1	5	0	0
Gallionellaceae	**56**	<1	5	0	0
Gallionella	**38**	0	0	0	0
Candidatus Nitrotoga	11	0	0	0	0
Sideroxydans	7	0	5	0	0
Unclassified Betaproteobacteria	0	<1	<1	0	5
Gammaproteobacteria	0	1	3	<1	5
Total no. of sequences	57	3076	15,689	19,747	119,631

V1, V4, and V6 refer to different variable regions of the 16S rRNA gene; 454 refers to the Roche 454 GS20 (V6) or GS FLX (V4) platform; Illumina refers to the Illumina GAIIx platform. Black, red, blue, green, and magenta text refer to Domain/Phylum, Class, Order, Family, and Genus level assignments, respectively. Taxa present at >20% abundance are shown in bold; relative abundances of <1% ranged from 0.1 to 0.99%; values of 0 correspond to <0.1%.

The association of Fe(III) oxides with organic materials and their accumulation in the semi-consolidated mat and puffball structures provides an explanation for Fe(III) reduction activity observed in the Fe(III) reduction experiments (**Figure 5**), with senescent FeOB and other bacterial cells and organics (e.g., originating from the surrounding forest soils) providing the electron donors for Fe(III) reduction. At the puffball site in particular, decomposition of organics coupled to Fe(III) oxide reduction can account for the abrupt increase in Fe(II) concentration within the puffball compared to the overlying water (**Figure 4B**). The fact that Fe(III) oxide reduction commenced immediately (no lag period) during anoxic incubation of these materials is consistent with the presence of ongoing FeRB activity. Incomplete (25–35%) Fe(III) oxide reduction was observed in both the mat and puffball incubations, in contrast to previous studies with electron donor (acetate/lactate) amended seep materials (not conducted in this study) in which near complete (≥80%) reduction has been documented (Emerson and Revsbech, 1994b; Blöthe and Roden, 2009). These results suggest that Fe(III) reduction was carbon-limited, which makes sense given that large quantities of Fe(III) oxide accumulate in the seep environment. Nevertheless, simple kinetic calculations indicate that partial Fe(II) regeneration via decomposition of organic carbon coupled to Fe(III) reduction has the potential to significantly promote Fe turnover in redox interfacial environments (Blöthe and Roden, 2009). Collectively, the results of this and a limited number of related studies in Fe seeps (Blöthe and Roden, 2009; Bruun et al., 2010), freshwater wetland surface sediments (Sobolev and Roden, 2002), and plant rhizosphere sediments (Weiss et al., 2003, 2005) provide plausible real-world examples of the type of closely coupled microbial

Table 5 | Relative abundance of different phylogenetic taxa obtained by cloning and sequencing and pyrosequencing of 16S rRNA genes from site 7 (puffball) using different sequencing platforms and primer sets.

Taxa	Percent of sequences				
	Clone lib	V4–454	V6–454	V1-Illumina	V4-Illumina
Bacteria/Firmicutes	10	0	0	0	0
Bacilli	6	0	0	0	0
Bacillales	6	0	0	0	0
Bacillaceae	6	0	0	0	0
Bacillus	6	0	0	0	0
Clostridia	4	0	0	0	0
Clostridiales	4	0	0	0	0
Unclassified Clostridiales	4	0	0	0	0
Blautia	4	0	0	0	0
Bacteria/Proteobacteria	**90**	**89**	**92**	**96**	**97**
Alphaproteobacteria	1	0	0	0	0
Rhizobales	1	0	0	0	0
Hyphomicrobiaceae	1	0	0	0	0
Rhodoplanes	1	0	0	0	0
Betaproteobacteria	**48**	**29**	**37**	**45**	**36**
Burkholderiales	**20**	**26**	**31**	**32**	**22**
Comamonadaceae	12	**23**	**28**	**31**	19
Comamonas	11	**20**	**21**	0	17
Hylemonella	1	0	0	0	0
Pseudorhodoferax	0	0	4	0	0
Unclassified Comamonadaceae	0	2	2	**31**	2
Unclassified Burkholderiales	8	0	0	0	0
Aquabacterium	8	0	0	0	0
Methylophilales	0	<1	<1	3	3
Methylophilaceae	0	<1	<1	3	3
Methylophilus	0	<1	<1	3	3
Nitrosomonadales	16	<1	5	0	0
Gallionellaceae	16	<1	5	0	0
Gallionella	1	0	0	0	0
Sideroxydans	15	0	5	0	0
Rhodocyclales	12	<1	<1	6	5
Rhodocyclaceae	15	<1	<1	6	5
Propionivibrio	7	<1	0	6	0
Rhodocyclus	5	0	0	0	0
Unclassified Rhodocyclaceae	0	<1	<1	0	5
Unclassified Rhodocyclales	0	2	<1	5	5
Deltaproteobacteria	14	**31**	14	**31**	**23**
Desulfovibrionales	10	**31**	14	0	**23**
Desulfovibrionaceae	10	**31**	14	0	**23**
Desulfovibrio	10	**31**	14	0	**23**
Desulfuromonodales	4	0	0	0	0
Geobacteraceae	4	0	0	0	0
Geobacter	4	0	0	0	0
Unclassified Deltaproteobacteria	0	0	0	**31**	0
Gammaproteobacteria	**27**	**29**	**35**	**18**	**33**
Aeromonadales	9	5	<1	<1	6
Aeromonadaceae	9	5	<1	<1	6
Aeromonas	9	5	<1	<1	6

(Continued)

Table 5 | Continued

Taxa	Percent of sequences				
	Clone lib	V4–454	V6–454	V1-Illumina	V4-Illumina
Alteromonadales	0	0	7	0	0
Alteromonadaceae	0	0	7	0	0
Marinobacter	0	0	7	0	0
Methylococcales	18	0	0	0	0
Crenotrichaceae	1	0	0	0	0
Crenothrix	1	0	0	0	0
Methylococcaceae	17	0	0	0	0
Methylobacter	14	0	0	0	0
Methylosarcina	3	0	0	0	0
Pseudomonadales	0	**23**	3	17	**25**
Pseudomonadaceae	0	**23**	<1	17	**23**
Pseudomonas	0	**22**	<1	17	13
Unclassified Pseudomonadaceae	0	<1	0	0	10
Xanthomonadales	0	<1	12	<1	<1
Xanthomonadaceae	0	0	11	0	<1
Dyella	0	0	11	0	0
Unclassified Xanthomonadales	0	<1	12	<1	2
Unclassified Proteobacteria	0	<1	6	2	4
Bacteria/Bacteroidetes	0	10	<1	<1	1
Sphingobacteria	0	10	<1	0	<1
Sphingobacteriales	0	10	<1	0	<1
Unclassified Sphingobacteriales	0	10	0	0	<1
Unclassified Sphingobacteria	0	<1	0	<1	<1
Unclassified Bacteria	0	0	7	3	<1
Total no. of sequences	80	2385	15,573	50,093	35,512

*See **Table 2** caption for details.*

Fe redox cycle documented previously for cocultures of aerobic FeOB and FeRB (Sobolev and Roden, 2002; Roden et al., 2004).

MICROBIOLOGICAL EVIDENCE FOR *IN SITU* MICROBIAL FE REDOX CYCLING

Significant numbers of culturable FeOB and FeRB were present in both the mat and puffball materials (**Table 2**). However, the observed FeOB and FeRB densities were generally <1% of total culturable aerobic and fermentative heterotrophs, comparable to results obtained in other studies in which active microbial Fe redox cycling was implicated (Weiss et al., 2003; Blöthe and Roden, 2009). To our knowledge the efficiency of conventional FeOB and FeRB culturing approaches compared to heterotrophs has not been documented, and the possibility exists that the former populations were underestimated in this and other studies, due to culturability issues. This assertion is supported by the clone library results, which provided strong support for a lithotroph-dominated microbial community centered around taxa related to known FeOB (**Table 3**). Sequences related at the species level (≥97% similarity in 16S rRNA gene sequence) to microaerophilic FeOB *Gallionella capsiferriformans* ES-2 and *Sideroxydans lithotrophicus* ES-1 (Emerson and Moyer, 1997) were the most abundant taxa in the mat and puffball libraries, respectively. In addition, both libraries contained significant numbers of sequences closely related (99%) to denitrifying FeOB previously identified in freshwater sediments (Buchholz-Cleven et al., 1997), many of which are known to be capable of microaerophilic Fe(II) oxidation (Benz et al., 1998). The puffball library also contained sequences identical to the microaerophilic FeOB *Comomonas* sp. IST-3 isolated from a groundwater Fe seep in Alabama (Blöthe and Roden, 2009). Other putative lithotrophs were identified, including sequences related (albeit distantly at 92%) to the reduced sulfur (S^0 and $S_2O_3^{2-}$) oxidizing *Sulfuricella denitrificans* in the mat, and to the CH_4 oxidizing *Methylobacter* sp. in the puffball. Whether or not sulfur or methane oxidation takes place in the seep is unknown.

The clone libraries also contained significant numbers of sequences related to known FeRB, including *Rhodoferax ferrireducens* (Finneran et al., 2003) in the mat, and *Aeromonas hydrophila* (Knight and Blakemore, 1998) and *Geobacter* sp. (Lovley et al., 2004) in the puffball. The puffball library also contained sequences related to *Desulfovibrio*, a sulfate-reducing taxon which includes organisms capable of dissimilatory reduction of Fe(III) and other oxidized metals (Coleman et al., 1993; Lovley et al., 1993). Collectively, sequences related to known FeOB and FeRB

accounted for 88 and 59% of total sequences in the mat and puffball libraries, respectively. These results confirm 16S rRNA gene clone library results for analogous groundwater seep environments (Haaijer et al., 2008; Blöthe and Roden, 2009; Duckworth et al., 2009; Bruun et al., 2010; Fleming et al., 2011; Gault et al., 2011; Johnson et al., 2012), and are consistent with the presence of active Fe redox cycling microbial communities in such environments.

BARCODE SEQUENCING OF 16S rRNA GENE AMPLICONS

The specialized environment of the groundwater Fe seep provided an opportunity to assess whether high throughput barcode sequencing approaches can provide increased insight into 16S rRNA gene-based inferences of microbial community structure and functionality compared to those obtained through conventional cloning and sequencing. The motivation for applying these approaches is that they afford the opportunity to obtain 100–1000 times more sequences compared to a typical clone library consisting of a few hundred clones or less. Acquiring a much greater number of sequences has the potential to both extend knowledge of microbial diversity as well as more confidently reveal the dominant components of a given community (Sogin et al., 2006; Huber et al., 2007; Cardenas and Tiedje, 2008). The latter consideration is most relevant to this study, given our focus on dissection of a representative Fe redox cycling microbial community.

The barcode sequencing results agreed well with the conventional clone libraries at the phylum/class level (**Figure 7**). In particular, the relative importance of Betaproteobacteria in both the mat and puffball materials indicated by the clone libraries was verified by the barcode sequencing. This result is in agreement with a combined clone library and V4–454 sequencing study of a groundwater Fe seep in Maine (Fleming et al., 2011). However, in contrast to the findings of Fleming et al. (2011), where the *Leptothrix* dominated FeOB community indicated by clone library composition was verified by barcode sequencing, the *Gallionella*/*Sideroxydans* dominated FeOB communities suggested by the mat and puffball clone libraries was only verified by the V6 barcode libraries, and was not observed in the other libraries (see **Tables 4** and **5**). Even in the case of the V6 libraries, the relative abundance of *Gallionella*/*Sideroxydans* sequences was considerably lower than that observed in the clone libraries (5 vs. 47% for the mat, 5 vs. 16% for the puffball). While the cause for this mismatch remains unknown, it must be acknowledged that current barcode sequencing approaches, like conventional cloning and sequencing (von Wintzingerode et al., 1997), is subject to various types of biases (including PCR bias) that may render accurate quantitative analysis of microbial community structure difficult or impossible (Berry et al., 2011; Zhou et al., 2011). This limitation provides a plausible (albeit disappointing) explanation for various other mismatches between the clone library and barcode sequencing results, as well as differences in community composition among the different barcode libraries (see Results). Additional comparisons of conventional cloning and barcode sequencing approaches will be required to evaluate whether or not these methodologies routinely provide a common picture of microbial community composition.

Despite the apparent limited overlap among taxa present in the clone and barcode libraries, the barcode sequence information could nevertheless be used to gain further insight into characteristics of the mat and puffball microbial communities. A series of BLAST searches was conducted with most abundant OTUs ($\geq$0.5% of total sequences) detected in the barcode libraries; only the V4–454 sequences were used for this analysis, as these reads were 3–4 times longer than the V6–454 and Illumina sequences, thereby affording greater phylogenetic resolution (BLAST analysis of the shorter reads revealed large numbers of high similarity hits that could not be rationally distinguished in terms of their ability to provide insight in Fe redox cycling components of the microbial community). The similarity between the V4–454 and clone library OTUs was determined in conjunction with this analysis. Several interesting results emerged (see **Tables 6** and **7**). First, many of the most abundant V4–454 OTUs were highly similar to known FeOB, including *Acidovorax* sequences closely related to the denitrifying FeOB *A. delafieldii* 2AN (Chakraborty et al., 2011) for the microbial mat; and *Comomonas* sequences related the aerobic FeOB *Comomonas* sp. IST-3 (Blöthe and Roden, 2009) together with *Aquabacterium* and *Pseudomonas* sequences closely related to denitrifying FeOB (Straub et al., 1996; Buchholz-Cleven et al., 1997; Muehe et al., 2009) for the puffball. The seep contains significant nitrate (ca. 0.02–0.2 mM), and active nitrate-reducing, Fe(II)-oxidizing enrichment cultures were obtained from both the mat and puffball materials (M. Blöthe, unpublished data). In addition, a nitrate-reducing, Fe(II)-oxidizing *Dechlorospirillum* species (unrelated to sequences reported here) was recently isolated from the seep materials (Picardal et al., 2011). It is unknown whether or not *A. delafieldii* 2AN or the nitrate-dependent FeOB described by Buchholz-Cleven et al. (1997) are capable of microaerophilic Fe(II) oxidation, but the fact that many such organisms are known to grow lithotrophically via Fe(II) oxidation under microaerophilic conditions (Benz et al., 1998) suggests that this could be the case.

Second, potential Fe(III)-reducing *Desulfovibrio* sequences (see previous section) closely related to *D. putealis* (Basso et al., 2005) were the most abundant OTUs in the puffball V4–454 libraries. This result is important in that it strongly suggests the proliferation of anaerobic bacteria within the puffball, which in turn is consistent with the geochemical measurements and *in vitro* Fe(III) reduction experiments (see above). We found no voltammetric evidence for the existence of dissolved sulfide in the seep waters, and the solid-phases present were uniformly orangish-brown with no evidence of black iron monosulfides. In addition, there was no production of a sulfide smell upon acidification of samples from the anaerobic incubations. Together these results indicate that the *Desulfovibrio*-related taxa present in the puffball materials could have been functioning as Fe(III) reducers. The apparent absence of sulfate reduction activity is consistent with the recent groundwater seep study of Bruun et al. (2010) where no significant sulfate reduction was observed during anaerobic incubation of seep materials without added electron donor.

In both of the above examples, the most abundant barcodes for Betaproteobacteria (*Acidovorax*, *Comomonas*, *Aquabacterium*)

Table 6 | BLAST matches to dominant (≥0.5% of total sequences) microbial mat (site 2) V4-454 sequences, and similarity between V4 454 and clone library sequences.

Abundance rank	%Total sequences	Cumulative % total	V4 amplicon RDP assignment	Relevant BLAST match	Acession No.	Similarity (%)	Physiology	Reference(s)	Clone library RDP assignment(s)	Similarity (%)[a]
1	56.32	56.3	*Acidovorax*	*Acidovorax delafieldii* strain 2AN	HM625980.1	100	Fe(II) Ox, NO_3^- red	Chakraborty et al. (2011)	*Rhodoferax* *Aquabacterium*	97.92 97.52
2	23.90	80.2	*Bacillus*	*Bacillus thioparus* strain BMP-1	DQ371431	100	$S_2O_3^{2-}$ Ox, O_2 red	Pérez-Ibarra et al. (2007)	No match	NA[b]
3	2.30	82.5	Unclassified Bacillaceae	*Bacillus thioparus* strain BMP-1	DQ371431	100	$S_2O_3^{2-}$ Ox, O_2 red	Pérez-Ibarra et al. (2007)	No match	NA
4	0.81	83.3	Unclassified Comamonadaceae	*Acidovorax delafieldii* strain 2AN	HM625980.1	97	Fe(II) Ox, NO_3^- red	Chakraborty et al. (2011)	*Rhodoferax* *Aquabacterium*	95.02 94.67
5	0.81	84.1	Unclassified Comamonadaceae	*Acidovorax delafieldii* strain 2AN	HM625980.1	97	Fe(II) Ox, NO_3^- red	Chakraborty et al. (2011)	*Rhodoferax* *Aquabacterium*	97.84 97.42
6	0.75	84.9	*Acidovorax*	*Acidovorax delafieldii* strain 2AN	HM625980.1	97	Fe(II) Ox, NO_3^- red	Chakraborty et al. (2011)	*Aquabacterium* *Rhodoferax*	97.53 97.12
7	0.52	85.4	*Stenotrophomonas*	*Stenotrophomonas maltophilia* strain CCUG 41684	GU945534.1	100	Aerobic heterotroph	Svensson-Stadler et al. (2012)	No match	NA

[a] *Determined by querying each V4 454 sequence against the full set of unique clone library sequences using the "Align two or more sequences" facility in BLAST; only matches with ca. 95% or greater similary are reported.*

[b] *Not applicable.*

Table 7 | BLAST matches to dominant (≥0.5% of total sequences) puffball (site 7) V4–454 sequences, and similarity between V4 454 and clone library sequences.

Abundance rank	% Total sequences	Cumulative % Total	V4 Amplicon RDP assignment	Relevant BLAST match	Acession No.	Similarity (%)	Physiology	Reference(s)	Clone library RDP assignment(s)	Similarity (%)[a]
1	28.88	28.9	*Desulfovibrio*	*Desulfovibrio putealis* strain B7-43	NR_029118.1	99	SO_4^{2-} red, Fe(III) red?	Basso et al. (2005), Lovley et al. (1993)	*Desulfovibrio*	99.10
2	16.73	45.6	*Comamonas*	*Comamonas* sp. IST-3	DQ386262.1	99	Fe(II) Ox, O_2 red	Blöthe and Roden (2009)	*Comamonas*	99.57
3	9.67	55.3	Unclassified Sphingobacteriales	*Pontibacter korlensis* strain AsK09	GQ503321.1	87	Aerobic heterotroph	Zhang et al. (2008)	No match	NA[b]
4	6.94	62.2	*Pseudomonas*	*Pseudomonas alcaligenes*, various strains		100	Aerobic heterotroph	Straub et al. (1996), Muehe et al. (2009)	No match	NA
5	4.54	66.8	*Pseudomonas*	*Pseudomonas stutzeri*, various strains		100	Fe(II) Ox, NO_3^- red	Straub et al. (1996), Muehe et al. (2009)	No match	NA
6	4.33	71.1	*Aeromonas*	*Aeromonas hydrophila* strain ATCC 7966	X60404.2	100	Fe(III) red	Knight and Blakemore (1998)	*Aeromonas*	100
7	2.90	74.0	*Pseudomonas*	*Pseudomonas*, various species		100	Aerobic heterotroph	Bergey's (2005)	No match	NA
8	1.43	75.4	*Aquabacterium*	Denitrifying Fe(II)-oxidizing bacteria	U51102.1	99	Fe(II) Ox, NO_3^- red	Buchholz-Cleven et al. (1997)	*Aquabacterium*	100
9	1.18	76.6	*Pseudomonas*	*Pseudomonas*, various species		100	Aerobic heterotroph	Bergey's (2005)	No match	NA
10	1.05	77.6	*Pseudomonas*	*Pseudomonas alcaligenes*, various strains		99	Aerobic heterotroph	Bergey's (2005)	No match	NA
11	0.84	78.5	*Comamonas*	*Comamonas* sp. IST-3	DQ386262.1	98	Fe(II) Ox, O_2 red	Blöthe and Roden (2009)	*Comamonas* *Aquabacterium*	98.29 97.86
12	0.59	79.1	*Pseudomonas*	*Pseudomonas alcaligenes*, various strains		100	Aerobic heterotroph	Bergey's (2005)	No match	NA
13	0.55	79.6	Unclassified Burkholderiales	*Comamonas* sp. IST-3	DQ386262.1	98	Fe(II) Ox, O_2 red	Blöthe and Roden (2009)	*Comamonas* *Aquabacterium*	97.87 97.45

[a] *Determined by querying each V4 454 sequence against the full set of unique clone library sequences using the "Align two or more sequences" facility in BLAST; only matches with ca. 95% or greater similarly are reported.*

[b] *Not applicable.*

and Deltaproteobacteria (*Desulfovibrio*) related sequences were ≥97% similar to one or more unique OTUs in the clone libraries. These connections suggest that barcode sequencing did in fact sample many of the key putative Fe redox cycling taxa present in the clone libraries, even though this fact was not necessarily evident from the RDP-based phylogenetic assignments. This phenomenon is best illustrated by the *Acidovorax* related sequences identified in the mat V4–454 library, which were 97–98% similar to *Rhodoferax* and *Aquabacterium* related sequences from the clone libraries. A general implication of these results is that detailed BLAST searching, as well as inquiries into the physiological properties of related taxa, will likely be required to make the best possible physiological inferences from barcode sequencing information.

Another interesting finding from the V4–454 BLAST searches is that the large number of Bacillaceae related sequences in the mat library were closely related to *Bacillus thioparans* BMP-1, an organism capable of chemolithoautotrophic growth coupled to thiosulfate ($S_2O_3^{2-}$) oxidation (Pérez-Ibarra et al., 2007). Although we do not know if $S_2O_3^{2-}$ oxidation takes place in the seep, the large number of sequences related to this taxon clearly suggests the possibility. This may not be a far-fetched suggestion, given that oxidative dissolution of authigenic iron sulfide minerals in Mississippian-age marine sediments provides the Fe(II) source for the seep (Schieber and Glamoclija, 2007). This result, as well as the recovery of numerous sequences related to putative nitrate-reducing FeOB, provides an example of how 16S rRNA gene surveys could motivate more detailed studies of metabolically unique (in this case lithotrophic) organisms in a given microbial community.

CONCLUSION

A combination of geochemical and microbiological data revealed the existence of an *in situ* "microbial ferrous wheel" in a circumneutral groundwater Fe seep. The wheel turns by virtue of the coupled activities of lithotrophic (aerobic and possibly nitrate-reducing) FeOB and dissimilatory FeRB across mm-to-cm scale redox gradients within semi-consolidated mat and floating puffball structures. The results confirm and extend previous findings in similar groundwater Fe seep and aquatic sedimentary environments, and provide a real-world example of a microbially driven Fe redox cycling system analogous to that documented previously for cocultures of FeOB and FeRB. The groundwater seep environment also provides useful clues as to the likely physical and metabolic arrangement of microbial Fe redox cycling communities within redox gradients in a wide variety of soil and sedimentary environments.

ACKNOWLEDGMENTS

We are indebted to Mitch Sogin and colleagues at MBL, and Noah Fierer and colleagues at the University of Colorado–Boulder, for facilitating the barcode sequencing of our 16S rRNA gene samples. This work was supported by the NASA Astrobiology Institute (University of California, Berkeley and University of Wisconsin–Madison nodes), and the U.S. Department of Energy, Office of Biological and Environmental Research, Subsurface Biogeochemical Research Program through the SBR Scientific Focus Area at the Pacific Northwest National Laboratory. Work in the Emerson laboratory at Bigelow was also supported by grants from the Office of Naval Research N00014-08-1-0334 and the National Science Foundation IOS-0951077.

REFERENCES

Achenbach, L. A., and Coates, J. D. (2000). Disparity between bacterial phylogeny and physiology. *ASM News* 66, 1–4.

Ashelford, K. E., Chuzhanova, N. A., Fry, J. C., Jones, A. J., and Weightman, A. J. (2005). At least 1 in 20 16S rRNA sequence records currently held in public repositories is estimated to contain substantial anomalies. *Appl. Environ. Microbiol.* 71, 7724–7736.

Basso, O., Caumette, P., and Magot, M. (2005). *Desulfovibrio putealis* sp. nov., a novel sulfate-reducing bacterium isolated from a deep subsurface aquifer. *Int. J. Syst. Evol. Microbiol.* 55, 101–104.

Bates, S. T., Berg-Lyons, D., Caporaso, J. G., Walters, W. A., Knight, R., and Fierer, N. (2011). Examining the global distribution of dominant archaeal populations in soil. *ISME J.* 5, 908–917.

Benz, M., Brune, A., and Schink, B. (1998). Anaerobic and aerobic oxidation of ferrous iron at neutral pH by chemoheterotrophic nitrate-reducing bacteria. *Arch. Microbiol.* 169, 159–165.

Bergey. (2005). "Bergey's manual of systematic bacteriology," in *The Proteobacteria*, Vol 2, 2nd Edn, eds G. M. Garrity, D. J. Brenner, N. R. Krieg, and J. T. Staley (New York: Springer), 2816.

Berry, D., Ben Mahfoudh, K., Wagner, M., and Loy, A. (2011). Barcoded primers used in multiplex amplicon pyrosequencing bias amplification. *Appl. Environ. Microbiol.* 77, 7846–7849.

Blöthe, M., and Roden, E. E. (2009). Microbial iron redox cycling in a circumneutral-pH groundwater seep. *Appl. Environ. Microbiol.* 75, 468–473.

Brendel, P. J., and Luther, G. W. (1995). Development of a gold amalgam voltammetric microelectrode for the determination of dissolved Fe, Mn, O-2, and S(-II) in porewaters of marine and freshwater sediments. *Environ. Sci. Technol.* 29, 751–761.

Brune, A., Ludwig, W., and Schink, B. (2002). *Propionivibrio limicola* sp. nov., a fermentative bacterium specialized in the degradation of hydroaromatic compounds, reclassification of *Propionibacter pelophilus* as *Propionivibrio pelophilus* comb. nov. and amended description of the genus *Propionivibrio. Int. J. Syst. Evol. Microbiol.* 52, 441–444.

Bruun, A. M., Finster, K., Gunnlaugsson, H. P., Nornberg, P., and Friedrich, M. W. (2010). A comprehensive investigation on iron cycling in a freshwater seep including microscopy, cultivation and molecular community analysis. *Geomicrobiol. J.* 27, 15–34.

Buchholz-Cleven, B. E. E., Rattunde, B., and Straub, K. L. (1997). Screening for genetic diversity of isolates of anaerobic Fe(II)-oxidizing bacteria using DGGE and whole-cell hybridization. *Syst. Appl. Microbiol.* 20, 301–309.

Canfield, D. E., Stewart, F. J., Thamdrup, B., De Brabandere, L., Dalsgaard, T., Delong, E. F., Revsbech, N. P., and Ulloa, O. (2010). A cryptic sulfur cycle in oxygen-minimum-zone waters off the Chilean coast. *Science* 330, 1375–1378.

Caporaso, J. G., Lauber, C. L., Walters, W. A., Berg-Lyons, D., Lozupone, C. A., Turnbaugh, P. J., Fierer, N., and Knight, R. (2010). Global patterns of 16S rRNA diversity at a depth of millions of sequences per sample. *Proc. Natl. Acad. Sci. U.S.A.* 108, 4516–4522.

Cardenas, E., and Tiedje, J. M. (2008). New tools for discovering and characterizing microbial diversity. *Curr. Opin. Biotechnol.* 19, 544–549.

Chakraborty, A., Roden, E. E., Schieber, J., and Picardal, F. (2011). Enhanced growth of *Acidovorax* sp. strain 2AN during nitrate-dependent Fe(II) oxidation in batch and continuous-flow systems. *Appl. Environ. Microbiol.* 77, 8548–8556.

Clement, B. G., Luther, G. W., and Tebo, B. M. (2009). Rapid, oxygen-dependent microbial Mn(II) oxidation kinetics at sub-micromolar oxygen concentrations in the Black Sea suboxic zone. *Geochim. Cosmochim. Acta* 73, 1878–1889.

Coby, A. J., Picardal, F., Shelobolina, E., Xu, H., and Roden, E. E. (2011). Repeated anaerobic microbial redox cycling of iron. *Appl. Environ. Microbiol.* 77, 6036–6042.

Coleman, M. L., Hedrick, D. B., Lovley, D. R., White, D. C., and Pye, K. (1993). Reduction of Fe(III) in sediments by sulphate-reducing bacteria. *Nature* 361, 436–438.

Costello, A. M., and Lidstrom, M. E. (1999). Molecular characterization of functional and phylogenetic genes from natural populations of methanotrophs in lake sediments.

Appl. Environ. Microbiol. 65, 5066–5074.

Cummings, D. E., March, A. W., Bostick, B., Spring, S., Caccavo, F. Jr., Fendorf, S., and Rosenzweig, R. F. (2000). Evidence for microbial Fe(III) reduction in anoxic, mining-impacted lake sediments (Lake Coeur d'Alene, Idaho). *Appl. Environ. Microbiol.* 66, 154–162.

Decho, A. W., Norman, R. S., and Visscher, P. T. (2010). Quorum sensing in natural environments: emerging views from microbial mats. *Trends Microbiol.* 18, 73–80.

Dewhirst, F. E., Chien, C.-C., Paster, B. J., Ericson, R. L., Orcutt, R. P., Schauer, D. B., and Fox, J. G. (1999). Phylogeny of the defined murine microbiota: altered schaedler flora. *Appl. Environ. Microbiol.* 65, 3287–3292.

Druschel, G. K., Emerson, D., Sutka, R., Suchecki, P., and Luther, G. W. (2008). Low-oxygen and chemical kinetic constraints on the geochemical niche of neutrophilic iron(II) oxidizing microorganisms. *Geochim. Cosmochim. Acta* 72, 3358–3370.

Duckworth, O. W., Holmström, S. J. M., Peña, J., and Sposito, G. (2009). Biogeochemistry of iron oxidation in a circumneutral freshwater habitat. *Chem. Geol.* 260, 149–158.

Edgar, R. C., Haas, B. J., Clemente, J. C., Quince, C., and Knight, R. (2011). UCHIME improves sensitivity and speed of chimera detection. *Bioinformatics* 27, 2194–2200.

Emerson, D. (2009). Potential for iron-reduction and iron-cycling in iron oxyhydroxide-rich microbial mats at Loihi Seamount. *Geomicrobiol. J.* 26, 639–647.

Emerson, D., Fleming, E. J., and McBeth, J. M. (2010). Iron-oxidizing bacteria: an environmental and genomic perspective. *Annu. Rev. Microbiol.* 64, 561–583.

Emerson, D., and Moyer, C. (1997). Isolation and characterization of novel iron-oxidizing bacteria that grow at circumneutral pH. *Appl. Environ. Microbiol.* 63, 4784–4792.

Emerson, D., and Revsbech, N. P. (1994a). Investigation of an iron-oxidizing microbial mat community located near Aarhus, Denmark – laboratory studies. *Appl. Environ. Microbiol.* 60, 4032–4038.

Emerson, D., and Revsbech, N. P. (1994b). Investigation of an iron-oxidizing microbial mat community located near Aarhus, Denmark: field studies. *Appl. Environ. Microbiol.* 60, 4022–4031.

Emerson, D., Weiss, J. V., and Megonigal, J. P. (1999). Iron-oxidizing bacteria are associated with ferric hydroxide precipitates (Fe-plaque) on the roots of wetland plants. *Appl. Environ. Microbiol.* 65, 2758–2761.

Finneran, K. T., Johnsen, C. V., and Lovley, D. R. (2003). *Rhodoferax ferrireducens* sp. nov., a psychrotolerant, facultatively anaerobic bacterium that oxidizes acetate with the reduction of Fe(III). *Int. J. Syst. Evol. Microbiol.* 53, 669–673.

Fleming, E. J., Langdon, A. E., Martinez-Garcia, M., Stepanauskas, R., Poulton, N. J., Masland, E. D. P., and Emerson, D. (2011). What's new is old: resolving the identity of *Leptothrix ochracea* using single cell genomics, pyrosequencing and FISH. *PLoS ONE* 6, e17769. doi:10.1371/journal.pone.0017769

Francis, C. A., and Tebo, B. M. (2002). Enzymatic manganese(II) oxidation by metabolically dormant spores of diverse *Bacillus* species. *Appl. Environ. Microbiol.* 68, 874–880.

Gault, A. G., Ibrahim, A., Langley, S., Renaud, R., Takahashi, Y., Boothman, C., Lloyd, J. R., Clark, I. D., Ferris, F. G., and Fortin, D. (2011). Microbial and geochemical features suggest iron redox cycling within bacteriogenic iron oxide-rich sediments. *Chem. Geol.* 281, 41–51.

Gillis, M., Vandamme, P., Devos, P., Swings, J., and Kersters, K. (2001). "Polyphasic taxonomy," in *Bergey's Manual of Systematic Bacteriology*, 2nd Edn, eds D. R. Boone and R. W. Castenholz (New York: Springer), 43–48.

Glazer, B. T., and Rouxel, O. J. (2009). Redox speciation and distribution within diverse iron-dominated microbial habitats at Loihi Seamount. *Geomicrobiol. J.* 26, 606–622.

Haaijer, S. C. M., Harhangi, H. R., Meijerink, B. B., Strous, M., Pol, A., Smolders, A. J. P., Verwegen, K., Jetten, M. S. M., and Den Camp, H. J. M. O. (2008). Bacteria associated with iron seeps in a sulfur-rich, neutral pH, freshwater ecosystem. *ISME J.* 2, 1231–1242.

Hamady, M., Walker, J. J., Harris, J. K., Gold, N. J., and Knight, R. (2008). Error-correcting barcoded primers for pyrosequencing hundreds of samples in multiplex. *Nat. Methods* 5, 235–237.

Hamaki, T., Suzuki, M., Fudou, R., Jojima, Y., Kajiura, T., Tabuchi, A., Sen, K., and Shibai, H. (2005). Isolation of novel bacteria and actinomycetes using soil-extract agar medium. *J. Biosci. Bioeng.* 99, 485–492.

Hiraishi, A. (1994). Phylogenetic affiliations of *Rhodoferax fermentans* and related species of phototrophic bacteria as determined by automated 16S rDNA sequencing. *Curr. Microbiol.* 28, 25–29.

Holland, H. D., and Kasting, J. F. (1992). "The environment of the Archean Earth," in *The Proterozoic Biosphere: a Multidisciplinary Study*, eds J. W. Schopf and C. Klein (Cambridge: Cambridge University Press), 21–24.

Huber, J. A., Welch, D. B. M., Morrison, H. G., Huse, S. M., Neal, P. R., Butterfield, D. A., and Sogin, M. L. (2007). Microbial population structures in the deep marine biosphere. *Science* 318, 97–100.

Hunter, K. S., Wang, Y., and Vancappellen, P. (1998). Kinetic modeling of microbially-driven redox chemistry of subsurface environments: coupling transport, microbial metabolism and geochemistry. *J. Hydrol.* 209, 53–80.

Jakobsen, R. (2007). Redox microniches in groundwater: a model study on the geometric and kinetic conditions required for concomitant Fe oxide reduction, sulfate reduction, and methanogenesis. *Water Resour. Res.* 43, W12S12, 11.

James, R. E., and Ferris, F. G. (2004). Evidence for microbial-mediated iron oxidation at a neutrophilic groundwater spring. *Chem. Geol.* 212, 301–311.

Johnson, K. W., Carmichael, M. J., Mcdonald, W., Rose, N., Pitchford, J., Windelspecht, M., Karatan, E., and Brauer, S. L. (2012). Increased abundance of *Gallionella* spp., *Leptothrix* spp. and total bacteria in response to enhanced Mn and Fe concentrations in a disturbed Southern Appalachian high elevation wetland. *Geomicrobiol. J.* 29, 124–138.

Kalyuzhnaya, M. G., Stolyar, S. M., Auman, A. J., Lara, J. C., Lidstrom, M. E., and Chistoserdova, L. (2005). *Methylosarcina lacus* sp. nov., a methanotroph from Lake Washington, Seattle, USA, and emended description of the genus *Methylosarcina*. *Int. J. Syst. Evol. Microbiol.* 55, 2345–2350.

Knight, V., and Blakemore, R. (1998). Reduction of diverse electron acceptors by *Aeromonas hydrophila*. *Arch. Microbiol.* 169, 239–248.

Kojima, H., and Fukui, M. (2010). *Sulfuricella denitrificans* gen. nov., sp. nov., a sulfur-oxidizing autotroph isolated from a freshwater lake. *Int. J. Syst. Evol. Microbiol.* 60, 2862–2866.

Konhauser, K. O., Hamade, T., Raiswell, R., Morris, R. C., Ferris, F. G., Southam, G., and Canfield, D. E. (2002). Could bacteria have formed the Precambrian banded iron formations? *Geology* 30, 1079–1082.

Konhauser, K. O., Newman, D. K., and Kappler, A. (2005). The potential significance of microbial Fe(III) reduction during deposition of Precambrian banded iron formations. *Geobiology* 3, 167–177.

Kysela, D. T., Palacios, C., and Sogin, M. L. (2005). Serial analysis of V6 ribosomal sequence tags (SARST-V6): a method for efficient, high-throughput analysis of microbial community composition. *Environ. Microbiol.* 7, 356–364.

Langley, S., Gault, A., Ibrahim, A., Renaud, R., Fortin, D., Clark, I. D., and Ferris, F. G. (2009). A Comparison of the rates of Fe(III) reduction in synthetic and bacteriogenic iron oxides by Shewanella putrefaciens CN32. *Geomicrobiol. J.* 26, 57–70.

Lovley, D. R., Holmes, D. E., and Nevin, K. P. (2004). Dissimilatory Fe(III) and Mn(IV) reduction. *Adv. Microb. Physiol.* 49, 219–286.

Lovley, D. R., Roden, E. E., Phillips, E. J. P., and Woodward, J. C. (1993). Enzymatic iron and uranium reduction by sulfate-reducing bacteria. *Mar. Geol.* 113, 41–53.

Lu, S. P., Gischkat, S., Reiche, M., Akob, D. M., Hallberg, K. B., and Küsel, K. (2010). Ecophysiology of Fe-cycling bacteria in acidic sediments. *Appl. Environ. Microbiol.* 76, 8174–8183.

Luther, G. W., Glazer, B. T., Ma, S. F., Trouwborst, R. E., Moore, T. S., Metzger, E., Kraiya, C., Waite, T. J., Druschel, G., Sundby, B., Taillefert, M., Nuzzio, D. B., Shank, T. M., Lewis, B. L., and Brendel, P. J. (2008). Use of voltammetric solid-state (micro)electrodes for studying biogeochemical processes: laboratory measurements to real time measurements with an in situ electrochemical analyzer (ISEA). *Mar. Chem.* 108, 221–235.

Muehe, E. M., Gerhardt, S., Schink, B., and Kappler, A. (2009). Ecophysiology and the energetic benefit of mixotrophic Fe(II) oxidation by various strains of nitrate-reducing bacteria. *FEMS Microbiol. Ecol.* 70, 335–343.

Muyzer, G., Teske, A., Wirsen, C. O., and Jannasch, H. W. (1995). Phylogenetic relationships of *Thiomicrospira* species and their identification in deep-sea hydrothermal vent samples by denaturing gradient gel electrophoresis of 16S rDNA fragments. *Arch. Microbiol.* 164, 165–172.

Neubauer, S. C., Emerson, D., and Megonigal, J. P. (2002). Life at the energetic edge: kinetics of circumneutral iron oxidation by

lithotrophic iron-oxidizing bacteria isolated from the wetland-plant rhizosphere. *Appl. Environ. Microbiol.* 68, 3988–3995.

Pace, N. R. (1996). New perspective on the natural microbial world: molecular microbial ecology. *ASM News* 62, 463–470.

Pace, N. R. (1997). A molecular view of microbial diversity and the biosphere. *Science* 276, 734–740.

Peine, A., Tritschler, A., Küsel, K., and Peiffer, S. (2000). Electron flow in an iron-rich acidic sediment – evidence for an acidity-driven iron cycle. *Limnol. Oceanogr.* 45, 1077–1087.

Pérez-Ibarra, B. M., Flores, M. E., and García-Varela, M. (2007). Isolation and characterization of *Bacillus thioparus* sp. nov., chemolithoautotrophic, thiosulfate-oxidizing bacterium. *FEMS Microbiol. Lett.* 271, 289–296.

Picardal, F. W., Zaybak, Z., Chakraborty, A., Schieber, J., and Szewzyk, U. (2011). Microaerophilic, Fe(II)-dependent growth and Fe(II) oxidation by a *Dechlorospirillum* species. *FEMS Microbiol. Lett.* 319, 51–57.

Planavsky, N., Rouxel, O., Bekker, A., Shapiro, R., Fralick, P., and Knudsen, A. (2009). Iron-oxidizing microbial ecosystems thrived in late Paleoproterozoic redox-stratified oceans. *Earth Planet. Sci. Lett.* 286, 230–242.

Pruesse, E., Quast, C., Knittel, K., Fuchs, B. M., Ludwig, W. G., Peplies, J., and Glöckner, F. O. (2007). SILVA: a comprehensive online resource for quality checked and aligned ribosomal RNA sequence data compatible with ARB. *Nucleic Acid Res.* 35, 7188–7196.

Quince, C., Lanzen, A., Davenport, R. J., and Turnbaugh, P. J. (2011). Removing noise from pyrosequenced amplicons. *BMC Bioinformatics* 12, 38. doi:10.1186/1471-2105-12-38

Rentz, J. A., Kraiya, C., Luther, G. W., and Emerson, D. (2007). Control of ferrous iron oxidation within circumneutral microbial iron mats by cellular activity and autocatalysis. *Environ. Sci. Technol.* 41, 6084–6089.

Revsbech, N. P., Larsen, L. H., Gundersen, J., Dalsgaard, T., Ulloa, O., and Thamdrup, B. (2009). Determination of ultra-low oxygen concentrations in oxygen minimum zones by the STOX sensor. *Limnol. Oceanogr. Methods* 7, 371–381.

Roden, E. E., and Emerson, D. (2007). "Microbial metal cycling in aquatic environments," in *Manual of Environmental Microbiology*, 3rd Edn, eds C. J. Hurst, D. Lipson, R. Crawford, J. Garland, A. Mills, and L. D. Stezenbach (Washington, DC: American Society for Microbiology), 540–562.

Roden, E. E., Sobolev, D., Glazer, B., and Luther, G. W. (2004). Potential for microscale bacterial Fe redox cycling at the aerobic-anaerobic interface. *Geomicrobiol. J.* 21, 379–391.

Scheiber, J. (2004). "Groundwater-fed iron-rich microbial mats in a freshwater creek- Growth cycles and fossilization potential of microbial features," in *35 th Lunar and Planetary Science Conference*, Abstracts of the Papers, Houston, 1369.

Schieber, J., and Glamoclija, M. (2007). "Microbial mats built by iron bacteria: a modern example from southern Indiana," in *Atlas of Microbial Mat Features Preserved Within the Silicilastic Rock Record*, eds J. Scheiber, P. Bose, P. G. Eriksson, S. Banerjee, S. Sarkar, W. Altermannn, and O. Catuneanu (Amsterdam: Elsevier), 233–244.

Schloss, P. D. (2010). The effects of alignment quality, distance calculation method, sequence filtering, and region on the analysis of 16S rRNA gene-based studies. *PLoS Comput. Biol.* 6, e1000844. doi:10.1371/journal.pcbi.1000844

Schloss, P. D., Westcott, S. L., Ryabin, T., Hall, J. R., Hartmann, M., Hollister, E. B., Lesniewski, R. A., Oakley, B. B., Parks, D. H., Robinson, C. J., Sahl, J. W., Stres, B., Thallinger, G. G., Van Horn, D. J., and Weber, C. F. (2009). Introducing mothur: open-source, platform-independent, community-supported software for describing and comparing microbial communities. *Appl. Environ. Microbiol.* 75, 7537–7541.

Schopf, J. W., Kudryavtsev, A. B., Sugitani, K., and Walter, M. R. (2010). Precambrian microbe-like pseudofossils: a promising solution to the problem. *Precambrian. Res.* 179, 191–205.

Smith, K. S., Costello, A. M., and Lidstrom, M. E. (1997). Methane and trichloroethylene oxidation by an estuarine methanotroph, *Methylobacter* sp. strain BB5.1. *Appl. Environ. Microbiol.* 63, 4617–4620.

Sobolev, D., and Roden, E. E. (2004). Characterization of a neutrophilic, chemolithoautotrophic Fe(II)-oxidizing β-proteobacterium from freshwater wetland sediments. *Geomicrobiol. J.* 21, 1–10.

Sobolev, D., and Roden, E. E. (2001). Suboxic deposition of ferric iron by bacteria in opposing gradients of Fe(II) and oxygen at circumneutral pH. *Appl. Environ. Microbiol.* 67, 1328–1334.

Sobolev, D., and Roden, E. E. (2002). Evidence for rapid microscale bacterial redox cycling of iron in circumneutral environments. *Antonie Van Leeuwenhoek* 81, 587–597.

Sogin, M. L., Morrison, H. G., Huber, J. A., Welch, D. M., Huse, S. M., Neal, P. R., Arrieta, J. M., and Herndl, G. J. (2006). Microbial diversity in the deep sea and the underexplored "rare biosphere." *Proc. Natl. Acad. Sci. U.S.A.* 103, 12115–12120.

Spring, S., Jäckel, U., Wagner, M., and Kämpfer, P. (2004). *Ottowia thiooxydans* gen. nov., sp. nov., a novel facultatively anaerobic, N_2O-producing bacterium isolated from activated sludge, and transfer of *Aquaspirillum gracile* to *Hylemonella gracilis* gen. nov., comb. nov. *Int. J. Syst. Evol. Microbiol.* 54, 99–106.

Stookey, L. L. (1970). Ferrozine – a new spectrophotometric reagent for iron. *Anal. Chem.* 42, 779–781.

Straub, K. L., Benz, M., Schink, B., and Widdel, F. (1996). Anaerobic, nitrate-dependent microbial oxidation of ferrous iron. *Appl. Environ. Microbiol.* 62, 1458–1460.

Straub, K. L., Hanzlik, M., and Buchholz-Cleven, B. E. E. (1998). The use of biologically produced ferrihydrite for the isolation of novel iron-reducing bacteria. *Syst. Appl. Microbiol.* 21, 442–449.

Svensson-Stadler, L. A., Mihaylova, S. A., and Moore, E. R. B. (2012). *Stenotrophomonas* interspecies differentiation and identification by *gyrB* sequence analysis. *FEMS. Microbiol. Lett.* 327, 15–24.

Taillefert, M., Bono, A., and Luther, G. (2000). Reactivity of freshly formed Fe(III) in synthetic solutions and (pore)waters: voltammetric evidence of an aging process. *Environ. Sci. Technol.* 34, 2169–2177.

von Wintzingerode, F., Gobel, U. B., and Stackebrandt, E. (1997). Determination of microbial diversity in environmental samples: pitfalls of PCR-based rRNA analysis. *FEMS Microbiol. Rev.* 21, 213–229.

Walker, J. C. G. (1984). Suboxic diagenesis in banded iron formations. *Nature* 309, 340–342.

Wang, J. J., Muyzer, G., Bodelier, P. L. E., and Laanbroek, H. J. (2009). Diversity of iron oxidizers in wetland soils revealed by novel 16S rRNA primers targeting *Gallionella*-related bacteria. *ISME J.* 3, 715–725.

Wang, Q., Garrity, G. M., Tiedje, J. M., and Cole, J. R. (2007). Naive Bayesian classifier for rapid assignment of rRNA sequences into the new bacterial taxonomy. *Appl. Environ. Microbiol.* 73, 5261–5267.

Weiss, J. V., Emerson, D., Backer, S. M., and Megonigal, J. P. (2003). Enumeration of Fe(II)-oxidizing and Fe(III)-reducing bacteria in the root zone of wetland plants: implications for a rhizosphere iron cycle. *Biogeochemistry* 64, 77–96.

Weiss, J. V., Emerson, D., and Megonigal, J. P. (2005). Rhizosphere iron(III) deposition and reduction in a *Juncus effusus* L.-dominated wetland. *Soil. Sci. Soc. Am. J.* 69, 1861–1870.

Widdel, F., and Bak, F. (1992). "Gram-negative mesophilic sulfate-reducing bacteria," in *The Prokaryotes*, eds H. Truper, M. Dworkin, W. Harder, and K. Schleifer (New York, NY: Springer-Verlag), 3352–3378.

Woomer, P. L. (1994). "Most probable number counts," in *Methods of Soil Analysis*, part 2, ed. J. Bigham (Madison, WI: Soil Science Society of America), 59–79.

Zhang, L., Zhang, Q., Luo, X., Tang, Y., Dai, J., Li, Y., Wang, Y., Chen, G., and Fang, C. (2008). *Pontibacter korlensis* sp. nov., isolated from the desert of Xinjiang, China. *Int. J. Syst. Evol. Microbiol.* 58, 1210–1214.

Zhou, J. Z., Wu, L. Y., Deng, Y., Zhi, X. Y., Jiang, Y. H., Tu, Q. C., Xie, J. P., Van Nostrand, J. D., He, Z. L., and Yang, Y. F. (2011). Reproducibility and quantitation of amplicon sequencing-based detection. *ISME J.* 5, 1303–1313.

Conflict of Interest Statement: The authors declare that the research was conducted in the absence of any commercial or financial relationships that could be construed as a potential conflict of interest.

Received: 06 March 2012; accepted: 18 April 2012; published online: 22 May 2012.

Citation: Roden EE, McBeth JM, Blöthe M, Percak-Dennett EM, Fleming EJ, Holyoke RR, Luther III GW, Emerson D and Schieber J (2012) The microbial ferrous wheel in a neutral pH groundwater seep. Front. Microbio. ***3****:172. doi: 10.3389/fmicb.2012.00172*

This article was submitted to Frontiers in Microbiological Chemistry, a specialty of Frontiers in Microbiology.

Copyright © 2012 Roden, McBeth, Blöthe, Percak-Dennett, Fleming, Holyoke, Luther III, Emerson and Schieber. This is an open-access article distributed under the terms of the Creative Commons Attribution Non Commercial License, which permits non-commercial use, distribution, and reproduction in other forums, provided the original authors and source are credited.